WL-TR-92-4045

AD-A255 379

ANGHT LABORATORY

PROCEEDINGS OF THE 1991 USAF STRUCTURAL INTEGRITY PROGRAM CONFERENCE

EDITORS:

Thomas D. Cooper WL/Materials Directorate Wright-Patterson AFB, Ohio John W. Lincoln ASD/Deputy for Engineering Wright-Patterson AFB, Ohio

Robert M. Bader WL/Flight Dynamics Directorate Wright-Patterson AFB, Ohio

July 1992

Final Report for Period 2-6 December 1991



Hyatt Regency San Antonio, Texas

Approved for public release; distribution is unlimited

MATERIALS DIRECTORATE
WRIGHT LABORATORY
AIR FORCE MATERIEL COMMAND
WRIGHT-PATTERSON AFB, OHIO 45433-6533

NOTICE

When Government drawings, specifications, or other data are used for any purpose other than in connection with a definitely related Government procurement operation, the United States Government thereby incurs no responsibility or any obligation whatsoever; and the fact that the government may have formulated, furnished, or in any way supplied the said drawings, specifications, or other data, is not to be regarded by implication or otherwise as in any manner licensing the holder or any other person or corporation, or conveying any rights or permission to manufacture use, or sell any patented invention that may in any way be related thereto.

This report has been reviewed by the Office of Public Affairs (ASD/PA) and is releasable to the National Technical Information Service (NTIS). At NTIS, it will be available to the general public, including foreign nationals.

This technical report has been reviewed and is approved for publication.

THOMAS D. COOPER, Chief Systems Support Division

Materials Directorate

If your address has changed, if you wish to be removed from our mailing list, or if the addressee is no longer employed by your organization, please notify WL/MLS, Wright-Patterson AFB, Ohio 45433-6533 to help us maintain a current mailing list.

Copies of this report should not be returned unless return is required by security considerations, contractual obligations, or notice on a specific document.

REPORT DOCUMENTATION PAGE

Form Approved

OMB No 0704 0188

Public reporting burden for this collection of information is estimated to average 1 hour per response, including the time for reviewing instructions, sharching existing only sources, gathering and maintaining the data needed, and completing and reviewing the collection of information. Send comments rejarding this burden estimate or any other is per tof this collection of information, including suggestions for reducing this burden, to Washington Headquarters Services, circectorate for information Operations and Reports, 1215 refferson Davis Highway, Suite 1204, Arlington, VA 22202-4302, and to the Office of Management and Budget, Paperwork Reduction Project (0704-0188), Washington, DC 20503

1. AGENCY USE ONLY (Leave bla		3. REPORT TYPE AND	
	July 1992	Final, 2-6 De	
4. TITLE AND SUBTITLE Proceedings of the 19 Program Conference	991 USAF Structural Int	tegrity	5. FUNDING NUMBERS PE 62101F
Program Conterence			PR 2418
6. AUTHOR(S)			TA 07
			WU 04
ASD/ENFS, and Robert	mpiler & Editor; John W M. Bader, WL/FIB, Edit		
7. PERFORMING ORGANIZATION I	NAME(S) AND ADDRESS(ES)		8. PERFORMING ORGANIZATION REPORT NUMBER
WL/MLS, WPAFB OH 454	33-6533		WL-TR-92-4045
9. SPONSORING/MONITORING AC	GENCY NAME(S) AND ADDRESS(ES)	10. SPONSORING/MONITORING AGENCY REPORT NUMBER
11. SUPPLEMENTARY NOTES			· · · · · · · · · · · · · · · · · · ·
12a. DISTRIBUTION / AVAILABILITY	STATEMENT		12b. DISTRIBUTION CODE
Approved for public r	elease; distribution i	ls unlimited.	
13. ABSTRACT (Maximum 200 wor	ds)		
	ilation of the papers ference held at the Hy		
2-0 December 1991.			
•			
14 SUBJECT TERMS Airfram	e Structural Integrity	Program F-16N	File 1 15. NUMBER OF PAGES
	ife Extension, CT114 T		
	ructures, Compressive		
17. SECURITY CLASSIFICATION OF REPORT	18. SECURITY CLASSIFICATION OF THIS PAGE	19. SECURITY CLASSIFIC OF ABSTRACT	ATION 20. LIMITATION OF ABSTRACT
UNCLASSIFIED	UNCLASSIFIED	UNCLASSIFIED	UNLIMITED

FOREWORD

This report was compiled by the Systems Support Division, Materials Directorate, Wright Laboratory, Wright-Patterson Air Force Base, Ohio. It was initiated under Task 24180704 "Corrosion Control & Failure Analysis" with Thomas D. Cooper as the Project Engineer.

This technical report was submitted by the editors.

The purpose of this 1991 Conference was to bring together technical personnel in DOD and the aerospace industry who are involved in the various technologies required to ensure the structural integrity of aircraft gas turbine engines, airframes and other mechanical systems. It provided a forum to exchange ideas and share new information relating to the critical aspects of durability and damage tolerance technology for aircraft systems. The Conference was sponsored by the Aeronautical Systems Division Deputy for Engineering and Materials and Flight Dynamics Directorates of the Wright Laboratory, Wright-Patterson Air Force Base, Ohio. It was hosted by the Air Force Logistics Command's San Antonio Air Logistics Center.

DTIC QUALITY INCPECTED 5

		1_	
Accesio	n For		
NTIS	CRA&I	Ä	
DTIC	•	Ð	
Unan e			
Justific	ation		
By Distrib	itioa /		···•··
Ä	vallability	Codes	_
Dist	Avail an Speci	•	
A-1			

TABLE OF CONTENTS

Page
AGENDAviii
INTRODUCTIONxiii
SESSION I - OVERVIEWS
F-16 Airframe Structural Integrity Program 1
F-16N Fuel Shelf Joint Fatigue Life Extension by Cold-Expansion of Fastener Holes 27
C-141 Wing Station 405 Risk Assessment
Phased Load Condition Generator for C-17 Full-Scale Durability Qualification Testing
Testing of a Major Structural Component (C401) on the B-2 Advanced Technology Bomber
C-130 Wing Durability Testing
SESSION II - STRUCTURAL ANALYSIS AND TESTING
Using Approximate Methods for Complex Damage Tolerance Problems172
Damage Tolerance on Swedish Fighter Aircraft
Challenger Initial Analysis Update233
Certification Methodology for Aircraft Primary Composite Structures274
CT114 Tutor Wing Flight Load Survey288
SESSION III - MATERIALS AND NONDESTRUCTIVE INSPECTION
Probabilistic Durability Evaluation of Alcoa 7050 Aluminum305
Composite Repair of Aircraft Structures - The Australian Experience323
Technology Development - Aircraft Repairs with Composite Materials
Post Impact Compressive Strength in Composites 378

Inspection of Aircraft Engine Components Using Automated Eddy Current and Pattern Recognition Techniques
Electronic Holography & Shearography NDE for Inspection of Modern Materials and Structures
SESSION IV - STRUCTURAL ANALYSIS, TESTING, AND FORCE MANAGEMENT
Predicting the Influence of Inherent Material Inhomogeneities on Notch Fatigue Life
A Review of the Problem of Short Fatigue Cracks
Models for Fastened Structural Connections
Probabilistic Design463
Durability Testing of T-37B Empennage Using a Random-Block Load Sequence484
Vibroacoustic Fatigue and Stress Corrosion Cracks in the Fuselage Skin of a Large Cargo Airplane
SESSION V - ENSIP AND HELICOPTER INTEGRITY
Damage Tolerance of Engine Blading - Analysis and Failure Evaluation Considerations
Application of ENSIP on an In-Service Commercial Engine
Friction Stresses Between Blade and Disk Dovetails - Possible Cause of Numerous Dovetail Problems
A Comparison of Fatigue Life Prediction Methodologies for Rotorcraft602
Uncertainties in Determining High Reliability for Helicopter Component Safe Life Design
SESSION VI - MECSIP AND FORCE MANAGEMENT
Nondestructive Testing as Applied to Integrity Assessment
Results from Two MECSIP Studies
Variability in Crack Growth Rate Data

Selection of Critical Point-in-the-Sky for Navy Aircraft	732
Damage Tolerance Management of the X-29 Vertical Tail	751
A Case History for Assessing Dynamic Environment on the SRAM T Missile	762

AGENDA

1991 USAF STRUCTURAL INTEGRITY PROGRAM

2-6 DECEMBER 1991

Hyatt Regency San Antonio, Texas

SPONSORED BY:

ASD/Deputy for Engineering

WL/Flight Dynamics Directorate

WL/Materials Directorate

HOSTED BY:

San Antonio Air Logistics Center Aircraft Directorate

Aircraft Structural Integrity Branch (SA-ALC/LADD)

AGENDA

TUESDAY, 3 DECEMBER 1991

	SESSION I - OVERVIEWS Chairman - R. Bader, WL/FIB
0830-0900	F-16 Airframe Structural Integrity Program C. Babish, ASD/YPEF
0900-0930	F-16N Fuel Shelf Joint Fatigue Life Extension by Cold-Expansion of Fastener Holes L. Reid, Fatigue Technology, Inc
0930-1000	C-141 Wing Station 405 Risk Assessment R. Bell and J. Cochran, Lockheed Aeronautical Systems Co R. Alford and D. Hammond, WR-ALC/LJLEA
1000-1030	REFRESHMENT BREAK
1030-1100	Phased Load Condition Generator for C-17 Full-Scale Durability Qualification Testing R. Eastin, Douglas Aircraft Corp
1100-1130	Testing of a Major Structural Component (C401) on the B-2 Advanced Technology Bomber K.D. Jordan, LTV Aircraft Products Group
1130-1200	C-130 Wing Durability Testing K.E. Brown and R.A. Waldbusser, Lockheed Aeronautical Systems Co W.O. Greenhaw, WR-ALC/MMSFRA
1200-1330	LUNCH AND PRESENTATION Future Outlook for the Air Force Materiel Command P. Panzarella, Technical Director, USAF Systems Command Headquarters (NO PAPER PUBLISHED)
	SESSION II - STRUCTURAL ANALYSIS AND TESTING Chairman - H. Wood, ASD/ENF
1330-1400	MacIntosh/VAX Based DTA Analysis R.D. Giese, OO-ALC/LACES (PAPER NOT SUBMITTED FOR PUBLICATION)
1400-1430	Using Approximate Methods for Complex Damage Tolerance Problems A. Nathan, Israel Aircraft Industries
1430-1500	Damage Tolerance on Swedish Fighter Aircraft P. Sindelar and M-O. Olsson, Forsvarets Materialelverk (Defence Materiel Administration)

1500-1530	REFRESHMENT BREAK
1530-1600	Challenger Initial Analysis Update C. Nguyen-Quoc and M. Schade, Canadair, Inc
1600-1630	Certification Methodology for Aircraft Primary Composite Structures E.F. Kautz, S.L. Huang, R.E. Vining, and R.M. Catanese, Naval Air Development Center
1630-1700	CT114 Tutor Wing Flight Load Survey B. Mercier, Bombardier, Inc Capt J. Peetsma, National Defense Headquarters Canadian Forces
1700-1730	Damage Tolerance Design Handbook Update Dr A.P. Berens and Dr J.P. Gallagher, University of Dayton Research Institute J. Coate, WL/MLSE (PAPER NOT SUBMITTED FOR PUBLICATION)
1730-1930	RECEPTION
	WEDNESDAY, 4 DECEMBER 1991
	SESSION III - MATERIALS AND NONDESTRUCTIVE INSPECTION Chairman - T. Cooper, WL/MLS
0830-0900	Probabilistic Durability Evaluation of Alcoa 7050 Aluminum J.G. Burns, WL/FIBEC
0900-0930	Composite Repair of Aircraft Structures - The Australian Experience L. Molent, Aeronautical Research Laboratory
0930-1000	Technology Development - Aircraft Repairs with Composite Materials Dr J. Chung, E-Systems
1000-1030	REFRESHMENT BREAK
1030-1100	Post Impact Compressive Strength in Composites E. Demuts, R. Sandhu, and J. Daniels, WL/FIB
1100-1130	Inspection of Aircraft Engine Components Using Automated Eddy Current and Pattern Recognition Techniques A. Fahr, C.E. Chapman, and A. Koul, National Research Council Canada A. Pelletier and D. Hay, Tektrend International, Inc
1130-1200	Electronic Holography and Shearography NDE for Inspection of Modern Materials and Structures D. Nethaway, Pratt & Whitney

1200-1330	LUNCH AND PRESENTATION Damage Tolerance - A Philosophical Discussion T. Swift, Chief Scientific & Technical Advisor, Fracture Mechanics/Metallurgy, Federal Aviation Administration (NO PAPER PUBLISHED)
	SESSION IV - STRUCTURAL ANALYSIS, TESTING AND FORCE MANAGEMENT Chairman - C. Petrin Jr., ASD/ENFS
1330-1400	Predicting the Influence of Inherent Material Inhomogeneities on Notch Fatigue Life A. Grandt Jr., T. Scheumann, and R. Todd, Purdue University A. Hickle, Alcoa
1400-1430	A Review of the Problem of Short Fatigue Cracks R. Carlson, G. Kardomateas, and P. Bates, Georgia Institute of Technology
1430-1500	Models for Fastened Structural Connections B. Szabó, Washington University Maj J. Bortman, Israel Air Force
1500-1530	REFRESHMENT BREAK
1530-1600	Probabilistic Design P. Roth, General Electric Co
1600-1630	Durability Testing of T-37B Empennage Using a Random-Block Load Sequence J. Unruh, D. Butts, and K. Schrader, Southwest Research Institute
1630-1700	Vibroacoustic Fatigue and Stress Corrosion Cracks in the Fuselage Skin of a Large Cargo Airplane W. Dunn and M. Kluesener, Consultants L. Shaw and L. Rogers, WL/FIBG
	THURSDAY, 5 DECEMBER 1991
	SESSION V - ENSIP AND HELICOPTER INTEGRITY Chairman - V. Spanel, ASD/YZE
0830-0900	Damage Tolerance of Engine Blading - Analysis and Failure Evaluation Considerations P. Domas, General Electric Co
0900-0930	Application of ENSIP on an In-Service Commercial Engine A. Tannock, Y. Valani, D. Craig, and S. Doan, Pratt & Whitney Canada, Inc H. Johnson, Pratt & Whitney Florida
0930-1000	Friction Stresses Between Blade and Disk Dovetails - Possible Cause of Numerous Dovetail Problems B. Kalb, General Electric Co
1000-1030	REFRESHMENT BREAK

1030-1100	Engine Front Frame Vibration Damping Capt V. Johnson, ASD/YZEE (PAPER NOT SUBMITTED FOR PUBLICATION)
1100-1130	A Comparison of Fatigue Life Prediction Methodologies for Rotocraft R. Everett Jr., National Aeronautics and Space Administration
1130-1200	Uncertainties in Determining High Reliability for Helicopter Component Safe Life Design W. Matthews, D. Neal, T. Rudalevige, and M. Vangel, US Army Laboratory Command
1200-1330	LUNCH AND PRESENTATION Airlift - Desert Storm Maj B. VanVliet, USAFR, Flight Control Division, Flight Dynamics Directorate, Wright Laboratory (NO PAPER PUBLISHED)
	SESSION VI - MECSIP AND FORCE MANAGEMENT Chairman - J. Turner, SA-ALC/LADD
1330-1400	Nondestructive Testing as Applied to Integrity Assessment B. Clinch, McDonnell Douglas
1400-1430	Results from Two MECSIP Studies C. Brooks, McDonnell Douglas
1430-1500	Variability in Crack Growth Rate Data E. Tuegel, McDonnell Douglas
1500-1530	REFRESHMENT BREAK
1530-1600	Selection of Critical Point-in-the-Sky for Navy Aircraft D. Crain, McDonnell Douglas M. McMahon, Naval Air System Command
1600-1630	Damage Tolerance Management of the X-29 Vertical Tail J. Harter, WL/FIBEC
1630-1700	A Case History for Assessing Dynamic Environment on the SRAM T Missile W. Buckey, ASD/YGEF
1700	ADJOURN

INTRODUCTION

This report contains the proceedings of the 1991 USAF Structural Integrity Program Conference held at the Hyatt Regency Hotel in San Antonio, Texas from 3-5 December 1991. The conference, which was sponsored by the ASD Deputy for Engineering and the Wright Laboratory Flight Dynamics and Materials Directorates, was hosted by the San Antonio Air Logistics Center Aircraft Directorate, Aircraft Structural Integrity Branch (SA-ALC/LADD).

This conference, as in previous years, was held to permit experts in the field of structural integrity to communicate with each other and to exchange views on how to improve the structural integrity of military weapon systems. This year, as in previous years, our friends from outside the U.S. borders provided the audience with outstanding presentations on activities within their countries. It is anticipated that this conference will include their contributions in the agenda of future meetings.

The sponsors are indebted to their hosts for their support of the conference. The sponsors are also indebted to the speakers for their contributions. In particular, thanks are due to the three luncheon speakers for their informative presentations. Mr Phil Panzarella, who will be the DCS, Engineering and Technical Management, for the Air Force Materiel Command provided an inspiring discussion of the merger of the Air Force Logistics Command and the Air Force Systems Command. Mr Tom Swift who is the Chief Scientific and Technical Advisor, Fracture Mechanics and Metallurgy, for the FAA made an excellent presentation on the role of damage tolerance for ensuring safety of aging commercial aircraft. Major Brian Van Vilet, USAFR, from the Wright Laboratory, Flight Dynamics Directorate, gave the audience an interesting perspective on life in the desert area during Desert Storm. As usual, much of the success of the conference is due to the efforts of Jill Jennewine and her staff from the Universal Technology Corporation. Their cooperation is appreciated. We are also grateful to Rita Scholes of WL/MLS for compiling the Proceedings and preparing the publication.

Robert M. Bader

R.M. Bader

WL/FIB

Thomas D. Cooper/

WL/MLS

John W. Lincoln ASD/ENFS

John M. Lincoln

F-16 AIRCRAFT

STRUCTURAL INTEGRITY







- BACKGROUND
- F-16 REQUIRED STRUCTURAL MODIFICATIONS
- F-16 POTENTIAL STRUCTURAL REPAIR ACTIONS
- F-16 LESSONS LEARNED
- SUMMARY



STRUCTURAL DESIGN CRITERIA

	DESIGN WEIGHT (LBS)	STRENGTH	SERVICE LIFE	MISSION MIX	×	
BLK 10/15	22500	S.5 6	8000 HR ROMT	55% A-A 20% A-G 25% GEN		
BLK 25/30 '	26910	S.D 6	8000 HR GOAL	28% A-A 57% A-G 15% GEN		
BLK 40 ²	28500	8 G.S	8000 HR ROMT	30% A-A 55% A-G 15% GEN	∘ ర	55% A-A ³ 30% A-G 15% GEN
BLK 50 •	28750	S.D 6	8000 HR ROMT	30% A-A 55% A-G 15% GEN	9 5	55% A-A ³ 30% A-G 15% GEN

1. ONLY MINIMAL STHUCTUHAL CHANGES INCORPORATED AT BLK 25/30 NOTES:

MAJOR STRUCTURAL IMPROVEMENTS INCORPORATED AT BLK 40 તાં

BLOCK 40/50 AIRFRAME ANALYZED FOR BOTH MISSION MIXES AND DESIGNED FOR WORST CASE က်

CORRECTIONS TO BLK 40 PROBLEMS HAVE BEEN INCORPORATED IN BLK 50



HISTORICAL PERSPECTIVE

F-16A/B

- DESIGN USAGE PREDICTED DURING FSD BASED UPON PREVIOUS FIGHTER AIRCRAFT EXPERIENCE
- ACTUAL USAGE HAS PROVEN TO BE SUBSTANTIALLY MORE SEVERE
- MORE EXTENSIVE AIR-TO-GROUND USAGE THAN EXPECTED
- EXTENT OF HIGH-G MANEUVERING ALLOWED BY AUTOMATIC ALPHA-G LIMITER FUNCTION OF FLIGHT CONTROL SYSTEM NOT ANTICIPATED :

F-16C/D - BLOCK 25/30

- PROGRAM PLANNED AND BUDGETFD BASED UPON USE OF A/B STRUCTURAL DESIGN WITH ONLY MINOR IMPROVEMENTS
- SEVERITY OF A/B USAGE AND IMPACT ON SERVICE LIFE NOT FULLY UNDERSTOOD
- LED TO RELAXING SERVICE LIFE REQUIREMENT TO 8000-HOUR GOAL



HISTORICAL PERSPECTIVE (CONT)

F-16C/D - BLOCK 40/42

- **USAGE FULLY DEFINED**
- SCHEDULE & FUNDING PROVIDED FOR MAJOR STRUCTURE REDESIGN
- 8000-HOUR SERVICE LIFE REQUIREMENT REESTABLISHED
- PROBLEM IDENTIFIED TO DATE ARE LARGELY THE RESULT OF CONCURRENCY INHERENT IN A P3 PROGRAM
- SERVICE LIFE TESTING OF BLOCK 30 ONLY IN FIRST LIFETIME WHEN BLOCK 40 DESIGN FROZEN
- SERVICE LIFE TESTING OF BLOCK 40 (AFT FUSELAGE) STARTED AFTER BLOCK 40 PRODUCTION
- FIXES TO BE PROVIDED IN ACCORDANCE WITH CONTRACTUAL CORRECTION OF DEFICIENCY (COD) CLAUSE

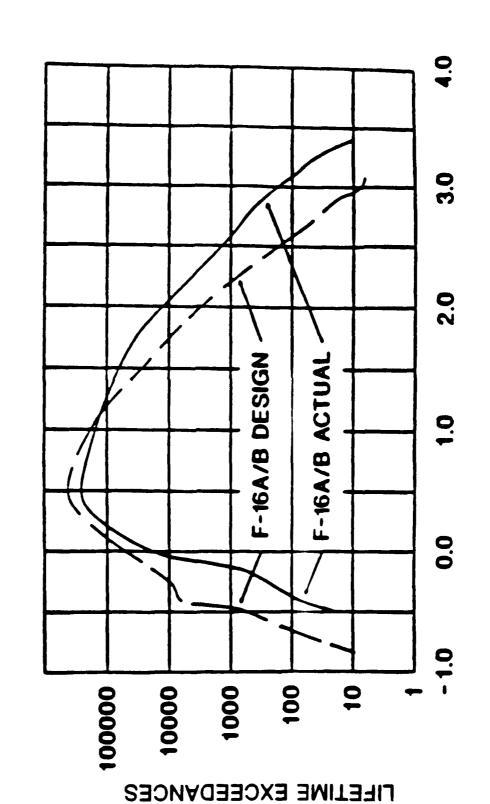
F-16C/D - BLOCK 50/52

STRUCTURAL IMPROVEMENTS INCORPORATED IN PRODUCTION



USAF F-16A/B ACTUAL AND DESIGN USAGE

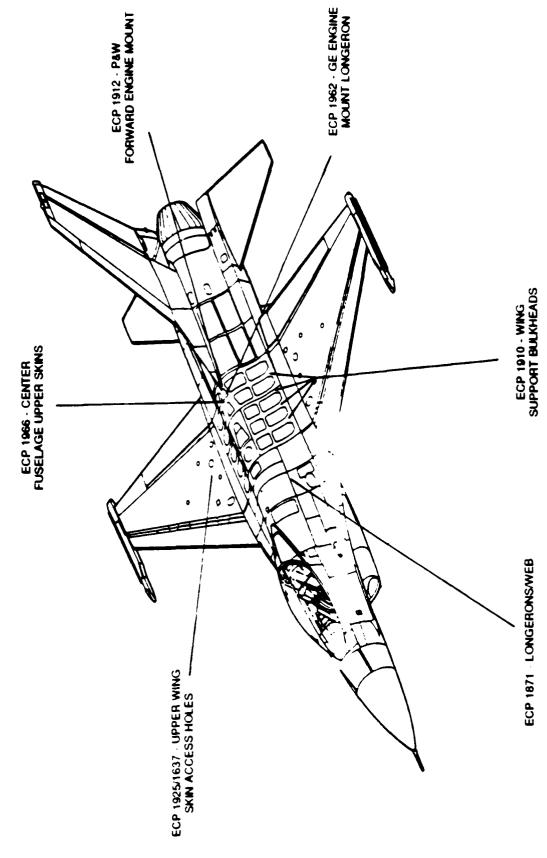
LIFETIME EXCEEDANCES VS WING BENDING MOMENT



BENDING MOMENT (MILLION INCH-POUNDS)



F-16 REQUIRED STRUCTURAL MODIFICATIONS





ECP 1910 - WING SUPPORT BULKHEADS

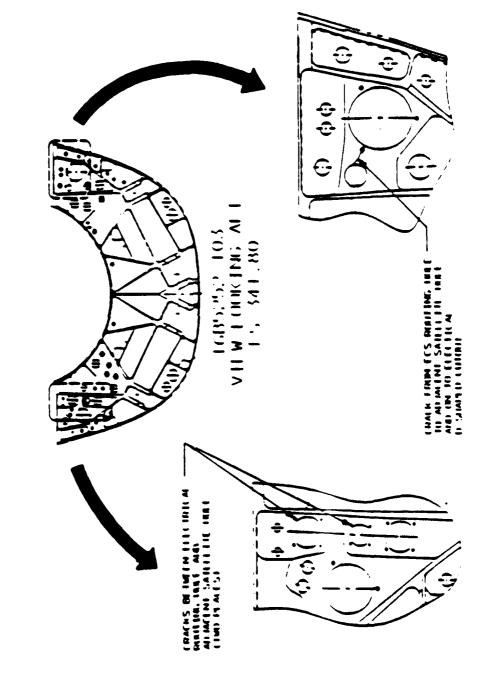
- TEST EXPERIENCE (BLOCK 30):
- · CRACKS FOUND IN F.S. 341 LOWER BULKHEAD AT 3988 HOURS
- CRACKS FOUND IN F.S. 357 UPPER BULKHEAD AT 3988 HOURS
- · CRACKS FOUND IN FUEL SHELF JOINT AT 7330 HOURS
- FIELD EXPERIENCE:
- · CRACKS FOUND IN SAME LOCATIONS ON SOME AIRCRAFT
- . USAF, USN, EPAF, FMS
- MODIFICATION:
- · COLDWORK SHEAR WEB PENETRATIONS
- REINFORCE SOME SHEAR WEB POCKETS
- · COLDWORK FUEL SHELF JOINT
- REPLACE F.S. 341 LOWER BULKHEAD WITH IMPROVED DESIGN

ECP 1910 - WING SUPPORT BULKHEADS



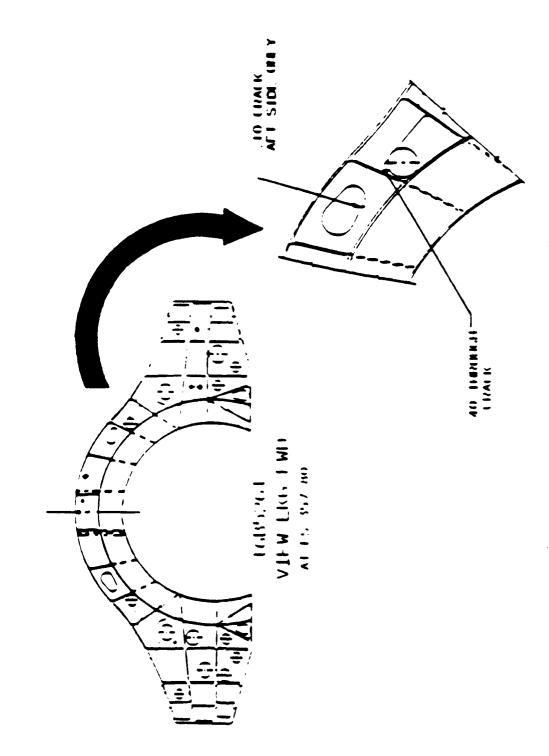


F.S. 341 LOWER BULKHEAD



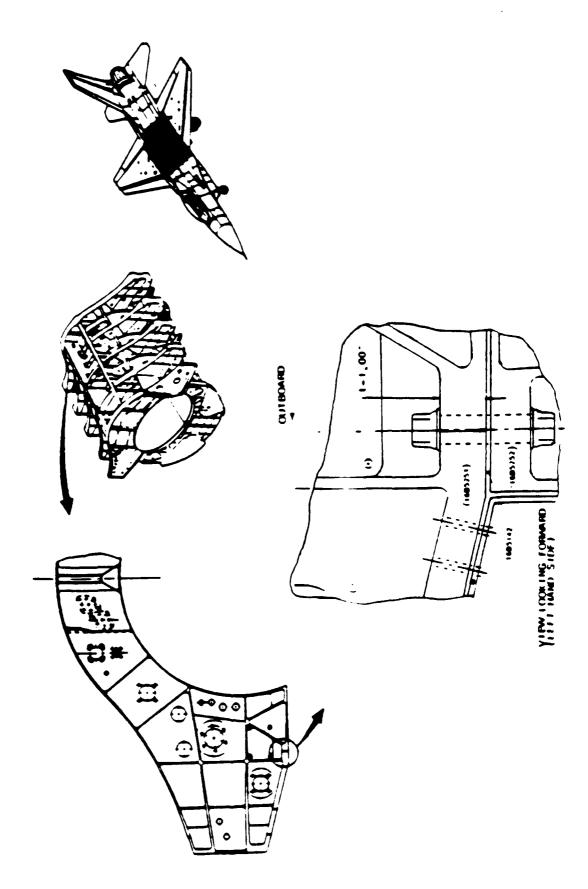


F.S. 357 UPPER BULKHEAD





FUEL SHELF JOINT





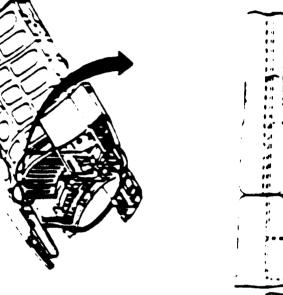


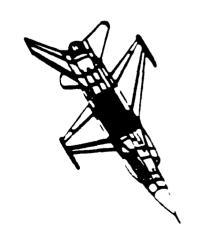
ECP 1871 - LONGERONS/WEB

- TEST EXPERIENCE (BLOCK 30):
- RHS FOUND FAILED AT 3988 HOURS
- LHS FOUND FAILED AT 5000 HOURS
- FIELD EXPERIENCE
- APPROXIMATELY 60 FAILURES HAVE BEEN REPORTED
- MODIFICATION
- . REPLACE LONGERONS WITH IMPROVED DESIGN
- · CHANGE MATERIAL TO 7475 T7351 ALUMINUM

ECP 1871 - LONGERONS/WEB











ECP 1966 - CENTER FUSELAGE UPPER SKINS

- TEST EXPERIENCE:
- BLOCK 30 CRACKS FOUND AT 7330 HOURS
- BLOCK 40 CRACKS FOUND AT 2317 HOURS
- FIELD EXPERIENCE NONE REPORTED
- MODIFICATION:
- REPLACE 16B5301 SKIN WITH IMPROVED DESIGN
- . ROUT SOME FLANGES
- . ADD EXTERNAL STRAPS
- . INSTALL INTERNAL REINFORCEMENTS

ECP 1966 - CENTER FUSELAGE UPPER SKINS

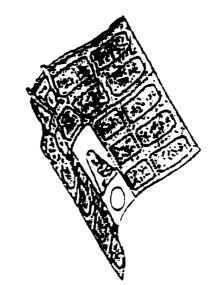


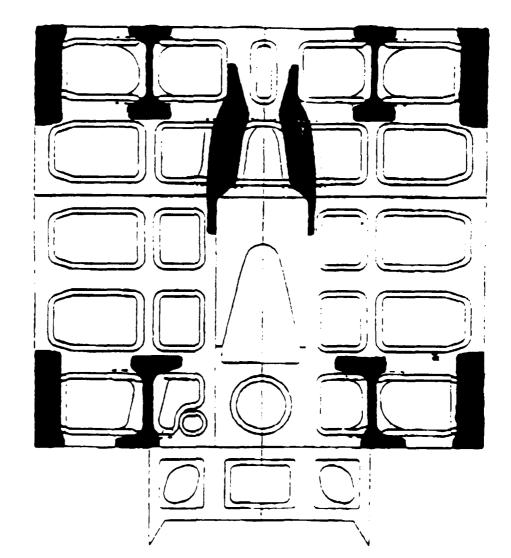
















TEST EXPERIENCE (BLOCK 40 COMPONENT):

• 1ST FAILURE AT 4000 HOURS

2ND FAILURE AT 5000 HOURS

FIELD EXPERIENCE - NONE REPORTED

MODIFICATION:

. REPLACE BACK-UP FITTING WITH IMPROVED DESIGN

. CHANGE MATERIAL TO HI ANIUM



ECP 1912 - P&W FORWARD ENGINE MOUNT





ECP 1962 - GE ENGINE MOUNT LONGERON



· CRACKS FOUND AT 10,000 HOURS

FIELD EXPERIENCE - NONE REPORTED

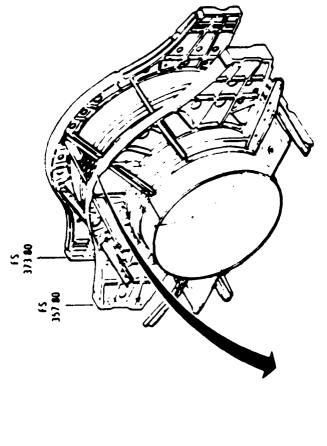
MODIFICATION:

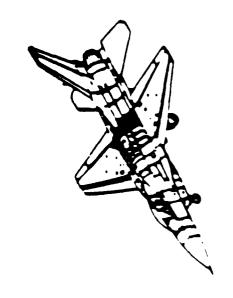
· COLDWORK HOLES

. REPLACE RIVETS WITH SHEAR PINS



ECP 1962 - GE ENGINE MOUNT LONGERON





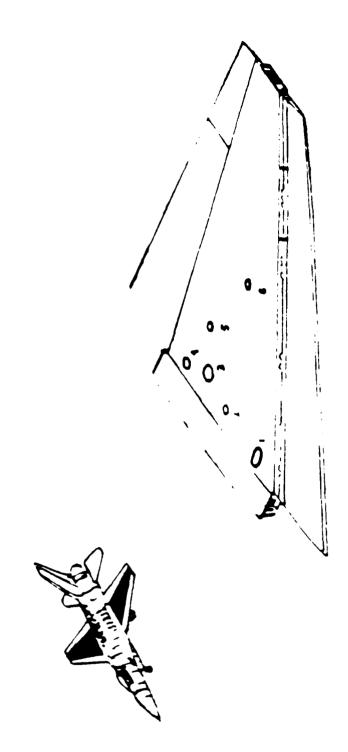




ECP 1925/1637 - UPPER WING SKIN ACCESS HOLES

- TEST EXPERIENCE:
- · BLOCK 30 1ST CRACKS FOUND AT 600 HOURS
- BLOCK 40 COMPONENT CRACKS FOUND AT 2000 HOURS
- FIELD EXPERIENCE:
- PRE-BLOCK 40 ECP 1637 REPAIRS FLEET-WIDE CRACKING
- BLOCK 40 NONE REPORTED
- MODIFICATION
- · ROUT SKIN STEP
- INSTALL EXTERNAL REINFORCEMENTS

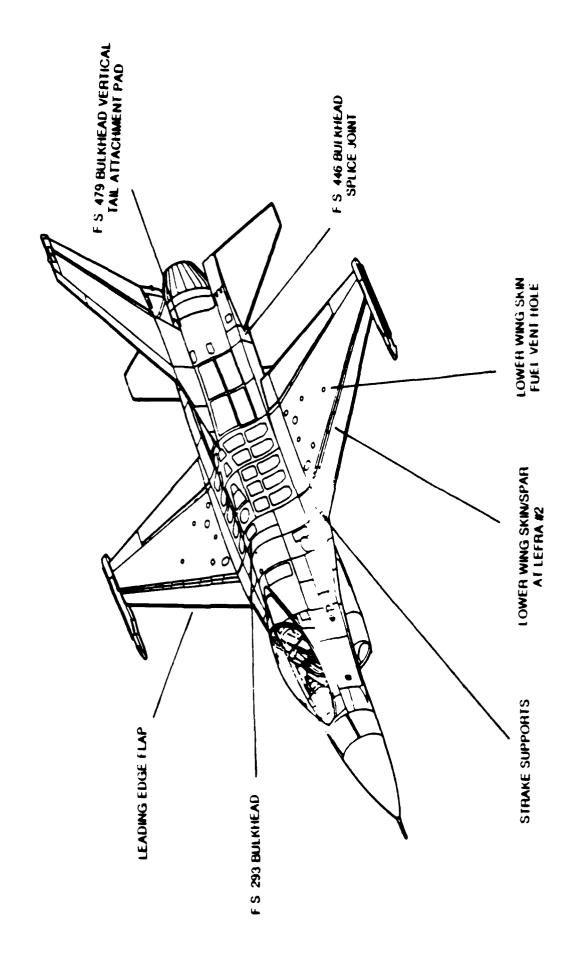
ECPs 1925/1637 - UPPER WING SKIN ACCESS HOLES







F-16 POTENTIAL STRUCTURAL REPAIR ACTIONS





F-16 LESSONS LEARNED

- USAGE OF PREVIOUS FIGHTER AIRCRAFT WAS FOUND NOT TO BE REPRESENTATIVE OF F-16 USAGE
- AIRCRAFT PERFORMANCE AND THE "ALPHA-g" LIMITER HAS PRECIPITATED UNPRECEDENTED USAGE SEVERITY
- OBTAIN EARLY FLIGHT LOADS RECORDER DATA
- DESPITE AIRCRAFT SIZE--THE WEIGHT WILL GROW
- CONDUCT A MINIMUM OF TWO LIFETIMES OF TESTING TO VALIDATE DURABILITY AND DAMAGE TOLERANCE CHARACTERISTICS
- ADDITIONAL FULL-SCALE DURABILITY TEST INVALUABLE TO PROGRAM



SUMMARY

- STRUCTURAL ANALYSIS & TESTING IS AN ON-GOING PROCESS
- KNOWN STRUCTURAL MODIFICATIONS ARE NEEDED NOW
- DEVELOPMENT ACTIVITIES BEING AGGRESSIVELY PURSUED
- RETROFIT PLAN BEING DEVELOPED AND COORDINATED WITH THE USER

F-16N FUEL SHELF JOINT FATIGUE LIFE EXTENSION BY COLD EXPANSION OF FASTENER HOLES

Presented at the
1991 USAF Aircraft Structural Integrity Program Conference
San Antonio, Texas

Len Reid

Vice President, Engineering Programs

Fatigue Technology Inc., Seattle, WA

Antonio Rufin

Senior Project Engineer

Fatigue Technology Inc., Seattle, WA

Abstract:

Fatigue cracks have been detected in U.S. Navy F-16N aircraft center fuselage bulkheads after 1200 to 1500 flight hours. Under a Navy-sponsored program, Fatigue Technology Inc. evaluated use of hole cold expansion as an effective method of extending the fatigue life of holes in the bulkhead fuel shelf joints. A series of spectrum fatigue tests were conducted on complex load transfer specimens simulating both production and rework hole configurations. X-ray diffraction and photoelastic evaluations confirmed inducement of residual compressive stresses during cold expansion. Minimum fatigue life improvement using cold expansion was 1.5: 1 in specimens with edge margins as low as 1.26.

1.0 INTRODUCTION

The U.S. Navy's 26 F-16N aircraft are flown in the role of aggressor/adversary aircraft at its Fighter Weapons School. Cracks have been detected by the Navy after 1,200 to 1,500 flight hours in critical center fuselage carry through bulkhead structure at FS 325,341,357 and 309. Most detected cracks are less than 0.030 inch in size around bolt holes and attachment points. Similar cracks in the fuel shelf area have since been detected in U.S. Air Force F-16's.

Under a recently completed program for AeroStructures, Inc., and the U.S. Navy, Fatigue Technology Inc., (FTI) evaluated use of its split sleeve cold expansion process as both a production

structural enhancement and a depot-level structural repair method for the highly stressed fastener holes in the fuel shelf area bulkhead at FS 341, as shown in Figure 1. The program was related to verification of structural integrity of the F-16N airframe in support of General Dynamics Corporation ECP 1909. Specific cold expansion processes used in this program included FTI's patented Cx system (split sleeve cold expansion plus ream to final hole size) and Cold Expansion to Size System, (Cx2s) in simulated production and rework configurations, respectively. An overview of the cold expansion techniques is presented next, followed by a detailed description of the test program.

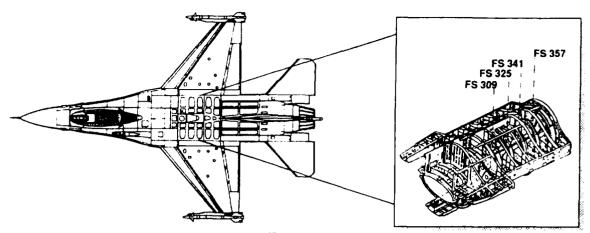


Figure 1
F-16 FS 341 Bulkhead Location

2.0 OVERVIEW OF COLD EXPANSION PROCESSES

High-interference cold expansion is a technique used by the aerospace industry to improve the fatigue life and durability of holes in metallic materials. The process, which has been exhaustively validated through test and in-service experience, provides fatigue and crack growth life improvement by creating residual compressive stresses around the hole. This condition significantly reduces the stress concentration at the hole as detailed in [1].

The basic FTI high-interference split sleeve cold expansion process [2], is accomplished by drawing an oversize mandrel through an internally prelubricated split sleeve to expand the metal around the hole (Figure 2). The sleeve protects the hole

from damage, ensures that the material is radially expanded, and enables one-sided (blind) processing. The depth of the resultant residual compressive stresses around the hole effectively shields the hole from the effects of applied cyclic tensile loading (Figure 3). From a fracture mechanics viewpoint, the sharp stress reduction means that the stress intensity factor at cracks emanating from the hole will also be reduced, thus inhibiting crack growth.

The cold expansion to size process [3] utilizes the elastic/plastic properties of the base metal with the specifications and tooling dimensions to size a hole to a prescribed interference or clearance dimension. Close tolerance holes are attained without additional final reaming of the material, making it particularly suited to rework of fastener holes.

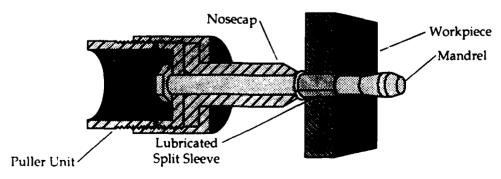
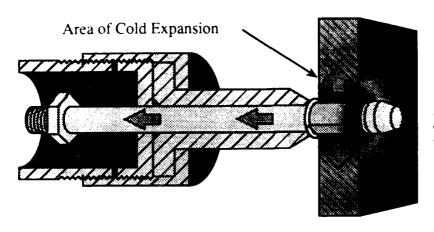


Figure 2
Basic Cx System Components



The permanently induced zone of compressive stress around the hole effectively extends fatigue life.

Figure 3
Basic Principles

3.0 TEST PROGRAM

The evaluation effort involved testing of complex load transfer test articles subjected to spectrum fatigue loads that reproduced the geometry and flight loads of the actual aircraft configuration. Naval Air Systems Command (NAVAIR) and FTI jointly developed and validated the 2-ft long load transfer test articles, consisting of a contoured 2124-T851 specimen and thin titanium straps.

A total of four hole conditions were evaluated to simulate the new production configuration and the rework requirements of these holes:

- 1. Baseline 9/16 inch diameter as-reamed, no cold expansion (NCx).
- 2. Production 9/16 inch diameter, cold expanded (Cx) and reamed.
- 3. Rework 19/32 inch diameter, cold-expanded to size (Cx2s).
- 4. Rework 5/8 inch diameter, cold-expanded to size (Cx2s).

An additional rework size of 3/4-inch diameter was deleted because the configuration may not meet structural integrity requirements. However, this may be replaced by an 11/16-inch diameter hole as part of a follow-on program.

The spectrum fatigue tests were supplemented with approximate stress and strain evaluations of the cold-expanded holes using X-ray diffraction and photoelasticity, respectively. The overall test matrix is shown in Figure 4.

Specimen Number(s)	Specimen Description	Test Type
A18NFn	9/16" NCx (three total)	Static + SCG (one static)
A18CFn	9/16" Cx (three total)	SCG only
A19CFn	19/32" Cx2s (three total)	Static + SCG (one static)
A20CFn	5/8" Cx2s (three total)	Static + SCG (one static)
A18CP1 A19CP1 A20CP1	9/16" Cx (19/32" Cx2s, 5/8" Cx2s)	Photoelasticity
A18NX1 / A18CX1 A19CX1 / A20CX1	9/16" NCx (9/16" Cx, 19/32" Cx2s, 5/8" Cx2s)	X-Ray Diffraction

Figure 4
Test Matrix

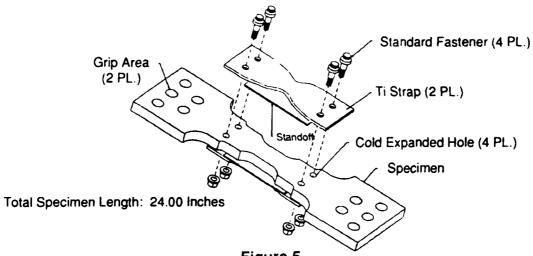


Figure 5
Spectrum Fatigue Test Article

3.1 Specimens

grip area.

The spectrum fatigue test articles consisted of a 2124-T851 aluminum specimen surrounded by two hourglass-shape titanium (Ti 6Al-4V) straps. The specimen and straps were fastened together by 4 bolts located at the test holes (see Figure 5). The assembly was designed to closely simulate hole and edge geometry and peak stresses due to the combined airframe bypass load, pin bearing loading on the holes, and bending stresses. In all cold-expanded specimens the split sleeves were oriented with the sleeve gap towards the end

The aluminum specimens originated from 3 material lots. The specimens were intermingled (each test configuration contained typically one specimen from each lot) to avoid statistical biasing. No apparent lot-to-lot variations were detected in the results.

The final test article design was the result of several design iterations that were individually evaluated by means of finite element analysis (FEA) and fully instrumented static

tests. The goal for bypass load-to-total load ratio at peak load in the specimen was 0.838 (a reduction of 5 percent from the calculated airframe ratio of 0.882, to preclude failures near the center of the specimen). The average value calculated from strain gage readings on one test article out of every group tested was 0.842 +/- 0.017.

The load spectrum included compression loads which would have caused the straps to buckle in a standard load transfer configuration. To avoid damage to the straps, the strap holes were machined

to an oval shape; the straps thus remained unloaded when the test article end loads were compressive. This solution was also made possible by the very light torque applied to the fasteners and the low-friction standoff sheet material (0.015-inch thick Micarta_{TM}) placed between the straps and the specimen. In addition to these measures, the straps were kept parallel and close to the specimen by means of two lightly fastened aluminum slotted plates (Figure 6).

One of the early test article con-

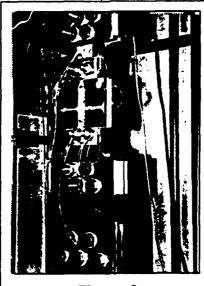


Figure 6
Test Article in Frame

figurations investigated in the program involved a direct application of bending moments by fastening a steel plate on one side of the specimen only (no straps). The plate was also designed to introduce the appropriate amount of bypass loading. However, this method failed to perform as expected due to the high grip/end fixture rigidity. Asymmetrically placed end shims failed for the same reason. Lateral offset concepts were therefore dropped.

The photoelasticity and X-ray diffraction specimens (Figure 7) were one-hole 1.00-inch thick facsimilies of the spectrum fatigue test specimens. They were designed for the specific purpose of revealing strain and stress distributions around the holes before and after cold-expansion.

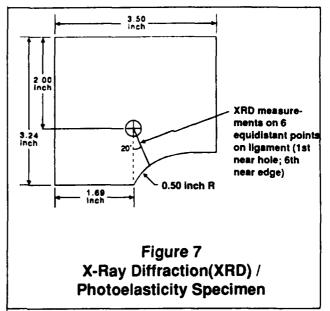
3.2 Test Equipment

Testing was performed using FTI's MTS 100-kip capacity closed-loop servohydraulic universal test frame. The spectrum waveform was generated by a Digital Equipment Corporation (DEC) PDP 11/23+ computer equipped with a MTS 442 test processor, from data provided by AeroStructures, Inc.

To minimize possible bending loads on the specimen due to slight grip and/or fixture non-coplanarity, an alignment verification check was performed. The test was conducted using an instrumented specimen from this program with straight-sided 0.100-inch thick, 4.00-inch wide Ti 6Al-4V straps. Strain gages at the center of the aluminum specimen showed a small amount of bending which was later practically eliminated (< 1.1 percent) with the addition of end shims.

3.3 Static Tests

The static tests were performed to monitor strains and specimen bypass loads. The first specimen of each hole configuration was instrumented with a



minimum of 2 uniaxial foil strain gages at its center and tested after assembly to peak tension and peak compression. The first specimen tested also had gages near the ends (front and back), and the straps had a single gage located near the center (one side only). The strain gages on this specimen and an additional gage at the center of each of the straps were used to verify the loads and check the strap unloading feature in compression.

A strain gage rosette used early in the program on an NCx specimen without straps showed that the principal strains in the ligament were closely aligned with the specimen axis. This result was subsequently confirmed by the crack growth patterns observed after fracture near the holes in both NCx and Cx specimens.

3.4 Spectrum Loads

The ASCII-format spectrum loads file supplied by AeroStructures, Inc. was a 100-equivalent flight hour block spectrum based on Top Gun aircraft 163270 (FS 341 upper bulkhead). The NAVAIR-defined peak tensile and compressive loads were 94,726 lb and 10,664 lb, respectively. The latter required scaling down the compressive portion of the spectrum, because the program had a pre-

established peak compression-to-peak tension ratio of 0.1605. These loads properly accounted for membrane and bending loads. Each spectrum pass represented 100 equivalent flight hours and encompassed a total of 12,685 segments. The average frequency was 7 Hz.

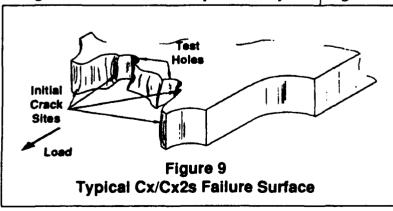
3.5 Crack Monitoring

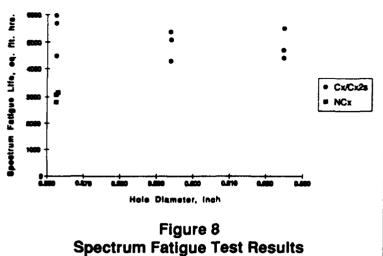
Direct visual access to the area in the immediate vicinity of the fastener holes

was was blocked by the straps and and fasteners. Crack growth measurements were instead made using Micro-Measurements (Measurements Group, Inc.) TK-09-CPA01 bonded crack growth gages. Each gage consists of a number of electrical resistor strands connected in parallel; crack growth through the specimen (and hence, gage), causes a change in total resistance which can be monitored through a signal amplifier. The gages allowed initial crack detections at about 0.030 inches away from the hole edge (the typical location of the first wire strand) and then in 0.010-inch increments, up to 10 increments.

3.6 X-Ray Diffraction and Photoelasticity Tests

X-ray diffraction testing was performed by Technology for Energy Corporation (TEC) on specimens representing the NCx and Cx/Cx2s hole configurations. TEC used multiple-tilt X-ray dif-





fraction equipment to measure residual tangential stresses on the front and back surfaces (mandrel entry and exit sides) at 6 points located as shown in Figure 7. The NCx specimen was intended as a control data point.

Measurements Group, Inc. applied their PS-8B (0.08-inch thick sheet grade) and PL-8 (castable grade, 0.100-inch typical thickness) high-sensitivity photoelastic coating [4] to 3 specimens (one for each Cx/Cx2s hole size). The holes were subsequently cold-expanded. The PS-8B bi-refringent sheets were permanently bonded to the mandrel entry and exit sides of the specimens. The castable material was used on the edge of the specimen nearest to the hole.

4.0 TEST RESULTS

Spectrum fatigue test results are summarized in Figure 8. Relative to the average of the NCx

> results, all Cx specimens lasted more than 1.5 times longer. The amount of fatigue life improvement attained by cold-expansion was essentially independent of repair hole size [5]. The typical appearance of a fracture surface for both Cx/Cx2s and NCx specimens is shown in Figure 9. Crack initiation was always at the hole, with

the secondary crack starting at the base of the fillet near the end of the specimen's lifetime (95 to 99 percent).

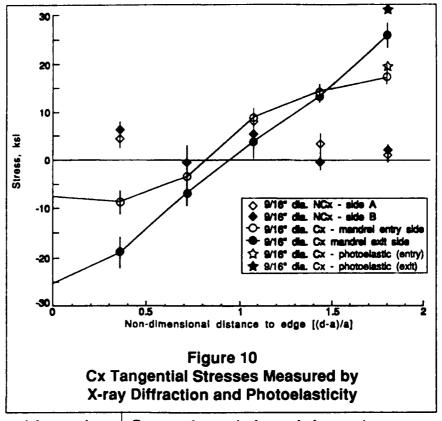
Typical tangential stress measurements obtained by X-ray diffraction are shown graphically in Figure 10. The vertical bars represent the absolute error margins as estimated by TEC [6].

The photoelastic specimens were meant primarily as a qualitative strain evaluation tool. The fringe order (taken from fringe color pattern changes on the specimen) is directly proportional to the difference between

principal strains. In general, special procedures and equipment not available for this program would have been needed to separate individual strain components, due to the biaxial nature of the cold expansion strain field. The only exception is on the contoured side of the specimens, where the tangential strains are nearly uniaxial and a simple fringe count revealed their magnitude. Maximum residual tangential edge strain and stress estimates (based on fringe counts) compared favorably with the X-ray diffraction measurements, as shown in Figure 10.

6.0 DISCUSSION

The test effort verified that a significant degree of fatigue life improvement can be achieved in this particular mechanical joint through cold expansion of the fastener holes. Results for the NCx (control) specimens correlated well with NAVAIR predictions drawn from aircraft data (2860 measured average equivalent flight hours, vs. 2,900 predicted hours).



Compared to typical open hole tests (e.g., as presented in [1]), the level of fatigue life extension was relatively moderate, probably as a result of the high applied stresses, filled hole configuration, and combined low edge margin and fillet stress concentration. Nevertheless, the results were determined by the Navy to justify the use of this process for repair of the F-16N fuel shelf joint.

The independence of the fatigue test results from hole size was unexpected and the cause has not been conclusively established. The residual tensile stresses at the edge were also found to vary little with hole size.

Finally, the correlation between X-ray diffraction and photoelastic stress measurements at the edge of the specimens show that X-ray diffraction (and to a lesser extent, photoelasticity) can be effectively used in this type of components to determine residual stresses with reasonable accuracy.

7.0 CONCLUSIONS

Cold expansion processes are being used extensively in fatigue-critical applications as a means to retard or preclude crack growth. The F-16N fuel shelf fastener holes presented unique challenges from a test standpoint in terms of loads and configuration which were successfully addressed in this program. Test results demonstrated the potential offered by the Cx and Cx2s processes to significantly improve the fatigue life of the specific fuel shelf joint evaluated in this effort.

ACKNOWLEDGEMENTS

This program was performed under contract 90102 to AeroStructures, Inc. Funding was provided by the NavalAir Systems Command. Their support is gratefully acknowledged.

REFERENCES

- 1. Phillips, J.L., "Sleeve Coldworking Fastener Holes", Vol. I, Air Force Materials Laboratory report AFML-TR-74-10 (1974).
- FTI Process Specification FTI 8101B (Cold Expansion of Fastener and Other Holes Using the Split Sleeve System (Cx) and Countersink Cold Expansion Nosecap (CCx)). (May 1984).
- 3. FTI Engineering Process Specification FTI 8201 (Cold Expansion to Size of Fastener and Other Holes Using the Split Sleeve System (Cx2s) and Countersink Cold Expansion Nosecap (CCx)). (January 1985).
- 4. Measurements Group, Inc. Bulletin S-116 E (1991).
- 5. Rufin, A.C., "F-16(N) Fuel Shelf Joint Test Program", Final Report, FTI Document 28006 (1991).
- 6. "Fatigue Technology Inc. Residual Stress Summary", TEC Report R-91-048 (1991).

WS 405 RISK ASSESSMENT C-141

1991 USAF STRUCTURAL INTEGRITY PROGRAM CONFERENCE SAN ANTONIO, TEXAS 2-5 **DECEMBER 1991**

D.O. HAMMOND - WR-ALC J.B. COCHRAN - LASC R.E. ALFORD - WR-ALC R.P. BELL - LASC

OVERVIEW

WHAT WE WILL SEE HERE TODAY IS HOW A STRUCTURAL ASSESSMENT OF THE C-141 WS 405 JOINT WAS FATIGUE CRACKING BEGAN MANIFESTING ITSELF IN THE WS 405 JOINT IN THE MID 1980'S AND REACHED GENERALIZED CRACKING BY 1989. THOROUGH DATA GATHERING THROUGH SPECIAL INSPECTIONS, FINITE ELEMENT MODEL ANALYSES, AND THE INDIVIDUAL AIRCRAFT TRACKING PROGRAM PROVIDED LASC WITH THE NECESSARY INFORMATION REQUIRED TO PERFORM A STRUCTURAL RISK ASSESSMENT. INVESTIGATION INTO A NUMBER OF AVAILABLE RISK ANALYSIS PROGRAMS WAS MADE AND A FINAL METHOD ESTABLISHED THAT RESULTED IN THE NECESSARY ANSWERS AROUND WHICH FORCE MANAGEMENT ACTIONS COULD BE RECOMMENDED. MADE USING STANDARD RISK ANALYSIS PROGRAMS EXPANDED TO ADDRESS THE PROBLEM AT HAND.

OVERVIEW

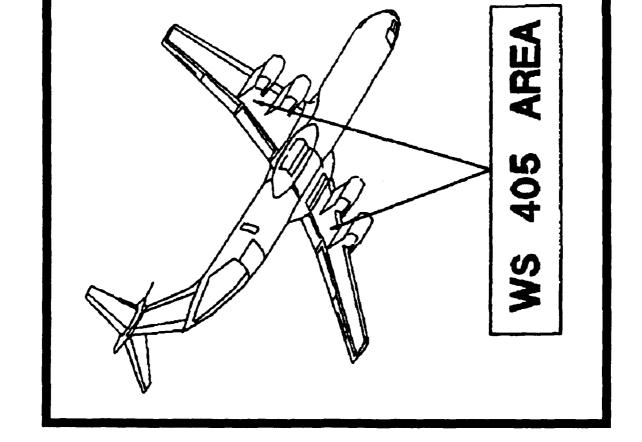
DATA SUMMARY

No. of Cracks, Usage, Distributions, FEM Models

RISK CALCULATIONS

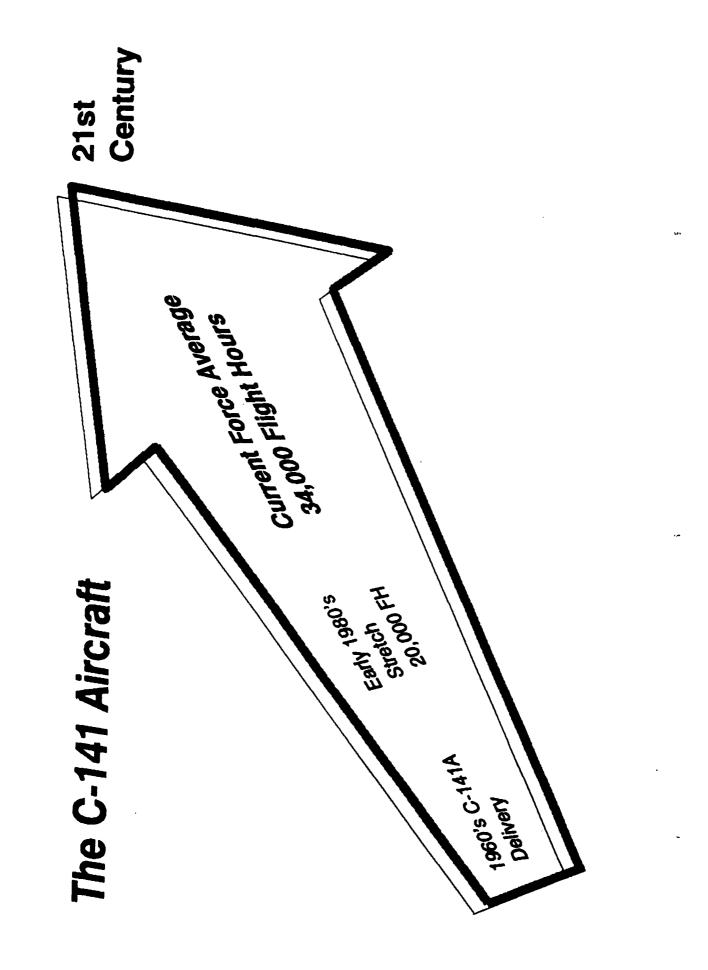
SUMMARY

Force Management Actions



THE C-141 AIRCRAFT

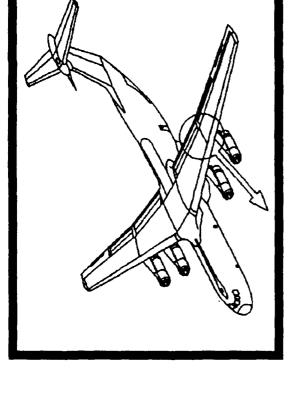
WORKHORSE OF MAC. TODAY, IT IS NOT INCONCEIVABLE TO EXPECT THE C-141 TO PROVIDE RELIABLE IS BASICALLY CONSTRUCTED OF 7075 T6 AL ALLOY AND WAS DESIGNED TO PROVIDE 30,000 FLIGHT HOURS THE FORCE IS CURRENTLY AVERAGING 34,000 FLIGHT HOURS. STRETCHED DURING THE 1970s, THE C-141B, WITH THE ADDITION OF AERIAL REFUELING CAPABILITY, RAPIDLY BECAME THE AIRLIFT WELL INTO THE 21ST CENTURY. WITH THIS IN MIND, THE CURRENT "TOOLS" OF STRUCTURAL ANALYSES MUST GO BEYOND THE SPECIFICS OF STRENGTH, DURABILITY AND FRACTURE MECHANICS AND INTO THE C-141A WAS PRODUCED AND DELIVERED TO THE AIR FORCE DURING THE 1960'S. THE AIRCRAFT THE REALM OF STATISTICS AND PROBABILITIES, I.E., RISK ASSESSMENTS. SERVICE.

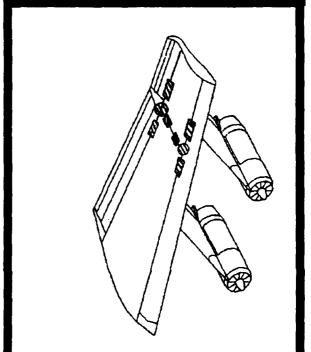


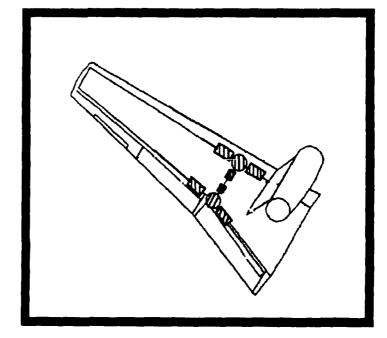
INNER/OUTER WING JOINT

DESIGN GOALS OF 30,000 HOURS BUT IS RAPIDLY DETERIORATING AS AIRCRAFT USAGE CONTINUES TO ACCUMULATE. WHEN FATIGUE CRACKING BEGAN TO MANIFEST ITSELF IN THE MID 1980S, ACTIONS BECAME NECESSARY TO ADEQUATELY MANAGE THE AIRCRAFT. INSPECTIONS, REDESIGNS, AND REPAIRS WERE ENGINEERED, BUT BY THE TIME A CORRECTIVE ACTION REPAIR PROGRAM COULD GET UNDERWAY, FATIGUE CRACKING ELEVATED THE JOINT CONCERN TO ONE OF SAFETY. IT IS THIS CONCERN THAT PROMPTED THE THIS JOINT HAS MET THE WING JOINT AT W.S. 405 JOINS THE OUTER WING TO THE INNER WING. RISK ASSESSMENT THAT THIS PRESENTATION DESCRIBES.

Inner / Outer Wing Joint Basic Repair







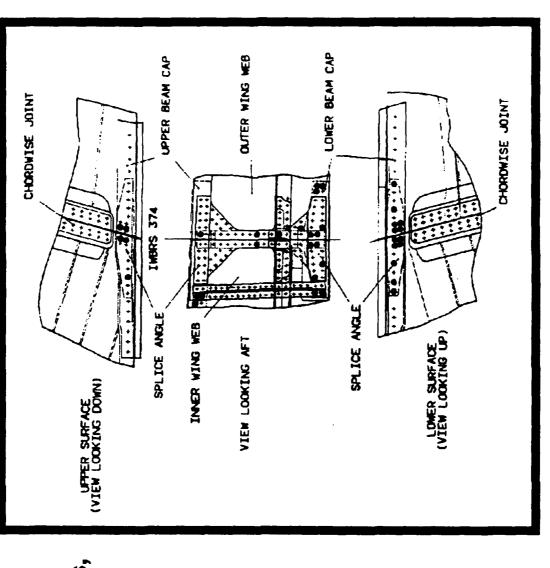
WS 405 CRACK SUMMARY

TCTO 528 IS THE TCTC 758 WAS A THE RESULT OF THE INSPECTION DATA CONFIRMED THE PRESENCE OF NOT ONLY MULTI-ELEMENT (MORE THAN ONE PART) CRACKING, BUT ALSO MULTI-SITE (MORE THAN ONE CRACK IN SAME PART IN SAME LOAD TRANSFER PATTERN) DAMAGE. THIS DATA ALSO CONFIRMED THAT APPROXIMATELY 50 PERCENT OF CRACKS THE NEXT TWO CHARTS SUMMARIZE CRACK LOCATION DATA AS REPORTED BY TCTO'S 1C-141-753, CURRENT (BHEC) REWORK OF FASTENER HOLES IN THE JOINT AREA AND INCLUDES INSPECTION OF THESE HOLES BY BHEC. FOUND BY TCTO 753 IN THE REAR BEAM LOWER CAP WERE IN EXCESS OF THE CRITICAL CRACK LENGTH. TCTO'S 753 AND 761 WERE DIRECTED BOLT HOLE EDDY INSPECTIONS OF THE LOWER REAR BEAM CAP ATTACHMENT TO THE TIE-DOWN FITTING. DIRECTED INSPECTION BY X-RAY OF THE FRONT AND REAR BEAM W.S. 405 JOINT AREA. -761, -758 AND -528.

STATEMENT OF CONDITION

Summary of Cracked Holes, C-141 Force, WS 405 at Front Beam

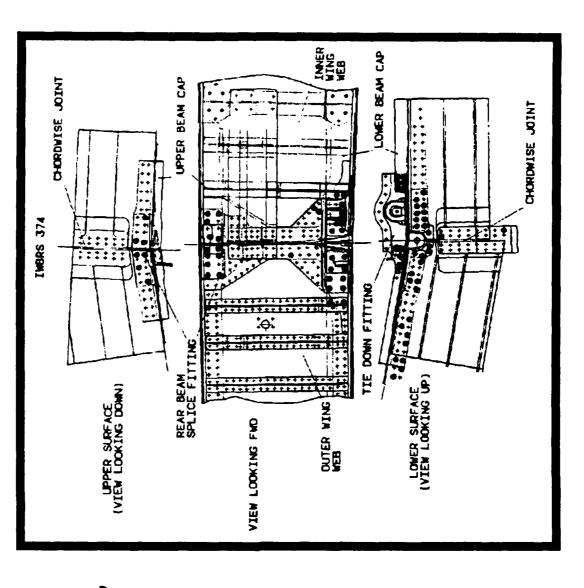
NDI: BHEC



STATEMENT OF CONDITION

Summary of Cracked Holes, C-141 Force, WS 405 at Rear Beam

NDI: BHEC



CRITERIA

OUR OBJECTIVE IN ALL OF THIS WAS TO DETERMINE A METHOD FOR EVALUATING THE SAFETY OF THE FORCE DURING THE FORCE MANAGEMENT PROGRAM INITIATED BECAUSE OF THE CRACKING PROBLEM

BE J. SIMPLY DEFINED BY US PROBABILITY OF THE LOAD EXCEEDING THE STRENGTH AT A GIVEN POINT IN TIME. RISK ANALYSIS WAS THE METHOD SELECTED, AND IT WAS

ONCE THIS RISK HAD BEEN CALCULATED, WE ADOPTED THE 1 X 10⁻⁴ FAILURE CRITERIA SPELLED OUT DURING A C-5 SAB REVIEW, "IF A STRUCTURAL MEMBER FAILS FOR WHATEVER REASON, THEN THE RISK OF CATASTROPHIC FAILURE ON A SINGLE FLIGHT OF NO MORE THAN ONE IN TEN THOUSAND IS ACCEPTABLE."

WS 405 RISK ASSESSMENT

Greater Than the Strength of the Structure RISK: The Probability of Experiencing A Load

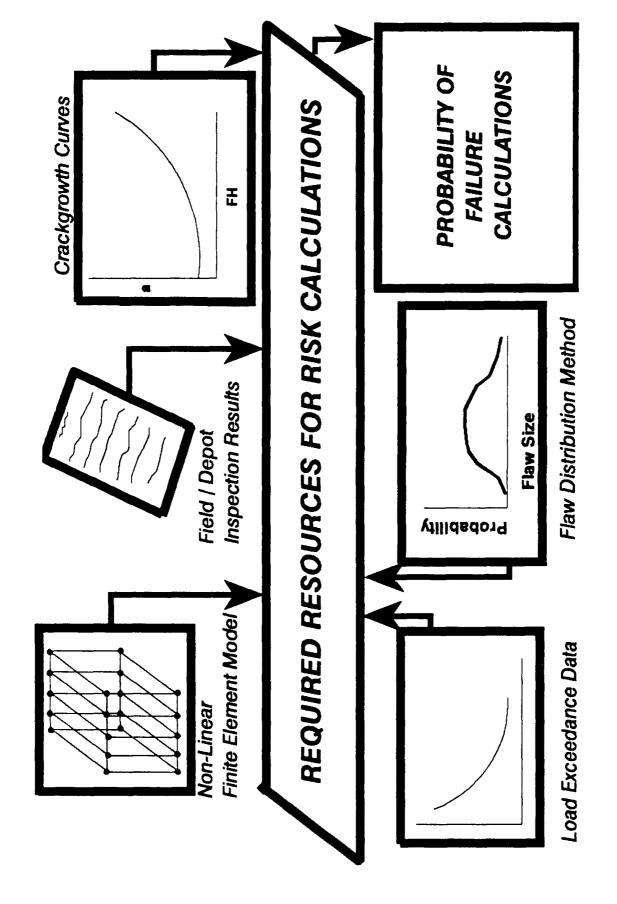
Scientific Advisory Board, in a September 1977 review of the C-5, endorsed the following statement:

whatever reason, then the risk of a catastrophic failure on a single flight of no more than one in ten "If a structural member fails for thousand is acceptable."

RESOURCES FOR RISK CALCULATION

THE REQUIRED RESOURCES FOR A RISK CALCULATION ARE SHOWN:

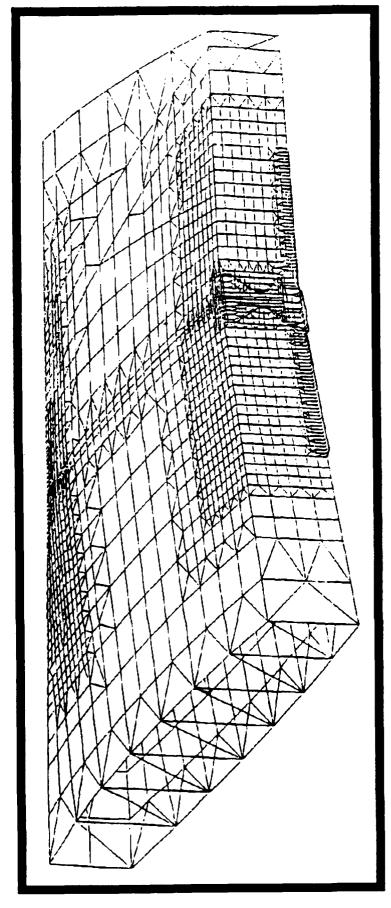
- FIELD/INSPECTION DATA RESULTS ARE REQUIRED TO DETERMINE THE INITIAL CRACKING DATA FROM WHICH THE REST OF THE ANALYSIS CAN PROCEED. ;
- CRACKGROWTH CURVES ARE REQUIRED TO REDUCE THE CRACK LENGTHS FOUND DURING THE LENGTHS FOR THE AVERAGE FLEET AIRCRAFT. INSPECTIONS TO ?
- FLAW DISTRIBUTION DATA IS NEEDED TO GENERATE THE STRENGTH DATA FOR THE COMPONENTS BEING ANALYZED. .
- THE DISTRIBUTION OF BOLT LOADS AND STRESSES IN THE VARIOUS COMPONENTS IS DETERMINED BY A NON-LINEAR FINITE ELEMENT MODEL. 4.
- THE PROBABILITY THAT THE AIRCRAFT WILL SUSTAIN OR EXCEED A GIVEN LOAD IS CALCULATED BY USING LOAD EXCEEDANCE DATA. ۍ.



NON-LINEAR FINITE ELEMENT MODEL

ACCOMPLISHED BY SETTING UP A LOAD VS. STIFFNESS CURVE FOR EACH BOLT LOAD AND ITERATING RUN BY RUN UNTIL AN ACCURACY WAS ACHIEVED WITHIN 10 POUNDS. THE MODEL REPRESENTS CALCULATIONS IN THIS AREA AND WAS LATER MODIFIED TO PERFORM THE NON-LINEAR CALCULATIONS. AS TO PERFORM A RISK ANALYSIS ON A MULTI-ELEMENT STRUCTURE, IT BECAME NECESSARY TO BUILD A LINEAR MODEL IS SUFFICIENT FOR CALCULATION OF BOLT FOR NORMAL SLOW CRACKGROWTH CALCULATIONS, BUT A NON-LINEAR MODEL IS REQUIRED FOR ANY PREDICTIONS WHERE PARTS ARE SEVERED. OUR MODEL CONTAINED 10,000 ELEMENTS AND EACH NON-LINEAR RUN TOOK APPROXIMATELY A DAY. SUBSEQUENT DATA REDUCTION TOOK ANOTHER THE MODEL HAD ORIGINALLY BEEN BUILT TO PROVIDE DATA FOR STANDARD CRACKGROWTH IT TURNED OUT, IT WAS ONLY NECESSARY TO PERFORM NON-LINEAR CALCULATIONS ON ABOUT 250 BOLTS. AN INVESTMENT OF SEVERAL THOUSAND HOURS. A NON-LINEAR FINITE ELEMENT MODEL. STRESSES LOADS AND THIS WAS

C-141 WS 405 FINITE ELEMENT MODEL **REAR BEAM VIEW**

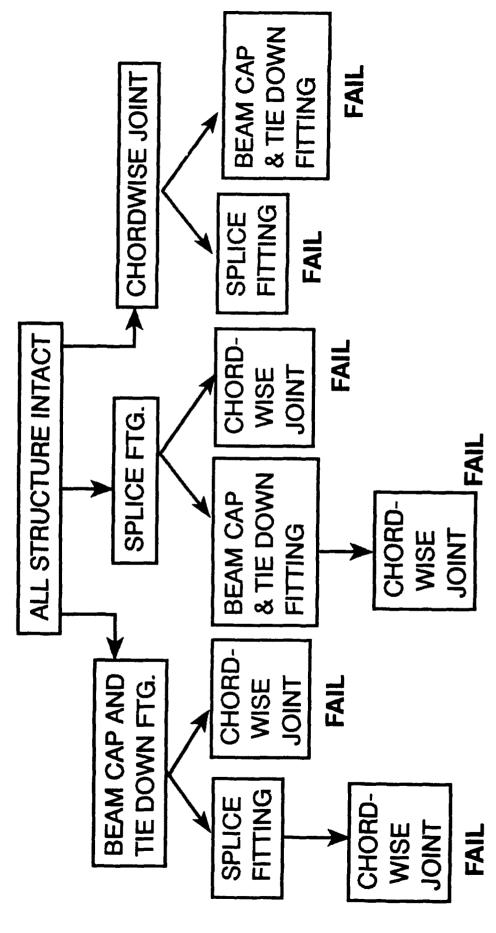


BLANK DECISION TREE

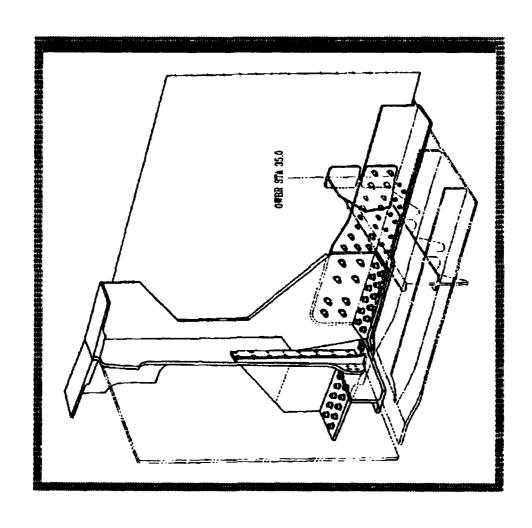
3 ELEMENTS WILL HAVE 6 POSSIBLE FAILURE AT THE EARLY COMBINATIONS AND 4 WOULD HAVE 24. WHEN YOU CONSIDER IT TAKES ONE DAY TO RUN THE FEM, ONE DAY TO REDUCE THE DATA TO PLOTS OF BOLT LOADS AND STRESSES, AND AT LEAST A COUPLE OF DAYS TO RUN TREE. ESSENTIAL TO SIMPLIFY THE FAILURE MODES TO EVERY EXTENT POSSIBLE. FAILURE IMPOSSIBLE THIS IS THE DECISION OR FAILURE TREE FOR WHICH WE DEVELOP PROBABILITIES. POSSIBLE BE Ø WOULD SUCH II ESTABLISH EVERY DETAIL OR FOR EXAMPLE, 5 1 NECESSARY CANNOT INCLUDE CALCULATIONS IN ANY REASONABLE TIME. SI II ANALYSIS, IS TREE II THE CRACKGROWTHS, THIS THE OBVIOUSLY, OF STAGES

THAT THE PICTURE OF THE WS 405 A SEPARATE ANALYSIS WAS AT THIS STAGE THE FAILURE TREE IS AN ESTIMATE OF WHAT THE FINAL RESULT BASED ON FEM DATA MADE LOOKING AT THE OUTBOARD SIDE OF THE JOINT THE BEAM CAPS, SPLICE FITTING AND CHORDWISE JOINT SEE HOWEVER, KNOWING THE RESULTS OF FIELD INSPECTIONS, AN EDUCATED GUESS CAN BE YOU CAN JOINT AGAIN SHOWS THE CRITICAL PARTS REPRESENTED BY THE DECISION TREE. THIS DECISION TREE ONLY REPRESENTS THE REAR BEAM AREA. ABOUT THE COMPONENTS THAT WILL NEED TO BE THOROUGHLY INSPECTED. CONDUCTED ON THE FRONT BEAM USING THE SAME METHODOLOGY. ARE SHOWN. WILL BE.

WS 405 RISK ASSESSMENT FAILURE DECISION TREE



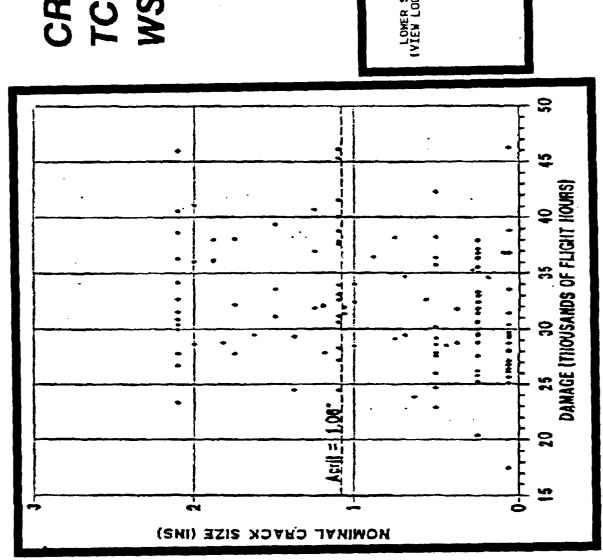
C-141 WS 405 REAR BEAM STRUCTURE



CRACK DATA

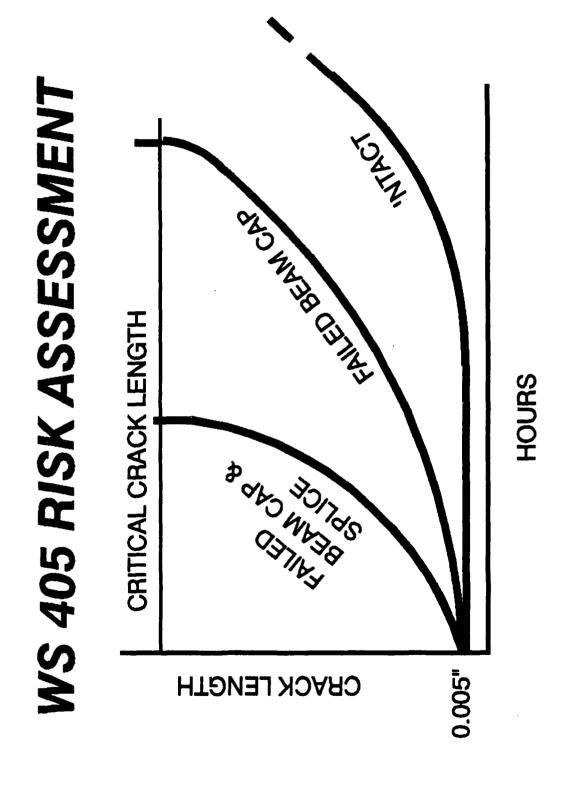
THIS WAS AN INSPECTION ALONG THE AFT TAB OF THE REAR BEAM CAP, CONCENTRATING ON THE AREA INSPECTIONS, USING THE LINEAR VERSION OF THE FINITE ELEMENT MODEL, THIS AREA HAD BEEN PIN OBTAINED, THE ANALYSIS WAS A REASONABLY GOOD PREDICTOR OF REALITY. THE CRITICAL CRACK LENGTH POINTED AS A POSSIBLE FAILURE AREA. AS CAN BE SEEN FROM THE DATA, WHICH WAS SUBSEQUENTLY SHOWN HERE IS FOR LIMIT DESIGN LOAD. THE CRACKS SHOWN ABOVE THE LINE ARE NOT CAPABLE OF SUSTAINING LIMIT LOAD. ONE PROBLEM, WHEN COMPONENTS HAVE CRACKS OF THIS SIZE, IS THAT THEY THIS CHART SHOWS THE DISTRIBUTION OF CRACKS DETERMINED DURING THE TCTO 753 INSPECTION. THIS WAS DEMONSTRATED DURING A SIMULATED TEST OF THE AREA. EARLY IN THE ANALYSIS AND PRIOR THE GROUND TIE DOWN FITTING WAS ATTACHED. SHED LOAD TO ADJACENT AREAS.

CRACKS FOUND BY TCTO 753 IN WS 405 AREA



CRACKGROWTH CURVE

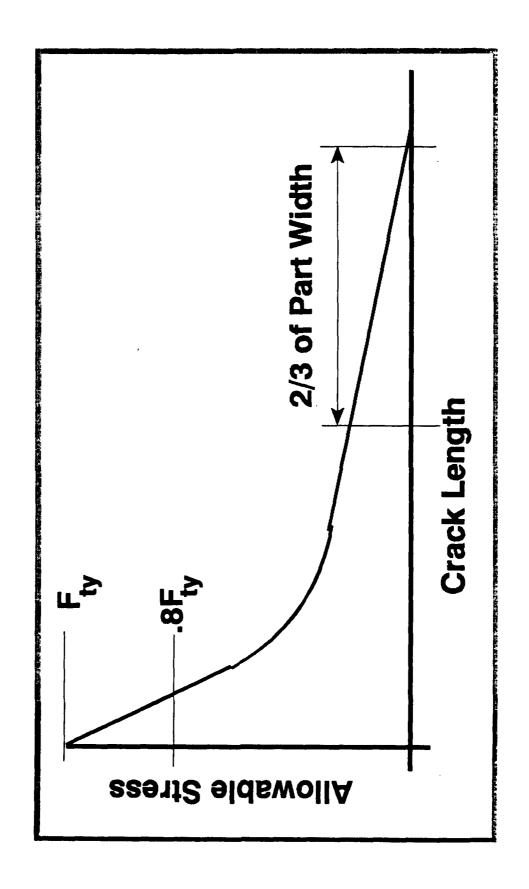
EACH BLOCK ON THE FAILURE DIAGRAM WILL REQUIRED A SEPARATE CRACKGROWTH CURVE DEVELOPMENT, AND EACH WILL REQUIRE A SEPARATE FINITE ELEMENT MODEL RUN. THESE CRACKGROWTH CURVES ARE ALSO FLIGHT HOURS WHEN THE INSPECTION WAS COMPLETED, THE FLEET DATA HAD TO BE NORMALIZED TO A IF YOU THIS IS SHOWN BY THE MIDDLE CURVE. FINALLY, IT CAN FAIL BECAUSE OF GREATLY INCREASED STRESSES WHEN BOTH USED FOR REDUCING THE FIELD INSPECTION DATA. SINCE EACH AIRCRAFT WAS AT A DIFFERENT SET OF THERE ARE THREE WAYS THE CHORDWISE JOINT (PANEL SPLICES) CAN FAIL. THIS IS REPRESENTED BY THE INTACT CURVE SHOWN TO THE FAR RIGHT. THE BEAM CAP AND THE MAJOR SPLICE FITTING HAVE FAILED. THIS CURVE IS SHOWN TO THE FAR LEFT. THESE CRACKGROWTH CURVES ARE TYPICAL OF THOSE FOR THE CHORDWISE PANEL SPLICES. SECOND, IT CAN FAIL DUE TO THE INCREASED STRESSES CAUSED BY A FAILED BEAM CAP. FIRST, IT CAN FAIL ALONE. RECALL THE DECISION TREE, COMMON TIME.



STRENGTH CURVE

A THEORETICAL CURVE OF THIS IYPE IS SHOWN USING THE APPROACH OF FEDDERSON. IT IS A PLOT OF CRACK LENGTH VERSUS ALLOWABLE STRENGTH. THE METHOD IS ABLE TO PREDICT STRENGTHS BOTH FOR THE LINEAR ELASTIC PORTION OF THE ALSO FOR THE AREAS OUTSIDE OF THIS RANGE. LASC HAS STANDARD PROGRAMS FOR CALCULATING THE CURVE BETWEEN 80 PERCENT OF THE YIELD STRENGTH OUT TO APPROXIMATELY 1/3 OF THE WIDTH, AND FRACTURE MECHANICS PORTION OF THESE CURVES. HOWEVER, THERE ARE A NUMBER OF TABLES WHICH CAN OBVIOUSLY, FOR COMPLICATED SHAPES WITH FASTENER HOLES, THE CURVE WILL EACH ELEMENT IN THE ANALYSIS REQUIRES A STRENGTH CURVE. DISCONTINUOUS INSTEAD OF SMOOTH AS SHOWN. BE USED.

Residual Strength Diagram For A Single Element



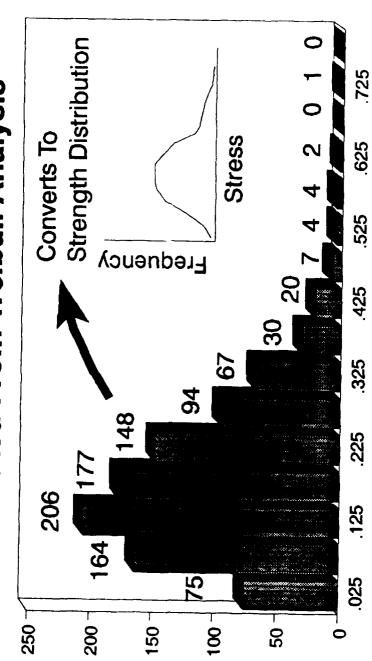
DISCRETE DISTRIBUTION

THIS CHART SHOWS A DISCRETE CRACK FREQUENCY DISTRIBUTION GENERATED FROM A WEIBULL WERE SIMULATED USING THE WEIBULL DISTRIBUTION BECAUSE OF ITS ABILITY TO MATCH SMALL SAMPLE ADDITIONALLY, DATA OBTAINED DURING THE REPAIR ACTIONS NOW IN PROGRESS CONTINUE TO MATCH THE THE DATA FOR THE CHORDWISE JOINT AND SPLICE FITTING DISTRIBUTIONS LIKE THIS NEED TO BE GENERATED FOR EACH ELEMENT AT EACH SELECTED TIME PERIOD IT ALSO TURNED OUT THAT AFTER NORMALIZING THE CRACK DATA, THE FIT WAS EXCELLENT. PREDICTED DISTRIBUTION. THE BEAM CAP ASSESSMENT WHICH WAS DONE PRIOR TO THE OVERALL RISK, USED A LOG NORMAL DISTRIBUTION. THE CAP DATA WAS SIMPLY UPDATED AND USED IN THIS ASSESSMENT. ELEMENT. SHOWN ON THIS CHART IS FOR A SINGLE POINT IN TIME AND FOR A SINGLE DISTRIBUTION OF THE INSPECTION DATA. FOR WHICH RISK IS TO BE CALCULATED THE DATA

ASSOCIATED ONE SUCH DISTRIBUTION CAN BE SEEN JUST UP AND TO THE RIGHT OF ITS DISTRIBUTION AND FREQUENCY DISTRIBUTIONS A STRENGTH THE CRACK FREQUENCY DISTRIBUTION. PROBABILITIES CAN BE DERIVED. THESE

WS 405 RISK ASSESSMENT

Typical Crack Frequency Distribution Generated From Weibull Analysis

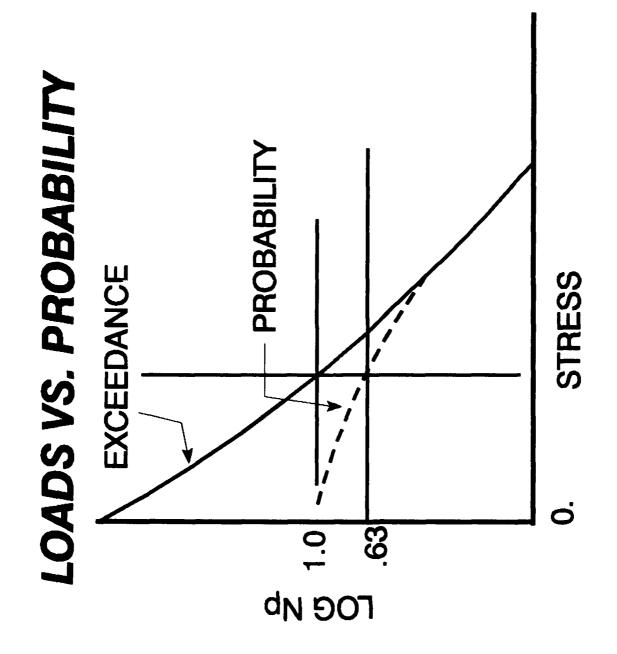


Crack Length (Inches)

Number of Cracks

LOADS CURVE

TYPE FOR EACH ELEMENT IN THE FAILURE TREE. FROM THIS DATA, THE STRESSES APPLIED TO THE THE X AXIS GIVES THE STRESSES FOR EACH PROBABILITY. OBVIOUSLY, THERE WILL BE A UNIQUE CURVE OF THIS THIS CHART SHOWS A TYPICAL LOADS EXCEEDANCE CURVE FROM WHICH PROBABILITIES WERE DERIVED. ELEMENTS ARE DERIVED. IF THESE STRESSES EXCEED THE ALLOWABLE STRENGTHS, THEN FAILURE OCCURS. THE PROBABILITY IS CALCULATED AS 1-e-N WHERE N IS THE NUMBER OF OCCURRENCES.



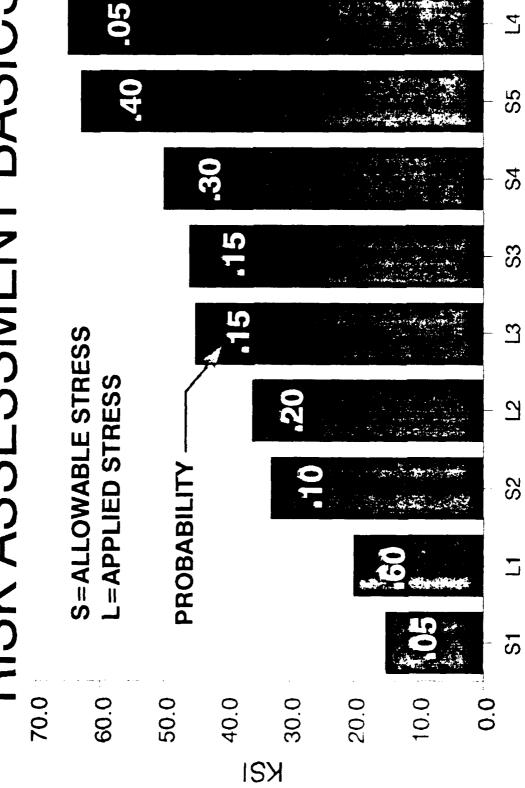
RISK EXAMPLE

THE NEXT CHART PRESENTS AN EXAMPLE OF HOW RISK CALCULATIONS UTILIZING THE PREVIOUSLY DISCUSSED PROCEDURES AND METHODS ARE CONDUCTED ON A SINGLE ELEMENT.

BE EASILY CALCULATED. THIS CALCULATION NEEDS TO BE CARRIED OUT FOR EACH ELEMENT ON THE FAILURE OUR EXAMPLE IS SIMPLIFIED SO THAT THE RESULTS CAN STRENGTHS AND EACH ELEMENT, WE NOW HAVE OBTAINED THE PROBABILITIES OF PROBABILITIES OF APPLIED STRESSES. TREE AT EACH TIME PERIOD.

LOOKING AT THE CHART, IT CAN BE SEEN THAT 5 PERCENT OF THE SPECIMENS HAVE A STRENGTH OF FAILURE IS 1.00. SIMILARLY, THE 10 PERCENT OF THE ELEMENTS WHICH HAVE STRENGTH S2, WILL OF FAILURE AT THIS POINT EQUALS .05 X 1 + .10 (.20 + .15 + .05). THE OTHER STRENGTHS AND EQUAL TO S1. IT CAN ALSO BE SEEN THAT ALL OF THE LOADS EXCEED IT, THEREFORE THE PROBABILITY THEREFORE, THE PROBABILITY LOADS ARE TREATED IN THE SAME MANNER, UNTIL THE OVERALL PROBABILITY OF FAILURE IS OBTAINED. EXPERIENCE LOADS OF L2, L3 AND L4, WHICH WILL CAUSE IT TO FAIL.

RISK ASSESSMENT BASICS



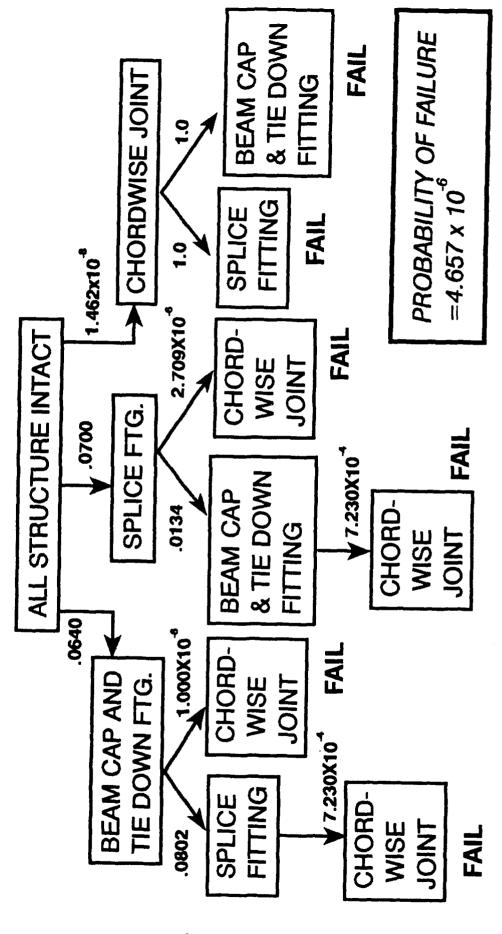
DECISION CHARTS

THE FIRST CHART SHOWS THE THE NEXT TWO CHARTS SHOW THE FINAL STEP OF CALCULATING THE RISK FOR A MULTI-ELEMENT SECOND CHART SHOWS THE PROBABILITY OF FAILURE OF THE JOINT AFTER THE X-RAY INSPECTION USING A PROBABILITY OF DETECTION CURVE DERIVED FROM THOSE SHOWN IN THE "HAVE CRACKS WILL TRAVEL" PROGRAM. THIS PROGRAM WAS FUNDED BY SAN ANTONIO AIR LOGISTICS CENTER AND IS STILL INSPECTION NUMBERS SHOWN ARE NOT THE ACTUAL CALCULATED NUMBERS BUT ARE MERELY FOR ILLUSTRATION PURPOSES. SITUATION EXISTING ON AN AVERAGE AIRCRAFT AT THE CONCLUSION OF 33,400 FLIGHT HOURS. NON-DESTRUCTIVE STRUCTURE USING ALL OF THE DATA DISCUSSED PREVIOUSLY AS INPUTS. WORLD REAL JO PERTAINING DATA OF SOURCE EXCELLENT PROBABILITIES AN

THE CHARTS ALSO SHOW WHICH AREAS OF THE WS 405 JOINT ABSOLUTELY HAVE TO BE PROTECTED TO ENSURE SAFETY.

& TIE DOWN PROBABILITY OF FAILURE **BEAM CAP** FAIL FITTING **★** CHORDWISE JOINT $=3.465 \times 10^{-3}$ FITTING FAIL SPLICE 1.0 8.325×10⁻⁷ **WS 405 RISK ASSESSMENT** FAILURE DECISION TREE 1.525X10⁴ CHORD-FAIL **BEFORE INSPECTION** ALL STRUCTURE INTACT JOINT WISE SPLICE FTG. 9060: / FAIL **₩** 9.000X10 & TIE DOWN **BEAM CAP** CHORD-.1100 FITTING **WISE** JOINT .1200 1.952X10⁴ FAIL CHORD-BEAM CAP AND **WISE** JOINT TIE DOWN FTG. \$ 9.000X10 FITTING CHORD-SPLICE WISE LOINT FAIL . 8 8

WS 405 RISK ASSESSMENT FAILURE DECISION TREE AFTER INSPECTION



SUMMARY

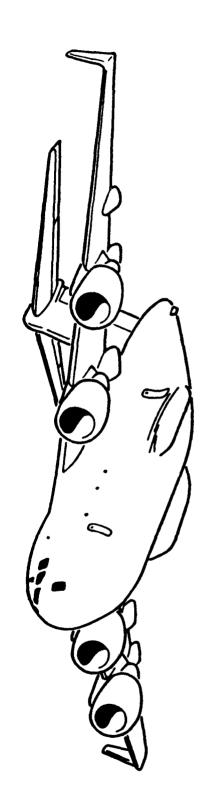
ALTHOUGH FINAL IN SUMMARY, THE RISK ASSESSMENT OF THE C-141 W.S. 405 JOINT HAS PROVIDED VALUABLE INPUT FOR DECISIONS REGARDING A REAL AIRCRAFT PROBLEM. A TEAM EFFORT BY LOCKHEED AND AIR FORCE ENGINEERS AND A SOUND, RELIABLE DATA BASE HAS GIVEN THE AIR FORCE A FORCE MANAGEMENT APPROACH ACTIONS AND TIMELINESS OF THESE ACTIONS ARE QUITE DETAILED, THIS FINAL CHART GIVES AN OVERVIEW OF THOSE ACTIONS. SPECIFICS ASSOCIATED WITH THIS ANALYSIS ARE OBTAINABLE ONLY FROM TO SAFELY EXECUTING CORRECTIVE ACTIONS TO THE WS 405 CRACKING PROBLEM. THE WARNER ROBINS C-141 ENGINEERING BRANCH (LJLE).

WS 405 RISK ASSESSMENT SUMMARY

- A Quantified Risk So Comparisons With Other Military Aircraft Could Be Made
- Created Decision Trees and Used Them to Identify the Area of the Joint Which Had To Be Protected
- Caused the Imposition of Flight Restrictions to the Aircraft
- Resulted in Steps to Expedite Inspections and Modifications to the Aircraft

PHASED LOAD CONDITION GENERATOR FOR C-17 FULL SCALE DURABILITY QUALIFICATION TESTING

)



1991 ASIP CONFERENCE 3-5 DECEMBER 1991 SAN ANTONIO, TEXAS R. G. Eastin Douglas Aircraft Co. Long Beach, Ca.

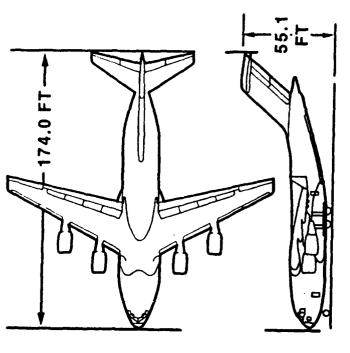
PHASED LOAD CONDITION GENERATOR FOR C-17 FULL SCALE DURABILITY TESTING

erate sequences of phased external load conditions. These sequences will be used testing. This presentation will review the primary motivation for developing this A Phased Load Sequence Generator System (PLSGS) has been developed to gento "simulate" the gust and taxi loading environments during C-17 full scale durability system, the main problems which had to be addressed, the methodology/approach used and the main features of the system. This will be done at a conceptual level. Details may be obtained from existing technical publications and the authors.

USAF/MCDONNELL DOUGLAS C-17A

MAX T.O. GROSS WEIGHT MAX PAYLOAD MAX INTERNAL FUEL CRUISE SPEED THRUST PER ENGINE AIRDROP

T 580,000 LB 172,200 LB 176,000 LB MACH 0.77 39,800 LB 110,000 LB



CAPABILITIES

	COMBATO OFF.	
AERIAL REFUELING		
AIRDROP & LAPES R		
SMALL AUSTERE AIRFIELD		
LOADING DRIVE ON/OFF]
CARGO	OUTSIZE	
	OVERSIZE & BULK	
LONG		

0

10

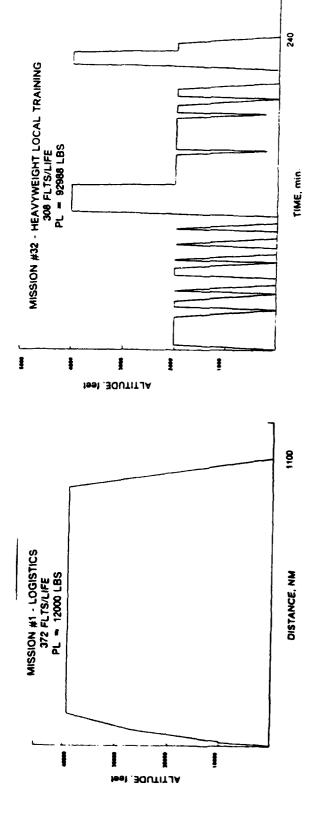
165 FT BASIC WING SPAN.

USAF/MCDONNELL DOUGLAS C-17A

is on a par with the C-5. The loadable cargo space is 88 feet long which includes the The C-17A is designed to meet unique operational requirements which include carrying and airdropping outsized cargo (e.g. large trucks and tanks), operating on 3000 to 4000 foot runways with 50 foot taxiways, enhanced ground maneuverability (e.g. backup ability), and a range of 2400 nautical miles with full payload. The overall length and wing span is close to that of a C-141 while the cargo hold cross section ramp which is loadable to 40000 pounds. It also has a single aft cargo door which opens both on the ground and in flight so that the full width of the aft opening can be utilized for airdrop or LAPES (Low Altitude Parachute Extraction System) of outsized combat equipment.

SPECIFIED SERVICE USAGE

35 Unique Peacetime Design Mission Profiles Specified



One Lifetime of Operation Consists of:

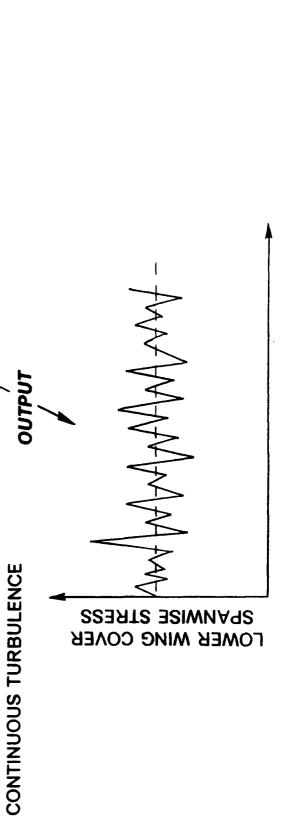
8564 Flights 30000 Flight Hours 18950 Landings (Includes Touch and Gos) 4200 Full Pressure Cycles 3200 Hours @ $V_E \ge 300$ KEAS & h ≤ 2000 feet 6050 Hours @ $V_E < 300$ KEAS & h ≤ 2000 feet

Ņ

SPECIFIED SERVICE USAGE

cycles per mission. One lifetime consists of 8564 flights, 30000 flight hours, and 18950 landings (including touch and gos). There are approximately 4200 full cabin pressure cycles with many lesser cycles associated with numerous moderate altitude transitions. The specified mission profiles also contain a significant amount of operation at 2000 feet and below. Approximately 30% of the total flight time is spent in this The specified service usage for the C-17A is given in terms of 35 unique design mission profiles. These vary from logistics missions, with the majority of time spent cruising at altitude and one ground-air-ground (GAG) cycle, to complex training missions, with the majority of time spent at low altitude and as many as eleven GAG environment with about one third of that spent cruising at 300 KEAS or greater.

)



GUST VELOCITY

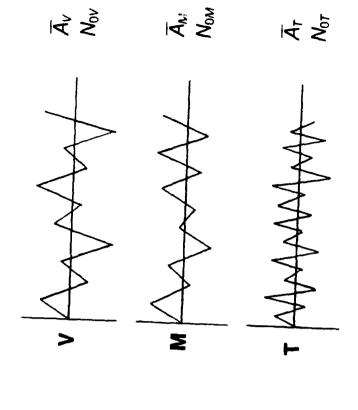
LINEAR AIRFRAME

)

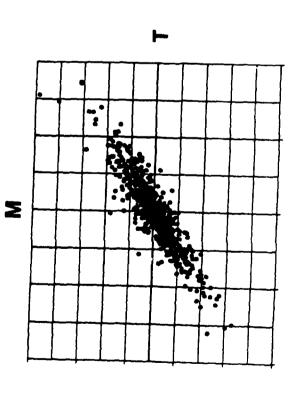
and internal stresses do not vary. However, if the airplane encounters turbulence the plane). Output from the system are external loads (e.g. wing shear, moment, and While flying through clean air the airplane is statically balanced and external loads result is a complex interaction involving external aerodynamic forces, aircraft inertia and the flexible airframe itself. This gives rise to dynamically varying external loads and internal loads/stresses. From an analytical standpoint we assume that the turbulence is a Gaussian random process which is input to a linear system (i.e. the airtorsion) which in turn give rise to internal loads/stresses. These represent a family of Gaussian random processes related by the same input turbulence and the linear system from which they emerge.

)

(Phasing and Variable N₀)



- $N_{0V} \neq N_{0M} \neq N_{0T}$
- STATISTICAL RELATIONSHIP OF
 M TO T IS PHASING



(Phasing and Variable N₀)

In considering response quantities, (e.g. wing shear, bending and torque), the time history response is characterized as Gaussian random. If the turbulence field that the airplane is flying through has a standard deviation of unity then the standard deviation of the response is denoted as \overline{A} and the characteristic response frequency is denoted as No. In general No is different for each response quantity and can vary significantly between different parts of the airframe. This characteristic is discussed later and presents a significant dilemma with respect to full scale testing where only one No over the whole airplane is really possible.

them together we can illustrate phasing characteristics. This can be predicted if we If we periodically sample two response quantities (e.g. moment and torque) and plot know the variance of each response quantity and covariance of each to the others. This information is presented in the form of a covariance matrix.

COVARIANCE MATRIX

)

$$\vec{A}_{1}^{2}$$
 \vec{A}_{21} \vec{A}_{31} \vec{A}_{N1}
 \vec{A}_{12} \vec{A}_{2}^{2} \vec{A}_{32} \vec{A}_{N2}
 \vec{A}_{13} \vec{A}_{23} \vec{A}_{3}^{2} \vec{A}_{N3}

- AND DIAGONAL N O VARIANCES RESPONSE COVARIANCES OFF DIAGONAL WITH SYMMETRIC
- COMPLETELY DESCRIBES RESPONSE QUANTITY INTERRELATION STATISTICS
- USED TO CREATE PHASED LOAD CONDITIONS (E.G. MOST LIKELY VALUE OF P2 GIVEN P, IS [A24/A?]P1)
- CAN BE COMPUTED IN CONJUNCTION WITH PSD ANALYSIS
- CAN BE ESTIMATED FROM STATISTICAL ANALYSIS OF RESPONSE TIME HIS-

COVARIANCE MATRIX

The covariance matrix is one of the key elements of the PLSGS. It is fundamental to creating phased load conditions (i.e ones which have a probability of occuring in flight). This matrix completely describes the statistical dependency of all response It is a symmetric matrix in which the diagonal elements are the variances of the quantities to each other. It can be determined in conjunction with Power Spectral Density (PSD) analysis or from an analysis of the time history of response quantities. response quantities and the off diagonal elements are covariances.

AIRCRAFT GUST RESPONSE PREDICTION

FREQUENCY OF EXCEEDANCE/UNIT TIME GIVEN BY,

$$N(y) = N_0 [P_1 \exp(-y\overline{A}/b_1) + P_2 \exp(-y\overline{A}/b_2)]$$

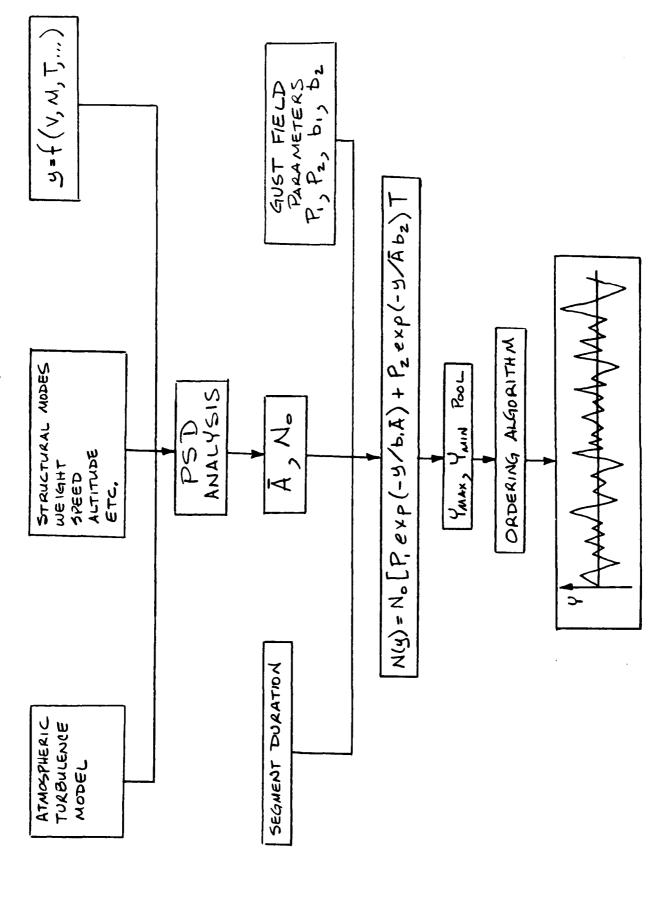
= INTENSITY PARAMETER OF NON-STORM TURBULENCE FIELDS RESPONSE QUANTITY STANDARD DEVIATION PRODUCED BY PROPORTION OF TIME SPENT IN NON-STORM TURBULENCE = INTENSITY PARAMETER OF STORM TURBULENCE FIELDS PROPORTION OF TIME SPENT IN STORM TURBULENCE A UNIT STANDARD DEVIATION TURBULENCE FIELD ZERO CROSSING FREQUENCY OF RESPONSE Ald d

- PSD TECHNIQUES USED TO COMPUTE A and Mo
- COVARIANCES MAY BE COMPUTED AS PART OF PSD ANALYSIS

AIRCRAFT GUST RESPONSE PREDICTION

The turbulence model is such that the frequency of exceedance/unit time at any given response level (y) is given by the "crossing count" formula. PSD techniques are typically used to compute A and No. These along with the crossing count formula are sufficient to completely describe the response spectra of each individual quantity. However, if the interrelationship of response quantities must be known, then covariances are needed. These can be easily computed as an extension to the basic PSD analysis.

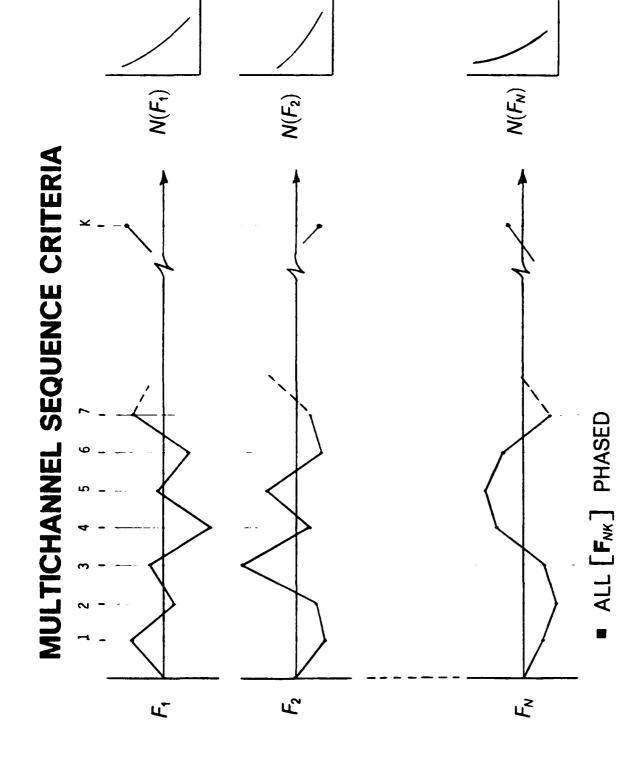
SINGLE CHANNEL SEQUENCES



SINGLE CHANNEL SEQUENCES

and other relevant ones as required. The output from the PSD analysis is \overline{A} and N_0 Single channel sequences have been and are routinely generated for coupon testing and control point analyses. This is done on a mission segment basis. A PSD analysis characteristics data and the linear relation between the desired response quantity ters for the segment altitude, and segment duration are used with the crossing count formula to establish a pool of sequence content. An ordering algorithm is then used is performed using an atmospheric turbulence model, structural and operational for the response parameter of interest. This, along with the gust probability parameto create a max-min sequence about any desired mean value.

ered and others. Additionally there is no N_o problem by definition and the content of For single channel sequences interaction between external loads and the effect on internal loads/stresses is handled easily in the PSD analysis. The computed A will account for any linear relationship between the response parameter being considthe sequence is "exact". Truncation can be performed using a simple range truncation algorithm without concern over biasing content or phasing.



■ ALL F_v EXCEEDANCES MATCHED

MULTICHANNEL SEQUENCE CRITIERIA

Considering a given flight segment and the sequence of load conditions, [F_{NK}], which are due to gust response there are two primary criteria which must be satisfied for it to be considered a valid sequence.

probable combination of loads, F_N as derived by the covariance matrix and an analysis of the overall sequence must result in a good approximation to the covariance First, the loads must be properly phased. That is, each load condition K must be a

a good approximation to the distribution given by the crossing count formula using \overline{A} and N_0 from the PSD analysis and P_1 , P_2 , b_1 , and b_2 for the segment altitude should Secondly, if we perform an exceedance analyses of each individual load sequence, be obtained.

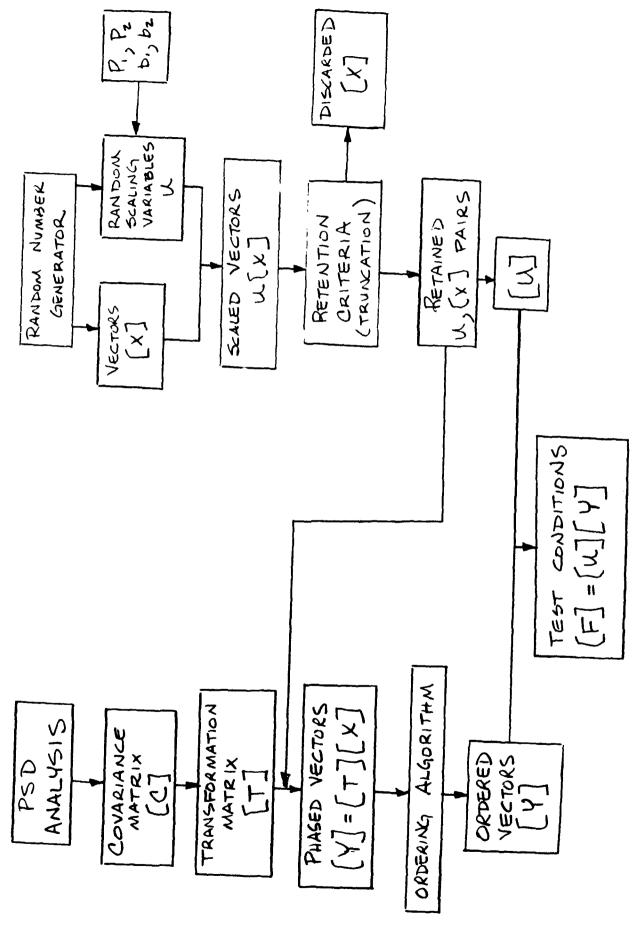
PLSGS DEVELOPMENT OBJECTIVES

- DEVELOP SYSTEM TO GENERATE SEQUENCES OF EXTERNAL LOAD **CONDITIONS REPRESENTING AIRCRAFT RESPONSE DUE TO GUST**
- USE SAME BASIC INPUT AS USED TO DEVELOP SINGLE CHANNEL SEQUENCES USED FOR ANALYSIS AND DEVELOPMENT TESTING (E.G. \overline{A} , N_0 , P_1 , P_2 , b_1 , b_2)
- SATISFY MULTICHANNEL SEQUENCE CRITIERIA
- DEVELOP AND INCORPORATE TRUNCATION SCHEME TO BE USED TO REDUCE THE NUMBER OF LOAD CONDITIONS IN THE SEQUENCE FOR **ECONOMY OF TESTING**

PLSGS DEVELOPMENT OBJECTIVES

phasing. Lastly we wanted to incorporate a compatible truncation scheme that could In setting out to develop the PLSGS there were several objectives that we wanted to meet. The overall objective was to develop a system that could be routinely used to generate discrete external load conditions for full scale testing which would be representative of aircraft response due to gust. The same basic input was to be used that was used to generate single channel sequences for analysis and development testing. Along with this we wanted the full scale sequences generated by the PLSGS to be consistent with the single channel analysis sequences. Ideally this means that if we look at any single response quantity within the full scale sequence we would like it to be identical to the single channel sequence. Satisfying the multichannel sequence critieria previously discussed insures this and also proper load-to-load be used to reduce the number of load conditions, as required, for economy of testing.

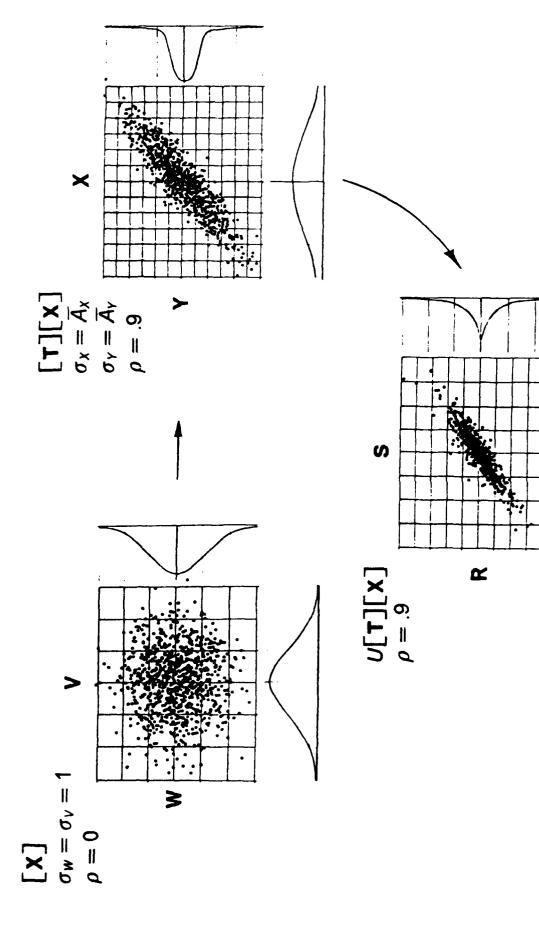
GENERAL PROCESS DESCRIPTION



GENERAL PROCESS DESCRIPTION

- 1. PSD analysis provides covariance matrix, C.
- Transformation matrix, T, is derived from covariance matrix.
- Vectors, X, are generated whose components are independent normally distributed random variables with unit variance. က
- Random scaling factors, U, are generated for each X using P₁,P₂,b₁, and b₂.
- 5. Truncation is performed using UX retention criteria.
- Vectors Y are generated from TX which are dependent normally distributed random variables with same covariance as given by C. 6.
- 7. Optimum ordering is determined using Y = TX.
- 8. Actual load conditions, F, are determined from UTX.

LINEAR TRANSFORMATIONS



LINEAR TRANSFORMATIONS

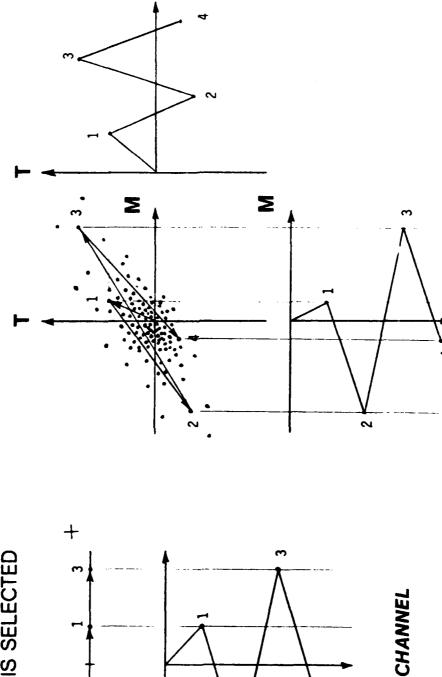
baseline random variables into random variables which are then ordered and used for testing. This is illustrated here for the two dimensional case. The components of ance. These are transformed using transformation matrix T into a new set of vectors whose components have the desired phasing but are still normally distributed. Each As previously summarized two linear transformations are performed to change the the X vectors are uncorrelated normally distributed random variables with unit varivector is then scaled by a random scaling variable, U, having an exceedance distribution given by:

$$N(u) = P_1 \exp(-u^2/b_1^2) + P_2 \exp(-u^2/b_2^2)$$

The resulting vectors now have the desired phasing and individual components have the required exceedance distributions. The only thing left to do is order them.

ORDERING

- ORDERING ALGORITHM IS ANALOGOUS TO THAT USED FOR CREATING SINGLE CHANNEL SEQUENCES
- UP TO 18 CONTROL LOADS EVALUATED BY ALGORITHM BEFORE LOAD CONDITION IS SELECTED



SINGLE CHANNEL

MULTICHANNEL

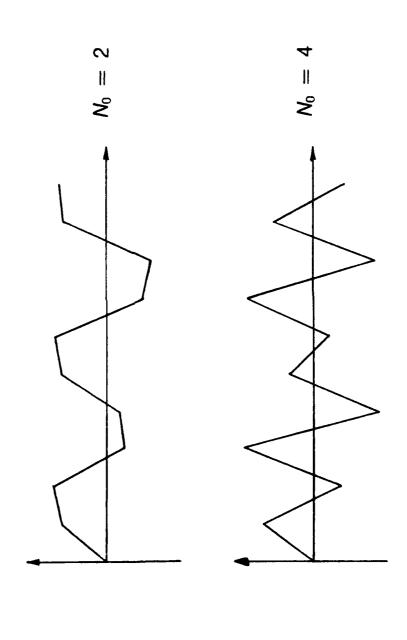
ORDERING

j

sequences. The algorithm alternates between signs as much as possible with the conditions just before and after. This results in ordering that closely resembles the comparable single channel sequences. The algorithm allows for up to 18 loads to be used as "control" loads. These are selected to be as representative as possible of groups of loads over different parts of the airframe. The remaining loads are slave ideal being that each load condition ends up opposite in sign to the same loads in The ordering algorithm is analogous to that used for creating single channel to these "control loads".

INDUCED AUTOCORRELATION

- BIASES ORDERING TO GIVE TWO CHARACTERISTIC ZERO CROSSING FREQUENCIES OVER THE MULTICHANNEL SEQUENCE
- CORRELATION AND EXCEEDANCES DISTRIBUTIONS ARE UNDISTURBED

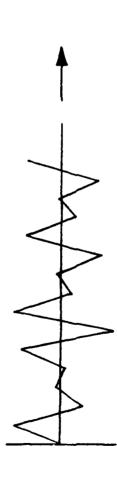


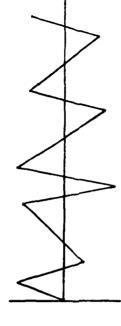
INDUCED AUTOCORRELATION

The ordering algorithm, left to itself, will tend to result in a multichannel sequence where every channel has the same zero crossing frequency. This is especially true experience. This results in a multichannel sequence having two characteristic zero induced auto correlation scheme may be used. This will bias the ordering such that selected loads will tend to dwell in sign for every other sign reversal the others when correlation is high. In order to induce some variation between channels which, in reality, may have significantly different (e.g. double) zero crossing frequencies, an crossing frequencies. The process preserves correlation and exceedances distrib-

TRUNCATING SEQUENCES

- REQUIRED FOR ECONOMY OF TEST
- **ELIMINATE NONDAMAGING SEQUENCE CONTENT**
- RANGE TRUNCATION (RT) APPROACH FOR SINGLE CHANNEL SEQUENCES





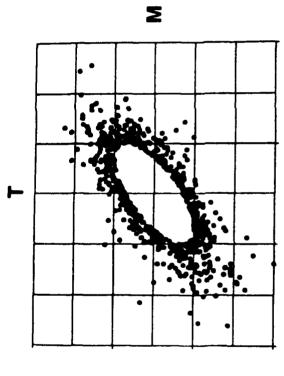
- RT PERFORMED AFTER ORDERING
- RT OF MULTICHANNEL SEQUENCES WILL DISTORT PHASING AND **EXCEEDANCES**
- ELLIPTICAL TRUNCATION METHOD ADOPTED

TRUNCATING SEQUENCES

nomical manner. The objective is to reduce the sequence length (i.e. number of Truncation is necessary so that testing can be accomplished in a timely and eco-A common measure of importance is the sequence's effect on fatigue crack cycles) without significantly affecting the impact of the sequence on the test article. Ideally the process will eliminate sequence content which is unimportant to the test. nucleation and/or crack growth. A common approach at DAC, for single channel sequences, has been to truncate based on a load or stress range (i.e. peak-valley difference). The range truncation ward and effective way of reducing single channel sequence length in a controlled manner. However, this method is not suited to multichannel sequences because it utions. A method, referred to as elliptical truncation, has been adopted which is as (RT) process is performed after the sequence has been ordered and is a straightformust be performed after ordering and it distorts phasing and exceedance distribeffective as the RT method but does not have its drawbacks.

ELLIPTICAL TRUNCATION

- LOAD CONDITION ELIMINATED IF F*C-1F = S < s
- ANALOGOUS TO SINGLE CHANNEL PEAK TRUNCATION



- APPLIED TO X
- CORRELATION IS UNDISTURBED
- "HIGH" LOAD EXCEEDANCE DISTRIBUTION IS UNDISTURBED

ELLIPTICAL TRUNCATION

The elliptical truncation method used is analogous to the peak truncation process for a single channel sequence. In two dimensions this can be looked at as eliminating all load conditions within a predefined elliptical radius, s. This process, in actual practice, is applied to the normal independent random variables, X to achieve global truncation without any transformation. Elliptical truncation does not disturb correlation and leaves the distribution of "high" loads untouched.

SUMMARY OF PLSGS

)

- ENGINEEERING SOLUTION TO PROBLEM OF "SIMULATING" DYNAMIC RESPONSE LOADING IN STATIC GROUND TEST ENVIRONMENT
- APPLICABLE TO ANY RESPONSE FOR WHICH A COVARIANCE MATRIX IS AVAILABLE
- "PHASING" ENSURED BY USE OF COVARIANCE MATRIX
- EXCEEDANCES FOR INDIVIDUAL LOADS ARE MATCHED "EXACTLY"
- GLOBAL ELLIPTICAL TRUNCATION USED TO REDUCE LOAD POINTS
- INDUCED AUTOCORRELATION USED TO DEAL WITH VARIABLE CROSS-ING FREQUENCY PROBLEM
- SEQUENCES USED FOR TEST ARE COMPATIBLE WITH SEQUENCES USED **FOR ANALYSIS**

SUMMARY OF PLSGS

The PLSGS provides an engineering solution to the problem of "simulating" dynamic response loading while constrained to using sequences of statically balanced test conditions. While the methodology was developed with airplane gust response in trix is available. Load phasing is ensured by use of the covariance matrix and exceedances for individual response quantities are closely matched. A truncation scheme is incorporated which will reduce the number of load conditions without biasing exceedances or phasing. Although the variable crossing frequency problem is not completely solved it is dealt with effectively using an induced autocorrelation scheme. Finally, the individual sequences which result are completely compatible and mind it is generally applicable to any dynamic response for which a covariance macomparable to those single channel sequences used for analysis.

REFERENCES

)

REPORT MDC-19211, THE PHASED LOAD SEQUENCE GENERATOR SYS-TEM, T. LERWICK, SEPTEMBER 26, 1990. A SYSTEM FOR GENERATING SEQUENCES OF PHASED GUST OR TAXI LOADINGS, R. G. EASTIN, TRYGVE R. LERWICK, SVEN M. SOEDEL, JOURNAL OF AIRCRAFT, TO BE PUBLISHED IN DECEMBER 1991.

REFERENCES

`)

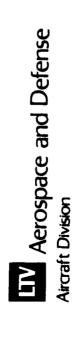
by Tryg Lerwick, provides a rigorous detail description of the method and also includes detailed mathematical derivations required to support the system. The second The PLSGS has been documented in two references. Report MDC-J9211, prepared reference is a less detailed description of the system and is scheduled to be published in the December 1991 issue of the Journal of Aircraft.

TESTING OF A MAJOR STRUCTURAL COMPONENT (C401) ON THE B-2 ADVANCED TECHNOLOGY BOMBER

by

K. D. Jordan
F. M. Grimsley (B-2 SPO)
V. W. Hall
C. E. Micheal
E. G. Nichols

1991 USAF STRUCTURAL INTEGRITY PROGRAM CONFERENCE San Antonio, Texas PRESENTED TO: 3-5 December 1991

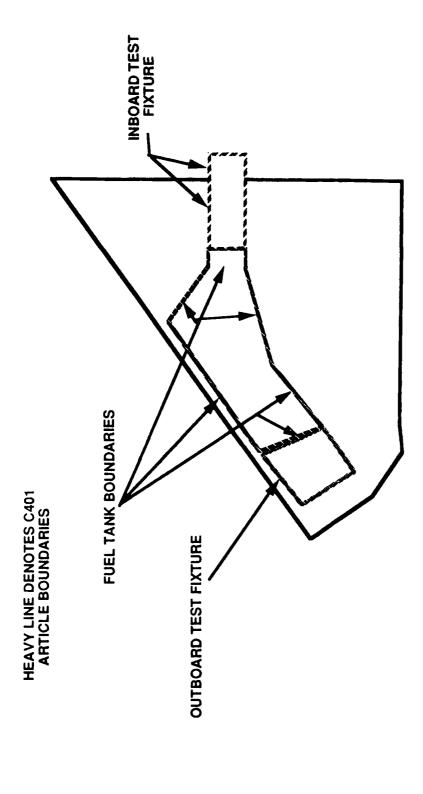


PURPOSE

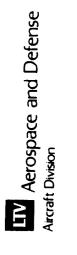
QUALIFY FUEL CONTAINMENT CAPABILITY OF INTEGRAL TANK

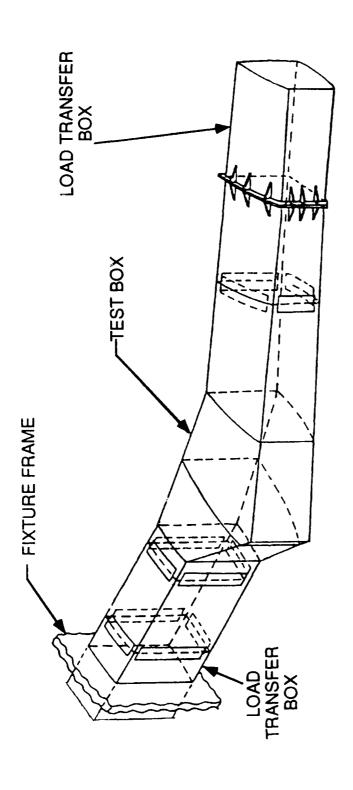
VERIFY STRUCTURAL INTEGRITY





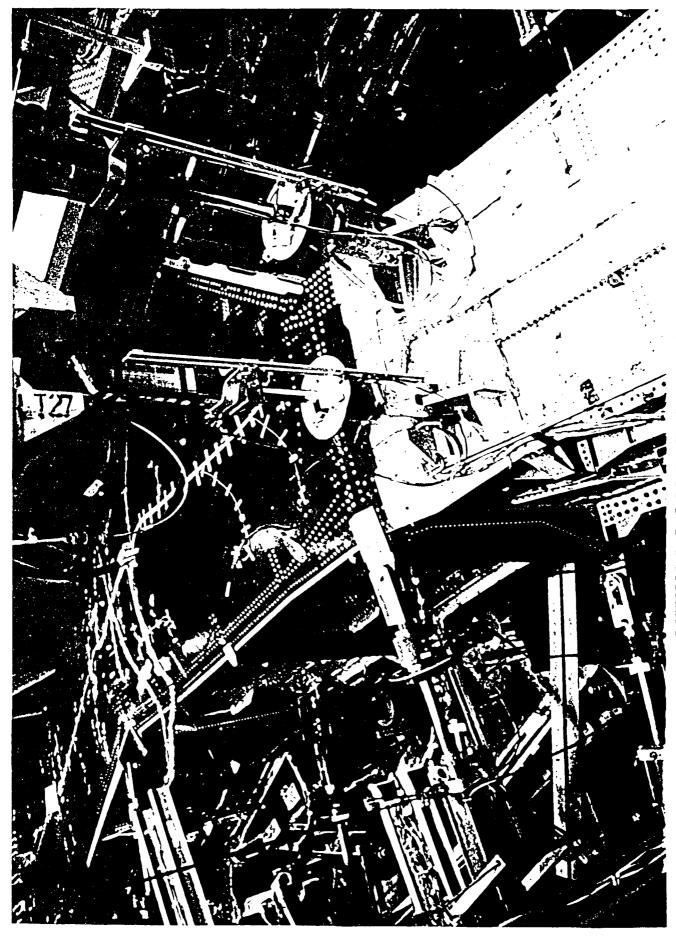
TEST ARTICLE VEHICLE LOCATION

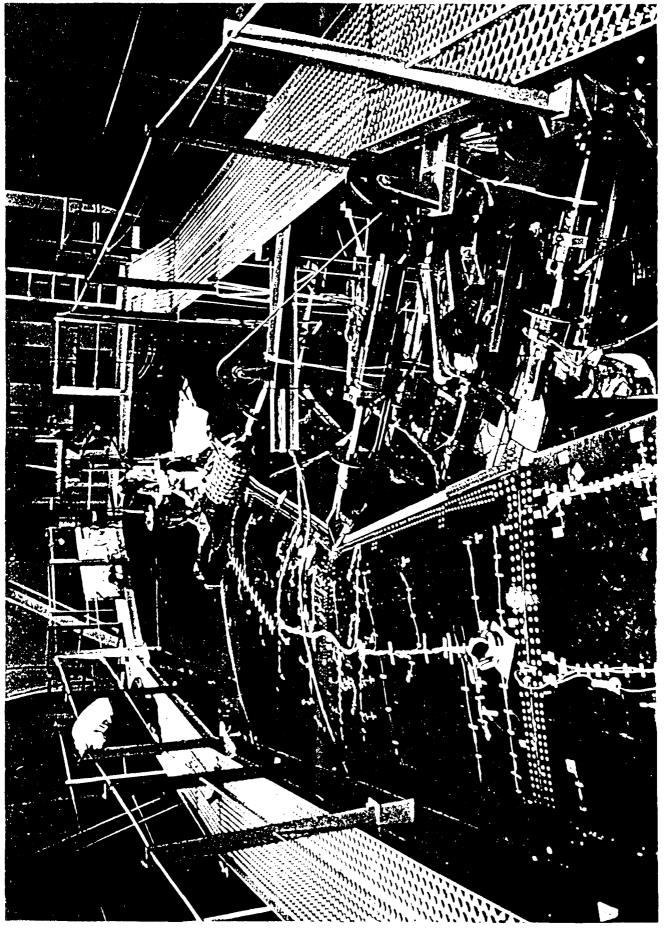




C401 TEST ARTICLE







DETERMINATION OF LOAD POINTS AND LOADS

GOAL: MINIMUM LOAD POINTS, ACCURATE INTERFACE

LOADS

CARVE-OUT OF MASTER NASTRAN MODEL

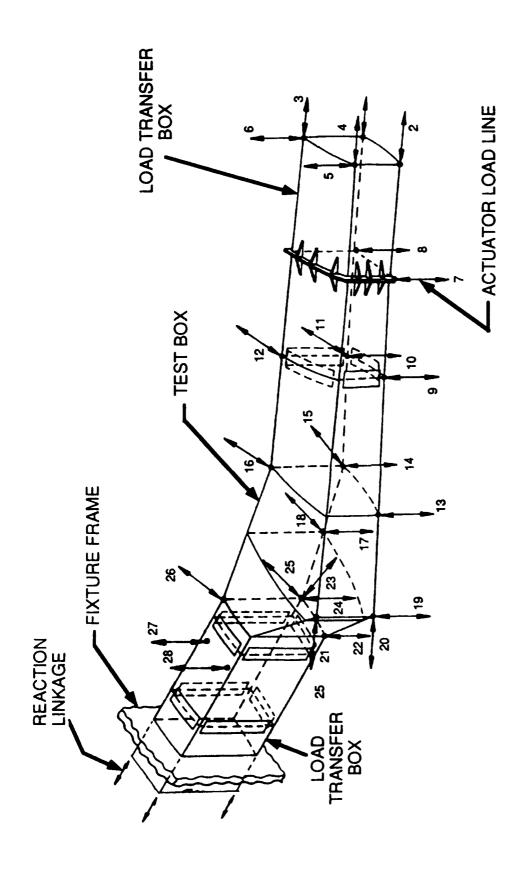
COARSE GRID MODEL TO MATCH VMT

FINE GRID MODEL TO TUNE INDIVIDUAL LOADS

GOOD MATCHING M AND T; V ACCEPTABLE

28 LOAD ACTUATORS REQUIRED

LW Aerospace and Defense Aircraft Division



LOAD JACK LOCATIONS

LIV Aerospace and Defense Aircraft Division

SPECTRUM DEVELOPMENT

- NORTHROP RESPONSIBILITY
- FLIGHT-BY-FLIGHT APPROACH
- GROUND HANDLING, LANDING, TAXI, GUST AND MANUEVER
 - **LOADS RANDOM WITHIN PHASE**
- PHASES IN SEQUENCE WITHIN FLIGHTS
- FLIGHTS RANDOMLY SEQUENCED

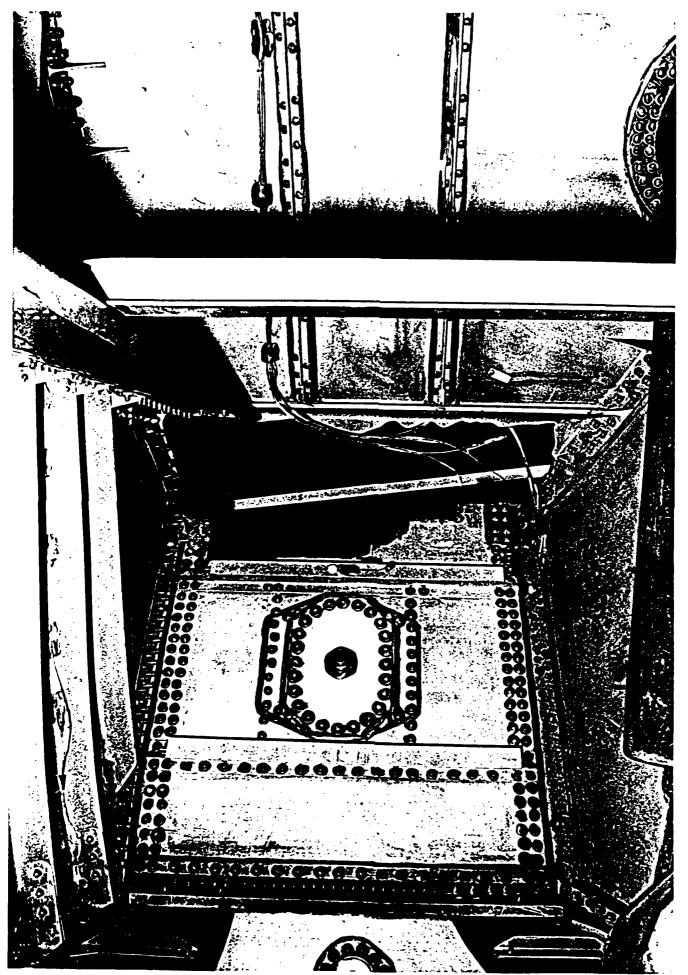


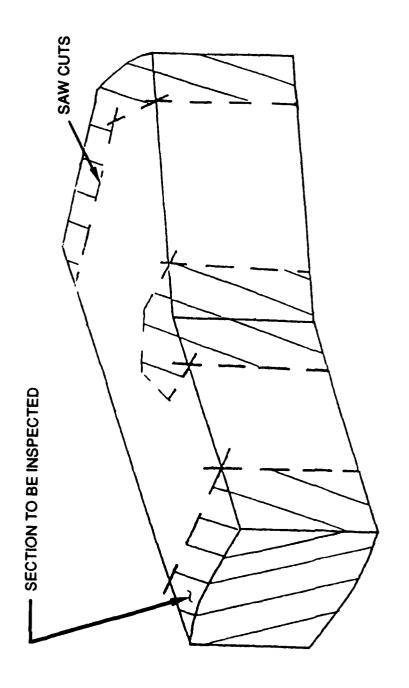
LOADING SEQUENCE

- PRESSURE TESTS
- STRAIN SURVEY
- DURABILITY TEST
- IMPACT DAMAGE
- RESIDUAL STRENGTH

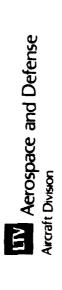


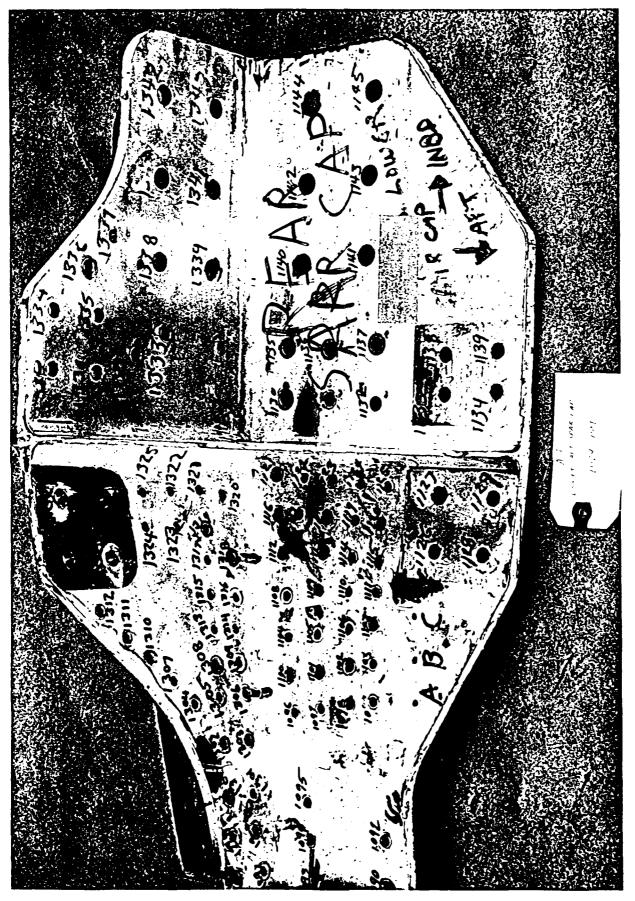






POST TEST TEARDOWN





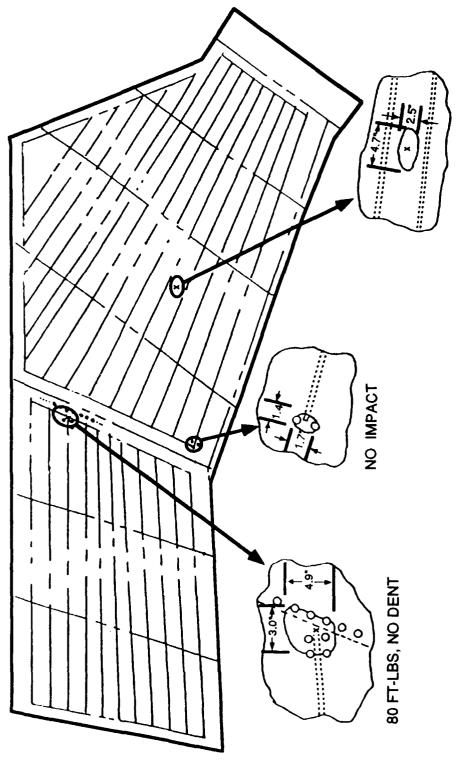
RESULTS

RESIDUAL STRENGTH OF 174% DLL

NO CLASS "B" LEAKS

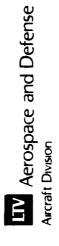
NO GROWTH OF IMPACT DAMAGE

LIV Aerospace and Defense Aircraft Division



64 FT-LBS, .16 IN. DENT (THROUGH)

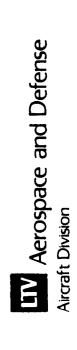
IMPACT DAMAGE LOCATIONS



RESULTS

TEARDOWN

- CONSERVATIVE HOLE QUALITY EFFECTS
- 5000 HOLES INSPECTED
- 3 CRACKS FOUND
- COMPOSITE INSPECTION INCONCLUSIVE
- FAILURE WAS TEST ARTICLE UNIQUE
- NO DESIGN CHANGES REQUIRED



INTRODUCTION

On Monday, saly 17, 1989, a historic event took place in the desert near Palindiae, California: the maiden flight of the B-2 Advanta. Textinalings (Stealth) Bomber, the post technologically advanced aircraft of our time. This event represented a major milestone in a development program which began almost 10 years ago. With all the pomp, circumstance and media coverage of a Hollywood gala, millions of people witnessed live coverage of first flight.

Just like all premier events, much work had been accomplished behind the scenes in order to ensure a successful debut. It is possible that the development testing of the B-2 is the most extensive test program ever accomplished during the history of aircraft design. This presentation will address one portion of development testing conducted by LTV Aircraft Products Group from November 1986 to December 1987. This test was referred to as the "C40! Box Test" and involved the static and durability testing of major production structure.

PURPOSE OF TEST

The primary test requirement was to qualify the fuel containment capability of an integral fuel tank by demonstrating that there would be no structural or material detects that would result in fuel leakage. This was accomplished by conducting pressure tests and durability testing to two lifetimes.

The second objective of the test was to verify the structural integrity of the section. This was accomplished by verifying the analytically predicted strains and their distributions and the predicted durability characteristics of the structure including major joints.

DESCRIPTION OF TEST ARTICLE

The test article consisted of a portion of the left hand wing structure of the aircraft. The outboard section consisted of a steel load transfer box which was used to apply some of the test loads to the next section inboard.

The next section was approximately 50 inches long. The inboard 27 inches of the structure was representative of the actual vehicle.

Inboard of the test fixture, was the test box built by LTV Aircraft Products. This section was the primary test structure and was structurally identical to the production article. Materials used are graphite epoxy, aluminum, and titanium. In addition to functioning as a fuel tank, the box acts as a spanwise load path. The box is approximately seventeen feet long and is comprised of the following major components:

- 1) Front and rear spars made of "T" shaped upper and lower caps enclosing a shear web. The web is pierced in several places by openings which allow access to the fuel tank.
- Primary full-depth ribs, three in number, span the gap between the front and rear spars. The construction of the two outboard full-depth ribs is similar to that of the spars, consisting of caps enclosing a shear web. The inboard full-depth rib, consisting of a straight and canted section, are machined from one-piece forgings and contain integral stiffeners.
- 3) Intermediate partial-depth ribs are located at 5 locations. They also span the distance between front and rear spars but do not extend the full depth of the

- airfoil. They are separated into upper and lower sections, tied together at intervals columns. The ribs are stiffened by vertical "T" sections.
- 4) Upper and lower skins serve as airfoil surfaces as well as the top and bottom of the fuel tank. They consist of multi-axial layers of graphite epoxy tape bonded into a sheet with integral blade-type, spanwise stiffeners on each inside surface. The skin stiffeners are fastened to the ribs with titanium butterfly clips and Hi-Lok fasteners.

The test box was sealed at assembly following production procedures. Most of the joined surfaces were coated with wet sealant prior to mate-up, fastener insertion, and torquing. Voids without access holes were packed with sealant prior to closure. Any voids which had entrances and exits were filled by injection after assembly. The final sealing operation was that of filleting inside corners of joined parts and covering fastener heads. All fasteners which project through the skins were sealed with Stat-O-Seals and "O" rings. For fasteners which exit the tank other than through the skins, the stat-o-seal was used and the fastener end which projects inside the box was coated with a dome-type sealant. In all cases, the sealant around the joints and fasteners present a double barrier to leak propagation.

The inboard section is approximately 10 feet long and extends 2 feet to the right of aircraft centerline. This section also represented actual vehicle structure.

The fifth and final section was a steel load transfer box which extended approximately 8 feet past the test structure. This box was rigidly mounted with the test fixture and served to react the majority of the applied loads during test. The entire test article cantilevered out from and was supported by the fixture while the test loads were applied.

DETERMINATION OF LOAD POINTS AND LOADS

A challenge presented early in this test program was how to accurately reproduce internal load distributions with a minimum of load points (for cost and safety concerns) while maintaining accurate structural interface loads. The approach taken by Northrop and LTV in this joint effort was to use a carve-out of the test article from the master NASTRAN model.

Initially, only vertical loads were applied to the model, but these proved insufficient and underscored the need for additional loading in the fore and aft directions, as well as horizontally in the spanwise direction. A coarse grid model was used in an iterative process of matching VMT between the test model and the master model. A grid point force balance (working outboard to inboard) resulted in the determination of load points and jack locations.

Once the jack locations had been fixed, a fine grid model was used to tune the individual loads to achieve the best match of internal load distributions. Throughout the process, constraints were placed on each jack so as to preclude local overloads of the structure.

The NASTRAN carve-out model was linear with no coupling due to non-linear deflections. The results showed good matching of bending moments and torsion, but the shears did not match well. This was acceptable since vertical shear did not play a significant role in sizing the structure. During the course of the test, good correlation was achieved between measured and predicted strains; measured deflections were within 5% of predicted at ultimate load. More importantly, good correlation existed between the C401 test and the forward box structure of the full-scale fatigue article.

TEST SET-UP AND LOADS

Twenty-seven hydraulic actuators were used to apply the flight loads to the test article during durability cycling. An additional actuator was used during strain surveys to introduce the correct load distribution into the lower rear spar cap. The locations of the actuators are shown in the figure. The actuators were hung from the fixture via gimbals and attached to the test article through specially made fittings containing self-aligning bearings. Four of the actuators apply the spanwise loads to the test article from the outboard end of the fixture. The remainder of the actuators apply loads which are approximately normal to the span line of the test article. All actuators operated in both tension and compression.

SPECTRUM DEVELOPMENT

Development of the test spectrum was the responsibility of Northrop. A flight-by-flight approach was used for airframe loads spectra development. Within each flight, service usage loads were established for each ground and flight phase. Static analyses were employed to obtain balanced loads for ground handling conditions. Landing and taxi loads were obtained from time history simulations using a dynamic model incorporating the appropriate rigid and flexible degrees of freedom. Both discrete and continuous runway profiles were considered for taxi. Gust loads were obtained using a similar dynamic model. Maneuver loads were determined from static aeroelastic analyses. Fuel tank pressurization loads were superimposed on air and ground loads where appropriate.

Each phase contained its associated loads, which were randomly sequenced within that phase. The phases were kept in their proper sequence within a given flight. As a result, the ground-air-ground load cycle was automatically included in its proper sequence. The flights, consisting of seven different mission profiles, were then randomly sequenced over the aircraft lifetime.

LOADING SEQUENCE

PRESSURE TESTS

The initial test of the specimen was a partial vacuum test to confirm the fuel sealant would not be dislodged from the corners and crevices of the tank. The empty specimen was loaded to the 0.0 G condition and a negative 2.5 PSIG pressure was applied with a vacuum pump. Seal integrity was verified by visual inspection with television borescope monitors and by observing the vacuum decay rate for a 15 minute period. A production proof pressure test was conducted to locate any leaks started by the vacuum test. The tank was pressurized to 5.2 PSIG and held for six minutes. No leakage or pressure drop was detected.

Fuel containment tests were conducted subsequent to the strain survey. The initial test was a proof pressure test to 8.0 PSIG in 2.0 PSIG increments simulating an in-flight refueling. The test article was loaded to an in-flight 1.0 G condition. The test was then repeated with the test article under a 1.09 G ground load, simulating a ground refueling. Tests to burst pressure, 12.0 PSIG, were conducted next as a continuation of the proof pressure tests. Pressure increments were 1.0 PSIG from 8 to 12 PSIG.

STATIC STRAIN SURVEY TESTS

Static tests to determine structural behavior and substantiate predicted analytical strains were conducted. Loads were applied in ten per cent increments to 100% of the desired load. Maximum strain survey loads were 60% of limit load.

DURABILITY TESTS

Durability testing involved a spectrum of repeated loads and pressure cycles. The spectrum was a repeating block of 335,434 cycles representing one-fifth of a lifetime. Total cyclic testing was for two lifetimes.

The spectrum was comprised of 106 flight or ground handling conditions, each produced in the test article by a unique arrangement of the 27 actuator loads. The computer controlled loading algebraically adds pairs of loading conditions together, multiplies them by a factor, and adds an on/off tank pressurization signal. The effect on the specimen is to superimpose the actuator loads of a base and a secondary flight condition upon one another, factor the sum to a desired percent of the load condition, and pressurize the test specimen as required.

Inspections were conducted at regular intervals determined by analyses of the fatigue critical areas of the test article.

At the end of two lives a composite damage tolerance test was conducted on the specimen. Two locations on the upper skin between internal ribs were selected as areas to be damaged. One area was centered between adjacent skin stiffeners. The other was centered over a single stiffener. Program damage tolerance requirements were visible damage (0.1 inch dent depth) up to a maximum of 75 foot-pounds. A one-inch diameter penetration was dropped with an impact energy of approximately 70 foot-pounds in order to generate a dent 0.1 inch deep. Both areas were ultrasonically inspected before and after impact to determine the extent of the damage.

RESIDUAL STRENGTH TESTS

At the completion of the impact test, the article was loaded to failure in an upgust condition. At 174% design limit load the lower forward cap of the inboard canted rib failed. Failure was caused by a fatigue crack around a fastener hole. This resulted in the test fitting which applied loads from actuators 19, 20 and 21 being separated from the specimen at the intersection of the canted rib and front spar.

POST TEST TEARDOWN

After the completion of all tests, the test article was partially disassembled and inspected. The article was separated into three sections by disassembly of the inboard and outboard joints. The forward box was then cut into four separate sections as shown in the figure. Two saw cuts were made inboard and outboard of the outboard and inboard ribs respectively. A third pair of cuts was made to remove a wedge from the aft spar area, centered at the kink. The wedge extended approximately halfway across the width of the box.

Each of the three sections were torn down to the detail level. All parts and fasteners were identified and marked as to orientation. Each fastener and detail part was inspected for delaminations, wear, cracks, galling, or yielding. All holes were dimensionally inspected at 0° and 90° orientations. Holes in metallic parts were inspected with eddy current while those in composite parts were inspected using zinc iodide techniques.

Composite surfaces were ultrasonically inspected. Metallic surfaces were fluorescent penetrant inspected. Any cracks found or indicated were opened and fractographically examined.

RESULTS

FUEL SEALING

The forward intermediate wing integral fuel tank passed the vacuum test, the pressure proof test and the durability test to two lifetimes with no class "B" leaks (seeps) or worse. A total of eleven seeps from around fastener heads were found at various times during testing. Most of these locations were on the lower wing skin surface. None of the seeps required repair per technical order leak classification procedures.

IMPACT DAMAGE

The two impact tests were performed after the box had been loaded to 150 per cent of design limit load in both the upgust and downgust conditions. The diagram shows the locations of impact and the resulting internal damage as determined by ultrasonic inspection. No additional damage was detected after loading to 174 per cent design limit load.

TEARDOWN INSPECTION

Two areas of interest were noted during the teardown and inspection of the wing assembly.

Many fastener holes in the C401 box were rough and exceeded the specified manufacturing tolerances. This was caused primarily by the use of one-step hole drilling methods. Due to changes in manufacturing methods the quality of the drilled holes in the production structure has shown marked improvement with succeeding articles. The C401 box is considered a conservative (worst case) representation of hole quality effects.

Eddy current inspections revealed three holes with radial cracks in their bores. Two were in hole numbers 603 and 702 in the aluminum canted rib. These were determined to have been caused by the static failure of the rib during the residual strength test. The third cracked hole, number 692 was in a 7075-T6 aluminum angle which joined the canted rib to the lower forward spar.

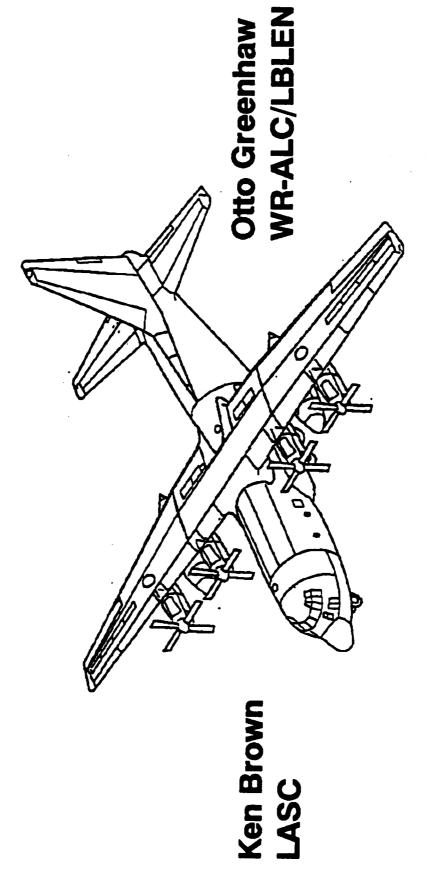
The initiation of the residual strength failure of the canted rib at the front spar was traced to an undetected crack that existed in the rib at the completion of durability cycling. A fractographic evaluation revealed that the crack initiated as a result of fretting between the steel splice angle (test fitting) and the aluminum canted rib. The crack initiated early (5% of cycles complete) and quickly propagated into an adjacent fastener hole. The crack then grew due to tensile and out of plane bending stresses to the edge of the canted rib.

Evaluation of the production design showed significant differences from the C401 test configuration at the failure location. These included omission of the leading edge support rib and a leading edge access door from the test. A second difference was the introduction of concentrated test loads by the jack attachment fittings at the test failure location. No protective sealant was used between the test steel splice fitting and the aluminum rib which is required in production. Lastly, the test steel splice fitting forms a single shear structural load path in the test as compared to the non-structural 7075-T76 splice plate used in production.

Each of these factors contributed to the development of the fatigue crack and failure of the canted rib. An assessment of the production design indicates that no fatigue problem would be expected to occur in this area. No design changes were instituted as a result of this test. However, this area is being closely monitored during the full scale durability test program.

Ultrasonic inspection of the stiffener and rib runouts revealed delaminations caused either by static failure during the residual strength test or by the prying loads imposed on these parts during disassembly to the component level. Considerable effort was required to free the skins and spar webs from the spar caps even after all the fasteners had been removed. The fuel tank sealant effectively bonded these parts together.

C-130 Wing Durability Testing



Ray Waldbusser WR-ALC/LBLEN

Overview

- Why This Test
- ▼ Test Description
- ► Test Repairs
- ► Future Plans For This Program (Unfunded)

OVERVIEW

previous fatigue tests of the C-130 wing have been conducted. Why was another test required? Three Why this test 0

the applied and setup physical test the A description of loadings. Test Description -

þe ğ will wi11 concepts the composite repairs selecting the repair of some for and criteria illustrated. discussed, Test repairs -

this program - Possible additional tests and evaluations which could be conducted as part of this program will be discussed. for plans Future

0

0

Why Another Test Program?

Sixteen Years Since Previous Test

Changes In The Airplane And Its Utilization

 Aircraft Were Approaching The Previously **Demonstrated Test Life**

WHY ANOTHER TEST PROGRAM?

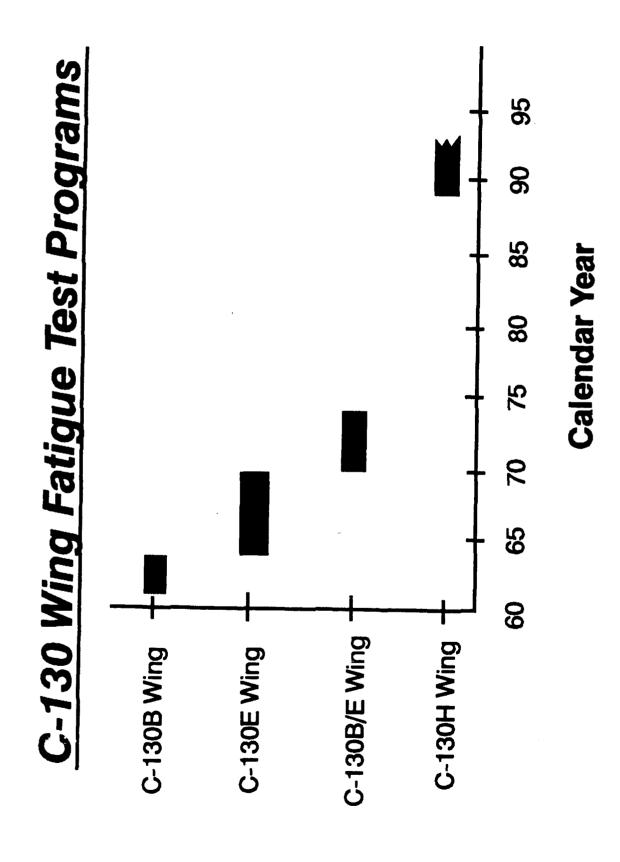
Three previous C-130 wing fatigue tests have been conducted; however, the last one completed sixteen years prior to the initiation of cycling on the present Many changes in fatigue test technology had occurred in this time, including the transition from block testing to flight-by-flight testing. had been program.

0

its utilization have been changed many times the airplane and during this period of years. The structure of

the C-130B/E wing fatigue test was stopped after 43,000 simulated flight block loading, some fleet aircraft were approaching a life not protected by this test. of Since hours

0



C-130 WING FATIGUE TEST PROGRAMS

wing cracks, and subsequent investigations after 18,500 simulated flight hours. The C-130B wing fatigue test was stopped resulted in reducing the ground loads spectrum. changes resulted from Several design

0

C-130E wing fatigue test was stopped after 23,000 simulated flight hours on the Design improvements 30,000 flight hours on the outer wing. resulted from the wing cracks which occurred. wing and center

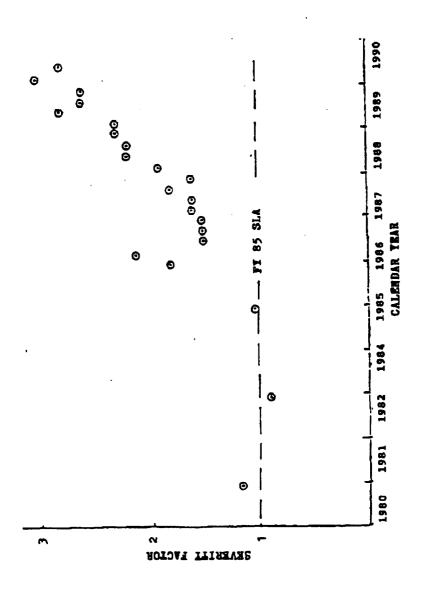
C-130B/E wing fatigue test was stopped after 43,000 simulated flight hours on outer wing have occurred the of significant redesigns Two subsequent to this test. center wing.

C-130H wing test has accumulated over 70,000 simulated flight hours on the Testing continues center wing and over 50,000 flight hours on the outer wing.

0

0

Increased Usage Severity



INCREASED USAGE SEVERITY

- C-130 usage has increased dramatically. Data points shown are from C-130E MAC AFTO forms. In recent years the severity of USAF 0
- altitude time, higher gross weights, more refueling time for tanker aircraft, more maneuvers, more severe maneuvers, etc. low These changes include increased

0

- These severe usages vary greatly between individual aircraft. 0
- present test was derived from C-130E MAC usage reported data for 1985 and part of 1986. the The spectrum being used for

A Changed Airplane

- Gross Weight Has Increased From 124,200 Lb. To 155,000 Lb.
- Utilization Of The Airplane Is Radically Different
- ► Gunships
- ► Low Altitude Time
- ▶ Maneuvers
- ► Aerial Refueling
- Structural Changes
- ► Three Major Center Wing Revisions
 - ► Five Major Outer Wing Revisions

A CHANGED AIRPLANE

the present military models the gross weight of the airplane has increased from 124,200 pounds to 155,000 pounds. to C-130s In changing from the original

0

0

modern military C-130s are used as gunships, helicopter tankers, and spend much this airplane has also witnessed radical changes in utilization. longer periods of time at low altitude and in severe maneuver environments. evolution of

changes, the wing structure was being above the through airplanes went changed in response: the As

- Three major center wing design revisions

Five major outer wing design revisions.

Durability Test Spectrum

Four Blocks Of 20,000 Flight Hours Each

Each Block Consists Of:

▶ 7351 Flights Applied in a Flight-By-Flight Sequence

▶ 1351 Missions

12,095 Touch-and-Go ➤ 26,968 Total Landings

14,873 Full Stop

9,066 Fuselage Pressure Cycles ► 600,234 Wing Cycles

DURABILITY TEST SPECTRUM

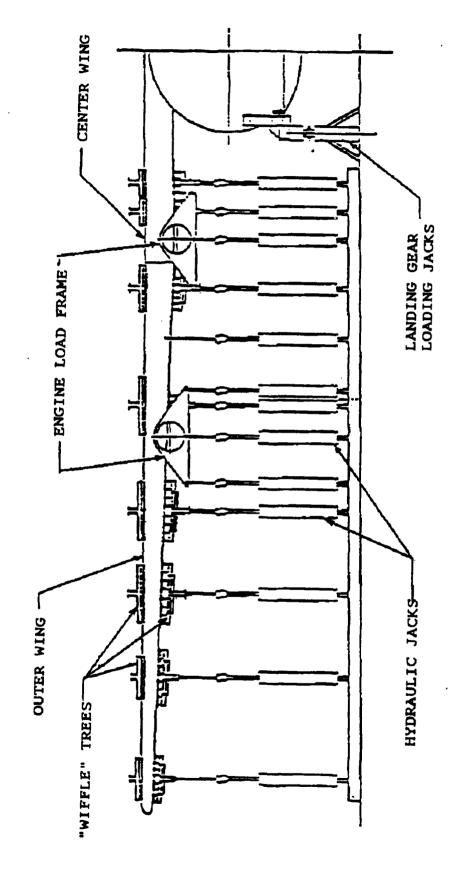
The test spectrum is derived as a block of 20,000 simulated flight hours. 0

The goal of the test is to apply this spectrum block four times. 0

Each block is composed of 7351 flights representing 13 different missions. O

those higher magnitude loads which occur less frequently than once per flight, are The ordering of flights is randomly selected, and the peak growth cycles, that is, randomly distributed between these flights.

Test Description



TEST DESCRIPTION

- Two wings are symmetrically loaded with shear, bending and torsion controlled. 0
- Cabin pressure is simulated Wing loads are reacted with a center fuselage section. in this fuselage section. 0
- each wing are applied through cradles at eight locations, through dummy engines at two locations, and at the external fuel tank supports. Loads to
- Loads are applied by servo-controlled hydraulic actuators. 0
- A fifty-one channel closed loop servo system controls these actuators. 0

Present Status

- Approximately 50,000 Flight Hours Have Been Simulated By Test
- Several Significant Cracks Have Been Detected
- Repairs Suitable For Service Use Have Been Provided For **Each Crack**
- These Repairs Have Been Proved By Subsequent Loading
- ▶ Inspections Have Been Provided As Necessary, Including **Development Of NDI Techniques**
- Detail Design Improvements Are Incorporated On Late Configurations
- A Proposed Follow-On Program Is Being Negotiated

PRESENT STATUS

continues on the test as we alternately apply flights, inspect, repair and Progress analyze. 0

o Each crack results in development work:

A suitable repair is designed.

This repair is installed on the test article with design changes made as necessary. Subsequent loading proves the design.

on service Technical Orders are issued as subject crack the safe and repairable length. detect required for inspection of service aircraft. NDI techniques are developed to aircraft at a

Production design changes are made as necessary to eliminate these problems from future airplanes. ı

A proposed follow-on program being negotiated could include: 0

Residual strength tests

Reserve operating capability tests

Teardown inspections

- Correlation analyses.

Repair Of Cracks

Existing Air Force Technical Orders (19%) ★ First Choice:

☆ Second Choice: New Repair Emphasizing Use Of Composites (9%)

New Repair Using Metallic Materials (72%) * Third Choice:

REPAIR OF CRACKS

Structural cracks are repaired by one of three methods.

Repaired according to one of the standard repairs presented in the C-130 Structural Repair Manual (T.O. 1C-130A-3). allows for test evaluation of the T.O. repair.) First Choice:

0

the use of composite Not only is the repair designed, developed and tested, but necessary NDI techniques are also developed. A new repair is designed emphasizing materials. Second Choice:

If this appears to have general application, it may be included repair is designed using metallic materials. in the Structural Repair Manual. A new repair Third Choice:

0

Composite Repairs

 Boron and Metal Combination Repair Center Wing Front Beam Lower Cap

Center Wing Lower Surface At The Fuselage Interface ► Graphite / Epoxy Repairs

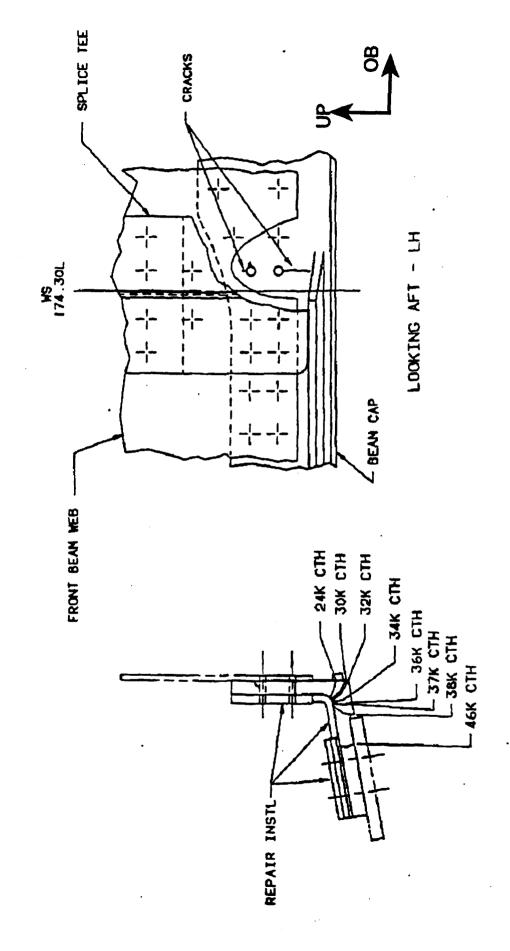
/ Prevent Mod: Center Wing Lower Surface At The Fuselage Interface

Boron / Epoxy Straps Added To Wing Stringers

COMPOSITE REPAIRS

be discussed for each of the following repairs. Much knowlege and The logic used in the material The NDI evaluation of the finished repairs has been an area of particular interest. NDI Various types of composite materials, sometimes in combination with metallic materials, has been gained in handling, fabricating and bonding these composite repairs. is also used to detect any continuing crack propagation. have been used in making test specimen repairs. will experience selections

Caposite Repair: Center Wing Front Beam Lower Cap



COMPOSITE REPAIR: CENTER WING FRONT BEAM LOWER CAP

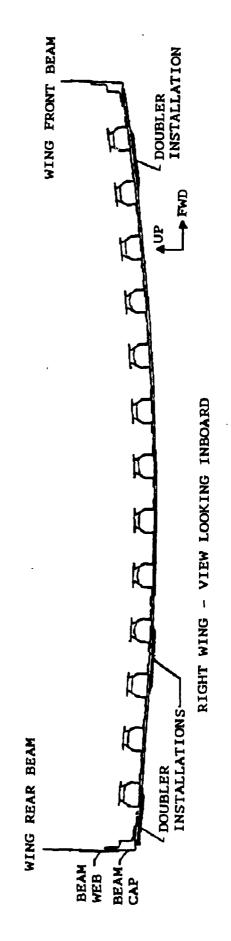
the vertical leg of the L/H lower spar cap at 24,000 in detected Were cyclic test hours. Two cracks 0

and a fastened and bonded a bonded boron/epoxy angle Cycling was resumed. made using aluminum strap. A repair was

the two cracks in the spar cap continued to grow down and aft under added and cycling was angle. At 46,000 CTH the crack was detected aft of the boron/epoxy fastened and bonded aluminum strap was Another boron/epoxy larger of resumed. angle.

0

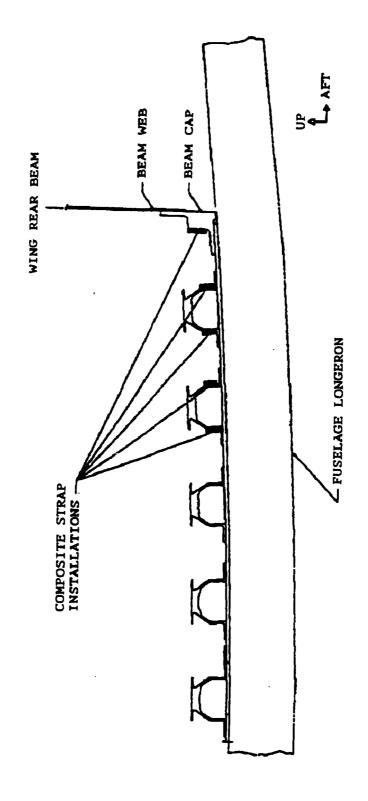
Composite Repairs: Center Wing Lower Surface



COMPOSITE REPAIRS: CENTER WING LOWER SURFACE

- detected at three locations on the center wing lower surface common to the fuselage intersection. Cracks were 0
- Graphite/epoxy patches were bonded to the wing panels at each of these locations. 0
- No further crack growth has been detected at any of these locations. 0

Composite Prevent: Center Wing Lower Surface



LEFT WING - VIEW LOCKING INBOARD

COMPOSITE PREVENT: CENTER WING LOWER SURFACE

- service aircraft in the wing lower surface at the intersection of the rear beam lower cap and the fuselage longeron. been detected on Cracks had 0
- this detected on the right side of the airplane at this location; "prevent" was added to the left side. Was crack 0
- Boron/epoxy straps were added to the test article at 26,000 cyclic test hours to reduce the local stress level and thus extend the useful life. 0
- Strains were significantly reduced and the area has remained crack free. 0

Inspections

- Inspections To Determine If Additional Inspections Each Crack Is Evaluated Against Existing Fleet **Are Required**
- NDI Techniques Are Developed As Required
- Safety Inspections Or Other Special Inspections Are Directed As Required

INSPECTIONS

the cracks detected on the test wing should be detected on service TCTOs issued by the ALC in response to the Individual Aircraft Tracking Program, a few cracks have been detected which are to be added to the IATP. While most of aircraft by

0

crack is evaluated to determine the appropriate methods of NDI for service use in detecting cracks at this locations. Each

crack location, calculated or measured crack growth, critical crack length, and inspections or other special inspections. Occasionally a few fleet airplanes are and anticipated airplane usage are considered in evaluating the need for safety inspected to determine if we have a test peculiar crack.

0

Future Program Planning

■ Residual Strength Testing

Residual Operating Capability Testing

■ Teardown Inspection

■ Correlation Analysis

FUTURE PROGRAM PLANNING

The following are being considered as program options after the completion of durability testing:

- loading to limit design load with the existing damage in the wing caused by the durability testing. testing strength Residual 0
- Residual operating capability testing applying normal operational flights as major structural members are progressively severed. 0
- the purpose of locating for disassembly limited ಹ ŧ Teardown inspection undetected cracks. 0
- Correlation analysis profiles of other usages of the C-130 will be evaluated against the test loading and the test cracking history. 0

Residual Strength Testing

Purposes:

Demonstrate Limit Load Capability of the Wing Structure With Large Cracks

Predicting Failure in Structure With Large Cracks Demonstrate The Analytical Techniques for

Program:

Apply Two Cycles of Fifty Percent of Limit Load While Conducting Strain Surveys

Apply Limit Load

RESIDUAL STRENGTH TESTING

demonstrate To Purposes:

that the wing, as it exists with large cracks and many hours of simulated usage, is capable of sustaining limit design load. To demonstrate that the analytical techniques which will be employed in structural management programs adequately predict the behavior of large cracks when subjected to a limit design load application. C-130

Program:

Remove repairs from selected existing cracks.

Install strain gages around the larger cracks.

Read the strain gages while applying two cycles of 50% of limit design load.

Apply limit design load.

Residual Operating Capability Tests

Purpose:

To Determine The Remaining Static Capability

Of Structure With Major Damage

Program:

Primary Structural Members Are Cut ROC I:

Simulated Flights Are Applied

Once Per Hundred Flight Load Is Applied

ROC II: Additional Structural Damage Injected

Simulated Flights Are Applied

One Cycle of 75% of Limit Load is Applied

RESIDUAL OPERATING CAPABILITY TESTS

Once the residual strength of the test wing has been demonstrated, the capability of the a limited period of time after sustaining for major structural damage will be demonstrated. operations airplane to continue normal

Three or four typical operational flights will be applied with the once per one-hundred flight load will be structural members will be completely severed by sawcut at critical being monitored for damage progression. If disabling damage is the after these flights, locations. structure Selected apparent applied. ROC I:

Several structural members will be completely severed by sawcut at critical one cycle of previous sawcut locations. β simulated followed ferry flights will be seventy-five percent of limit design load. the ţ٥ adjacent possibly O. operational Additional locations, ROC II:

Teardown Inspection

Purpose:

To Locate Any Cracks Undetected By The Various Inspection Methods Being Used

Program:

Inspect Using Laboratory Inspection Methods Select Critical Areas And Typical Areas Disassemble As Necessary

TEARDOWN INSPECTION

inspected by a number of techniques: visual, presently being x-ray, eddy current, ultrasonic, etc. wing is test The 0

o A more thorough inspection is to be conducted:

for teardown will be selected based on specific criteria, possibly areas, possibly because they are typical areas, critical are because they Areas

These selected areas will be disassembled to the extend necessary to perform the desired inspections.

ı

etching, and other Bolt hole eddy current, magnification aided visual, inspection techniques will be used to detect cracks. ı

Correlation Analysis

■ Compare Local Loadings To Desired Loadings At Significant Cracks

■ Calculate Test Demonstrated Life For Other C-130 Utilizations

CORRELATION ANALYSIS

There are always questions loads being too large, too small, locally introduced, out of phase, too few or too many; therefore, any known deviations of the test loads, whether by design or by spectra loading differs from analytical spectra. accident, will be compared with the analytical loads. Test

0

The spectrum of loads used for this test represented one particular usage of the C-130 - USAF Military Airlift Command, 1985-1986. Various other USAF utilizations airplane will be compared to the test results on both a fatigue analysis and a fracture analysis basis. of the

0

Conclusions

The Test Has Successfully Demonstrated An Adequate Life For The C-130 Wing

Very Severely Utilized Wings Are Scheduled For **Center Wing Replacement**

Composite Repairs Were Successfully Used

/ NDI Procedures Were Developed As Required

CONCLUSIONS

- present production C-130 wing has been demonstrated to have an adequate service life free of disabling cracks when used with the USAF MAC profiles. 0
- the more severe usages being experienced by some USAF aircraft will result life. A modified center wing in the form of retrofit kit is presently being produced to upgrade these aircraft. service shorter considerably of

0

- composite repairs were successfully installed on the test article. Techniques and procedures for installing and inspecting these repairs were developed. 0
- of the cracks that were detected required the development of NDI procedures for fleet monitoring of aircraft. Several

0

USING APPROXIMATE METHODS FOR COMPLEX DAMAGE TOLERANCE PROBLEMS

BY ARNOLD NATHAN TASHAN ENGINEERING CENTER ISRAEL AIRCRAFT INDUSTRIES LTD

PRESENTED TO THE 1991 USAF STRUCTURAL INTEGRITY PROGRAM CONFERENCE

SAN ANTONIO, TEXAS
3 DECEMBER 1991



USING APPROXIMATE NETHODS FOR COMPLEX DAMAGE TOLERANCE PROBLEMS

Arnold Nathan: TASHAN Engineering Center, Israel Aircraft Industries

1.0 INTRODUCTION:

In a damage tolerance substantiation effort of either a military or commercial aircraft, many critical locations must be analyzed. An integral part of the analysis is the calculation of the stress intensity factor which depends upon the applied stress, the crack size and a "geometric" correction factor, commonly referred to as β :

$K_T = \sigma \sqrt{\pi a} B$

Numerous methods exist to help calculate the stress intensity correction factor. Handbook solutions are available for standard crack configurations. Simple methods such as compounding and superposition help easily and quickly obtain solutions when multiple geometric or loading influences exist. Nevertheless, most "real life" problems include complexities not easily found in the standard handbooks, nor easily solved with the aforementioned simplistic methods. Thus, time consuming mathematical approaches or finite element models are necessary.

It is specifically these "non standard" problems which are the subject of this paper. Time and monetary constraints may prohibit lengthy and complex solutions. Combining the five following ingredients, the stress intensity of complex problems may be calculated in a fraction of the time with minimal error:

- 1) standard handbook solutions
- 2) simplistic methods
 - (compounding, superposition, stress distribution, etc)
- 3) physical understanding of the standard B solutions
- 4) physical understanding of the load path
- 5) engineering judgment

In short, it is the purpose of this work to demonstrate the accuracy of certain shortcuts, approximations, and engineering judgments and thus give the analyst some useful tools to get quick and reasonable results for complex cases.

Section 2 begins with a simple example to demonstrate the general approach. Some basic assumptions and methodologies are verified to build a foundation for more complex problems. Once certain insights are developed, they may be applied to more complicated geometries. The "engineering judgment" solution is compared to known solutions or finite element results to determine the reliability of the approximation. Upon successful correlation between the approximate method and the finite element solution, a physical understanding of various influences is developed and confidence is built in applying appropriate assumptions. More complex crack configurations may be solved in an efficient and relatively accurate manner.

2.0 DEMONSTRATION OF THE ENGINEERING APPROXIMATIONS

2.1 Example 1: Crack by a notch

A relatively simple example of a crack by an elliptical notch (See Figure 2.1) will first be presented to demonstrate the general approach. A solution to this problem exists in Reference 1 and is compared to the approximate results:

Approximate Method:

- Step 1: Calculate the stress concentration, K_t, of a notch in a semi-infinite plate from Reference 2
- Step 2: Calculate β at the notch using the stress distribution method (See Footnote 1 below).
- Step 3: As the crack grows away from the notch, the local stress is decreasing. Reference 4 attempts to calculate the reduction in local stress across the cross section away from the notch. Thus for small cracks assume a diminishing stress distribution per Reference 4. Then calculate β per Footnote 1 below:

$$K_{I} = 1.12\sigma_{remote} K_{t} \alpha \sqrt{\pi a}$$
 (Equation 2.1)

thus
$$\beta = 1.12K_{+}\alpha$$
 (Equation 2.2)

(Note that the a calculated in Reference 4 is given as a factor C and includes a factor of 1.12 which we have already included in the above Equation 2.2)

See Figure 2.2 for a comparison of the approximate method results to the solution given in Reference 1 for a crack by a 0.5" radius notch.

Footnote 1

Stress Distribution Method to Calculate Stress Intensity (Taken from the USAF Damage Tolerance Design Handbook - Ref. 3)

Note: To be used for small cracks only

$$K_{I} = 1.12\sigma_{local}\sqrt{\pi a}$$

In the immediate vicinity of the stress concentration, $\boldsymbol{K}_{t}\colon$

$$K_{I} = 1.12\sigma_{remote} K_{t} \sqrt{\pi a}$$
 (thus $\beta = 1.12K_{t}$)

As the crack grows into area where $K_{\ensuremath{\mathbf{t}}}$ is diminishing:

$$K_{I} = 1.12\sigma_{\text{remote}} K_{t} \alpha \sqrt{\pi a}$$
 (thus $\beta = 1.12K_{t} \alpha$)

 α = Ratio by which K_{t} has thus far diminished

2.2 Example 2: Continuing Damage

Taking the engineering judgment one step further, the case of a broken ligament and a crack emanating from the other side of the nole, may be solved (See figure 2.3). This is an extremely common problem in any damage tolerance substantiation analysis, for which no simple solution is available. Assuming that there is also the influence of finite width, the problem may be approached as follows:

- Step 1: Return to the Reference 1 stress intensity solution for a crack by an elliptical notch. Assume a notch radius of curvature equal to the radius of the hole and a notch length equal to the broken ligament plus the diameter of the hole (See Figure 2.4)
- Step 2: Assume an edge crack finite width effect (Reference 5)
- Step 3: Compound (multiply) the notch and finite width β 's (Divide out a factor of 1.12 because this edge effect appeared both in steps 1 and 2)
- Step 4: For larger cracks, the crack no longer feels the hole and an edge crack solution with the crack sized equal to "d+D+a" will give reasonable results (See figure 2.5)

A numerical example is in order with a comparison between the approximate approach above and a PROBE "p-version" finite element solution. (See Figure 2.6 for the PROBE finite element model. See Reference 6 for explanation of PROBE "p-version" finite elements).

Broken ligament, d = 1.5" radius of hole, r = 0.5" crack length, a = 0.5"

Approximate Solution:

Notch length, b, = 1.5" +1" = 2.5"

Notch radius = 0.5"

From the ellipse geometry calculate:

$$c = \sqrt{b \times r} = 1.118$$
"

 β_{NOTCH} (per Reference 1) = 2.80

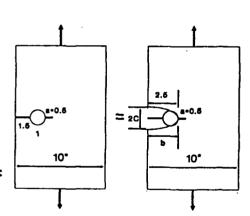
β Edge Crack Finite Width (Reference 5) = 1.78

$$K_{I} = \sigma \sqrt{\pi a \beta} = 1 \sqrt{(\pi.5)} (1.78 \times 2.80) / 1.12 = 5.57 \text{ KSI} \sqrt{\text{IN}}$$

Finite Element Solution:

KI = 5.30 KSI√IN

Difference of Results: = 5%



2.3 Example 3: Multi-Cracking from Single Fastener Hole

The question of Multi-site damage has been addressed by both the military and commercial damage tolerance requirements. With the recent emphasis on the problem of aging aircraft, multi-site damage has gained increased awareness. Nevertheless, the relatively simple problem of two different sized cracks emanating from a single hole (see figure 2.7), is far from trivial. Our standard handbook solutions include the case of 2 equal sized cracks growing from a hole, but do not offer a solution for our more general case.

An approximate approach is summarized for various cases in Table 2.1. Examples to justify the methodology for the various cases will follow in this section.

In Table 2.1 we first differentiate between the "lead crack" and the "opposite crack". The "lead crack" is the one for which we are calculating the stress intensity factor. The opposite crack is on the other side of the hole and has an influence on the stress field of the "lead crack".

Secondly, we differentiate between different crack sizes: (with "a" equal to crack size and "r" the radius of the hole)

- small crack 0.2 > a/r
- medium crack $0.2 \le a/r \le 1.0$
- large crack **a/r** > 1.0

The guiding principles used in the approximations of Table 2.1 are the following:

- 1) At a certain size, a crack by a hole is so large that the crack tip is out of the stress concentration influence of the hole, and does not know if there is a crack and a hole behind the crack tip or just one large crack.
- 2) An "opposite" crack which is very small will not influence the crack tip stress field of the lead crack.
- 3) A small or medium sized "lead" crack by a hole, is influenced by a significant sized crack at the other side of the hole. Nevertheless, the dominating two influences on this "lead" crack are the stress concentration caused by the radius of the hole and the fact that additional cross section is absent at the other side of the hole. Thus, if both of these effects can be amply accounted for, the stress intensity of the "lead" crack should be reasonable.

TABLE 2.1: Calculation of K $_{\mbox{\scriptsize I}}$ of Lead Crack with Opposing Crack at Hole

			
CATEGORY	SKETCH	LOGIC	JUSTIFICATION
Lead Crack: - large Opp. Crack: - small - medium - large	opposite lead opposite lead opposite lead	Lead crack does not feel the hole and may be treated as one long crack opposite lead	See example Section 2.3.1 which results in difference of about 3% between approx method and the more rigorous solution
Lead Crack: - small - medium Opp. Crack: - small	opposite lead	Lead crack does not feel the opposite side	See example Section 2.3.2 which results in negligible errors when ignoring the small opposite crack
Lead Crack: - small - medium Opp. Crack: - medium - large	opposite lead opposite lead opposite lead opposite lead	Lead crack feels the radius of the hole and also is effected by additional missing material at the other side of the hole due to the opposite crack. Use elliptical notch stress intensity factor with the final radius of curva- ture equal to the hole radius and: 2b = a + D **Opp** **Opp**	See example Section 2.3.3 which results in differences of 3-5% between approx method and the finite element solution

NOTE: Large crack a/r>1; Medium crack 0.2sa/rs1; Small crack a/r<.2

The following sections present examples to justify the methodology, assumptions and approximations presented in Table 2.1.

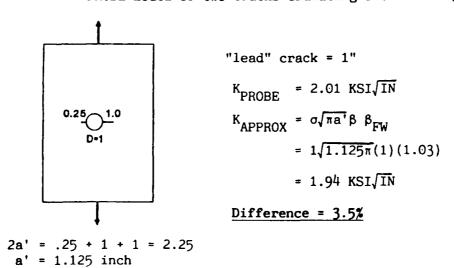
2.3.1 Category 1 (of Table 2.1) - Approximation Justification

"Large lead crack does not feel the hole and may be treated as one large crack the size of the hole and the two cracks" (See sketch by category 1 of Table 2.1)

Example 1: Verify assumption by comparing to known solution, i.e., 2 equal sized cracks emanating from a hole in an infinite plate

Difference = 3%

Example 2: Verify assumption by comparing to PROBE "P-version" finite element solution (See Figure 2.8 for typical PROBE model of two cracks emanating from a hole)



2.3.2 Category 2 (of Table 2.1) - Approximation Justification

"Lead crack does not feel opposite crack when the opposite crack is small"

Example: Verify the assumption by comparing 2 known solutions which will clearly demonstrate that if the opposite crack is small it doesn't effect the lead crack.

Compare the case of 2 small cracks emanating from a hole to the case of 1 small crack by a hole, and note the effect of the opposite crack on the lead crack.

Difference = 1%

2.3.3 Category 3 (of Table 2.1) - Approximation Justification

"A crack by a hole with a significant sized "opposite" crack may be approximated by a crack by an elliptical notch of length equal to the opposite crack and the hole with the end radius of the notch equal to the radius of the hole" (See sketch Category 3 of Table 2.1)

Example 1: Verify the assumption by comparing to a PROBE "p-version" finite element solution

opposite crack = 0.3"

opposite crack = 0.5"

"PROBE" Solution
$$K_I = 1.85 \text{ KSI}\sqrt{IN}$$

Approximate Method:

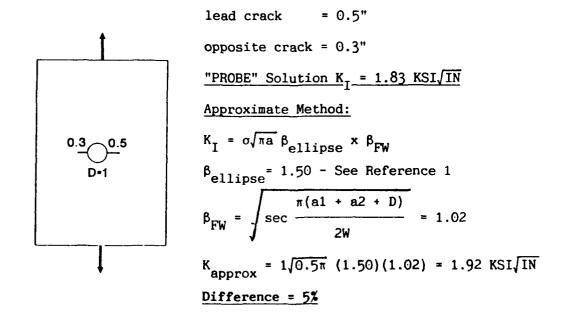
$$K_I = \sigma \sqrt{\pi a} \beta_{ellipse} \times \beta_{FW}$$

$$\beta_{ellipse} = 1.82 - \text{See Reference 1}$$

$$\beta_{FW} = \sqrt{\sec \frac{\pi (a1 + a2 + D)}{2W}} = 1.02$$

$$K_{approx} = 1\sqrt{0.3\pi} (1.82)(1.02) = 1.80 \text{ KSI}\sqrt{IN}$$
Difference = 2.5%

Example 2: Verify the assumption by comparing to same PROBE "p-version" finite element solution - but looking at the other crack



2.4 Example 4: Lug

In this section, the case of a lug will be studied (see sketch Figure 2.9a). One critical location is the lug hole. The stress intensity of the lug hole has been studied extensively in the literature and will not be addressed in this work. Another location which is also prone to fatigue cracking is the radius which is sometimes placed near the base of the lug. It is this area which will be addressed in this paper.

The radius near the base of the lug is characterized by a significant stress concentration and a complex non-linear cross sectional stress distribution. A PROBE "p-version" finite element model was built (Figure 2.9b) and the stress distribution calculated across Section A-A (Figure 2.10).

Approximate methods will be used to calculate the stress intensity near the base of the lug, and will be compared to the values calculated with a "cracked" PROBE finite element model(Figure 2.11).

2.4.1 Small Cracks

For small cracks, the local stress distribution approximation will be used (See footnote 1 - Section 2.1 of this paper):

$$K_{\rm I} = 1.12\sigma_{\rm local}\sqrt{\pi a}$$

where σ_{local} is calculated by the uncracked PROBE model(Figure 2.9b)

A comparison of the approximate method and the PROBE finite element solution is presented in the table below:

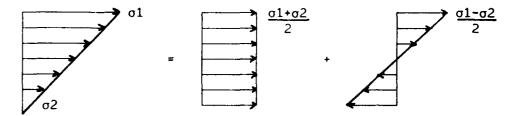
Table 2.2: Lug Radius - Comparison Approximate and PROBE Solutions for Small Crack Sizes

Crack Size (inch)	β from PROBE	1.12 × olocal	% Difference
0.08	2.40	2.28	5%
0.10	2.28	2.16	5%
0.20	2.18	2.04	6%

2.4.2 Intermediate Sized Cracks

Let's look again at the lug cross sectional stress distribution presented in Figure 2.10. For small cracks we were able to use the stress distribution method of Reference 3, but this approach is limited to small cracks only. For intermediate size cracks, a linear stress distribution will be assumed which "more or less" follows the stress distribution curve in the intermediate crack size ranges (Fig 2.12). We may have a tendency to make this linear stress distribution slightly above the true stress distribution in the area of interest to compensate for the missing high stresses at the notch radius. It is reemphasized that this linear stress approximation may only be valid for a range of crack sizes which are in the area characterized by the linear stress approximation (See Figure 2.13).

With the linear stress distribution already defined, a stress intensity calculation is straightforward. The linear stress distribution may be separated into pure tension and bending components:



The stress intensity solution for an edge crack in tension or bending is given in all stress intensity handbooks. The principle of superposition may be used to combine the stress intensity factors of the two different loading cases.

Summary of the approximate approach for the intermediate crack sizes:

- STEP 1: Draw a linear stress distribution which approximates the true non-linear stress distribution for the crack length in question. (See footnote 2 below)
- STEP 2: Separate the linear stress distribution into tension and bending components
- STEP 3: Calculate K_{T} for each tension and bending component
- STEP 4: Superimpose the 2 stress intensity factors

This approximate method was used and compared to a PROBE finite element model which included a crack (Figure 2.11). The results of the comparison are presented as Figure 2.14. A 3-6% stress intensity solution difference is calculated for crack sizes ranging from 0.4"-0.75".

Footnote 2: This approach will not result in a reasonable answer if the linear approximation only characterizes a very small portion of the true stress distribution curve and totally misses the vast majority of the curve prior to the crack size in question.

3.0 CONCLUSION

It was the purpose of this paper to demonstrate how engineering insight and judgment may be used along with basic damage tolerance tools to attack the "non-standard" crack configurations. All assumptions were compared to more accurate solutions to develop a feeling for the validity of the approximate approach. The cases of continuing damage, multiple cracking and complex stress distributions were all solved in a relatively quick and simplistic manner using no more than standard handbook solutions along with superposition, compounding and the stress distribution method. Even with the most gross approximations, the error in β remained well under 10% if reasonable judgment was applied.

Reference 7 is recommended as a useful source to help develop the physical understanding and insights needed to find approximate fracture mechanics solutions.

4.0 REFERENCES

- 1. Tada, H.; Paris, P.; and Irwin, G., <u>The Stress Analysis of Cracks</u> Handbook, Second Edition, Paris Productions Inc., 1985.
- 2. Peterson, R., <u>Stress Concentration Factors</u>, John Wiley and Sons, 1974.
- 3. Gallagher, J.P.,; Giessler, F.J.; and Berens, A. P., "USAF Damage Tolerance Design Handbook", AFWAL-TR-82-3073, 1984.
- Schijve, J., "The Stress Intensity Factor of Small Cracks at Notches", Delft University Report No. LR-330, also ICAF Doc. No. 1246, 1981.
- 5. Rooke, D.P. and Cartwright, D. J., <u>Compendium of Stress Intensity Factors</u>, Her Majesty's Stationary Office, 1976.
- 6. PROBE Finite Element Computer Program, NOETIC Technologies Corporation, 1985.
- 7. Broek, D., The Practical Use of Fracture Mechanics, Kluwer Academic Publishers, 1988.

FIGURE 2.1 CRACK BY NOTCH

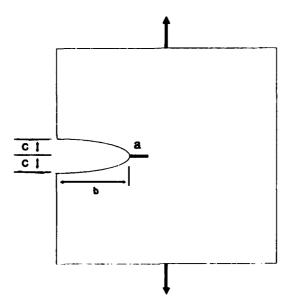


FIGURE 2.2: CRACK BY A NOTCH APPROXIMATE VS. KNOWN B SOLUTION

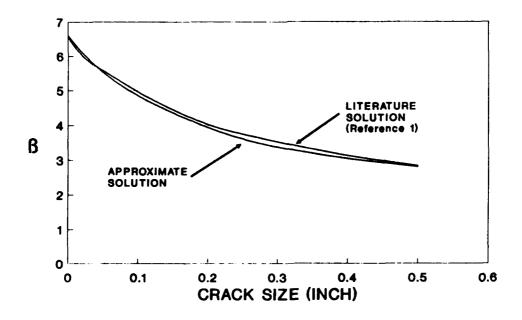


FIGURE 2.3: CONTINUING DAMAGE BROKEN LIGAMENT AND CRACK FROM OTHER SIDE OF HOLE

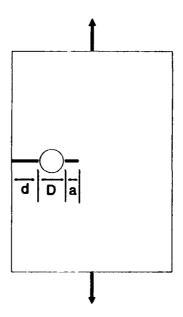


FIGURE 2.4: NOTCH ASSUMPTION FOR BROKEN LIGAMENT CASE

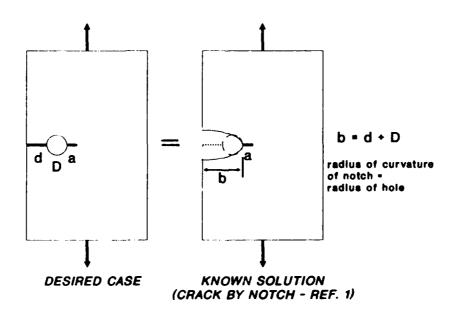


FIGURE 2.5: BROKEN LIGAMENT - LARGE CRACK EDGE CRACK APPROXIMATION

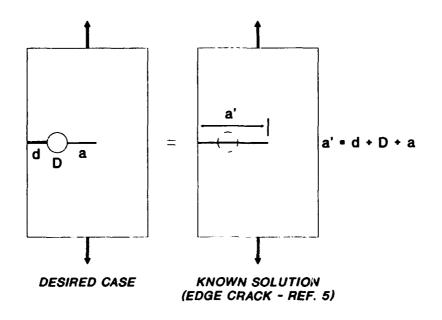


FIGURE 2.6: PROBE CONTINUING DAMAGE FINITE ELEMENT MODEL (1/2 model due to symmetry - not to scale)

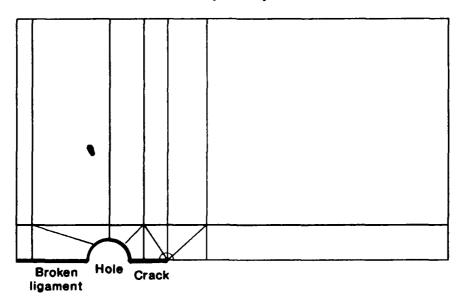
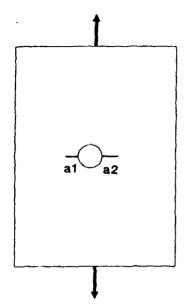


FIGURE 2.7: MULTI-CRACKING FROM SINGLE HOLE



LEAD CRACK - CRACK OF INTEREST

OPPOSITE CRACK - CRACK EMANATING
FROM OTHER SIDE

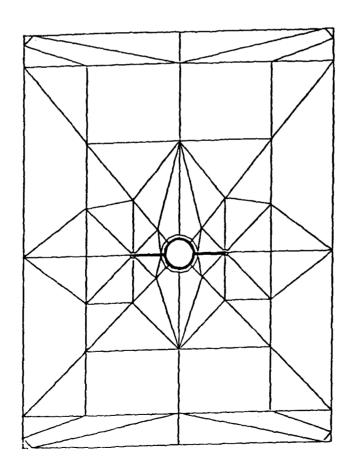
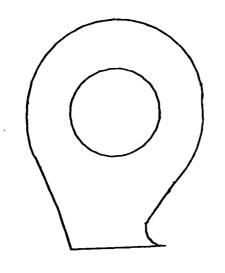
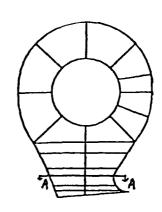


FIGURE 2.8: TYPICAL PROBE MODEL WITH TWO CRACKS FROM A HOLE



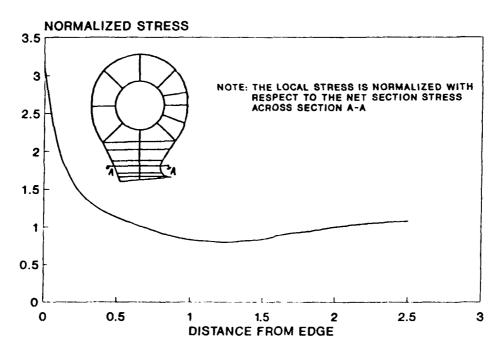


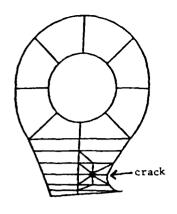
a) Sketch of Lug

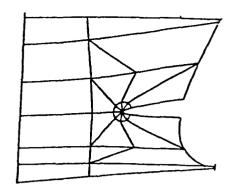
b) PROBE Finite Element Model of Lug

FIGURE 2.9: LUG EXAMPLE

FIGURE 2.10: LUG EXAMPLE LOCAL STRESS DISTRIBUTION - SECTION A-A







Blow up of Cracked Area Including Scaled Displacements

FIGURE 2.11: "CRACKED" PROBE MODEL OF LUG

FIGURE 2.12: LUG EXAMPLE LINEAR APPROX OF STRESS DISTRIBUTION

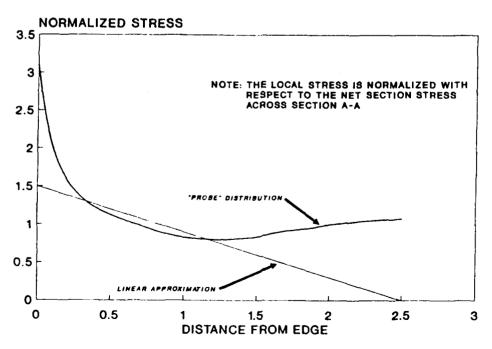


FIGURE 2.13: LUG EXAMPLE APPLICABILITY OF LINEAR APPROXIMATION

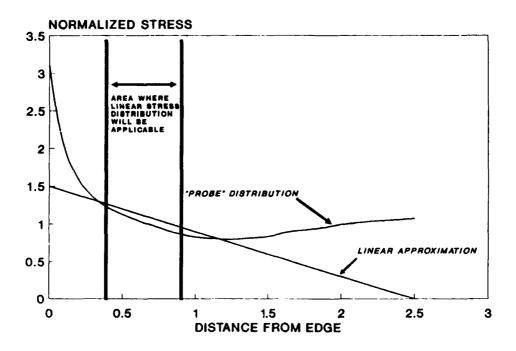
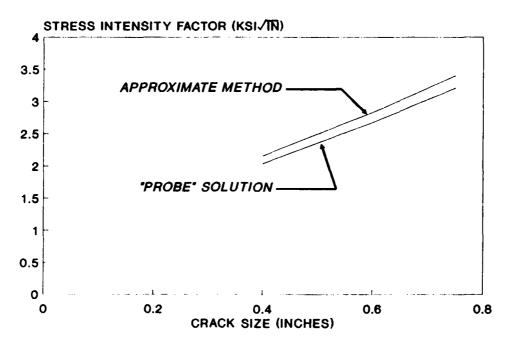


FIGURE 2.14: COMPARISON OF K FOR LUG
INTERMEDIATE CRACK SIZE



1991 USAF Structural Integrity Program Conference, 3 December 1991, San Antonio TX

Damage Tolerance on Swedish Fighter Aircraft

Pavel Sindelar
FFA - The Aeronautical Research Institute of Sweden,
S- 161 11 BROMMA, Sweden

and

Mats-Olof Olsson FMV - Defence Materiel Administration 115 88 Stockholm, Sweden

OUTLINE

Background

Damage Tolerance Assessment of the Viggen Fighter

Part I 1980-83

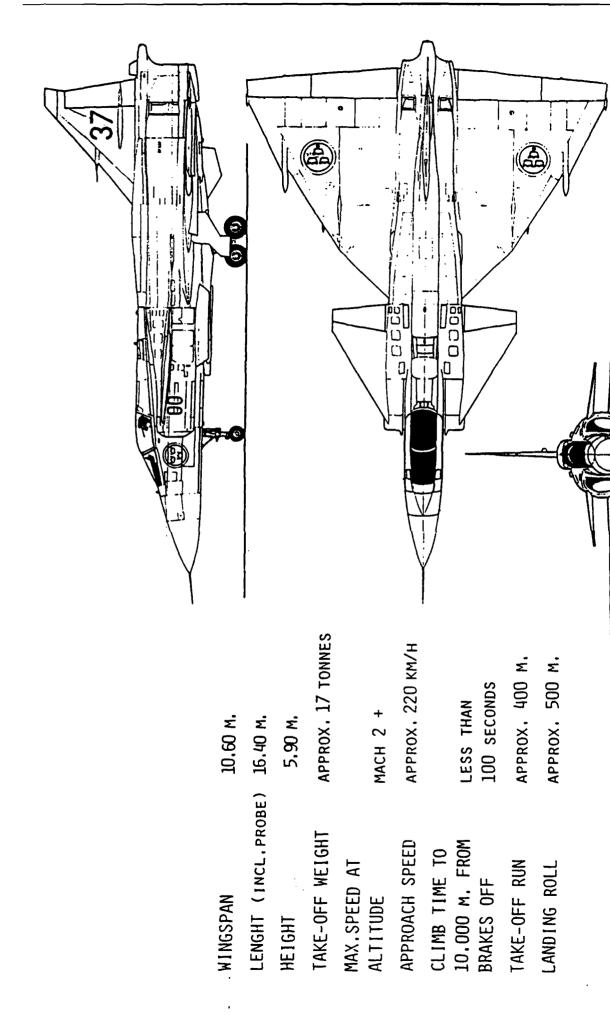
Part II 1986-89

Service Life Extension

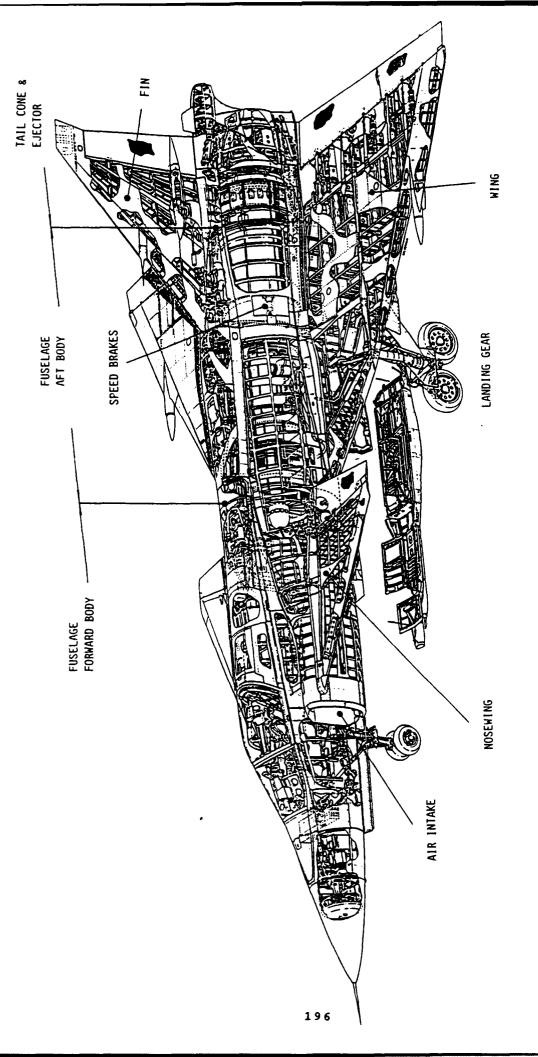
1990 -

Background

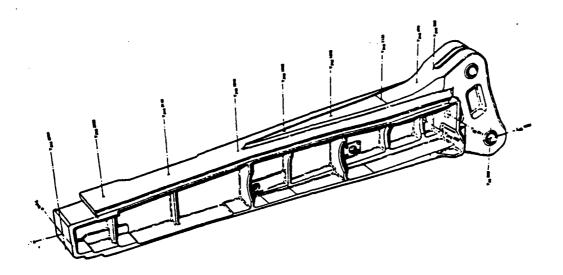
- Viggen crashes 1975-76
- 3-aircraft have been lost within a period of several months after ca 250-300 FLH
- Wing failure due to fracture of the mian spar in the root area
- Early fatigue crack initiation at a complex stress concentration in the lower spar flange



JA 37 AIRCRAFT THREE-VIEW DIAGRAM

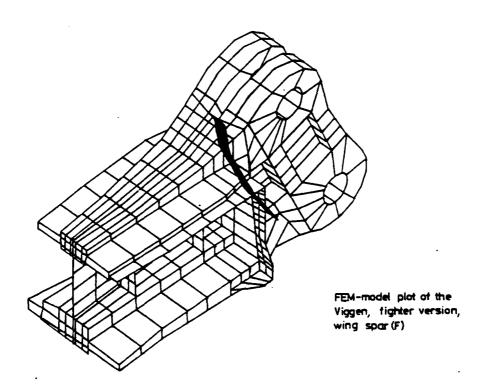


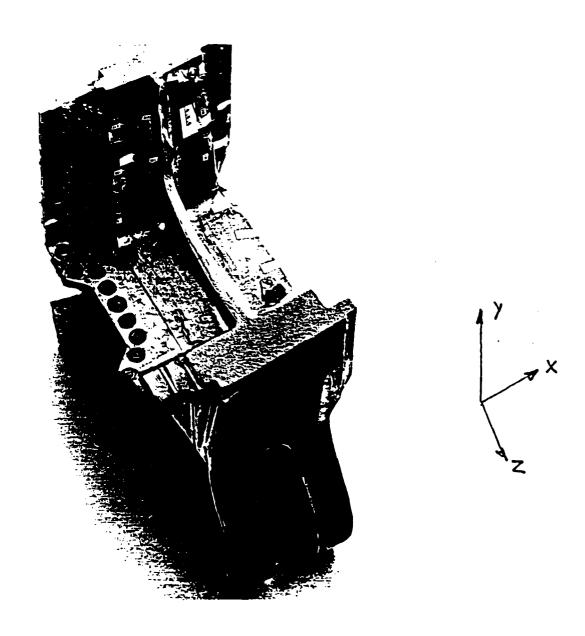
JA 37 STRUCTURAL ARRANGEMENT



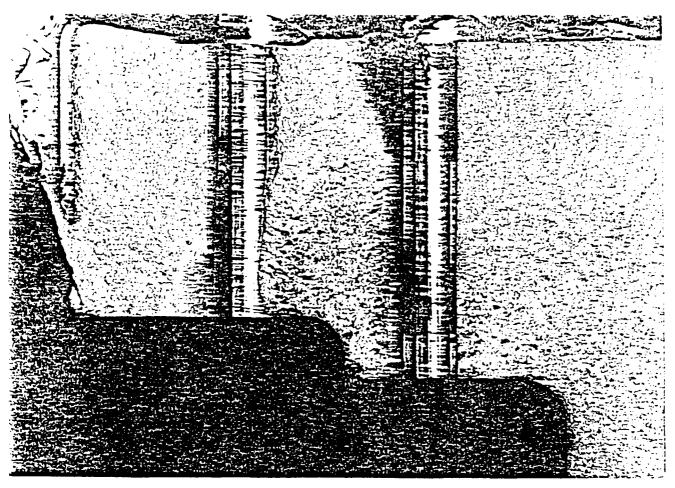
The wing spar (F) of the fighter version of Viggen

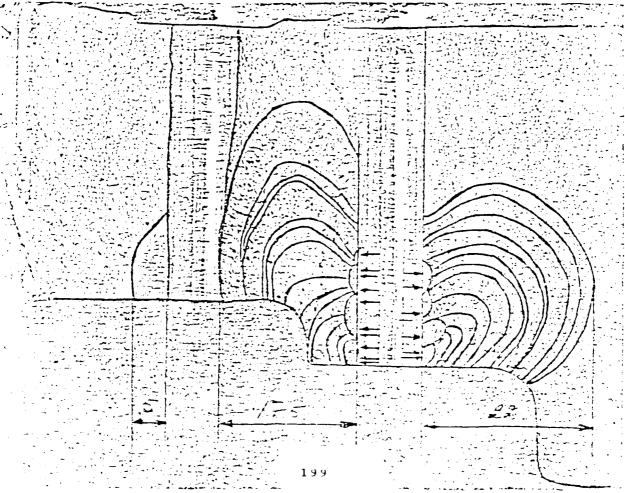
JAJT. HUNUDBALK V. VINGE VOIL 17 9





Viggen - Fatigue Fracture of the main spar of the wing





Viggen - Fatigue crack initiation and propagation in the main wing spar-

Cause:

The fatigue tests carried out earlier were locally not representative for production aircraft

Actions:

- cold working of the holes
- geometry modifications

Learned Lesson:

The successive changes of the structure in the last stage of development should be carefully evaluated with respect to the performed fatigue test representativeness

Damage Tolerance Assessment of the Viggen Fighter

A cooperative project of FFA and SAAB-SCANIA-Aerospace Division under the direction of FMV

Part I 1980 - 1983

Overall Objective

Adopting the USAF philosophy in achieving the structural safety, the Damage Tolerance Requirements MIL-A-83444 are thoroughly applied with the objective to gain an adequate experience in the proposed methodology with respect to the needs of a prospective methodology utilization in the development of future Swedish military aircraft.

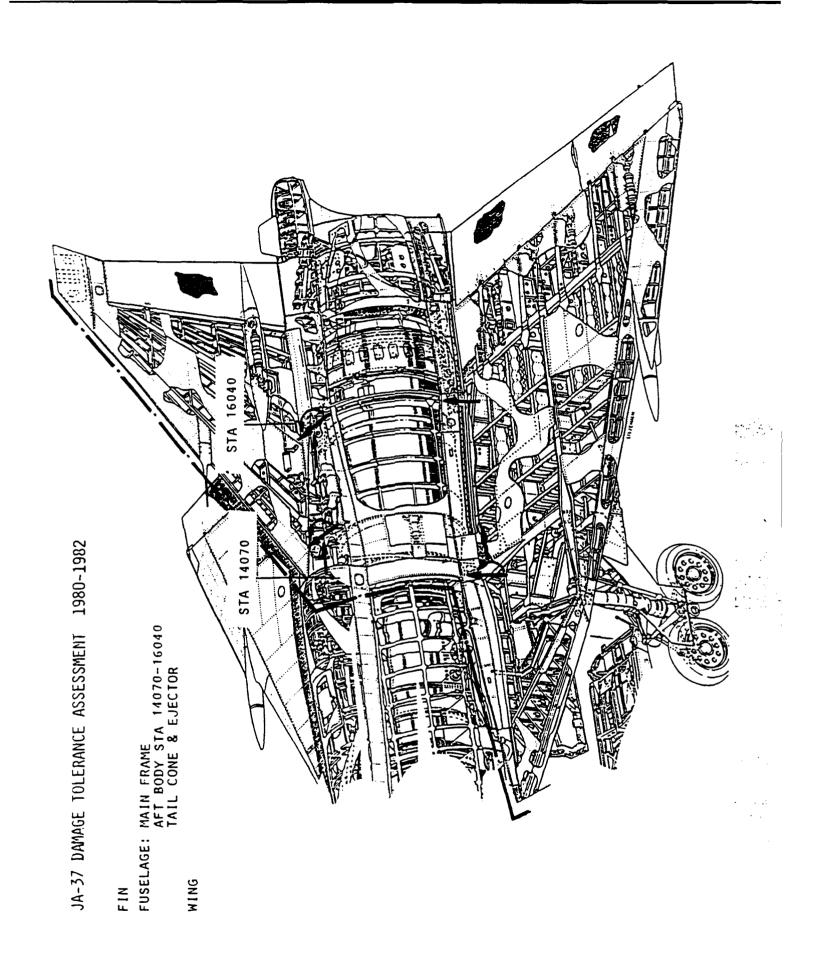
PHASES OF THE APPLIED WORK METHODOLOGY

1:ST REVISION OF AVAILABLE DATA

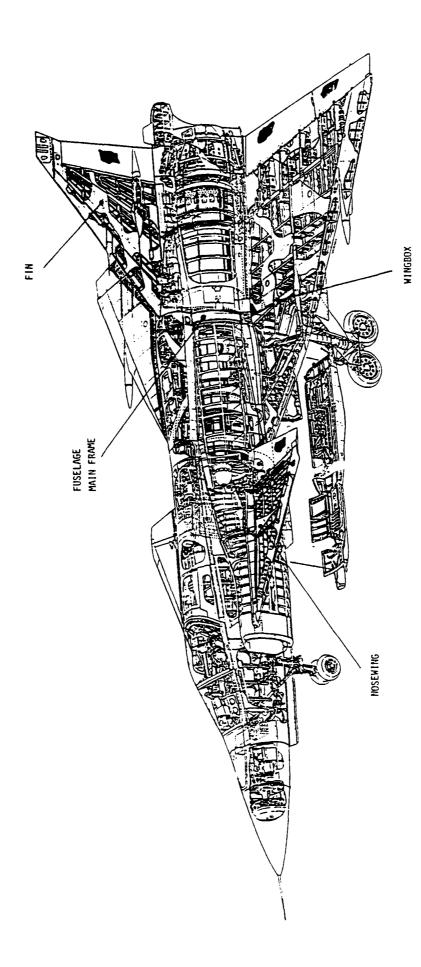
- STUDY OF STRUCTURAL DESIGN
- LOADING SPECTRA DEVELOPMENT
- METHOD AND RESULTS OF DESIGN ANALYSIS 1.E. STATIC STRENGTH, FATIGUE
- RESULTS OF DESIGN VERIFICATION TESTS
- DATA COMPLETION

2:ND DAMAGE TOLERANCE ASSESSMENT

- IDENTIFICATION OF SAFETY OF FLIGHT STRUCTURES
- CLASSIFICATION OF STRUCTURE
- 1) SLOW CRACK GROWTH STR.
- 11) MULTIPLE LOAD PATH-FAIL SAFE STR.
- III) CRACK ARREST FAIL SAFE STR.
- DEFINITION OF CRITICAL AREAS
- DETAIL STRESS ANALYSIS
- LOCAL STRESS SPECTRA DEVELOPMENT
- CRACK GROWTH ANALYSIS
- DAMAGE TOLERANCE VERIFICATION TESTS
- INSPECTION PROCEDURES
- MAINTENANCE PROGRAM
- MODIFICATIONS

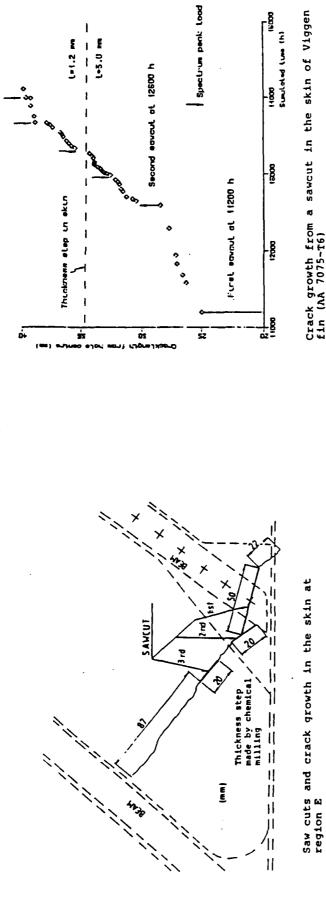


JA-37 TAIL COME & EJECTOR CLASSIFICATION OF SUSSEMUCTURES COUCE CANCE CAROLIN STR.
CAUCE ADPEST
FAIL SWE STR. JA-37 FIRE THE MOST CRETICAL ANEAS PANEL STOR CRACE GROWIN STR. PRINTERS. JA-37 CLASSIFICATION OF SUBSTRUCTURES FIN ATTACHEMENT JA-57 FUSELAGE AFT BOOK B-STATION 14878-15818 CLASSIFICATION OF SUBSTAUCTURES DET-SHE WASTER THROUGH THAT IS --- SLOW CRACE GROWIN STR mily a mily in the later of the control of the cont A11 114

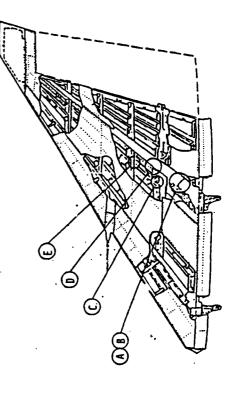


JA-37 FULL SCALE FAIIGUE/DAMAGE TOLERANCE TEST PROGRAM

Viggen - Full scale Damage Tolerance test on the FIN

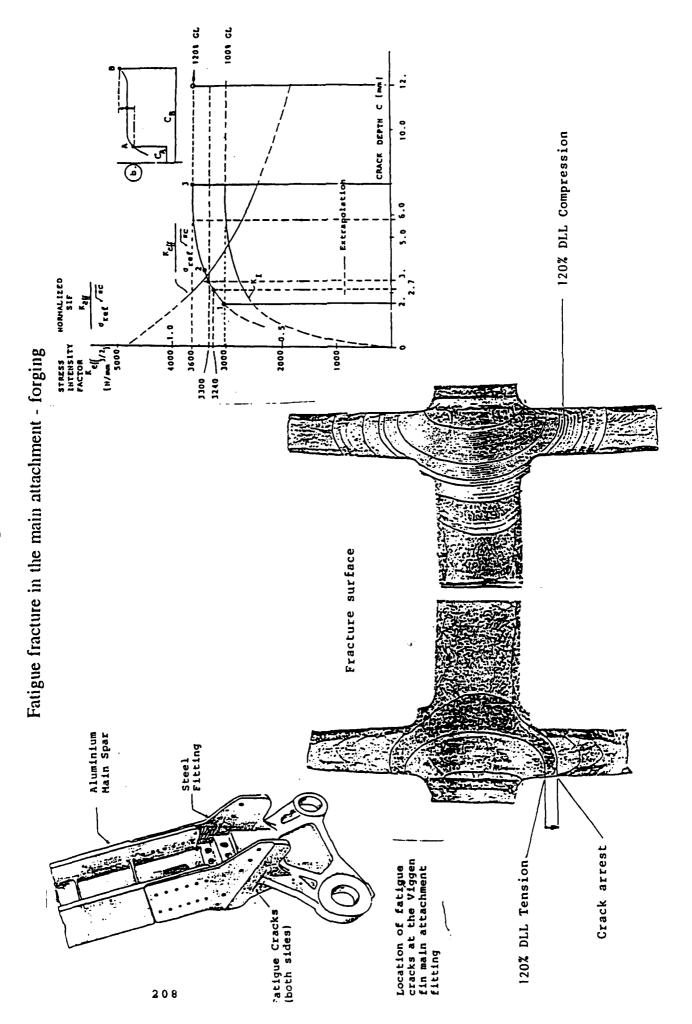


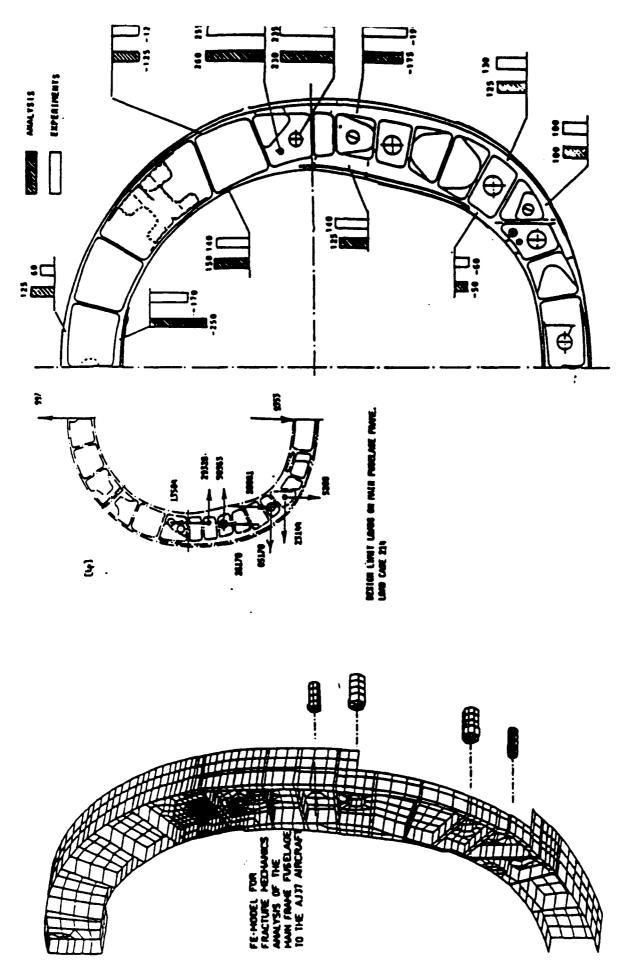
Crack growth from a sawcut in the skin of Viggen fin (AA 7075-T6)



Fin design and location of cracks

- Full scale Damage Tolerance test on the FIN Viggen





Calculated and measured stresses in main fuselage frame for load case 214

Major results

- Slow crack growth in the main attachment of the fin has been verified
- Fail safe -crack arrest capabilities have been demonstrated in the most critical area of the Fin-box
- Relatively high stress levels have been found in the main wing attachment frame
- The Damage Tolerance Philosophy has been officially adopted by the Swedish Airforce to be applied in development of the future Swedish military aircraft

STATIC 92 - 95 JAS 39 GRIPEN: STRUCTURAL TEST PROGRAM SUMMARY 5 8 8 87 FATIGUE & DAMAGE TOLERANCE 98 DAMAGE TOLERANCE B FATIGUE 211

Damage Tolerance Assessment of the Viggen Fighter

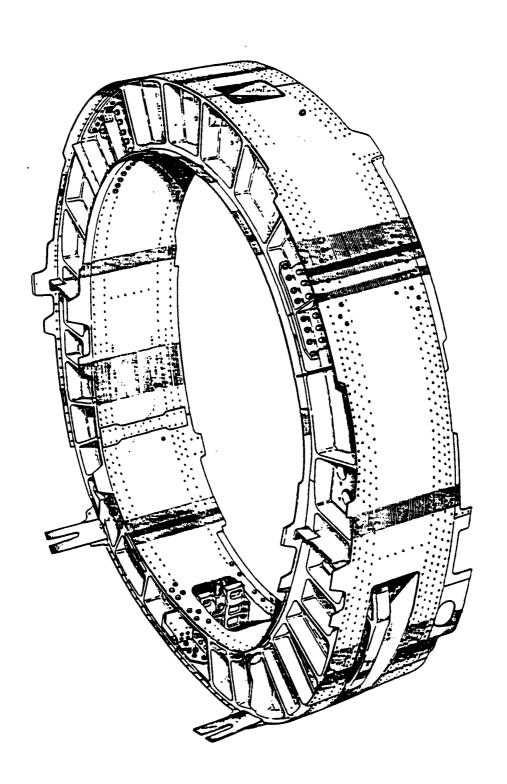
Part II 1986 - 1989

- conducted at the FFA with support of Saab-Scania Aerospace Division

Main Objective

to assess damage tolerance of four versions of the main wing attachment frame

Viggen - The main wing attachment frame



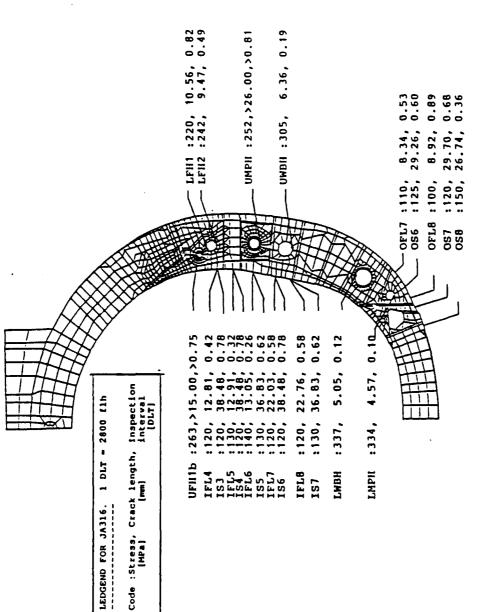
Methodology

Analysis/Fracture Control

- Extensive FE-analyses applying substructuring technique and advanced Self-Adaptive FE method
- Iterative solutions of contact problem occurring in the area of load transfer between the wing attachment frame and wing spar
- three dimensional solution of stress intensity factors in specific cases applying Self-Adaptive FE-code
- Linear Fracture Mechanics applied

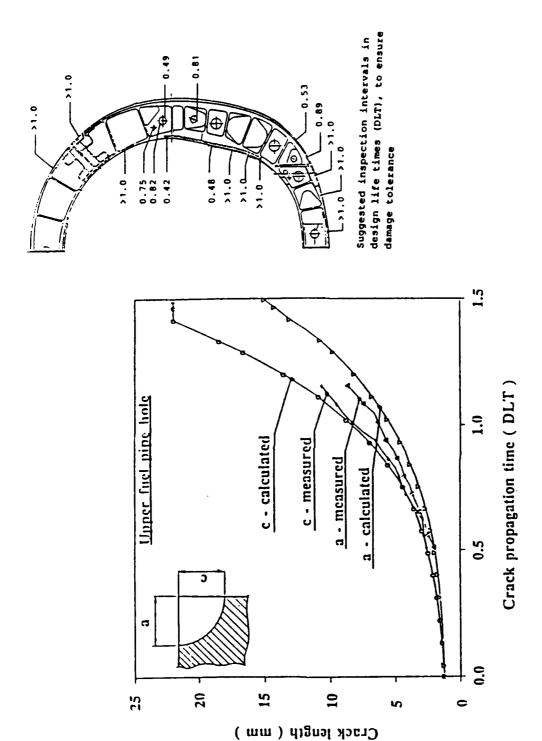
Tests

- Coupon tests
- full scale damage tolerance test of **one version** of the main wing attachment frame

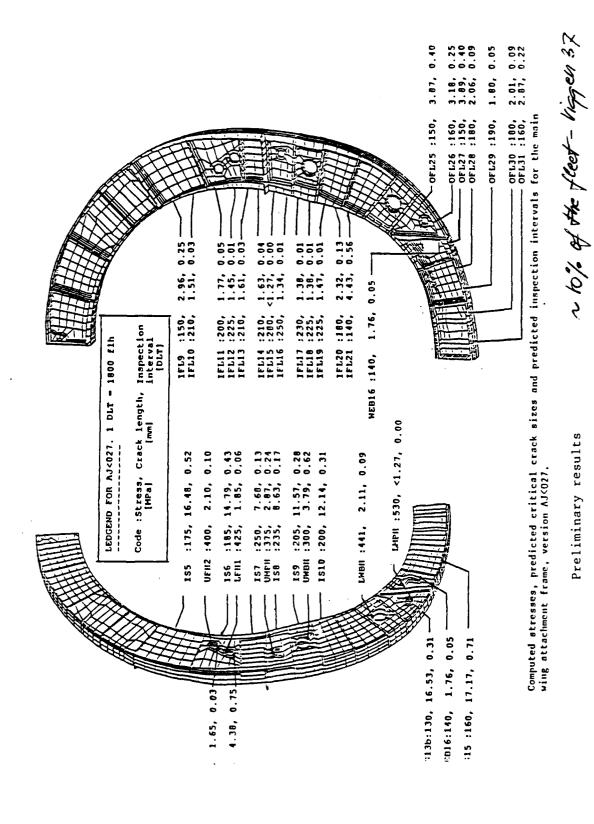


Computed stresses, predicted critical crack sizes and predicted inspection intervals for the main wing attachment frame, version JA316.

Preliminary results



Comparison between predicted and measured crack length as function of time (design lifetimes)



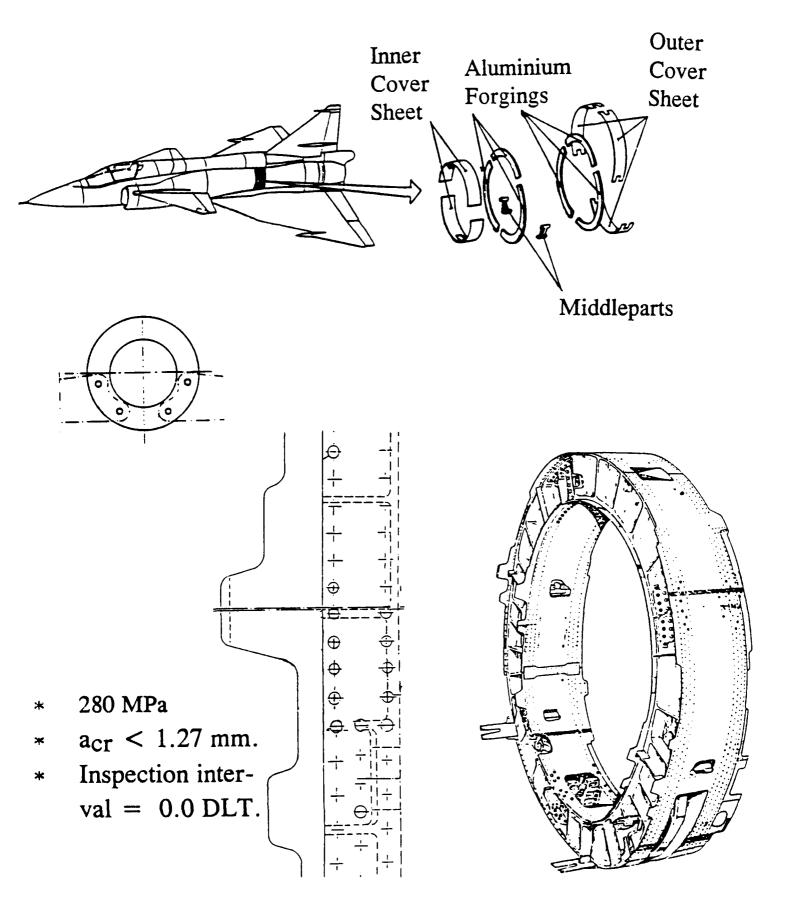
Preliminary results

217

Major results

- a good correlation between calculated and measured stresses in the region of high stress levels and concentration
- relatively good correlation between predicted and measured crack growth
- except the frame version examined in the full scale test relatively short critical crack lengthes < 2.5 and corresponding short inspection intervals have been obtained
- Particularly one of the four frame versions analyzed appeared as seriously critical

* Service Life Extension



* Inspections?

- Very small cracks
- Complex structure

* Proof test?

- No transition point
- Very high loads and short intervals

* Conservatism?

Input data - Spectrum - Stresses - Material data - Others - Massumptions - Initial quality - Failure criteria - Others

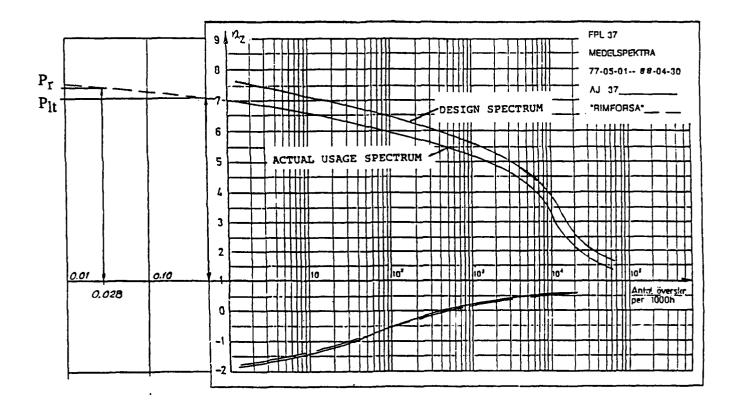
* Other options?

* Input Data:

-Spectrum: Usage nz spectrum gave:

$$P_r = 7.6 g$$
 (min(once in 20 DLT),(1.2*P_{lt}))

$$P_{lt} = 7.1 g$$
 (once in a DLT)



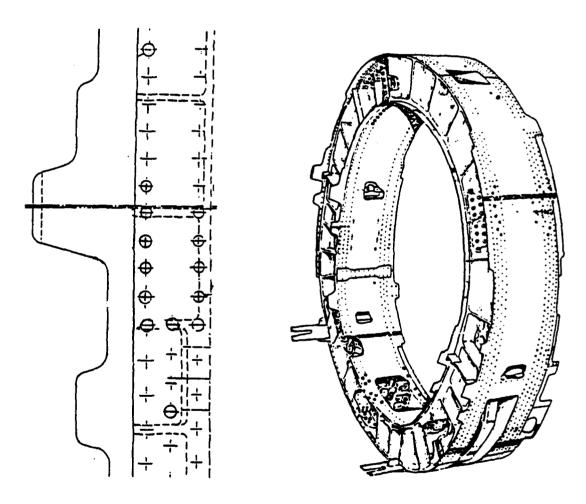
$$a_{cr} = 1.69 \text{ mm}, c_{cr} = 2.36 \text{ mm}.$$

Prop time to failure
$$= 0.05 DLT$$

* Input Data:

- Stresses: Detailed study gave:

Stress reduction from 280 MPa to 228 and 257 MPa for the two fastener columns.



=>

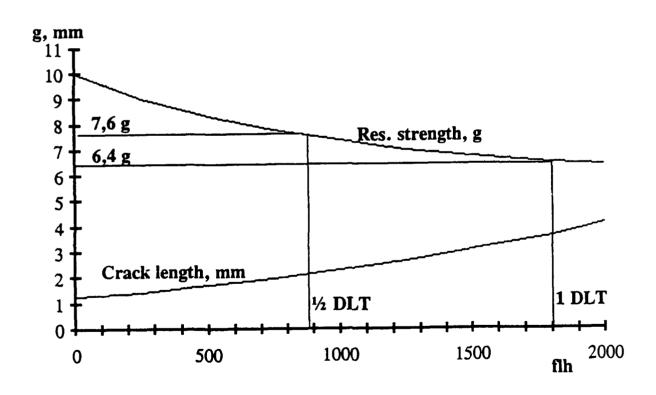
 $a_{cr} = 2.11 \text{ mm}, c_{cr} = 3.05 \text{ mm}.$

Prop time to failure = 0.11 DLT

* Input Data:

- Mat. data: Empirical retardation factor of 4.5, based on test results gave:

=>
$$a_{cr} = 2.11 \text{ mm, } c_{cr} = 3.05 \text{ mm.}$$
Prop time to failure = 0.5 DLT



ai =1.27 mm gave 6.4 g failure load at 1 DLT.

* Assumptions

- Init. quality: $a_i < 1,27 \text{ mm}$?

Two fatigue tested sections of a frame has been torn down.

- 4 DLT of testing
- ~650 rivet/bolt holes

=> Cracks < 1.0 mm in 6 holes.

- Failure crit: K_c (plain strain) too conservative?

- Very small cracks
- Stresses close to yieldstress

- Back to safe life?

- Leave the "slow crack growth, non inspectable" ?

- Fail safe
- Failure of one of the two forgings

* Fail safe

- Aerodynamic effects:
 - Flutter
 - Changed V-shape
 - Changed alpha

_

- No damage on aux. systems:
 - Hydraulic
 - Fuel
 - Electrical
 - Propulsion
 - Flight control

_

- Detectable/Inspectable

* Sufficient res. strength

- Load transfer: Measurements + FEM-calculations show < 60 % increase of stresses in the intact frame.

- Dyn. factor: FEM-calculations give

Df ~ 1.4 (No damping cons.)

- Cracks in intact frame:

Crack with $a_i = 0.127$ mm has grown during 1 DLT.

* Results:

- At failure:

Fail safe up to > 7.6 g OK.

- After failure:

Inspection interval 75 flh.

=>

Flight safety based on fail safe is demonstrated.

Inspections for broken frame:

- After overloads > 6.5 g.
- Every 60 flighthours

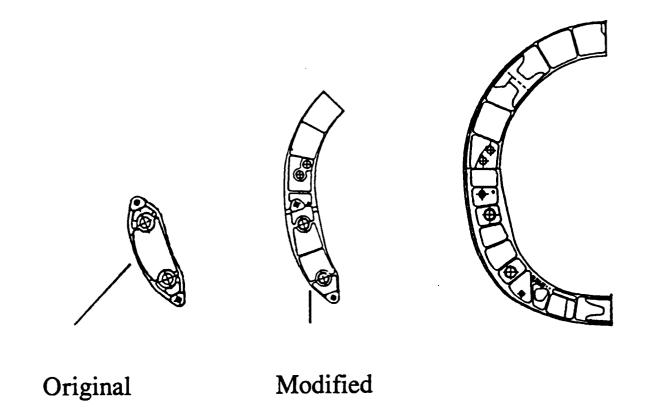
* Ongoing actions:

- Detailed usage analysis
- => Actual stress spectra.

- Statistic evaluation of reported overloads
- => Plt and Pr expressed in terms of stresses.

- Failure criteria
 - JR, KR, CTOD/CTOA
 - Others
- => Less conservatism

* Modification of the middlepart



- Stress reduction of ~ 40 %
- Increases the weight with ~ 50 kg, close to c.g.

- * Future, regarding the rest of the structure:
- Much lower stresses.
- Most of the structure has been fatigue tested 4 + 2 DLT, the last two with increased load level.
- => Hope to be able to demonstrate DT slow crack growth.
 - Studying CRP/BRP reinforcement methods.

* Concluding remarks

- Reliable method
 - Service life extension

- Flight safety demonstrated

Presented to

1991 USAF Structural Integrity Program Conference

3 — 5 December 1991 San Antonio, Texas

þ

(Cathy) Nguyen-Quoc Hoang-Thuy Bombardier Inc., Stress Engineer Canadair Group

Acknowledgement

- R. Banister P. Newman
- M. Schade
- M. Jolicoeur
- Capt. C. McRae

Ę



1991 USAF STRUCTURAL INTEGRITY PROGRAM CONFERENCE

SYNOPSIS: CHALLENGER INITIAL ANALYSIS UPDATE

C. Nguyen-Quoc; M. Schade

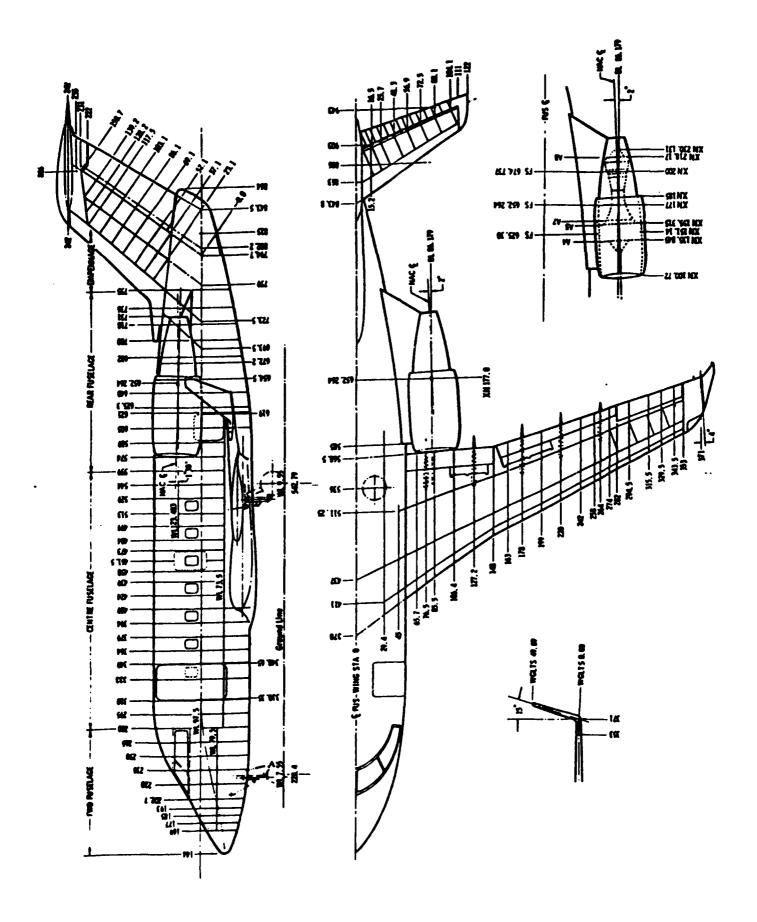
The aim of this Initial Analysis Update is to provide the Challenger customer with an economical and accurate damage tolerance review of the aircraft structure when they intend to operate the aircraft differently from the basic design Challenger. The original Challenger (CL-600-1A, 3A) was designed for Executive or VIP usage. Recently, Canadian D.O.T. and DND have operated the aircraft with the Navaid, Electronic Warfare and Low Level flight roles and mission profiles. To reevaluate the damage tolerance analysis of the whole aircraft structure, an Initial Analysis Update (Task 4a ASIP) has been implemented through the ASIP program. The Initial Analysis Update mainly describes a Damage Tolerance Methodology used to justify the A/C Inspection Interval when the aircraft fleet changes its roles and mission profiles. spectrum combining all the load factors from pre take-off to post landing can be derived based upon the new mission profile/role. A damage comparison between the basic design profile and the new role can be performed at the typical control points of the aircraft. Subsequently, the aircraft Inspection Interval which raised the Time Limits/Maintenance check can be reevaluated. The methodology used has been automated and supported by a package of computer software developed for the Regional Jet and Challenger program.

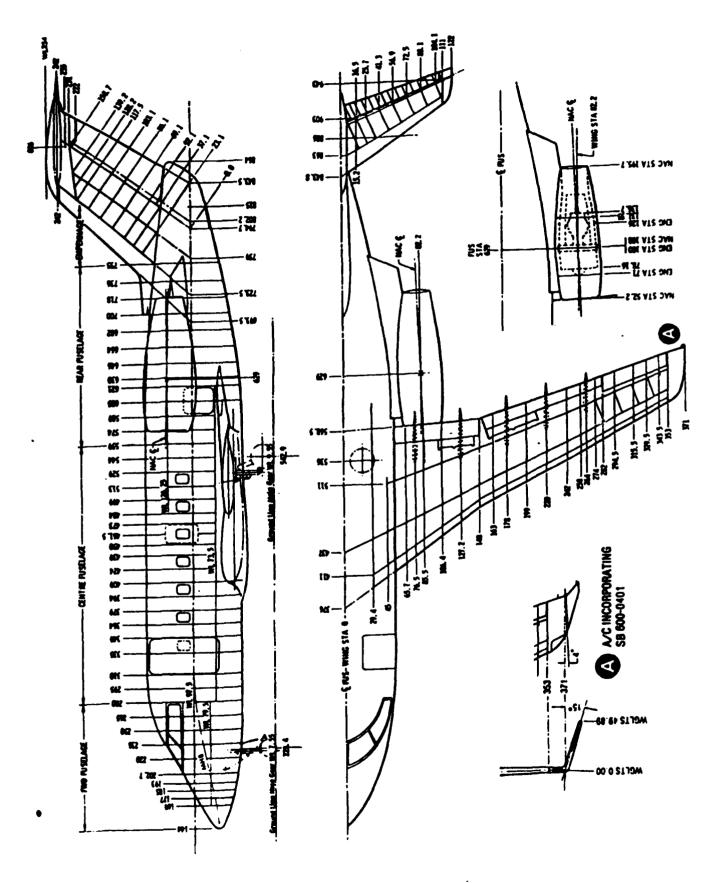
Presentation Overview

- Challenger background
- CC-144 ASIP requirement
- Task IV Final Anaylsis (4a)
- Lessons Learned
- Conclusions and Discussions

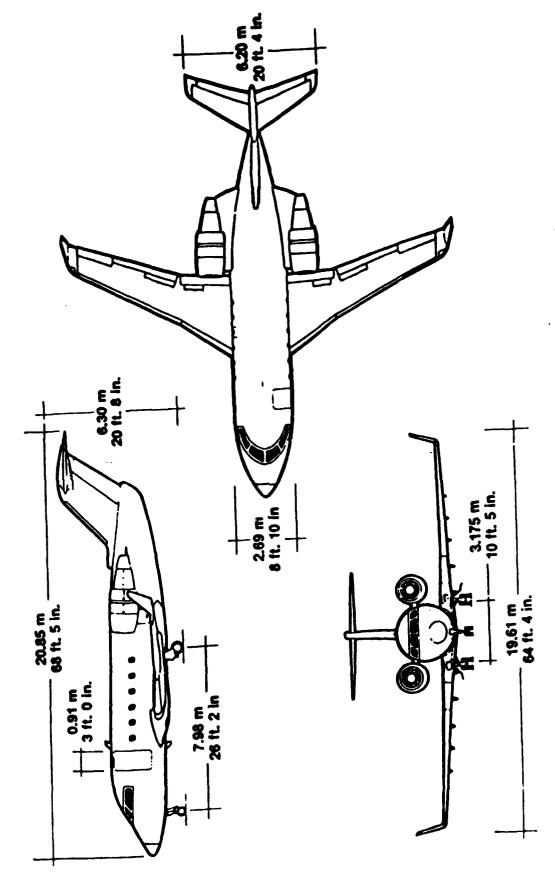
Challenger Background

- The Challenger was designed to meet FAR 25 Amendment 45 requirements
- First model CL-600 was certified in Nov. 1980
- Second model CL-601 was certified in Feb-March 1983
- Challenger have an economical life of 30,000 hours as a business jet
- DND purchased 16 Challenger aircraft and designated CC-144 to both models
- CC-144 operating roles
- Administrative airlift (Executive)
- · Electronic Warfare (EW)
- Avionic Test Bed (AT
 - Coastal Patrol (C









Current CL-600-1A11 Envelope

Max. Take-off Weight Max. Landing Weight Max. Zero Fuel Weight

Max. altitude

Vmo/Mmo Max/Min. Temperatures

Max. Occupants

41,250 lb. (with winglets)

36,000 lb.

28,500 lb.

41,000 ft

360 kds/0.835 m

Sea level: +50°C (ISA +35°C)/ -40°C (ISA -55°C)

Twenty-two (Nineteen Passengers)

Current CL-600-2B16 Envelope

43,100 lb. (*44,600 lb. with optional weight increase) Max. Take-off Weight

36,000 lb.

Max. Landing Weight

29,500 lb. (31,000 lb. with optional weight increase) Max. Zero Fuel Weight

41,000 ft.

Max. Atttude

Vmo/Mmo

360 kts/0.835 m

Sea Level: +50°C (ISA +35°C)/-40°C (ISA -55°C) Max/Min. Temperatures

Twenty-two (Nineteen Passengers)

Max. Occupants

• Note: Increase from 44,600 lb. to 45,100 lb. expected to be approved by Transport Canada October 1990

Structural Substantiation

Z

1

Structural Testing (CL-600)

- with a conservative structural life limit imposed pending approval Although structure designed as Damage Tolerant, initial type approval was to pre-amendment 25-45 standard (FAR 25.571) of the damage tolerance testing and analysis
 - Objective was to demonstrate safe fatigue life of 30,000 hours with a test factor of 5
- (upper and lower panels) and horizontal vertical stabilizer joint characteristics with support from wing development testing Nastran math model used to predict loading/structure **lesting**

Complete Airframe Fatigue Test (CL-600)

- Supplied majority of structural data crack growth
- Test rig designed to induce loads typical of several flight regimes, including pressurization cycles (up to 45,000 ft.)
 - Initial testing (1 life), flight by flight spectra to investigate natural

]

1

]

J

Structural Substantiation (Cont.)

1

Complete Airframe Fatigue Test (Cont.)

- A further 30,000 hours testing with induced cuts for damage tolerance assessment
- Application of limit load to damaged structure
- Results closely matched Nastran model predictions for crack growth/residual strength
- Test completed at 60000 hours

Complete Airframe Static Test (CL-600)

- 12 limit load tests
- 12 threshold tests at 85% ultimate
- 6 ultimate tests

Additional Tests (CL-600)

- Many sub-assemblies were tested for static and residual strength
- All flight surfaces were limit load tested prior to first flight



Ì

Additional Tests (Cont.)

Windshield and Empennage were tested to bird strike requirements (4 lb. bird for windshield; 8 lb. bird for empennage)

Sonic fatigue tests performed for engine/rear fuselage area

Engine mount tested to five life times (safe life)

Damage Tolerance (CL-600)

Submissions of test data and analysis, through MSG-2 procedures, provided damage tolerance approval in January 1985 (FAA). Transport Canada approved damage tolerance on all variants in November 1987

Structural life limitations provided in Maintenance Manual Chapter V (Document PSP 605)



コココココココニューコー

Landing Gear (CL-600)

- Multiple main and nose landing gear static, fatigue, and drop tests were performed by Dowty
- Analyses were made for landing gear failures (effects on emergency egress, fuel tank integrity, bursting tyre in wheel bin)



11111111111111

Additional Items for CL-601

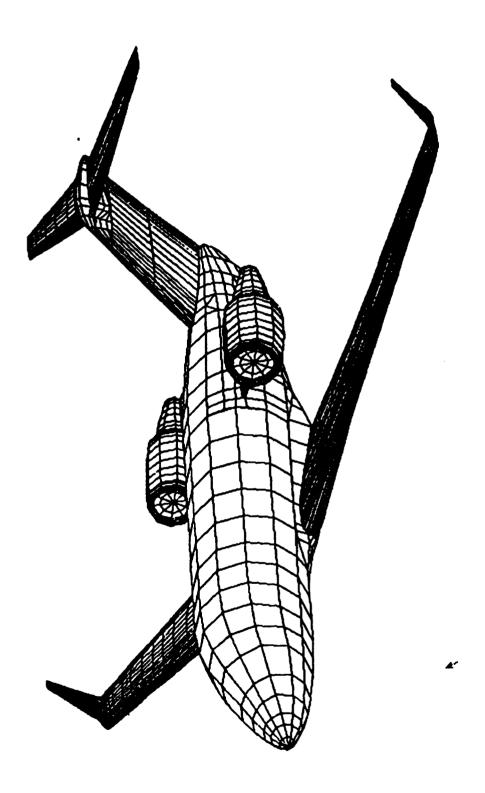
- Aft fuselage changes examined for static strength, damage tolerance and rotor burst
 - Modified flight profile for damage tolerance analysis
- Engine mounts tested to damage tolerance requirements
- Tests for winglet and outer wing modifications
- Main landing gear redesigned for improved life limit



Additional Items for CL-601-3A

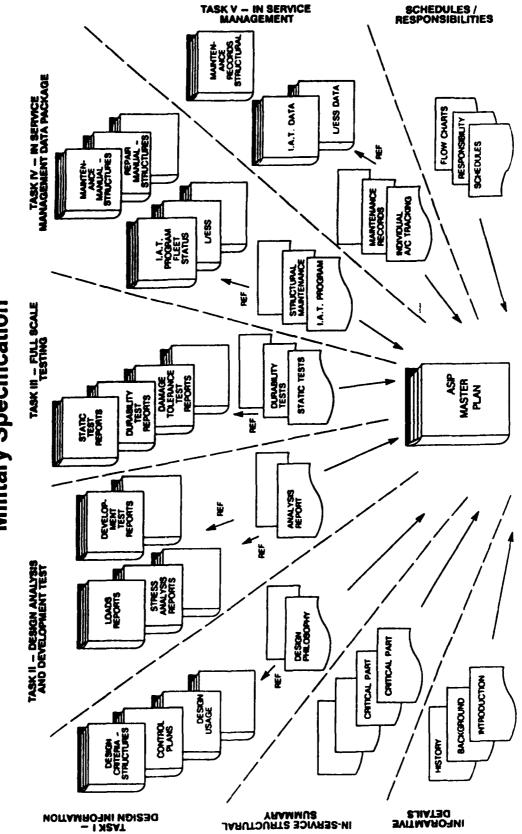
Effects on damage tolerance analysis considered for shorter time to altitude or higher weight to altitude performance





CC-144 ASIP Requirement

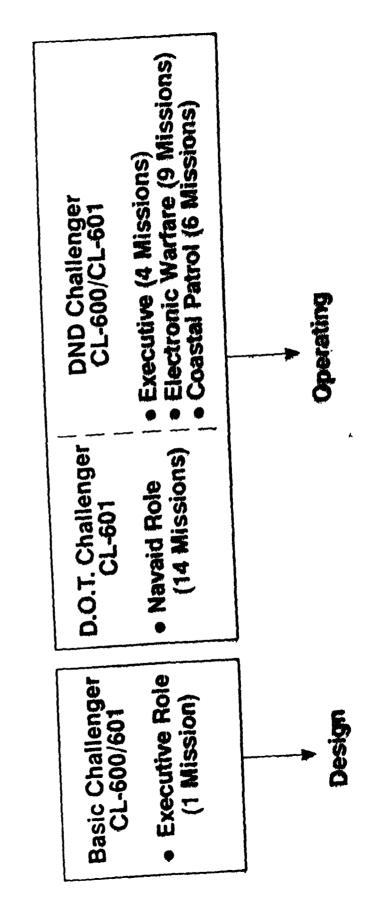
D-12-010-013/SG-000 Military Specification





- "New" roles/mission profile
- Mission aircraft performance data
- Mission mass distribution
- Mission definition
- Load factors derivation
- Fatigue loads data
- Stress transfer functions
- Stress history
- Range paired stress spectrum
- Crack growth for control points
- Define inspection interval factors
- Justify Design Maintenance Manual

Task IV — Final Analysis (4a)
Role(s)/Mission Profiles



Task IV — Final Analysis (4a) Load Factors Derivation

- Vertical gust occurrence/magnitude ESDU 69024
- Lateral gust occurrence /magnitude
 ESDU 69024
- Vertical manoeuvre occurrence/magnitude MIL-A-8866B
- Take-off & landing vertical acceleration

. Challenger Initial Analysis Update

Task IV — Final Analysis (4a)
Load Factors Derivation (Cont.)

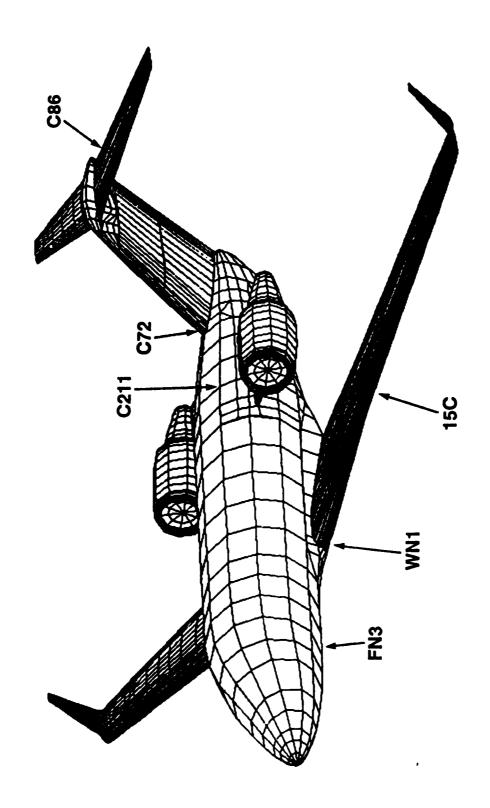
- Taxi-turn acceleration MIL-A-8866B
- Engine run-up
- Sinking speed
- Brakes and reverse thrust

Task IV — Final Analysis (4a)
Fatigue Loads System

Task IV — Final Analysis (4a)

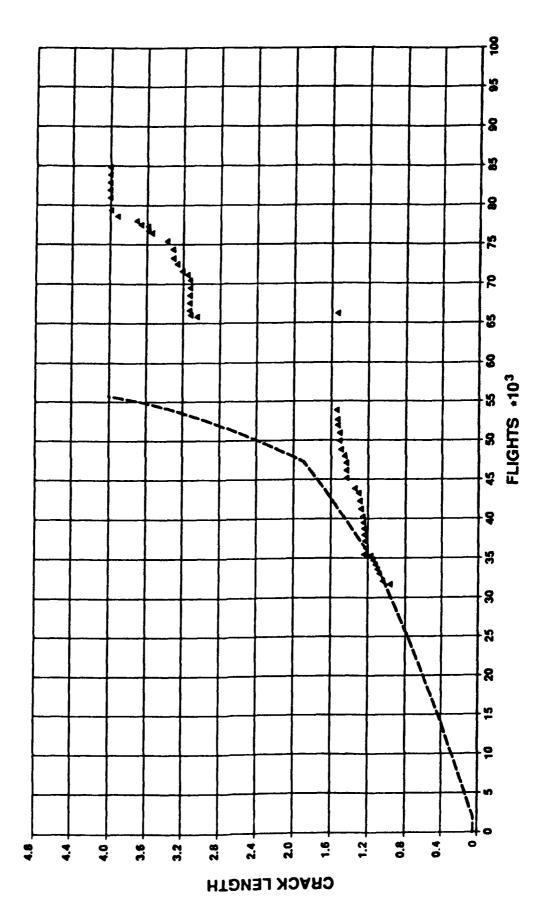
Stress Transfer Functions

- Six (6) Control Points
- 2 on the Wing
- 2 on the Fuselage
- 1 on the V/S
- 1 on the H/S
- FEM Stress-load transfer function

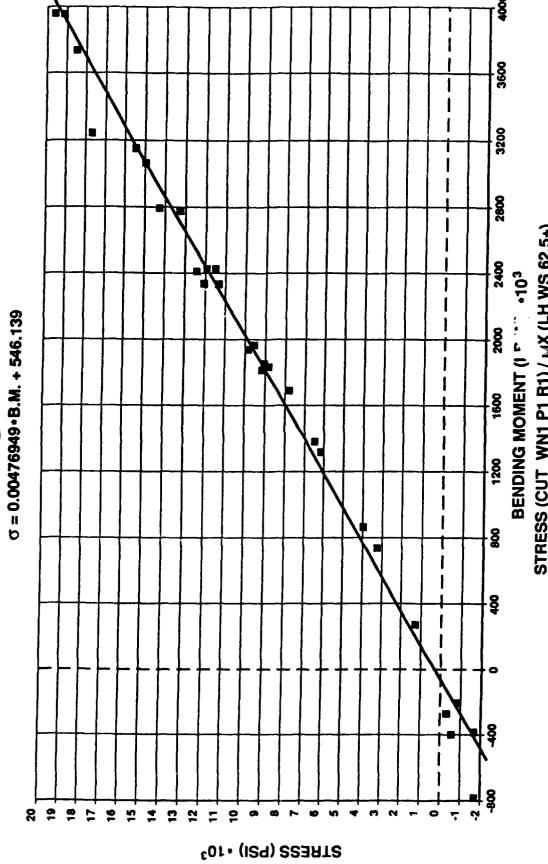


Forward Fuselage Control Point FN3





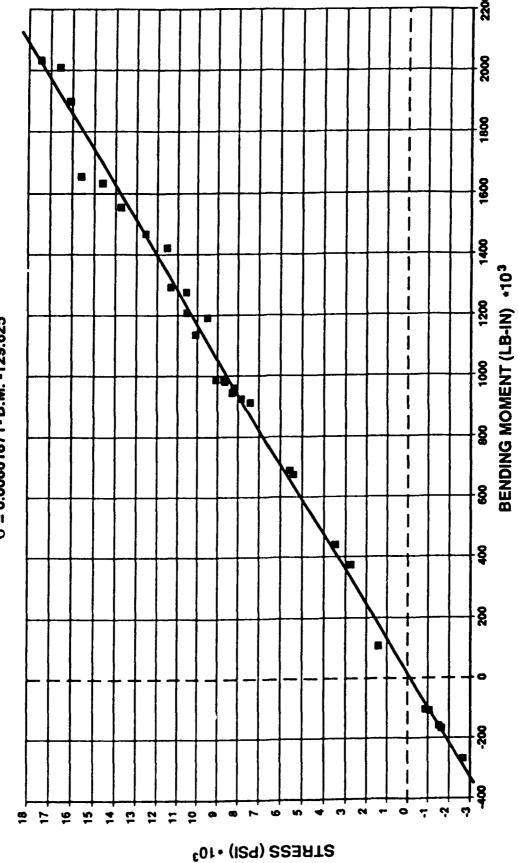




STRESS (CUT WN1 P1 R1) / MX (LH WS 62.5+)

Outboard Wing Control Point



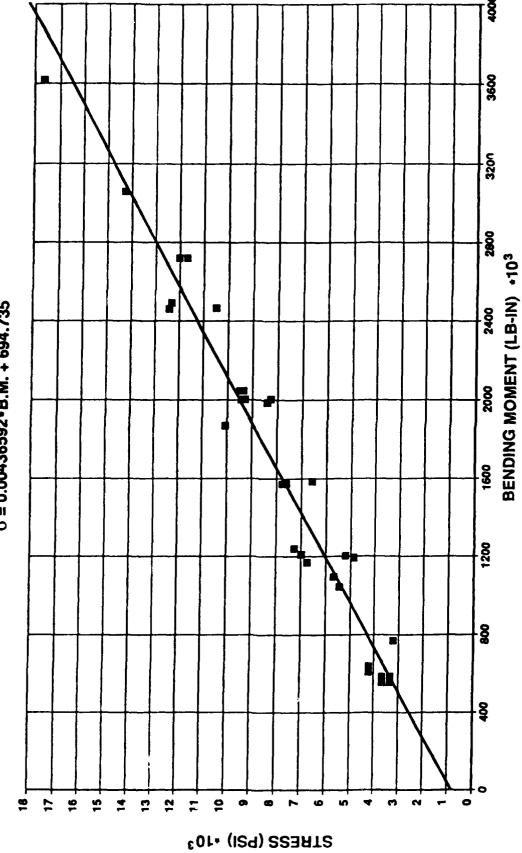


42803

STRESS (CUT 15C P1 R1) / MX (LH WS 148.-)







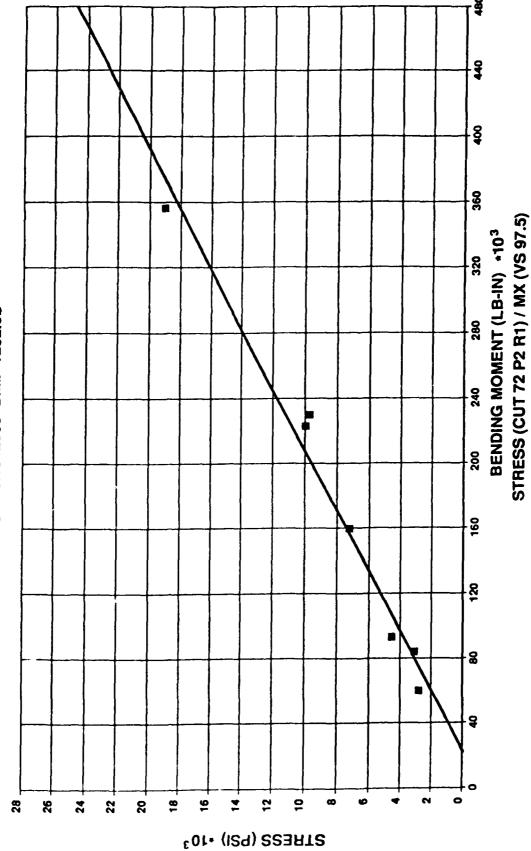
\$30

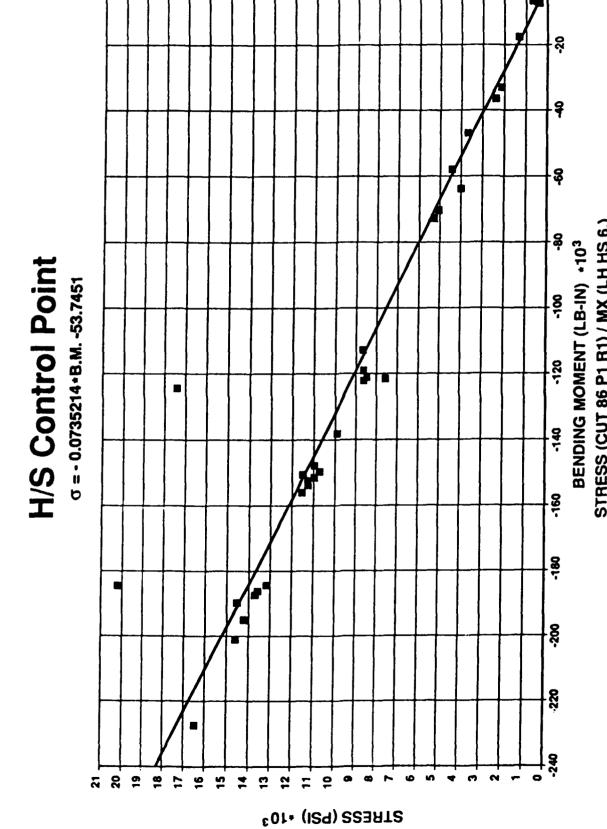
STRESS (CUT 211 P2 R1) / MY (FS 621)

261



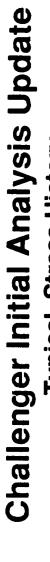


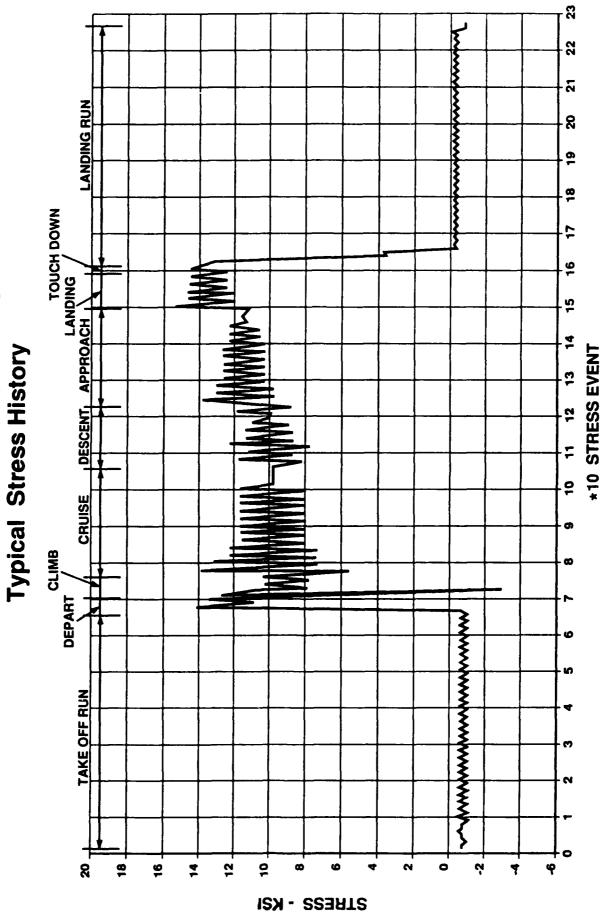




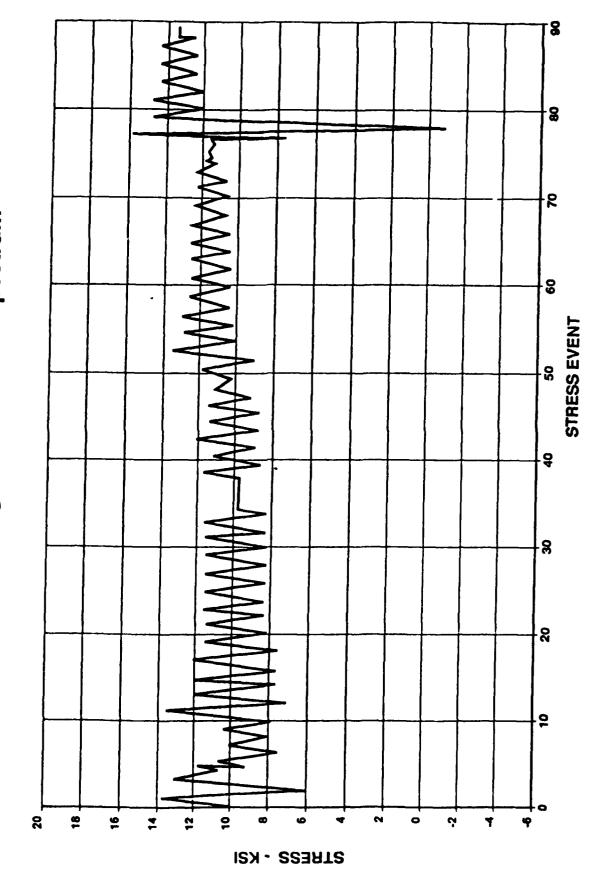
STRESS (CUT 86 P1 R1) / MX (LH HS 6.)

- Stress sequence derived from
- Unit load and load factor definitions
- Stress transfer function
- Range paired stress spectrum
- Ground air ground (GAG) cycle
- Peak valley range paired





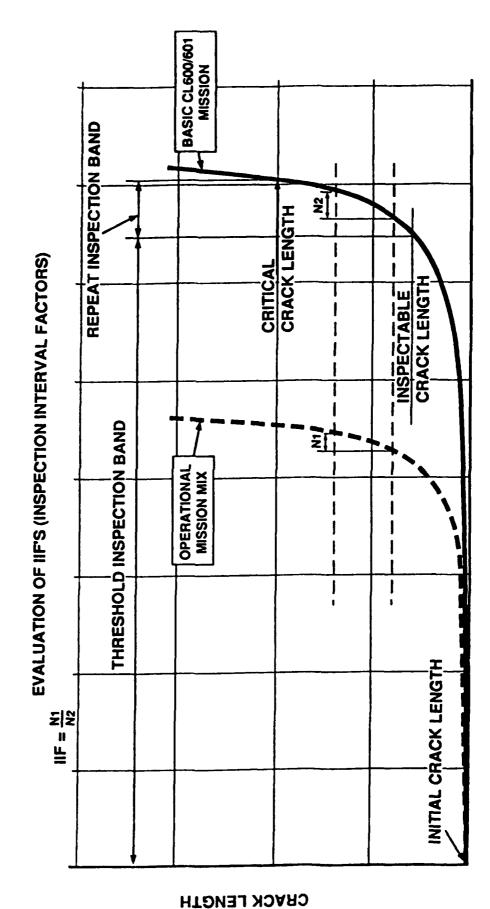
Challenger Initial Analysis Update Typical Range Paired Stress Spectrum



. Challenger Initial Analysis Update

Task IV Final Analysis (4a)

Crack Growth for Control Points



NUMBER OF FLIGHTS

- Challenger Initial Analysis Update

Task IV — Final Analysis (4a)

A/C Component	Control Point	Incremental Crack	Design Mission	Navaid Mission	¥
		Length		Mix	
Wing	NA L	0.20 - 2.10	3912.6	4719.0	1.21
	15C	0.50 - 2.30	11380.1	12566.4	1.10
Fuselage	FN3	0.05 - 4.00	29027.5	60491.7	2.08
	211	1.00 - 1.50	10389.2	34573.2	3.33
Vert. Stab.	072	0.10 - 0.11	579.9	55628.6	95.93
		0.20 - 0.25	631.5	55569.8	88.01
Horl. Stab.	980	0.50 - 0.55	776.2	6042.7	7.79
		1.00 - 1.10	467.0	4146.3	8.89
		1.30 – 1.50	533.9	4956.6	8.95

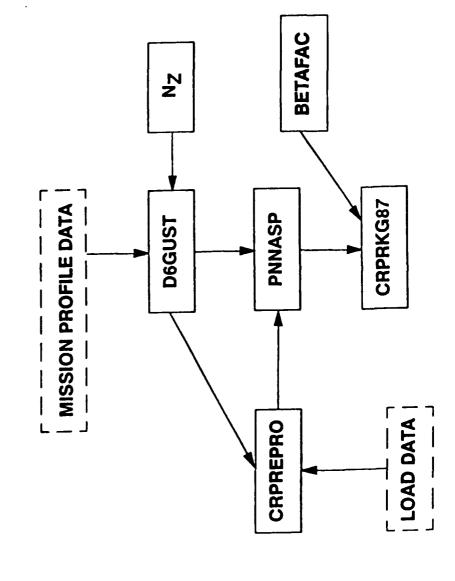
. Challenger Initial Analysis Update

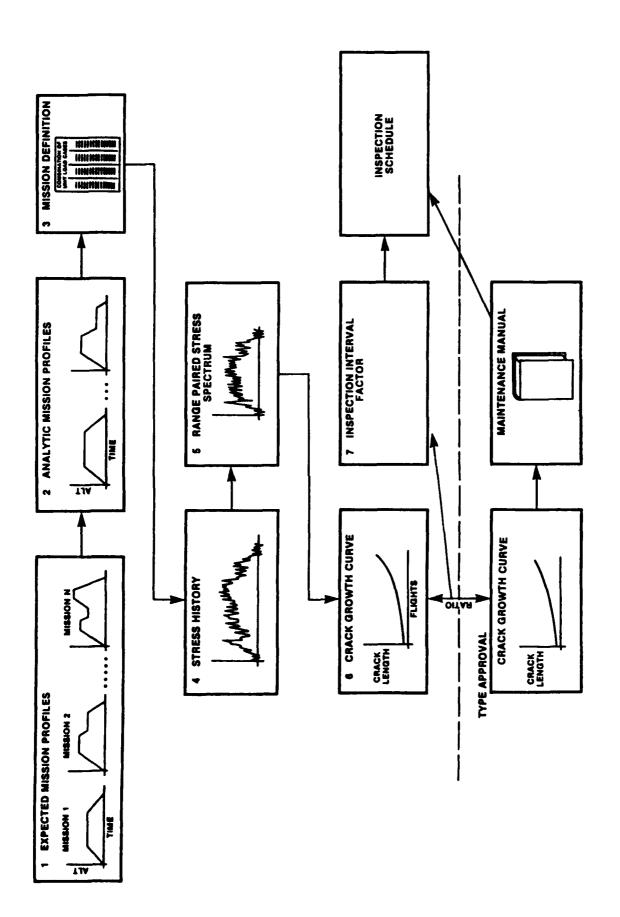
Task IV — Final Analysis (4a)

IIF Between Design & IEST A/C

A/C Component	Control Point	Incremental Crack Length	Design Mission	IEST Mission Mix	프
Wing	WN1 15C	0.20 - 2.10 0.50 - 2.30	3912.6 11380.1	3196.8 8906.4	0.82
Fuselage	FN3 211	0.05 - 4.00 1.00 - 1.50	29027.5 10389.2	23594.4	0.95
Vert. Stab.	072	0.10 - 0.25	3851.4	79304.4	20.59
Hori. Stab.	980	0.50 – 1.50	6390.8	31766.4	4.97

Task IV – Final Analysis (4a) Damage Tolerance Package





-

Lessons Learned

- Accuracy of mission definition
- Spectrum complication
- Software update

Conclusions and Discussions

- Challenger Initial Analysis Update has provided Canadair with the most economical and efficient way to update the Damage Tolerance Analysis
- Additional study required for:
- **Equivalent spectrum**
- Control points for future aircraft (E.C. & R.J.)

CERTIFICATION METHODOLOGY FOR AIRCRAFT PRIMARY COMPOSITE STRUCTURES

bу

E. F. Kautz, S. L. Huang, R. E. Vining, and R. M. Catanese Naval Air Development Center Warminster, Pennsylvania

The recommendations in this paper are not to be construed as the official position of the Naval Air Systems Command on certification of composite structures.

ABSTRACT

This paper discusses the results of a Navy sponsored research and development program that investigates the issues associated with certifying the structural integrity of aircraft constructed with advanced composite materials. Recommendations for material design allowable development, preproduction component design tests, and a full-scale static and fatigue test certification process are given.

INTRODUCTION

Structural certification test procedures for Navy fixed wing piloted aircraft are contained in Military Specifications MIL-A-8860 through MIL-A-8870. These specifications, when combined with other applicable documents which are modified and amplified for specific aircraft model types, define the ground tests required to demonstrate the airworthiness of an aircraft for its planned service life.

By specification, current Navy certification test procedures for metal aircraft require that (1) a full-scale static test article successfully withstand minimum loads of 150% design limit, and (2) a full-scale fatigue test article demonstrates an airframe life of at least two times the design service life when subjected to repeated loads for the most critical flight conditions. These two requirements, when successfully completed in conjunction with other applicable tests, such as drop tests, elevated temperature tests, and cabin pressure tests, typically satisfy strength and rigidity requirements for final structural certification. Pre-production component design tests, when conducted by airframe manufacturers, are typically performed for the purpose of early verification of the static and fatigue strength capability of final or near final structural designs of critical structural areas. These tests are not an inherent part of the final certification process.

A concern that both government and industry share is the significant variability of composite materials in both static strength and fatigue life. Consequently, the need to establish appropriate certification test procedures that will insure the structural integrity of aircraft manufactured with composite airframe parts throughout their entire service life is a priority goal. Presented in this paper is a summary review of a recent study that was conducted to evaluate the scatter in static strength and fatigue life of composite structures. The characteristics of composite structure behavior are discussed in three major areas:

Mechanical Properties Variability Environmental Sensitivity Impact Damage

ANALYSIS OF MECHANICAL PROPERTIES VARIABILITY

Two separate investigations were conducted to define mechanical property constants for composite aircraft structures. In the first investigation, scatter (variability) in demonstrated static and fatigue strength were determined for unnotched, open hole, and bolted-joint specimens. In the

second investigation, static strength and fatigue life scatter were determined for bonded, co-cured, and impact-damaged composite structures.

Two airframe manufacturers, Northrop Corporation and the McDonnell Aircraft Company (MCAIR), both under contract to the Naval Air Development Center (NAVAIRDEVCEN), performed the investigations and reported the findings of their work for unnotched, open-hole, and bolted-joint specimens in references (1) and (2), respectively, and for bonded, co-cured, and impact-damaged specimens in references (3) and (4), respectively. Northrop selected the two parameter Weibull distribution to describe the scatter in static and fatigue strength. The shape parameter (α) was used to describe the scatter. MCAIR chose the normal distribution in analyzing the static and fatigue strength scatter of the composite specimens. Scatter for the normal distribution was described by the coefficient of variation (CV). For direct comparison of the Northrop data with MCAIR, a transformation (approximate) of CV to an equivalent α by the method of moments was made.

In addition, both Northrop and MCAIR also assessed the effects of loading direction, test environment, specimen geometry, and laminate lay-up on static strength scatter. As shown in table 1, additional scatter in static strength was attributed by Northrop for loading direction (compression versus tension) and for test environment (elevated temperature wet versus room temperature wet and dry). MCAIR, however, did not observe any effects of these variables on scatter. From these observations, the need to fully investigate factors affecting scatter for all loading condition variables as an inherent part of the material design allowables development test program is recommended. The results of each contractor's analysis of static strength scatter (a) are shown in Table 2.

Table 1

OBSERVED EFFECTS ON STATIC STRENGTH SCATTER

Variable	Northrop	MCAIR
Loading Direction	Yes (1)	No
Test Environment	Yes (2)	No
Specimen Geometry	No	No
Laminate Lay-Up	No	No

- (1) Test results show tension scatter was significantly less (95% confidence) than compression scatter.
- (2) Room temperature dry and wet (RTD/RTW) scatter was significantly less (95% confidence) than elevated temperature wet (ETW) scatter for tension loading.

Table 2

STATIC STRENGTH SCATTER

Composite Structure	NORTHROP	MCAIR
	α	α (CV)
~~~~~~~~~~~~~~~~~~~~~~~~~~~~~~~~~~~~~~		
Bolted Construction	20	19 (0.065)
Bonded Construction	9	16 (0.076)
Co-Cured Construction	-	16 (0.078)
Impact Damaged	12	30 (0.043)

Note: As a decreases, scatter increases.

The results of the MCAIR and Northrop studies are very similar for bolted construction. The results for bonded and co-cured construction and for impact damaged specimens, however, are significantly different. This difference may be attributed, in part, to the different number of test results analyzed. In the bolted construction studies, more than 2,000 data points were used. For the other conditions, most cases had less than 200. Therefore, on the strength of the large sample for bolted construction and since this type of construction represents the type of structure found in typical primary airframes, only the bolted construction data is used in this paper to demonstrate a static strength certification procedure for composite structures. A value of  $\alpha = 20$  has been selected for this purpose. The actual  $\alpha$  values used in a specific aircraft development program should be established during the material design allowable phase. In the case of metal structures,  $\alpha$  values ranging from 25 to 35 (references (4), (5), and (6)), have been exhibited. For comparison purposes, a value of  $\alpha = 30$  is used in this paper for metal structures.

Fatigue life scatter for composite structures, as determined by Northrop and MCAIR, are given in table 3:

Table 3

FATIGUE LIFE SCATTER

Composite Structure	a (Northrop)	a (MCAIR)
Bolted Construction	1.25	1.0
Bonded Construction	1.25	1.0
Co-Cured Construction	-	1.0
Impact Damaged	-	1.4

A value of  $\alpha$  = 1.25, representing the typical fatigue life scatter found in bolted composite construction, is used in this paper for demonstrating a fatigue life certification procedure. A value of  $\alpha$  = 7.5 is used for metal structure (reference 1).

The comparison of Weibull shape parameters clearly show the scatter in static strength and fatigue life is greater in composite structure than in metals. Consequently, appropriate test loads and demonstrated lifetime requirements must be established for composites to achieve an equivalent acceptable level of confidence currently enjoyed with metal structures. Our goal is to ensure every Navy aircraft will safely reach its planned service life.

#### ENVIRONMENTAL SENSITIVITY

Composites have demonstrated significant sensitivity to the operational environment, in particular, the synergistic effects of temperature and moisture. For structures which are subject to matrix controlled failures, the influence of the environment takes on additional significance. Consequently, the certification process for composite structures must consider these effects.

The issue of strength degradation due to the environment is currently addressed during the certification process by the development and use of strength reduction (knockdown) factors. These factors, expressed as percent reduction in room temperature strength, give measurable values for establishing acceptable design allowables that reflect reduced load carrying capabilities due to the critical environment.

The Navy emphasizes the need to use strength knockdown factors associated with a hot/wet environment for compression and a cold/dry environment for tension loads. These factors, along with factors for material properties variability, are typically included in all pre-production component design verification tests as well as in the full scale static and fatigue tests. The use of knockdown factors is intended to provide an acceptable level of confidence that the required room temperature strength needed to certify the structure for the critical environmental condition(s) is adequately defined. In reference (2), typical graphite/epoxy knockdown values are 15% for compression and 6% for tension.

#### IMPACT DAMAGE

Composite laminates exposed to low-velocity impact damage have demonstrated the potential to sustain extensive internal damage without exhibiting visual signs on the impacted surface, reference 7. To counter the onset of any reduction in the strength of the laminate, the Navy has established an impact damage requirement that has been included in the detailed specifications for recent aircraft development programs (e.g., V-22, A-6 Re-wing program). This impact damage requirement states that a laminate exhibiting a specified threshold of visible impact damage on its surface must be able to sustain design ultimate load fully compensated for environment and material properties variability. For the purposes of this requirement, the threshold of visible surface damage has been defined as any indentation that is clearly visible to the unaided eye up to a distance of five feet (1.5 meters). Typically, a 0.05 inch (0.13 centimeter) indentation will be visible to the naked eye at that distance. The requirement also states that the internal damage can not grow.

#### RECOMMENDATIONS FOR CERTIFICATION TESTING

#### MATERIAL DESIGN ALLOWABLES

#### STATIC STRENGTH DESIGN ALLOWABLES

A primary objective of static testing is to establish design allowables for the environmental service envelope. For composite structures, these allowables may be determined by testing coupons that represent the specific material(s) being used by the airframe manufacturer in the fabrication of the aircraft. Unidirectional coupons (i.e., coupons with 0° or 90° fiber orientations) and multi-directional laminate coupons are recommended for testing. The unidirectional tests are performed to establish mechanical properties such as Young's modulus, shear modulus, and Poisson's ratio. To obtain theses properties, tests should include longitudinal and transverse tension, compression, and shear. Multi-directional laminate tests are recommended for a minimum of five different lay-ups found in the aircraft primary structure. These strength tests should include unrotched tension and compression, open hole tension and compression, filled hole compression, bearing, and bearing/bypass configurations.

Test coupons must be environmentally conditioned to establish strength to temperature/moisture relationships for the entire environmental service envelope. Sufficient replicates of each test condition must be performed to generate an acceptable statistical data set for establishing statistical constants. In references (1) and (2) a minimum of fifteen replicates was recommended. The specific test conditions and the number of replicates required in an aircraft development program must be established early in the program and approved by the procuring agency. B-basis design allowables can then be developed for each loading condition from these test results. B-basis allowables for lay-ups not tested should be determined using a combination of analysis and the available test data in conjunction with the established statistical constants. Examples of typical test matrices are shown in tables 4 and 5.

Table 4

UNIDIRECTIONAL LAMINATE - STATIC STRENGTH ALLOWABLES TEST MATRIX

Loading Mode	Loading Mode Laminate Fiber Orientation		Environments		
Tension	0°	LTD	RTD	ETW	
Tension	80°	•	•	•	
Compression	00	•	•	•	
Compression	90°	•	•	•	
Shear	± 45°	•	•	•	

#### Legend:

LTD = Low Temperature Dry RTD = Room Temperature Dry ETW = Elevated Temperature Wet

Table 5 MULTI-DIRECTIONAL LAMINATE - STATIC STRENGTH ALLOWABLES TEST MATRIX

Test Type	Loading Mode	Laminate	En	vironmen	ts
Unnotched	Tension	L1 - L5	LTD	RTD	ETW
Unnotched	Compression	L1 - L5	•	•	•
Open Hole	Tension	L1 - L5	•	•	•
Open Hole	Compression	L1 - L5	•	•	•
Filled Hole	Compression	L1 - L5	•	•	•
Bearing	Tension	L1 - L5	•	•	•
Bolt	20% LT-Tension	L1 - L5	•	•	•
Bearing	30% LT-Tension	L1 - L5	•	•	•
By-Pass	50% LT-Tension	L1 - L5	•	-	•
Bolt	20% LT-Compression	L1 - L5	•	•	•
Bearing	30% LT-Compression	L1 - L5	•	•	•
By-Pass	50% LT-Compression	L1 - L5	•	•	•

Legend: L1 - L5 = Lay-up 1 through Lay-Up 5

LTD = Low Temperature Dry

RTD = Room Temperature Dry

ETW = Elevated Temperature Wet

LT = Load Transfer

= Load Transfer

#### FATIGUE STRENGTH DESIGN ALLOWABLES

Fatigue tests are performed to determine the fatigue threshold strain, that is, the strain levels below which fatigue failure will not occur. As in static design allowable development, fatigue allowables are determined by testing coupons that have been fabricated from the specific material(s) that are to be used in the aircraft production. The manufacturing processes used for these coupons must be consistent with those employed on actual airframe parts.

Laminate tests are recommended as follows: Perform fatigue tests for the critical environment on no-hole and open-hole coupons to establish the fatigue threshold. A minimum of four strain levels should be tested to establish the fatigue threshold. A minimum of six replicates of each test condition is further recommended. Pooling techniques should be used to determine scatter in the test data since investigation results to date indicate the independence of scatter from strain level. Analysis of test data should be performed using the Weibull distribution. B-basis strain life curves may be constructed using computed a values. The fatigue allowable strain is thereby defined as the threshold strain on the B-basis curve.

#### STRUCTURAL DESIGN DEVELOPMENT TESTING

#### STATIC TESTS

Pre-production static tests are used to verify analysis, provide confidence in the design allowables, evaluate design details, and provide test results for use in the interpretation of subsequent full-scale airframe static test data. Design verification tests range in complexity from relatively simple elements to full-scale components such as wing torque box structure and landing gear back-up structure. The actual number and type of tests required will depend upon the aircraft design but must include specimens that are representative of each major critical component and type of construction used in the airframe.

A building block approach to design verification testing is essential for composite structures because of the relatively high variability in mechanical properties exhibited by composite materials, the reduction in mechanical properties due to moisture absorption, and their multiplicity of potential failure modes.

The essence of the building block approach is as follows:

Select critical areas for test verification based upon stress analysis of the aircraft structure and by consideration of structural 'hot spots' that have occurred in previous aircraft development programs. Determine the most critical failure mode for each area selected and establish the test loads and environment which will produce similar failures. Special attention should be given to matrix controlled failure modes such as delamination, debonding and potential failures caused by out-of-plane loading. The sensitivity of composite matrix dominated failure modes to the temperature/moisture environment makes environmental test simulation a key issue in a design development program. The approach for static testing

should be that the test environment selected is the one that produces the failure mode which sustains the lowest loads.

Design and test a series of elements, each element representing a single area and single mode of failure. These initial specimens will generally be of low complexity. From this point on, a series of sub-component specimens should be designed and tested which simulate progressive structural design complexity. The extent of this test effort will be different from aircraft to aircraft, however, the number of replicates for each test specimen must be sufficient to identify the critical failure mode and provide a reasonable estimate of the mean load carrying capability of the element/sub-component. Both damaged (representing undetected impact damage) and undamaged elements must be tested

Design and test full-scale components representing major portions of the aircraft structure such as wing torque box structure, landing gear support structure, arresting gear support structure, and horizontal tail support structure. For certification of these development structures, design verification test loading must be established such that the test data and failure mode will be applicable to the full-scale static test airplane. The importance of applying proper load distributions and boundary conditions can not be over emphasized. Extensive strain gage coverage of the test specimens is necessary since the certification process requires correlation of measured strains on the static test aircraft with strains measured on the appropriate design verification test specimens.

Prior to testing elements and sub-components, predicted failure modes and failure loads must be determined. All specimens should be loaded to failure and strains (at failure) determined for each specimen type. Premature failure or failure in an unanticipated failure mode are indications of deficiencies in the design and/or analysis. Such events require in-depth evaluations to implement necessary corrections before proceeding to tests at the next level of complexity. Where multi modes of failure are observed in a certain specimen type, additional tests are recommended to determine the most critical failure mode and the associated mean strength.

Composite structures must demonstrate the same strength reliability as conventional metal structures. Traditionally, metal structures have been required to demonstrate the ability to sustain 150% design limit load (DLL). On the assumption that the test article represents a mean fleet aircraft and the scatter in static strength is known, the reliability to sustain maximum service loads can be calculated (Reference 1). Typically, the maximum service load experienced by Navy fighter aircraft in service is approximately 125% DLL. A 95% confidence reliability at 125% DLL demonstrated by a single metal structure ( $\alpha$  = 30) tested to 150% DLL is computed at 0.99274. To demonstrate the same reliability with 95% confidence (temperature and environmental effects ignored), a single composite structure where  $\alpha = 20$  must sustain 164% DLL. If the test is performed under ambient temperature and dry conditions, the effects of the temperature and moisture absorption on static strength must also be considered. Consequently, the minimum acceptable test failure load must account for static strength variability and environmental effects. For example, if an environmental knockdown factor of 15% is used to account for

compression failure strength of composites under hot and wet conditions, and if the scatter in the compression static strength data was described by  $\alpha$  = 20, then the minimum acceptable test failure load for a compression failure should be 193% DLL instead of the traditional 150% DLL for metal structures.

#### FATIGUE TESTS

Due to the large scatter in composite structure fatigue life, a two lifetime fatigue test will not demonstrate the same reliability as demonstrated with metal structure. A composite structure could require testing to more than fifty (50) lifetimes to achieve the same reliability. Since this is not practical, tests of all-composite components should be performed using the load enhancement factor approach described in reference 1. In this approach, all loads in the test spectrum are increased by a factor sufficient to demonstrate the desired fatigue reliability in a two lifetime fatigue test. Load enhancement factors may be calculated using procedures described in reference 1. For the typical composite fatigue life where  $\alpha=1.25$ , and for a static strength where  $\alpha=20$ , the load enhancement factor is 1.15. All loads in the fatigue test are multiplied by this factor and a two lifetime test performed.

In the certification of mixed metal-composite structures, i.e. structures with both metal and composite components, the higher loads dictated by the load enhancement approach may cause premature failure in the metal components before substantiation of the fatigue strength of the composite components can be accomplished. Consequently, a two lifetime unfactored test to demonstrate adequate metal fatigue life is recommended followed by a two lifetime test using the load enhancement factor to substantiate the fatigue life of the composite components. This approach, as might be suspected, has a significant disadvantage in that it might require costly repair and/or replacement of metal components.

An alternate test method to certify mixed metal-composite structure was proposed in reference 1. In this test method, occasional high loads are introduced into the spectrum. The number and magnitude of these high loads are selected to demonstrate the same composite fatigue reliability as the load enhancement approach (all loads increased), while maintaining metal fatigue life at a constant value due to beneficial retardation effects. Consequently, the composite parts and the metal parts are tested adequately in fatigue with minimal risk of premature and unwanted failures of the metal parts. This approach significantly reduces the problems associated with fatigue testing of mixed metal composite structure and should be explored in more detail and verified experimentally.

#### FULL-SCALE TESTING

#### STATIC TESTS

By specification, test conditions that do not require test to failure must be successfully performed to at least 150% DLL without failure. For each test condition, prior to testing, the critical areas must be identified and

the environmental strain allowables clearly defined. During static testing, measured strains in composite structure at 150% DLL must not exceed the previously defined design allowable strains. These measured strains (in the critical areas) must agree with the strains measured on the design verification test specimen(s). These comparisons are required to provide confidence that the full-scale static test article does in fact have the strength characteristics demonstrated by the design verification test article.

Typically, the Navy requires full-scale static testing to failure for the most critical condition. An inherent part of this test program is the definition of critical area(s), failure load, failure mode, failure strain, and environmental design allowable strains prior to actual testing. Additionally, the minimum acceptable failure load required to demonstrate the required reliability shall be established for the predicted failure mode. As previously discussed in the section on structural design development static tests, definition of the minimum acceptable failure load must account for static strength variability and the effects of the critical environment. If, for example, the static strength  $\alpha$  for the predicted failure mode is 20 and the environmental knockdown factor is 15%, the minimum acceptable failure mode to demonstrate a reliability of 0.99274 is 193% DLL. A test is considered acceptable when the failure load is equal to or exceeds the minimum acceptable failure load and when measured strains at 150% DLL do not exceed allowable strains for the worst case environment. Direct agreement of full-scale test strains with those measured on the design verification specimen(s) in all critical areas must also be established.

When the test structure includes metal(s) and composite(s), the failure of a metal part prior to satisfactory demonstration of the static strength of the composite part(s) requires extrapolation of measured strains in the critical areas of the composite structure to the point corresponding to the minimum acceptable failure load. The extrapolated strains must not exceed the mean failure strains obtained from the results of successful design development tests. All significant test variations from analytical predictions require thorough investigation and reporting to the procuring activity for review and approval.

#### FATIGUE TESTS

The load enhancement factor approach as described earlier may be used for an 'all-composite' structure. For mixed metal-composite structure a two lifetime unfactored test to demonstrate adequate metal fatigue life is recommended followed by a two lifetime test using the load enhancement factor to substantiate the fatigue life of the composite components.

#### CONCLUSIONS

Static strength certification of composite and mixed composite/metal structures can be achieved (with the same degree of confidence now attained for all-metal structures) using the procedures presented in this paper.

A comprehensive certification plan must be developed by the airframe manufacturer and approved by the contracting agency before the structural

design is finalized. All testing in a composite aircraft development program must be considered as part of the certification process.

The highest test load used for certification of a composite structure depends on the strength scatter for the particular material and type of construction used and on the failure mode of the structure which sustains the final failure.

Fatigue certification of mixed composite/metal structure is difficult to achieve by a single test due to significant scatter of composites. The method of introducing occasional high loads in the load spectrum should be investigated further and experimentally validated.

The certification process for composite structures demands a thorough, timely, and well planned program to achieve reliability goals.

#### REFERENCES

- 1. Whitehead, R. S., Kan, H. P., Cordero, R., and Saether, E. S., 'Certification Testing Methodology for Composite Structures,' Report NADC-87042-60, October 1986, Volumes I and II.
- 2. Sanger, K. B., 'Certification Testing Methodology for Composite Structures,' Report NADC-86132-60, January 1986.
- 3. Kan, H.P., Cordero, R., and Whitehead, R.S., 'Advanced Certification Methodology for Composite Structures,' Northrop Corporation, NADC Contract No. N62269-87-C-0259, Report to be published.
- 4. Rapoff, A.J., Dill, H.D., and Sanger, K.B., 'An Improved Certification Methodology for Composite Structures,' McDonnell Aircraft Company, NADC Contract No. N62269-87-C-0258, Report to be published.
- 5. Lincoln, John W., 'Certification of Composites for Aircraft,' Paper presented at the 1986 USAF ASIP Meeting, Sacramento, CA.
- 6. Whitehead, R. S. 'Lessons Learned for Composite Aircraft Structures Qualification,' paper presented at the 1987 Aircraft/Engine (ASIP/ENSIP) Conference, San Antonio, TX, 1-3 December 1991.
- 7. Bhatia, N. M., 'Impact Damage Tolerance of Thick Graphite/Epoxy Laminates,' Report No. NADC-79038-60, January 1979.

#### CT114 TUTOR WING FLIGHT LOAD SURVEY

by

Mr. Bruno Mercier Military Aircraft Division Bombardier Inc. Capt. John F. Peetsma Directorate Aerospace Support Engineering National Defense Headquarters

1

#### SUMWRY

A flight test program to measure the wing loads and strains on the Canadian Forces CT114 Tutor was recently completed. This program was conducted to assess the wing design loads and to better define the wing load spectrum. This is part of the CT114 ASIP activities to provide data for safe airframe operation up to the Tutor retirement date.

This paper first gives an overview of the load measurement system. It reviews the basic concepts used for measuring the loads and discusses the results of the load calibration. Key elements that have a direct impact on load measurement are highlighted.

The paper then describes the data acquisition, processing and verifications carried out during the flight tests. Activities such as the verification of signal saturation, calibration checks, response to reference manoeuvres and derivation of load offsets are discussed. These activities are considered important as they determine the accuracy and reliability of the loads measured. In view of the data verifications, preliminary results for severe flight conditions are discussed.

#### 1.0 INTRODUCTION

The Tutor Wing Flight Load Survey was undertaken in 1987 to assess the wing design loads and to better define the wing load spectrum. This in-flight investigation was mainly justified by the fact that the wing loads had never been measured in-flight and that a flight load survey of the Tutor tail carried out in 1978-80 indicated loads in excess of the design limits (Ref.1).

In both above flight load surveys, load measurement was accomplished by numerically combining strain gauge responses, as originally described in NACA 1178 (Ref.2). The application of this technique involves extensive strain gauging, load calibration and large capacity data acquisition and processing systems. Experience has shown that this technique is subjected to a number of problems such as the hysteresis and nonlinearity of the structure or the drift of the strain gauge sensitivity and offset. During the Tutor Wing Flight Load Survey, effort was made to understand these problems and minimize their effect on the measured loads. Several data verification techniques were used during the flight tests to keep track of the accuracy of the loads and to ensure that the recorded data was free of discrepancies.

The paper first describes the technique used to measure the loads, how it was applied and what difficulties were encountered. The paper then gives a description of the data verifications carried out during the flight test phase followed by a discussion on the measured wing loads for two severe manoeuvres. Finally, the paper concludes with a discussion on the achievement of the program's objectives and on the lessons learned.

#### 2.0 LOAD MEASUREMENT SYSTEM

Flight load measurement is accomplished by numerically combining strain gauge responses in order to isolate the desired load components (Ref.2). Figure 1 illustrates the load measurement principle. A structure is first strain gauged. Various load cases are applied to the strain gauged structure to simulate the expected operational loads. The recorded applied loads and strain gauge responses are used to develop the regression models that will best predict the loads. These regression models, referred to as load equations, are then used to convert the in-flight strain gauge responses into flight loads.

For the Tutor Wing Flight Load Survey, it was decided to measure the shear, bending and torque at both left and right wing roots and at three additional right hand wing stations, as shown in Figure 2. This selection of loads allows for the comparison between left and right wing loads and for the comparison of the measured wingspan load distribution against the analytical prediction.

#### 2.1 Strain Gausing

Figures 3 and 4 show the location of the strain gauge bridges installed to record the wing loads. Primary and secondary bridges were installed at each location, for a total of 116 channels. Each strain gauge bridge was connected in either axial or shear Wheatstone bridge compensated for temperature. All strain gauge bridges were wired to the left or right wing root connectors for interfacing with the load calibration data acquisition system or with the flight data acquisition system.

#### 2.2 Load Calibration

The load cases used to calibrate the wings are summarized in Figure 5. These load cases exercised the wing up to 40 % of the maximum design shear/bending and up to 27% of the design torque. They also permitted the investigation of unwanted effects such as local loading, carry-over loads and longitudinal loads. These effects are discussed below with the load equation derivation.

The following scheme was used to perform the calibration load cases:

- a) A calibration loading rig mainly consisting of a base grillage was designed to hold the test aircraft by its fuselage jacking points and to hold the loading actuators in place, as shown in Figure 6. This scheme was adopted because any calibration load cases could easily be repeated at any time during the flight tests. However, it put a restraint on the magnitude of the asymmetric shear loads that could be applied without damaging the fuselage jacking points.
- b) The vertical loads were applied at the spar/rib intersections through simple wood and rubber pads. Up loads were transferred through the lower skin. Down loads were transferred through the upper skin with the use of collar assemblies. Pure torque loads were also applied with collar assemblies. Contour boards were not used since the chordwise load position must be known. Longitudinal aft loads were applied through the flap and aileron hinges.

In addition to the wing loads, the end loads and bending loads at the aileron and flap hinges of the right wing were recorded. Each of these loads was obtained from a single bridge configured to isolate the desired load. These hinges were calibrated by applying end loads, bending loads and combined end/bending loads.

#### 2.3 Data Acquisition

The data was recorded with a 11 bit ground based data acquisition system. Shunt tests were performed during the calibration period to ensure there was no gain drift from the signal conditioner.

For each calibration load case, three loading/unloading cycles were performed. Loads and strain gauge responses were recorded at every 20% increment/decrement of the maximum load, for a total of 30 samples per load case.

For each strain gauge and each load case, a linear regression was then performed between the strain gauge response and the load. The slope of this regression, referred to as influence coefficient, measures the strain gauge sensitivity to a given load. The regressions resulted in an influence coefficient matrix of 116 by 58, defining the response of each strain gauge to each load case. The regression coefficient ( $R^2$ ) computed with each regression was also kept as a measure of the variance of the strain gauge responses.

#### 2.4 Load Equation Derivation

Each load equation is obtained by performing a multiple linear regression between the load and the strain gauge responses. A set of load cases and strain gauges must therefore be selected for each regression. The following criteria were used to select each set:

- a) The strain gauge had to be located at the wing station where the load was measured;
- b) The load cases had to be outboard of the strain gauges used and sufficiently far away to not cause local loading effects. Local loading was verified by plotting a given strain gauge response versus the position of the load application point, as shown in Figure 7;
- c) Primary and secondary strain gauges were not used in the same load equation since they often had the same sensitivity to bending and torque loads. Mixing of strain gauges with the same sensitivity in the same load equation can cause the regression to be close to an indeterminate system. This can result in load equations having two strain gauges that cancel each other, a situation that can result in large errors;

d) Strain gauges with a  $R^2$  value below 0.990 were avoided in 75% of the load cases used in a given regression. The other 25% of strain gauge/load case combination had  $R^2$  values above 0.950:

The sensitivity of the strain gauges to an applied load on the opposite side of its location, referred to as carry-over load, was also verified. Carry-over bending cases were limited to 5% of the design limit bending. However, carry-over torques up to 27% of design limit were applied. It was found that no strain gauges presented significant sensitivity to these carry-over loads.

The regression analysis was then performed using the following iteration procedure:

- a) The regression was first carried out with all strain gauge/load case combinations that met the above criteria.
- b) The contribution of each strain gauge in a given load equation was weighted by the modified T-value as defined in Ref.3. The T-value of a strain gauge is a measure of its standard error, its sensitivity to the loads and its uniqueness in measuring the loads;
- c) The strain gauge with the least contribution was rejected;
- d) The regression was carried out again;
- e) Steps b), c) and d) were repeated until 3 strain gauges were left.

The probable error of each iteration was then plotted against the number of strain gauge participating in a given load equation. Figure 8 shows the probable error plot for the torque equations. The load equations with the least number of strain gauges and with no significant deterioration of the probable error were selected for the final evaluation of their accuracy.

#### 2.5 Load Equation Evaluation

To verify how well each load equation isolates each load component, the ratio of calculated load over applied vertical load, referred to as combined influence coefficient, was plotted as a function of the load application point position. Figure 9 shows examples of this type of plot for a bending equation and a torque equation. Equations with no errors throughout the calibration envelope would have all its points falling on the solid lines drawn on these plots. As a result of these plots, the torque equations showed the worst deviations from the solid lines, followed by the shear equations and the bending equations.

The accuracy of the load equations was further verified by performing load cases that were not part of the calibration cases. These cases, referred to as assurance tests, featured distributed load and longitudinal load cases. Table 1 lists the type of load cases that were performed and the maximum errors produced. These load cases showed that most load equations were sensitive to longitudinal loads.

An additional evaluation of the accuracy of the load equation was performed by combining the strain gauge response obtained during the calibration load cases in order to simulate typical flight load distributions, as described in Ref.4. Three flight load distributions were simulated. Design limit aft longitudinal loads were also superposed to these three flight load distributions. Table 2 lists the maximum errors obtained for these cases. These results showed two limitations to the load equations:

- a) The errors are not proportional to the magnitude of the loads applied. For small applied loads, the errors were generally the same as for large applied loads.
- b) For the highest longitudinal load conditions, the load equations deviated by up to approximately 10% of the design loads.

Attempt was made to reduce these problems by rederiving load equations with different combinations of strain gauges that appeared to have lower hysteresis and less sensitivity to longitudinal loads. The resulting load equations still had approximately the same limitations.

For the measurement of most high load conditions, these limitations were judged acceptable. However, they did show that the load equations were fairly inaccurate for small load conditions.

#### 3.0 FLIGHT TESTING

The flight test phase was generally divided into the planning of the test envelope and missions, the preparation of the instrumentation, the solo missions performed at Canadian Forces Base (CFB) Cold Lake/Alberta and the formation missions performed with the Snowbirds Aerobatics Team at CFB Moose Jaw/Manitoba.

A great deal of effort was spent on the preparation of the instrumentation and on the data verification performed during the tests. This section focuses on these two aspects which proved to be critical to the validity of the load measured and thus to the achievement of the project's objectives.

#### 3.1 Data Acquisition

Aircraft CT114081 had already been used during a tail load survey carried out in 1978-80 and was therefore selected as the test aircraft. A Standard Aircraft Instrumentation System (SAIS) had already been designed for that aircraft so it was adapted to record 83 strain gauge channels and 30 flight parameters at a rate of 132 samples per second for mission durations of up to approximately 60 minutes.

Figure 10 gives an overview of the main data acquisition steps. The system featured the following important characteristics:

- a) 10 VDC excitation was used for the strain gauges, as for the load calibration data acquisition;
- b) The system monitored and recorded the excitation voltage;
- c) The signals were lowpass filtered at 20 Hz before amplification and offsetting to the 0 to 5 VDC signals required for encoding into 11 bit words;
- d) On-board recording was used all the time. Real time telemetry was used for selected flights or as available.

#### 3.2 Data Processing

Figure 11 shows the basic data reduction processes performed in the flight test control room. The real time processing included decommutation of the telemetered signal, conversion into engineering units, load calculation using the load equations and plotting of the data on strip chart. Real time monitoring of the flight data was used to judge the severity of the manoeuvres flown and to time mark and identify the relevant portions of the mission.

Post-mission playback of the aircraft tape was used when the data was not telemetered properly or when there was a requirement to quickly display new load equations between missions.

Before final processing of the aircraft tape, a number of verifications were carried out on selected portions of the flight data. These verifications are further discussed below.

#### 3.3 Signal Saturation

Saturation of the signal occurs when the signal exceeds the upper or lower limit managed by the encoder (0 or 5 VDC). Figure 12 shows examples of saturated signals. The information is lost during saturation and this information is often of the most interest.

At the beginning of the flight tests, many saturation problems were encountered with the strain gauges. This was caused by difficulty in estimating the ranges and the offsets correctly. The correction of the saturation problems proved to be time consuming and sometime resulted in downtime of up to two weeks.

#### 3.4 Calibration Checks

Four calibration checks were carried out during the flight test phase. The first check was performed before the first mission to ensure that the flight data acquisition system gave the same results as the load calibration data acquisition system. The other three checks were carried out during the flight tests and after the last mission to check for any deterioration of the load measurement system. Table 3 describes the type of calibration cases used.

The strip charts were used to quickly check which load equations were not working. However, they did not show the response of each bridge participating in an equation.

To fully assess the status of the load measuring system, software was written to derive the influence coefficients for each strain gauge and the combined influence coefficients for each load equation (refer to 2.0 Load Measurement System above).

The comparison of these coefficients with the coefficients derived during the load calibration permitted identification of the load equations or strain gauges which were not behaving properly. In some cases, new equations had to be rederived. Table 4 gives typical accuracy obtained from the calibration checks. As observed during the load calibration, the worst equations were the torque and the shear equations.

#### 3.5 Response to Rollercoaster Manoeuvre

A reference manoeuvre referred to as the rollercoaster was flown one to three times per mission for all non-Snowbirds missions. A typical time history of the normal acceleration and airspeed for this manoeuvre is shown in Figure 13.

The rollercoaster manoeuvres was used to track the response of the strain gauges and load equations at a specific point in the sky used as a reference. The point in the sky was established at:

Normal Acceleration: 2.0 g
Aircraft Weight: 7000 lb
Airspeed: 250 knots
Altitude: 10,000 ft

Software was written to curve fit selected strain gauge and load equation responses with Nz*W (normal acceleration times the weight) and Q (dynamic pressure). The time history of a typical fit is shown in Figure 14. This curve fit also gave us an estimation of the zero load offset.

The responses of the load equations at the reference points in the sky were plotted to show the wingspan shear, bending and torque distributions, as shown in Figure 15. These distributions were used as a final check to ensure that the load equations generally behaved as expected.

The position of the wing load center during the reference points in the sky was also used to check the load equations. The load center position is found by dividing the wing root bending by the shear and by dividing the wing root torque by the shear. Figure 16 shows typical load centers for reference points in the sky flown during the flight tests.

#### 3.6 Strain Gauge Offsets

Blocks of data were recorded on a regular basis before take-off and after landing with the aircraft in static leveled condition and engine to idle. These ground blocks were used in conjunction with the rollercoaster to establish the zero load offsets. The difference between the average response from the ground blocks and the zero load offset from the rollercoasters was estimated for each load equations. These deltas were then used for the missions that did not contain any rollercoasters.

#### 3.7 Response to Symmetric Pull Up

The response of the best set of load equations during severe manoeuvres was then looked at more closely. Figure 17 shows the time history of the root bending and torque equations for a typical 7 g symmetrical pull up. The amplitude of the load cycle for the right side is within 10% of the left side, although a balance condition was expected. Furthermore, the measured load extrapolated to a 7.33 g condition is within reasonable limits of the design condition. However, a more rational extrapolation that takes into account the aircraft weight, CG location and elevator deflection will be carried out before the design conditions are assessed.

#### 3.8 Response to Rolling Pull Out

Figure 18 shows the time history of the root bending and torque equations for a typical 5 g left rolling pull out. The manoeuvre is initiated by a right spiral dive in order to set the load factor to 5 g. Abrupt deflections of the aileron to the left is applied. This results in a sudden nose down torque on the right wing. A g relief then follows the peak roll acceleration. This relief results in a bending and a torque relief on both wings. The torque relief on the left wing significantly limits the nose up torque induced by the aileron up deflection.

As for the symmetrical pull up, the measured rolling pull out loads will be extrapolated to the design conditions. This extrapolation will consider, as a minimum, the aircraft weight, CG location, load factor, aileron position, roll rate and roll acceleration.

#### 4.0 DISCUSSION AND CONCLUSION

Although calibrated strain gauge load measurement is fairly simple in theory, it's application to a full scale structure such as a wing requires a great deal of effort in the following areas:

- a) Strain gauging,
- b) Fabrication and use of a loading rig,
- c) Data acquisition and processing, and:
- d) Calibration checks and data verifications during the flight tests.

The results obtained during the Tutor Wing Flight Load Survey have confirmed that a strain gauge calibrated load measurement system has some limitations in accuracy and cannot be used blindly throughout the flight test envelope. The best set of load equations that could be derived during this project still remained inaccurate at predicting small shear and torque loads. These limitations were judged acceptable for the purpose of verifying the wing design loads. However, they might not be acceptable for the purpose of deriving fatigue spectrum.

The load equations also proved to be very sensitive to common problems that are typical of in-flight strain measurement such as signal saturation, drifting of the strain gauges sensitivity and offset, and; deterioration of the strain gauges. However, these problems can be detected early by carrying out a number of data verifications before and during the flight tests. The calibration checks and the response to rollercoaster proved to be essential at detecting and troubleshooting the load equations that did not work properly. The results of these data verifications also served to gain confidence in the flight data for the post flight data analyses.

#### List of References

- [1] AGARD Conference Proceeding No. 375, TUTOR (CL-41A) Tail flight Load Survey by A. Paquin and J. Skotnicki, April 1984
- [2] MACA Report 1178, Calibration of Strain-Gauge Installation in Aircraft Structures for the Measurement of Flight Loads, by T.H. Skopinski, W.S. Aiken Jr. and W.B. Huston, 1954
- [3] NASA Technical Paper 1748, A Modified T-Value Method for Selection of Strain Gages for Measuring Loads on a Low Aspect Ratio Wing, M.H. Tang and R.G. Sheldon, 1980
- [4] NASA Report TM 56047, A Study of the Effect of Radical Load Distributions on Calibrated Strain Gage Load Equations, July 1977

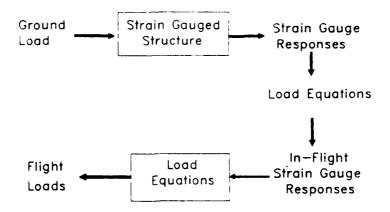


Figure 1 Load Measurement Principle

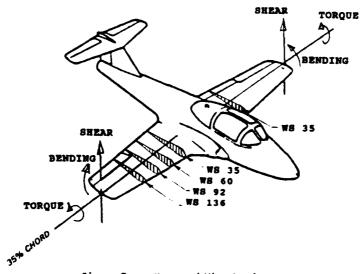


Figure 2 Measured Ving Loads

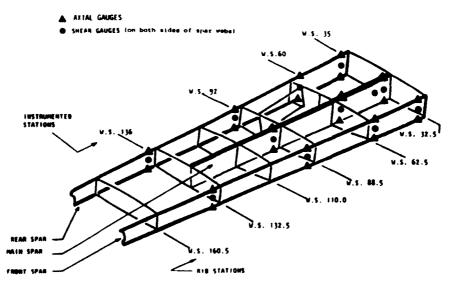
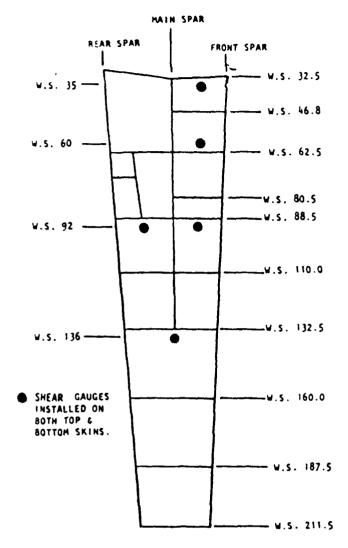


Figure 3 Spar Cap and Spar Web Strain Gauge Locations



TYPE OF LOAD	MAGNITUDE
	17 %
	40 %
	26 %
	27 %
	40 %

Figure 4 Skin Strain Gauge Locations

Figure 5 Calibration Load Cases

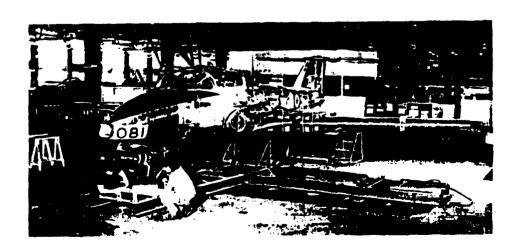


Figure 6 <u>Calibration Loading Rig</u>

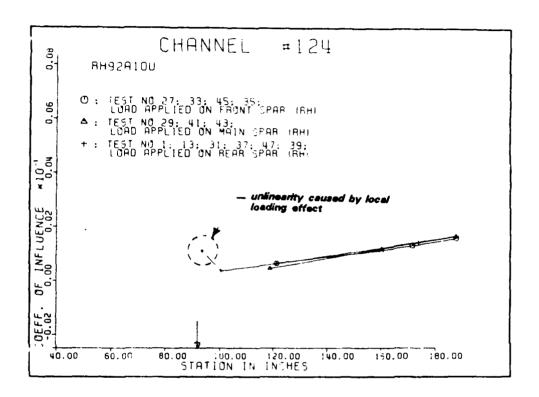


Figure 7 Example of an Influence Coefficient Plot

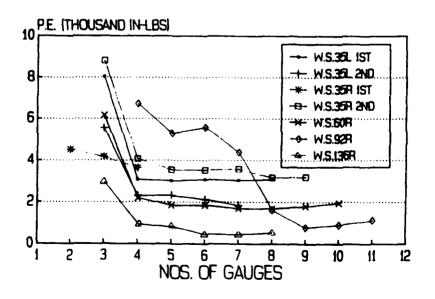


Figure 8 Probable Error for the Torque Equations

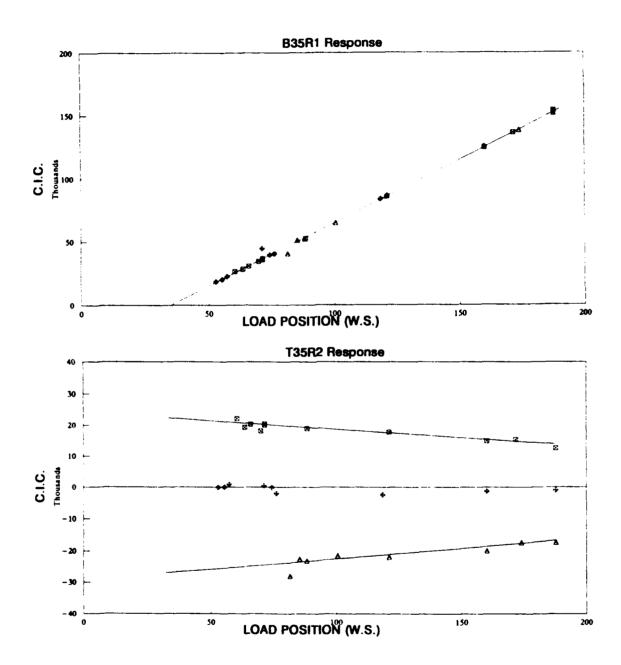


Figure 9 <u>Examples of Combined Influence Coefficient Plots</u>

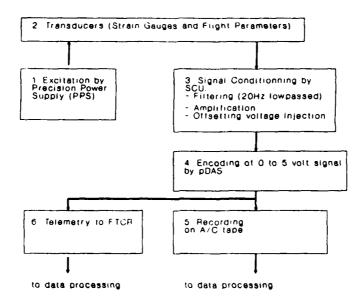


Figure 10 Data Acquisition

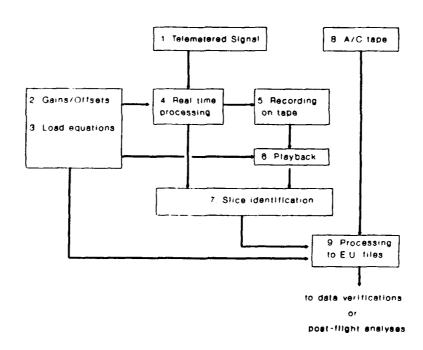


Figure 11 Data Processing

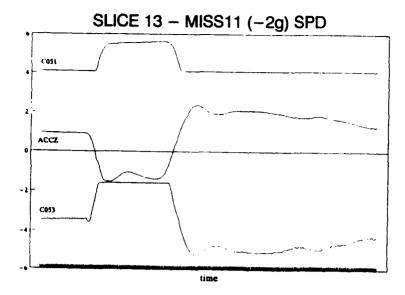


Figure 12 <u>Examples of Saturation</u>

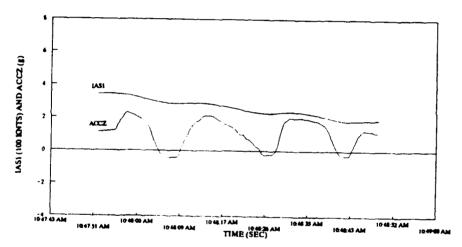


Figure 13 Rollercoaster Manoeuvre

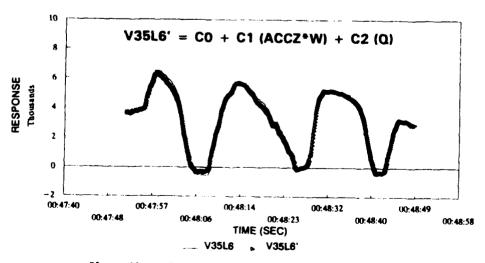


Figure 14 <u>Example of Curve Fit Time History</u>

## 2.0 g / 250 knts / 7000 lbs

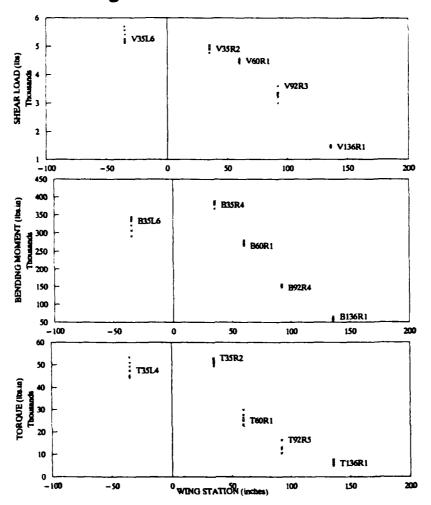


Figure 15 <u>Vingspan Load Distribution</u>

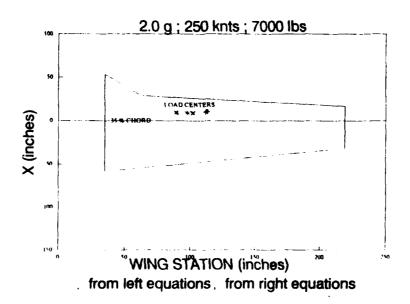


Figure 16 <u>Heasured Wing Load Center</u>

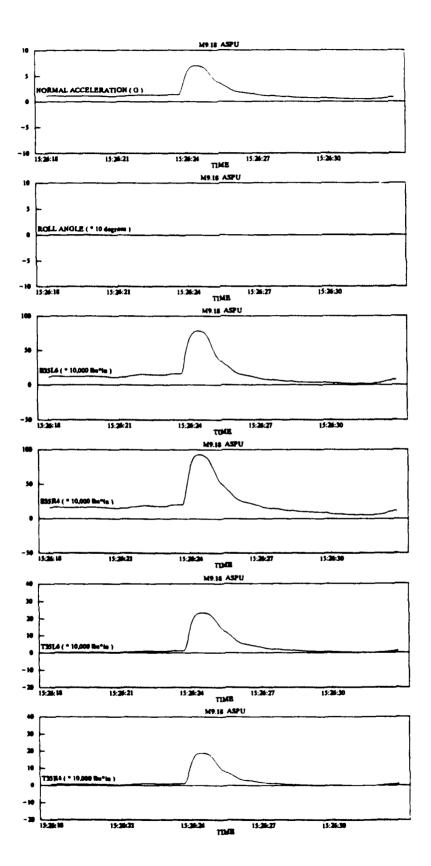


Figure 17 Symmetric Pull up Root Bending and Torque

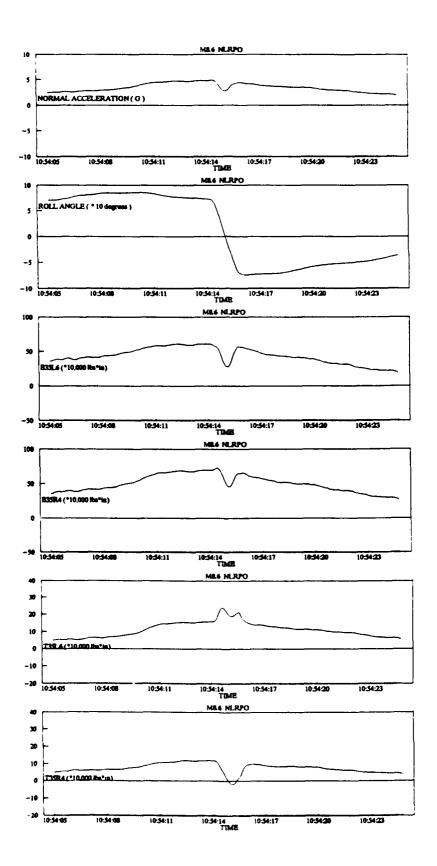


Figure 18 Rolling Pull Out Root Bending and Torque

ltem	Load Condition	Load Magnitude (% of design)	Shear Equations Max Error	Besding Equations Max Error	Torque Equations Max Error
1	Distributed Shear and Torque	20 %	- 5.5 %	+ 6.3 %	+ 0.83 %
2	High Distributed Shear (no Torque)	4() %	+ 4.1 %	+ 0.95 %	4500 lbs*in
3	Load (no Shear and no Torque)	40 %	78 lbs	- 5200 lbs*in	3400 lbs*in

Table 1 Load Equation Accuracy for the Assurance Tests

Item	Type of Load	Shear Equations		Beading Equations * 1000 fbs*in		,	Torque Equations 1000 ibs*in	
		Applica	Error	Applied	Error	Applied	Errot	
1	Rolling Pull out W/O Longitudinal Load	+14700	-309	+1272	-12.2	+45.3	+4.8	
2	Flap Manoeuvre W/O Longitudinal Loads	+ 7600	-219	+628	-7.6	-8.5	-6.4	
3	Flap Manoeuvre with Longitudinal Loads	+7600	-1280	+628	-413	-8.5	-11.8	

NOTE: (+) for vertical up load and nose up torque

Table 2 Load Equation Accuracy for the Flight Load Distribution Cases

Item.	Description of Load Cases	Shear (ibs)	Torque (* 1000 lbs*in)
1	Symmetric Shear at Front Spar/ W.S. 160	+1400	+21,560
2	Symmetric Shear at Rear Spar/ W.S. 160	+1000	-18,480
3	Pure Torque at Right W.S. 160	0	+16,940
4	Pure Torque at Left W.S. 160	o	+ 16,940
5	Pure Torque at Right W.S. 80	0	+113,622
6	Pure Torque at Left W.S. 80	0	+113,622

NOTE: (+) for vertical up load and nose up torque

Table 3 <u>Calibration Checks performed during</u> the Flight Test Phase

Load	2nd Ground Ch	ck Calibration
Equation	Max Error	Error
No.	(%)	(%)
V35L6	+ 8	- 0.86
V35R2	+ 3	- 5.2
V60R1	+ 11	- 1.7
V92R3	+ 11	+ 5.1
V136R1	+ 8	+ 1.4
B35L6	+ 1.6	- 5.6
B35R4	- 3.2	- 0.92
B60R1	+ 5.7	- 1.6
B92R4	+ 4.9	- 0.10
B136R1	+ 6.3	- 0.33
T35L4	+ 11	+ 4.4
T35R2	+ 9.0	- 3.4
T60R1	+ 11	- 4.0
T92R5	+ 9.1	- 1.2
T136R1	- 7.0	- 0.70

Table 4 Typical Accuracy from the Calibration Checks

# PROBABILISTIC DURABILITY EVALUATION OF ALCOA 7050 ALUMINUM

JOSEPH G. BURNS JAMES L. RUDD JAMES A. HARTER WL/FIBEC PAUL E. MAGNUSEN ANDREW J. HINKLE ROBERT J. BUCCI ALCOA

## 1991 USAF STRUCTURAL INTEGRITY PROGRAM CONFERENCE

#### Slide #1. TITLE

This is a briefing on the work the Flight Dynamics Directorate of the Wright Laboratory is performing in the area of structural durability. The work that is being presented is a collaborative effort with Alcoa, but concentrates on the work performed by the Air Force. The probabilistic approach that is described in this briefing was developed by Dr Sherrell Manning of General Dynamics/Fort Worth Division under contract with the Flight Dynamics Directorate.



## **OUTLINE**

- Background / Objective
- Deterministic Durability
- Probabilistic Durability
- Test Program
- Results
- Conclusions

#### Slide #2. OUTLINE

This briefing consists of a description of the background of the Air Force - Alcoa collaborative effort, followed by the objectives of this effort. Then a summary of the deterministic and probabilistic approaches to durability analysis will be presented. Next, the test program the Flight Dynamics Directorate conducted on Alcoa's 7050 thick plate aluminum will be described. The results of this test program are summarized and conclusions are made.



## BACKGROUND

- Air Force / Alcoa Collaborative Effort
- Current Production Techniques for 7050-T7451 are better than previous techniques (1984)
- Better Material Quality for Current Techniques (Less Microporosity)
- Longer Fatigue Lives for Round-Bar Specimens
- Question: Does Longer Fatigue Life Occur for Structural Details?

#### Slide #3. BACKGROUND

Alcoa's current production techniques for 7050-T7451 thick plate aluminum are better than they were in the past (1984). The difference is that the current techniques produce a better quality aluminum characterized by less microporosity. Testing by Alcoa showed that simple round bar specimens made of aluminum produced with the current production techniques showed longer fatigue lives than those produced with the old production techniques. The question that arizes is will structural components also show an increase in life with an increase in material quality?



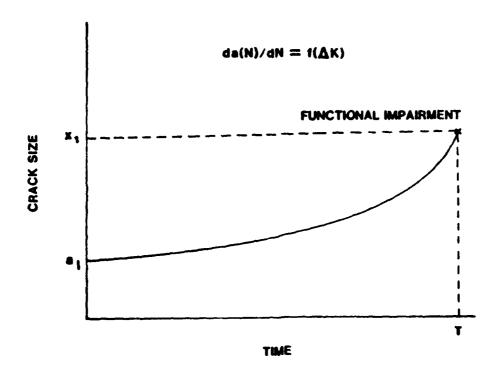
## **OBJECTIVES**

- Determine Effect of Material Quality on Structural Durability
- Assess Capability of Probabilistic Fracture Mechanics Approach to Predict Structural Durability
- Assess Benefits of Probabilistic Approach

#### Slide #4. OBJECTIVES

The Flight Dynamics Directorate has three main objectives in performing this research. The first objective is to determine the effect material quality has on structural durability. It would seem reasonable that a structure made with better quality material would last longer than one made with material of a lesser quality. However, it is not known just what role material quality plays in structural durability once the material has been machined, since the machining and assembly processes are sources of flaw introduction. The second objective is to evaluate the probabilistic fracture mechanics appoach that was developed by General Dynamics under contract with the Flight Dynamics Directorate. The third objective is to assess the benefits of this probabilistic approach.

### **DETERMINISTIC APPROACH**

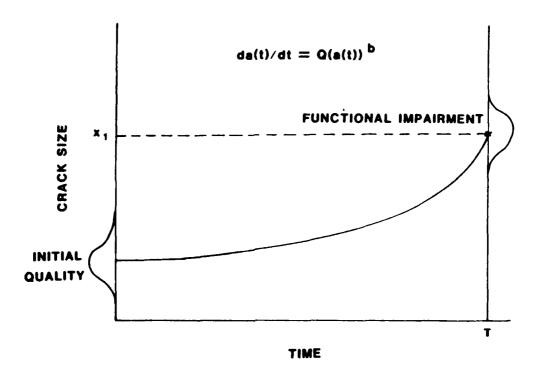


#### Slide #5. DETERMINISTIC APPROACH

In the deterministic durability approach, a flaw of a given size is assumed to be present in a structural detail. The growth of this flaw is then modeled deterministically using the loading that the structure is expected to see in service. The crack growth rate is a function of the change in stress intensity factor (function of stress, geometry and crack length). The flaw is analytically grown until it reaches a size that would cause functional impairment which would be characterized by fuel leakage, loss of cabin pressure, etc. The requirements are that functional impairment shall not occur before two design service lifetimes.

#### PROBABILISTIC APPROACH

#### **DETERMINISTIC CRACK GROWTH**



Slide #6. PROBABILISTIC APPROACH (DETERMINISTIC CRACK GROWTH)
In one probabilistic approach to durability, the starting crack size that is assumed to be present in the structural detail is a distribution of crack sizes. This distribution of crack sizes is determined by a deterministic exponential back extrapolation model that makes use of the crack size versus time relationship for a number of test specimens. This distribution of initial crack sizes is referred as the Equivalent Initial Flaw Size (EIFS) distribution. This distribution is then analytically grown forward in time in the same deterministic manner in which it was back extrapolated. This is used to determine the distribution of crack sizes at any service time.



## Test Program

- 2 Qualities of 7050 Aluminum
  - "Old" Quality 1984 production techniques
  - "New" Quality Present production techniques
- 2 Specimen Types
  - 2 Open Hole
  - 24 Open Hole
- F-16 400 hour spectrum
- 4 Maximum Stress Levels

#### Slide #7. TEST PROGRAM

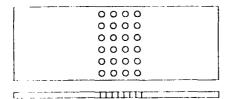
In the test program that was performed in this effort, two different qualities of 7050 thick plate aluminum were tested. "Old" quality material that was produced using 1984 production techniques was tested along with "New" quality material that was produced using current production techniques. Two different specimen types were tested. The first type was a specimen containing two open holes in tandem, and the second specimen type contained 24 open holes arranged in four rows of six. Both specimen types were 3/8 inch thick in the test section and all holes had a 0.25 inch diameter. Testing of a third specimen type (butt joint) was planned, but did not produce successful failures. This specimen is currently being redesigned. Each specimen was tested using an F-16 400 hour lower wing spectrum. This spectrum was used because of its exceptional marking of the test specimen fracture surfaces. A total of four different maximum stress levels were used in the test program.



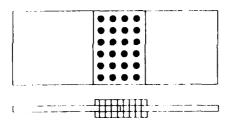
### Test Program



max stress (ksi)	32	34	37	40
# of specimens	39	60	40	60



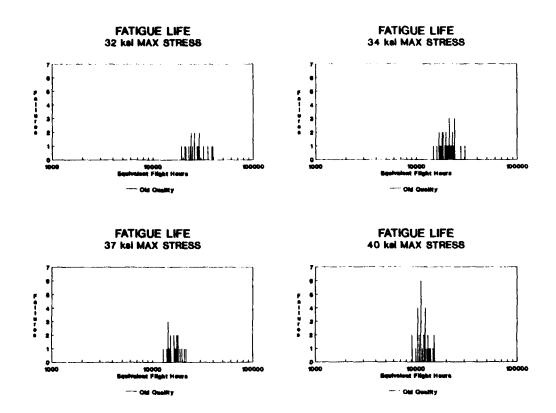
max stress (ksi)	32	34	37	40
# of specimens	_	12	12	-



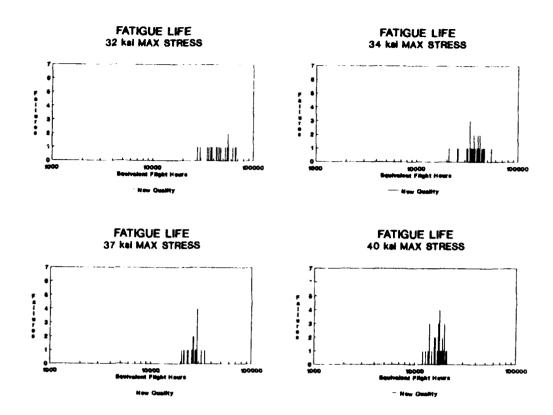


### Slide #8. TEST PROGRAM

This figure shows the specimen types that were used in the test program and the numbers of specimens that were tested at each stress level. Approximately half of the test specimens at each stress level were "old" quality and the other half "new" quality. All test results that are presented are for the two-holed specimens only.



Slide #9. FATIGUE LIFE - "OLD QUALITY"
This figure shows the number of "old" quality specimen failures that occurred versus equivalent flight hours for the two holed specimens. Equivalent flight hours is plotted on a logarithmic scale.



Slide #10. FATIGUE LIFE - "NEW QUALITY"

This figure shows the numbers of "new" qualityspecimen failures that occurred versus equivalent flight hours for the two-holed specimens. In comparing the "new" quality and the "old" quality results for each maximum stress level, it is seen that the "new" quality material gives distributions of longer lives at each maximum stress level.

### MATERIAL QUALITY COMPARISONS

(MEAN LIFE, HRS.)

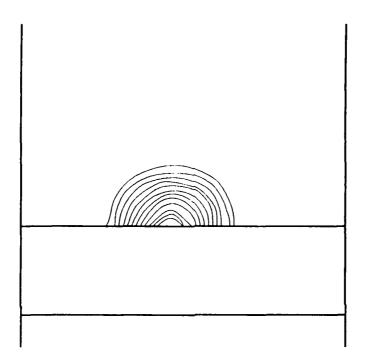
MATERIAL	σ = 32 KSI	σ = 34 KSI	σ = 37 KSI	σ = 40 KSI
QUALITY	0 = 32 K31	0 = 34 N31	0 = 37 K31	0 = 40 KSI
"NEW"	46,200	44,200	26,500	16,800
"OLD"	26,800	20,500	16,600	11,800
"NEW"	1.72	2.16	1.60	1.42

### Slide #11. MATERIAL QUALITY COMPARISONS (MEAN LIFE)

This table shows the lagarithmic mean life for each quality material at each stress level. This table shows that the "new" quality material yielded an increase in fatigue life ranging from 42 percent to 116 percent.

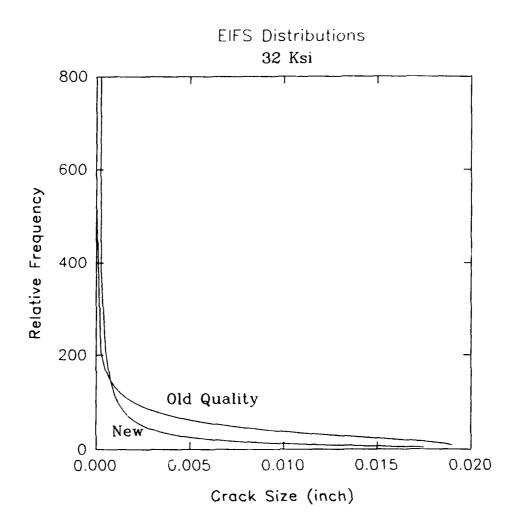


### FRACTURE SURFACE



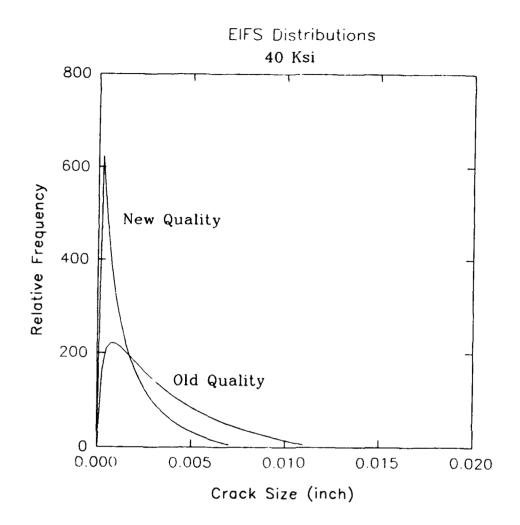
### Slide #12. FRACTURE SURFACE

This figure shows how the F-16 400 hour spectrum marked the fracture surfaces of the specimens. The fracture surfaces of the specimens were marked once each time through the spectrum. Therefore, each marker band represents 400 flight hours. In the probabilistic durability analysis, the furthest point on each marker band in the direction of crack propagation from the initiation point was recorded to produce crack length versus time data. These data were then used to calculate the Equivalent Initial Flaw Size (EIFS) for each specimen. The EIFSs were then pooled to produce the EIFS distribution for each quality specimen at each stress level.



Slide #13. EIFS DISTRIBUTIONS (32 KSI)

This figure compares the distributions of Equivalent Initial Flaw Sizes for the "old" and "new" quality specimens that were tested at a maximum stress level of 32 ksi. As can be seen from this figure, both qualities show distributions ranging from 0 to about 0.02 inch. As expected, the "new" quality specimens have a higher relative frequency of crack sizes skewed toward 0 than the "old" quality specimens. Also, the "new" quality specimens possess a thinner and shorter tail than the "old" quality at larger crack sizes.



### SLIDE #14. EIFS DISTRIBUTIONS (40 KSI)

This figure compares the distributions of Equivalent Initial Flaw Sizes for the "old" and "new" quality specimens that were tested at a maximum stress level of 40 ksi. As can be seen from this figure, the distributions have shorter, thicker tails at the larger crack sizes than the 32 ksi case. Also, the largest relative frequency of crack sizes are shifted to slightly larger crack sizes than the 32 ksi case. Consistent with the 32 ksi case, the "new" quality specimens show higher relative frequency at the smaller crack sizes and lower relative frequency at larger crack sizes (thinner tails) than the "old" quality specimens.



### MATERIAL QUALITY COMPARISONS (EIFS, INCH)

MATERIAL QUALITY	32 KSI (1/10,000)	40 KSI (1/10,000)
"NEW"	.0179	.0074
"OLD"	.0192	.0113
"NEW"  "OLD"	.932	.655

### Slide #15. MATERIAL QUALITY COMPARISONS (EIFS)

This table compares the values of the largest crack sizes that would be expected to be present in a structural component containing 10,000 cracks for each material quality and stress level. As is seen by this table, the "new" quality material produces smaller Equivalent Initial Flaw Sizes than the "old" quality material.



### MEAN LIFE COMPARISONS

### **32 KSI**

MATERIAL	REPAIR SIZE05"		REPAIR SIZE25"	
QUALITY	DET.	PROB.	DET.	PROB.
'NEW'	7,600	30,400	9,600	44,800
OLD.	7,600	13,400	9,600	25,200
NEW.	1.00	2.27	1.00	1.78

### Slide #16. MEAN LIFE COMPARISONS (32 KSI)

This figure compares the flight hours it would take a structural component containing a crack of an initial size to grow to a repair size of 0.05 inch and 0.25 inch for both deterministic and probabilistic analyses. These flight hours were determined starting with a 0.005 inch crack for the deterministic approach and the Equivalent Initial Flaw Size Distributions for the probabilistic approach. The probabilistic values are the times at which a crack of the given repair sizes would be expected to be present 50 percent of the time. These calculations were performed for each material quality at a maximum stress level of 32 ksi.



### MEAN LIFE COMPARISONS

### **40 KSI**

MATERIAL	REPAIR SIZE05°		REPAIR SIZE25"	
QUALITY	DET.	PROB.	DET.	PROB.
'NEW'	2,800	13,600	3,600	20,400
.OFD.	2,800	8,800	3,600	14,400
NEW.	1.00	1.55	1.00	1.42

### Slide #17. MEAN LIFE COMPARISONS (40 KSI)

This figure compares the flight hours to repair for the deterministic and probabilistic approaches with a maximum stress level of 40 ksi. As is seen from the tables at both stress levels, the "new" quality material takes considerably longer (42% - 127% longer) to reach the repair crack sizes for the probabilistic cases because of the difference in material quality. The deterministic cases however do not account for material quality. Also, the probabilistic lives are much longer than the deterministic lives. This is a result of the conservatism of the deterministic analysis and will vary depending on the confidence level chosen for the probabilistic analysis.



### **CONCLUSIONS**

- ADVANTAGES OF PROBABILISTIC APPROACH:
  - ACCOUNTS FOR INITIAL FATIGUE QUALITY
  - GIVES INFORMATION ON EXTENT OF DAMAGE
- DISADVANTAGES OF PROBABILISTIC APPROACH
  - LARGE DATABASE NEEDED
  - SUBJECTIVE
- BETTER QUALITY MATERIAL YIELDS:
  - SMALLER EIFSs (7 35%)
  - LONGER STRUCTURAL LIVES (42 116%)

### Slide #18. CONCLUSIONS

There are both advantages and disadvantages to the probabilistic approach. The most significant advantage of the probabilistic approach is that it accounts for the initial fatigue quality of the structural component. The probabilistic approach also gives a feel for the number of cracks that would be expected to be present in a structure containing a number of details that were subjected to the same loading. The disadvantages of the probabilistic approach are the need for a large database to determine the Equivalent Initial Flaw Size distributions, and the subjectivity of the method of measuring the crack size versus time. It is also concluded that a structure built with better quality materials does yield smaller Equivalent Initial Flaw Sizes and longer structural lives. More testing needs to be performed to better assess the capabilities and benefits of this probabilistic approach.

### COMPOSITE REPAIR OF AIRCRAFT STRUCTURES The Australian Experience

### By L. Molent Aeronautical Research Laboratory Melbourne Australia

ARL has pioneered the use of composite repairs to metal structures. This work has established Australia as a leading exponent of this technique in the world. Whilst initially developed for military aircraft the technique is now being applied more widely to civil aircraft. In view of the growing number of problems in the ageing aircraft fleet, economical restraints, and fracture criticality of modern designs, there is great potential for this technique to gain much wider use.

This presentation will highlight some examples of bonded composite repairs, and briefly address the philosophy behind their design.

Presented at:

1991 USAF STRUCTURAL INTEGRITY PROGRAM CONFERENCE

San Antonio, Texas 3-5 December 1991

### 1.0 INTRODUCTION

In military applications the Aeronautical Research Laboratory, Australia, has pioneered the use of bonded repairs to fatigue and corrosion related damage. This has proved to be an effective and highly cost efficient method as compared to conventional repairs. Numerous such repairs have successfully been conducted over the past 15 years, see Table 1.

The high acquisition costs associated with the purchase of modern transports and military aircraft has resulted in greater utilization of existing aircraft fleets. This trend, of operating aircraft approaching or exceeding their original design life, has been reflected in an increased number of structurally significant defects. Many joint airline, industry and airworthiness actions have addressed this issue. The recent incident, involving the Aloha B-737, dramatically illustrated the consequences of undetected multi-site damage (MSD). Essentially this failure, of the fuselage, occurred due to numerous small cracks along a fastener line linking together, causing the residual strength of the structure to be exceeded.

At present there is concern that, when repairing MSD, the close proximity of a large number of mechanically fastened repairs may lead to a compromise in the damage tolerance of the structure even though, in isolation, each repair may be satisfactory. The challenge is to develop alternative repairs to remedy such concerns. One alternative is the use of bonded composite repair techniques.

Repairs using bonded composites have numerous advantages over conventional mechanically fastened repairs [1,2]. Adhesive bonding does not result in stress concentrations due to additional fastener holes. This is particularly important for some modern military aircraft, designed under fracture mechanics principles and using finite element techniques, which produce highly structure, but without the inherent conservatism of conventional methods. In some cases, these designs cannot tolerate increased, or additional, stress concentrations, such as those produced by mechanically fastened repairs. Furthermore, composites are readily formed into complex shapes, permitting the repair of irregular components. The high degree of anisotrophy has the advantage of eliminating the parasitic stiffening of the structure in other than the desired direction. This is particularly relevant, considering current aviation practice, to the repair of MSD, which lead to the close proximity, and therefore potential interaction, of several mechanically fastened repairs. Lastly, in service damage monitoring is possible, with the appropriate fibre matrix system, by direct inspection through the repair using conventional eddy-current methods. In addition, the repair materials are themselves fatigue and corrosion resistant.

For a cracked structure a bonded repair significantly reduces the amplitude of the stress intensity factor and as a result

dramatically reduces crack growth. In many cases crack growth can be completely eliminated [1,2]. This reduction in the stress intensity factor is achieved by two mechanisms. The first is a general reduction in the net sectional stresses resulting from the addition of the repair. The second mechanism is due to the high modulus fibers attempting to hold together the adjacent crack faces, i.e. crack opening. Unlike mechanical repairs which contain some free length between the first set of fasteners and the crack, determined by tearout considerations, in a bonded repair, as the crack opens the adhesive is immediately subjected to shear resulting in transfer of load into the repair. Thus the crack opening displacements are smaller and consequently crack growth rates are substantially reduced.

Bonded repair can also be very economical to perform. In many cases repairs can be performed without access to internal surfaces, without the need to disassemble or unfurnish structure. This leads to significant man hour savings. Generally, precision tooling and frames are not required. The Australian experience has shown that application time is significantly less than for the conventional alternatives.

### 2.0 RECENT EXAMPLES OF BONDED REPAIRS

- a. C130. Stress corrosion cracking in the integral wing skin stiffeners has been a major problem. Originally, mechanically fastened repairs were conducted with limited success. In many cases crack growth continued and the stress corrosion was accelerated. A simple bonded repair was designed to prevent crack growth and protect the surface from further corrosion. In the past 15 years over 1000 such repairs have been conducted. Although the surface treatment used was basic by today's standards, no crack growth or repair degradation has been detected.
- b. Macchi. A machining error during manufacture of undercarriage wheels lead to under-dimensional wall thicknesses and subsequent fatigue cracking. A boron/epoxy reinforcement was placed at points of maximum stress, to reduce the stress concentration. This in turn lead to an increase in life from 60 landings to 1000 [3].
- c. Mirage III. A severe fatigue cracking problem developed in the lower wing skin of several Australian aircraft [4]. The region of cracking was from a fuel decant hole close to the intersection of the main spar and the root rib. A boron/epoxy repair was chosen, as its highly directional properties would introduce no local elevation of stress in the loaded spar, and eliminate mechanical damage that would occur from fasteners. Also the repair could be implemented in field conditions without wing removal. One hundred and eighty wings were repaired/reinforced in this manner. No degradation or crack growth were detected. Recently, an independent committee estimated that this procedure saved the Australian government 700 million dollars, by delaying the procurement of the F/A-18 replacement aircraft by five years.

- d. F-111C. Secondary bending in the upper wing pivot fitting integral stiffeners, resulted in compressive yielding under high positive loads. As a result subsequent negative loads produced high positive strains, due to the tensile residual component. This in turn lead to fatigue cracking. Due to the low fracture toughness of the D6AC steel, mechanically fastened repairs/reinforcements were precluded. A boron/epoxy doubler was designed to reduce the stress in the critical region by some 30% [5,6]. Full scale testing confirmed this result, and currently five reinforced aircraft have successfully completed certification testing under cold proof load conditions. This is the largest bonded composite repair program ever undertaken, each doubler consisting of inexcess of 120 plies. The reinforcement is conducted in-situ under field conditions.
- e. B-727. In order to demonstrate the durability of bonded repairs and surface treatments, several patches were bonded to environmentally aggressive locations on a B-727, at that time belonging to Ansett Airlines. The patch material chosen for this exercise was aluminum. Locations chosen included wing and vertical tail leading edges, and lower fuselage areas. Inspections conducted over the last seven years in service revealed that, although erosion of the aluminum had occurred, no evidence of bond degradation were found.
- f. Lap Joint Repairs. In light of concerns over MSD, a laboratory program to evaluate the efficiency of a bonded repair, to fuselage lap joints containing MSD, was conducted [7,8]. This showed that an order of magnitude increase in life could be achieved by bonding a boron/epoxy doubler over the lap joint. Completely severed lap joints, repaired in this manner, achieved lives greater than design requirements under aggressive environments. In order to gain further confidence in the durability of this repair scheme, a demonstrator doubler was bonded to the fuselage of a B-727 aircraft belonging to Australian Airlines. This currently has completed two years service without detectable degradation of the bonded doubler. This program was partially funded by the FAA.
- g. B-767. A relative new aircraft belonging to Ansett Airlines, was found to contain extensive corrosion damage surrounding fastener holes in the lower section of a keel beam. The damage was larger considered repairable by the manufacturer. that conventional solution was repair by replacement. As replacement components were not available, ARL was approached by the Airline to consider a bonded repair. Believing a bonded repair to be feasible, a boron/epoxy doubler, some 3ft in length and 2ins, wide was bonded to the lower inner face of the keel beam. This was intended to replace the loss strength of the beam, once the corroded material had been removed. In the worst case one third of the beam flange material, surrounding a hole, had been removed. This repair has been in service for three years, and has now a supplemental type certificate from the Australian Civil Aviation Authourity (CAA).
- h. B-747. As a further durability exercise, nine boron/epoxy patches were recently bonded to environmentally aggressive

- locations of a Boeing 747-300 aircraft owned by Qantas Airlines [8]. These locations were also chosen for their known high probability of being damaged, and included, wing and vertical tail leading edges, fuselage lap joints, upper flap surfaces, and engine cowlings. Both ambient and hot setting adhesives were used. These patches will be monitored periodically to assess the integrity of the bond.
- i. B-747. In collaboration with Boeing, four areas on the 747-400 forward fuselage fatigue test article were repaired using bonded composite doublers [9]. Locations chosen for repair allowed direct evaluation of their effectiveness by comparison to mirrored locations containing similar, yet unrepaired, cracks. These were: skin cracks at STA 560, cracks in lower corner of door 2, frame cracking lower STA 560, and frame cracking upper STA 360. The test article completed a additional 20,000 pressure cycles without any detectable crack growth.

### 3.0 DESIGN CONSIDERATIONS

In considering a bonded composite repair for a given situation, careful attention should be given to the following:

- a. Geometrical Limitations. Such factors as sharp radii and short transfer lengths may prevent the use of a bonded repair. Being of relatively large diameter, boron fibre for instance, is not readily formed around corners less than approximately 3 in. radius. Presence of protruding head fasteners may also impede application.
- b. Accessibility. Poor accessibility may prevent implementation of repair application equipment, such as vacuum bags and heating elements. Also the effects on the surrounding structure should be assessed when using heat curing adhesives. This may include the need to vent fuel cells with nitrogen, if an elevated temperature cure is to be conducted.
- c. Material Considerations and Selection. Materials selected for a repair should not degrade the parent material, for example, by introducing galvanic corrosion. Also consideration must be given to residual stresses induced, due to the differences in thermal expansion of the two materials [11]. Generally the stiffest possible material and lay-up (i.e. uni-directional) is chosen, to minimize neutral axis offset and aerodynamic interference. The choice of adhesives is critical [12]. The adhesive should have high shear modulus, shear strain capacity, peel resistance, be highly durable and cure at relatively low temperature to minimize residual stresses caused by thermal expansion mis-match between the two adherents. Modern structural film adhesive are simple to handle and generally meet these requirements.
- d. Design for Low Adhesive Stresses. Firstly, the designed repair should achieve significant stress intensity reduction at the crack tip to retard crack growth. Wherever possible, the repair should

reduce the stress intensity factor below the fatigue threshold of the material. Importantly, particularly for durability, the adhesive stresses must be kept low, generally below 40 MPa (9 Ksi). To achieve this the repair is tapered at the ends to reduce peel and shear stresses. The damage tolerance of the repair needs to be considered in the design phase. 'Handbook' solutions are available [13] for simple geometries, but as the complexity and loading of a structure increases, the finite element method of analysis should be used [14,15].

- e. Application Process. Consideration must be given to the mechanism to be used to pressurize and heat the repair. When using positive pressure, this induced load must be reacted, either through the structure or some convenient static fixture. When using vacuum pressurization there may be risk of contaminations being drawn from fastener holes and cracks, and air ingress through these areas may also lead to void formation in the adhesive. The choice of heaters and number thereof, is determined by the complexity and thickness of the structure. Care must be taken in locating the monitoring thermocouples, to ensure that no hot or cool spots exist, as these may adversely effect the cure of the repair. The temperature distribution should be verified prior to conducting the repair.
- f. Surface Preparation and Treatment. The importance of surface cleaniless cannot be overstated for any adhesive bonding process and is paramount to any successful application. The presence of contaminants or oxides severely inhibits adhesive bonding. general, the surface is degreased to remove surface contaminants, by direct application of a solvent, then abraded to expose fresh, chemically active, material. Following this, the surface is chemically treated to promote bonding. Treatments such as silane solution or non-tank anodizing, aim at the removal of surface oxides, and the promotion of an oxide layer resistant to hydration, with a microstructure which enhances interlocking of the adhesive with the surface. These steps must be preformed in sequence, as the standard of the subsequent steps depends on the latter. Care must also be taken to ensure that the surface of the repair material is meticulously clean.
- g. Quality Control. An essential step in the repair process. With any composite/adhesive system there are many protective surface films, by which the accidental inclusion of any, would lead to repair failure. Steps must be in place to ensure that an artisan preforms the required surface preparation to strict standards. Temperature and pressure must also be carefully monitored to attain proper cure, and hence, full material strength.

### 4.0 PREFERRED SYSTEM

Based on the performance of past repairs, ARL has defined standard procedures and preferred material for field repair purposes. In general, boron/epoxy doublers, epoxy/nitrile adhesive (eg. FM73),

and a surface treatment based on silane solution are used. Some of the reasons supporting this selection are as follows:

- a. Boron/epoxy has high directional stiffness and strength, with high shear and peel properties. It is readily formable at low temperatures and pressures to accommodate complex curvatures. The relatively high thermal expansion is compatible with that of aluminum and steel. As this material is non-conductive, conventional NDI methods can be used to monitor damage beneath the repair. The material is also chemically inert and as such provides corrosion protection to the repair area.
- b. Film epoxy/nitrile adhesives come in their own carriers, ensuring uniformity of thickness and are easy to handle. They possess moderately high moduli and shear yield strain, and exhibit high plastic shear strain and peel strength with reducing temperature. Their ability to gel at relatively low temperatures aids in the reduction of thermally induced stresses. Durable bonds can be achieved with relatively simple surface treatments. These materials are also resistant to most fluids commonly used in the aircraft environment.
- c. Numerous laboratory programs [14] and past repairs have demonstrated that good strength and durability can be obtained using a 1% solution of silane in deionized water, prepared fresh and used within a few hours of mixing. The solution is required to wet the surface for a period of 15 minutes, applied either by spray or clean brush. This is followed by 15 minutes of drying at approximately 80 degree C (using an oven, or heat gun for field applications). This system involves no hazardous chemicals, is environmently safe and can be applied in-situ. Silane does not encourage corrosion or hydrogen embrittlement of materials. This factor was critical in the case of the F-111 repair, in which aluminum, D6AC steel and fasteners were simultaneously treated. No other known system could be used for this application without the risk of contamination between metals.

Coupled to the surface treatment, the following steps are performed:

The surface is degreased using methly ethyl ketone (MEK) or other solvents with rapid evaporation rates. This is followed by a light grit-blasting, using 50 micron alumina grit, to expose the metal. The grit is never recycled and nitrogen is used to propel the grit, to avoid contamination by water and oils commonly found in compressed air sources. As a grit blasted surface finish is clearly visible, this is an important aid towards ensuring good surface preparation. Hand abrasion is avoided, if possible, as it is difficult to specify the degree of abrading, and embeds contaminants in grooves and scratches during the process.

Gamma-glycidoxypropyltrimethoxysilane

Similarly, solvent wiping after abrading acts to spread contaminants.

The surface of the boron/epoxy is thoroughly solvent cleaned and then lightly grit blasted to remove all the release agents which may be present on the surface.

In cases involving the repair of cracked components, the common practice of 'stop drilling' is not pursued. The reason for this is that the hole would create greater unsupported lengths, than the original crack, for the bridging repair fibers and reduce their effectiveness in preventing crack opening displacement. Also, it is generally acknowledged that the plastic zone at the crack tip induced by fatigue, plays a significant role in retardation of growth rates. Stop drilling would remove this zone. These arguments are supported by a study in [16].

### 5.0 CONCLUSION

There are many advantages and economies in the use of bonded composite repairs. Work over the last fifteen years have demonstrated the superior crack retardation attained from bonded composites. Numerous successful repairs have been conducted and are performing well in-service. With the increasing awareness of the ageing aircraft problem, more bonded repair applications will become evident. There is always the need to address the durability and serviceabilty of repair systems, and to this end several demonstrator programs, using bonded repairs, are in progress with commercial airlines and military agencies.

### 5.0 References.

- [1] Baker A.A., 'Repair of Cracked and Defective Metallic Aircraft Components with Advanced Fibre Composites: An Overview of Australian Work', Composite Struc. 2 1984, pp 153-181.
- [2] Jones, R., Molent, L., Baker, A.A. and Davis M.J. 'Bonded Repair of Metallic Components: Thick Sections', Theo. and Applied Fracture Mech 9 1988 pp 61-70.
- [3] Baker A.A., 'A Summary of Work on Applications of Advanced Fibre Composites at ARL, Australia', Composites 9 1978, pp 11-16.
- [4] Baker, A.A, et al, 'Repair of Mirage III Aircraft Using BFRP Crack Patching Technique', Theo. and App. Frac. Mech. 2 1984, pp 1-15
- [5] Molent, L., Callinan, R.J. and Jones, R., 'Design of an All Boron Epoxy Doubler For the F-111C Wing Pivot Fitting: Structural Aspects', Composite Struct. 11 1, pp 57-83, 1989.
- [6] Baker, A.A., et al, 'The Development of a Boron/Epoxy Doubler System for the F-111C Wing Pivot Fitting: Materials Engineering Aspects', Proc. Inter. Conf. on Aircraft Damage Assessment and

- Repair', Melbourne, Aust., 1991, pp 221-230.
- [7] Molent, L., Wallace, G. and Currie, A., Crack Growth and Repair of Multi-Site Damage of Fuselage Lap Joints', ARL-STRUC-TM-534, Melbourne, Aust., Feb. 1990.
- [8] Jones, R., et al, 'Bonded Repair of Multi-Site Damage', Proc Inter. Symp. on Structural Integrity of Aging Airplanes', Atlanta, Georgia, Mar. 1990.
- [9] Bartholomeusz, R.A., Paul, J.J. and Roberts, J.D., 'Application of Bonded Composite Repair Technology to Civil Aircraft: 747 Demonstrator Program', Proc. Inter. Conf. on Aircraft Damage Assessment and Repair, Melbourne, Aust., 1991, pp 216-220.
- [10] Molent, L. and Roberts J.D., 'Bonded Repair Application to the Boeing 747-400 Pressure Test Article: August 1990', ARL-STRUC-TM-573, Melbourne, Aust. 1990.
- [11] Baker A.A., Davis, M.J. and Hawkes, G.A, 'Repair of Fatigue Cracked Aircraft Structure with Advanced Fibre Composites: Residual Stress and Thermal Fatigue Studies', Proc. ICAF Conf. 1979.
- [12] Baker, A.A., 'Evaluation of Adhesives for Fibre Composite Reinforcement of Fatigue Cracked Aluminium Alloys', SAMPE Journal Mar/Apr. 1979.
- [13] Hart-Smith, L.J., 'Analysis and Design of Advanced Composite Bonded Joints', NASA CR-2218, 1974.
- [14] 'Bonded Repair of Aircraft Structure', ed.'s Baker, A.A. and Jones, R., Matinus Nijhoff Press, 1988.
- [15] Jones, R., Davis, M.J. Callinan, R.J. and Mallinson, G.D., 'Crack Patching: Analysis and Design', J. Struct. Mech., 10(2), 1982, pp175-188.
- [16] Labor, J.D. and Ratwani, M.M., 'Development of Bonded Composite Patch Repairs For Cracked Metal Structure', NADC-79066-60-Vol I, Nov. 80.

TABLE 1
SOME APPLICATIONS OF BONDED REPAIRS TO METALLIC STRUCTURES

Aircraft	Problem	Remarks
¹ C130	Stress Corrosion Cracking in aluminium wing skin stiffeners	Over 1000 repairs, no growth in 15 yrs. Approx. Savings A\$67M
Macchi	Fatigue Cracking in Magnesium Alloy Wheels	Life from 60 to 1000 Landings.Savings A\$2M
Mirage III	Fatigue Cracking in Lower Aluminium AU4SG Skin	180 Wings Repaired or Reinforced. Approx. Savings A\$28M, ('90 A\$700M procure./5yrs)
Mirage III	Fatigue Cracks in Fin Aluminium AU4SG Skin	No Growth in 8 yrs.
F-111C	Secondary Bending in D6ac Wing Pivot Fitting Leading to Fatigue Problem.	Developement Phase. 5 Aircraft Reinforced. 30% Strain Reduction.
F-111C	Stress Corrosion Cracking in 7075T6 Fuselage Console Truss	No Growth in 8 yrs.
F-111C	Stress Corrosion Cracking in 7075T6 Bulkhead.	Recent Repair.
F/A-18	Cracking in Fatigue Test 7150T6 Bulkhead	No growth in 10,000 SFH
P-3	Lightening Burn in Fuselage Skin (Graphite patch repair)	No crack initiation in 11 yrs.
B-727	Durability Exercise. Several Al. Patches	No Delamination in 8 yrs Service
B-727	Simulated Damage in Fuselage Lap Joint	No Degradation in 2 yrs Service
B-767	Corrosion Damage in Fuselage Keel Beam	No Degradation in 3 yrs Service
B-747	Durability Exercise 9 Patches	1 year in service
B-747	Cracks in Fuselage Fatigue Test Article. 4 Repairs.	No Growth in 20,000 SFH

¹ standard RAAF repair



## TECHNOLOGY DEVELOPMENT -

# AIRCRAFT REPAIRS

## WITH COMPOSITE MATERIALS

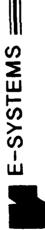
DR. JAYCEE CHUNG 1991 USAF ASIP CONFERENCE

STRUCTURE TAKES A LONG TIME TO REPAIR. THIS MEANS A HIGH REPAIR COST NEW ONE. PROBLEMS FOR THE CONVENTIONAL REPAIR ARE: 1) IT DOUBLER/TRIPLER OR REPLACING THE DAMAGED STRUCTURE WITH A CONVENTIONAL REPAIR OF A DAMAGED METALLIC AIRCRAFT WITH A LONG AIRCRAFT DOWN-TIME AND 2) IT IS HEAVY. IS EITHER REINFORCING THE DAMAGED STRUCTURE WITH

### PROBLEM

- METALLIC REPAIR OF METALLIC ACFT STRUCTURE
- TAKES TOO LONG (LONG ACFT DOWN-TIME)
- IS TOO EXPENSIVE (HIGH PDM COST)
- IS TOO HEAVY

COMPOSITE OF PROVIDES BETTER THE DETAILS FOLLOWS. REPAIR, REPAIR OF METALLIC AIRCRAFT STRUCTURE STRUCTURAL INTEGRITY WITH LOWER COST. ADVANTAGES OF COMPOSITE REPAIR ARE AS COMPARED TO THE CONVENTIONAL METALLIC



# GREENVILLE DIVISION

# COMPOSITE REPAIR OF METALLIC ACFT STRUCTURE

- PROVIDES BETTER STRUCTURAL INTEGRITY THAN METALLIC REPAIR
- COMPOSITE PATCHES ARE STRONGER AND STIFFER
  - SAVES WEIGHT AND VOLUME
- PREVENTS CRACK INITIATION AND PROPAGATION
  - PREVENTS CORROSION
- PATCH EASILY CONFORMS TO COMPLEX GEOMETRY
- SAVES REPAIR COST
- SHORTER DESIGN/REPAIR HOURS
  - SHORTER AIRCRAFT DOWN-TIME

COMPOSITE MATERIALS AND PROCESSES, SURFACE PREPARATION AND BY METALLIC STRUCTURES IS ACCOMPLISHED UTILIZING CURRENTLY AVAILABLE TECHNOLOGIES, SUCH AS ADHESIVE BONDING PROCESSES, AND FRACTURE MECHANICS REPAIR OF TECHNOLOGY COMPOSITE

OF IMPLEMENTATION E-SYSTEMS IS PRESENTLY IN THE PROCESS OF THE TECHNOLOGY FOR PRODUCTION REPAIR.

EXPERIMENT AND REPAIR DEMONSTRATION ARE THE SCOPE OF THIS THIS IS SOME OF THE WORK PERFORMED UNDER THE COMPOSITE BY DESIGN/ANALYSIS PROCEDURE DEVELOPMENT, VERIFICATION REPAIR TECHNOLOGY DEVELOPMENT/IMPROVEMENT PROGRAM PRESENTATION.

# SCOPE OF PRESENTATION

1. ANALYSIS

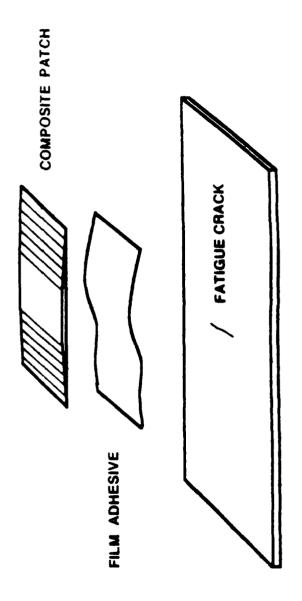
2. EXPERIMENT

3. REPAIR DEMONSTRATION

FOR THIS STUDY, A 7075-T6 ALUMINUM PANEL OF 5"W X 15"L X 0.1"T CONFIGURATION WAS SELECTED FOR METALLIC STRUCTURAL COMPONENT TO BE REPAIRED. A COMPOSITE PATCH WAS DESIGNED TO MEET THE AF163-2 FILM ADHESIVE WAS CHOSEN AND MODELED AS A BONDING COMPONENT BETWEEN THE COMPOSITE PATCH AND ALUMINUM PANEL. THE ALUMINUM PANEL FOR EACH CASE. LOAD REQUIREMENTS FOR

MATERIAL PROPERTIES AND CONFIGURATION SELECTED. EACH HYBRID MATH MODEL WAS COMPRISED OF 607 FINITE ELEMENTS (F.E.'s) AND NODAL POINT OF THE COMPOSITE PATCH F.E.'s TO A CORRESPONDING 586 ADHESIVE WAS MODELED WITH 2-D SPRING ELEMENTS CONNECTING A A CRACK ELEMENT FOR AN ALUMINUM PANEL TO BE REPAIRED, 260 2-DIMENSIONAL SPRING ELEMENTS FOR AN ADHESIVE USED, AND REPAIRS, HYBRID MATH MODELS WERE DEVELOPED BASED ON THE COMPOSITE PATCH WERE MODELED WITH Q-4 F.E.'S , AND THE TO ANALYTICALLY PREDICT THE EFFECTS OF THE COMPOSITE F.E.'S FOR A COMPOSITE REPAIR PATCH. THE PANEL AND PANEL F.E.'s. NODAL POINT OF THE

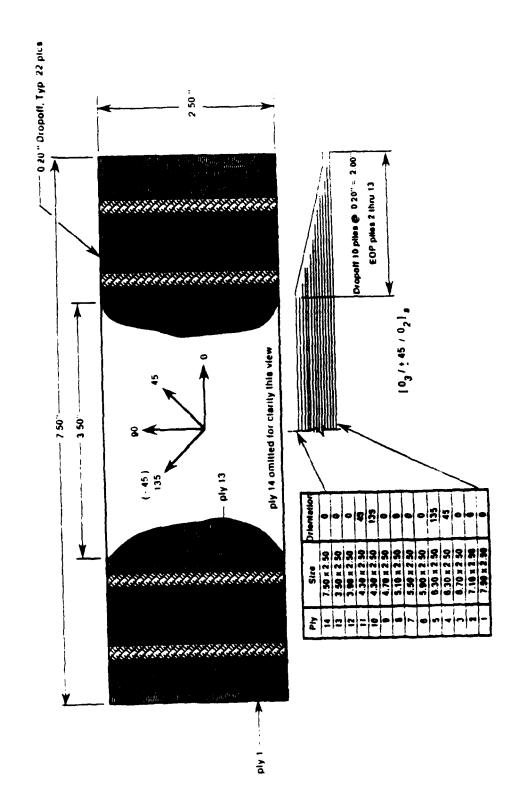
## HYBRID MATH MODEL



7075-T6 AL.UMMUM

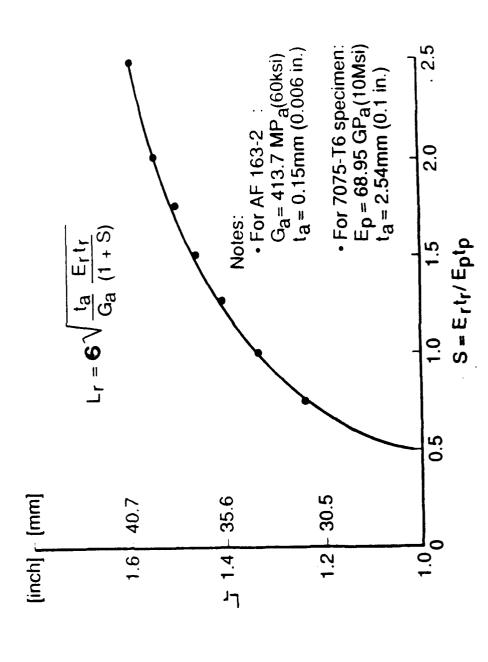
[03/±45/02]S AND [010]. THE COMPOSITE MATERIAL SYSTEMS CHOSEN FOR THE STUDY WERE TEXTRON 5521/4 BORON/EPOXY (B/EP) STIFFNESS (2) COMPOSITE MATERIAL SYSTEMS WERE USED IN TWO DIFFERENT LAY-UP CONFIGURATIONS, I.E., LAMINATES OF COMPOSITES. BOTH REQUIRE 250°F CURING TEMPERATURE. AND ICI FIBERITE 7714A/3500 GRAPHITE/EPOXY (GR/EP) DEPENDING UPON PATCH MATERIAL AND CONFIGURATION, THE PATCH VARIES. (2) OMI

# PATCH LAY-UP CONFIGURATION

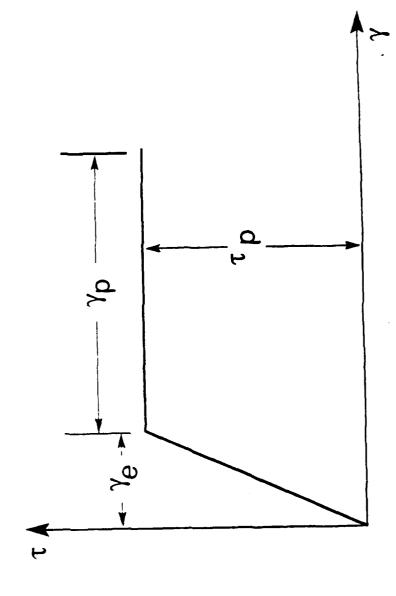


OF MINIMUM PATCH LENGTH IS A FUNCTION OF STIFFNESS RATIO (PATCH-TO-ALUMINUM PANEL) FOR GIVEN PHYSICAL PROPERTIES THE A PATCH DESIGN CHART WAS DEVELOPED FOR THE REPAIR. THE ALUMINUM PANEL AND ADHESIVE.

# MINIMUM PATCH LENGTH REQUIRED

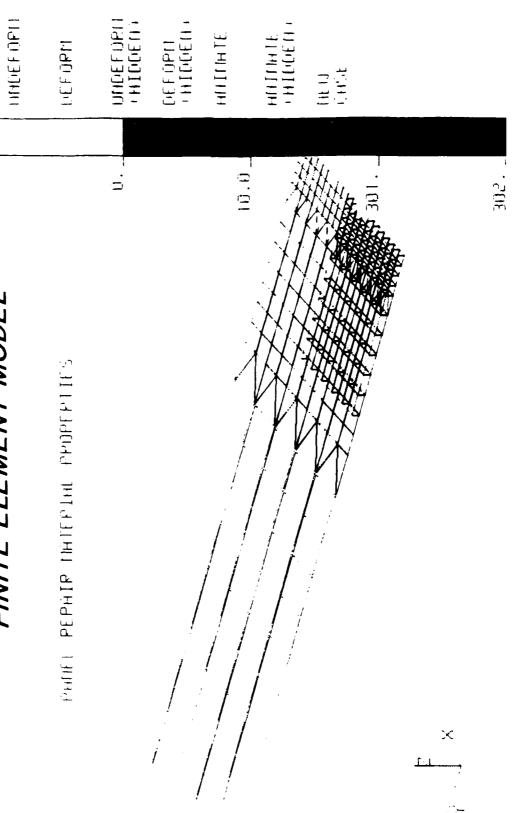


### BILINEAR APPROXIMATION OF ADHESIVE PROPERTIES



300 (SHOWN IN BILINEAR ADHESIVE PROPERTIES), THE SPRING ELEMENT LOAD AND WAS ELIMINATED TO SIMULATE DISBOND BETWEEN THE COMPOSITE PROPERTIES OF THE COMPOSITE PATCH, SPRING ELEMENT REACHED THE MAXIMUM SHEAR STRESS POINT DURING THE COMPUTER ANALYSIS, WHEN CONSTRUCTED WITH APPROXIMATELY 1,200 FINITE ELEMENTS ADHESIVE AND ALUMINUM PLATE, A HYBRID MATH MODEL WAS PATCH AND ALUMINUM PANEL. PHYSICAL SPRING ELEMENTS. THE BASED ON ď

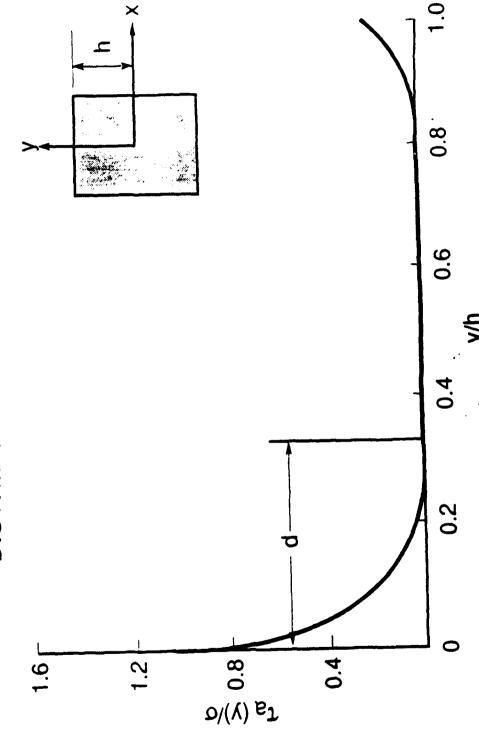
### FINITE ELEMENT MODEL



COLOP CODE BY MATERIAL ID

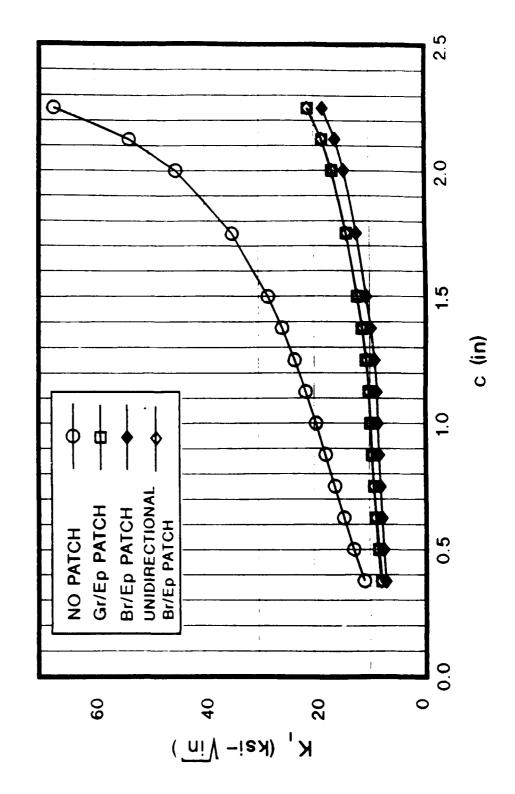
SHEAR MODEL SHEAR STRESS IN ADHESIVE WAS PLOTTED ALONG THE CENTER-LINE OF THE CRACK-LINE NORMALIZED STRESS IN ADHESIVE IS HIGH IN VICINITY OF CRACK-LIN! PATCH TERMINATION. THE ANALYSIS RESULTS WERE LATER FROM THE COMPUTER ANALYSIS RESULTS, A TYPICAL BETWEEN THE CRACK AND PATCH TERMINATION. CONFIRMED BY A SERIES OF TESTS.

### TYPICAL SHEAR STRESS DISTRIBUTION IN ADHESIVE



THE MAIN PURPOSE OF COMPOSITE REPAIR OF CRACKED METALLIC SHOWED A DRASTIC REDUCTION OF INTENSITY FACTOR WITH INSTALLATION OF A COMPOSITE STRUCTURE IS TO KEEP THE STRESS INTENSITY FACTOR LOW. HYBRID MATH MODEL ANALYSIS SHOWED A DRASTIC REDUCTION STRESS

## STRESS INTENSITY REDUCTION



3M AF163-2 ALONG WITH TEXTRON 5521/4 B/EP AND ICI FIBERITE 7714A/3500 COMPOSITE PRIMERS ADHESIVE AND AMERICAN CYANAMID BR-127 PRIMER WERE CHOSEN SEVERAL COMPOSITE MATERIALS, ADHESIVES, AND SURFACE PREPARATION TECHNIQUES AVAILABLE FOR REPAIRS OF METALLIC STRUCTURES. FOR THIS STUDY, COMPOSITE MATERIALS. THERE ARE GR/EP



# COMPOSITE-TO-METALLIC REPAIR MATERIALS

• GRAPHITE/EPOXY - 250° F CURE ICI-FIBERITE HYE16714A, 7714A/3500 HERCULES ULTRA HIGH MODULUS/1919

• BORON/EPOXY - 250° F CURE

TEXTRON 5521/4 TEXTRON 5505/4 ADHESIVES - 250° F

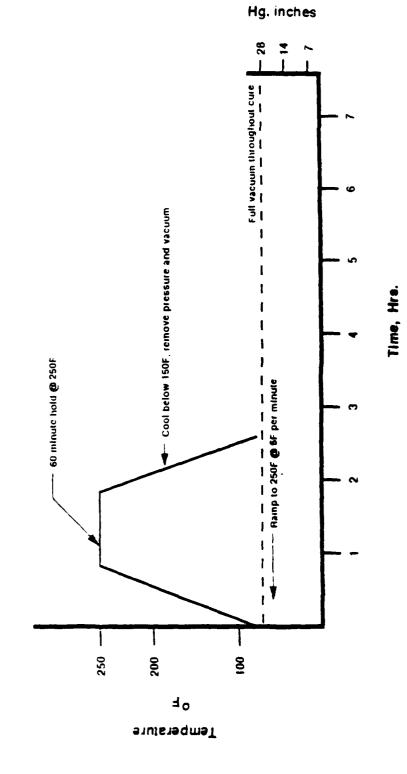
3M AF 163-2, 126 AC FM 73, 87-1 ADHESIVE PRIMERS

3M EC-3924

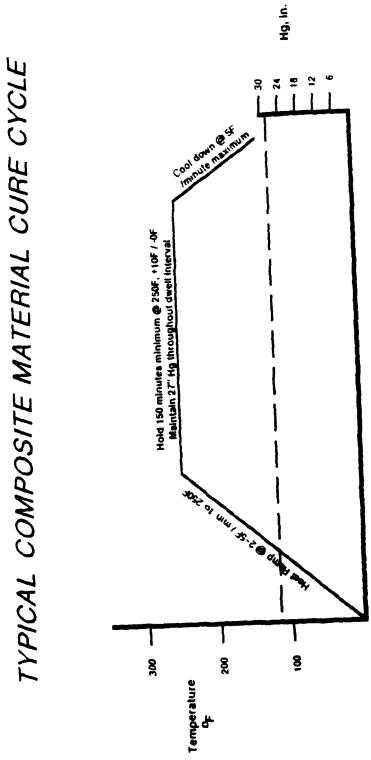
AC BR-127

THIS REPAIR. 250 °F. BONDING THE ADHESIVE REQUIRES AN HOUR CURING TIME AT CURE CYCLE CAN BE USED FOR PRE-CURE/ADHESIVE

## TYPICAL ADHESIVE CURE CYCLE



THAN ADHESIVE CURING TIME. THEREFORE, CO-CURING TIME IS DETERMINED BASED ON COMPOSITE MATERIAL CURING TEMPERATURE. NORMALLY, COMPOSITE MATERIAL CURING TIME IS THEREFORE, CO-CURING DEPENDING UPON MATERIAL SYSTEM, EACH COMPOSITE MATERIAL REQUIRES A CERTAIN PERIOD OF CURING TIME AT ITS CURE TIME REPAIR LONGER



- 1. Process to be controlled with ingoing thermocoupie.
- 2. Apply 27" His vacuum to part. Maintein full vacuum through
  - 3. Heat at 2 to 5 Degrees F perminute to 250F, +10F / -0F.
- 4. Hold part at 216F under full vacuum for 160 milnutes miln
- g. Cool part under hall veguents below 1967 as 6 degrees part

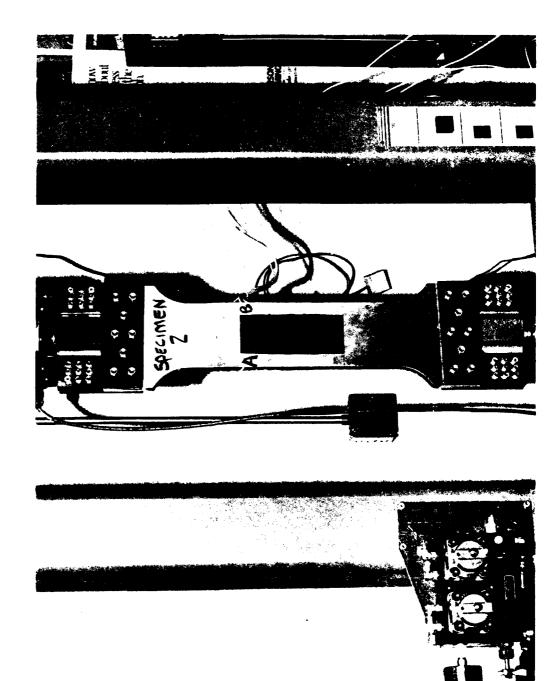
ANALYSIS, A SERIES OF COUPON TESTS WERE ON THE HYBRID MATH MODEL CONFIGURATION, CONDUCTED. BASED ON THE HYBRID MATH MODEL CONFIGURATION, TEST ARTICLES WERE FABRICATED WITH AND WITHOUT COMPOSITE PATCHES INSTALLED. FOR VALIDATION OF

### DEVELOPMENT TEST



32.1 THE COUPON SPECIMENS WERE TESTED UNDER CONSTANT AMPLITUDE CYCLIC LOADS OF 10 KSI AT R=0 AND FIGHTER AIRCRAFT FLIGHT LOAD SPECTRA AT MAXIMUM STRESS LEVELS OF 21.4 KSI AND 32. KSI.

# A COMPOSITE-REPAIRED FATIGUE TEST SPECIMEN



REPAIR, B/EP COMPOSITE PATCH REDUCES STRESS INTENSITY FACTOR STRONGER THAN B/EP SLIGHTLY MORE THAN GR/EP COMPOSITE PATCH, BECAUSE STIFFNESS PLAYS A STIFFER COMPOSITE PATCH PROVIDES A LONGER LIFE. IN TERMS COMPOSITES FOR A GIVEN NUMBER OF PLIES. IN CASE OF CRACK BOTH ANALYTICAL AND EXPERIMENTAL RESULTS SHOWED THAT A STRUCTURAL REINFORCEMENT, THE CASE MAY BE MAJOR ROLE IN REDUCTION OF STRESS INTENSITY FACTOR. FROM WHAT IS SEEN IN CRACK REPAIR. STATIC FAILURE LOAD, GR/EP COMPOSITES ARE UNCRACKED DIFFERENT

IT IS BELIEVED TO BE DUE TO RETARDATION EFFECTS ON METALLIC RESULTS THAN CONSTANT AMPLITUDE CYCLIC LOAD TEST RESULTS. FLIGHT LOAD SPECTRUM TESTS PROVIDED THE SAME OR BETTER

### COMPOSITE REPAIR

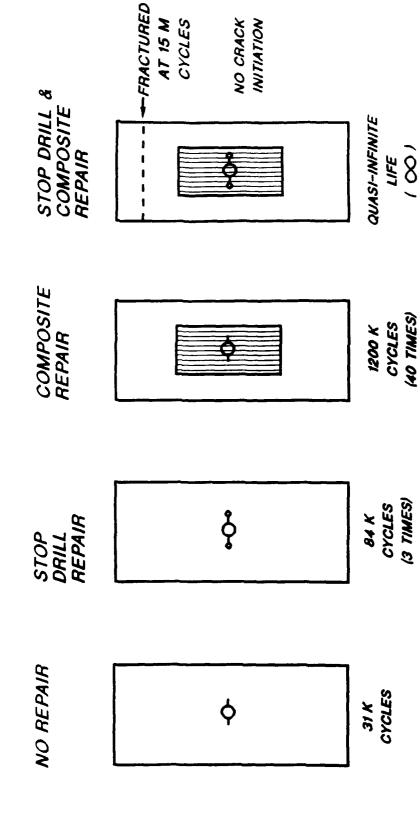
		NUMBER OF CYCLES	F CYCLES	
REPAIR PATCH	42	PREDICTION	TEST	DIFF.
B/Ep 14-plies	1.75	600,600 (20)*	977,500 (31)*	1.63
B/Ep 10-plies	1.65	495,200 (16)	753,100 (24)	1.52
Gr/Ep 14-plies	1.24	407,800 (13)	625,600 (20)	1.53
Gr/Ep 10-plies	1.08	335,600 (11)	423,100 (13)	1.25
No Patch	N/A	30,700 (1)	31,800 ( 1)	1.04

* : LIFE GAINS WITH REPAIR

AND WITH IMPROVEMENT IN SURFACE PREPARATION STOP-DRILL REPAIR PROVIDED APPROXIMATELY THREE (3) TIMES LIFE EXTENSION IS ADHESIVE BONDING, PRESENTLY 40 TIMES EASILY ACCOMPLISHED. EXTENSION. LIFE

AT OCCURRED ELSEWHERE STOP-DRILL/COMPOSITE REPAIR (FAR RIGHT FIGURE) PROVIDED A QUASI-INFINITE LIFE EXTENSION: FAILURE OCCU 15 MILLION CYCLES AS DEPICTED IN VIEWGRAPH.

### LIFE COMPARISON



E-SYSTEMS AD LAB TEST

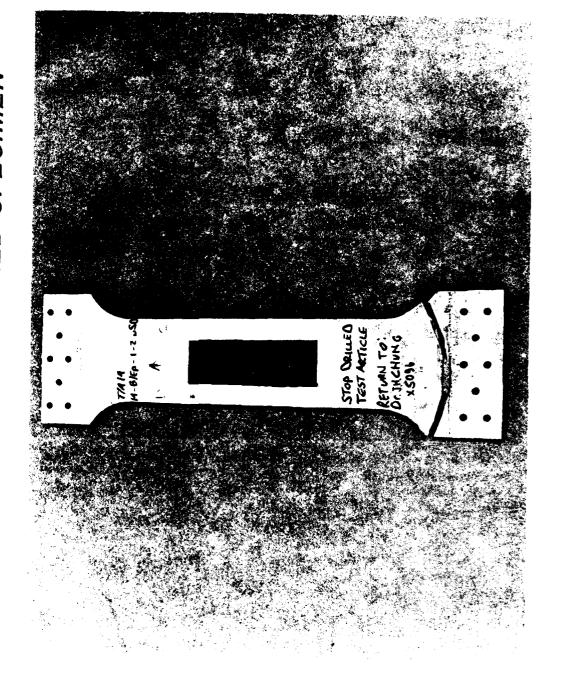
COUPON: AL 7075-76

PATCH : BORON-EPOXY GRAPHITE-EPOXY

10AD : 10 KSI (R=0)

IS HOLES MODE 9 N INDICATION OF CRACK INITIATION FROM THE STOP-DRILLED SHOWN IN THIS VIEWGRAPH. AN X-RAY INSPECTION SHOWED A STOP-DRILL/COMPOSITE REPAIRED TEST ARTICLE FAILURE UNDER THE COMPOSITE PATCH

### AND COMPOSITE-REPAIRED SPECIMEN FAILURE MODE OF A STOP-DRILLED



INSTALLATION WAS PERFORMED IN STRINGER 29 OF A C-18 (B-707). FOUR (4) HOURS. A PDM HANGAR ON F.S. 1060 AND THE DEMONSTRATION REPAIR TOOK DEMONSTRATION OF REPAIR PATCH

# IN-HANGAR REPAIL, DEMONSTRATION ON A C-18 (B-707)



FUSELAGE LAP JOINT. A 24-PLY 6"W X 16"L B/EP COMPOSITE PATCH WAS INSTALLED ON A FUSELAGE LAP JOINT OF THE AIRCRAFT. THE REPAIR TOOK FIVE (5) HOURS. FIELD REPAIR DEMONSTRATION WAS PERFORMED ON A C-18 (B-707)

# C-18 (B-707) FIELD REPAIR DEMONSTRATION



FLOOR INSTALLED ON AN IN-SERVICE 880 PATCH IS PRESENTLY INSPECTED WAS A COMPOSITE PATCH BEAM OF A C-135. PERIODICALLY.

# A COMPOSITE PATCH-INSTALLED C-135 F.S. 880 BEAM



COMPOSITE REPAIR SAVES SUBSTANTIAL AIRCRAFT MAINTENANCE COSTS WHILE PROVIDING BETTER STRUCTURAL INTEGRITY THAN CONVENTIONAL METALLIC REPAIR.



### SUMMARY/CONCLUSION

## COMPOSITE REPAIR PROVIDES :

- BETTER STRUCTURAL INTEGRITY
- COST-EFFECTIVENESS FOR ACFT REPAIR
- MAINTENANCE COST SAVINGS FOR USERS



### COMPRESSIVE STRENGTH IN COMPOSITES POST IMPACT

EDVINS DEMUTS
RAGHBIR S. SANDHU
JOHN A. DANIELS

FLIGHT DYNAMICS DIRECTORATE, WRIGHT LABORATORY, USAF Low Velocity Impact Resistance of Two Composites

E. Demuts and R. S. Sandhu USAF, Wright Laboratory, Flight Dynamics Directorate

### ABSTRACT

The need for safe composite airframes requires reliable criteria and requirements guiding the design of damage tolerant structures. The objective of this experimental investigation was to generate low velocity impact data of AS4/3501-6 graphite epoxy (Gr/Ep) and IM6/CYCOM3100 graphite bismaleimide (Gr/BMI). The impact response of both materials is presented here. The damaged area and the post impact compression strength (PICS) were determined at room temperature of moisture non preconditioned specimens of five thicknesses, varying from 9 to 97 plies, and having a nominal 10/80/10 layup. The size of specimens was 7"x10" (17.8 cm x 25.4 cm) during impact introduction and 5"x10" (12.7 cm x 25.4 cm) during PICS tests. The thinner specimens (9, 26, 48 plies) were subjected to an impact that caused a 0.1" (2.54 cm) deep dent while each of the thicker specimens (74 and 96 plies) received a 100 ft-lb (136 joules) impact. During the impact introduction, the specimens were clamped between two rigidly supported steel plates each having a 5" (12.7 cm) square opening whose center coincided with those of the specimen and the free falling impactor. Because the impactor velocity just before striking the specimen was set to be approximately 16 ft/sec (4.88 m/sec), the mass of the impactor determined the impact energy. The extent of the damage was found by the use of ultrasonic through transmission NDI. For PICS determination a fixture was used that prevents specimen edge translation while permitting specimen edge rotation and specimens interior The thinner specimens (9 and 26 plies) indeed failed buckling. in buckling.

The most predominant conclusions of this investigation are:

1. the damaged area caused by impact was greater in the Gr/BMI
than in the Gr/Ep although Gr/Ep absorbed a greater amount of
impact energy than Gr/BMI; 2. the undamaged per ply compression
strength of both materials is a strong function of laminate
thickness while the per ply PICS is not; 3. the undamaged per
ply compression strength of Gr/BMI is about 25% greater than that
of Gr/EP but the PICS of both material systems is about the same.



# INTRODUCTION / NEED

- STRENGTH, STIFFNESS, DURABILITY, SAFETY STRUCTURAL INTEGRITY
- SAFETY = DAMAGE TOLERANCE
- DESIGN OF DAMAGE TOLERANT STRUCTURES REQUIRES IMPACT RESISTANCE DATA
- LOW VELOCITY IMPACT RESISTANCE OF GR/EP
- CHARACTERIZED
- AFGS 87221A, JUNE 1990
- NEED IMPACT RESISTANCE DATA FOR OTHER MATERIALS



### OBJECTIVE

POST IMPACT PROPERTIES ON DRY SPECIMENS AT RT COMPRESSION STRENGTH (PICS) DAMAGED AREA

• TWO MATERIALS
AS4/3501-6 GR/EP
IM6/CYCOM3100 GR/BMI

 $\blacksquare$  (% OF 00/ $\pm$ 450/900) 10 / 80 / 10 **ONE LAYUP** 

L11-57.PS Mon Nov 25 11:10:37 1991



### APPROACH

- **EXPERIMENTAL DATA**
- FOUR TEST SERIES
- A. BASIC MECHANICAL PROPERTIES
- UNDAMAGED LAMINATE COMPRESSIVE STRENGTH
- C. TRIAL TESTS 0.1 IN. DEEP DENT
- D. IMPACT TESTS (NDI, DENTS, PICS)
- FIVE LAMINATE THICKNESSES (ti)
- 9, 26, 48, 74 AND 96 PLIES
- IMPACT BY FREE-FALLING IMPACTOR 16 FT / SEC, 1" DIA.

L11-58.PS Mon Nov 25 07:54:16 1991



### **APPROACH**

**SPECIMEN SIZES** 

 $(3/4" \text{ TO } 1") \times (5" \text{ AND } 10") \times (8 \text{ AND } 16 \text{ PLIES})$ 

5" x 10" x t_i;

i = 1, 2, 3 i = 1, 2, 3, 4, 5 C. & D. 7" x 10" x ti;

CLAMPED BETWEEN TWO STEEL PLATES SPECIMEN SUPPORT DURING IMPACT

5" x 5" OPENING

RECORDED QUANTITIES

HISTORY OF LOAD AND ABSORBED ENERGY

IMPACTOR VELOCITY

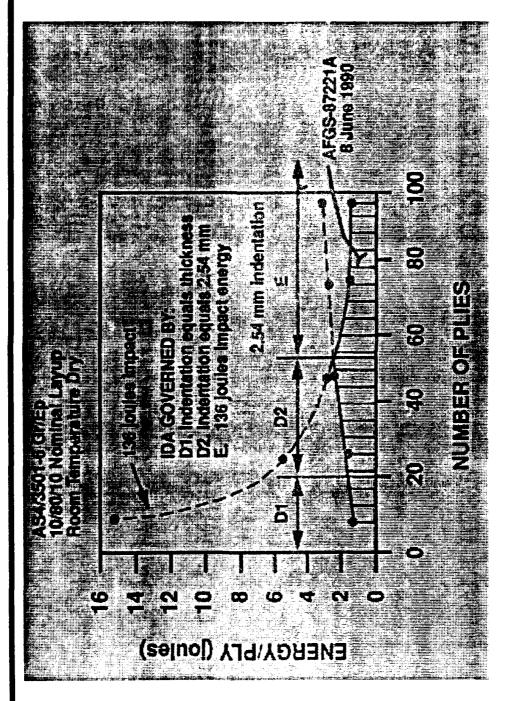
TEST TEMPERATURE

OTHERS

Mon Nov 25 11:16:30 1991



# INITIAL DAMAGE ASSUMPTION



1.PS Mon Nov 25 08:24:07 1991



## MANUFACTURING

GR / BMI POSTCURED AT 400 P FOR FOUR HOURS

FIBER VOLUMES

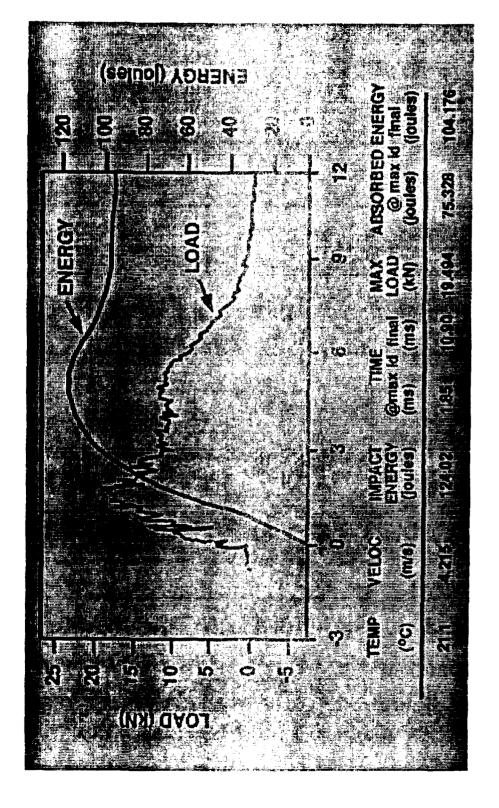
63% AS4/3501-6

57 % IM6 / CYCOM3100

**ULTRASONIC THROUGH TRANSMISSION** QUALITY OF SPECIMENS, DAMAGED AREAS



## TYPICAL IMPACT LOAD AND ENERGY HISTORIES



L11-62.PS Mon Nov 25 09:23:22 1991

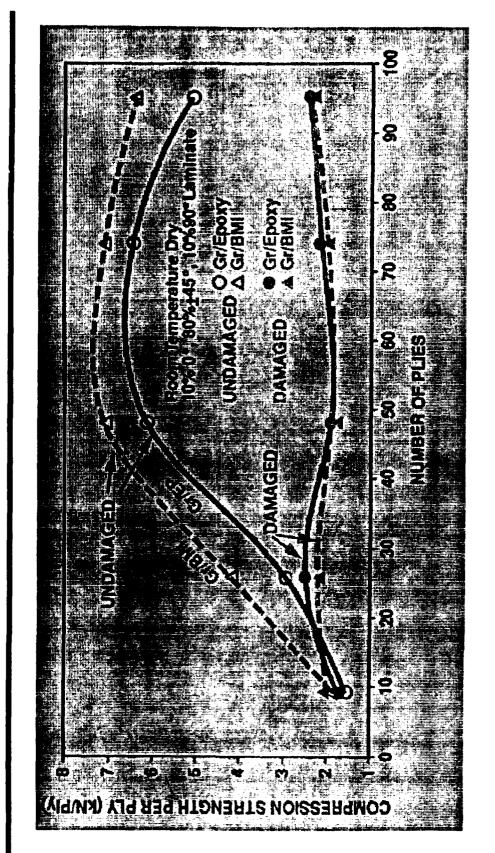


# SUMMARY OF TEST RESULTS

	a e e e e e e e e e e e e e e e e e e e	
VICE NY, E		
SIVCKING NO OF PLES		



## LAMINATE COMPRESSION STRENGTHS PRE - & POST IMPACT





## CONCLUSIONS

• ENERGY ABSORBED BY IM6 / CYCOM3100 IS LESS THAN THAT BY AS4 / 3501-6

IS GREATER THAN THAT OF AS4 / 3501-6 DAMAGED AREA OF IM6 / CYCOM3100

- STRONG FUNCTIONS OF THICKNESS - WEAK FUNCTIONS OF THICKNESS PER PLY COMPRESSION STRENGTHS OF BOTH COMPOSITES WHEN UNDAMAGED WHEN DAMAGED BOTH COMPOSITES HAVE ABOUT THE SAME IMPACT RESISTANCE

**ABOUT THE SAME MAGNITUDE** 



### **PAYOFFS**

- **EXTENDS LOW VELOCITY IMPACT DATA FROM** GR/EP TO GR/BMI
- TRANSITIONS DATA TO SPEC AUTHORITY (ASD / EN)
- APPROPRIATE GUIDELINES HELP TO DESIGN SAFE OR DAMAGE TOLERANT AIRFRAMES
- REQUIRES COORDINATION WITH MANUFACTURING, **NDI AND TESTING FACILITIES**

INSTITUTE FOR AEROSPACE RESEARCH

### LABORATORY TECHNICAL REPORT

LTR - ST - 1834

### INSPECTION OF AIRCRAFT ENGINE COMPONENTS **USING AUTOMATED EDDY CURRENT AND** PATTERN RECOGNITION TECHNIQUES

A. FAHR, C.E. CHAPMAN, A. PELLETIER, AND D.R. HAY

RAPPORT TECHNIQUE DE LABORATOIRE

INSTITUT DE RECHERCHE AÉROSPATIALE

28 JUNE 1991

OTTAWA, CANADA

### TABLE OF CONTENTS

	page
1. INTRODUCTION	1
2. INSPECTION SYSTEM	2
<ul><li>2.1. Hardware Components</li><li>2.2. Control Software</li><li>2.3. Pattern Recognition Software</li></ul>	2 3 3
3. EXPERIMENTAL PROCEDURES	4
<ul><li>3.1. Test Component</li><li>3.2. Inspection Procedure</li><li>3.3. Pattern Recognition Analysis</li><li>3.4. Crack Verification Tests</li></ul>	4 4 5 5
4. RESULTS AND DISCUSSIONS	5
4.1. Machine vs Human 4.2. Correlations with Crack Size	5 6
5. CONCLUSIONS	7
6. FURTHER WORK	7
7. REFERENCES	7
ACKNOWLEDGMENTS	8
LIST OF FIGURES	8

### Inspection of Aircraft Engine Components Using Automated Eddy Current and Pattern Recognition Techniques

A. Fahr and C.E. Chapman

Structures and Materials Laboratory
Institute for Aerospace Research
National Research Council Canada
Ottawa, Ontario, Canada.
K1A 0R6

A. Pelletier and D.R. Hay

Tektrend International Inc., 2755 Pitfield Boulevard, St. Laurent Montreal, Quebec, Canada. H4S 1T2

### 1. INTRODUCTION

Aircraft engine components operated under "safe-life" criteria are retired from service at the end of their "safe-life" period even though many parts may be substantially free of significant defects. Components operated under "damage tolerance" criteria are retired for cause on the basis of accumulated damage revealed by nondestructive evaluation procedures. The U.S. Air Force MIL STD 1783 establishes requirements for turbine engine structural integrity (1).

The successful implementation of damage tolerance concepts, based on MIL STD 1783, requires the use of sensitive nondestructive evaluation (NDE) techniques that can be used to inspect many parts reliably and economically. Of the few NDE methods available for the inspection of engine components, automated eddy current techniques show promise in terms of sensitivity, reliability and speed. The U.S. Air Force has implemented the new philosophy relying on totally automated eddy current systems designed for routine inspection of engine parts (2).

One of the major problems limiting the life of aircraft engines is the occurrence of low cycle fatigue (LCF) cracks in the fastener bolt holes of compressor discs, spacers and other rotating parts. Figure 1 illustrates a compressor disc and Figure 2 shows scanning electron micrographs of typical LCF cracks in the bolt holes of compressor discs. Inspection according to damage tolerance criteria requires repeatable detection (90% probability of detection with 95% confidence) of cracks with characteristic dimensions of 0.125 mm

(0.005"). At such levels, it is difficult to distinguish the actual flaw signal from the noise in the eddy current signal as both are of similar amplitude. If thresholding methods are used by a human analyst or implemented by means of electronic instrumentation, detectability can be low. However, in certain cases, searching for structure in the noisy waveform can provide indications of defects that escape detection by thresholding techniques. One way of achieving this is by using pattern recognition analysis.

Previous attempts to use pattern recognition for eddy current enhancement have focused on the interpretation of the impedance plane figure by using image processing techniques (3). In the present approach, raw waveforms are used so that waveform rather than image processing methods can be applied with a considerable reduction in processing time.

A fully automated inspection and decision making system which utilizes a standard eddy current instrument, an automated XYZ table and an advanced pattern recognition software package has been developed and integrated. The system has been used to inspect fastener bolt holes in aircraft engine rotating parts and the preliminary inspection results on a J 85 CAN 40 compressor disc are presented in this report. The effectiveness of pattern recognition in recognizing defective bolt holes has been compared with the conventional visual analysis of EC signals by an experienced operator. The results have been verified by pry opening of all the bolt holes and examination under a scanning electron microscope.

### 2. INSPECTION SYSTEM

With technical and financial support from IAR, Tektrend International Inc. has designed and manufactured an Automated Real-time Intelligent Eddy-current System (ARIES). An integrated systems approach was adopted combining and optimizing automated scanning, eddy current data acquisition, computer-based interpretation and display of results. ARIES consists of three main hardware components, control software and an advanced pattern recognition package as described in the following sections. The complete ARIES system is shown in Figure 3.

### 2.1. Hardware Components

The eddy current (EC) sensing device is a commercial Elotest Model B1 SD instrument equipped with a spirning probe. The instrument has a frequency range of 10 Hz to 10 MHz and a gain range of -12 to 90 dB. For automatic EC probe positioning, a Techno XYZ table, driven by three stepping motors, is employed. The table has a working surface of 75cm X 75cm and the probe head is capable of reaching any point in a 50cm X 50cm surface area with a positioning accuracy of 0.005mm.

Both the EC instrument and the XYZ table are linked to a Hewlett Packard Vectra RS/20 computer with a 80386-20 MHz microprocessor, 80387 coprocessor, 2 MBytes of RAM, 100 MBytes of hard disc storage with 17 msec access time and VGA graphics. The table is fully controlled by the RS/20 through a serial link and the ARIES control software.

The EC instrument is also connected to the RS/20 through a serial digital link to transmit set-up information and an analog link to transmit the EC signals. An RTI-800 analog-to-digital (A/D) board with a transient sampling rate of up to 7 kHz is provided with a high-capacity RAM for EC signal acquisition and storage. A SKY 321-PC digital signal processor (DSP) board is installed for high-speed, real-time processing of the EC signals.

The system operates at a traversal rate of 8 mm/sec between holes with a dwell time of 6 sec in each hole taking two eddy current readings at six different vertical levels and provides a large volume of data at high data rates. The digital EC signals are displayed on the screen and saved on hard disc.

### 2.2. Control Software

The RS/20 operating system is MS-DOS Version 4.01. Menu-driven software has been developed for operating the system using the "C" language with some specific A/D modules programmed in assembly language. The system can be operated in manual or automated modes and can play back data files or create prints. The main menu is displayed in Figure 4

In eddy current testing, defect indications are measured as the change of impedance which consists of a resistive component (real term) and an inductive reactance component (imaginary term). The real component represents the amplitude of the EC signal while the imaginary component indicates the phase angle. The two parts are usually combined and displayed as an impedance plane Lissajous readout as shown in Figure 5-a. ARIES shows the phase (Figure 5-b) and amplitude (Figure 5-c) components as well as the impedance plane representation. These signals are displayed on the screen, in real time, along with the pattern recognition classification results as illustrated in Figure 5 for a bolt hole crack. Alternatively, the overall inspection results can be displayed in graphic form and defective bolt holes identified using a different colour code as illustrated in Figure 6.

### 2.3. Pattern Recognition Software

Pattern recognition is a branch of artificial intelligence which uses statistics and mathematics to store patterns in a computer and to compare new patterns with those that have been stored. The objective of pattern recognition is to classify unknown patterns into known classes on the basis of measurements.

ICEPAK (Intelligent Classifier Engineering PAKage) is a commercial pattern recognition package developed by Tektrend International Inc. A pattern recognition process using ICEPAK consists of four steps; data acquisition, data transformation, feature extraction and classification as shown in Figure 7. During development of a classifier, a training and testing phase is also required. A detailed description of these steps is provided in Ref 4.

Briefly, acquisition of data, data transformation and extraction of features are parts of the fact gathering process to present the data in optimal formats for processing by the computer. Recognition is achieved by making measurements on patterns to be recognized and then deriving features from these measurements. These features form the input to a classification procedure that gives a class or group assignment for each pattern.

The raw signals from physical measurements are processed using a number of signal processing techniques including filtering, windowing and Fast Fourier Transformation to provide additional information that would be unobtainable by analyzing the raw signal alone. Up to 108 features of the signal from time, power, phase, cepstral and autocorrelation domains can be automatically selected based on their discriminating ability. There is also provision for up to 20 additional user-defined features.

ICEPAK uses five procedures to classify signals and details of the algorithms used in each procedure are provided in Reference 4. The classifying procedures are:

- a- Linear Discriminant Function (LDF)
- b- K-Nearest Neighbour (KNB)
- c- Empirical Bayesian (EB)
- d- Minimum Distance (MD) and
- e- Neural Network (NN)

The system is first trained on known signals and optimal features and classifying procedures are selected by optimization of classification (recognition) rate. Together, the features selected and the classifying procedure are part of a classifier. The classifier is then used to classify unknown signals.

### 3. EXPERIMENTAL PROCEDURES

### 3.1. Test Component

An aircraft engine compressor disc, similar to that shown in Figure 1, was used to evaluate the performance of the automated eddy current system. The disc had been retired from service due to the development of low cycle fatigue cracks in the tie bolt holes. The disc material was AM-355, a precipitation hardened martensitic stainless steel and it was known, from experience, that cracks grow radially with the majority growing inwards towards the centre of the disc. There were forty 4.7mm diameter bolt holes in the disc, thirty five of which were available for inspection since part of the disc had been already removed for other purposes.

### 3.2. Inspection Procedure

Eddy current inspections were carried out by placing the disc on the scanning table and calibrating the XYZ scanner to establish accurately the position of each hole. Calibrations are saved in files and can be used for future inspection of discs of the same nominal

dimension. Stepping the probe to the centre of the hole at the twelve o'clock location registers the coordinates of this reference position. The same procedure was repeated for the bolt holes at the three, six and nine o'clock locations. The computer then establishes, trigonometrically, the position of the forty holes.

A 4.4mm diameter differential spinning probe with a frequency range of 50kHz-2.5MHz was employed for bolt hole inspections. The instrument frequency and gain were adjusted to 660 kHz and 42 dB respectively, settings which were found to be optimal for this inspection. The bolt holes were inspected at five different depths and eddy current signals corresponding to each level were digitized and stored.

### 3.3. Pattern Recognition Analysis

For automated decision making using pattern recognition, the system was first trained using known signals from cracked and crack free bolt holes obtained in previous disc inspections. Important features of the training signals were automatically selected on the basis of their discriminating capability and classifiers were assessed in terms of the optimal recognition rate that can be achieved. Of the first four classifiers evaluated, the K-nearest neighbour procedure with three features produced an optimal recognition rate of 95% during training. The optimal features were related to the signal amplitude and partial power in the power and autocorrelation domains. The neural network procedure was not available at the time of these experiments and therefore was not included in this study. The optimal features and classifying procedure were stored away and were used with ARIES to identify, in real time, defective bolt holes.

### 3.4. Crack Verification Tests

After inspection and classification, all bolt holes were examined using optical and scanning electron microscopes and the actual location and size of cracks were determined. For this purpose, a 1x1 inch region surrounding each bolt hole was cut out, a notch was introduced in the side opposite to the suspected crack area and the sample was then pried open. The specimens that did not reveal a crack on the fractured surfaces were further examined on the bolt hole surface to make sure that the crack was not missed during the pry opening operation.

### 4. RESULTS AND DISCUSSIONS

### 4.1. Machine vs Human

To compare the performance of the automated decision making capability of ARIES to the success rate achieved by an inspector, the eddy current Lissajous figures from the bolt holes were examined by an experienced inspector. The inspection results are given in column A of Table I which indicates that 13 bolt holes contained cracks.

The inspector was then asked to identify the cracked bolt holes by visual analysis of the projection of the EC signal on X and Y axes which are related to amplitude and phase. The results are shown in column B of Table I indicating that 17 bolt holes contained cracks. The higher detection level using the partitioned signals is due to the fact that for very small cracks, the amplitude of the associated signals is at a level similar to the background noise. However, there is a slight change in the phase angle that can be seen on the phase signal.

Finally, the ICEPAK pattern recognition package was employed using the optimal classifier established during training and the system identified 29 bolt holes as being defective. The results of the automated classification using ICEPAK are illustrated in column C of Table I. The subsequent destructive tests and examinations under an SEM indicated that, in fact, 33 of the bolt holes had cracks. The SEM results are given in column D of Table I.

As seen in Figure 2 under SEM, the service-induced low cycle fatigue cracks have smoother fracture surfaces than those of tensile rupture created during the pry opening. The crack size ranged from a few microns up to about 1mm in length. The shape and location of cracks varied and examples of different crack geometries observed are illustrated in Figure 2. Most cracks initiated from the surface and propagated radially inward toward the centre of the disc. There were also some totally internal cracks as well as outward propagating cracks. As seen in Figure 2-c, some crack had multiple initiation sites.

The automated eddy current inspection with human interpretation resulted in 16 misses, some as large as 0.5mm. With the aid of pattern recognition, a larger number of cracks were detected, some as small as 0.05mm, and only four cracks were missed, all less than 0.1 mm in length. In addition to the improved detection levels, the use of pattern recognition results in a considerable savings in terms of inspection time and manpower. While the visual interpretation of repetitive EC signals by an operator is time consuming, automated classification using pattern recognition can be performed, displayed in real-time and recorded for future reference.

### 4.2. Correlations with Crack Size

Quantitative measurement of crack size using eddy current response is of considerable interest and has been the subject of numerous theoretical and experimental studies (e.g. 5,6). However, due to numerous factors, related to material, crack geometry, instruments, settings, signal processing, etc., that influence the EC signals, accurate sizing of defects using eddy current is not possible. Nevertheless, correlations between EC signal characteristics and crack size can be obtained and utilized to provide an estimate of the size of unknown defects under similar experimental conditions.

Figure 8 illustrates correlations between the EC signal amplitude and phase angle with the depth of the crack as measured on SEM micrographs. For the material and inspection conditions of this study, the trend is that the EC signal amplitude does not change

significantly until the crack size is about 0.5mm deep, after that it increases with increasing crack depth. On the other hand, the phase angle of the EC signal shows an increasing trend with the crack size until it reaches a maximum level and then starts to decrease. This decrease of the phase angle after the maximum is attributed to the weakening of the induced field at larger depths which is governed by the operating frequency.

The trends indicate that, if only the signal amplitude is used for crack detection, it is likely that some small cracks will remain undetected. Both amplitude and phase information are required to increase the detection level for small cracks and pattern recognition takes advantage of multi-feature analysis to recognize such small cracks.

### 5. CONCLUSIONS

A standard eddy current instrument, an automated XYZ table and an advanced pattern recognition software package have been integrated into ARIES, a system to inspect fastener bolt holes of aircraft engine components. The use of pattern recognition analysis provided significant improvement in the sensitivity, reliability and speed of inspection. It was possible to indicate the presence of service-induced fatigue cracks as small as 0.05mm in the bolt holes of a compressor disc in real-time.

The correlations between the EC signal amplitude and phase angle with the crack size indicate that both the amplitude and phase information are required to increase the detectability for small cracks. Pattern recognition uses these and other optimal features of the EC signal for improved detection results.

### 6. FURTHER WORK

A more extensive research program involving several service-retired components is currently underway to determine the probability of detection of various inspection procedures and to establish their significance with respect to damage tolerant design and maintenance of aircraft engine components. Automated eddy current inspection using pattern recognition analysis is one of the procedures being evaluated in this study.

### 7. REFERENCES

- 1. Engine Structural Integrity Program (ENSIP), U.S. Air Force Military Standard 1783, 30 November 1984.
- 2. The Role of NDI in the Certification of Turbine Engine Components, R.G. Taylor, S. I. Vukelich, T. D. Cooper, AGARD Conference Proceeding No. 462, Impact of Emerging NDE-NDI Methods on Aircraft Design, Manufacture and Maintenance, Published May 1990.
- 3. Feasibility of Using Adaptive Learning Networks for Eddy Current Signal Analysis, R.

Shankar, c.L. Brown, A.N. Mucciardi and T.J. Davis, Report TPS77-723, Electric Power Research Institute, Palo Alto, 1978.

- 4. Intelligent Classifier Engineering Package, User's Manual, Tektrend International, 2755 Pitfield, St. Laurent, Montreal, Quebec, H4S 1G3, Canada.
- 5. An Eddy Current Method for Flaw Characterization From Spatially Periodic Current Sheets, S.M. Nair and J. H. Rose, Proceeding of Review of Progress in Quantitative NDE, Vol. 9A, Plenum Press, 1990.
- 6. Sizing Radial Cracks in Bore Holes Using Eddy Current, J. Bernardi, A. Seretti, R, Samson, F. Hardy and E. Neron, Proceeding of the 4th European Conference in Nondestructive Testing, Pergamon Press, 1987.

### **ACKNOWLEDGMENTS**

The work was carried out with NRC/IAR support under Structures and Materials Laboratory Sub-program 318: Automated Inspection and Handling. The authors would like to thank Dr. W. Wallace, Dr. A.M. Charlesworth and Dr. A. Koul of the IAR Structures and Materials Laboratory and Mr. V. Lacasse of Tektrend International Inc. for their valuable contributions to this work.

### LIST OF FIGURES

- Figure 1. A photog aph of the compressor disc similar to that used in the present investigation.
- Figure 2. Examples of cracks seen in the bolt holes of compressor discs.
- Figure 3. A photograph of the automated intelligent eddy current scanning system.
- Figure 4. The main menu of the ARIES system.
- Figure 5. A computer display of digital eddy current signals from a bolt hole crack. (a) Impedance plane (Lissajous) presentation of EC signals (b) phase component and (c) amplitude component.
- Figure 6. A computer display of the compressor disc showing the bolt holes with detectable cracks.
- Figure 7. Pattern recognition steps.
- Figure 8. Correlations between the EC signal amplitude and phase angle with crack size.

Table I

Comparison Between Human Interpretation and Pattern Recognition

dole No. Automated Eddy Current Inspection SEM Human Interpretation Pattern Recognition				
	Lissajous (A)	Partitioned (B)	·(C)	(D)
1			*	*
1 2 3 4 5 6 7			*	*
3			*	*
4		•.	*	*
5	*	*	*	*
ס 7	*	*	*	*
, 8	*	*	*	*
8 9	•	•	-	••
ío				*
11			*	*
12	*	*	*	*
13	*	*	*	*
14	*	*	*	*
15	*	*	*	*
16			*	*
17		<u>.</u>	*	*
18	*	*	*	*
19 20	*	<b>*</b>	*	*
20 21			*	*
22			•	*
	. Material was	removed and not	available for ins	spection
28	•	*	* .	*
29		*	*	*
30			*	*
31			*	*
32	.9.		.de.	
33 34	*	*	*	*
35	*	*	*	*
36	•	•	*	*
37			<b></b>	*
38		*	*	*
39			*	*
40	*	*	*	*
Total	13	17	29	33

^{*} Indicates crack is detected

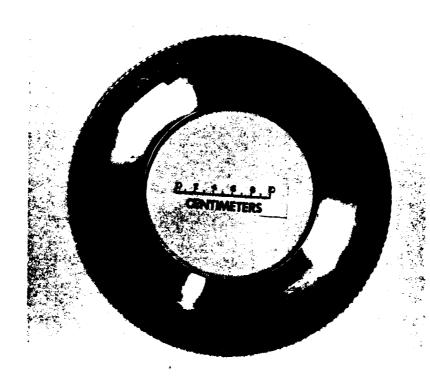


Figure 1. A photograph of the compressor disc similar to that used in the present investigation.

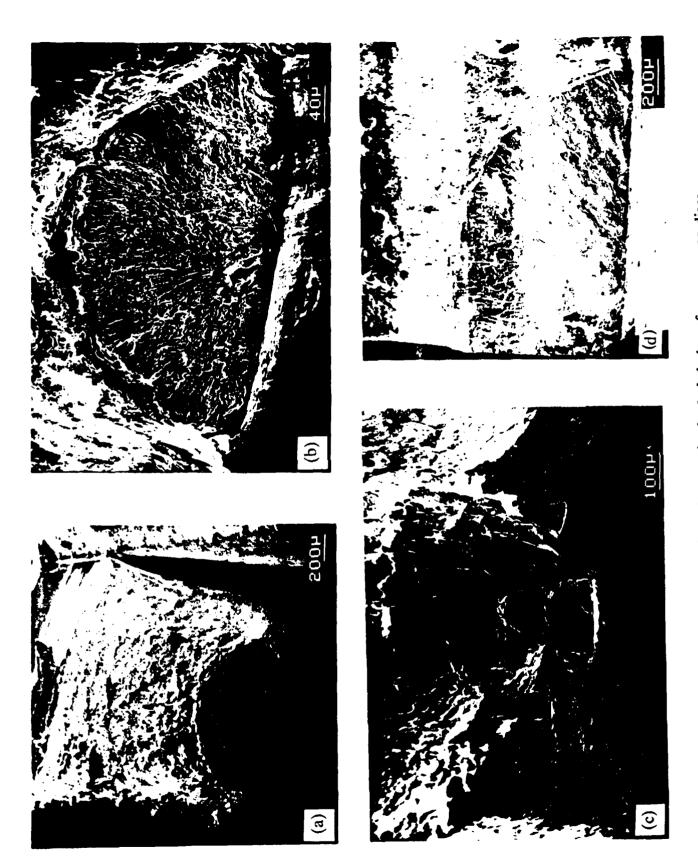


Figure 2. Examples of cracks seen in the bolt holes of compressor discs.

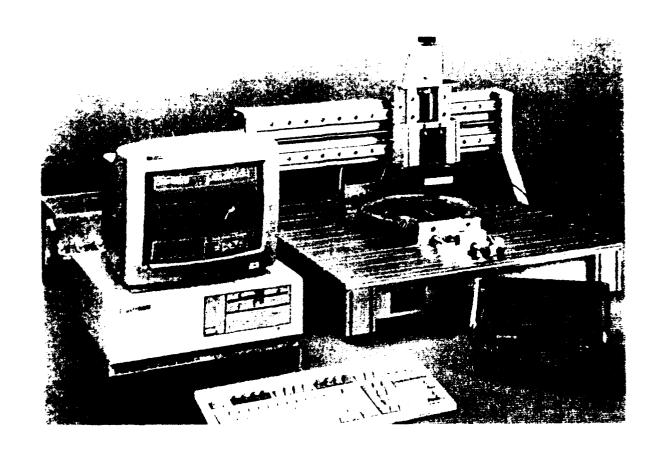
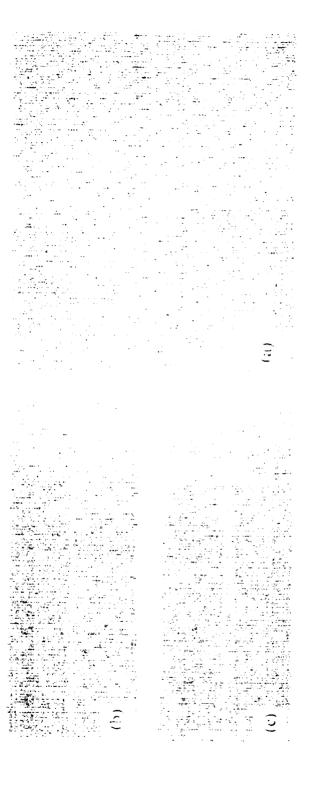


Figure 3. A photograph of the automated intelligent eddy current scanning system.



Save Class results

Figure 4. The main menu of the ARIES system.



Impedance plane (Lissajous) presentation of EC signals (b) phase component and Figure 5. A computer display of digital eddy current signals from a bolt hole crack. amplitude component.

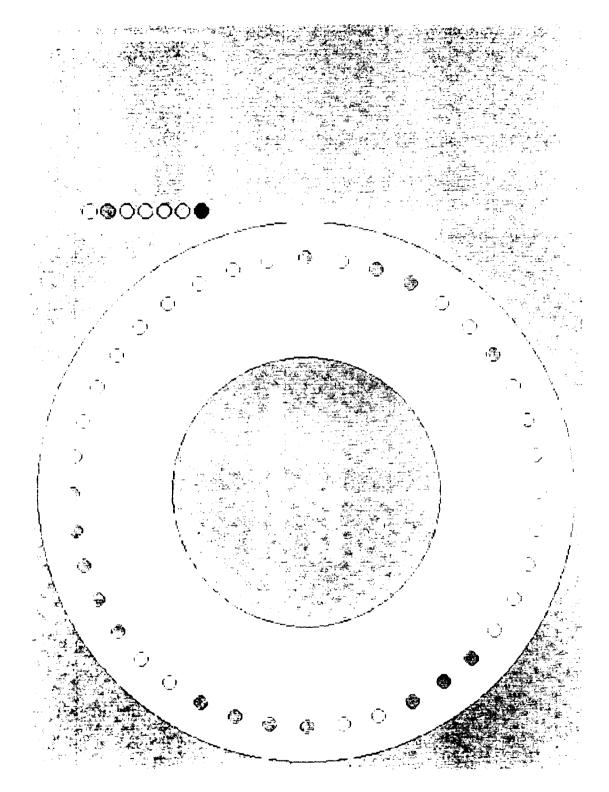


Figure 6. A computer display of the compressor disc showing the bolt holes with detectable cracks.

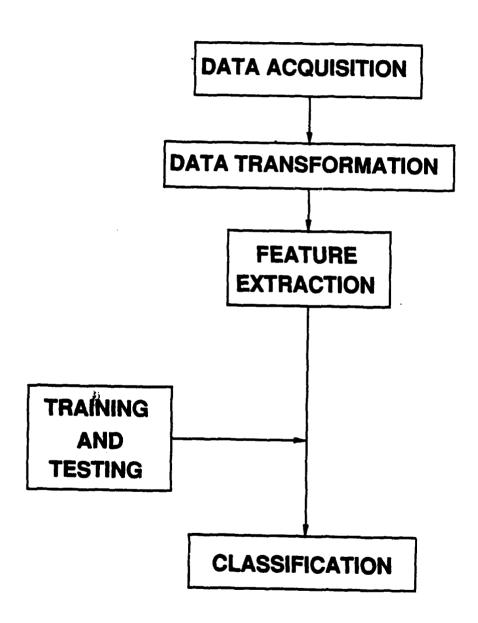


Figure 7. Pattern recognition steps.

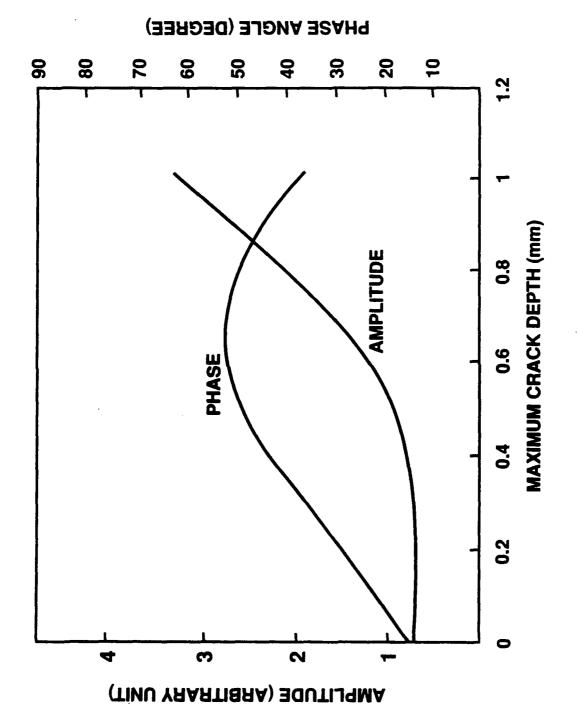


Figure 8. Correlations between the EC signal amplitude and phase angle with crack size.

### ELECTRONIC HOLOGRAPHY & SHEAROGRAPHY NDE MODERN MATERIALS AND STRUCTURES FOR INSPECTION OF

D.H. NETHAWAY PRATT & WHITNEY



1991 USAF STRUCTURAL INTEGRITY PROGRAM CONFERENCE **DECEMBER 3-5, 1991** 

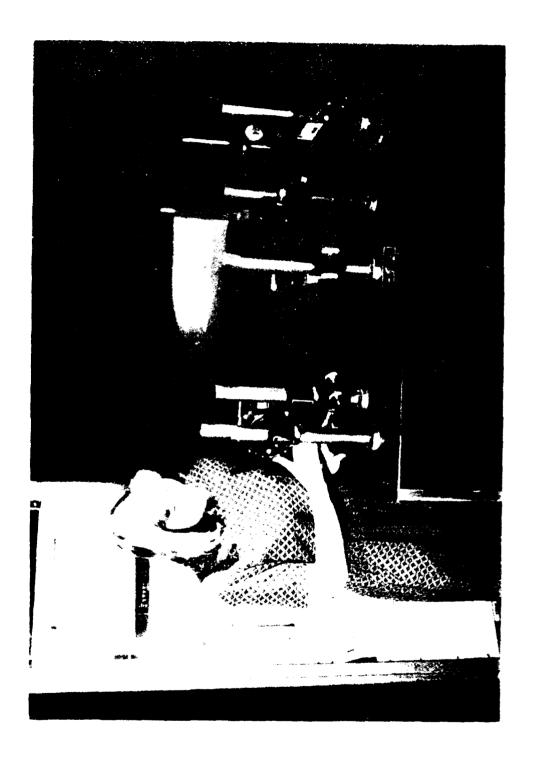
## ELECTRONIC HOLOGRAPHY & SHEAROGRAPHY NDE

### Outline

- Background
- System definition
- Component applications
- Jet engines
- Rocket engines
- Summary

## SYSTEM DEFINITION

## Pratt & Whitney System



## General Definition

delaminations in bonded and composite structures by sensing anomalies in the deformation of the structure An Optical NDE method that can detect unbonds and under steady-state or dynamic loading

## Holography vs. Shearography

### Similarities

- Laser
- Stress structure during inspection
- Image processing

### Differences

- Optical arrangement two beams vs. one
- Holography measures deformation Shearography slope
- Holography greater sensitivity
- Shearography less sensitive to environmental disturbances

## Holography vs. Shearography

Debond Under Load:

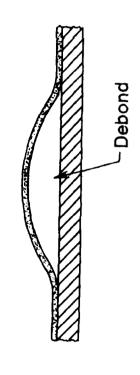
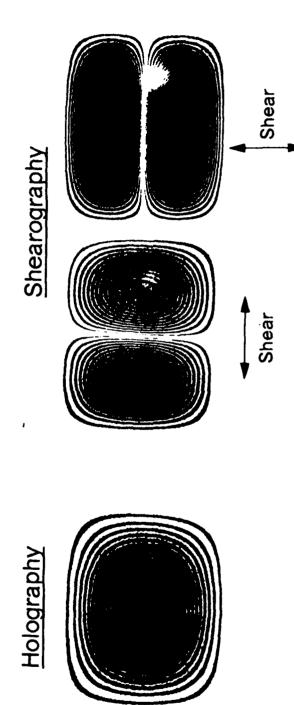


Image:



# "Electronic" Holography/Shearography

Elimination of film and processing has lead to

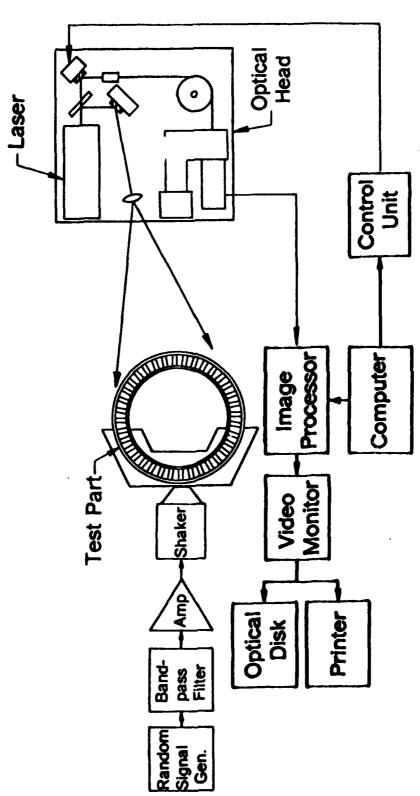
- Decrease in inspection time film = 10 mins vs electronic < 1 second
- Environment protection no chemicals
- Implementation into production facilities, logistics centers, and field (on-wing) applications

### How It Works

- Illuminate area
- Stress structure
- Vibration
- Mechanical shaker
  - Acoustic
- Pressure reduction
  - Temperature
- View enhanced image on monitor
- Defects defined

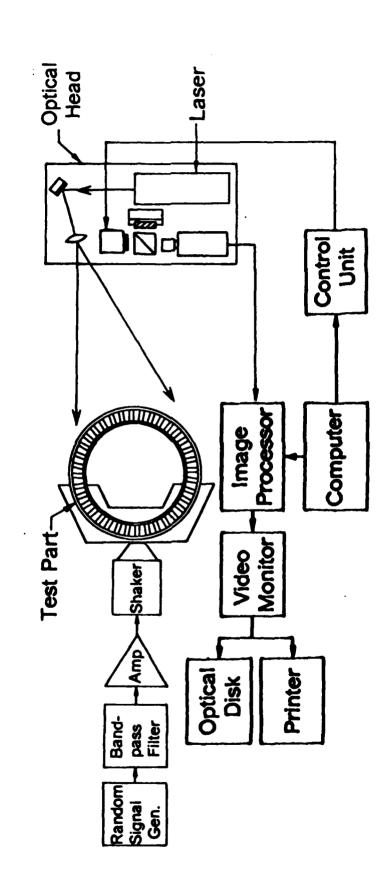
## SYSTEM DEFINITION

### Schematic



## SYSTEM DEFINITION

### Schematic



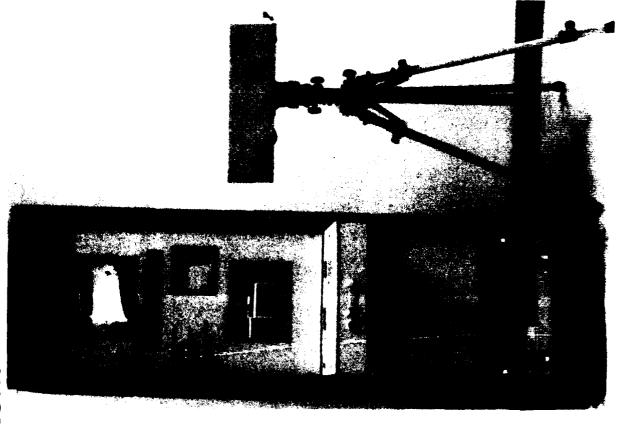
### SYSTEM DEFINITION

### Pratt & Whitney System

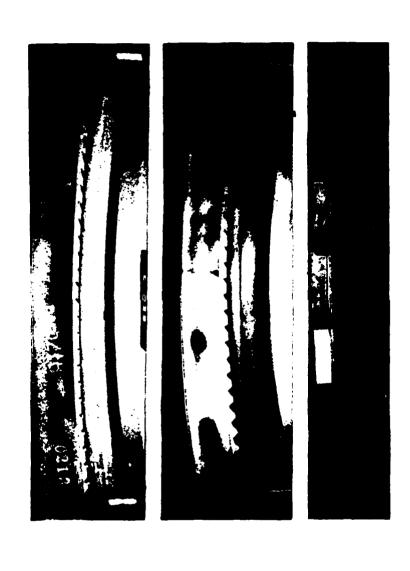
- Compact optical head
- Incorporates diode pumped, solid state laser
- Air cooled
- 140 mW output power
- Guaranteed for 10,000 hours of operation
- Completely portable
- Shearing optics permit amount of shear to be adjusted for optimal resolution
- Image processor uses frame averaging routine instead of frame subtraction
- Software capabilities
- Real-time highlighting of flaws in color
- Scanning fringe to aid in visualizing small flaws
- On-screen measurement of flaw size
- Automatic flaw recognition

### ELECTRONIC SHEAROGRAPHY NDE

Portable System

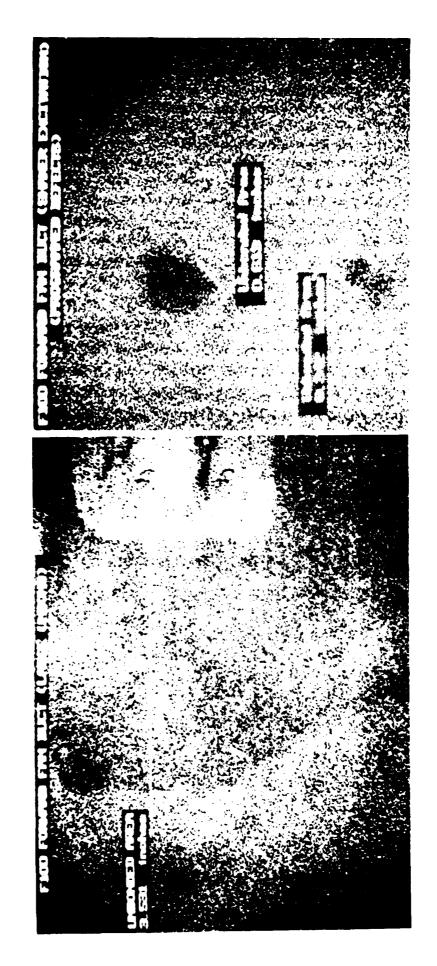


## Fiber Metal and Plasma Sprayed Abradable Seals

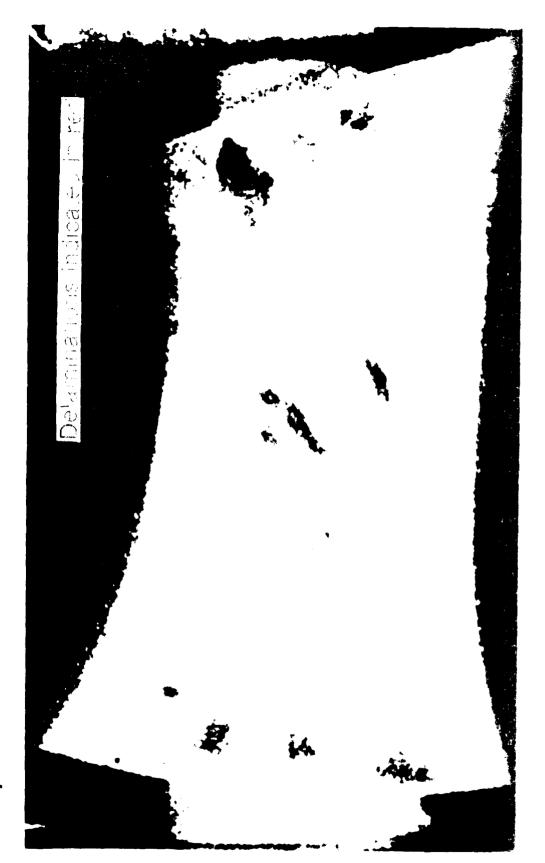


DARK AREAS INDICATE REGIONS OF UNBOND

### Honeycomb Duct



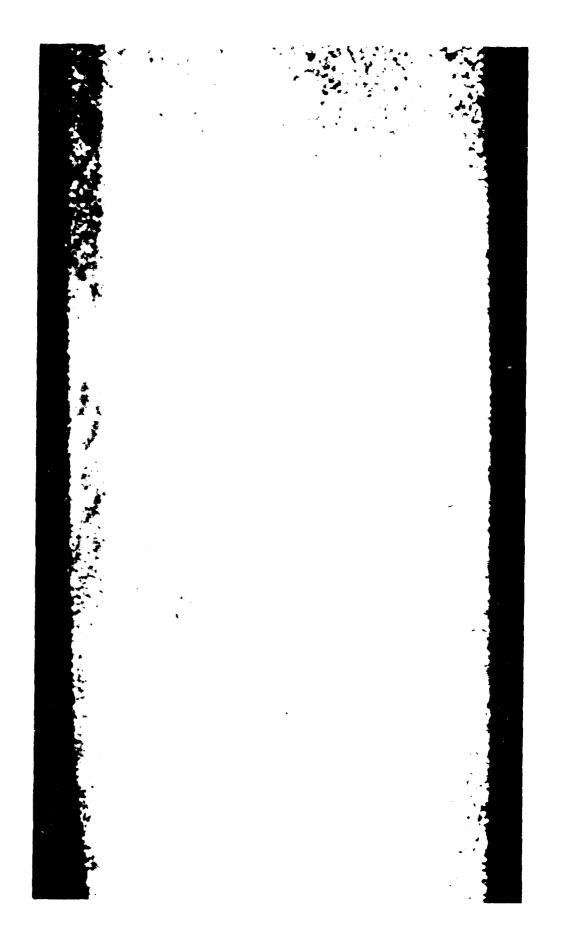
Composite Vane



### Two-Pack Composite Vanes



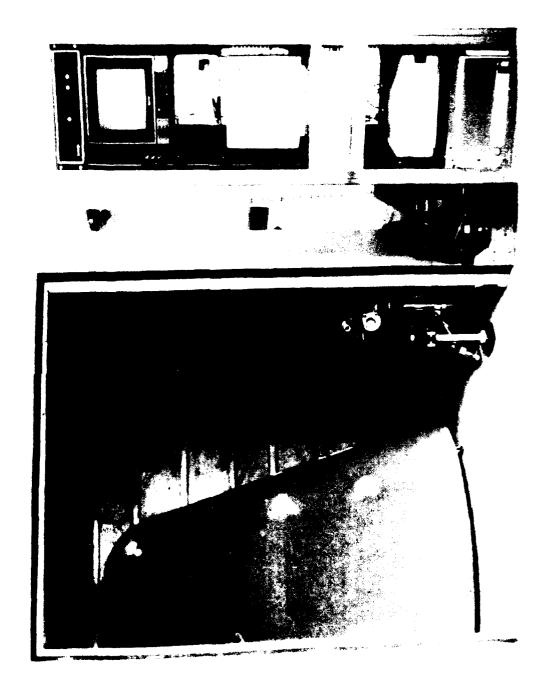
PW2037 Fan Composite Exit Vane



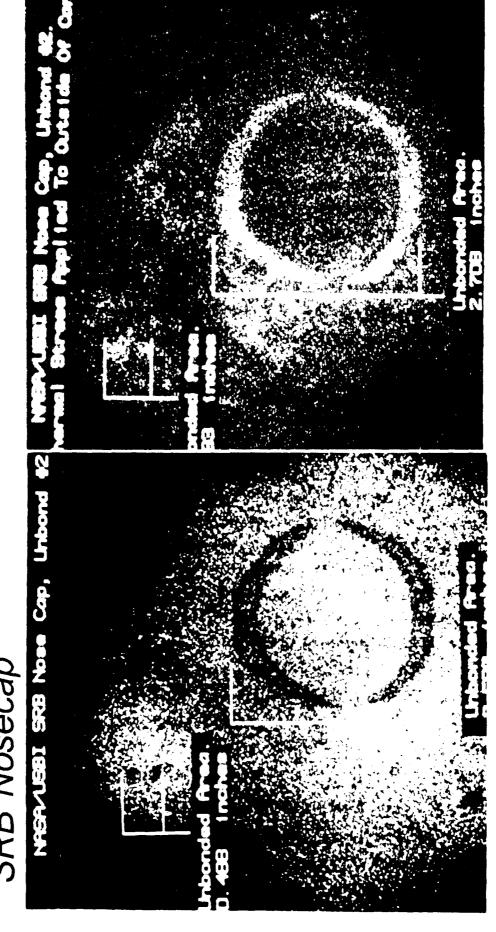
Composite External Flap



### SRB Nosecap



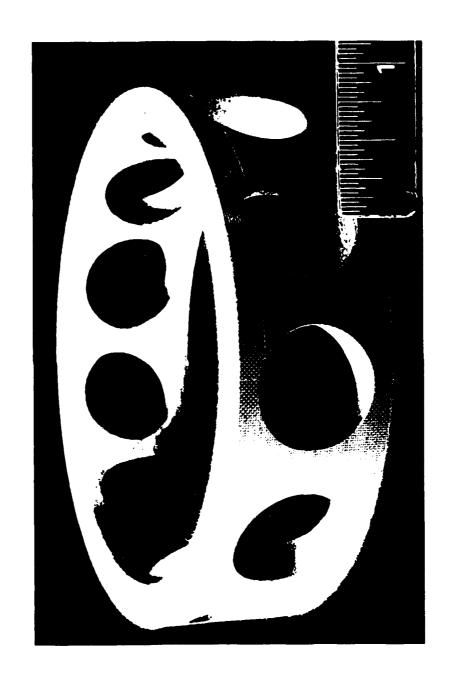
### SRB Nosecap



Thermal

Pressure Reduction

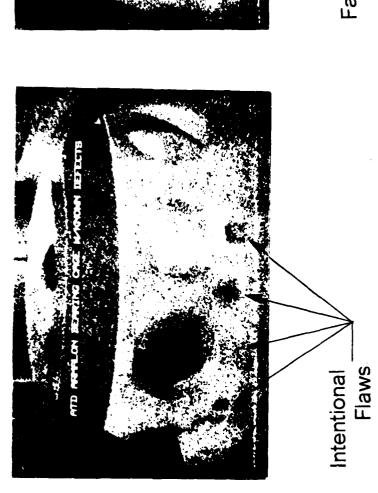
## ATD Teflon Impregnated, Glass Fiber Bearing Cage

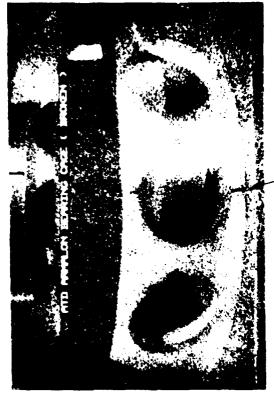


SSME-ATD Teflon Impregnated, Glass Fabric Bearing Cage

Cage With Known Flaws

Cage Failed During Load Testing





Failure Location -

### SUMMARY

### Electronic Holography/Shearography

Large field of view

Can inspect flat or highly contoured surfaces

Rapid inspection rate

Detect "touching" disbonds and delaminations

Results easy to interpret

On-site support

### Predicting the Influence of Inherent Material Inhomogeneities on Notch Fatigue Life

A. F. Grandt, Jr.¹,
A. J. Hinkle²,
T. D. Scheumann³, and R. E. Todd³

### **ABSTRACT**

This paper summarizes a fracture mechanics analysis developed to study the effect of initial size and spatial distribution of inherent material inhomogeneities on fatigue life. Calculations were performed for a set of experiments conducted previously to determine the influence of microporosity size and frequency on the fatigue life of notched 7050-T7451 aluminum specimens. The favorable comparison between the numerical and experimental results indicates the analysis method could be used to predict the benefits to fatigue life obtained by reducing the size and distribution of initial inhomogeneities such as those due to microporosity.

Professor and Head, and ³Graduate Research Assistants, School of Aeronautics and Astronautics, Purdue University, W. Lafayette, IN 47907 USA. T.D. Scheumann is currently employed by The Boeing Company.

² Staff Engineer, Alcoa Laboratories, Aluminum Company of America, Alcoa Center PA 15069 USA

### INTRODUCTION

The objective of this paper is to describe a fracture mechanics analysis to calculate the fatigue lives of notched components which contain initial material inhomogeneities, and to describe how to use this analysis to predict the influence of material quality on fatigue life. The analysis is based on prior work [1-5] which resulted in a computer model to predict the growth and coalescence of multiple fatigue cracks. The flaw configuration studied previously consists of a hole in a wide plate. Multiple surface and/or corner cracks are located along one side of the hole and are assumed to be partelliptical in shape. A remote cyclic stress is applied perpendicular to the crack plane, and the multi-degree-of-freedom analysis predicts the initial growth, coalescence, and propagation to failure of the final dominant flaw as shown schematically in Fig. 1. The numerical model employs stress intensity factor solutions developed by Newman and Raju for single surface and corner cracks [6], while interaction between individual cracks is predicted by a stress intensity factor solution obtained especially for coalescing corner cracks at fastener holes [2]. Prior work with the model demonstrated that it gives excellent predictions for intentionally introduced fatigue cracks which have relatively large initial dimensions [3-5]. The model had not previously been applied to small naturally occurring cracks which are the subject of the current investigation.

Alcoa Laboratories have conducted various experimental programs to investigate the influence of material quality on fatigue life [7-9]. Open hole fatigue specimens of aluminum alloy 7050 thick (6 in.) plate were machined from the quarter-thickness (low microporosity) and mid-thickness (high microporosity) plate locations [9]. The fatigue specimens were 0.125 inch (3.2 mm) thick, 1.0 inch (25.4 mm) wide, and 9.0 inches (229 mm) in length. Two 0.189 inch (4.75 mm) diameter holes drilled 1.0 inch (25.4 mm) apart along the specimen centerline were used to increase the likelihood that microporosity would be present on the surface of the hole. The specimens were cycled to failure (complete fracture of specimen through one hole) at three different axial stress levels. Examination of the fracture surfaces with a scanning electron microscope (SEM) indicated that fatigue cracks initiated from material micropores rather than from machining flaws. At each stress level fatigue life increased with a reduction in the size and frequency of crack initiating micropores.

### **Analysis of Experimental Results**

The original numerical algorithm assumes the initiating inhomogeneity to behave as an ideal elliptical crack. While this assumption gives reasonable fatigue life predictions for the 42 experiments considered in this investigation it may not for other situations such as initiation starting from particles or extremely small microporosity. To investigate different initiation sites the work of Trantina and Barishpolsky [10] was incorporated into the current analysis procedure. They conducted an elastic-plastic finite element analysis for estimating the stress intensity factor for small cracks which originate at voids or inclusions within a large body. The problem they examined consisted of an ellipsoidal void or inclusion which contains an equatorial crack of length b as shown in Fig. 2. The void height is h, its width is 2R, the crack extends a uniform length b around the void equator (x-y plane), and a remote stress  $\sigma$  is applied in the z direction perpendicular to the plane of crack growth. An effective stress intensity factor for this flaw geometry is given in Ref. 10 by the following expression:

$$K = \beta \sigma \sqrt{\pi b}$$
 [1]

where the dimensionless geometric term  $\beta$  is given by

$$\beta = \frac{2}{\pi} + B(1.12 \,\mathrm{K_t} - \frac{2}{\pi} - 1)(\frac{R}{b+R})^{10} + (\frac{R}{b+R})^{1.8} \quad . \tag{2}$$

Here  $K_t$  is the elastic stress concentration factor for the ellipsoidal void or inclusion (without the crack), and is a function of the aspect ratio h/2R. The constant B in Eq. 2 is given by B = 1 for a void, B = 2 for a bonded cracked inclusion, and by B = 0.3 for an unbonded inclusion. Note that for a void with B = 1, and for a crack size b >> R,  $\beta$  reduces to  $2/\pi$ , the well known result for a penny shaped crack in an infinite body. In this case, the void no longer influences the crack tip stress intensity factor. At the other extreme, when b << R,  $\beta$  equals  $1.12BK_t$ . Since 1.12 is the  $\beta$  value for an edge crack in a semi-infinite plate, this result effectively reflects the influence of the void on small cracks simply by the magnification in local stress caused by the void  $K_t$  (recall B=1 for a void).

Several points had to be considered before the Trantina-Barishpolsky solution could be applied to the microporosity encountered in the present experiments. First, one must account for the fact that the inhomogeneities are located along the bore of a hole, rather than at the center of a large body as assumed in Ref. 10. In addition, the inhomogeneities of interest are not necessarily circular in the x-y plane (perpendicular to the applied stress), nor is the crack length the same in the x and y directions.

These points are incorporated into the analysis by defining the following effective stress intensity factor:

$$K = \frac{K_{T-B}}{K_{penny}} K_{N-R} . ag{3}$$

Here  $K_{T-B}$  is the Trantina-Barishpolsky stress intensity factor solution computed by Eqs. 1 and 2 for a cracked void or inclusion in a large body,  $K_{penny}$  is the stress intensity factor solution for a circular penny shaped crack (i.e. no void) in an infinite body, and  $K_{N-R}$  is the Newman and Raju [6] stress intensity factor solution for a surface or corner crack located along the bore of a hole. To account for noncircular cracks, crack growth in the major and minor flaw directions was analyzed by defining  $K_{penny}$  with respect to the major and minor axes respectively.

The microvoids are assumed here to be precracked ellipsoids (B = 1), with the measured microvoid dimensions consisting of the sum of the void radius R and the crack length b. The void  $K_t$  would depend on the aspect ratio h/2R, and possibly on the "roughness" of the void surface. Specifying the crack length b involves deciding what portion of the initial inhomogeneity is cracked at the start of the test (i.e. the ratio R/(b+R) in Eq. 2). Since neither the void  $K_t$  nor the initial crack size b were known a priori, the effect of these two parameters on fatigue life was examined numerically. Figure 3 shows the influence of the void  $K_t$  and the initial crack size parameter R/(b+R) on the predicted fatigue life for a typical specimen. Note that the initial portion of the defect which is assumed to be cracked, reflected by the term R/(b+R), plays a modest role on life. When b >> R, the void loses its local influence, and the result from the original life analysis is obtained. When the initial crack size b is small, life decreases with increasing  $K_t$  as one would expect. Based on these calculations, and the likelihood that the microvoids could influence the growth of small cracks, it was decided to fix R/(b+R) = 0.9, and let  $K_t = 10$  for the current calculations.

The number of cycles N_p required for the dominant crack to grow to a size which had a crack growth rate of 0.01 inch/cycle (2.5 mm/cycle) was computed, and is compared in Fig. 4 with the actual measured fatigue life N_a. Only the shortest fatigue life is reported when multiple computations were performed for situations which involved cracks on opposite sides of the hole. The 0.01 inch/cycle crack growth rate was used here to define the predicted fatigue life, and it is expected that specimen fracture would occur within a few cycles after reaching this relatively fast growth rate. Therefore, for all practical purposes the predicted life N_p given in Fig. 4 represents the total specimen life to fracture. Note that the predictive model agrees quite well with the experimental results.

### Predictive Study of Initial Inhomogeneity Size, Location and Type

One goal for the current research was to develop a fatigue crack growth model which could be used to predict the effects of changes in initial material quality on the fatigue life of structural components. The initial inhomogeneity size and location distributions may be measured from the fracture surfaces of lot release tests [7] or determined from nondestructive inspection methods such as acoustic microscopy. Either the original algorithm or the modified algorithm may be used to study the effect of changes in the size and location of micropores. However, as process improvements continue to decrease the size and frequency of micropores in the material, constituent particles will most likely be the next inhomogeneity to initiate fatigue cracks [8]. The incorporation of the Trantina-Barishpolsky analysis is important because it allows different types of initiation sites to be compared.

To demonstrate how this model can be used to predict fatigue life, the following question was examined using a parametric study. "When do the micropores become small enough that constituent particles become the initiation sites?" The specimen configuration examined previously was considered to contain a quarter-circular (a=c) corner crack or a semi-circular surface crack located along the hole bore at midplane. The remotely applied cyclic stress was assumed to be 20 ksi (138 MPa) with a stress ratio of 0.1. Two types of initial defects were considered: a micropore with B=1.0 and a cracked inclusion with B=2.0 in Eq. 2. The initial void crack size parameter R/(b+R) was fixed at 0.9 as before and K_t was assumed to be 10. The fatigue lives corresponding to various initial size assumptions are shown in Figure 5. Note that this figure shows that for an equal area, the particle is more damaging than the pore, and that the corner is a more damaging location.

While constituent particle size varies with different processing procedures, a reasonable size range is 5 to 15  $\mu$ m in radius, which correspond to areas of 80 - 700  $\mu$ m². As shown in Fig. 5, particles of this size placed at the hole corner location have fatigue lives similar to pores with areas of 240 - 2200  $\mu$ m² located at the midplane hole location. By chance, tests conducted for another program [8], have demonstrated that this analytical study gives reasonable results. One specimen failed at 80,700 cycles due to the presence of a 710  $\mu$ m² micropore area located near the midplane of the hole. Figure 5 predicts a fatigue life of approximately 80,000 cycles for a midplane pore (surface void) of this size. A second specimen failed at 79,500 cycles due to a 324  $\mu$ m² constituent particle located at the hole corner. Figure 5 predicts that a 240  $\mu$ m² corner particle would cause failure at this life, which again agrees fairly well with the observed

value of 324  $\mu$ m². (The fracture surfaces for these two specimens are given in Fig. 6, and show the difference between the interior porosity and corner particle initial inhomogeneities.)

### **SUMMARY AND CONCLUSIONS**

A fatigue crack growth analysis has been performed for a series of experiments conducted to determine the effect of microvoid location and density on the fatigue life of notched specimens machined from 7050-T7451 aluminum plate. A computer program written previously to predict the life of multi-cracked holes was modified to consider the influence on the stress intensity of initial void crack interaction.

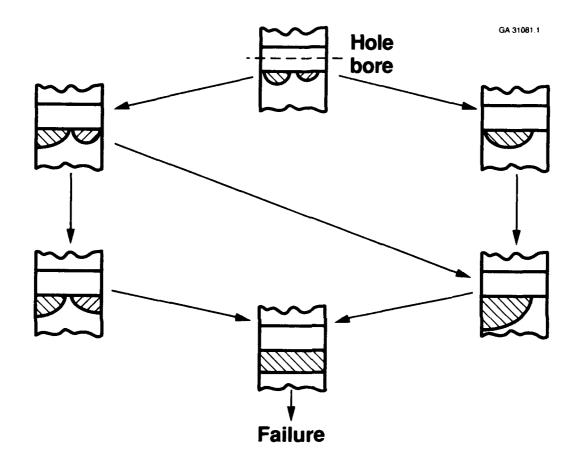
The original crack growth algorithm gave excellent life estimates for the data considered here, although the original analysis treated the microvoid "crack starters" as planar elliptical cracks, and did not consider the local stress concentration caused by the void. When a stress intensity factor analysis by Trantina and Barishpolsky [10] for small cracks which occur at voids or inclusions was added to the analysis scheme, similar life estimates were obtained, indicating that the initial crack assumption was quite reasonable for the current tests. A key advantage of incorporating the Trantina-Barishpolsky defect analysis, however, is the capability to compare initial inhomogeneity types.

It is felt that the good agreement obtained between experiment and analysis suggest that the present algorithm is a useful tool to predict the effect of altering discontinuity size, spacing, and type on the life of notched components. One such hypothetical configuration was examined to demonstrate the type of parameter studies possible with the current analysis tool.

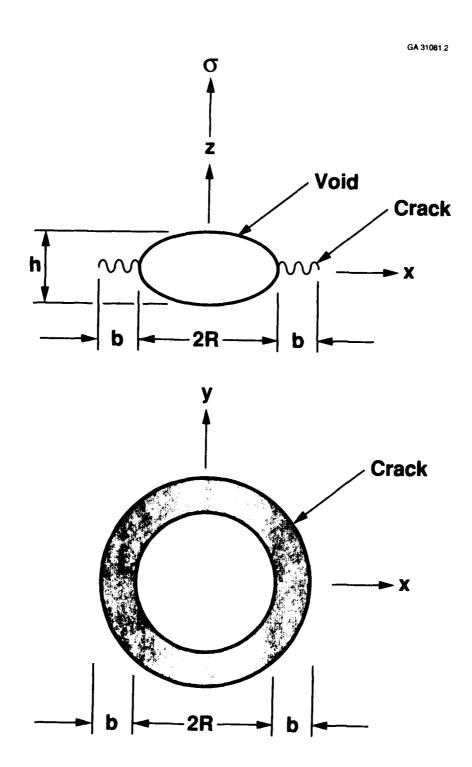
Consideration of the "small" crack problem was limited here to use of the Trantina-Barishpolsky stress intensity factor analysis for small void cracks, and the broader issue of "small" versus "large" crack material response remains to be studied. Although good results were obtained in the current analysis by extrapolating a linear fit of the "large" crack da/dN versus  $\Delta K$  data to the low  $\Delta K$  regime, it is recommended that small crack data be used when available.

### REFERENCES

- 1. R. Perez and A. F. Grandt, Jr. "Coalescence of Multiple Fatigue Cracks at a Notch," Proceedings, American Society of Civil Engineering EMD Specialty Conference, Purdue University, May 1983.
- 2. B. J. Heath and A. F. Grandt, Jr. "Stress Intensity Factors for Coalescing and Single Corner Flaws Along a Hole Bore in a Plate", *Engineering Fracture Mechanics*, Vol 19, No. 4, 1984, pp. 665-673.
- 3. A. F. Grandt, Jr., R. Perez, and D. E. Tritsch, "Cyclic Growth and Coalescence of Multiple Fatigue Cracks," *Advances in Fracture Research*, Proceedings of the 6th International Conference on Fracture, New Delhi, India, December 1984, Vol. 3, pp. 1571-1578.
- 4. A. F. Grandt, Jr., A. B. Thakker, and D. E. Tritsch, "An Experimental and Numerical Investigation of the Growth and Coalescence of Multiple Fatigue Cracks at Notches," *Fracture Mechanics: Seventeenth Volume, ASTM STP 905*, 1986, pp. 239-252.
- 5. T. H. McComb, J. E. Pope, and A. F. Grandt, Jr. "Growth and Coalescence of Multiple Fatigue Cracks in Polycarbonate Test Specimens," *Engineering Fracture Mechanics*, Vol. 24, No. 4, 1986, pp. 601-608.
- 6. J. C. Newman and I. S. Raju, Stress Intensity Factor Equations for Cracks in Three-Dimensional Finite Bodies, NASA Technical Memorandum 83200, Langley Research Center, Hampton, Virginia, August 1981.
- 7. P. E. Magnusen, A. J. Hinkle, W. Kaiser, R. J. Bucci, and R. L. Rolf, "Durability Assessment Based on Initial Material Quality," ASTM Journal of Testing and Evaluation, Nov. 1990, pp 439-445.
- 8. P. E. Magnusen, A. J. Hinkle, R. L. Rolf, R. J. Bucci, and D. A. Lukasak, "Methodology for the Assessment of Material Quality Effects on Airframe Fatigue Durability," *Fatigue 90*, Honolulu, HA, 1990, July 15-20.
- 9. A. J. Hinkle, P.E. Magnusen, R. L. Rolf, and R. J. Bucci, "Effect of Microporosity on Notched Specimen Fatigue Life," Structural Safety and Reliability, Vol. 2, pp 1467-1474, 1989. Edited by A. H-S Ang, M. Shinozuka, G.I. Schuleller, American Society of Civil Engineers, New York, Proc. of ICOSSAR '89, the 5th International Conference on Structural Safety and Reliability, San Francisco, CA, August 1989.
- G. G. Trantina and M. Barishpolsky, "Elastic-Plastic Analysis of Small Defects-Voids and Inclusions," *Engineering Fracture Mechanics*, Vol. 20, No. 1, 1984, pp. 1-10.

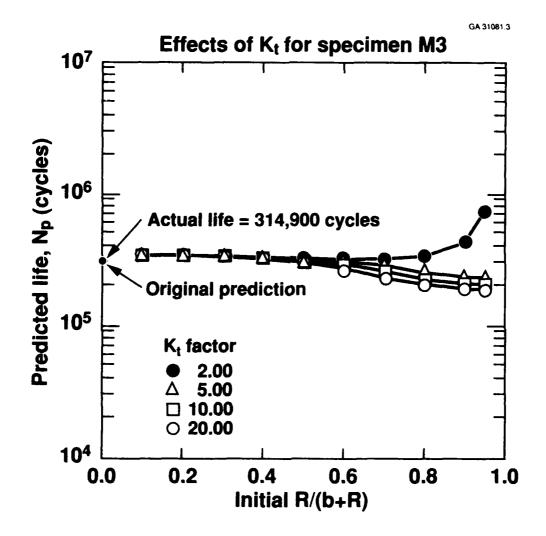


Schematic Representation of Various Ways in which Two Surface Surface Cracks at a Hole Can Transition into a Single Through-Thickness Crack Figure 1



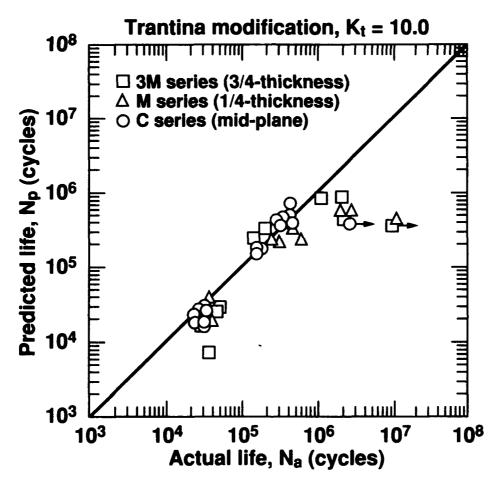
Schematic Representation of Cracked, Ellipsoidal Void Analyzed by Trantina and Barishpolsky.

Figure 2

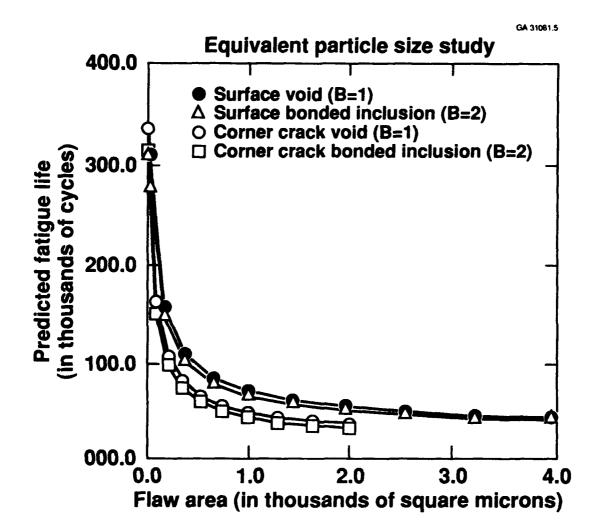


Parametric Study Showing Influence of Void K_t and Initial Amount of Void Precrack on Predicted Fatigue Life for Specimen M3 Figure 3

GA 31081.4



Comparison of Predicted and Measured Fatigue Lives Employing the Trantina-Barishpolsky Stress Intensity Factor Analysis for Voids with  $K_t$  = 10.0 Figure 4



Results of Parametric Study Showing Influence of Initial Void or Inclusion Area and Location on Fatigue Life
Figure 5



a) Interior porosity of 710 μm².
 Actual life: 80,700 cycles,
 Predicted life: 80,000 cycles.



b) Corner particle of 324 μm².
 Actual life: 79,500 cycles.
 Predicted life: 74,500 cycles.

### Verification of Trantina-Barishpolsky Analysis for Type of Inhomogeneity Figure 6

### A Review of the Problem of Short Fatigue Cracks

by

### R.L. CARLSON, G.A. KARDOMATEAS

School of Aerospace Engineering, Georgia Institute of Technology

and

### P. BATES

### Georgia Tech Research Institute

### Abstract

A review of published results indicates that the description of short fatigue crack behavior as "anomalous" is inappropriate. This designation is a consequence of the use of correlation procedures which are not valid. An understanding of short fatigue crack growth behavior appears to require that two effects must be considered. The first of these concerns the role of obstruction to closure upon unloading. For a given range of stress intensity factor, obstruction to closure is generally less for short cracks than for long cracks. A second involves the fact that the linear fracture mechanics relation between the stress intensity factor range and the cyclic plastic zone is not generally valid for short cracks.

### Introduction

Most considerations of short fatigue crack behavior begin with reference to results obtained by Pearson [1]. Pearson discovered that short cracks could grow under loading which was below the threshold range of stress intensity factor. This behavior was subsequently described as "anamolous", and it has since been the subject of numerous investigations.

The objectives of this paper are to summarize the progress which has provided a characterization of the basic features of short fatigue crack behavior, and to identify problems which remain to be resolved.

### Short Fatigue Crack Features

To provide an overall perspective of short fatigue crack behavior within the context of fatigue in general, it is helpful to refer to the Kitagawa diagram [2] shown in Figure 1. Fatigue, crack nucleation and growth pass through distinct regimes which can be charac-

terized by crack length. The relation of the fatigue failure loading boundary to crack length is illustrated in Figure 1. In the plot of stress range versus crack length, the boundary is divided into three regimes which are depicted as two straight lines in regimes I and III and a curve in regime II. Stress range values below the boundary correspond to cases in which cracks are arrested. Above the boundary, crack growth occurs.

The ordinate value of the boundary in regime I corresponds to the endurance limit. The line in regime III represents the value of stress range,  $\Delta \sigma$ , corresponding to the threshold value of the stress intensity range,  $\Delta K$ , in the relation

$$\Delta K = Y(\Delta \sigma) \sqrt{\pi a} ,$$

where Y is constant for the given crack configuation and a is the crack length.

If the dashed lines were extended and used as the boundary in regime II, predictions would be nonconservative because cracks are observed to grow below these lines. The boundary in regime II is, therefore, represented by the solid curve connecting the two straight lines. The primary emphasis here will be on regime II. Before proceeding to this topic, however, few general remarks about the regimes in the Katagawa diagram will be made.

Crack initiation and initial growth are dependent on microstructural features such as inclusions, grain boundaries and texture [3,4,5,6,7]. At the left end of regime II cracks of the order of a microstructural feature such as grain size have exhibited discontinuous growth rates [4,5]. They alternately sprint, for example, through a grain and then are retarded at barriers such as grain boundaries. The transition from regime II so regime III occurs at different values of crack length for different alloys. It has been suggested that transition length depends on the grain size and the yield strength [8,9]. Experimental results have indicated that the length at the transition from regime II to III occurs at a length of the order of ten times a characteristic microstructural feature such as grain size [9].

It has also been observed that in comparing two alloys, the one with the greater endurance limit can have the lower threshold for crack growth [6,10]. This reversal in resistance behavior may create difficulties in developing correlations between crack initi-

ation and crack growth behavior [11,12]. Efforts to use fracture mechanics as a basis for extrapolating back to the initial phase of fatigue damage may, therefore, involve issues which require further study.

Recent results indicate that the anomalous designation is inappropriate, and is a consequence of the use of correlation procedures which are not valid. A clarification of short fatigue crack growth behavior appears to require that two effects must be considered. One concerns the role of obstruction to closure upon unloading. For a given range of stress intensity factor, obstruction to closure is generally less for short cracks than for long cracks. A second mechanism involves the fact that the relationship between the stress intensity factor range and the cyclic plastic zone size used for long cracks is not valid for short cracks.

Although most attention has been directed toward consideration of these two mechanisms, a third potentially important mechanism should be mentioned. Nakai and Ohji [13] and Nakajima, et al [14] have presented test results for "anomalous" short crack behavior which they contend was solely the result of corrosive action. That is, for the test conditions developed, they ruled out both crack tip plasticity effects and closure effects. Since corrosion fatigue failures are often observed in service, this behavior should not be ignored.

### Correlation Limitations

In fatigue crack growth the application of LEFM leads to the use of  $\Delta K$  to compute the cyclic plastic zone size at the crack tip. In 1967 Rice [15] predicted that because the use of  $\Delta K$  underestimates the size of the cyclic plastic zone size for short cracks, they should grow faster than long cracks for the same  $\Delta K$  value. This can be illustrated by considering an edge crack in a wide plate for which

$$\Delta K = 1.1(\Delta\sigma)\sqrt{\pi a} ,$$

where  $\Delta K$  is the stress intensity factor range,  $\Delta \sigma$  is the applied stress range and a is the crack length. When plots of short and long crack data are made, this is the type of equation used. If a short crack is one tenth the length of a long crack, it follows that the

ratio of the applied stress ranges for the same  $\Delta K$  is

$$\frac{\Delta \sigma(\text{short})}{\Delta \sigma(\text{long})} = 3.16 \ .$$

Clearly, the stress level for the short crack can be much larger than that for the long crack.

For long fatigue cracks,  $\Delta K$  serves as a valid correlation parameter. Also, the cyclic plastic zone  $r_{cyc}$  can be calculated from  $\Delta K$ , and it also can be considered a suitable correlation parameter. For short cracks  $\Delta K$  is no longer suitable, but  $r_{cyc}$ , if properly determined, may still be an acceptable correlation parameter. Nisitani, et al [16] have proposed that the short crack growth rate, da/dN, is proportional to the cyclic plastic zone size. They then assume that

$$rac{r_{cyc}}{a} \simeq rac{\Delta \sigma}{\sigma_0}$$
 ,

where a is the crack length and  $\sigma_0$  is the yield strength. They then derive the relation

$$\frac{da}{dN} = D\left(\frac{\Delta\sigma}{\sigma_0}\right)^n a$$

for short cracks. The constants D and n must be determined from tests. Although this equation has been used to correlate short crack test data, it does not provide a continuous transition from short to long cracks. Separate growth rate equations are required for short and long cracks. Also, it does not, as K does, provide a description of component geometry and loading.

The determination of the size of the plastic zone in front of the crack tip is not as simple as may generally be believed. Larsson and Carlsson [17], Rice [18] and Leevers and Radon [19] have shown that an accurate determination of the plastic zone size requires the use of a second term of the Williams' series [20]. The additional term results in the addition of the uniform stress which is parallel to the line of the crack, and it can be either tensile or compressive. This uniform stress depends on the specimen geometry and the details of loading. For an edge crack in a finite width plate, for example, the stress is tensile and increases with increasing crack length to plate width ratio beyond a value of about 0.6. For ratios of less than 0.6 a compressive stress which increases with decreasing ratio is developed [19]. Computations for very short cracks have not been presented.

Although the short fatigue crack presents special problems with regard to the high level of loading encountered, it may be possible to develop a satisfactory correlation parameter which includes additional terms of the Williams' series. Thus, a replacement of  $\Delta K$  with

$$\Delta K (1 + \ldots)$$

may provide an improved representation of the cyclic plastic zone developed. The additional terms beyond unity could be expected to decrease with increasing crack length.

### Obstruction to Clossure Effects

Much of the recent work on short crack growth has focused on the effect of closure obstruction. It is reasoned that closure obstruction is less for short cracks and that all that is required is the adoption of an effective  $\Delta K$  to account for the observed behavior. Blom, et al [6] present results of an elastic-plastic analysis which support the reduction in closure obstruction conjecture. A number of researchers have adopted this approach, and they have presented results of correlations which show agreement with experimental data [6,12,21]. The results of Swain, et al [12] indicate that the Newman closure model [22] provides the adjustment in  $\Delta K$  required to correlate short crack data with long crack data except for the case of R = -1. For this case the short cracks grew faster than the long cracks. This observation would appear to be consistent with data obtained for negative R by Yu, et al [23] and by Tack and Beevers [24]. They found that the crack growth rate for tests with the same maximum stress increased with decreasing (more negative) R. This implies that compressive excursions, which are usually neglected, can affect closure obstruction.

It may appear that the use of an effective stress intensity factor range evades the question of its validity for describing the plastic yielding developed for short cracks. The rationale for the use of an effective  $\Delta K$  may, however, be viewed as being analogous to Irvin's plastic zone size correction to the crack length [25].

### Discussion

The applicability of the closure methods will probably depend on the extent to which the test data used to implement the analyses can successfully incorporate the inelastic features of short crack behavior. These inelastic features and the closure mechanisms are, of course, coupled. The degree of coupling can be expected to depend upon the R ratio value. For high R, for which a short crack may remain open throughout a loading cycle, closure obstruction would not be involved. For low values of R, however, the inelastic deformation at the crack tip is an integral part of the crack extension process which leads to the formation of closure obstructions. The complicating effects of negative R have been discussed above.

It was noted earlier that the level of load applied in the short crack experiments may result in the net stress being a large proportion of the yield strength. Components in aircraft which are subjected to this level of loading on a sustained basis could be expected to have very short lives for longer cracks. Such loading is not likely to be exprienced, however, as such high loads would occur on only an intermittent basis. This leads to the conclusion that the effects of intermittant loading should be studied. Some spectrum loading tests on short cracks have been conducted recently [12,26]. Some future tests should also, however, be conducted for simpler loading conditions. Considerable insight has been gained, for example, from tests in which is maintained constant except for a single overload. Tests of this type could reveal the development of retardation, or possible arrest effects which could have an impact on service applications involving short cracks. It has, for example, been shown by McEvily and Yang [27] that the form of closure obstruction can change abruptly during loading. They presented convincing evidence that indicates that even though crack closure obstruction prior to an overload is of the plane strain form, obstruction during the transient retardation interval occurs at the specimen faces; i.e., under plane stress conditions. It has been noted that this behavior can be expected to have an impact on closure models which are applied to variable amplitude loading for long cracks [28]. The possible effects on short cracks is at present a matter for conjecture.

Finally, the possible complicating effects of corrosion should be recalled. Service failure tabulations in which the causes of failure have been identified have indicated that corrosion fatigue occurs frequently. Access of corrosive agents to the tip of cracks can be expected to be easier for short cracks than for long cracks. This access may also be facilitated by

the fact that opening loads tend to be lower for short cracks than for long cracks. The complications for this problem involves a coupling of all of the mechanisms present; i.e., enlarged plastic zone size, closure obstruction and corrosion.

### **Conclusions**

- 1. Since the mechanisms for crack nucleation, short crack growth and long crack growth are different, attempts to extrapolate back from long growth behavior to the earlier regimes may not be possible.
- 2. Characterization of short crack growth as "anomalous" is based on the use of invalid correlation procedures. Because of the high levels of loading encountered with short cracks, the linear elastic fracture mechanics relation between cyclic plastic zone size and stress intensity factor range is not generally applicable.
- 3. It may be possible to adopt an elasticity based, multiple parameter solution as a correction for the crack tip plastic zone size. This may lead to the development of an acceptable correlation parameter for short crack growth under high R ratio loading.
- 4. For low R values some closure obstruction may develop. Then an acceptable correlation parameter must incorporate both the inelastic and closure effects properly.
- 5. The high level of loading used in short fatigue crack tests in the laboratory is not likely to be encountered on a sustained basis in service. Such high loads occur on only an intermittent basis, so the behavior of short crack growth under variable amplitude loading needs to be thoroughly investigated to evaluate the impact of the problem.
- 6. Evidence has been presented which indicates that the form of closure obstruction can vary for long cracks under variable amplitude loading. If such variations occur for short cracks, the development of simple closure models may be difficult.
- 7. In many service failures there is evidence that crack growth has occurred in conjunction with corrosion. The possible coupled effects of enlarged plastic zone, closure obstruction and corrosion should be recognized as a potential service problem.

### References

1. Pearson, S., "Initiation of Fatigue Cracks in Commercial Aluminum Alloys and Subsequent Propagation of Very Short Cracks", Eng. Fracture Mechanics, Vol. 7, pp.

- 235-247 (1975).
- 2. Kitagawa, H. and Takahashi, S., "Applicability of Fracture Mechanics to Very Small Cracks or Cracks in the Early Stages", *Proc. ICM-2*, ASM, pp. 627-631 (1976).
- 3. Schijve, J., "The Practical and Theoretical Significance of Small Cracks An Evaluation", Proc. Second Int. Conf. on Fatigue and Fatigue Thresholds, pp. 751-771 (1984).
- 4. Gregory, J.K., Gysler, A. and Luetjering, G., "The Influence of Texture on Fatigue Microcrack Propagation in an Al-Zm-Mg-Cu Alloy", *ibid*, pp. 847-856.
- 5. Newman, P.T. and Beevers, C.J., "The Initiation and Growth of Microcracks in Nickelbase Superalloys", *ibid*, pp. 785-796.
- Blom, A.F., Hedlund, A., Zhao, W., Fathulla, A., Weiss, B. and Stickler, R., "Short Fatigue Growth Behavior in Al 2024 and A 7475", The Behavior of Short Fatigue Cracks (Ed. K.J. Miller and E.R. delosRios), Mechanical Eng. Public., pp. 37-66 (1986).
- Kendall, J.M., James, M.N. and Knott, J.F., "The Behavior of Physically Short Fatigue Cracks in Steel", ibid, pp. 241-258.
- 8. Radhakrishnan, V.M. and Mutoh, Y., "On Fatigue Crack Growth in Stage 1", ibid, pp 87-99.
- 9. Taylor, D., "Fatigue of Short Cracks: the Limitations of Fracture Mechanics", *ibid*, pp. 479-490.
- 10. Bolingbroke, R.K. and King, J.E., "A Comparison of Long and Short Fatigue Crack Growth in a High Strength Aluminum Alloy", *ibid*, pp. 101-114.
- 11. Rudd. J.L., Yang, J.N., Manning, S.D. and Garver, W.R., "Durability Design Requirements and Analysis for Metallic Airframes", *Design of Fatigue and Fracture Resistant Structures*, ASTM STP 761, pp. 133-151 (1982).
- 12. Swain. M.H., Everett., R.A.Jr., Newman, J.C.Jr., and Phillips, E.P., "The Growth of Small Cracks in 4340 Sovel", Amer. Helicopter Soc. National Technical Specialists Meeting on Advanced Rotorcraft Structures, Williamsburg, Va. (1988).
- 13. Nakai. Y. and Ohji, J., "Short Surface Crack Growth in Corrosion Fatigue", Proc. Fourth Int. Conf. on Fatigue and Fatigue Thresholds, pp. 1605-1610 (1990).

- 14. Nakajima, M., Kato, Y. and Kitaoka, Y, "Corrosion Fatigue Characteristics of Small Surface Cracks in a High Strength Steel", *ibid*, pp. 1611-1616.
- 15. Rice, J.R., "Mechanics of Crack Tip Deformation and Extension by Fatigue", Fatigue Crack Propagation, ASTM STP 415, pp. 247-309 (1967).
- 16. Nisitani, H. and Goto, M., "A Small-crack Growth Law and its Application to the Evaluation of Fatigue Life", The Behavior of Short Fatigue Cracks (Ed. K. J. Miller and E. R. de los Rios), Mechanical Eng. Public., pp. 461-478 (1986).
- Larsson, S. G. and Carlsson, A. J., "Influence of Non-singular Stress Terms and Specimen Geometry on Small-scale Yielding at Crack Tips in Elastic-plastic Materials",
   J. Mech. Phys. Solids, Vol. 21, pp. 263-277 (1973).
- 18. Rice, J.R., "Limitations to Small Scale Yielding Approximation for Crack Top Plasticity", J. Mech. and Phys. of Solids, Vol. 22, pp. 17-26 (1974)
- 19. Leevers, P.S. and Radon, J.C., "Inherent Stress Biaxiality in Various Fracture Specimen Geometries", Int. Journal of Fracture, pp. 311-324 (1983).
- 20. Williams, M.L., Journal of Applied Mechanics, Vol. 58, pp. 109-114 (1957).
- 21. Larsen, J.M. and Jira, J.R., "Small Crack Closure Measurements in Titanium Alloys", Experimental Mechanics, pp. 82-87 (1991).
- 22. Newman, J.C.Jr., "A Crack Closure Model for Predicting Fatigue Crack Growth Under Aircraft Spectrum Loading", Methods and Models for Predicting Fatigue Crack Growth under Random Loading, ASTM STP 748, pp. 53-84 (1981).
- 23. Yu, M.T., Topper, T.H. and Au,P., "The Effects of Stress Ratio, Compressive Load and Underload on the Threshold Behavior of a 2024-T351 Aluminum Alloy", Proc. Second Int. Conf. on Fatigue and Fatigue Thresholds, pp. 179-190 (1984).
- 24. Tack, A.J. and Beevers, C.J., "The Influence of Compressive Loading on Fatigue Crack Propagation in Three Aerospace Bearing Steels", Proc. Fourth Int. Conf. on Fatigue and Fatigue Thresholds, pp. 1179-1184 (1990).
- 25. Irwin, G.R., "Plastic Zone Near a Crack and Fracture Toughness", Sagamore Ordinance Materials Conference, Syracuse University (1961).
- 26. Swain, M.H., Newman, J.C.Jr., Phillips, E.P. and Everett, R.A., "Fatigue Crack Initiation and Small Crack Growth in Several Airframe Alloys", *Proc. Fourth Int. Conf.*

- on Fatigue and Fatigue Thresholds, pp. 1079-1084 (1990).
- 27. McEvily, A.J. and Yang, Z., "Fatigue Crack Growth Retardation Mechanisms of Single and Multiple Overloads", *ibid*, pp. 23-36.
- 28. Carlson, R.L., Kardomateas, G.A. and Bates, P.R., "On the Effects of Overloads in Fatigue Crack Growth", Accepted for publication in *Int. Journal of Fatigue* (1991).

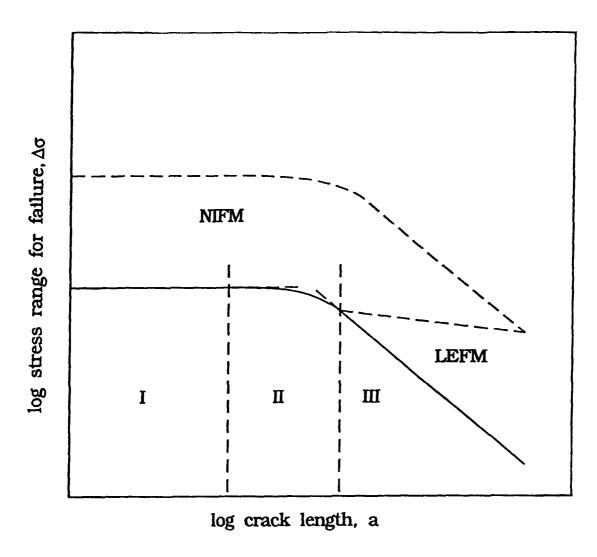


Figure 1. The Kitagawa Diagram.

#### 1991 USAF Structural Integrity Program Conference San Antonio, Texas 2-5 December 1991

#### MODELS FOR FASTENED STRUCTURAL CONNECTIONS

Dr. Barna A. Szabó Professor of Mechanics Washington University, St. Louis, MO 63130

> Dr. Jacob Bortman Major, Israeli Air Force

#### SUMMARY

This is a report on research conducted in the Center for Computational Mechanics of Washington University in St. Louis. The principal objective of this work is to improve safety of flight and minimize maintenance costs through effective utilization of computers.

Many investigators have been and are being concerned with the question: how to obtain correct numerical solutions to mathematical problems which are supposed to represent physical systems or processes? A great deal of progress has been made in this area, especially during the 1980's. It is now known that for a very large class of problems, which includes most problems in structural and mechanical engineering practice, exponential rates of convergence and very accurate estimates of error can be obtained by proper design of finite element meshes and increase of the polynomial degree of elements (see, for example, [1]). On the other hand, very little attention has been paid to the much more important questions: Is the mathematical problem properly formulated? – Is it adequate for the purposes of a particular decision-making task?

Consider, for example, the problem of deciding whether a titanium repair patch on a stiffened panel, made of laminated composites, is adequate or not. The panel shown in Fig. 1 was actually tested by the McDonnell Aircraft Company in

[†] The work reported has been sponsored by the Air Force Office of Scientific Research under research grant No. 88-0017 and the Israeli Air Force.

St. Louis. The test was designed for determining stiffness and strength. Consider now four mathematical models of this mechanical system:

Model 1: Plane elasticity, the fasteners represented by elastic springs.

Model 2: Plane elasticity, the fasteners represented by nonlinear springs, the properties of which are determined by coupon tests. Note that Model 1 is a special case of Model 2.

Model 3: Effects of bending and stability are considered in addition to the in-plane forces, and nonlinear fastener connections. Note that Model 1 and Model 2 are special cases of Model 3.

Model 4: Same as Model 3, but local failure of the panel is considered also. The first three models are special cases of Model 4.

The question is: Which of these models should be used? The answer depends on the range of loading and the desired accuracy. Model 1 generally does not represent reality well, but is much easier to use than the other models. Model 2 is generally accurate until buckling or local failure occurs. Model 3 is quite sophisticated (and expensive), and Model 4 involves a choice of failure theories, thereby introducing another set of modeling problems and requiring information which is not readily available.

The essential point is that a single model does not provide sufficient information for deciding whether the model itself is adequate or not. A particular mathematical model must be viewed as a member of a hierarchic system of models. The proper choice of a model from the hierarchic sequence is such that the data of interest are independent, up to the desired level of accuracy, from a priori restrictions imposed on the model.

A properly formulated hierarchic system of models makes it possible to approximate any real system or process up to the limits of our ability to represent the natural laws controlling that process by mathematical relationships.

The particular focus of the work reported here was the development of advanced models for fastened structural connections. The structural and strength responses of airframes are both very strongly influenced by the design and quality of fasteners. In present modelling practice fasteners are often treated poorly, even conceptual errors are not uncommon in the mathematical description of fasteners. As a consequence, expensive and time-consuming testing programs are

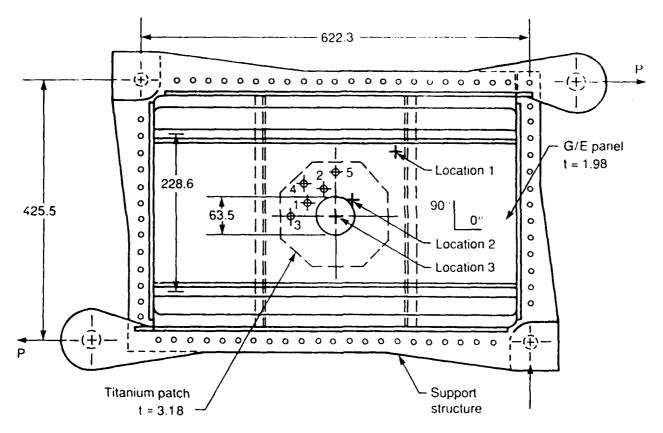


Fig. 1. Example: Shear test of a composite panel.

The dimensions are in millimeters.

required, essentially for overcoming the inadequacies of mathematical models and their numerical treatment.

#### Structural models

A model of fastened structural connections must provide reliable information about the distribution of forces in fastener groups. This is possible only if the force-displacement relationships of fasteners and their dependence on installation, aging and manufacturing tolerances are represented by the model.

The force-displacement relationships are generally nonlinear. Force-displacement curves, of the form  $F = k_f(\Delta) \Delta$ , can be obtained by inexpensive coupon tests. For a mathematical model to account for such nonlinearities, a simple and rapidly converging iterative procedure must be employed. In the first step linear stress-strain relationship is assumed.

Considering membrane action only, in the first step of the iteration fasteners are represented by a pair of rigid disks, connected to the upper plate and lower plate by distributed springs (see Fig. 2.) The mathematical representation of the

springs is:

$$T_n^{(U)}(\theta) = -k_n^{(U)} \left( u_n^{(U)}(\theta) + U \cos \theta \right)$$

$$T_n^{(L)}(\theta) = -k_n^{(L)} \left( u_n^{(L)}(\theta) + D \cos \theta \right)$$

$$F = k_f (U + D)$$

where the superscript U (resp. L) represents the upper (resp. lower) plate; the angle  $\theta$  is the angle measured from the line of action of the fastener force F, and

- $T_n$  is the normal traction acting on the fastener bore. (Force per length squared units).
- $k_n$  is the spring rate of a distributed spring between the rigid disk and the plate. (Force per length cubed units).
- un is the normal displacement (positive inward) of a point on the fastener bore.
- U is the displacement of the rigid disk in the upper plate.
- D is the displacement of the rigid disk in the lower plate.

The investigation has shown that structural models need not account for the fact that fasteners transmit forces in compression only, that is when  $(u_n^{(U)}(\theta) + U\cos\theta) > 0$  (resp.  $(u_n^{(L)}(\theta) + D\cos\theta) > 0$ ). Lumping the spring stiffnesses is adequate.

#### Strength models

In strength models either the maximal stress in the vicinity of fasteners or stress intensity factors must be computed. Knowing the magnitude and orientation of the fastener force F, from the structural model, computation of the stresses or stress intensity factors either by the finite element method or the boundary element method is straightforward.

#### Implementation and Examples

The numerical procedure has been implemented into a research computer program named NONLFAS which was used for evaluation of some practical demonstration problems. The commercial p-version finite element code MSC/PROBE† was employed to calculate the coefficient matrices of the upper and lower plates.

[†] The MacNeal-Schwendler Corporation, Los Angeles, CA 90041-1777.

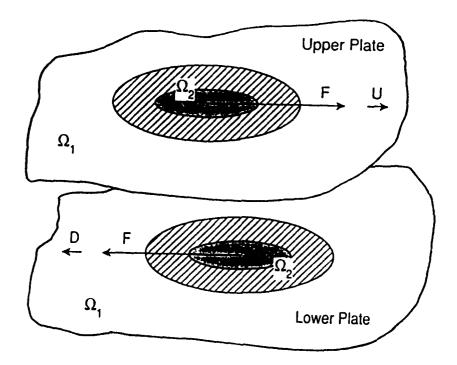


Fig. 2. Schematic representation of plate connections.

Experimental test measurements were employed for assessing the accuracy of the model. Three typical cases were investigated:

- (a) A ten-fastener doubler which was loaded into the nonlinear region;
- (b) An orthotropic shear panel with circular hole, simulating damage, repaired by an octagonal titanium plate (see Fig. 1);
- (c) A tensile orthotropic panel with a 4.0 inch diameter hole repaired by a trapezoidal titanium plate.

The model predictions were found to be in a good agreement with the experimental results reported in the literature. In all cases quality control and error estimation calculations based on p-extensions were performed. Based on these model problems, it was concluded that for structural analysis a relatively coarse mesh can be used with  $p \le 5$ . For strain and stress analyses, as well as for fracture mechanics computations, higher p-levels are needed, however. In certain cases, mesh refinement beyond the mesh required for representing the geometric details of a fastened connection was also needed to achieve the required accuracy.

#### Conclusions

It was found that there are two important parameters which affect the load distribution between the fasteners: the fastener stiffness and the level of initial

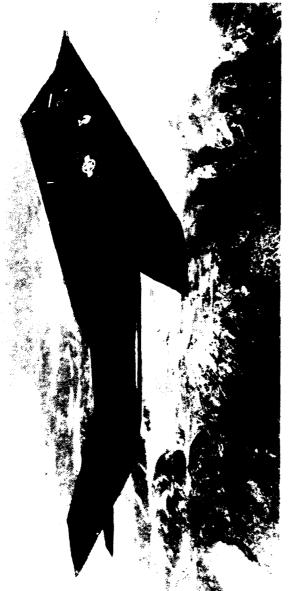
clearance at each fastener. Both of these parameters are controlled by the manufacturing and the installation processes.

- (1) The fastener stiffness: It was found that in all cases there were two saturation points with respect to the fasteners' stiffness, called the "weak" and "stiff" points, beyond which the fasteners may be considered as infinitely weak or stiff, respectively. In order to understand the sensitivity of the loads with respect to fastener stiffness one should first locate the stiffness of the investigated case relative to these two points.
- (2) The initial clearance: Two increments of initial clearance were specified. A high level (relative to the original displacement) to represent a poor installation where the fastener may be considered almost absent, and a low level which corresponds to a minor flaw in installation. In both cases, the behavior was found to be similar: for the tensile cases, the largest load change was always at the same fastener location where the increment of clearance was specified, and the load change decayed with the distance from that fastener. For the shear case, moment considerations controlled the load redistribution.

The procedure employed in this investigation can be modified for analyzing other types of connections. For example, connections by adhesives could be treated in similar fashion: modeling the plates by two-dimensional elements which are attached by nonlinear elements that would represent the adhesive behavior. Again, for purposes of efficiency, first the linear degrees of freedom should be condensed out, and only then should the nonlinear equations be solved.

#### REFERENCES

- [1] Szabó, B. and Babuška, I., Finite Element Analysis, John Wiley & Sons, Inc., New York (1991).
- [2] Bortman, J. "Nonlinear Models for Fastened Structural Connections Based on the p-Version of the Finite Element Method" D. Sc. Dissertation, Sever Institute of Technology, Washington University, May 1991.
- [3] Bortman, J. and Szabó, B. A., "Analysis of Fastened Structural Connections" to appear in AIAA Journal.
- [4] Bortman, J. and Szabó, B. A., "Nonlinear Models for Fastened Structural Connections" to appear in Computers and Structures.



### Probabilistic Design

Philosophy for Implementation

**USAF Structural Integrity Program Conference** 1991

Dr. Paul G. Roth GE Aircraft Engines December 4, 1991 (513) 774-5014

### PRDS (Probabilistic Rotor Design System) Contract Awarded by USAF WL/POTC -- F33615-90-C-2070

**USAF** program monitors:

Sqr. Ldr. Mike E. McIntyre (513) 255-2351 Ted G. Fecke (513) 255-2081

Focusing on advanced gas turbine engine disks

- 1. Identify limitations of current design practices
- 2. Develop a probabilistic methodology for design based on controlled risk of failure
- 3. Validate the methodology
- 4. Generate proposal for incorporation into an evolving ENSIP an Exploration of the Philosophy Not a Program Overview . .

### In Designing . . .

s can be controlled	
Some things can t	absolutely

If they are not, failures are possible

E.G. Core speed Analysis quality Uncertainties are not meaningfully statistical

Some things can be controlled only within limits

If they are too far out, failures are probable

E.G. Material cleanliness Surface integrity Fatigue capability Uncertainties may sometimes be statistically quantified

# Traditional Design Practices Address Concerns by Compounding Conservatism

- Max loads
- Min properties
- Safety factors

Successful but Why and by How Much?

Can We Afford Excessive Caution?

Sometimes but Probably Not Always --

# GEAE Life Managenient Analysis

Problems have been rare

- Life Management Programs (LMP) characterizes nine classes

	Analysis	Process	Materials	Quality	Systems
Tolerances too large	×				
Parts out of blueprint				×	
Manufacturing damage		×		×	
Fretting	×		×		
Material inclusions		×	×	×	
Assembly				×	
Temperatures not understood	×				
Stresses not understood	×				
Secondary failure					×

T2623.04 - 911113

# Analysis Verification Programs

- Analysis problems essentially confined to early days
- Methods validated under controlled conditions
  - Thermal
- Stress
- · Burst
- LCF
- Sharp crack fracture mechanics
- Probabilistic fracture mechanics
- Statistical combination
- NDE
- Analysis not fundamentally limited, but considerable data required

# Processes, Measurements and Usage Remain Concerns Given Accurate Analysis -- Variability in Materials,

Concerns cautiously managed

Probabilistically . . . by holding failure probability low Traditionally . . . by compounding conservatism

### Attention hierarchy

Major mechanisms	LCF
	Flaw induced cracking
Minor mechanisms	Yield (disk growth)
	Ultimate strength (burst)
Next on the list   Creep	Creep

# PRDS Uses Traditional Analysis Approaches but Eats Away at Margins When Meaningful

### Risk Is Quantifiable and Validatable Under Controlled Conditions

- Non-statistical contributors:
- Analysis inaccuracy
- Poor systems understanding
- Missed quality checks
- Operational variability

- Statistical contributors:
- Tolerances
- Instrumentation errors
- Engine build variability
- Mission mix
- Basic material properties
- Material flaws
- · Surface damage
- NDE detectability

T2623.07 - 91111

## Interpretation and Application of Risk Based Design Criteria

• Risk is a condition of uncertainty . . . probability theory called on for quantification

- Assumes predictability even in randomness

Statistical distributions derived from basics or inferred by sampling

Applied to predict subsequent sampling

· Probability theory works well in physics, chemistry, genetics and gambling

Repeated and repeatable sampling possible

 Application of probability theory to aircraft or engines or even to single disks requires a different interpretation

- Risks must be inferred from studies of simpler models

They can not be realistically validated

Consequently, decisions are qualitative despite quantitative language

Probabilistic methods require: extrapolation, validation, interpretation

#### Extrapolation

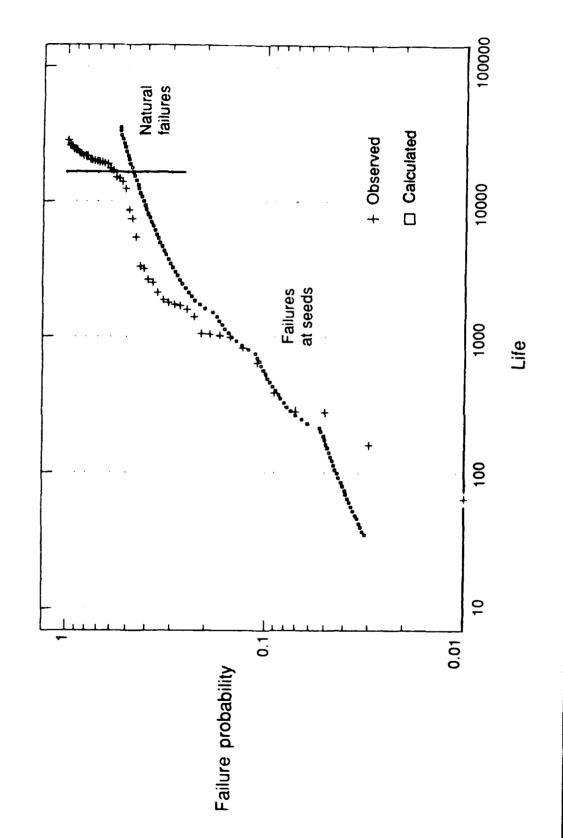
- Extrapolation . . . unavoidable
- Directly demonstrating design probability levels of 1/10,000 (or even 1/1,000) not possible
- Reasonable extrapolations given tight distributions
- Often attainable when sources of variability adequately identified
- Broad distributions a concern
- Critical applications more sensitive to extrapolation
- May be complicated by size effect translations

T2623 09 - 911113

#### Validation

- Validation . . . have to put the pieces together properly
  - Many examples show importance of getting it right
- Probabilistic analysis can be validated under controlled conditions
  - All analyses are defended this way
- Validation is usually restricted to probabilities between 1% and 99%
  - Probabilistic fracture mechanics demonstrated for seeded material . . . translation of results to more realistic flaw levels is very direct
- Current design practices, by contrast, lack quantitative validation

Probabilistic Fracture Mechanics

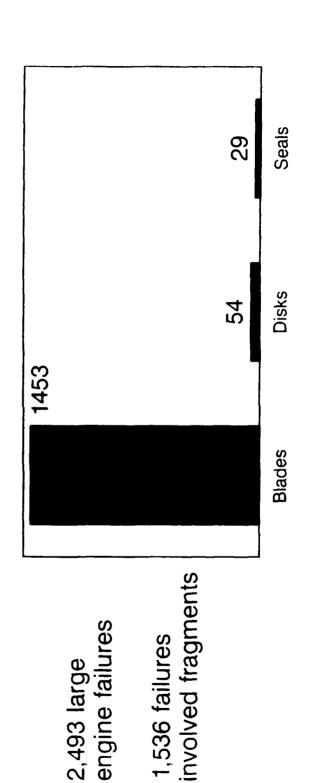


#### Interpretation

- Interpretation . . . surprises always possible
  - Not eliminated by current practices
- Nor by probabilistic approaches
- When the relevant failure modes are treated properly, risk will remain low
- If unrecognized failure modes appear, risk will be managed
  - Ability to react improved by PRDS-required level of analysis

### FAA/NAPC Statistics

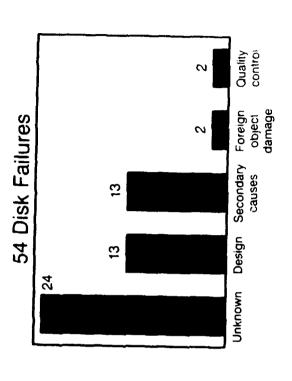
- engine rotor failures that occurred in U.S. commercial FAA/NAPC reports: statistics on aircraft gas turbine aviation during 1972-1987
- Disk failures comprise only a small percentage of large commercial engine failures (2.2%)

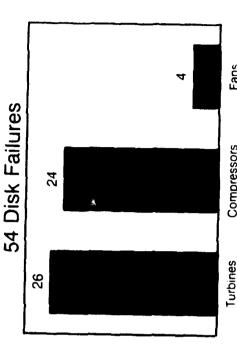


T2623.12 911113

### FAA/NAPC Statistics

- Some failures are attributed to design problems . . . many are not
- Fatigue or flaw induced cracking may be the dominant failure mode
  - 43 of the 54 disk failures occurred during takeoff and climb
- 24 of the 54 could not be explicitly assigned a cause
- Thermal stresses are likely significant drivers
- Hot disks more inclined to cracking than cold disks





12623 13 - 911113

- Assume a fleet of engines each to be operated to 20,000 flights, 3 hours per flight
- fleet is to provide 272.6 million hours of service Consistent with current levels of reliability, this with no more than 54 disk failures
- Running it like an LCF testing program, an upper bound on the acceptable design level of risk at 20,000 cycles can be calculated

1.188 failures 100 engines engine lifetime 20,000 flights 3 hours flight 272.6 million hours 54 failures

Note: Additional assumptions needed to infer design limits for individual disks

- In reality, commercial aviation is not an LCF test program
- The average life of the fleet is considerably less than the assumed 20,000 cycle design life
- Problems have occurred . . . have been managed and eventually eliminated
- It follows that the initial design risk at 20,000 cycles must have been considerably higher than 1/100
- But that it has been dynamically lowered by good life management

# Definition of Appropriate Risk

- but decisions must be made which affect everyone Concerning risk, no decision pleases everyone.
- Government constituted to make the minimum decisions required by society
- Government often responsible for balancing the risk equation
- Given analysis methodology which is validated and adequately supported by data . . . specification of 1/100 as a 20,000 cycle design limit is probably appropriate for now

T2623.16 - 911113

# But Shouldn't We Be Pushing for Greater Safety?

- Adding one zero to the design limit (making it 1/1,000) may be a reasonable near term goal
  - Its practicality depends on cost/benefit tradeoffs
- Adding even more zeroes to disk limits will probably not, however, reduce real engine risk if other elements of the system assume dominance

T2623 17 - 911113

#### Conclusions

- Current design practices work but may be wasteful
- Since risk isn't quantified, we don't really know
- Probabilistic design is preferable given tools which are validated and given adequate definition of the statistical inputs
- PRDS should be able to control recognized failure modes
- Also, while PRDS will not eliminate surprises, it should help in managing them
- 20,000 cycles would match commercial disk failure experience Based on FAA statistics, an engine risk of 1/100 at
- limit (though 1/1,000 may be a reasonable near term goal) - This suggests 1/100 at 20,000 as an appropriate design
- Requiring even lower rates (1/10,000 or 1/100,000) will accomplish little unless other system elements are concurrently improved

#### PRDS Status

- Program development underway
- Application and validation to begin next year

T2623 19 · 911113

#### RANDOM-BLOCK LOAD SEQUENCE DURABILITY TESTING OF T-37B EMPENNAGE USING A

# KURT SCHRADER • DEVIN BUTTS • JAMES UNRUH

Division of Engineering and Material Sciences
Southwest Research Institute
San Antonio, Texas
December 1991

### INTRODUCTION_

Final Results and Conclusions ☑ Data Collection and Monitoring ☑ Load Sequence Development ✓ Load Application Evaluation ☑ Laboratory Test Setup Durability Testing Objective External Loads Source ☑ T-37B SLEP Overview

## T-37B SLEP OVERVIEW.

Objective: Structural Life Extension for

8000 Additional Flight Hours

SABRELINER

SOUTHWEST RESEARCH INSTITUTE

**W** Modification

**Tooling** 

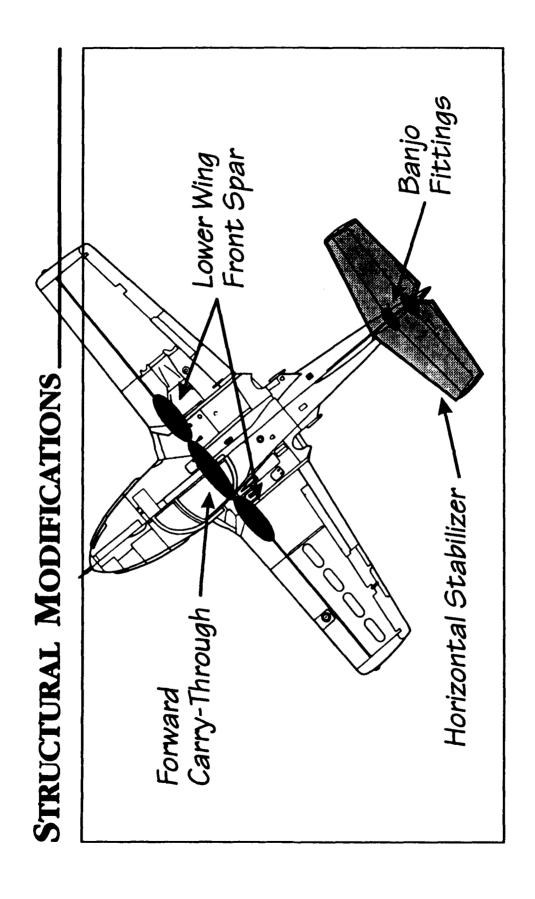
Analysis

**u** Design

**If** Testing

**域** Kit Production

**If** Flight Demonstration



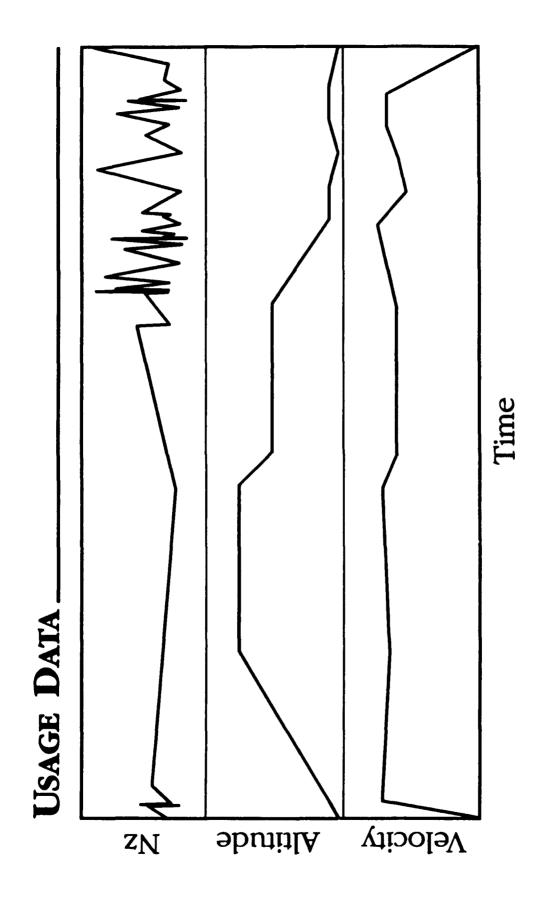
# DURABILITY TESTING TASKS.

For Install Modified Components on T-37B Aircraft

Test to Two Lifetimes (16,000 Hours)

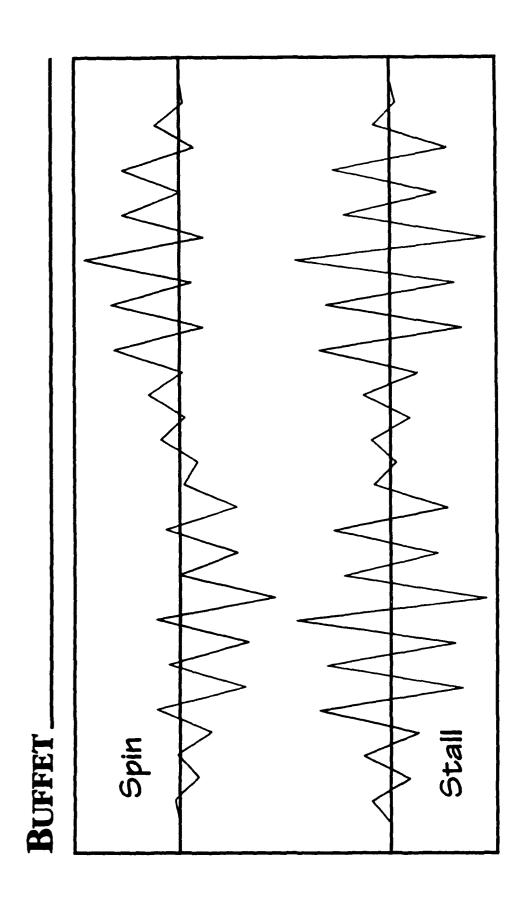
W Use Actual Usage Spectrum

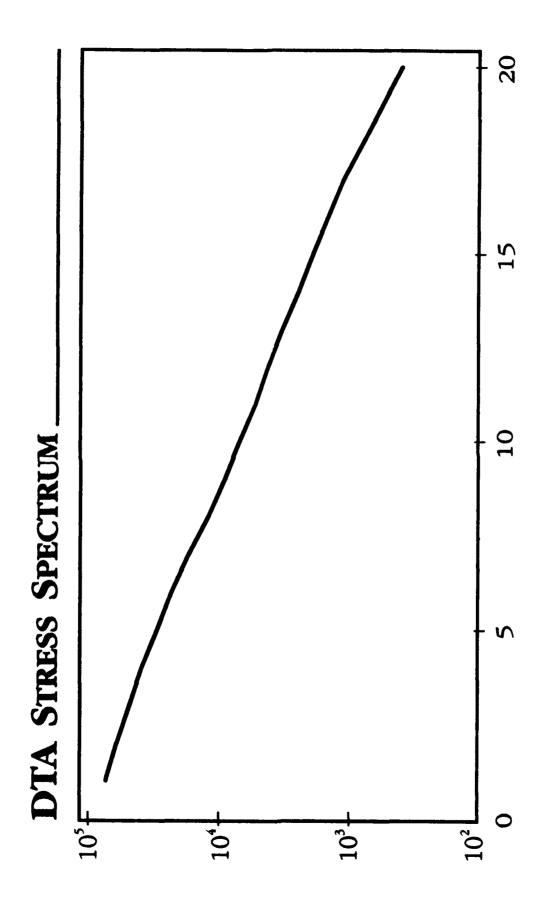
**G** Conduct Structural Inspections



# EXTERNAL LOADS SOURCE

- **M** Buffet Environment During Specific Maneuvers
- M Aft Tailcone Natural Frequency Vibrations
- Inertial Loading Induces Internal Stresses
- Demonstrated During Cessna DTA and SwRI Flight Test
- Published Stress Spectrum In Cessna DTA Report





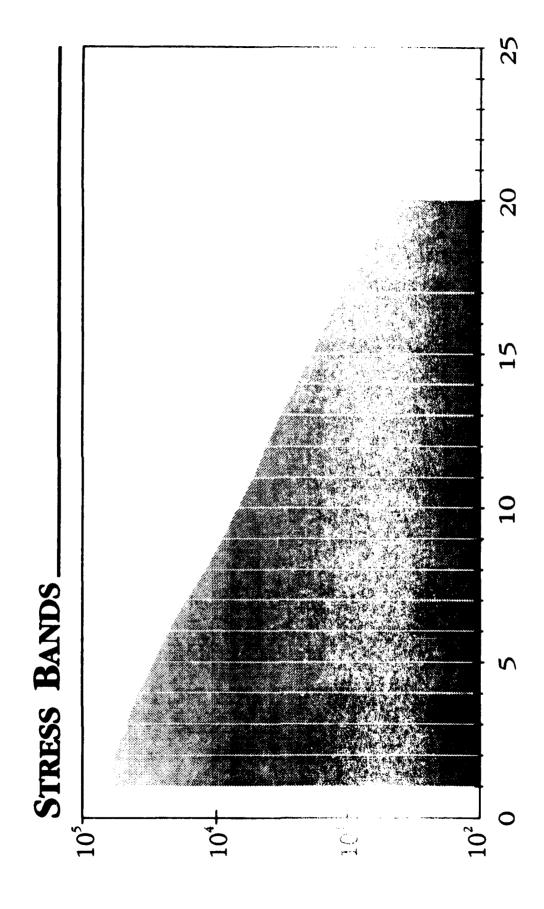
## LOAD APPLICATION EVALUATION.

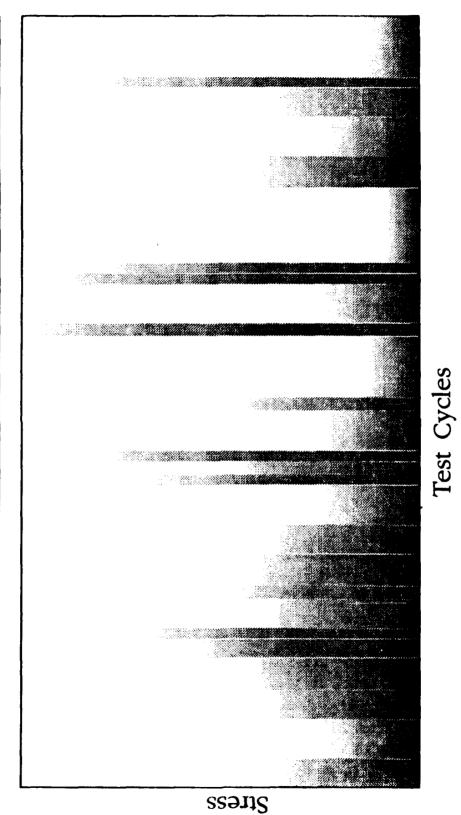
- Excitation of Torsional Mode to Produce Desired Stresses
- Unmodified Structure Subjected to Development Tests
- Instrumentation on Forward BanjoIn Demonstration of Capability
- ☑ Development of Stress Relationships

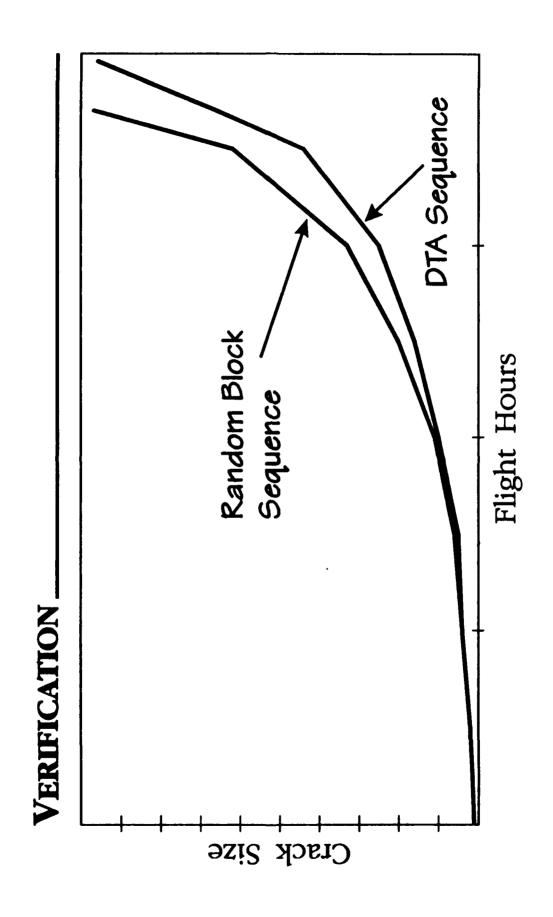
### > Strain Gages Φ Φ Strain Gage -FORWARD BANJO INSTRUMENTATION.

# RANDOM-BLOCK LOAD SEQUENCE DEVELOPMENT

- Published Stress Spectrum
- ☑ Discrete Occurrences in Individual Stress Bands
- Festablish minimum-maximum cycles per block
  - ~ Adequate Randomization
- ∼ Limitation of Control Equiptment
- **G** General Randomization of All Blocks
- **If** Verification of Random-Block Sequence







### LABORATORY TEST SETUP_

Test Article and Fixture

F Hydraulic Actuator and Control System

If Fixed Frequency Coupled with Random-Block Amplitude Time History

Gain Desired Signal Multiplier Signal Senerator M FORCING FUNCTION.

### DATA COLLECTION_

- Signal Conditioning
- **E** Digital Tape Recorder for Backup
- ☑ Data Collection Using Two Computers
  - ~ Peak/Valley Detection in Real-Time for Single Channel
- ~ Rapid Digitization of 16 Channels for Final Analysis

### DATA MONITORING_

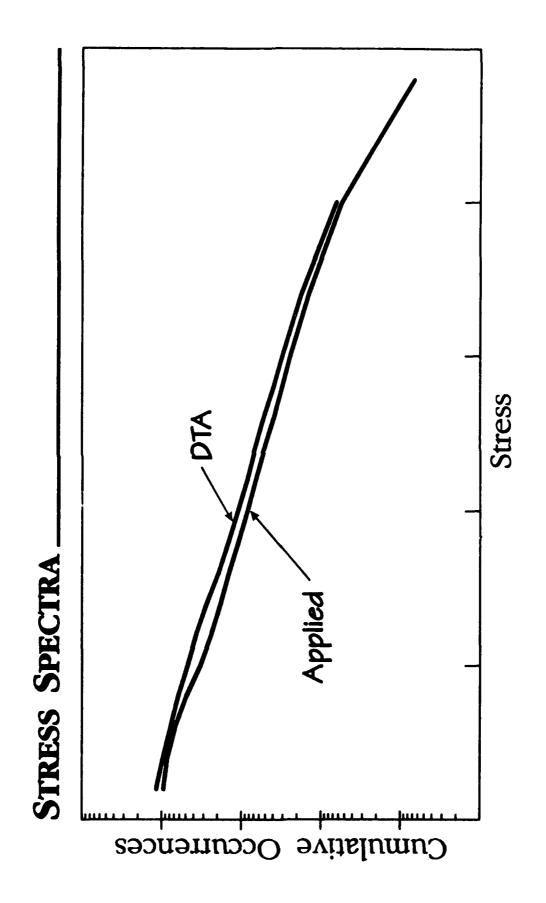
Assement of Each 1,000 Flight Hour Test Block

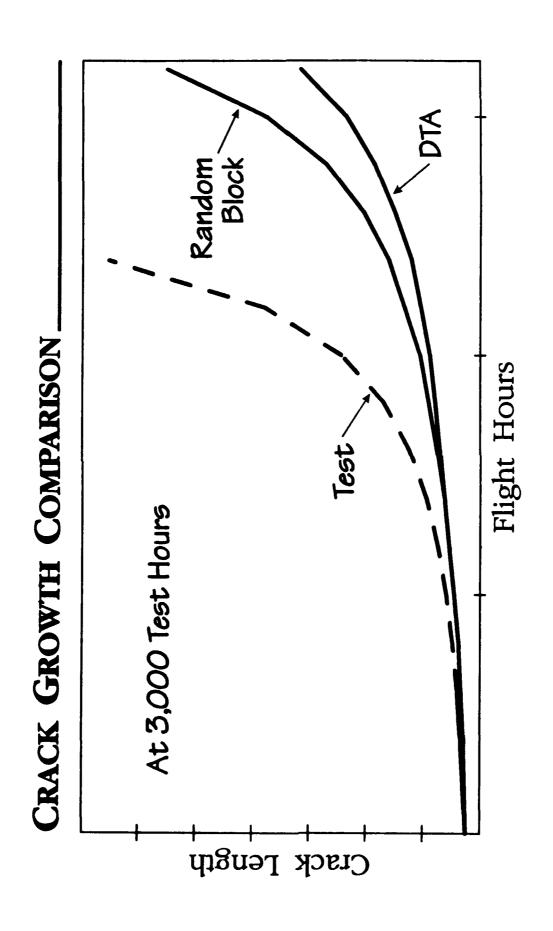
~ Control Gage Stress Spectra Comparison

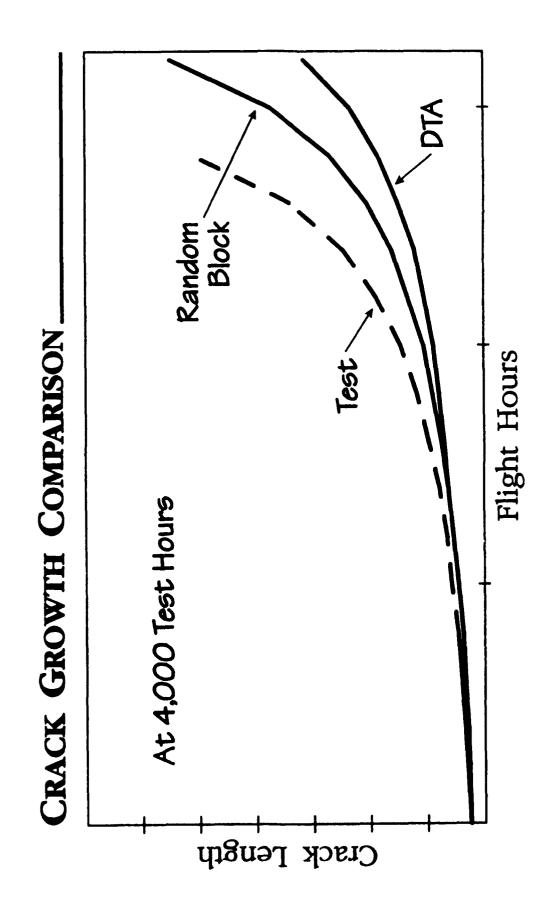
~ Crack Growth Comparison

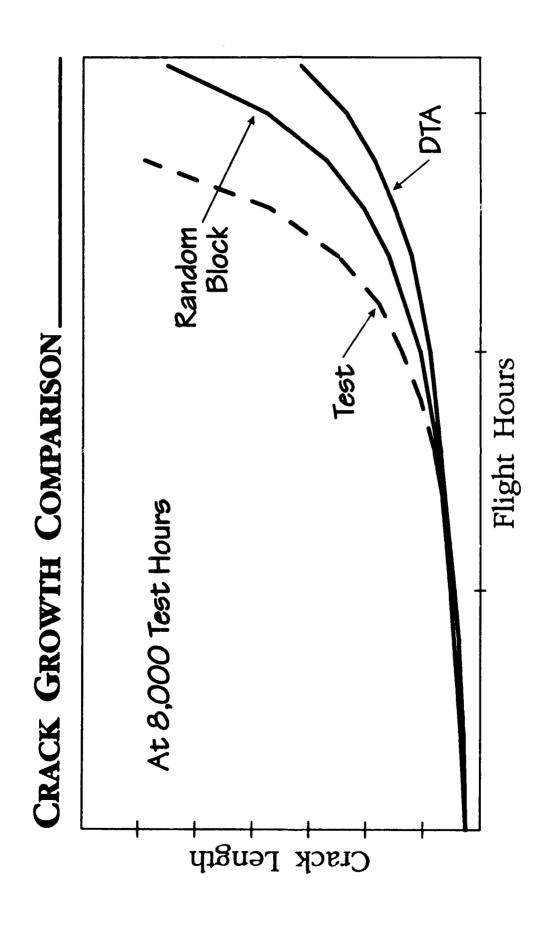
Adjust to Subsequent 1,000 Flight Hour Test Block Based on Projected Crack Growth

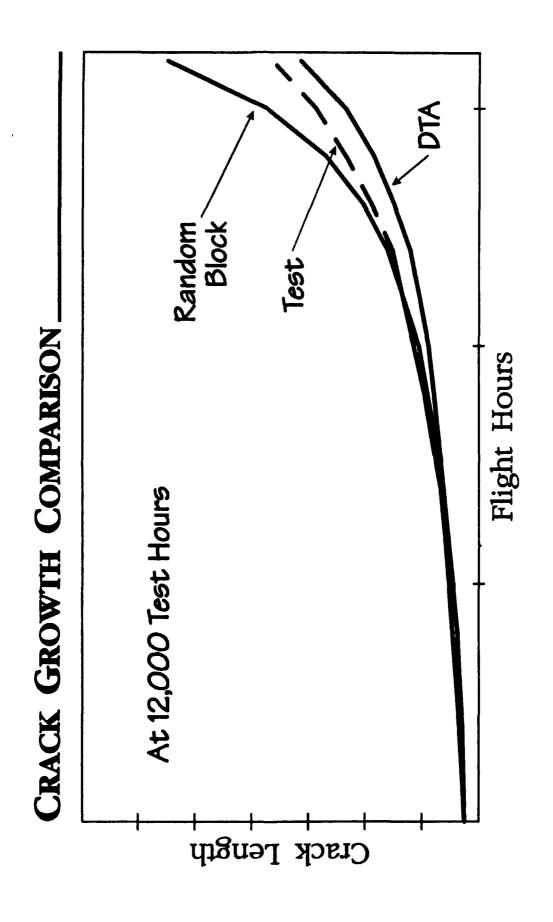
Digitization of Channels | Force | Acceleration | Strain Gages Conditioning Signal DATA ACQUISITION SYSTEM. Tape Backup Test Fixture Real Time Peak

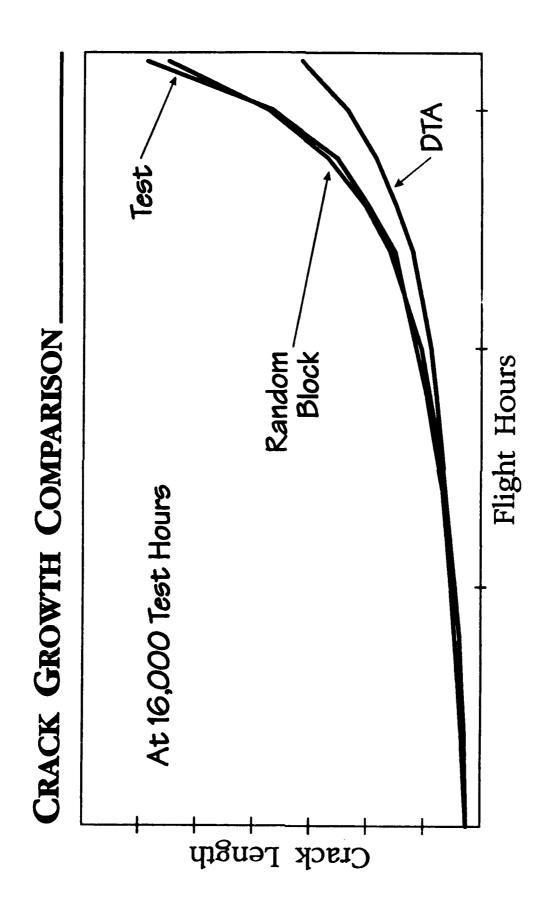












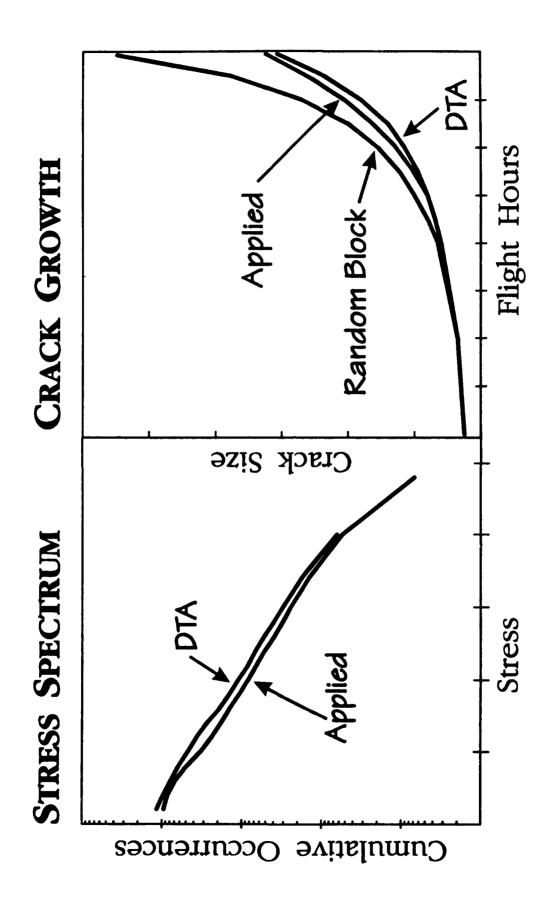
# FINAL RESULTS AND CONCLUSIONS.

Final Stress Spectrum and Crack Growth

If No Observed Cracking at Completion of Test

If Demonstration of Dynamic Input to Produce Desired Stress Spectrum

W Subjected Test Article to an Equivalent of 16,000 Flight Hours in Two Weeks



### VIBROACOUSTIC FATIGUE AND STRESS CORROSION CRACKS IN THE FUSELAGE SKIN OF A LARGE CARGO AIRPLANE

### W. Dunn**, L. Shaw* and L. Rogers**

### 1. Abstract

In August 1986, a 48 inch long skin crack was discovered in the forward fuselage of a large cargo airplane. An inspection of other airplanes identified similar, but very short cracks in 58 of 77 airplanes. The greater majority of cracks are associated with the row of fasteners joining external fairing support structure to the fuselage skin.

Initial investigations resulted in clarifying the type of problem but did not fully identify the cause of cracking. It appears that the cracks are the result of corrosion fatigue and stress corrosion. Because of the stress corrosion high crack growth rate, most of the crack faces studied showed large areas of intergranular separation and only small areas of fatigue structions.

A video holography program graphically identified the many panel responses as higher order thin skin vibration modes. At frequencies up to 1000 hz, panel modes of up to 5 peaks per panel were observed in the fringe patterns generated by the video holography technique.

A modal analysis (ground vibration test, GVT) program has been performed to identify lower frequency frame and stringer global (shell) modes as well as higher frequency panel modes.

An acoustic survey of engine noise, including the multiple pure tone harmonics, has been performed to identify the external acoustic patterns impinging upon the entire fuselage. Eleven other airplanes were tested to define the overall acoustic levels of the engines exciting the forward fuselage.

Fractographic, finite element analyses and material characterization studies are being performed to support the above programs investigating the skin cracks occurring in the large cargo airplane.

A flight test will also be performed to quantify the skin responses (acceleration and strain versus frequency) for selected flight and ground operations.

Additional flight data may be gathered and evaluated in conjunction with the above data to establish the effectiveness of practical crack controlling measures in this potentially high maintenance cost area. Based on the combined results of all of the efforts, the most cost effective measures will be recommended for fleet repair/retrofit of this aircraft.

^{*} US Air Force/Wright Laboratory/FIBG, Wright-Patterson AFB

^{**} Consultant

### 2. Background

The forward fuselage cargo area side walls are of frame, stringer and skin construction. The frames and stringers are made of 7075-T6 aluminum and the skin is 7079-T6 clad (one side) aluminum. Straps of 6AL-4V annealed titanium are bonded to the skin at frame and mid-bay locations. The skin is nominally 0.068 inches thick and the titanium straps are 0.016 inches thick. The material characteristics for the skin and straps are those for sheet material. The skin radius in the cargo area is 143.0 inches and the in-flight operating pressure is 8.3 psi. The frame spacing is 20 inches and the stringer spacing is nominally 8 inches. External fairing lower support structure is attached to the skin with a row of fasteners which are 1.57 inches above the adjacent row of stringer fasteners. The fairing lower support structure and row of fasteners is referred to as the waterline 295 area.

Most of the cracks have been located along waterline 295 with a few located at other stringers above the waterline 295 area. This observation led others to suspect that the source of initial cracking is the result of acoustic excitation of the frames, skin and fairing by engine fan noise when the engines are operated at takeoff rated thrust. It was suggested that global frames modes were responding to the engine fan noise, resulting in high cycle-low stress fatigue cracks of the skin along waterline 295.

A structural dynamic response and engine acoustic excitation test program was developed to define quantitatively, the structural dynamic response and engine acoustic source parameters relating to the skin cracking situation. This program consisted of defining modal responses using video holography techiques, a modal analysis (GVT) and an acoustic survey of the engines operating at and near takeoff rated thrust. Supporting efforts include analysis of existing data, fractographic examination of available crack surfaces and performance of a material characteristics program. A flight test program is recommended to identify and quantify other sources of acoustic excitation as well as other sources of loadings of the fastener holes along the waterline 295 area. Solutions and recommended fixes will then be developed and evaluated.

### 3. Video Holography Modal Analysis (GVT)

The video holography study was conducted by Mr. Gene Maddux, et al. of WL/FIBG as a prelude to the large conventional modal analysis to determine the response of the forward fuselage to engine noise. Since the size and complexity of the fuselage dictates the use of a large number of accelerometers and microphones for the modal analysis and acoustic survey, this preliminary study was very helpful. Ground-based modal analysis techniques needed to perform this type of survey have been used for many years; however, the sheer size and nature of this structure suggested the addition of this relatively new video holography technique. This technique provides a real-time view on a video monitor of the resonant responses of the structure as it is excited by the shaker or loudspeaker. Areas of antinodal

response are seen as series of dark fringes (contour lines) surrounded by bright areas corresponding to nodal lines. Local modes are those that are more or less confined to the region bounded by two adjacent stringers and two frames. Global modes, frame modes as they are sometimes called, consist displacements that involve essentially rigid body movements of many of the local regions. For local modes, the stringers and frames act as boundary conditions and the skin behaves somewhat like a slightly curved plate. Conversely, the global modes of interest are governed primarily by the stiffness of the frames and have very little coupling with local modes. One of the goals of this test program was to determine the predominate modal behavior the forward fuselage in the range corresponding to the acoustical excitation (350-500 Hz) produced by the engines.

The test equipment consisted of a shaker and power amplifier and the following special equipment: a Retra 1000 Video Holography system, a Panasonic NV 8950 VHS VCR, a Polaroid Freeze Frame image recorder, and a Wavetek Model 650 Variable Phase Synthesizer.

These tests were conducted at the Stewart Air National Guard base at Newburgh, New York. It is probably the first time that a video holographic survey has been conducted from inside the test specimen. The excitation was provided by a 25 pound-force shaker mounted to an overhead frame as shown in figure 1 and later by a loudspeaker located outside of the airplane in the vicinity of the The primary concern in using the video holography survey area. technique was unwanted rigid body motion and vibrations of the airplane relative to the laser source. The fringe patterns used to determine the resonant frequencies and mode shapes are created by extremely small changes of distance (a few microinches) between the holography module and the surface of the airplane during a 0.33 second period (the frame rate of the video camera). Low frequency (less than 10 Hz) variations of relative motions of 30 microinches or less can be tolerated through the use special optical processing techniques. To minimize the extraneous motion, two 5000 pound concrete blocks on the aircraft were used to provide a somewhat stable platform for the video holography system. The video holography camera was located about 350 cm from the fuselage wall. During holographic data acquistion periods, the attending personnel were limited to two people. The hangar air conditioners were turned off during the tests to prevent excessive motions caused by air loads acoustic coupling to the airplane.

In order to record the largest area possible with the 5 milliwatt laser in the video holography module, the surface of the airplane skin between frames and stringers was covered with a thin layer of low-mass retroreflective material as shown in figure 2. It returns about 1700 times as much light as a flat-white surface under the same illumination. The uncoated areas on the stringers and frames appear dark in the video images and are used as reference points to identify the locations of various areas of interest. The numerous cables in front of the coated areas did not obstruct the view of the mode shapes.

During the test, the shaker was used to excite the structure with a few sine sweeps from 8 to 1000 Hz and the resulting modal response viewed on the monitor and taped for subsequent review.

Sine dwell excitation was then used to record each resonant frequency and associated mode shape of interest. This was accomplished by first, manually sweeping the frequency until a fringe pattern developed, indicating a resonant condition. The frequency was then fine tuned until a maximum number of fringes (maximum amplitude response of the structure) appeared in the area of interest. This resonant frequency was recorded and a hard copy made of the mode shape using the Polaroid Freeze Frame unit with 35 mm black and white film. A film with an ASA rating of 200 was chosen to require about a fifteen second exposure time. Instead of "freezing" a single frame, the picture recorded is an average The unwanted low frequency fringes would drift of live fringes. randomly in the field of view during the exposure while the mode shape fringes remained almost stationary. The resulting photos do not have the resolution normally associated with video holography but have more than sufficientdetail to analyze the behavior of the structure. Observing the fringes in real time on the monitor is much better than looking at video taped or hard copy versions of This process was repeated for each major resonant data. condition. In order to get reasonably detailed pictures of the various mode shapes and complete the study in a finite length of time, the camera was positioned to cover a maximum area of about two square meters, the response recorded and then moved to the next location.

The results of the tests showed that there is a striking difference between the fringes generated during a sweep of the fuselage and those for a simple plate specimen. Some portion of the former is at resonance at virtually every frequency. usual test procedure calls for defining a resonant mode by maximizing a fringe pattern. With the fuselage, one portion of the view will contain several distinct fringe patterns each of which may be increasing or decreasing at the same time as the frequency is swept. A single pattern may reach a maximum, decrease and then increase to a new maximum over a wide frequency range without a significant change in shape. For a simple specimen, each succesive mode is visible as a suddenly developing fringe pattern with no observable fringes between resonances. Furthermore, each mode shape is unique and definable (a number of sinusoidal half-waves in each direction). For the fuselage, once the local modes become the predominant response (above 250 Hz), the same mode often seems to appear at several frequencies. For any video holography location, the global modes were found to lie between 10 and 200 Hz. An 80 Hz mode shape is shown in figure 3. The local modes were uniformly scattered from 250 to 750 Hz with the strongest response in the 400-550 Hz range. A 493 Hz mode shape is shown in figure 4. More than thirty modal images were converted to hard copy for each video holography position and at least that many more could have been chosen. The external acoustical excitation produced almost identical results as the shaker when the frequencies were above 350 Hz. This system did not have enough power to sufficiently excite the frame modes.

This effort was very successful in terms of providing guidance for planning the full modal analysis effort. The video holography recordings showed high modal densities and sometimes peculiar modal coupling, both of which significantly modified the

amount and location of conventional instrumentation planned for the modal analysis phase. Copies of the video taped sine sweeps were reviewed many times by our instrumentation and test engineers at Wright-Patterson. This type of preliminary test can be equally helpful for many future modal analyses.

### 4. Modal Analysis (GVT)

The modal analysis (GVT) was conducted on an airclane at Kelly AFB, Texas in late August 1991. The video holography results assisted greatly in reducing the number of accelerometers needed to perform the test.

The test equipment consisted of: a Zonic 7000/VAX Workstation II; two Ling Model 6C shakers (251b) with PCB Model 208A03 Force Transducers and approximately 172 Vibrametric M1000 Accelerometers. Since the Zonic used could only record and process 64 channels at a time, the modal analysis tests were divided into four phases. One for longitudinal (fore and aft along the stringers) response, one for frame response, one for panel response and one for fairing/panel response (see figures 5 through 8).

A combination of the accelerometers from these four phases were used to record responses during engine runs of idle, 80% N1, 90% N1, TRT and a slow deceleration of the engines from TRT (see figure 9).

During the modal survey, the shakers were excited with a random signal of 0 to 1000 Hz content. The resulting modes are very complex as shown in figure 10 for the panel response at 444.7 Hz and in figure 11 for the frame response at 442.7 Hz. The video holography results must be used to interpret the results, although phasing is easy to distinguish in the modal results. The panel response is presented in vector output and the frame response is depicted in connected peak line output. The frame response is primarily frame web lateral response and can be interpreted only when the structural layout is known and the video holography results are available to define local web lateral responses. Figure 12 shows a transfer function for one of the reference accelerometers on a panel and a shaker forcetransducer. Figure 13 shows transfer functions for an accelerometer on the fairing and both shaker force transducers. As can be seen in these transfer functions which are relatively flat, that there are very many modes which interact and make the data reduction very tedious.

The modal survey results support the video holography results in that the global modes are low in frequency and do not interact or couple with the higher frequency (above 400 Hz) panel modes.

### 5. Acoustic Survey

Eleven airplanes were tested for variations in engine noise from one airplane to another. Four microphones were placed within one foot of each other on the left side of the forward fuselage to record the engine fan noise. Multiple microphones were used to guard against loss of data and to maintain confidence in the data since these were very quick installations, on the order of 10-15 minutes. The power spectra of the 90% N1 and TRT engine noise

levels for low frequencies are shown in figures 14 and 15 for all eleven airplanes.

A typical set of sound pressure level spectra are shown in figure 16. Each spectrum of the four microphones are displayed for four engine power settings: idle, 80% N1, 90% N1 and TRT. Notice the engine rpm harmonic "multiple pure tone" peaks. Alegation, such peaks do not show up in the idle spectra since the fan blade tip speeds are not supersonic. The frequency of the harmonic peak is equal to the rated rpm/60 times the N1 percentage times the number of the harmonic, e.g. 58.33x0.90x8 equals 420 Hz.

To evaluate the influence of "delta frequency" on the power spectra, several runs were made for different "delta frequency" with the results shown in figures 17a to 17d. As can be seen, the smaller "delta frequency" is the better choice for describing the spectral characteristics of the engine noise and is sufficient to cover engine speed (rpm) hunting.

One airplane was instrumented with 27 microphones along the length of the fuselage in three rows. A sound pressure level spectrum for a forward microphone is shown in figure 18. Note the multiple pure tone peaks of engine fan harmonic noise. A SPL spectrum for an aft microphone is shown in figure 19. Note the elevated sound pressure levels between 1000 and 3000 Hz, which is due to the noise from the auxilary power units running in the aft fuselage. A contour map of the overall sound pressure levels measured at the 27 microphones is shown in figure 20.

Nothing unsual was noted during the test and the results are as expected.

Two strain gages were placed on the fuselage skin near fasteners along waterline 295. The microstrain output of these gages were very low throughout the acoustic survey tests, on the order of only a few microstrains. It is not apparent that the strains alone are large enough to cause fatigue cracking of the skin.

### 6. Analysis of Available Flight Test Data

As part of the effort to better understand the forward fuselage skin cracking problem, a review of data collected on previous test programs was undertaken. The tests were conducted between February and November 1988.

The data was checked for stationarity and randomness. and trend tests were performed on representative strain gage data. The results indicate the data is stationary. Power spectra of the data indicate narrow band noise responses exist at harmonic frequencies of the engine rpm. Autocorrelations of the data show little or very weak periodicity exists over the long run (see Therefore, the stationarity and randomness are figure 21). acceptable for basic statistical analyses. A microphone sound pressure level spectrum is shown in figure 22. Note, the three sharp peaks are considered to be extraneous noise. These peaks do not show up in the strain gage response power spectrum shown in figure 23. However, the responses in the frequency ranges of 280 to 350 Hz and 410 to 510 Hz are considered to be significant. The transfer functions shown in figure 24 for these frequency ranges are very flat. This result correlates well with the video holography and modal analysis results which show many local modes responding collectively in these frequency ranges.

A statistical analysis was performed to determine the peak value, mean value (average) and standard deviation of two strain gages for various operating conditions. Data from ground engine run-up tests and level flight at 300 KCAS at 30000 feet tests were used in the statistical analysis. The analysis started by digitizing the tape recorded strain gage responses at 3750 samples per second. This assured a frequency bandwidth to 1000 Hz. Using statistical values based on the constant time width sampling above would be expected to generated a mean of zero for an AC signal. To avoid this problem and to give a better feel for the average value of a strain peak, the peaks in the signal were counted. absolute values of the peaks were used to determine the statistical parameters and avoid a near-zero mean. A "peak" was defined as the highest (or lowest) point between zero crossings. Taking the absolute value of the peaks yielded the strain distribution as shown in figure 25.

The dominant frequency of the strain cycles was estimated (on the average) by using the total number of peaks determined by the process described above, dividing by two, and then dividing by the length of the sample record (in seconds). The dominant average frequency for the engines operating at takeoff rated thrust was Since the engines were operating at peaks per second. approximately 95 percent of rated rpm at takeoff rated thrust for these tests, this yields an eighth engine rpm harmonic frequency For the remainder of the other of 443 cps, which is close. operating conditions, it is not possible to tell if the dominant frequency is tracking a particular engine order because the engine speeds were not recorded. The dominant average peaks per second ranged from 318 pps to 611 pps. Based on the video holography and modal analysis results, these frequencies suggest that local mode responses dominate the strain gage data. Strain levels for ground engine run-up and flight are presented in two bar charts. Figures 26 and 27 compare 70% N1, 80% N1, 90% N1 and TRT ground run-up conditions to the flight condition of 15000 feet and 300 KCAS for strain gages 3665 and 3608 under tight and loose fastener conditions. These fasteners are in the fairing support structure. Each of these plots indicate increasing amplitude with engine speed. The strain level at straight and level flight is less than or equal to the strain level at 70% N1. Note also that the mean the peaks is considerably less than the largest (maximum) The standard deviation is almost as large as the mean and indicates a lot of variability in the data. The data reveals no consistent pattern as to whether the tight or loose fastener condition causes higher peak strain levels and the differences are Also, the mean values for tight and generally small. Therefore it is concluded that fasteners are almost identical. tight or loose lower fairing attachment angle fasteners make no difference on the strain level.

The strain levels during a takeoff were also studied. Data was available only for strain gage 3665 with tight fasteners. It was found that the dynamic strain levels increased during the roll down the runway. Maximum strain levels were approximately 5-16% higher than TRT with brakes locked. However, the levels dropped

sharply upon climb initiation. The levels during landing were also measured with tight fasteners for strain gage 3665. The levels are generally 40-50 microstrain, about 50-60% of the level at TRT.

An order analysis (waterfall plots) was performed on various transducer outputs recorded during slow ramping of the engine from idle to TRT, referred to as slow accels. Because there is no rpm reference, the waterfall plots were displayed as a function of time from 0 to 120 seconds, the duration of the slow accel. Strong order tracking would indicate that the vibratory response could be caused by engine unbalance or acoustic excitation at pure tones. Some weak order tracking does occur, as shown by accelerometer 3709 in figure 28, but this is the exception rather than the rule. The majority of the waterfall plots show bands or groupings of resonant frequencies, typical of ring-stiffened shells. The bands of responses that appear on most accelerometer and strain gage waterfall plots have approximate center frequencies of 300, 450, 650 and 950 Hz. The absence of strong order tracking suggests that the response is resonant, although the levels are not high.

### 7. Fractographic and Material Characteristics Tests

Fractographic examination of crack specimens from the forward fuselage, waterline 295 area, indicate the cracks progress primarily by stress corrosion. Once the net section stress exceeds the material yield stress, the cracks progress by net section overload. The specimen in figure 29a showed multiple initiation sites and crack growth by a stress corrosion mechanism and very high local stresses. Figure 29b shows the edges of the fastener hole (black arrows) and the probable crack initiation site E. Figure 29c is an enlargement of area E showing a mixed intergranular and ductile failure mechanism. Figure 29d is a enlargement of area G showing a hint of exfoliation and ductile failure. Figure 30 is a fractograph of a laboratory induced ductile overload failure for use during fractographic comparisons to distinguish between ductile overload, fatigue and stress shows the difference corrosion failures. Figure 31 fractographic views of low and high alternating stresses. Notice that the lower the stress level the less distinguishable the fatigue striations are, although the fracture faces are flat indicating intragranular fracture. Similarly, a lack striations has been observed on the fracture faces of 2024-T3 aluminum fatigued in a vacuum. This suggests that very low stress cycling at very low frequencies with the crack area subjected to a very corrosive environment may result in fracture faces that may not exhibit discernable striations.

Strength testing of coupons from the skin material indicate the material is representative of high strength 7079-T6. Fatigue and stress corrosion tests of the skin material are currently in progress and still to be completed. It appears that the crack stress intensity thresholds for fatigue and stress corrosion are low enough that the pressurization ground-air-ground cycles may be enough to cause corroded flaws and corrosion pits to grow in a fatigue mode and/or stress corrosion cracking mode.

### 8. Finite Element Analyses

A finite element model is being developed of a section of the forward fuselage and selected local bays to predict global and local mode shapes and frequencies as well as strain distributions during pressurization of the cargo area. Figure 32 is a wire layout of the local bays modeled for the finite element analysis. Strains around the fastener hole, using a very fine mesh of nodes, will be determined for dynamic and static pressures applied to the fusewage skin. Appropriate static loading boundary conditions will be applied to the panel model when predicting static loading condition strains around the fastener hole. The forthcoming results will be useful in better understanding the results of the above efforts, in better planning of future flight tests and in evaluating the structural integrity of the skin and frames of the forward fuselage.

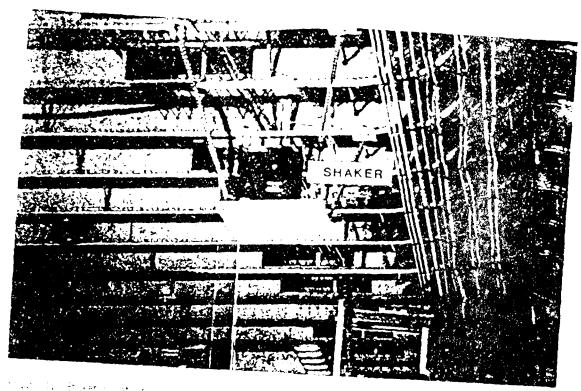
### 9. Future Flight Tests

Flight tests are needed to conduct static and dynamic strain surveys of the skin to evaluate all of the above gathered data to establish the effectiveness of practical crack controlling measures in this potentially high maintenance cost area. Based on the results of all of the efforts, the most promising measures will be recommended for application to this airplane.

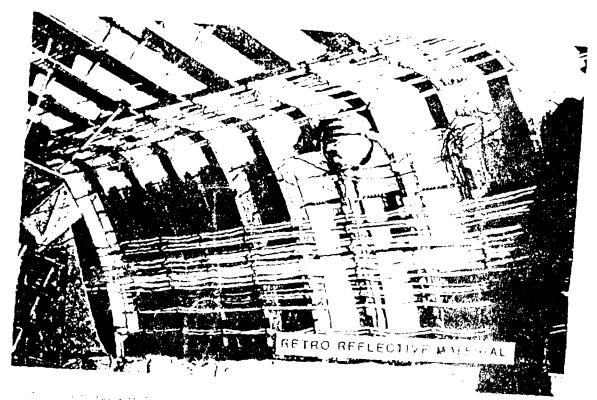
### 10. Summary

The video holography program was very instrumental in panel resonant responses and defining local optimizing instrumentation for the modal analysis program. The modal survey results confirmed the complexity of the frame and panel responses. The acoustic survey verified the consistency of engine fan noise from airplane to airplane and the acoustic tests snowed small sound pressure level variations along the length of the The fractographic efforts confirmed the stress fuselage. corrosion aspect of the cracking problem although a few minor fatigue striations were noted. Finite element analyses, material characteristics and additional flight tests are establish the mechanism of crack growth involving other forward fuselage skin loadings. The skin loadings from the engine fan noise do not appear to be the primary crack initiation and growth mechanism although the noise levels appear to be sufficient to degrade the corrosion resistant barrier of the sealants around the fasteners and between the skin and stringers and fairing support structure. Further, the noise levels do appear to be significant the failures of fairing intermediate structure and will investigated during future flight tests.

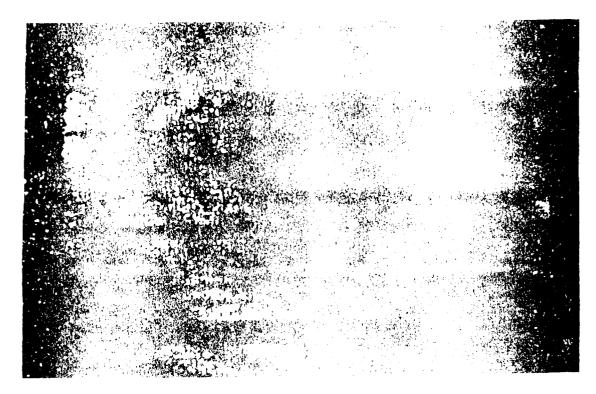
All of the above efforts are interrelated and the results therefrom are very useful and necessary in understanding the cracks occurring in the forward fuslage skin of a large cargo airplane.



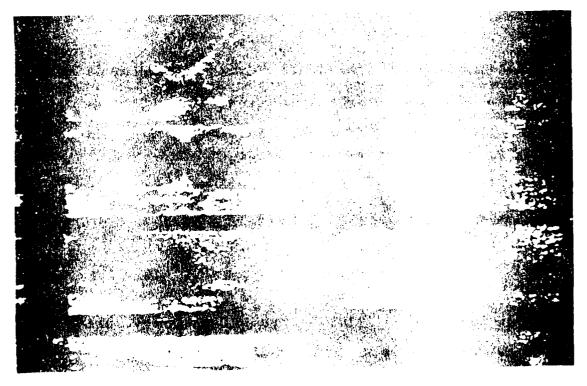
The transfer of the second



e e en en en e



Fluore S



.

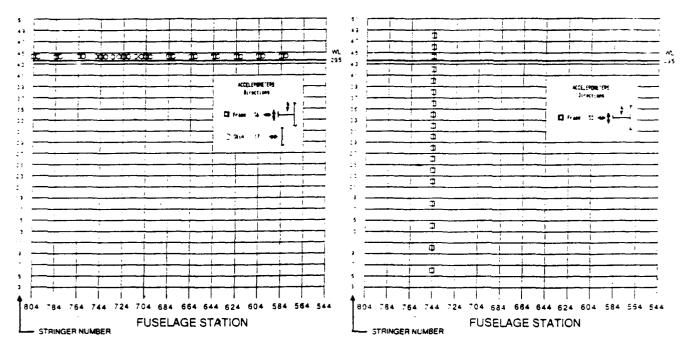


Figure 5. 6VT _ Longitudinal Accelerometer Locations

Figure 6. 6VT - Frame Accelerometer Locations

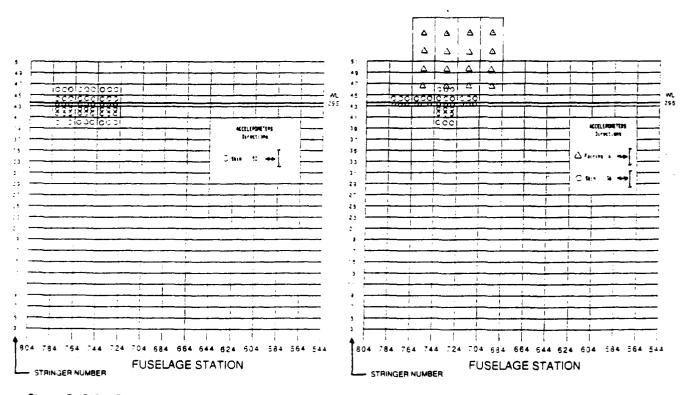


Figure 7. 6VT - Panel Accelerometer Locations

Figure 8. 6VT - Fairing Accelerometer Locations

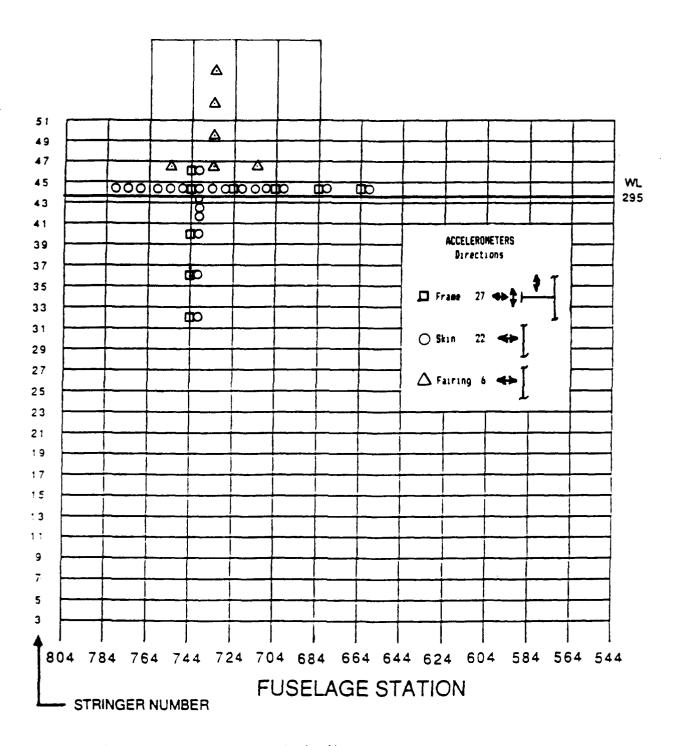


Figure 9. Engines Operating - Accelerometer Locations

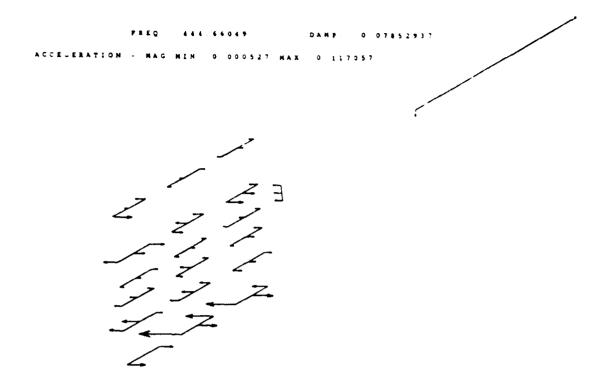


Figure 10. Panel Response at 444.7 Hz

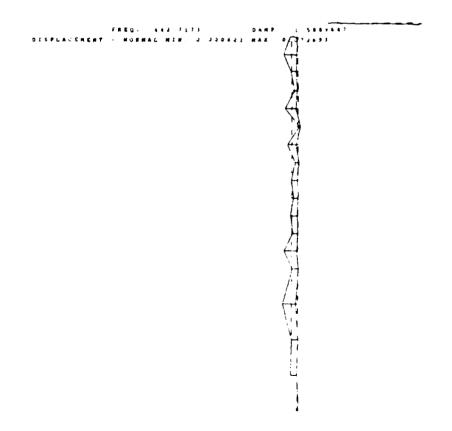


Figure 11. Frame Response at 442.7 Hz

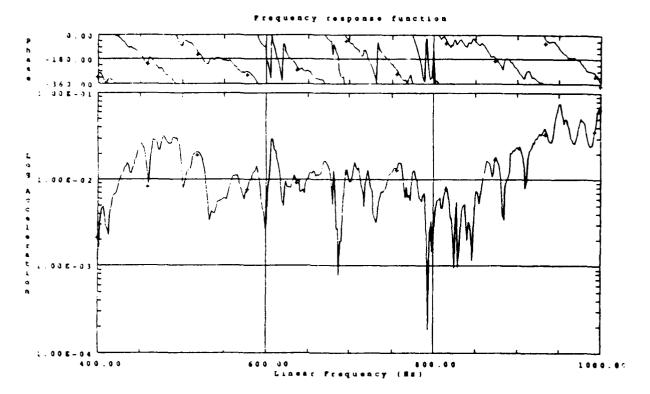


Figure 12. Transfer Function for Reference Accelerometer

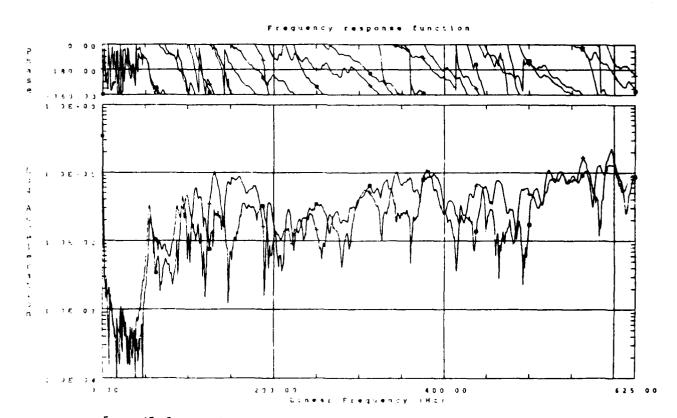


Figure 13. Transfer Function for Fairing Accelerometer

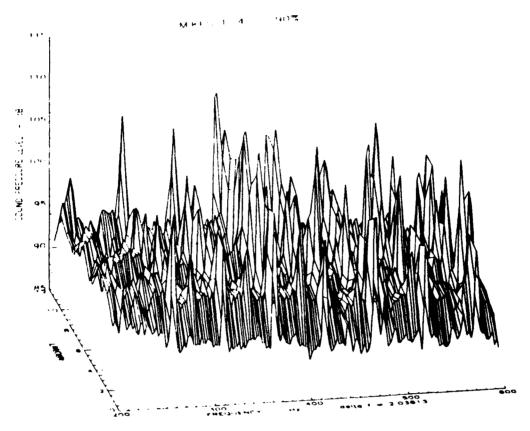


Figure 14. Engine 90% N1 SPL Spectra for Eleven Airplanes

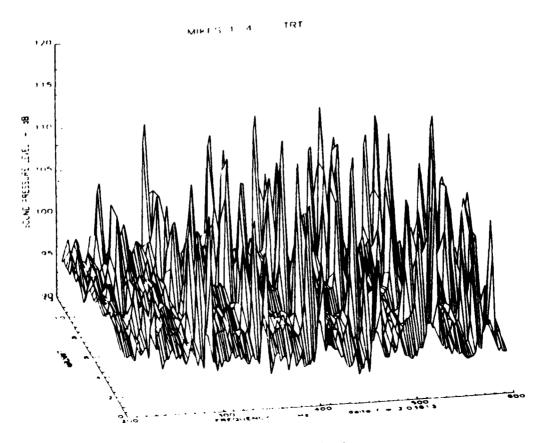
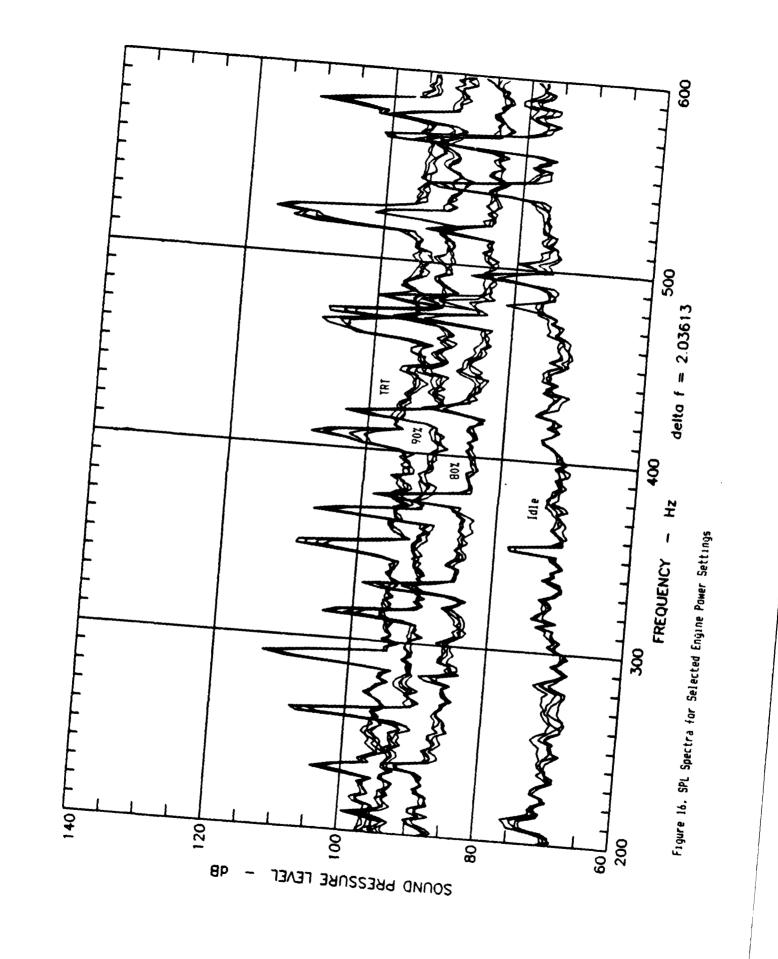
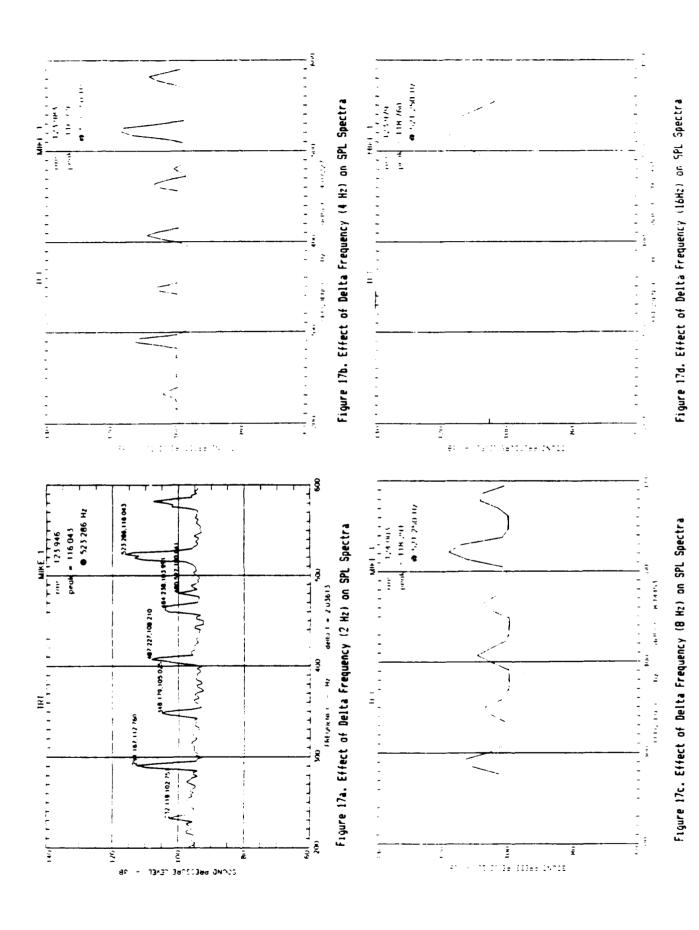


Figure 15. Engine TRT SPL Spectra for Eleven Airplanes





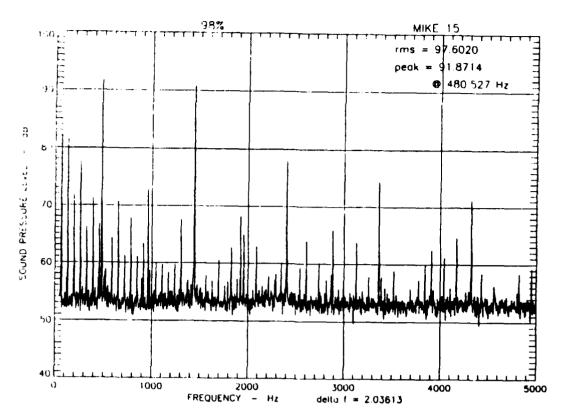


Figure 18. SPL Spectrum for a Forward Microphone

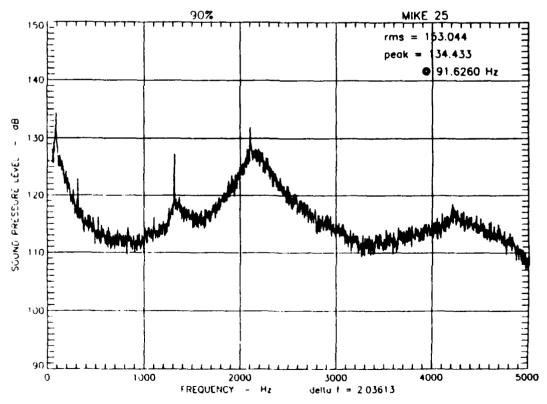


Figure 19. SPL Spectrum for an Aft Microphone

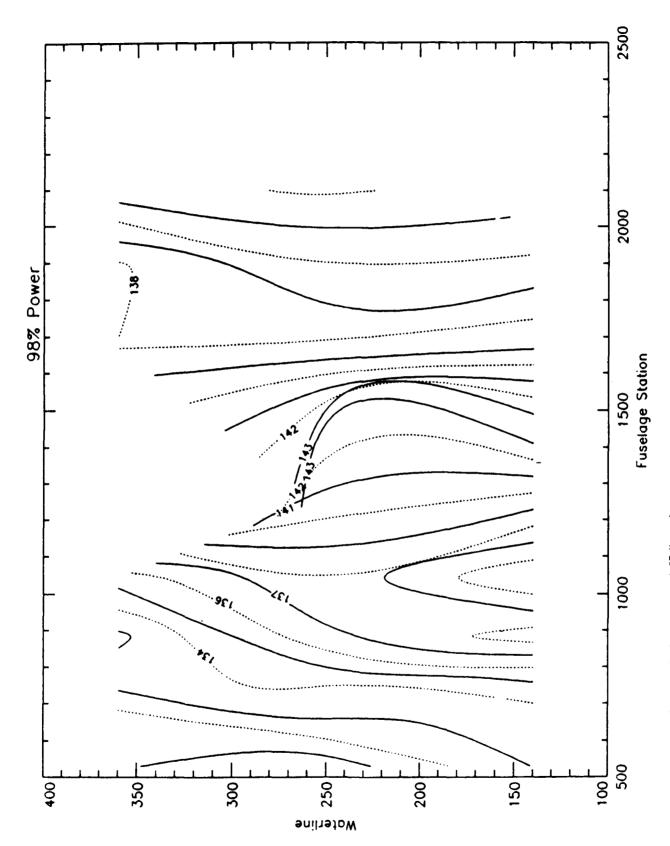


Figure 20. Overall SPL Contour Map of 27 Microphones

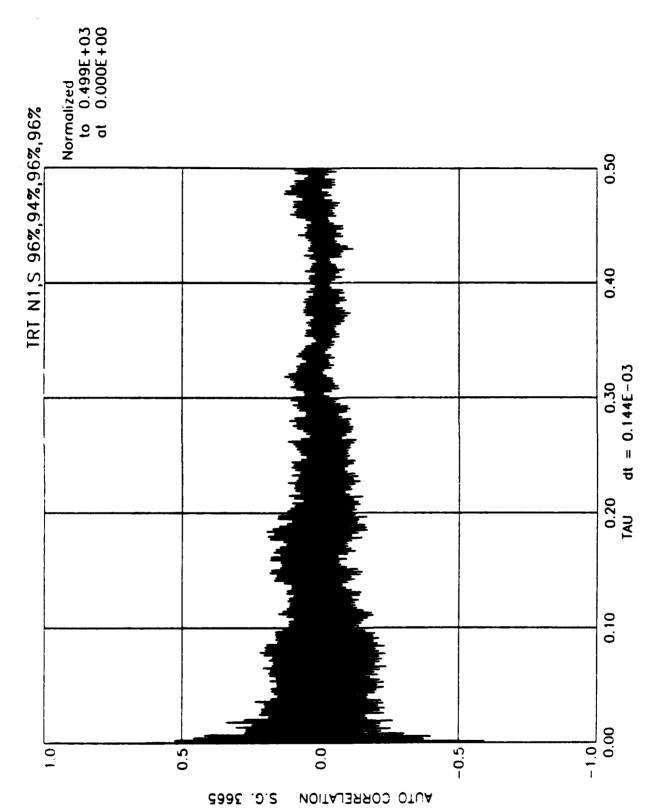


Figure 21. Autocorrelation of Strain Gage 3665 Strains

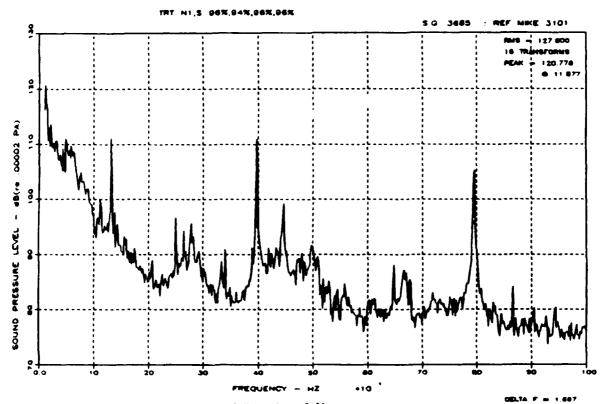


Figure 22. SPL Spectrum for External Microphone 3101

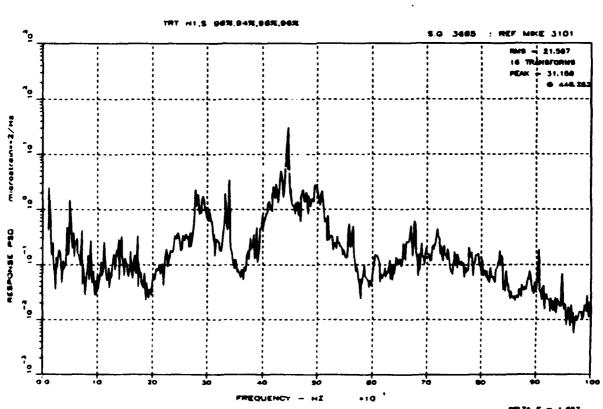
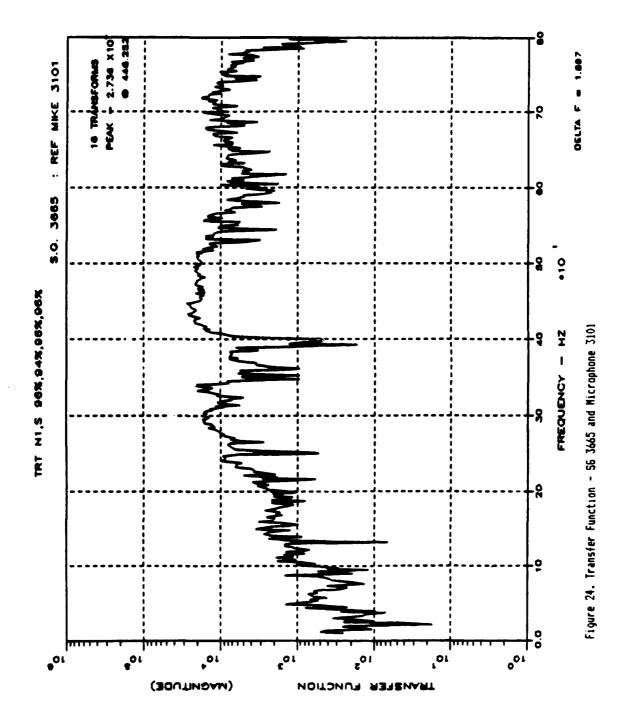
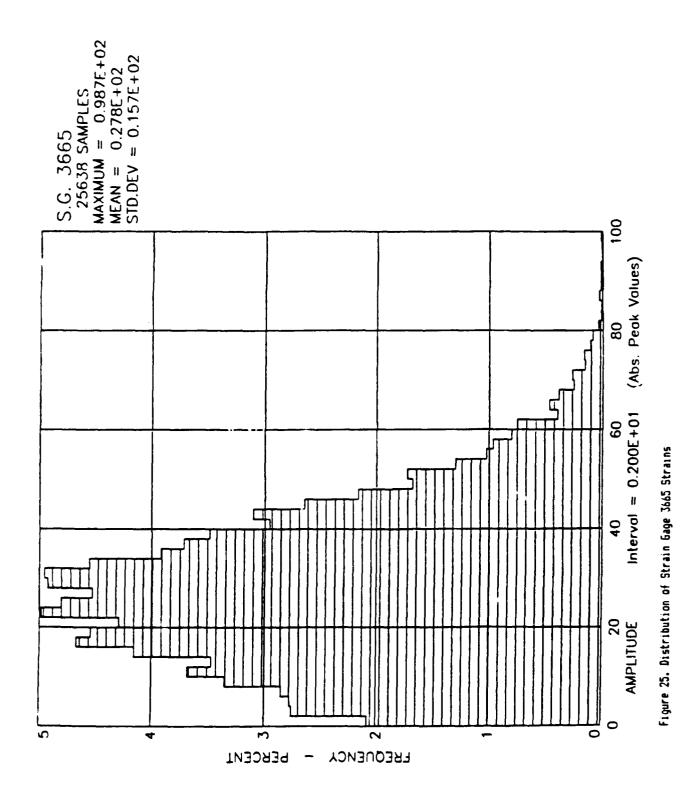
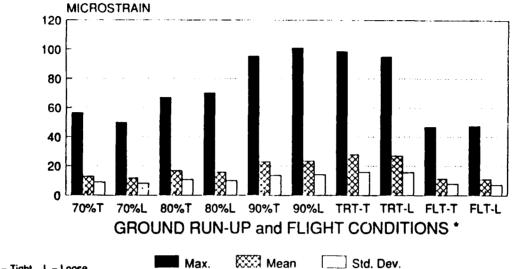


Figure 23. Response PSD for Strain Gage 3665 Strains





#### S.G. 3665 **TIGHT AND LOOSE FASTENERS**



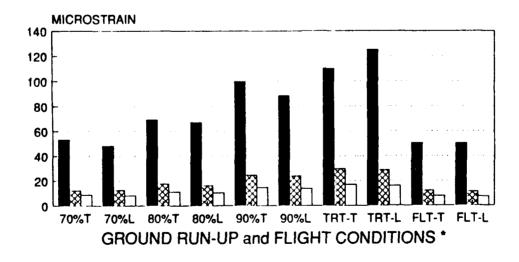
*T = Tight L = Loose *FLT = 300 KCAS 15,000 ft.

Mean

Std. Dev.

Figure 26. Response of SG 3665 for Ground and Flight Tests

#### S.G. 3608 **TIGHT AND LOOSE FASTENERS**



₩₩ Mean

*T = Tight L = Loose

*FLT = 300 KCAS 15,000 ft.

Figure 27. Response of S6 3608 for Ground and Flight Tests

Max.

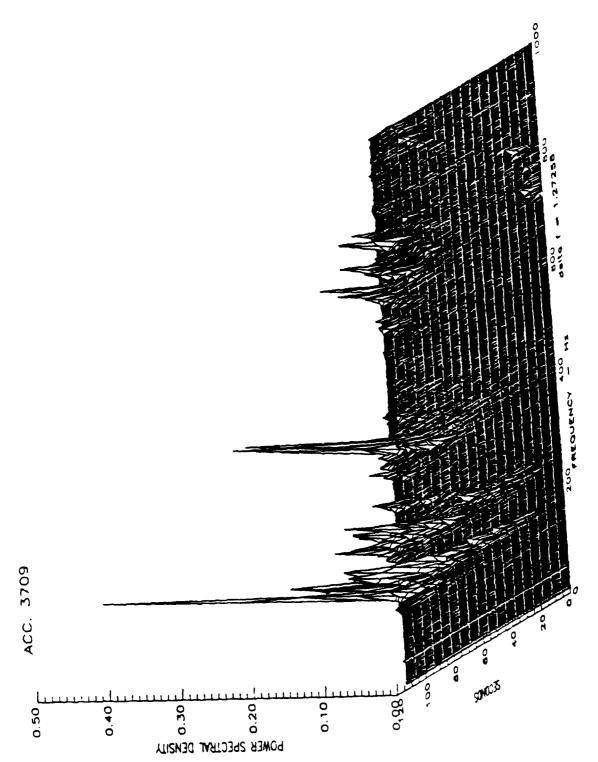


Figure 28. Waterfall of Acceleration PSDs for Accelerometer 3709 for Slow Accel of Engine to 181







1982 Period Merry appropriate by the property of the propriate of the property of the property



Figure 29. Scunnung Electron Microscope Views on a forward Fuselage Stin Chack

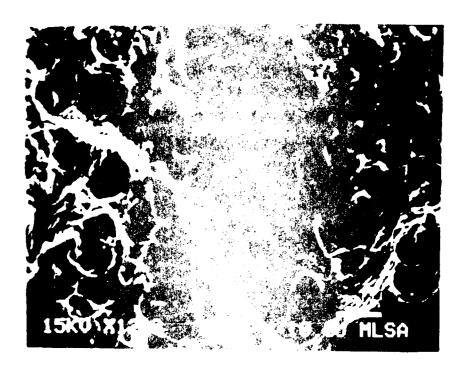
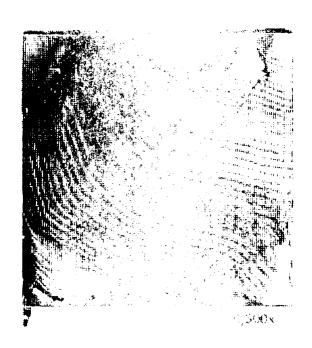


Figure IN. A Baltimore of The a Swetcle Overload Topography



- SPECTRE STATE OF THE STATE OF T

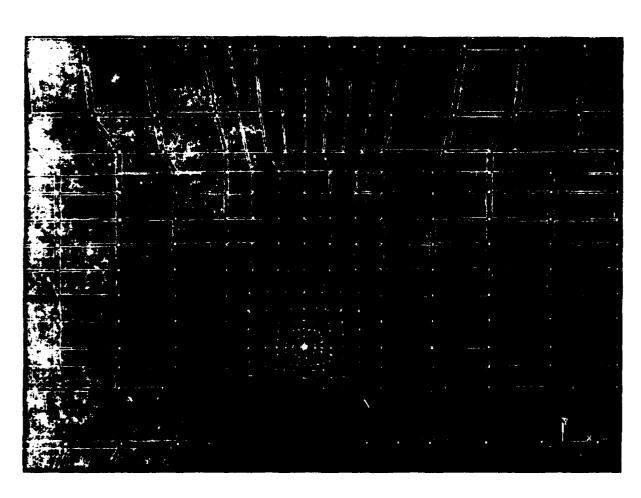


Figure 72. Wire Layout of Finite Elizant Analysis Panel Model

# Damage Tolerance of Engine Blading

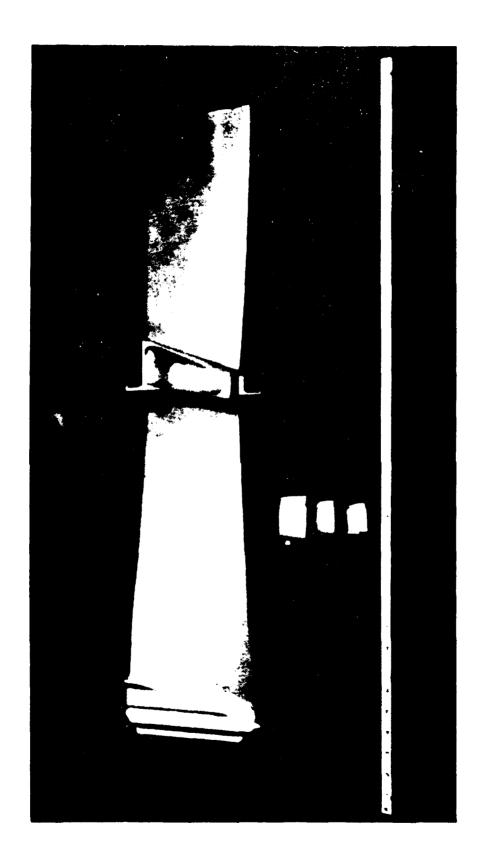
Analysis and Failure Evaluation Considerations

USAF Structural Integrity Conference December 3-5, 1991 San Antonio, TX

Dr. P.A. Domas Life Management Programs GE Aircraft Engines

#### Overview

- Application of damage tolerance to turbine engine blading
- Titanium
- Fan and compressor
- Fracture mechanics modeling
- Successes
- Limitations
- Correlations using fractography



## **ENSIP** and Damage Tolerance

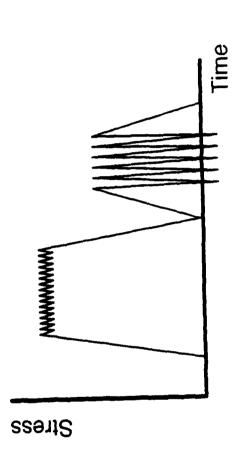
- ENSIP (Mil-STD-1783) has driven engine damage tolerance improvement
- More damage tolerant materials
- Improved Fracture Mechanics methods
- Improved NDE methods and understanding
- More tolerant rotating structures
- Concepts and some ENSIP tools can be applied to blades

# Blade Damage Tolerance (D/T) Considerations

- Damage potential high (FOD/DOD, erosion, corrosion)
- Potential resonant vibration loading (high frequency)
- Subject to HCF/LCF interaction
- Uncertainties limit D/T concept applications
- Location and type of damage
- Loading magnitude and frequency
- Load variation with time and crack length

### HCF/LCF Interaction

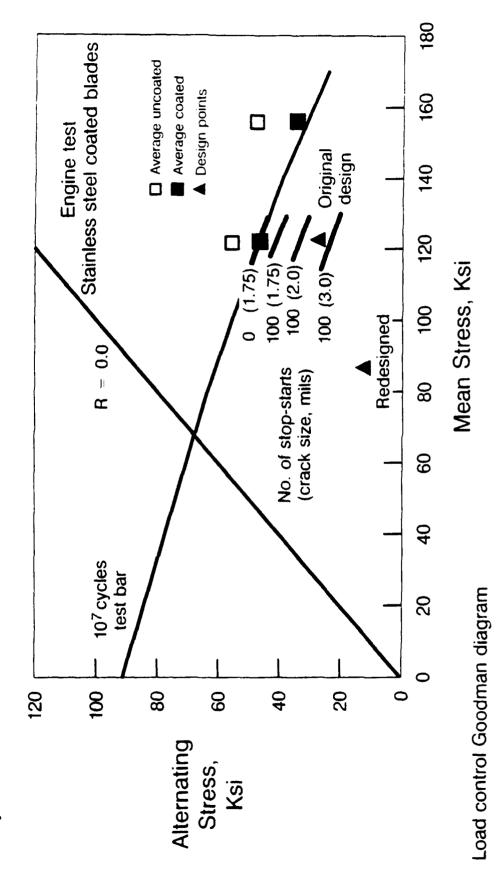
- "Low" amplitude, "high" mean stress, high frequency • High Cycle Fatigue loading elements
  - Superimposed on Low Cycle Fatigue elements - "High" amplitude, "low" R-ratio, low frequency
- Non-linear interaction can occur



# Fracture Mechanics Based HCF/LCF Models

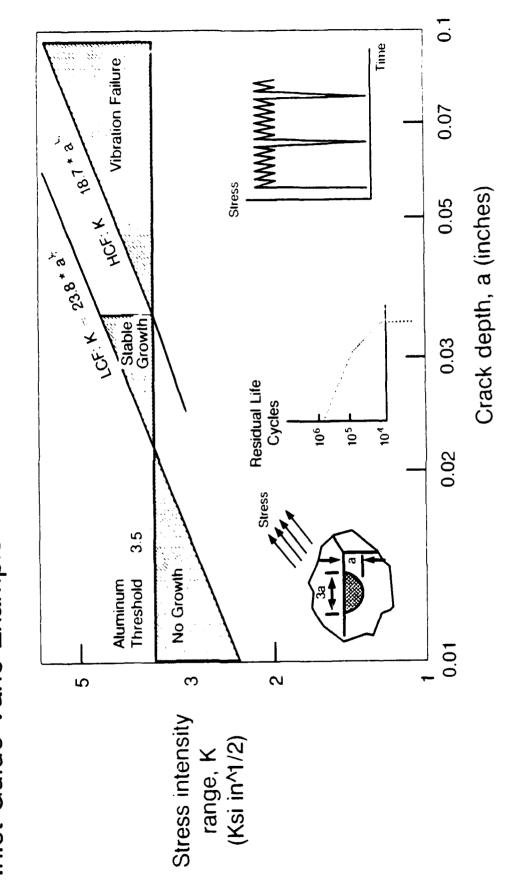
- For "Crack-like" damage, F/M model shows promise
- Applied engine example:
- Stainless steel coated blades
- Test cell airfoil failure 100 cycles after stall
- Stresses below Goodman Diagram limits
- Fracture Mechanics model correlated with failure
- "HCF allowable" reduced by "Stop-start" (LCF) cycles
  - Cracked coating provided "damage"

Fracture Mechanics Model for Airfoil Failure Explained HCF/LCF interaction on coated blade

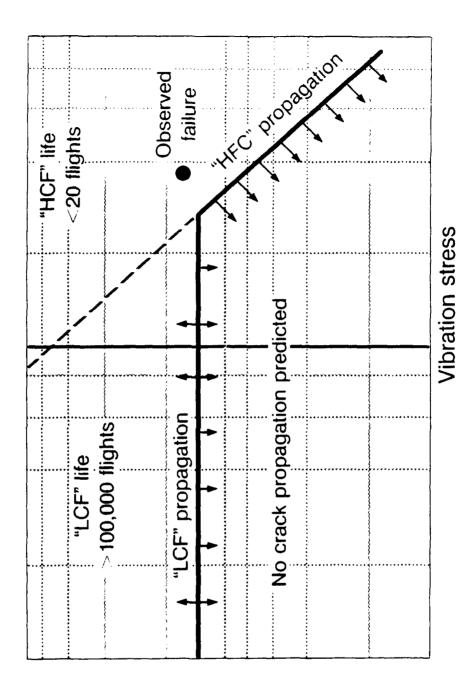


T2619 07 - 911007

High Frequency HCF -- Limits LCF Stable Growth Inlet Guide Vane Example



## Correlation with FOD Initiated Failure Ti-6AI-4V Fan Blade

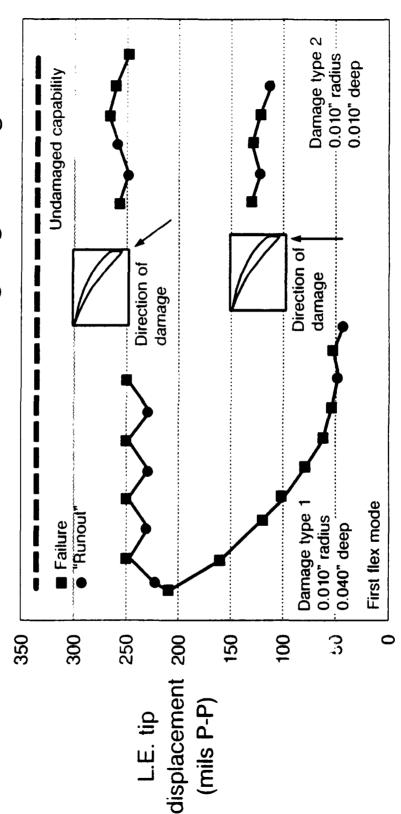


12619.09 - 911007

Crack size

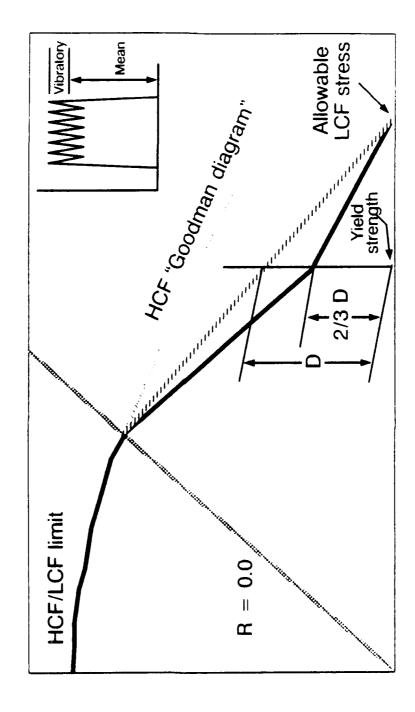
F.O.D. Fatigue Data Study Summary Compressor Rotor Blade

Ti-6-2-4-2, artifical leading edge damage, 70F



**Tests** 

### Fracture Mechs. Based HCF/LCF Design Guidelines Modified "Goodman Diagram"



Mean stress

1261911 911007

Vibratory

stress

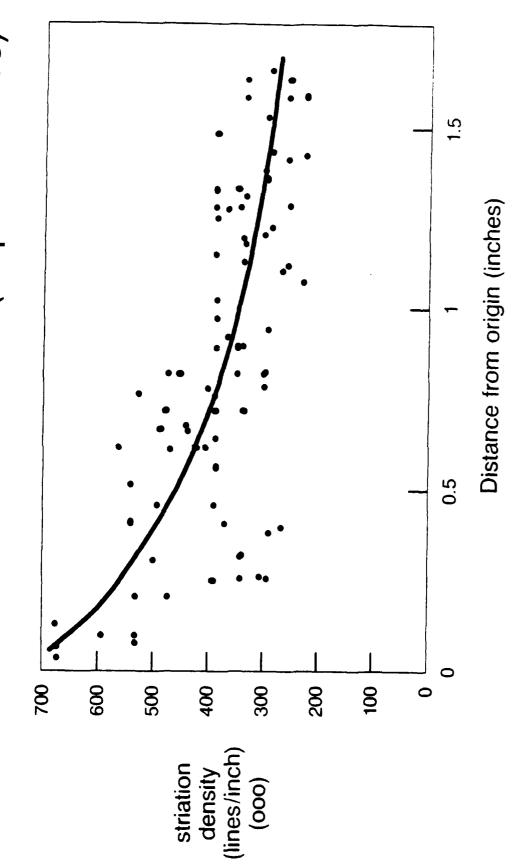
### Fracture Mechanics Models -- Validation Correct Fractography Interpretation Essential

### Fan Blade Example

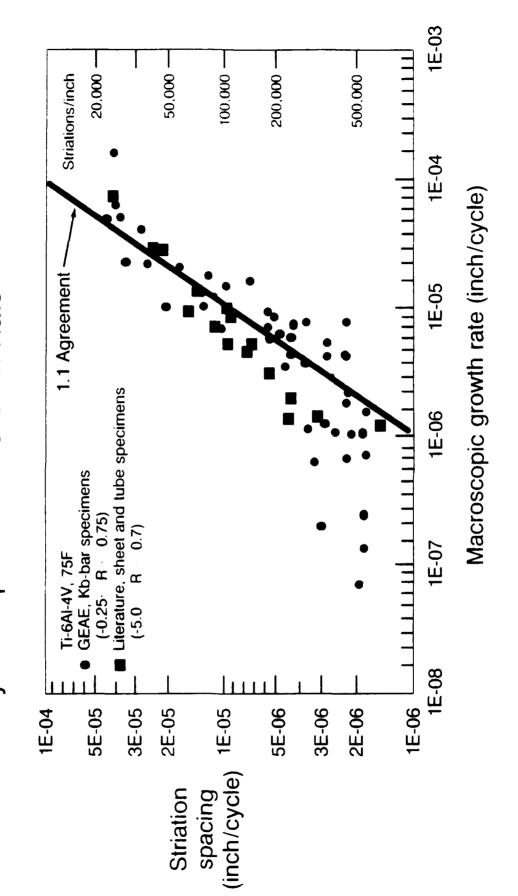
- Field failure analysis:
- Characteristic blade striation density behavior
  - At limits of fractographic resolution
- Level maintained across fracture surface
- Previous large engine fan blade F/M analysis:
  - HCF components "kick-in" sequentially
- Striation formation not "one-to-one" with missions
- Behavior predictable by Fracture Mechanics

T2519 12 · 911007

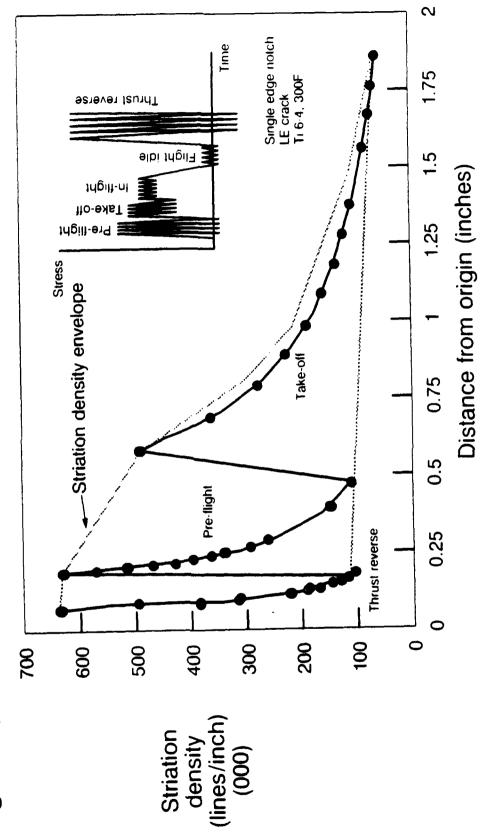
Failed Fan Blade Striation Data (Representative)

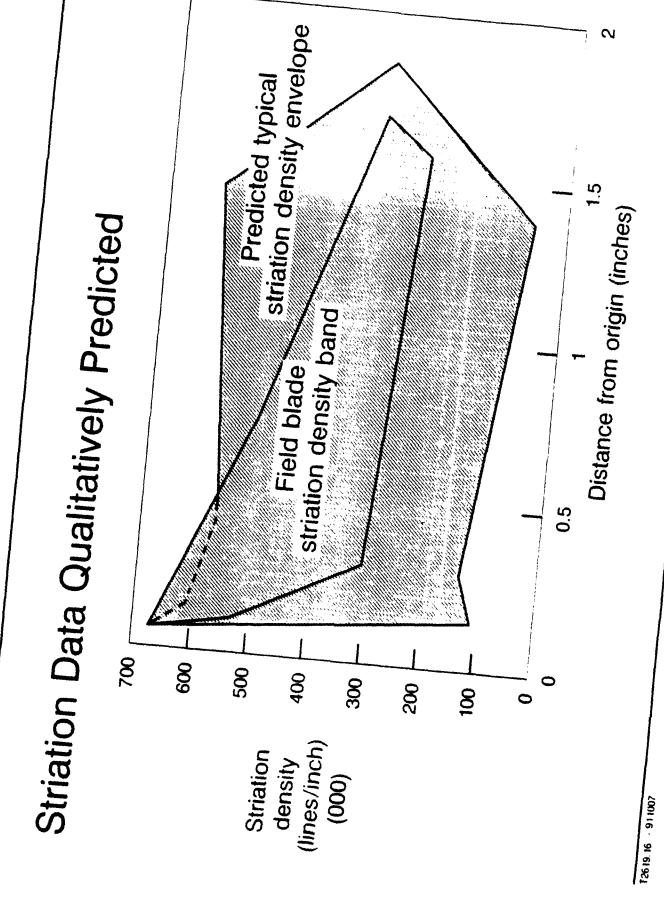


### Comparison of Macro and Micro Crack Growth Rates Striation density vs. Experimental Growth Rate



Large Engine Fan Blade Leading Edge Example Blade Striation Density Illustration





#### Summary

- Fracture mechanics a useful tool
- But major limitations exist
- Uncertain loading spectrum
- Uncertain sources/types of damage
- HCF/LCF interaction
- Design "Avoidance" is current methodology
- Probabilistic fracture mechanics . . . potential solution?



#### APPLICATION OF ENSIP COMMERCIAL ENGINE ON AN IN-SERVICE

### Presenter: Archie Tannock Pratt & Whitney Canada

**Authors:** 

H. Johnson (PWA), Y. Valani, S. Doan, R. Adamson, D. Craig (P&WC)

1991 USAF Structural Integrity Program Conference

#### 6240300

# PRESENTATION OVERVIEW

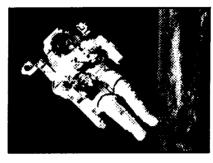
- Background
- ENSIP assessment
- Design criteria
- Manufacturing and quality control (NDI assessment)
- Material characterization
- Component testing
- Accelerated engine test (a.m.t)
- Engine life management (tracking and SMP)

#### Summary

## UNITED TECHNOLOGIES



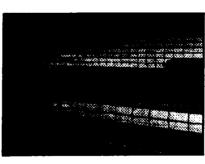
Defence & Space



Controls



Industrial



Building



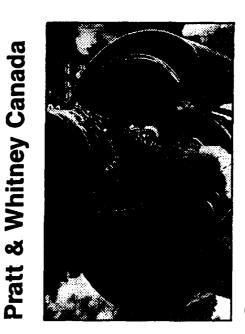
### POWER GROUP



**Commercial Business** 

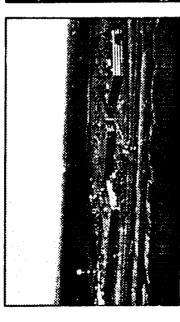


Operations



**Government Business** 

### P&WC FACILITIES



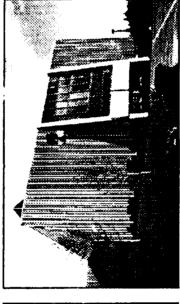
Plant 1 - Longueuil, QC



Plant 5 - St. Hubert, QC

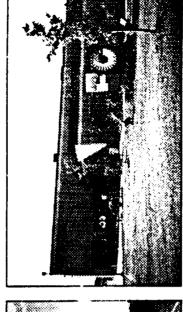


Plant 21 - Mississauga, Ont.



Plant 41 - Halifax, N.S.

Plant 2 - Longueuil, QC



Plant 22 - Mississauga, Ont.

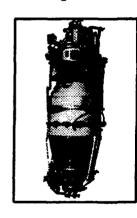
5007100

## WORLD MANDATE: CIVIL & MILITARY

MARKET, DESIGN, MANUFACTURE & SUPPORT



**Small Turbofans** 

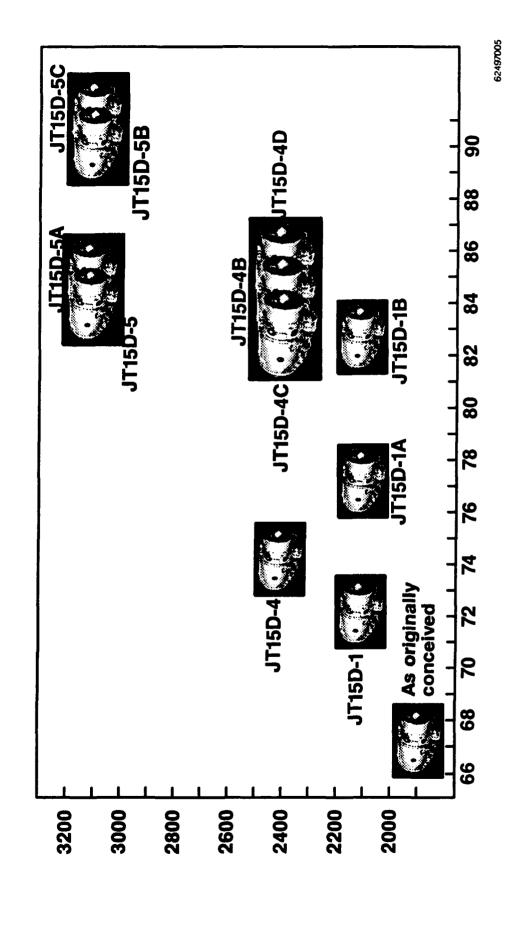


**Turboprops/Turboshafts Auxiliary Power Units** 



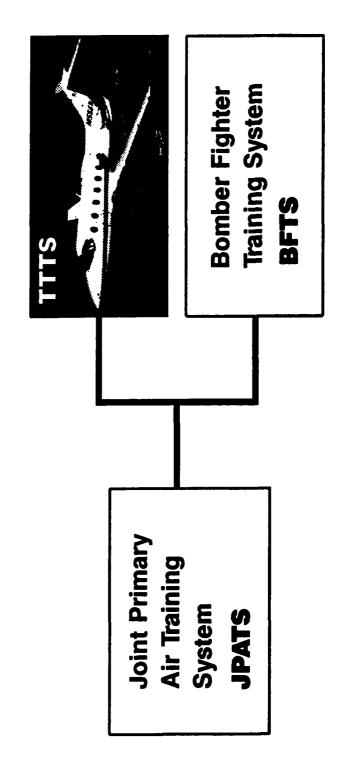
**APUs** 

#### VELOPMENT FAMILY



# USAF STRUCTURAL INTEGRITY PROGRAM CONFERENCE

Trainer aircraft masterplan



#### 62497029

# TANKER TRANSPORT TRAINING SYSTEM (TTTS)

- **USAF** required modern missionized business jet
- (Beechjet 400T → Jayhawk T1A) 1990 contract awarded to Beech
- Powered by Pratt & Whitney Canada JT15D-5B turbofan

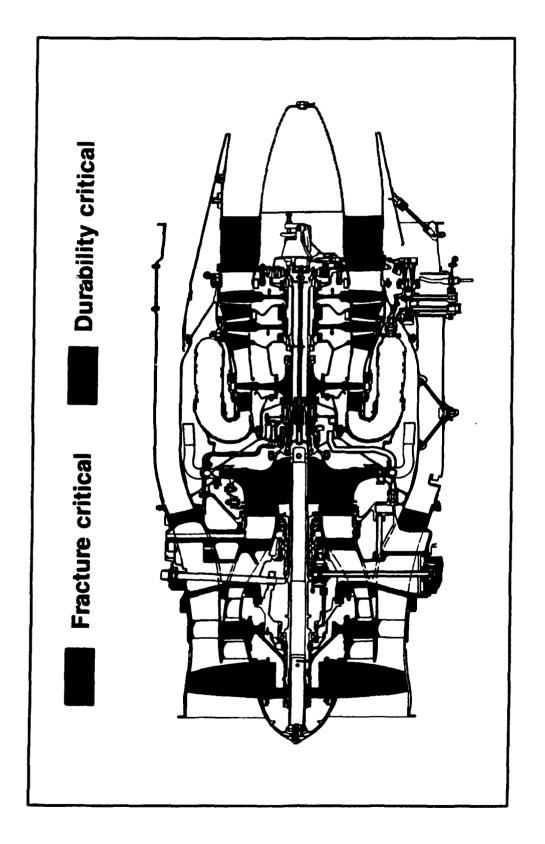
# MIL-STD-1783 FOR THE PRATT & WHITNEY CANADA JT15D-5B ENGINE

## TAILORED ENSIP - TTTS

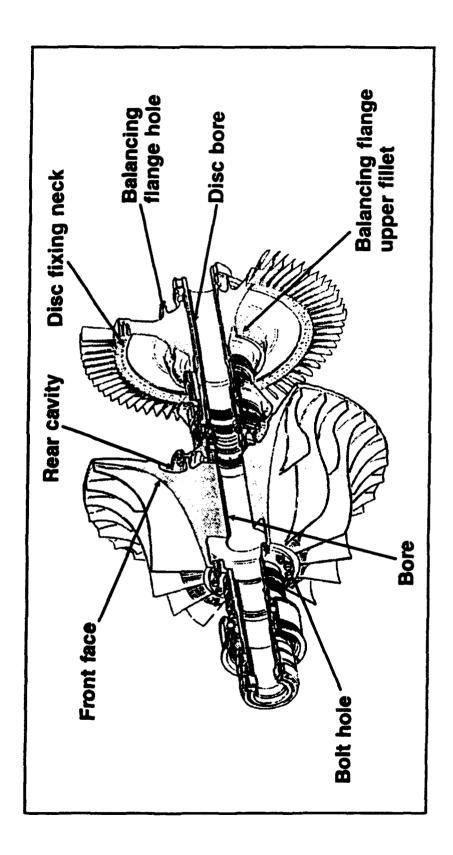
TASK I	TASK II	TASK III	TASK IV	TASK V
DESIGN	DESIGN ANALYSES MAT'L CHARACTERISTIC AND DEV. TESTS	COMPONENT AND CORE ENGINE TESTS	GROUND AND FLIGHT ENGINE TESTS	ENGINE LIFE Management
- ENSIP master - Durability and damage tolerance control - Diagnostic consideration - Material and process characterization Operational Requirements - Design service life and design usage requirements - Design criteria	Design duty cycle     Durability and damage tolerance analysis     Diagnostics analysis     Manufacturing and quality control     Material characterization	• Damage tolerance tests	Accelerated mission test (AMT)     Critical parts list update	Update analysis     Structural     maintenance     plan     Individual     engine     tracking     FLTF     Durability and     damage     tolerance     control plan     implementation

## DESIGN CRITERIA

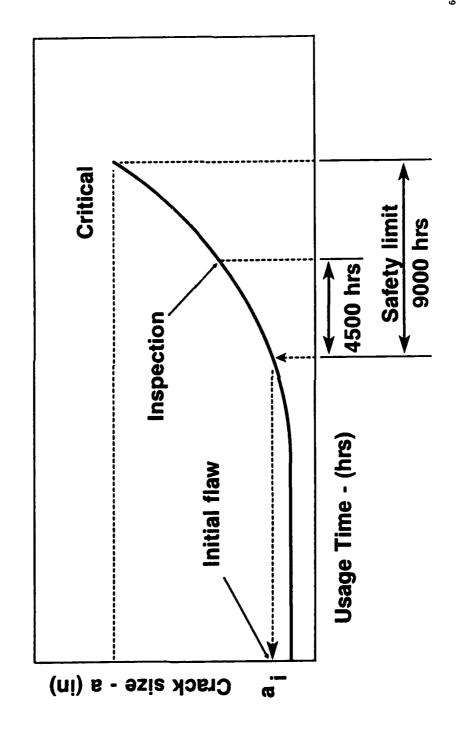
- JT15D-5B designed to meet FAR 33 reqt's
- Assess engine components against TTTS mission(s) for:
  - 18000 hrs durability
- (To achieve safe 4500 hrs inspection - 9000 hrs damage tolerance interval)



# CRITICAL SENSITIVE LOCATIONS



## DETERMINATION OF INITIAL FLAW SIZE



#### NON-DESTRUCTIVE INSPECTION MANUFACTURING AND QUALITY CONTROL

- NDI specimens
- Determination of POD for ultrasonic, FPI and **Eddy current inspection methods**

## MATERIAL CHARACTERIZATION

DA/DN vs AK CURVES

• Full characterization:

**AISI 410** 

Inconel 625 **AMS 4439** 

**Incoloy 901** Waspaloy®

Partial characterization:

Ti 6-4

Ti 6-2-4-2 Ti 6-2-4-6β

#### 62497015

### DAMAGE TOLERANCE TESTS COMPONENT VERIFICATION

Spin pit:

Fan hub

High turbine disk

Low turbine 1 disk

Impeller

Structures rig:

Fan shaft

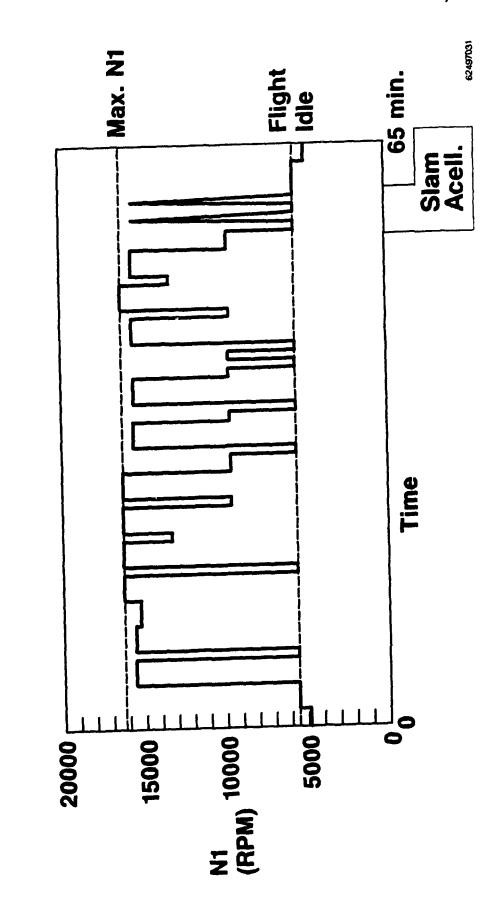
Gas generator case

Low turbine support case

## ACCELERATED MISSION TEST (AMT)

- AMT objectives
- To demonstrate engine durabilityTo provide Pacer engines

# JT15D-5B ACCELERATED MISSION CYCLE (AMT)

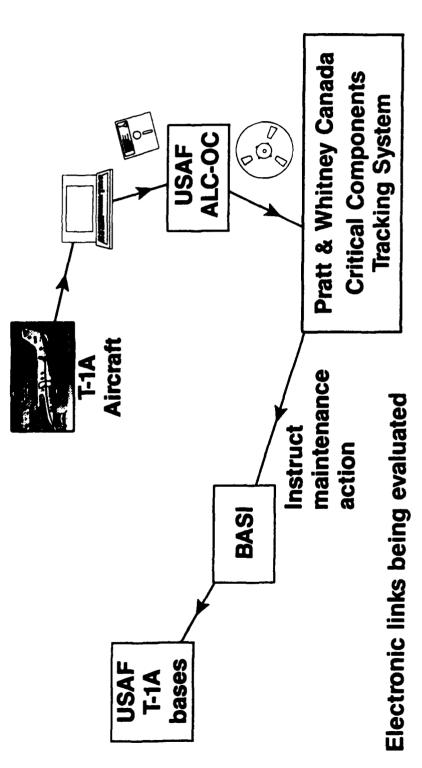


### **AMT STATUS**

- Test on one engine completed
- Engine in excellent condition
- Test on second engine almost complete

# ENGINE LIFE MANAGEMENT

SIMPLIFIED DATA FLOW DIAGRAM OF TRACKING SYSTEM



62497028

#### 62497025

## LIFE MANAGEMENT

### CRITICAL COMPONENTS TRACKING SYSTEM (CCTS)

- AMT LCF calibration complete
- Mission simulations
- Crack growth algorithms in development
- Preliminary design review with USAF
- 14th November 1991

# MAINTENANCE PLAN (SMP)

tasks to ensure safe inspection and Integrates results of all the ENSIP replacement intervals

#### 62497024

#### SUMMARY

- JT15D substantial service and development experience made it suitable for tailored **ENSIP application**
- Application of ENSIP philosophy can reduce life cycle costs
- Expertise for future programs

#### APPENDIX 1

#### APPLICATION OF ENSIP ON AN IN-SERVICE COMMERCIAL ENGINE" SYNOPSIS

The P&WC JT15D-5 twin spool engine was introduced in commercial service in 1984. It is the most recent development of the JT15D family of engines which were first introduced into service in 1970. In 1990 the JT15D-5 powered BEECHJET was selected for the USAF Tanker Transport Trainer System (TTTS). Although the engine has been in service for 6 years, the USAF requested that the engine be assessed using the ENSIP philosophy.

This paper will show P&WC's approach taken in applying ENSIP to an "off the shelf" engine and how it differs from the usual ENSIP application at the design phase.

The paper will also address P&WC's compliance with ENSIP tasks not covered under our commercial lifting philosophy, e.g:

- Development of a Master Plan based on design and field experience with JT15D-5.
- Durability and Damage Tolerance Assessment on all fracture and durability critical components.
- NDI Probability of Detection (POD) data.
- Accelerated Mission Test.
- Engine Usage/Critical Parts Tracking Program.
- Structural Maintenance Plan.

The conclusion will address our lessons learned and their effect on our future philosophy.

27THJUNE

#### LIFE MANAGEMENT PROGRAMS FRICTION STRESSES BETWEEN BLADE AND DISK DOVETAIL POSSIBLE CAUSE OF NUMEROUS DOVETAIL PROBLEMS GE AIRCRAFT ENGINES **BARRY J. KALB USAF STRUCTURAL INTEGRITY CONFERENCE** DECEMBER 3-5,1991 SAN ANTONIO, TX

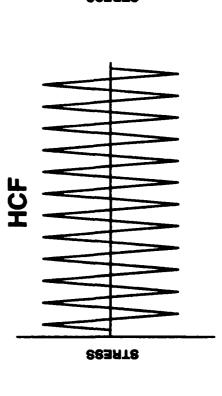
### DOVETAIL CRACKING

- CRACKING HAS OCCURRED IN A NUMBER OF AXIAL BLADE DOVETAILS ON BOTH FANS AND COMPRESSORS
- IN MANY OF THE DOVETAIL CRACKING PROBLEMS, THE CRACKING HAS OCCURRED AT THE EDGE OF CONTACT BETWEEN THE BLADE AND THE
- CRACKING HAS PRIMARILY BEEN ATTRIBUTED TO HIGH CYCLE FATIGUE (VIBRATORY STRESS) DUE TO THE APPEARANCE OF THE FRACTURE
- A NEW CAUSE OR MAJOR CONTRIBUTOR TO THE CRACKING HAS BEEN IDENTIFIED:

# FRICTION STRESSES BETWEEN THE BLADE AND DISK DOVETAILS

### **DOVETAIL CRACKING**

- BEFORE DISCUSSING THE EFFECT OF FRICTION, LET'S ADDRESS THE QUESTION OF THE APPEARANCE OF HIGH CYCLE FATIGUE (HCF) ON THE FRACTURE SURFACE
- SPECIMEN TESTING FOLLOWED BY FRACTOGRAPHY HAS SHOWN THAT BOTH LOADING SPECTRUM SHOWN BELOW PRODUCE A FRACTURE SURFACE TYPICAL OF HCF
- **CRACK INITIATION MECHANISM OF SPECTRUM ON RIGHT IS** PRIMARILY LCF

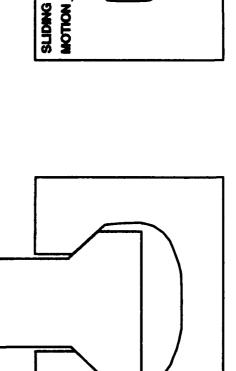


### **DOVETAIL CRACKING**

- SLIDING ALWAYS OCCURS BETWEEN BLADE AND DISK DOVETAIL PRESSURE FACES FOR AXIAL DOVETAIL SLOTS
- DISK HOOP STRAIN OPENS AXIAL DOVETAIL SLOTS, ALLOWING **BLADE TO MOVE RADIALLY OUT**
- NORMAL FORCE BETWEEN DISK AND BLADE DOVETAIL COMBINED WITH SLIDING MOTION PRODUCES A SHEARING LOAD

**ORIGINAL DOVETAIL POSITION** 

**DEFLECTED DOVETAIL POSITION** 

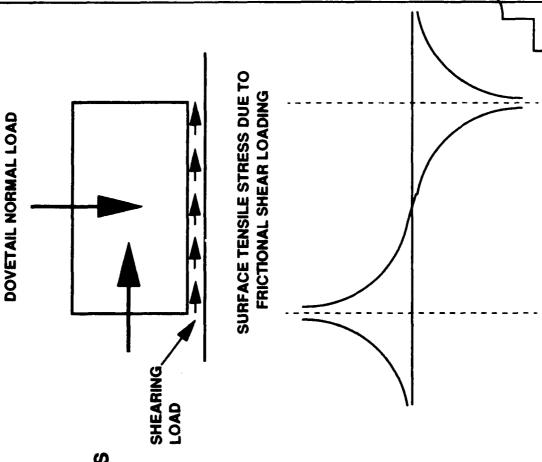


#### **FRICTION STRESS**

TENSILE SURFACE STRESSES
INTRODUCED TO SURFACE AS A
RESULT OF SURFACE SHEAR LOADS

STRESSES ARE COMPRESSIVE AT LEADING EDGE OF BLOCK SLIDING MOTION

STRESSES ARE TENSILE AT TRAILING EDGE OF BLOCK SLIDING MOTION CRACKING WOULD OCCUR AT TRAILING EDGE WHERE TENSILE STRESSES OCCUR, WHICH IS CONSISTENT WITH CRACKING LOCATION ON PARTS



### **LITERATURE DATA**

- REVIEW OF LITERATURE HAS SHOWN THAT FRICTION LOADING SIGNIFICANTLY INCREASES THE LOCAL STRESS
- MATHEMATICAL SOLUTIONS TO THE SLIDING CONTACT PROBLEM HAVE **BEEN CONDUCTED FOR VARIOUS GEOMETRIES**
- HAVE NOT FOUND SOLUTION FOR RECTANGULAR BLOCK ON SURFACE
- SOLUTION FOR CYLINDER SLIDING ON A FLAT PLATE SHOULD SERVE **AS A LOWER BOUND TO THE DOVETAIL PROBLEM**
- STRESS = 2 * AVERAGE CONTACT STRESS * FRICTION COEFFICIENT
- FRICTION STRESS FOR HIGH CONTACT STRESSES AND HIGH FRICTION **COEFFICIENT ARE SIGNIFICANT**

### **LITERATURE DATA**

NORMAL LOADING

● FATIGUE TESTS THAT INCLUDED
THE EFFECT OF FRICTION LOADING
AND LOCAL SLIDING WERE
CONDUCTED TO VALIDATE THE
STRESS EFFECT ON LCF LIFE

SHOES SHOES SHOES SHOES SHOES SHOES SHOES

SKETCH OF RIG SHOWN AT RIGHT

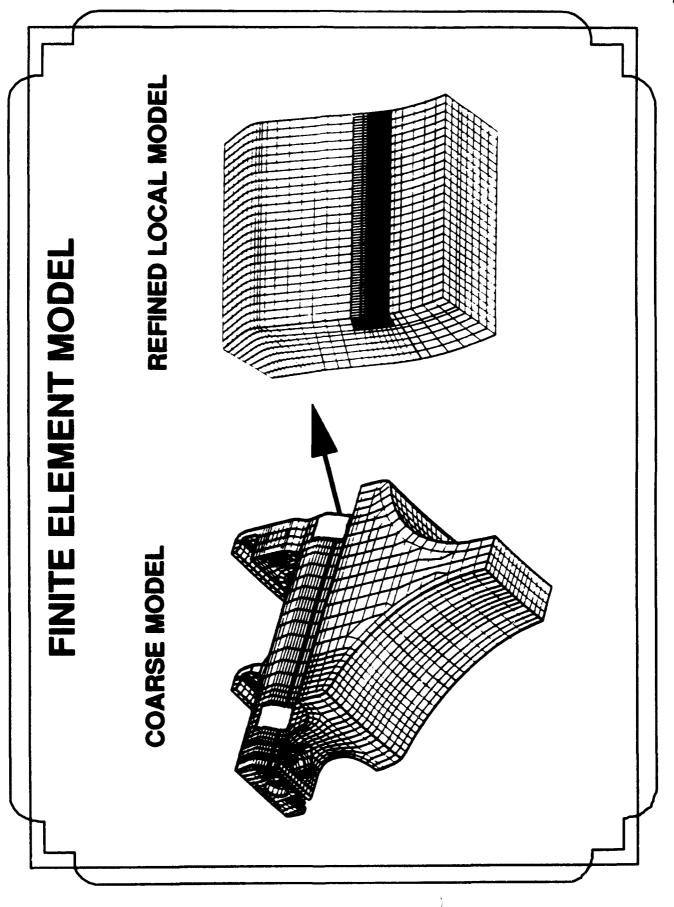
▶ FATIGUE PREDICTIONS CORRELATED WELL WITH CALCULATED STRESSES FOR SMALL DISPLACEMENTS FOR LARGE DISPLACEMENT, EXCESS WEAR ACTUALLY REMOVED DAMAGED MATERIAL, EXTENDING THE FATIGUE LIFE

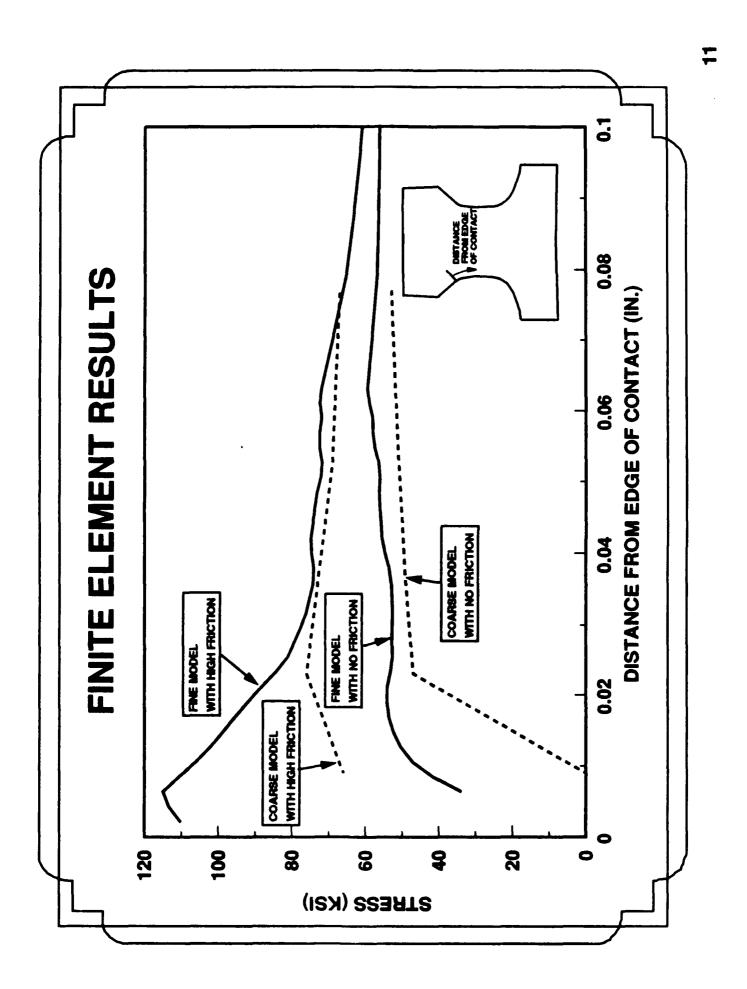
# **ANALYTICAL MODELING TECHNIQUES**

- RECOGNIZING THAT FRICTION STRESSES WILL OCCUR, ANALYTICAL MODELING TECHNIQUES WERE DEVELOPED TO UNDERSTAND THE STRESSES AND REDESIGN INCLUDING THEM
- TWO ANALYTICAL MODELING TOOLS PROVED EFFECTIVE PREDICTING THE LOCALLY HIGH FRICTION STRESSES
- FINITE ELEMENT MODELS WITH REFINED GRID
- PHOTOELASTIC MODELING WITH SIMULATED HIGH FRICTION
- TWO APPROACHES WILL BE DISCUSSED IN GREATER DETAIL IN THE PAGES TO FOLLOW

### FINITE ELEMENT MODELS

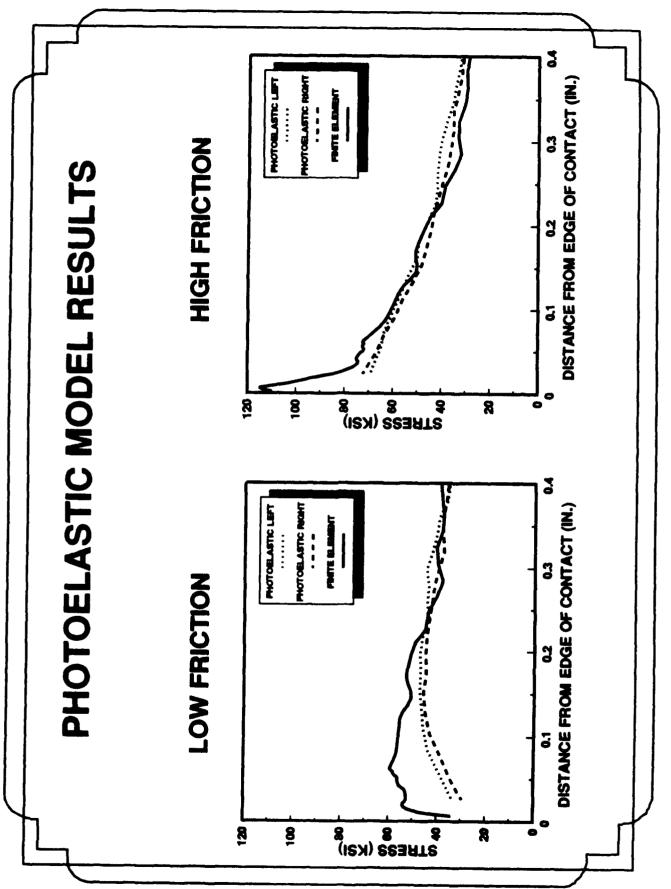
- FINITE ELEMENT MODELS CONSTRUCTED WITH FRICTION LOADING INCLUDED BETWEEN THE BLADE AND DISK DOVETAIL
- STANDARD MODELS SHOWED IMPACT OF FRICTION, BUT WERE TOO COARSE TO ACCURATELY MODEL LOCAL FRICTION EFFECTS
- EXTREMELY FINE MESH MODELS, WITH ELEMENT SIZES APPROACHING .001", USED TO REPRODUCE LOCAL STRESS DISTRIBUTION
- SAMPLE MODEL AND TYPICAL STRESS RESULTS SHOWN OF THE FOLLOWING PAGES





### PHOTOELASTIC MODEL

- PHOTOELASTIC MODELS CONSTRUCTED WITH BOTH HIGH AND LOW FRICTION LOADING INCLUDED BETWEEN THE BLADE AND DISK DOVETAIL
- HIGH FRICTION LOADING SIMULATED BY BONDING SANDPAPER TO THE PHOTELASTIC MODEL ON THE PRESSURE FACES
- PHOTOELASTIC PREDICTED STRESSES COMPARED WITH CORRESPONDING FINITE ELEMENT ANALYSES
- PHOTOELASTIC STRESSES AT THE POINT OF CONTACT COULD **NOT BE READ FROM THE FRINGE ORDERS**
- STRESSES AWAY FROM THE POINT OF CONTACT WERE IN EXCELLENT AGREEMENT WITH THE THE FINITE ELEMENT RESULTS, SHOWING THE EFFECT OF FRICTION



# **ANALYTICAL MODELING SUMMARY**

- FRICTION LOADING CAN SIGNIFICANTLY RAISE THE STRESS LOCALLY BOTH FINITE ELEMENT AND PHOTOELASTIC MODELS PREDICT THAI
- LOWER DOVETAIL CONTACT PRESSURES WOULD RESULT IN LOWER FRICTION STRESSES AND MAY PREVENT THE DOVETAIL CRACKING
- **DUSE OF LUBRICANTS TO REDUCE THE COEFFICIENT OF FRICTION CAN ALSO HELP KEEP STRESSES LOW**
- DIFFICULT TO MAINTAIN LUBRICANT OVER LONG PERIOD OF
- DOVETAILS USING ANALYTICAL TOOLS THAT INCORPORATE THE MORE PERMANENT FIX HAS BEEN EXPLORED BY RESHAPING EFFECT OF FRICTION

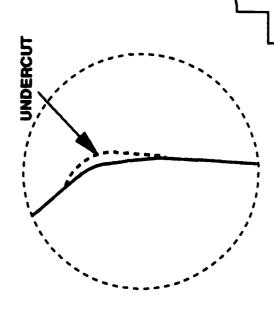
## DOVETAIL UNDERCUT DESIGN

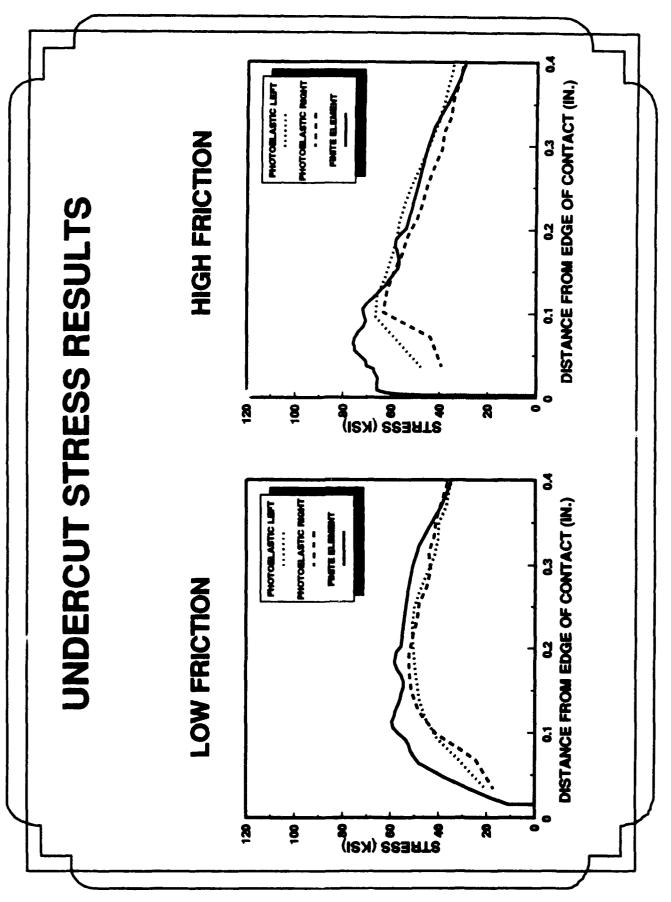
WITH ANALYTICAL TOOLS THAT INCORPORATE FRICTION, DOVETAIL GEOMETRIES CAN BE RESHAPED TO MINIMIZE THE EFFECT OF FRICTION

AN UNDERCUT, STARTING AT THE EDGE OF PRESSURE FACE, INTERRUPTS THE SURFACE TENSILE STRESS DUE TO FRICTION LOADING

UNDERCUT GEOMETRY, SIMILAR TO SKETCH, EVALUATED USING BOTH FINITE ELEMENT AND PHOTOELASTIC MODELS

BOTH ANALYSIS APPROACHES SHOW SIGNIFICANTLY LOWER STRESS LEVELS WITH THE UNDERCUT INCORPORATED





# **DOVETAIL CRACKING SUMMARY**

- FRICTION LOADING HAS BEEN IDENTIFIED AS A POSSIBLE CAUSE OF NUMEROUS DOVETAIL CRACKS OCCURING AT THE EDGE OF THE PRESSURE FACE
- FINITE ELEMENT MODELS, WITH VERY FINE MESH, AND PHOTOELASTIC MODELS HAVE BEEN SHOWN TO BE USEFUL ANALYTICAL TOOLS TO PREDICT THE EFFECT OF FRICTION
- RECOGNIZING THE EFFECTS OF FRICTION, THESE ANALYTICAL TOOLS CAN BE USED TO RESHAPE THE DOVETAIL GEOMETRY TO BE LESS SENSITIVE TO FRICTION STRESSES
- IN ADDITION, PRELIMINARY LCF/HCF TESTING OF THE UNDERCUT **GEOMETRIES HAS SHOWN A SIGNIFICANT LIFE BENEFIT**

# NASA TECHNICAL MEMORANDUM 102759 AVSCOM TECHNICAL REPORT 90-B-011

# A COMPARISON OF FATIGUE LIFE PREDICTION METHODOLOGIES FOR ROTORCRAFT

R. A. Everett, Jr.

**DECEMBER 1990** 

National Aeronautics and Space Administration

Langley Research Center Hampton, Virginia 23665-5225



### **SUMMARY**

Because of the current U.S. Army requirement that all new rotorcraft be designed to a "six nines" reliability on fatigue life, this study was undertaken to assess the accuracy of the current safe life philosophy using the nominal stress Palmgrem-Miner linear cumulative damage rule to predict the fatigue life of rotorcraft dynamic components. It has been shown in the past that this methodology can predict fatigue lives that differ from test lives by more than two orders of magnitude. A further objective of this work was to compare the accuracy of this methodology to another safe life method called the local strain approach as well as to a method which predicts fatigue life based solely on crack growth data. Spectrum fatigue tests were run on notched( $K_T$ =3.2) specimens made of 4340 steel using the Felix/28 variable amplitude spectrum ( a shortened form of a standard loading sequence for 'fixed' or semi-rigid helicopter rotors). Two other spectra which resulted from a simple rainflow reconstruction of Felix/28 were also tested.

Both linear cumulative damage methods predicted the fatigue lives of the Felix/28 tests fairly well, being slightly on the unconservative side of the test data. The crack growth method, which is based on "small-crack" crack growth data and a crack-closure model, also predicted the fatigue lives very well with the predicted lives being slightly longer than the mean test lives but within the experimental scatter band. The crack growth model was also able to predict the change in test lives produced by the rainflow reconstructed spectra.

### Introduction

One of two principle philosophies is currently used for the fatigue design of flight vehicles. These two philosophies are usually identified as safe life and damage tolerance. The safe life philosophy dates back to 1924 when Palmgren(ref. 1) published his work on linear cumulative damage in the life evaluation of ball bearings. In 1945, in an independent study by Miner (ref. 2), the same concept was applied to the design of aircraft components. The damage tolerance philosophy was introduced in the 1960's by the U.S. Air Force(ref. 3) in an attempt to prevent catastrophic accidents resulting from a less than perfect manufacturing process. In the damage tolerance philosophy, new structures are assumed to contain small cracks. Up to the current time the damage tolerance philosophy has been used exclusively on fixed-wing aircraft while all current rotorcraft have been designed using a safe life approach.

Because of two studies(ref. 4 and 5) done about a decade apart, the safe life approach using the Palmgren-Miner(P/M) linear cumulative damage rule has been questioned as being the most reliable approach to predicting fatigue life. In the work in reference 4 by Jacoby, the predicted lives of one-third of about 300 tests on all types of structures and materials were considered to be on the unconservative side. The work in reference 5, the hypothetical pitch link problem formulated by the American Helicopter Society, showed variations in predicted fatigue life from 9 to 2,594 hours. The current round-robin on fatigue life prediction in the American Helicopter Society(AHS) using a statistical reliability analysis is an effort aimed, in part, at investigating the adequacy of the safe life methodology. The AHS round-robin was instituted to increase future fleet readiness and flight safety which strongly depend on the degree of reliability and maintainability that can be designed into rotorcraft flight critical components. The current U.S. Army fatigue-life specification for new rotorcraft is the so-called "six-nine" reliability, or probability of failure of one in a million. The work reported in this study is a parallel effort to the AHS round-robin but focuses more on

the actual methodologies used to predict fatigue life rather than the reliability aspect of the problem.

To make an assessment of the several methods that are used to predict fatigue life, a test program was designed to evaluate the several methodologies. The test spectrum chosen for the tests was the standardized rotorcraft spectrum called Felix/28(ref. 6). This spectrum will be described in a later section in the paper. This spectrum was chosen since very little experience exists in the rotorcraft community in synthesizing load histories from actual flight records as reported in a recent study by Berens et. al. in their report on helicopter fatigue methodology(ref. 7). Two other forms of Felix/28 were also used in the spectrum tests. Both of these spectra were developed using the results of a rainflow counting analysis on the Felix/28 spectrum.

The three analysis methods that were used to calculate fatigue life were the nominal stress P/M, the local strain P/M, and a total-life fracture mechanics analysis developed by Newman(ref. 8). The nominal stress P/M method was chosen since it is the primary method currently used by the rotorcraft community. The local strain method was recommended in a recent study on helicopter fatigue methodology(ref. 7), since it assesses the stress(strain) state at discontinuities such as holes where the fatigue damage process occurs. The total-life analysis was chosen since it is a method that calculates fatigue life based solely on fatigue crack growth from "small" initial cracks(10 to 20 microns in length).

### Test Program

Both spectrum-fatigue and constant-amplitude-fatigue test data were needed for this study. The spectrum fatigue tests were needed as a point of reference to assess the ability of the several methodologies in predicting fatigue life. Constant amplitude test data were also needed for fatigue life calculations using the P-M nominal stress linear cumulative damage rule. This

section describes the test specimen used for these tests and explains how the fatigue tests were performed.

### Material and Specimen Configuration

The material selected for this study was AISI 4340 steel since it is often used in making dynamic components of rotorcraft. The material was supplied in the annealed condition with a plate thickness of 3/8 inch. All specimens were heat treated to Rockwell C scale values between 43 and 45 by a one hour soak at 840 C then tempering in a vacuum at 440 C for two hours followed by furnace cooling in nitrogen gas. The resulting tensile strength was 212 ksi which was calculated from an average of five tests.

The test specimens were machined to the configuration shown in Figure 1 before they were heat treated. The specimens were machined from the plate leaving a surface finish of 32 rms with the longitudinal axis of the specimen being aligned in the rolling direction of the plate. The hole dismeter of 0.25 inches was machined using several progressively larger drill sizes with the last drill removing only 0.002 inches maximum to minimize residual stresses. The surface finish of the hole after machine polishing was 8 rms.

The elastic stress concentration factor (based on net section stress) as determined from the boundary force method (ref. 9) is 2.42. The same value is given by Peterson in his book on stress concentration factors(ref. 10).

### Constant Amplitude Tests

All constant amplitude fatigue tests were run in servo-hydraulic, electronically controlled test stands. All tests were run at a stress ratio, R, of zero with cyclic frequencies between 10 and 20 hertz. Loads signals were controlled to within one percent. All fatigue lives reported herein were to specimen failure. Maximum net-section stress values ranged from 50 to 170 ksi.

Table 1 presents data for all constant amplitude tests. Figure 2 shows the constant amplitude fatigue tests plotted on a typical stress versus life cycle (S/N) curve. The endurance limit for these tests was estimated to be about 55 ksi.

### Spectrum Tests

The spectrum fatigue tests were also performed using servo-hydraulic, electronically controlled test stands. For these tests a computer that was used to input the sequence of peak and trough commands to the testing machine also checked to assure that each commanded peak or trough was attained (to within 0.5% of range) before proceeding with the remainder of the sequence.

The load spectrum chosen for these tests was a helicopter load sequence developed in a collaborative effort by three European countries(ref. 6). Two standardized spectra were developed by this effort. One spectrum, called Helix, is a loading sequence representative of hinged or articulated rotors. The other spectrum, called Felix, represents a load sequence for fixed or semi-rigid rotors. A shortened version of Felix called Felix/28 was chosen for these tests. The full Felix sequence has slightly more than two million load cycles through one pass of the spectrum while Felix/28 has only 161034 cycles.

As with all fatigue test load spectra many modifications are made to the recorded flight loads before the final version of the test load sequence is established(ref. 11). A Westland Helicopter Ltd. Lynx and a MBB-BO-105 were the two helicopters whose load sequences were used in developing Felix. The Felix spectrum is scaled in Felix units with the maximum load in the sequence being 100. In arriving at the final version of Felix all alternating loads below 16 Felix units were omitted. The ground load at landing is -28 Felix units. The Felix/28 spectrum was developed by further omitting all alternating loads that were below 28 Felix units. The full Felix version contained 22 unique maneuvers. In creating Felix/28 if any of these 22 maneuvers were eliminated because of the further load omissions, these

maneuvers were retained by redefining these maneuvers to have only one load cycle of the highest load at or below 28 Felix units.

Four unique flights each at three different flight lengths make up the 140 flights which represent one pass through the spectrum. The three different flight lengths are 0.75, 2.25, and 3.75 hours. All 140 flights combined represent 190.5 flight hours. The four unique flight types are made up of loading sequences that represent training, transport, anti-submarine warfare, and search and rescue missions. Figure 3 shows a typical load sequence for the transport mission.

Three forms of the Felix/28 spectrum were run during this test program. Each spectrum was run at several different maximum stress levels. Besides the actual Felix/28 sequence, the other two test spectra were load sequences developed from a rainflow cycle counting of the Felix/28 spectrum. Tests were run on these spectra to assess how important load interaction effects are on fatigue life in the Felix/28 spectrum. In one load sequence, called the low-high sequence in this study, the loads were applied in the order from the lowest load range, as determined by the rainflow counting method, to the highest load range. This load sequence is given in Table 2 and shown schematically in Figure 4. The other loading sequence was the reverse order of the low-high sequence and was called the high-low sequence. Since the low-high sequence gave fatigue lives that were slightly longer than the Felix/28 spectrum, the high-low sequence was run to see if shorter lives would result.

### Fatigue Life Prediction Methodologies

In this next section, an explanation of the three techniques used in this study to predict fatigue life is presented. The two safe-life methods calculate a total fatigue life without explicitly considering crack growth in the analysis. As opposed to these methods, the Total-Life Analysis uses only crack growth data to predict total fatigue life with the initial crack

length,  $a_i$ , being determined from a microscopic examination of crack initiation sites( $2a_i = 0.0006$  in.).

### Palmgrem-Miner Nominal Stress Approach

The rotorcraft industry mostly uses the nominal stress, Palmgren-Miner linear damage accumulation rule (P/M) to calculate the design fatigue life of rotorcraft dynamic components. The linear cumulative damage rule states that fatigue failure occurs when the summation of the so-called cycle ratios (n/N) is equal to one. In the nominal stress approach, the nominal applied stress is used with a cycle counting technique to group the flight loads into discrete load levels so the numerators (n) of the cycle ratios can be defined. In the design of rotorcraft the denominator(N) is determined from fatigue tests on the actual part being designed. Usually six tests are run at different stress levels and a curve is faired through each point to define the endurance limit(ref. 12). The curve shape used in fairing through the test points is usually established from coupon S/N test data. The design endurance limit is the lowest of several "statistical" reductions taken on the mean endurance limit. The statistical reductions often considered are eighty percent of the mean, one standard deviation from the mean, and three standard deviations from the mean. Usually the lowest of the several reductions considered is taken as the design endurance limit. In this report the denominator of the cycle ratio(N) was determined from coupon S/N data at a stress ratio of zero.

Since the fatigue load cycles from the flight loads data are at many different R ratios, these loads(stresses) are "corrected" to stress values that give the equivalent damage as the flight load stresses but at the R ratio of the S/N data. Some form of the Goodman diagram is normally used for this "correction". In this study a linear Goodman correction was used. The fatigue life is then calculated by summing all the cycle ratios for the different stress levels determined from the counting technique and this sum is inverted and multiplied by the number of cycles per pass in the load spectrum to calculate fatigue life. In equation form this becomes

In using the nominal stress P-M analysis for fatigue life prediction there are at least three parts of the analysis where different approaches can be used. First, a counting technique must be used to group the flight stresses into discrete stress levels to form the cycle ratios. In this study a rainflow counting technique has been used which has been programmed as a computer algorithm(ref. 13). The rainflow count of Felix28 is given in Table 2. Second, an S-N curve is needed for the denominator of the cycle ratios. In this study as stated previously, constant amplitude tests were run at a stress ratio of zero to provide this information (see Fig. 2 and Table 1). In the computer algorithm that was written for the nominal stress P-M analysis, the S-N data were put in an equation which is linear on a log-log plot as shown in figure 5. The horizontal line shown in figure 5 represents the endurance limit which was determined from the three tests that were runouts(see Table 1). The stress levels of these three tests were averaged to define the endurance limit at 55.83 ksi. All tests were used to calculate the log-linear line shown in figure 5 except for the three runout tests and tests that were below the endurance limit. Third, the flight stresses were corrected by a linear Goodman correction to give a set of stresses that gave an equivalent damage as the actual spectrum stresses but at the stress ratio used in the constant amplitude tests.

### Local Strain Approach

The local strain approach uses the P/M linear cumulative damage rule, but seeks to define the fatigue damage in a more rigorous manner by relating the fatigue life to the local strain and local mean stress. This approach also is able to account for load interaction effects since the strain for a current load cycle depends on the prior load cycles deformation(ref. 14). Instead of using a S-N curve to determine the denominator of the cycle ratios, a local strain life relationship is used which relates the local strain amplitude,  $\epsilon_{\rm a}$  to the cycles to failure, N*. This relationship is usually developed from constant amplitude fatigue tests on unnotched specimens.

For a mean local stress of zero this relationship can be expressed as

$$\epsilon_{\mathbf{a}} = \frac{\sigma_{\mathbf{f}}}{E} (2N^*)^{\mathbf{b}} + \epsilon_{\mathbf{f}}' (2N^*)^{\mathbf{c}}$$
 (2)

fit parameters. These curve fit parameters are often called the fatigue strength coefficient, fatigue strength exponent, fatigue ductility coefficient, and fatigue ductility exponent, respectively. An equation which corrects the above calculated life for a nonzero local mean stress is

$$N = N* (1 - \sigma_o / \sigma_f')^{-1/b}$$
 (3)

where  $\sigma_0$  is the local mean stress.

The numerators in the cycle ratios, n, are determined by taking the flight load peaks and valleys and turning them into a sequence of local stress-strain hysteresis loops. These local stress-strain hysteresis loops are then grouped into similar strain ranges to form the cycle ratios (n/N) used to calculate the fatigue life. It is the forming of the stress-strain hysteresis loops where the load interaction effects of the flight loads are taken into account.

The local stress and strains corresponding to each flight load peak and valley can be determined experimentally or estimated through approximate equations(ref. 15). If the equation method is used the flight loads(or stress, S) are often related to the local stress and strain using Neuber's rule in the form

$$\sigma \in -\frac{(K_{T}S)^{2}}{F}$$
(4)

where  $\sigma$  and  $\epsilon$  are the local stress and strain, and  $K_{\widehat{T}}$  is the elastic stress concentration factor. A cyclic stress-strain relationship such as

$$\epsilon = \sigma/E + (\sigma/A)^{1/S}$$
 (5)

where A is the cyclic strength coefficient and s is the cyclic strain hardening exponent, is then combined with the Neuber rule to determine the local strain for each flight load peak and valley in the load sequence. The corresponding local stress can then be determined from Neuber's rule and the local stress-strain hysteresis loops are formed.

A rainflow counting of a given flight load sequence will give the same cycle counting results in terms of the the number of cycles(n) at a given nominal stress as the method for generating the hysteresis loops stated above(ref. 15). These nominal stresses can then be converted to local stresses using Neuber's rule as previously stated. Computer algorithms have been developed for performing this type of rainflow counting(ref. 13). A computer program has also been developed for predicting fatigue life from a simplified version of the local strain approach. In this approach upper and lower bounds are placed on the mean stress of each load cycle and fatigue lives are calculated using equations 2 through 5 to determine upper and lower bound values of fatigue life(ref. 13). This approach was used in this study in determining the fatigue life from the local strain methodology.

A computer algorithm, called UPLO, developed by Khosrovaneh and Dowling (ref. 13) was used for calculating the upper and lower bounds on fatigue life. The curve fit parameters needed in equations 2, 3, and 5 are given in Table 4. The range and mean stress values for Felix28 needed by UPLO were determined by a rainflow computer algorithm(ref. 13).

### Damage Tolerance Approach

In the damage tolerance approach to structural integrity, a safe inspection interval or safe operating life is calculated from crack growth considerations. A safe inspection interval is determined for structures where the structure can be inspected and a safe operation life is determined for structures that can not be inspected. Concepts from fracture mechanics which

relate crack growth rates to the stress intensity factor range are used to calculate the safe operating interval or life. In this approach, life is calculated by integrating a crack growth rate versus stress intensity factor relationship like

$$da/dN - C(\Delta K)^{m}$$
 (6)

where da/dN is the crack growth rate and  $\Delta K$  is the stress intensity factor. To calculate a safe inspection interval the initial crack size used in the integration is 0.05 inches(ref. 3). To calculate a safe operation life the initial crack size used in the integration is 0.005 inches. In the calculation of the safe operating life the crack growth life must be greater than the design life of the structure.

In this study, a modified damage tolerance approach was used to predict the total fatigue life of the test specimen. The main difference between the total life analysis(TLA) and the more widely accepted approach, explained above, is that crack-closure concepts(ref. 8) are used to define an effective  $\Delta K$  and the initial crack length was determined from a previous "small" crack study on 4340 steel(ref. 16). From crack-closure considerations,  $\Delta K$  in equation 6 is replaced by  $\Delta K$  effective. In this work the effective stress intensity factor is defined as

$$\Delta K_{eff} = (S_{max} - S_o)(\pi a)^{1/2} F \qquad (7)$$

where  $S_0$  is the crack-opening stress as calculated from the analytical closure model developed by Newman(ref. 8) and F is the boundary correction factor which accounts for the effects of structural configuration on the stress intensity factors. To

calculate the crack growth rate, equation 6 becomes

$$da/dN = C[(S_{max} - S_0)(\pi a)^{1/2} F]^m$$
 (8)

Total life is calculated by numerically integrating equation 8 from the initial crack length to failure as

$$N = \sum_{i}^{a_{f}} C[(S_{max} - S_{o})(\pi a)^{1/2}F]^{m}$$
(9)

where  $\mathbf{a_i}$  is the initial crack length as determined from the small crack studies and  $\mathbf{a_f}$  is the final crack length at failure. Cycles are summed as the crack grows until  $K_{\text{max}} - K_{\text{c}}$ , where  $K_{\text{c}}$  is the fracture toughness. When  $K_{\text{max}} - K_{\text{c}}$ , the summation of the load cycles, N, becomes the total fatigue life.

The total fatigue life as determined by the TLA method was calculated from a computer algorithm developed by Newman. For this study the initial crack length used to predict the fatigue life was 0.0006 inches. This value was taken from a small crack study on 4340 steel(ref. 16) in which initial defect sizes at 34 crack initiation sites were evaluated by scanning electron microscopy of the fracture surfaces. The largest value was about 0.002 inches, the median value was about 0.0006 inches, and the smallest was about 0.00008 inches.

### Comparisons of Predicted and Test Lives

Figure 6 shows the results for the Felix/28 spectrum tests and the rainflow counted sequence tests. The data are plotted as the maximum stress in the spectrum versus the load cycles to failure. Table 3 shows these test results in tabular form at the several different maximum stress values. Figure 6 shows that at the higher stress levels the low-high sequence gave fatigue lives that were slightly longer than the Felix/28 lives, while the high-low sequence gave slightly shorter lives than the Felix/28 lives. The test results also show that as the maximum stress level in the spectrum is reduced the lives for the three different test spectra appear to converge. In reference 6 it was noted that Felix/28 test lives should be viewed with caution at the higher stress levels, whereas, the lives near the endurance limit simulated the full Felix spectrum test results fairly well. The current tests also show that for this material and hole configuration a maximum stress

in the spectrum of 100 ksi will give test lives at about one pass through the spectrum while a runout is at about a maximum stress of 65 ksi in the spectrum.

In figure 7 the Felix28 spectrum test results are shown as well as the analytical life predictions from the nominal stress P-M analysis, local strain P-M, and the TLA analysis as explained above. The P-M analysis life predictions follow the trend of the Felix28 test data very well, although the predictions are slightly on the unconservative side. It should be noted that these lives were based on a mean regression line through the S-N data of figure 2. The mean regression line is shown in figure 5. In general, rotorcraft fatigue lives are based on a reduction from this mean curve. This will be discussed in more detail later.

The local strain P-M life predictions as calculated by the UPLO program also follows the trend of the Felix28 data very well. Similarly to the nominal stress P-M analysis, the local strain predicted lives are slightly unconservative when compared to the test data where the maximum stress in the test spectrum is at the higher values. However, at the lower stress values the local strain predicted lives fall within the scatter of the test results.

The life predictions from the TLA analysis also follows the trend of the test data very well. These predicted lives are also slightly longer than the mean test lives but are within the experimental scatter.

Since the nominal stress P-M method cannot account for any load interaction effects, it will predict the same fatigue lifes for all three spectrums. As stated previously, the local strain P-M method does account for load interaction effects. However, in this study since the bounded analysis of the UPLO computer program was used to predict fatigue lives, it is not clear how successful the local strain analysis would be in predicting the load interaction effects of these spectra. As can be seen in figure 8, the maximum difference in lives that could be produced by the local strain method due to load sequence effects was similar to the difference in lives observed for the two reconstructed sequence tests.

The TLA analysis, like most analyses that calculate crack-growth rates, accounts for load interaction effects. As can be seen in figure 8, different fatigue lives are predicted for the lo-hi and hi-lo load spectra by the TLA method. For the lo-hi spectrum the lives predicted by the TLA fall within the scatter of the test data. For the hi-lo spectrum, the TLA predicts lives that approximate the upper bound of the test life scatter. It must be recalled that these life predictions made with the TLA were done using the median value(0.0006 inches) of the initial defect size determined from a previous test program on the same batch of 4340 steel(ref. 16).

If any of the three methods used in this study were used for predicting the design fatigue life of an aircraft, some type of reduction would be taken from the mean life curves shown previously. Figure 9 shows such possible reductions as well as a life prediction curve using the initial crack size most often used in damage tolerance analysis(0.05 inches, ref. 3). If the nominal stress P-M analysis were used for design, one possible reduction would be to reduce the mean S-N curve to 80% of the mean stresses and calculate fatigue lives based on the 80% S-N curve(ref 12). Fatigue lives predicted by this procedure are shown in Figure 9. Since this "design" life curve falls on the conservative side for practically all test data this would appear to be an acceptable design life curve.

Figure 9 also shows a life prediction "design" curve as calculated by the TLA method( $a_i$ = 0.002 inches). These lives were calculated using the largest inclusion particle dimensions found in reference 16. While this "design" curve also predicts lives on the conservative side of the test data, it predicts an endurance limit between 40 and 45 ksi which is nominally 10 ksi less than the 80% P-M prediction and about 20 ksi less than the one runout test.

To place in perspective the effect of using the current damage tolerance initial crack size(0.05 inches) on predicting total fatigue life, a curve from these calculations is also shown on figure 9. Very conservative lives would be predicted using the 0.05 inch initial crack size.

### Conclusions

The following conclusions have been reached from this study on 4340 alloy steel, quenched and tempered to  $45~R_{\odot}$ :

- 1. Both the nominal stress and the local strain Palmgren-Miner linear cumulative damage rules predicted the fatigue lives under the Felix/28 standardized helicopter spectrum with reasonable accuracy.
- 2. Two simple load sequences(low-high and high-low) from rainflow counting of Felix28 showed different lives than the actual Felix/28. The nominal stress P-M linear cumulative damage rule produces the same life prediction for both reconstructed sequences. The maximum difference in lives that could be produced by the local strain method due to load sequence effects was similar to the difference in lives observed for the two reconstructed sequence tests.
- 3. The Total Life Analysis(TLA) which uses crack-closure concepts in predicting total fatigue life using crack-growth data alone (initial crack size of 0.0006 inches) also predicted the Felix28 test data very well. Since this analysis can take into account load interaction effects, it also predicted the total fatigue lives of the simple rainflow reconstructed spectra with reasonable accuracy.

### REFERENCES

- 1. Palmgren, A., <u>Ball and Roller Bearing Engineering</u>, translated by G. Palgrem and B. Ruley, SKF Industries, Inc., Philadelphia, 1945, pp. 82-83.
- 2. Miner, M.A., "Cumulative Damage in Fatigue", Journal of Applied Mechanics, ASME, Vol.12, Sept. 1945, pp. A-159-164.
- 3. Gallagher, J.P.; Giessler, F.J.; and Berens, A.P.: USAF Damage Design Handbook, Guidelines for the Analysis and Design of Damage Tolerant Aircraft Structures, Air Force Wright Aeronautical Laboratorie, AFWAL-TR-82-3073, 1984.
- 4. Jacoby, G., Comparison of Fatigue Life Estimation Processes For Irregularly Varying Loads, Proceedings of 3rd conference on Dimensioning, Budapest 1968.
- 5. Arden, R.W., Hypothetical Fatigue Life Problem, presented at the Specialists Meeting on Helicopter Fatigue Methodology, Midwest Region of the American Helicopter Society, preprint no. 18, 1980.
- 6. Edwards, P.R. and Darts, J.: Standardised Fatigue Loading Sequences for Helicopter Rotors (Helix and Felix) Partl, Background and Fatigue Evaluation, Royal Aircraft Establishment TR 84084.
- 7. Berens, A.P.; Gallagher, J.P.; Dowling, N.E.; Khosrovaneh, A.K.; Thangjitham, S.: Helicopter Fatigue Methodology, Vol. I Analysis Methods, USAAVSCOM TR 87-D-13A, 1987.
- 8. Newman, J.C.Jr.: A Crack-Closure Model for Predicting Fatigue Crack Growth under Aircraft Spectrum Loading, ASTM STP 748, 1983.
- 9. Tan, P.W.; Raju, I.S.; and Newman, J.C.: Boundary Force Method for Analyzing Two-Dimensional Cracked Plates, ASTM STP 945, 1988.
- 10. Peterson, R.E.: <u>Stress Concentration Factors</u>, John Wiley & Sons, New York, 1973.
- 11. Fowler, K.R. and Wantanabe, R.T.: Development of Jet Transport Airframe Fatigue Test Spectra, ASTM STP 1006, 1989.
- 12. Thompson, G.H.: Boeing Vertol Fatigue Life Methodology, presented at the Specialists Meeting on Helicopter Fatigue Methodology, Midwest Region of the American Helicopter Society, preprint no. 22, 1980.
- 13. Khosrovaneh, A.K. and Dowling, N.E.: Fatigue Loading History Reconstruction Based on the Rain-Flow Technique, NASA CR-181942, 1989.
- 14. Socie, D.F.: Fatigue-life Prediction Using Local Stress-Strain Concepts, Expermental Mechanics, SESA, Feb. 1977.

- 15. Dowling, N.E.: A Review of Fatigue Life Prediction Methods, SAE/DOC Symposium on Durability by Design, SAE paper no. 871966, 1987.
- 16. Swain, M.H.; Everett, R.A.; Newman, J.C., Jr.; and Phillips, E.P: The Growth of Short Cracks in 4340 Steel and Al-Li 2090, paper no. 7 in AGARD Report 767, 1989.

Table 1. Constant amplitude fatigue test data for R = 0.

S max (ksi)	Cycles-	to-failure		
50	5993030			
52.5	3757353,	10000000(	run-out)	
55	2577077	10000000(run-out)		
60	206790,	116768,	10000000	(run-out)
65	97278,	81773		
70	308435,	61361,	58233	
80	80827,	49277	37095,	34059
	28099	•	·	
120	7434,	7306.	7056	
175	1531,	1336,	1325	

Table 2. Rainflow Low-High Load Sequence Derived From Felix28

NOMINAL STRESS	NOMINAL STRESS	NUMBER OF
RANGE	MEAN	CYCLES
(KSI)	(KSI)	
•		
2.80	25.59	354
2.80	32.83	334
6.42	29.21	416
10.04	29.21	609
10.04 10.04	36.45 40.07	1228 810
13.66	36.45	2
17.28	18.35	140
17.28	32.83	78
20.91	32.83	2061
20.91	36.45	90
24.53	-7.00	140
24.53	18.35	140
24.53	36.45	2040
28.15	29.21	833
31.77	25.59	346
35.39	25.59	7904
35.39	29.21	56
35.39	32.83	71072
35.39	43.69	2529
39.01 39.01	21.97 25.59	3014 42825
39.01	29.21	6393
39.01	43.69	252
42.63	25.59	480
42.63	29.21	207
42.63	36.45	1274
46.25	21.97	274
46.25	25.59	6239
46.25	29.21	4274
46.25	40.07	604
49.87	3.86	268
49.87	25.59	956
49.87	29.21	2179
53.49	25.59	2
53.49	29.21	116
57.12 57.12	25.59 29.21	5 185
60.74	29.21	25
64.36	25.59	7
64.36	29.21	8
64.36	32.83	75
67.98	29.21	9
71.60	29.21	16
75.22	25.59	7
78.84	18.35	5
78.84	25.59	1
82.46	21.97	128
82.46	29.21	16
89.70	25.59	8

Table 3. Spectra Fatigue Test Data

## a) Felix/28 Spectrum

S max (ksi)	Cycle	s-to-failure		
65	41000000(re	un-out)		
70	11031000			
73.3	4396500			
80	3128200,	2898600,	2095100,	1177900
	1032500	841860	552600,	404510
85	121080	·	·	
86.7	176308			
90	227510,	179180		
93.3	279190			
100	187490,	175650,	107580	
120	52079,	41228		

### b) Rainflow Low-High Spectrum (of Felix/28)

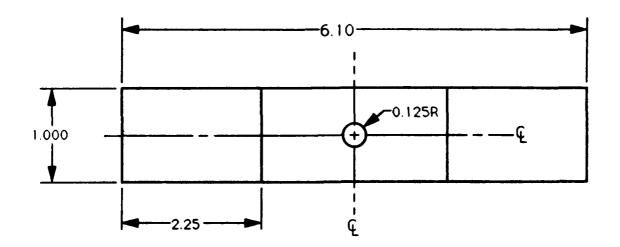
70	42290000(run-out)			
80	2116500	·		
90	4112834,	3176269,	629160	
100	577140,	219872,	214420	
120	206495,	65124,	49055	

# c) Rainflow High-Low Spectrum (of Felix/28)

80		592808,	422226,	2440630	
90		551120,	532280,	484260,	325150
100	•	49790.	230500,	62559	
120		34915	33825		

Table 4. Local Strain Curve Fit Parameters

σf	fatigue strength coefficient	290 ksi
b	fatigue strength exponent	-0.091
έf	fatigue ductility coefficient	0.48
c	fatigue ductility exponent	-0.60
A	cyclic strength coefficient	305 ksi
s	cyclic strain hardening exponent	0.15



Note: Dimensions in inches

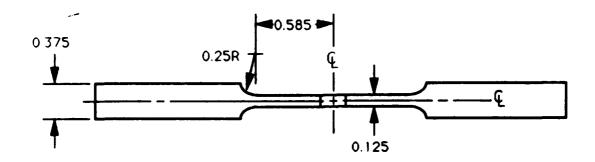


Fig. 1. Fatigue test specimen configuration

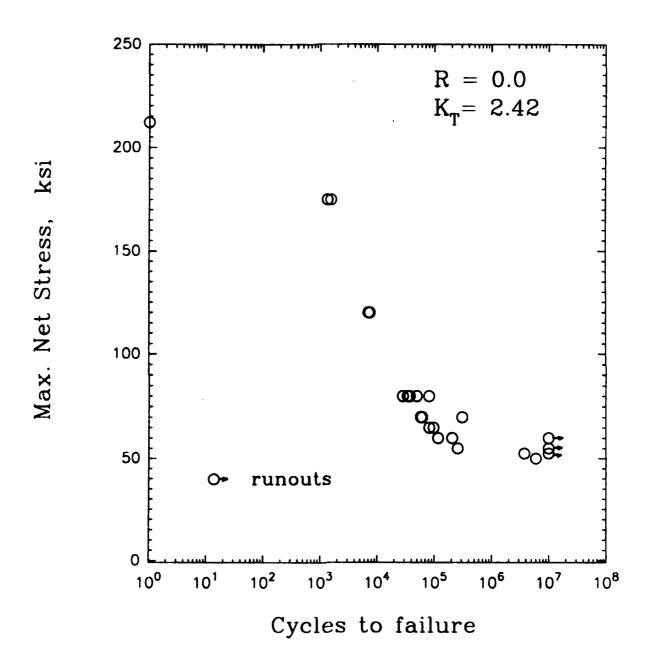
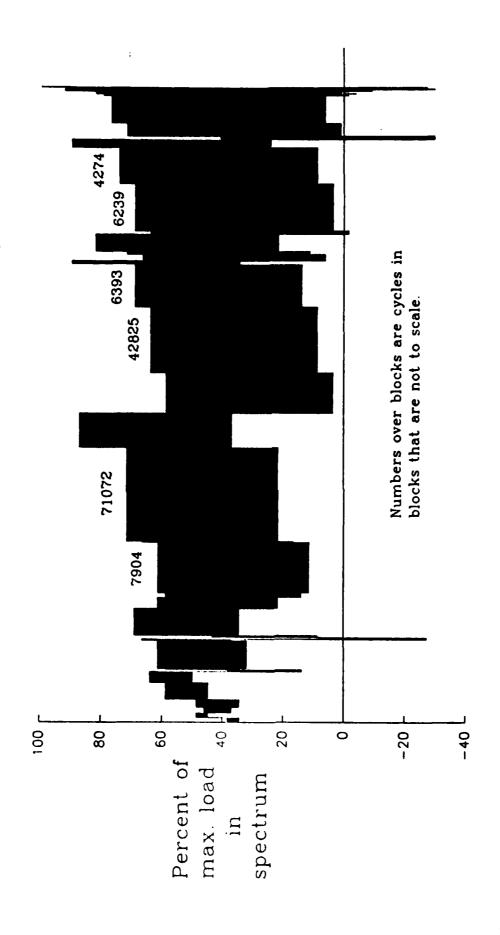


Fig. 2 Constant amplitude test data.



Fig. 3 Felix28 long transport flight (3.75 hrs).



Rainflow low-high load sequence derived from Felix28 Fig. 4

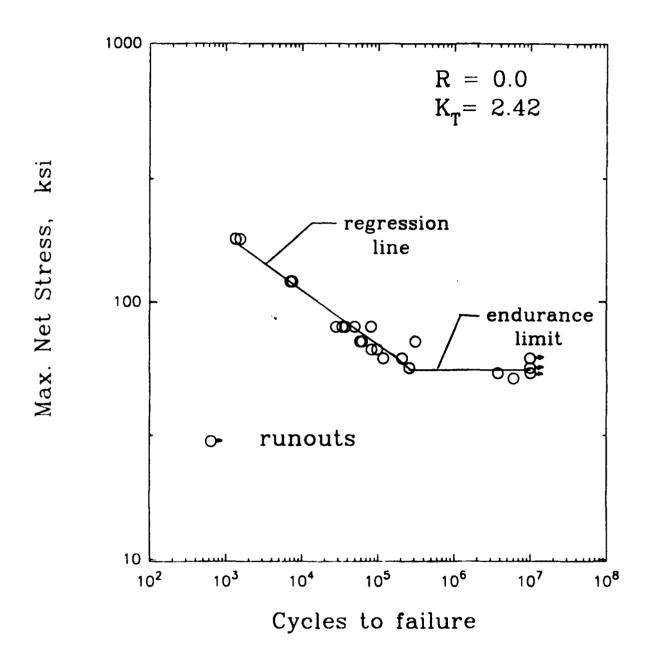


Fig. 5 Regression analysis of constant amplitude data

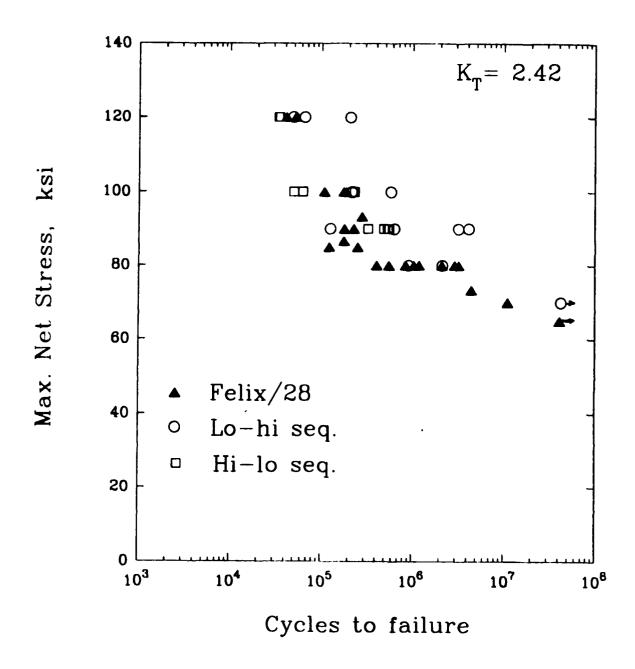


Fig. 6 Spectrum test data.

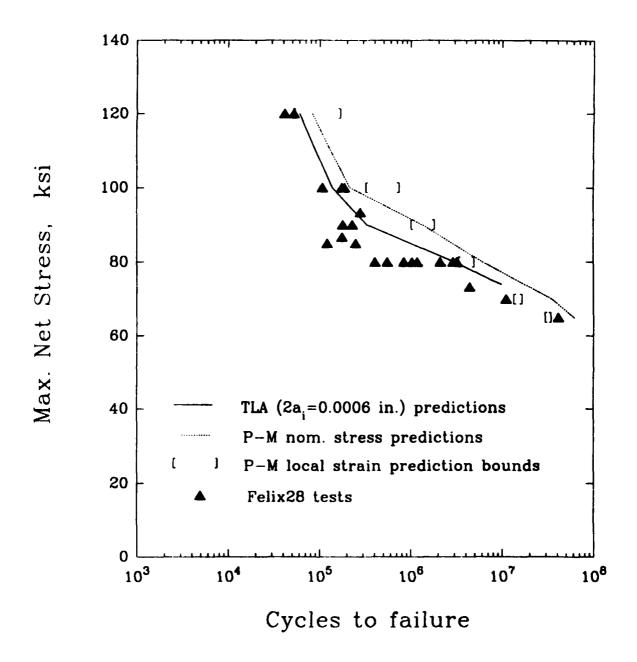


Fig. 7 Fatigue life predictions for Felix28 tests.

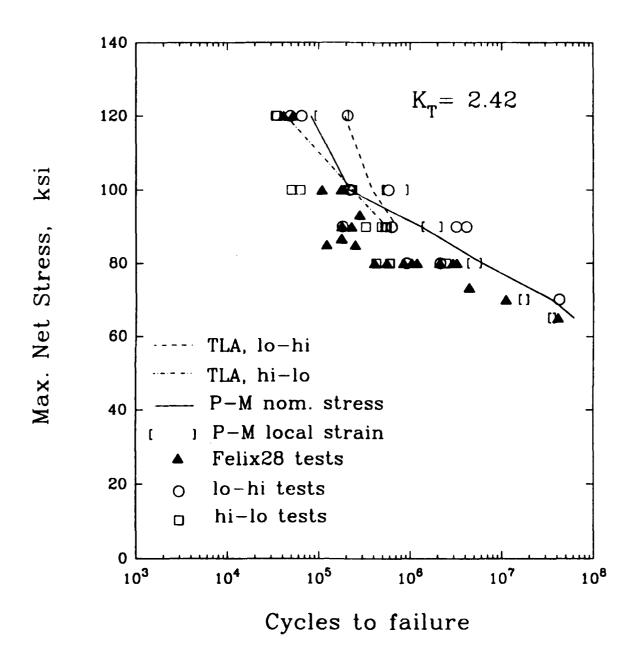


Fig. 8 Fatigue life predictions for lo-hi and hi-lo spectrum tests.

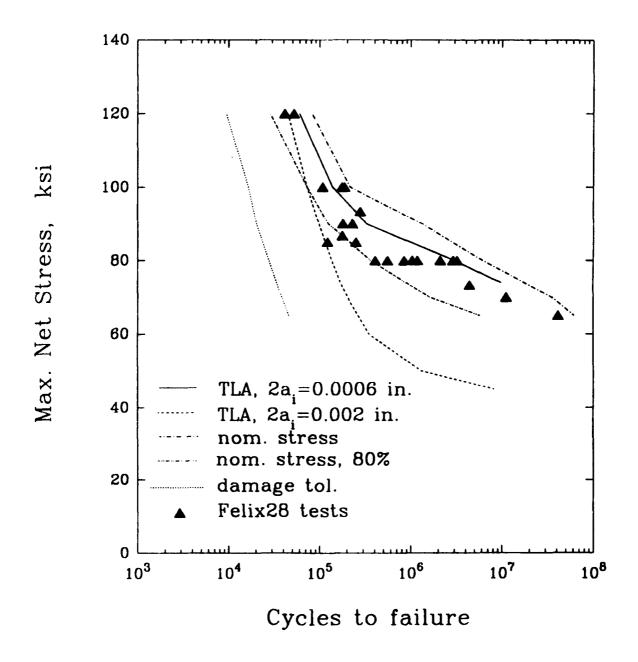


Fig. 9 Effect of conservative assumptions on fatigue life predictions for Felix28 tests.

NASA Litera Anti-Anti-Anti-Anti-Anti-Anti-Anti-Anti-	Report Docume	ntation Page			
1. Report No. NASA TM-102759 AVSCOM TR-90-B-011	2. Government Accession	No	3 Recipient's Catalog	j No.	
4. Title and Subtitle	- di		5. Report Date	•	
A Comparison of Fatigue Life Pro Methodologies for Rotorcraft	ediction		December 1990	, 	
			6. Performing Organi	zation Code	
7 Author(s)			8. Performing Organi	zation Report No.	
R.A. Everett, Jr.					
			10. Work Unit No.		
9. Performing Organization Name and Addre	nec .		505-6? -0-04		
NASA Langley Research Center,		5-5225	11. Contract or Grant	No.	
U.S. Army Aviation Research and					
Aerostructures Directorate			13. Type of Report an	d Period Covered	
Hampton, VA 23665-5225 12 Sponsoring Agency Name and Address					
National Aeronautics and Space A	Administration		Technical Mem	orandum	
Washington, DC 20546-0001 U.S. Army Aviation Systems Co	mmand		14. Sponsoring Agenc	y Code	
St. Louis, MO 63166	immand				
15 Supplementary Notes R. A. Everett, Jr.: Aerostruc	ture Directorate IIS		<i>(</i> 1)		
Langley Research Center, Ha		AMIA (AVSCO	и),		
Paper to be published in the	Journal of the America	can Helicopter So	ciety.		
		•	•		
16. Abstract					
Because of the current U.S. Army					
on fatigue life, this study was und					
the nominal stress Palmgrem-Min dynamic components. It has beer					
differ from test lives by more than	n two orders of magn	itude. A further o	objective of this w	ork was to	
compare the accuracy of this meth					
	well as to a method which predicts fatigue life based solely on crack growth data. Spectrum fatigue tests				
were run on notched ( $K_T = 3.2$ ) specimens made of 4340 steel using the Felix/28 variable amplitude spectrum (a shortened form of a standard loading sequence for "fixed" or semi-rigid helicopter rotors).					
Two other spectra which resulted					
Both linear cumulative damage m	ethods predicted the f	fatigue lives of the	e Felix/28 tests fa	irly well, being	
slightly on the unconservative sid	le of the test data. Th	e crack growth m	ethod, which is b	ased on "small-	
crack" crack growth data and a cr					
predicted lives being slightly long crack growth model was also able					
spectra			<u> </u>		
17 Key Words (Suggested by Author(s))		18 Distribution Statem	nent		
	ım loading				
Fatigue life	Linglace	fied - Unlimited			
Helicopter Crack growth			Category - 39		
19 Security Classif (of this report)	20 Security Classif (of thi		21 No of pages	22. Price	
Unclassified	Unclassified		31	A03	

# Uncertainties in Determining High Reliability For Helicopter Component Safe Life Design

William Matthews Donald Neal Trevor Rudalevige Mark Vangel

U.S. Army Materials Technology Laboratory Watertown, Massachusetts 02172-0001

### Synopsis

This paper identifies the uncertainties in determining high component reliability at a specified lifetime from a case study involving the fatigue life of a helicopter component. Reliabilities are computed from results of a simulation process involving an assumed variability of the load and strength in determining fatigue life. The uncertainties in the high reliability computation are then examined by introducing small changes in the variability for the given load and strength values in the study.

Results showed for a given component lifetime a small increase in variability of load or strength produced large differences in the component reliability estimates. Among the factors involved in computing fatigue lifetimes, the component reliability estimates were found to be most sensitive to variability in loading. Component fatigue life probability density functions were obtained from the simulation process for various levels of variability. The range of life estimates were very large for relatively small variability in load and strength.

The substantial sensitivity of these estimates may be indicative of the typical sensitivity of high reliability estimates in a broader class of structural design problems including applications of composite materials.

# Contents

1	Introduction	1	
2	The Coupon Test SN Curve The Component SN Curve		
3			
4 Spectrum Load		3	
5 Miner's Rule			
6	Simulation Procedures in Determining Component Reliability	4	
	6.1 Bootstrap Method Applied to Coupon SN Curve Computation	4	
	6.2 Reliability Estimates From SN Component Curve Simulations	5	
	6.3 Load Uncertainties Effect on Reliability Computations	6	
	6.4 Reliability Sensitivity From Uncertainties in Miner's Rule	6	
7	Working SN Curve	7	
	7.1 Reduction Factors for Working Curves	7	
8	Results and Discussions	8	
9	Conclusions	11	

### 1 Introduction

Methodology to substantiate helicopter fatigue life has received considerable attention during the last decade. This interest was stimulated by the substantial variability in the results from the study on the American Helicopter Society pitch link problem ¹. Recently, further interest has resulted from the U.S. Army's introduction of a structural fatigue reliability criterion for rotorcraft. This criterion has been interpreted ² as a requirement for a component lifetime estimate to have a reliability of .999999.

Helicopter safe life reliability methodology has recently been the subject of several papers 3, 4, 5, 6 and an American Helicopter Society subcommittee round robin 7.

The authors ⁸ have investigated the sensitivity of high reliability estimates from simple stress-strength statistical model computations. Results showed substantial variability in reliability estimates even for almost undetectable differences in the assumed probability density functions (PDF's) representing the stress and strength data.

In this paper the uncertainties in determining high reliability for helicopter component safe life design are studied by introducing a simulation process to identify the effects of a small amount of variability in the design variables for determining the lifetime estimate. The reliability values are determined for a generic uniaxial steel structure loaded in tension similar to a helicopter pitch link component by applying Miner's linear damage rule 9. The six component fatigue test values were obtained from Arden 1 where the maximum applied stress (S) on the component is tabulated with respect to cycles to failure (N). In order to obtain an SN curve to represent the component fatigue test results, a separate regression analysis was applied to a larger set of coupon tests of a steel for which the results are tabulated in Bury 10. The assumed spectrum load used in determining the lifetime estimate was obtained from

¹Arden, R. W., "Hypothetical Fatigue Life Problems", Proceedings of the American Helicopter Society Midwest Region Helicopter Fatigue Methodology Specialists' Meeting, March 1980.

²Arden, R. W. and Immen, F. H., "U.S. Army Requirements for Fatigue Integrity", Proceedings of the American Helicopter Society National Technical Specialists' Meeting on Advanced Rotorcraft Structures, Williamsburg, VA October 1988.

³Amer, K. B., "A New Philosophy of Structural Reliability, Fail Safe Versus Safe Life", Journal of the American Helicopter Society, Vol 34(1), January 1989.

⁴Krasnowski, B. R., "Designing Rotorcraft Dynamic Components to Reliability Requirements", Presented at the National Fatigue Specialists' Meeting, American Helicopter Society, Scottsdale, Arizona, October 1989.

⁵Spigel, B. S., "Safe Life Design for Rotorcraft", Journal of the American Helicopter Society Vol 36(1), January 1991.

⁶Thompson, A. E. and Adams, D. O., "A Computational Method for the Determination of Structural Reliability of Helicopter Dynamic Components" Presented at the American Helicopter Society Annual Forum, Washington D.C., May 1990.

⁷Everett, R. A., Bartlett, F. D., and Elber, W., "Probabalistic Fatigue Methodology for Six Nines Reliability", AVSCOM Technical Report 90-B-0091 NASA Technical memorandom 102757, December 1990.

⁸Neal, D. M., Matthews, W. T., and Vangel, M. G., "Model Sensitivity in Stress-Strength Reliability Computations", MTL TR 91-3, Jan 1991.

⁹Miner, M. A., "Culmulative Damage in Fatigue", Journal of Applied Mechanics, 12 (1945) pp. A150-A164

¹⁰ Bury, K. V., Statistical Models in Applied Science, John Wiley & Sons, 1975 pg. 598.

Berens ¹¹. Note that only the six component fatigue test values are from Reference 1, and the remaining test values are from References 10 and 11.

### 2 The Coupon Test SN Curve

This section describes the procedure for determining an SN regression curve to represent coupon fatigue test data ¹⁰ shown in Figure 1. The assumed functional representation ¹² of the data is

$$S = S_{\infty} + (S_u - S_{\infty})e^{-\beta(\log_{10}N)^{\gamma}}, \tag{1}$$

where S is the maximum applied stress and N is the number of cycles required for the coupon to fail.  $S_{\infty}$  is the coupon endurance limit representing the case when  $N \to \infty$  and  $S_{\mathbf{u}}$  represents the static strength of the coupon (i.e., the strength for N=1). The shape of the SN curve is determined by  $\beta$  and  $\gamma$ .  $S_{\infty}$ ,  $S_{\mathbf{u}}$ ,  $\beta$ , and  $\gamma$  were determined from application of an IMSL computer code ¹³ for solving nonlinear regression problems. The resultant SN curve is shown in Figure 1 (solid line) with the individual coupon fatigue test values.

A review of the literature on the determination of component fatigue life showed various functional representations similar to Equation 1 have been applied where N is the independent variable and S is the dependent (response) variable. This is counter to the conventional functional representation of test data where S would be the independent variable in the analysis since a fixed cyclic load (stress) value is applied and a resultant (dependent) number of cycles to failure is recorded. In order to obtain N as the dependent variable, Equation 1 can be inverted resulting in the following.

 $\log_{10} N = e^{\{\log[-\log((S-S_{\infty})/(S_{\omega}-S_{\infty}))]-\log\beta\}/\gamma}.$  (2)

Although Equation 2 is recommended in determining the functional representation of the data, Equation 1 was applied in this study since it is commonly used in engineering fatigue analysis and the qualitative measure of the relative uncertainties in determining the reliability at a specified lifetime are not affected by the SN curve assumption.

In order to simplify the analysis, the fatigue data from Reference 10 was normalized with respect to the estimated  $S_{\infty}$  value determined from the initial application of regression analysis. Another SN curve was then obtained from the normalized data, where  $\beta$ ,  $\gamma$ , and  $S_{u}$  were obtained for a known  $S_{\infty}$  of 1. The resultant SN(N) curve is shown in Figure 2. The figure also shows the regression results SN(S) from the application of Equation 2.

¹¹Berens, A. P., "Helicopter Fatigue Methodology", Vol. 1, University of Dayton Report, AVSCOM TR-87-D-13A, Dec. 1987.

¹²Weibull, W., Fatigue Testing and Analysis of Results, Pergamon Press, New York, 1961.

¹³ "RNLIN", IMSL Stat/Library: FORTRAN Subroutines for Statistical Analysis, Vol 1. ch. 2 pp. 239-247 April 1987.

### 3 The Component SN Curve

Usually the shape of the component SN curve is obtained from a prior coupon SN(N) curve as shown in Figure 2. The location (ordinate position) of the curve is determined from extrapolating the individual component values as shown in Figure 3 to  $N=10^8$  cycles. The original component values in Reference 1 have been rescaled so that they have scales similar to the S values in Figure 2. The extrapolation process involves vertically positioning the coupon SN curve (Figure 2) to agree with the individual component values and then extending the curves to  $N=10^8$  cycles.  $S_i$  values are obtained for  $N=10^8$  and the component curves' mean stress position at N is

$$S_m = \sum S_i/n \tag{3}$$

where n is the number of component test results. The solid line in Figure 4 shows the representative component  $SN_c$  curve and component test data. Since there are usually only six component test results available because of the costs in component testing, the above procedure is often applied. Using the more extensive, less expensive coupon test results to determine the shape of the SN curve assumes similar material, test, and environment for both coupon and component.

### 4 Spectrum Load

The normalized spectrum loading used in the fatigue life analysis is shown in Figure 5A. The loading was obtained from a rainflow count of a modified combat history described in Reference 11. The spectrum was determined by the number of loads within discrete range increments. The spectrum is simplified to five loads  $\{L_i\}_1^5$  by expanding the size of the range increments and including the appropriate cycle count  $\{n_i\}_1^5$  within each expanded range. The normalization procedure involved dividing each  $L_i$  by the smallest damaging load  $S_{\infty}$  (endurance limit). This simplification was adequate for identifying the spectrum effects in this study.

### 5 Miner's Rule

In order to obtain the lifetime estimate from the simplified fatigue load (L) and the normalized material strength (S) data shown in Figures 5A and 5B, the following linear damage rule 9 is applied where

$$DF = \sum_{i=1}^{5} \frac{n(i)}{N(i)},\tag{4}$$

is the damage fraction for each pass or repetition of the spectrum. This representation of operation hours is described in Reference 11. The n(i)'s are the number of cycles corresponding to the applied load L(i) shown in Figure 5A. The N(i) values are obtained from the SN curve in Figure 5B where the corresponding  $S_i$  values are identified in the figure by the L(i) values obtained from the spectrum loads in Figure 5A. In addition, the rule requires that

$$N_P \cdot DF = 1 \tag{5}$$

in order to determine the maximum number of passes  $(N_P)$  that can occur prior to the component failure.

### 6 Simulation Procedures in Determining Component Reliability

### 6.1 Bootstrap Method Applied to Coupon SN Curve Computation

The Bootstrap method ¹⁴ a simulation process, was introduced in the fatigue life reliability analysis in order to examine the effects of uncertainties used in determining the coupon SN curve and the resultant component reliability. From a single set of data, only one reliability estimate can be obtained. However, even with all conditions the same, one would expect to determine a different reliability estimate from another set of data. The Bootstrap method provides a technique for estimating the variability among random sets of data generated under equivalent conditions, using data from only a single random sample. The idea is to create arbitrarily many 'new' datasets by sampling with replacement from the original data. If there are n values in the original data, then a new dataset is created by selecting n values from among these observed data, allowing data values to be selected more than once. The probability distribution of the reliability calculated from these datasets, which are created by taking random samples from the single observed dataset, provides an estimate of the actual probability distribution of reliability which could, in principle, be determined from future datasets.

The material fatigue testing involves obtaining the number of cycles to failure for a specified applied load (S) shown as the individual data points in Figure 1. The Bootstrap method involves selecting a random set of 9 values independently with replacement from the set of cycles to failure values  $\{N_j(i)\}_{i=1}^9$ , for each  $j^{th}$  applied stress from  $\{S_j\}_{1}^{12}$  as shown in Figure 1 and obtained from Reference 12. The result is a new set  $\{N_j^*(i)\}_{1}^9$  for each of the  $S_j$  values. The new set is called the "bootstrap" sample, where some values can be repeated once, twice, or more times. The new set is then used in the regression procedures described in Section 2 in order to obtain a new SN curve (S in Equation 1).

In Figure A1, the results of the Bootstrap application show a 90% confidence band on the original SN(N) curve. Results in Figure A2 show the individual SN(N) curves obtained for the Bootstrap samples. The results from Figures A1 and A2 indicate that there is more variability for large or small N values than for the central region of the curve which is consistent with determining confidence bands on regression curves.

For calculation of the effects of coupon SN curve uncertainties, a damage fraction  $(DF^*)$  value is computed from application of Miner's rule in Section 5. The above procedure is repeated  $M_B$  times, so that a set of  $\{DF_k^*(i)\}_1^{M_B}$  are obtained. The component reliability R can then be obtained from the application of Miner's rule by counting the number  $(N_B)$  times  $N_P \cdot DF < 1$ ,  $k = 1, 2, ..., M_B$ , where  $N_P$ , the number of passes, is specified. The computed component reliability R from uncertainties in

¹⁴Efron, B., "Bootstrap Methods: Another Look at the Jackknife", Annals of Statistics, 7 (1979), pp. 1-26.

coupon testing procedure is written as

$$R = N_B/M_B \tag{6}$$

where  $M_B$  is the number of repeated applications of the bootstrap procedure.

### 6.2 Reliability Estimates From SN Component Curve Simulations

The following simulation procedure was applied in order to identify the effects of uncertainties in the location of the component  $SN_c$  curves on the reliability estimates. The uncertainties are assumed because of the potential differences in loading, material, surface conditions, and geometry between the coupon and component in obtaining the fatigue data. Also contributing to the uncertainties are: the extrapolation of the component fatigue data from determining  $S_i$ 's in Figure 3 and the availability of only six values in computing  $S_m$  (mean of the curve) in Figure 4. Examination of potential inaccuracies in the reliability computations due to assuming that the component and coupon SN curve shapes are similar was not included in the simulation process. Introducing variability in the curve's location was sufficient for showing sensitivity in the reliability computation. In the simulation process a random set of M  $S_m^*$  values were obtained. These values are normally distributed about the  $S_m$  value in Figure 4 from the following,

$$S_m^{\bullet}(i) = S_m(1 + V_S \cdot Z_i), \quad i = 1, 2, ..., M$$
 (7)

where the  $Z_i$ 's are the data values randomly selected from a standard normal distribution with a mean of 0 and a variance of 1. The  $V_S$  value is the coefficient of variation (CV) with mean equal to  $S_m$  and an assumed variance representing a set of  $S_i$  values similar to those in Figure 3. In Figure A3 a representative normally distributed set of  $S_m^*$  values are shown for  $V_S = .01$  and .02. The newly obtained mean values  $(S_m^*)$  are now used in vertical positioning of the component SN curve in Figure 4 so that M SN curves can be obtained from Equation 1 by the following,

$$S_{i}^{*} = S(S_{\infty}, S_{u}, \beta, \gamma) + \Delta P_{i}, i = 1, 2, ..., M,$$
(8)

where  $\Delta P_i = S_m^*(i) - S_m$ . M damage fraction values (DF_i) are obtained from applying the procedures described in Section 5 and the schematics in Figures 5A and B using the newly available  $S_i^*$  values.

From Miner's rule, compute  $N_P \cdot DF_i^*$ , i = 1, 2, ..., M and record the number  $(N_S)$  of times  $N_P \cdot DF_i^* < 1$  for a given  $N_P$  value, where  $N_P$  represents the specified number of passes. The component reliability R can be written as

$$R = N_S/M. (9)$$

Note, in order to obtain .999999 reliability,  $M = 1 \times 10^6$  simulations would be required.

### 6.3 Load Uncertainties Effect on Reliability Computations

A simulation procedure similar to that in Section 6.2 was applied in order to identify the sensitivity in computing component reliability by introducing uncertainties in the assumed spectrum loads (see Figure 5A). There exist potential errors involved in assuming a specific load spectrum ¹⁵. They are the results of: an inaccurate measuring device, the location of the device, and assuming load patterns determined from short periods of data recording which differ from the actual loads the component would be subject to during its operational lifetime.

Application of the simulation process involved only modeling uncertainties in the L values, with n(i)'s remaining constant for a given load. Introducing the same amount of variability in each  $\{L(i)\}_1^5$  values was sufficient to show the sensitivity of the reliability estimates to uncertainties in the loading.

Initially, the simulation involves obtaining M1 sets, where the  $j^{th}$  set  $\{L_j^*(i)\}_{i=1}^5$  is determined from the following,

$$L_i^{\bullet}(i) = L(i)(1 + V_L \cdot Z_i), i = 1, 2, ..., 5$$
 (10)

where j = 1, 2, ..., M1 and  $Z_j = j^{th}$  random value from a standard normal N(0,1) distribution.  $V_L$  is the coefficient of variation representing an assumed variability in load L(i).

For each of the  $j^{th}$  simulation, the original five loads  $\{L(i)\}_1^5$  in Figure 5A, are modified resulting in a new set  $\{L_j^*(i)\}_1^5$  from Equation 10. The distibution of  $L_j^*(1)$  for all j, for example, would be similar to that for  $S_m$  in Figure A3.

In the simulation process, each  $j^{th}$  modified set  $L_j^*$  and its associated  $N_j^*$  determines a damage fraction value DF_j as described in Section 5 and Figures 5A and B. In order to obtain component reliability values from the load variability, Miner's rule is then applied in the following manner. Record the number  $(N_L)$  of times  $N_P \cdot DF_i^* < 1$  for j = 1, 2, ...M1, where  $N_P$  is described in Section 6.1. The component reliability R is then written as

$$R = N_L/M1. (11)$$

### 6.4 Reliability Sensitivity From Uncertainties in Miner's Rule

A simulation procedure similar to those in Sections 6.2 and 6.3 is applied to the Miner's rule relationship in Equation 5. This was done in order to examine the effects of a possible error in assuming that if the damage fraction in Equation 4 equals 1, the component will fail. In order to identify the effects of this uncertainty in computing component reliability R, the following simulation process was performed.

Initially, the value 1 in Equation 5 is replaced by a set of random numbers  $\{CR_i\}_{1}^{M2}$  resulting in  $N_P \cdot DF < CR_i$  where

$$CR_i = 1 + V_M \cdot Z_i, i = 1, 2, ..., M2$$
 (12)

and  $V_M$  and  $Z_i$  are the assumed coefficient of variation and standard normal as previously defined in 6.2 and 6.3.

¹⁵Gunsallus, C.T., Hardersen, C.P., and Stennett, P.G., "Investigation of Fatigue Methodology", US-AAVSCOM TR 87-D-17, Army Aviation Applied Technology Directorate, Ft. Eustis, VA, May 1988.

The reliability R is determined from recording the number  $(N_z)$  of times that,

$$N_P \cdot DF < CR_i \tag{13}$$

and then defining

$$R = N_Z/M2. (14)$$

where M2 is the number of simulations.

### 7 Working SN Curve

The adjustment of the mean component  $SN_c$  curve from a limited amount of component test data results in a certain amount of variability in estimating the location of the curve. In order to account for this variability, and in some instances other uncertainties in the fatigue analysis process, a component  $SN_c$  curve reduction factor is often introduced which results in a new working  $SN_w$  curve as shown in Figure A4. There is no standard method for obtaining a working curve in the helicopter industry ¹⁶. The working curve in Figure A4 was obtained by a uniform reduction in all  $S_c$  values. This approach maintains the same curve shape as in the original  $SN_c$  curve, i.e., the coupon SN curve shape. This approach is consistent with the use of the coupon curve shape in the extrapolation process for each component data value, Figure 3, by which the original component curve  $S_m$  value, Figure 4, is obtained. In Figure 3, a schematic of this uniformity is shown where for N = 1 and  $N = 10^8$  show an equal amount of assumed dispersion in the  $S_i$  values.

### 7.1 Reduction Factors for Working Curves

Some of the reduction factors commonly used by the helicopter manufacturers are discussed in References 15 and 16. In some cases a simple multiplication factor is used to obtain working curve values,  $S_w$ , that is,

$$S_w = S_c - P \cdot S_m \tag{15}$$

where  $S_c$  represents the strength values from the component curve  $SN_c$  for various P values in the range of .20 to .50.  $S_m$  was previously defined in Equation 3.

Another reduction procedure involves defining

$$S_{w} = S_{c} - 3 \cdot SD \tag{16}$$

where SD, the standard deviation, is often determined from an assumed standard coefficient of variation for a particular material to represent the  $S_i$  values shown in Figure 3 and in Equation 3. A typical value for the coefficient of variation for steel is 7%. The SD value is then written as  $SD = .07 \cdot S_m$ . One other commonly used definition involves determining SD from the actual  $S_i$  values, that is  $SD = \sqrt{(\sum (S_i - S_m)^2/(n-1))}$  and substituting the SD value in Equation 16.

¹⁶Noback, R., "State of the Art and Statistical Aspects of Helicopter Fatigue Substantiation Procedures", Helicopter Fatigue Life Assessment, AGARD CP NO 297 North Atlantic Treaty Organization, March 1981.

The working curve was introduced in this paper in order to evaluate its capability to include the possible variability in the reliability estimates from the simulation results.

### 8 Results and Discussions

In this section, results from the simulation procedures are shown in both tabulated and graphical form. Variability is introduced in combination and individually for all of the following four factors: the spectrum load, the mean SN curve, Miner's rule, and the bootstrap process.

In Table 1 all four factors were varied for a range of CV values (% variability) from 1% to 5% except for the bootstrap simulation where the variability is obtained from coupon test results. The component reliability results are tabulated as a function of the corresponding CV values assumed in the simulation procedures. The results were obtained by systematically randomly selecting values from each of the four factors so that  $1 \times 10^6$  distinct factor combinations are obtained for computing the damage fraction (DF) in Section 5. The  $1 \times 10^6$  DF values were applient to Equation 13 resulting in the computed reliability values in the table.

In order to apply the simulation procedures, a 1% variability was introduced for each of the factors and the number of passes ( $N_P = 3425$ ) was selected in order to obtain a base line reliability value of .999999. This value was selected because of the helicopter industry's interest in obtaining high component reliability of .999999.

The results in Table 1 show a substantial instability when comparing the reliability estimate of .999999 versus .989676 for the respective 1 and 2 percent variabilities. The implication of these results is that in one case one in a million failures could occur compared to 10324 failures in a million in the other. This substantial difference for such a small increase in the inherent variability in the assumed fatigue life models shows a severe sensitivity in computing high reliability when there is a small degree of uncertainty in determining spectrum loads, SN curves, and assuming a failure requirement from Miner's rule. The results from increasing the variability from 3% to 5% show a corresponding reduction in reliability values. The R = .81606 for 5% variability is a very large reduction from the original .999999 for 1% variability. The CV values in Table 1 represent a range of potential parameter uncertainties in the fatigue life model.

In Table 2, reliability values are tabulated as a function of the combined and individual variability of the four factors. This was done in order to examine the effects of the individual factor variability on computing component reliability. The 1% variability was applied to all factors resulting in R = .999999 when  $N_P$  is equal to 3425 (as in Table 1 at 1%). The 2% variability was applied to each factor individually with 1% variability for the other two factors. The bootstrap process was applied in all of the cases. Introducing a 2% CV in the spectrum load (SPL) shows a substantial reduction in the reliability estimate from .999999 to .996404. The 2% variability in the component  $SN_c$  curve (MSN) shows a smaller reduction of .999999 to .999440

indicating that, based on the particular spectrum considered, the spectrum load uncertainties could result in greater instability in the reliability values. Small variations in the Miner's rule assumption (Equation 13) do not appear to be as as critical in the reliability computations. Increasing the variability from 3% to 5% shows a continued decrease in reliability estimates except for the case of Miner's rule variability which has a very small reduction. The 5% variability on the spectrum load shows a value R = .862469 which is only 5.7% greater than the case where all factors were varied simulataneously as shown in Table 1 for 5% variability.

In Table 3, reliabilities are obtained for the individual factors, spectrum load (SPL) and location component SN curve (MSN). In order to obtain the R = .999999 value for 1% variability on each of the factors the number of passes ( $N_P$ ) was 3700 for SPL and 4425 for MSN. The lower  $N_P$  value for SPL is consistent with the results in Table 2 since the R values for SPL were lower than those for MSN when  $N_P$  was 3425. In addition, it is obvious that a lower number of cycles of operation would usually increase the reliability value. The bootstrap method application resulted in a value of R = .999977 when combined with a 1% variability in MSN. This indicates that the method is not introducing any substantial variability compared to the SPL and MSN contribution in determining R. This is expected because of the small amount of variability in the SN curves shown in Figures A1 and A2. In addition, the range of cycle values contributing the most in determining the damage fraction has the least amount of variability.

Table 4 shows the reliability results from reducing the  $S_m$  value in Figure 4 and Equation 3 by the tabulated percentage in order to examine the possible material mean strength loss from environmental effects such as corrosion. New values equal  $(1-p/100)S_m$  where p is the tabulated percent reduction factor. In the case where p=0, R=.999999 was obtained varying the  $SN_c$  curve by 1% with  $N_P=4425$  which is in agreement with the result in Table 3. This variability in the  $SN_c$  curve (MSN) was maintained for each of the reduced  $S_m$  values. When p=1, then  $.99S_m$  was used in the simulation process to obtain a reliability value equal to .999852 compared to .999999 for no reduction in  $S_m$ . This result is not as substantial a reduction in R as the case where the  $S_n$  value is reduced by 5% and R=.324206. The overall results indicate that loads that previously did not increase the damage fraction are now significant contributers in reducing the component reliability. If there is a potential for material strength loss due to, for example, corrosion, then high reliability estimates are substantially reduced by small mean strength reduction.

Table 5A shows the deterministic fatigue lifetime values obtained from the application of various working curves described in Section 7. This computation was introduced to evaluate the curves relative effectiveness in accounting for the uncertainties in estimating the component  $SN_c$  curve. This evaluation involves comparing results from Tables 5A and 5B. In the table, a .50 reduction from Equation 15 shows a lifetime of .325 which is a very conservative estimate compared to the 6150 passes obtained from using the original component curve without a reduction. The least conservative lifetime estimate is 2000 which was obtained from reducing the component curves by three standard deviations (SD). SD was obtained by using the  $S_i$ 

values in Figure 3 and Equation 3. This estimate was less conservative than the 1225 lifetime value obtained using an assumed CV = .07. The extrapolation process shown in Figure 3 may account for the relatively low SD estimate for the case when the life value is 2000. The other reduction factors result in a predictable decrease in the life estimate with an increase in the reduction percent P.

In Table 5B, simultaneous variability on the component curve (MSN) and the spectrum load (SPL) for .999999 reliability shows shows a reduction in the lifetime value with increasing variability, which is consistent with prior results. By comparing results from Tables 5A and 5B, the effectiveness of the working curve in obtaining .999999 reliability can be identified. That is, for example, a 1% variability shows 3425 indicating that any of the working curves could provide the required reliability although the curve obtained from the 3SD reduction would be the least conservative acceptable method. Introducing 2% variability shows a life estimate of 1850 which, in this case, requires using the 3SD reduction procedure where SD is obtained from assuming a .07 CV value. If the variability is assumed to be 5% then a lifetime value of 50 is obtained which would require a working curve reduction factor of .44 in order to provide the .999999 reliability. If a 5% variability in the loading and SN curve can exist, then most of the working curve procedure can be an undesirable method for obtainint high reliability.

Using Equation 7 in Section 6.2, the results of introducing a 1% uncertainty in the positioning of the component curve is shown in Figure 6 as a probability density function for the lifetime estimate  $(N_P = 1/DF)$  determined from Equation 4. A 7.3% coefficient of variation was obtained with a mean life of 6194. The inner range,  $N_P \pm 3$ . SD, is 4964 to 7689 when the function is assumed to be log-normal. This is a substantial variability in the life estimate for a very small amount of variability in the the location of the SN curve.

In Figure 7, a density function for the life estimate was obtained from an assumed 5% variability using the same procedures, as described above. In this case the CV was 37.5% with a mean equal to 6621. The inner 3SD range is 2065 to 18587 for the lifetime value estimates. This exceptionally large dispersion in the life estimates for a moderate amount of variability (5%) in the location of the mean curve indicates instability in estimating lifetime values. Note, by taking the log of the data a normal function was obtained indicating that the fatigue estimate can be represented by a log-normal distribution.

In Figure 8, a computation similar to that described in Figure 6 was performed in order to determine the difference in life values between the 1% and .0001% points corresponding to reliabilities of .99 and .999999 respectively. A 1% variability in the spectrum was assumed in the computation of  $N_P$ . A CV of 10.8% was obtained with a mean of 6.13. Results show a life of 4795 for the lower reliability of .99 and 3689 for the higher reliability of .999999 showing a 23% decrease in the lifetime estimate.

Figure 9, where a 5% variability in the spectrum was introduced, shows a log-normal distribution of lifetime values similar to that in Figure 7 for the SN_c curve

variability. The inner range of 1075 to 31956 again shows the substantial variability in the life estimate indicating a serious instability in the fatigue life computation approach when even small uncertainties exist in assuming a specified spectrum load. Load spectrum and fatigue strength CV's in the range of 7% to 13% are being considered by the helicopter industry. ¹⁷ A comparision of the reliabilities of .99 and .999999 for the respective lifetimes showed 1702 and 448 passes which is a 74% decrease in lifetime. This is a much greater percent decrease than that of the 1% variability case in Figure 8. This assumed variability is probably more realistic than that of 1% which was previously assumed. In fact, reviewing the literature indicates that 5% variability may be much lower than that which actually occurs in assuming the spectrum load distribution.

Comparison of these figures show uncertainties in safe life fatigue design in terms of changes in design lifetime for a fixed reliability whereas the results of Tables 1 to 4 show variability in terms of changes in reliability for fixed lifetimes.

Although only a simple case has been considered, the modeling and simulation processes are capable of dealing with more complex safe life fatigue designs. Such designs could include more complex load spectra and additional parameters in the fatigue life model. The value of any high reliability based analyses, whether simple or complex, appears in question in view of the very substantial sensitivity of the reliability and lifetime results from this study.

### 9 Conclusions

A small amount of variability (uncertainty) in load or strength in the safe life fatigue model can result in a substantial reduction in high reliability values for a specified lifetime of a component. These uncertainties also can result in very unstable lifetime estimates for a given reliability. In contrast, the small variations assumed in the Miner's Rule criterion, and the variability in the SN coupon curve determination, caused a minimal amount of change in the reliability estimates.

A small percent reduction in the strength values in the component SN curve (for example, corrosion effects) can result in a large decrease in the reliability values.

Introducing working curves in the fatigue life computation is only effective when there is a small amount of variability in the SN component curve, or the reduction factor was very large.

In view of the sensitivity of the safe life reliability criterion of .999999 to the modest variability considered in this analysis, it appears that the .999999 reliability is ineffective as a criterion to ensure safety for a specifed service life. In summary, this paper has identified a potential problem associated with obtaining a meaningful quantatative measure of reliability for a fatigue loaded component.

¹⁷Schneider, G. and Gunsallus, C., "Continuation of the AHS Round Pobin on Fatigue Reliability and Damage Tolerance", presented at the American Helicopter Society 47th Annual Forum, Phoenix, Arizona, May 1991.

Table 1: Reliability Vs Factor Variability: Lifetime = 3425

% Variability *	Reliability
1.0	666666
2.0	989676
3.0	.937250
4.0	.872101
5.0	.816061
Simultaneous Variability assumed for the following: spectrum load, mean curve, Miner's rule = factor(1) and the Bootstrap process on defining mean curve	Simultaneous Variability assumed for the following: spectrum load, mean curve, Miner's rule = factor(1) and the Bootstrap process on defining mean curve

Table 2: Reliability Vs Individual Factor Variability: Lifetime = 3425

% Variability (P) on		Reliability	
Individual Factors *	SPL	NSW	MR
1.0	666666	666666	666666
2.0	.996404	.999440	866666
3.0	.967356	.992375	
. 0.4	.912587	.972164	766666.
5.0	.862469	.941979	.999994
* 1% variability is applied to all factors except for individual increase in factor variability (P) in first column Bootstrap process also included	ariability is applied to all factors except for ind increase in factor variability (P) in first column Bootstrap process also included	s except for in ) in first colum included	dividual n

Table 3: Reliability Vs Individual Factor Variability / Lifetime

% Variability	Reliat	Reliability (R)
	SPL•	MSN **
1.0	666666	666666.
2.5	969376	.965875
5.0	.828010	.818789
·	3700 Lifetime value	
*	** 4425 Lifetime value	
Note: Application resulted in R = .99	Note: Application of Bootstrap process simulation resulted in R = .999977 with 1% variability for MSN	ss simulation ibility for MSN

Table 4: Reliability Vs Percent Reduction MSN: Lifetime = 4425

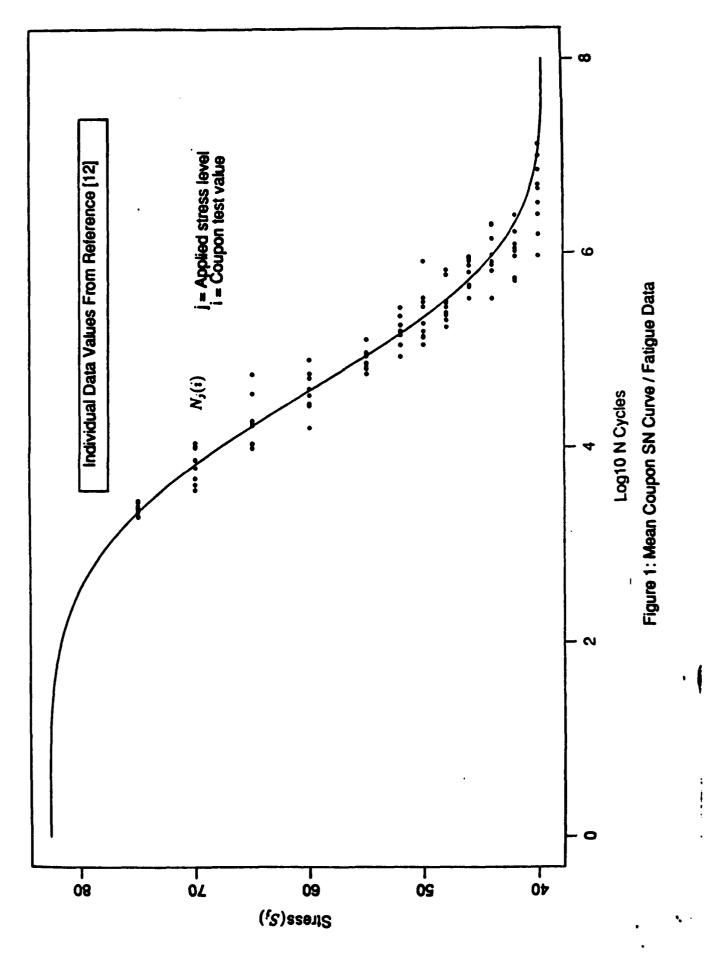
Reliability	666666	.999852	.995542	.946600	.720650	.324206	Note: 1% Variability on MSN
% Reduction	0.0	1.0	2.0	3.0	4.0	5.0	Note: 1% Vari

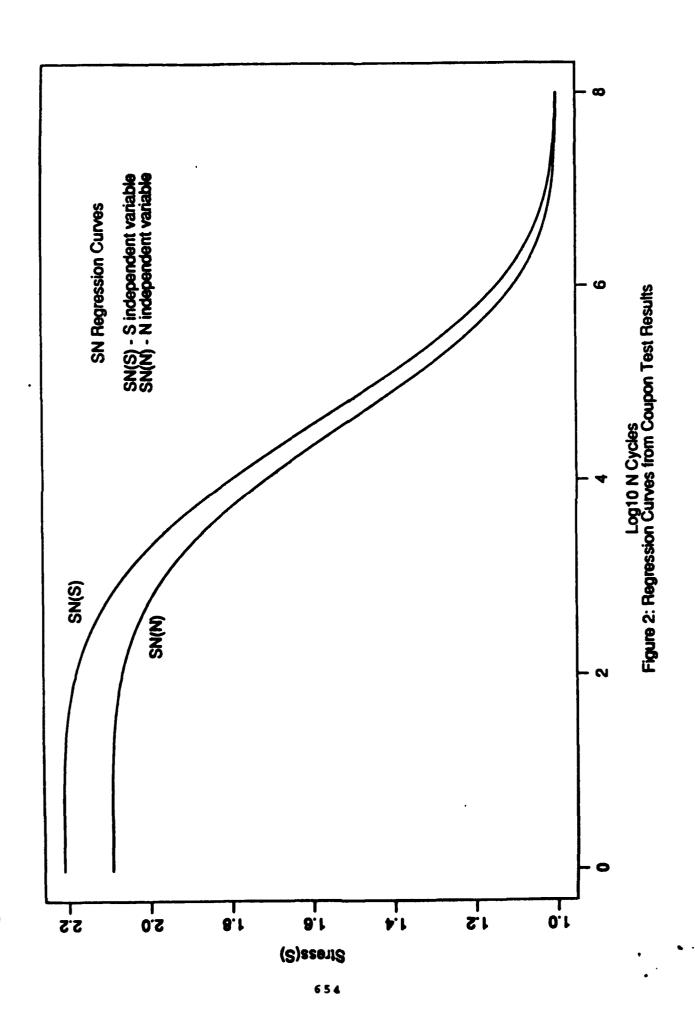
Table 5A: Lifetime Values From Application of Working Curves

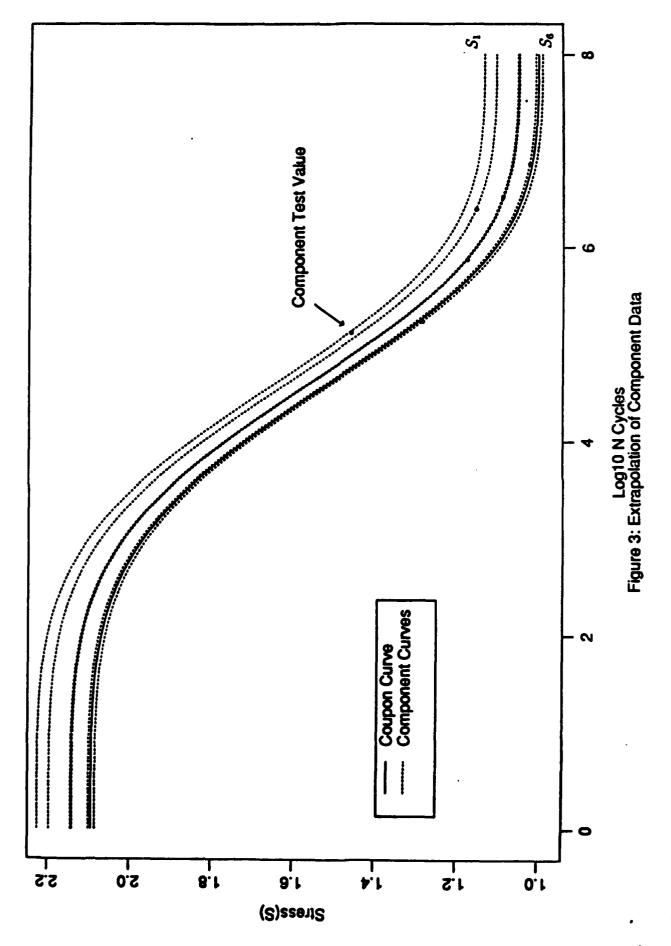
Working Curve (Adjustment on S)	Lifetime Values
.50	.325
44.	48
.30	200
.25	820
.20	1355
S - 3(sd) ••	1225
S - 3(sd)	2000
:. AN	6150
<ul> <li>Percent Reduction of (P) on S:</li> <li>where (1-P)S is location of working curve and</li> <li>S is mean component strength at endurance limit</li> </ul>	tion of (P) on S: n of working curve and ength at endurance limit
** Standard deviation determined from assuming 7% coefficient of variation for S	lermined from assuming f variation for S
*** NA: No adjustment of SN curve	ment of SN curve

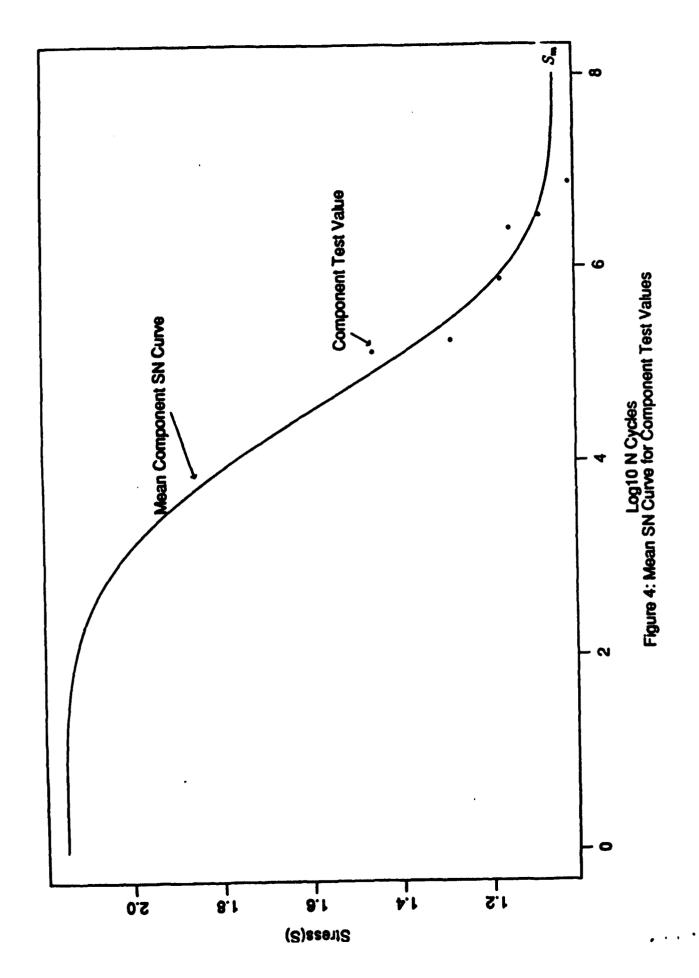
Table 5B: Lifetime Values with .999999 Reliability Variability on MSN and SPL

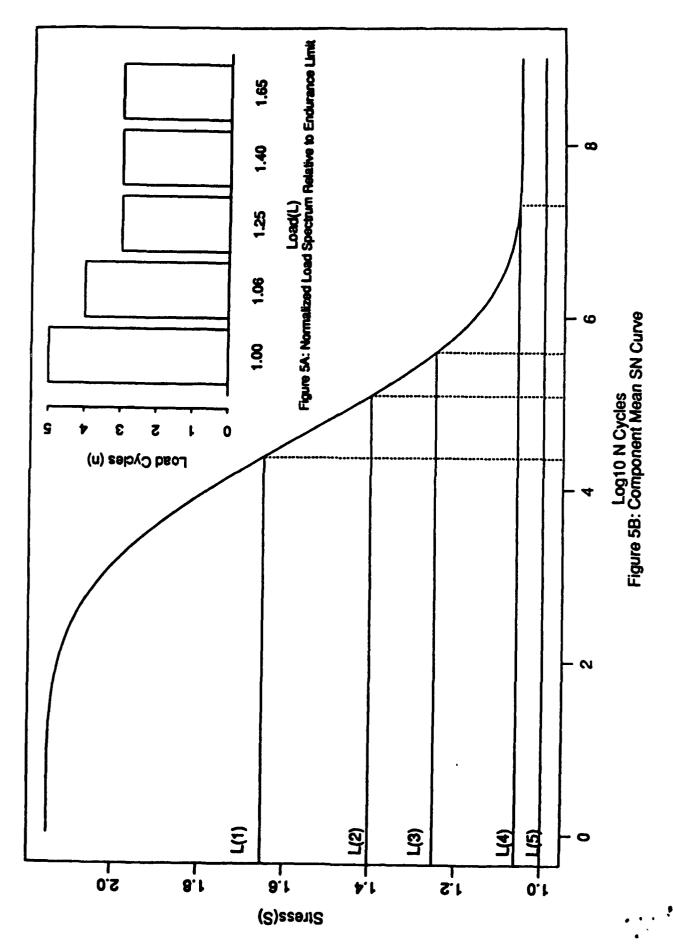
Lifetime Value	3425	1850	875	350	95
% Variability	1.0	5.0	3.0	4.0	5.0

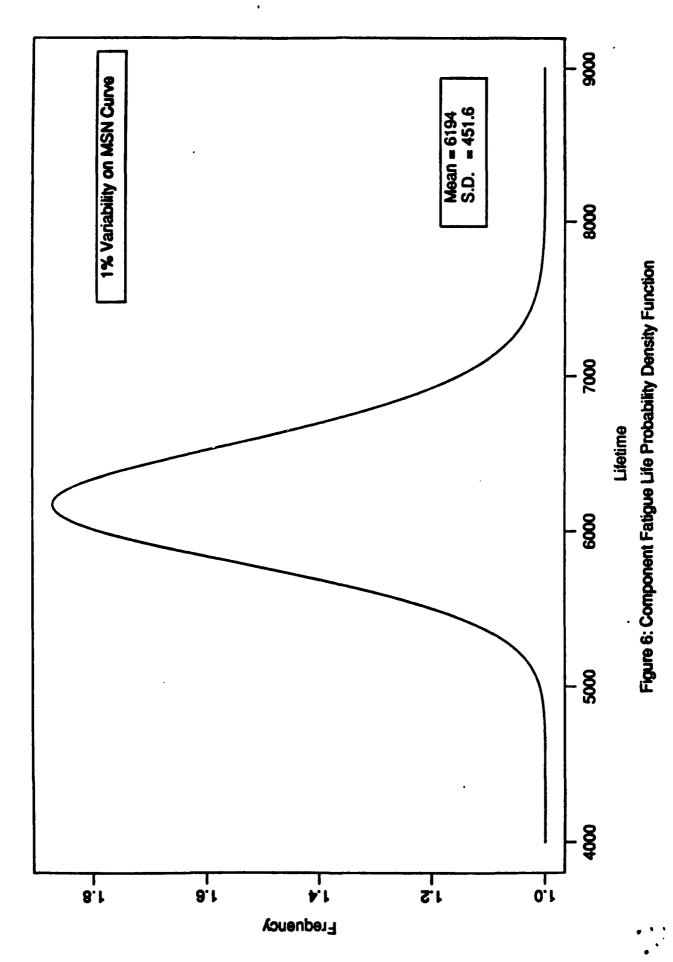












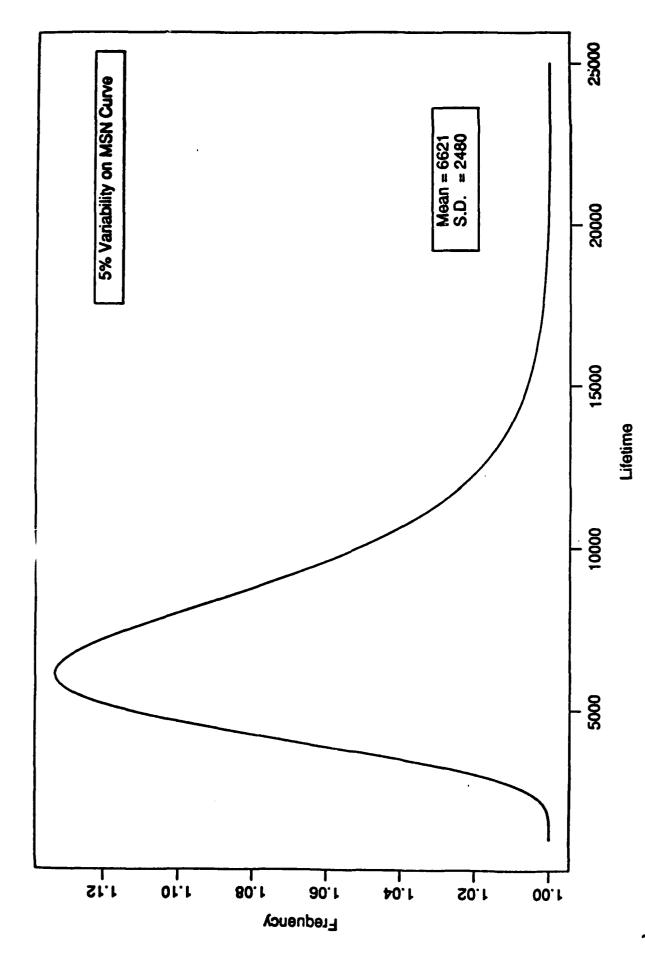
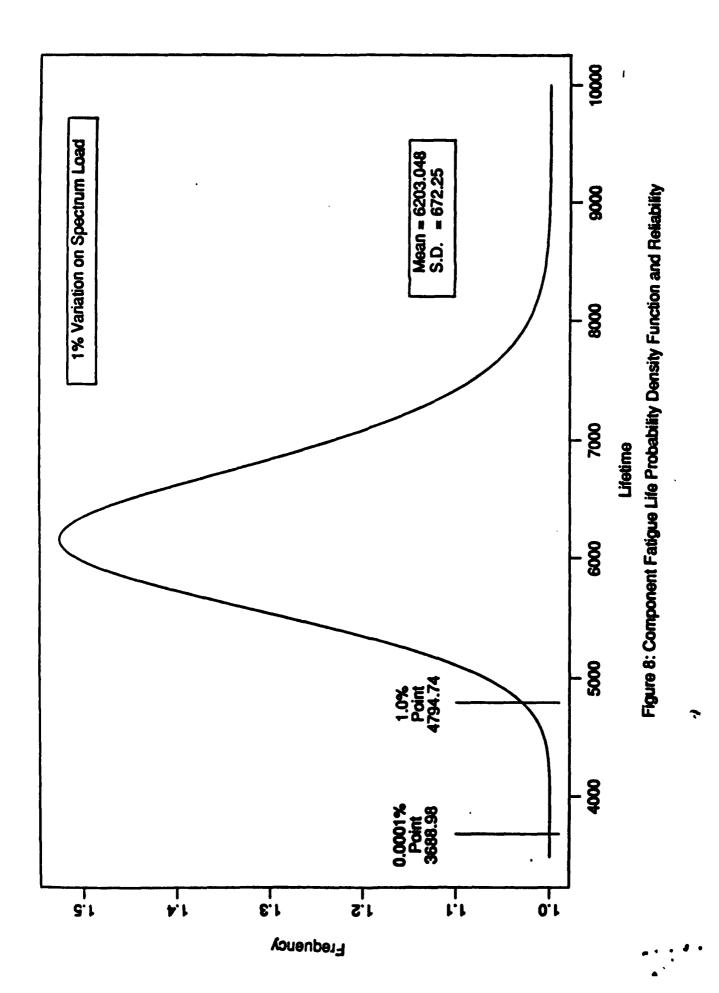
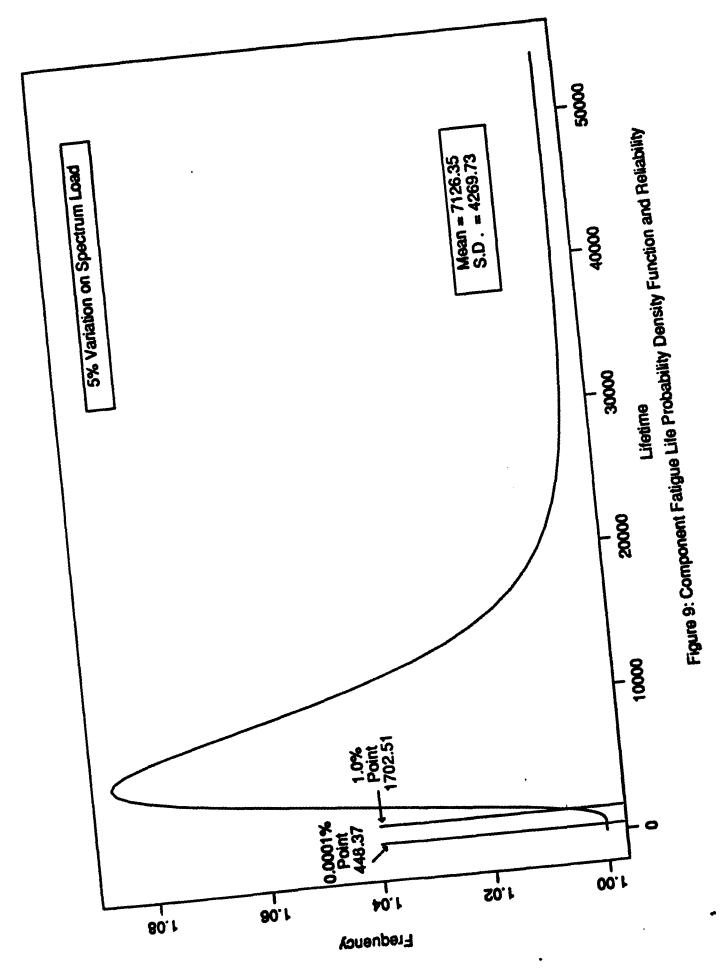
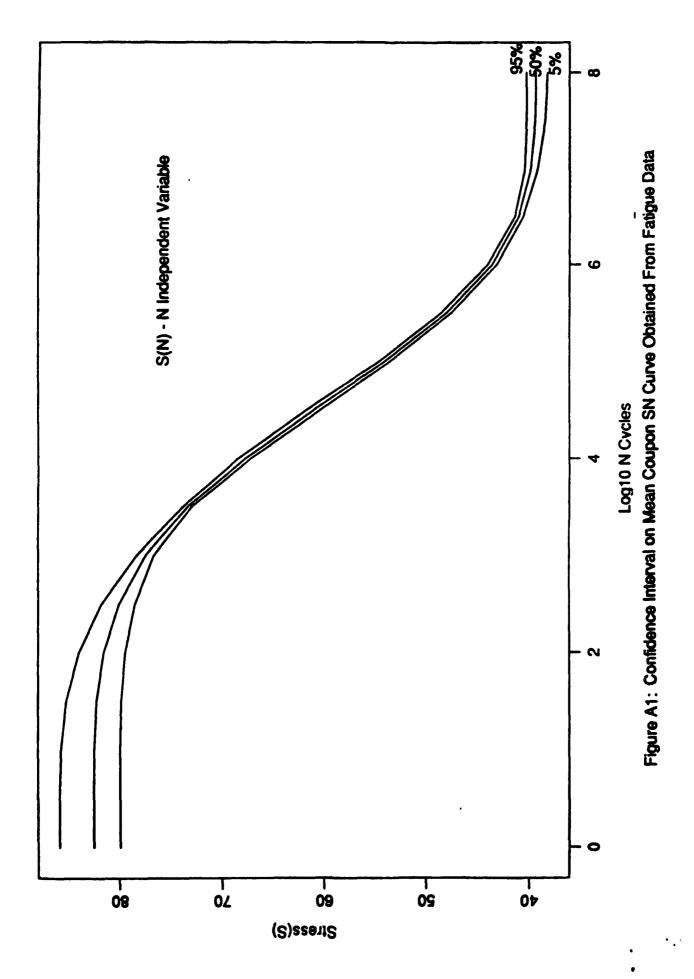
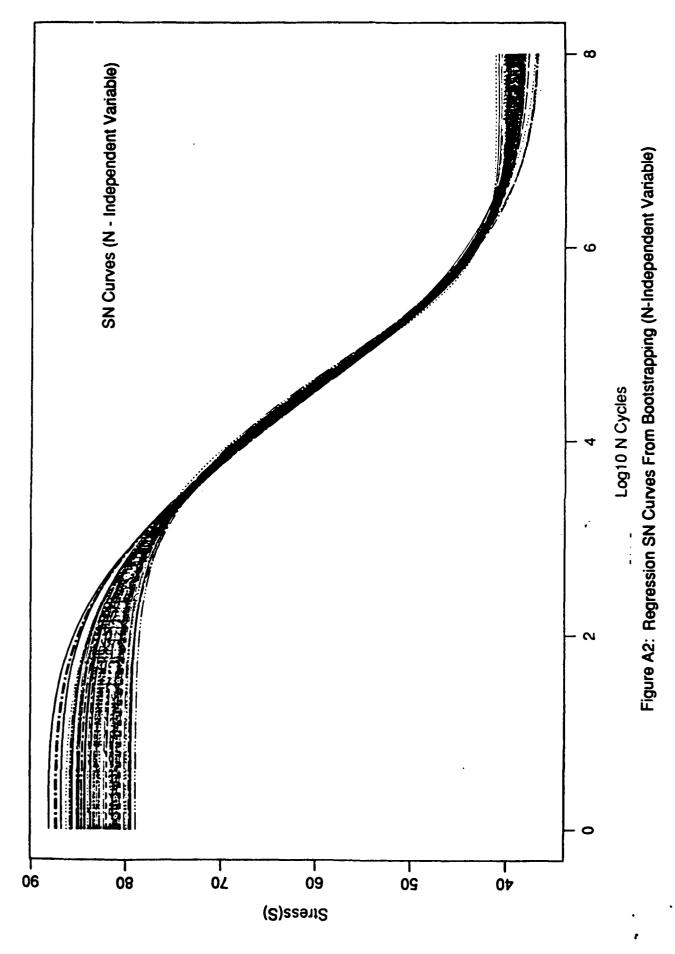


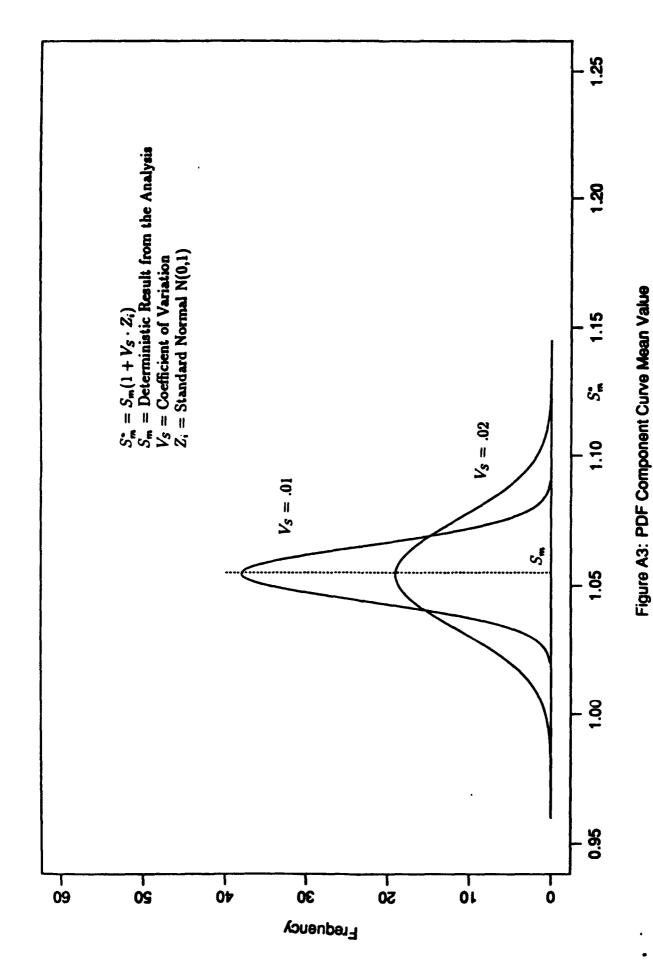
Figure 7: Component Fatigue Life Probability Density Function











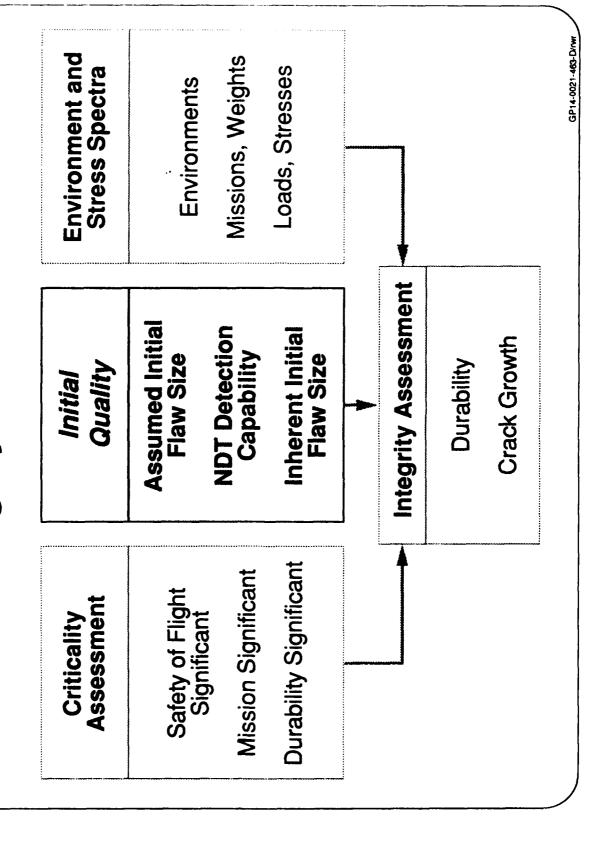
## Nondestructive Testing As Applied to Integrity Assessment

Robert J. Lord

McDonnell Aircraft Company

McDonnell Douglas Corporation Saint Louis, MO. GP:4-0021 460 Day

## Integrity Databases



2040 1000 1100

flaw size since that is used as the assumed initial flaw size during Damage tolerance life depends on, among other factors, initial damage tolerance analysis.

nondestructive testing (NDT) method used to inspect the For the purpose of this discussion, component initial quality can be defined in two ways. The detection capability of the component is one approach. Or, the inherent initial quality, defined by raw material quality and manufacturing process quality, may be used to define component initial quality.

### GP14-0021-465-D

### Probability of Detection Test Program

- Fabricate Representative Specimens
- Material
- Geometry
- Flaws of Interest
- Flawed and Unflawed
- Gather Inspection Data
- Appropriate NDT Method
- Production Inspection System
  - Production Inspectors
- Calculate Probability of Detection

NDT detection capability is quantified as probability of detection (POD), a statistical concept based upon actual test data. A typical POD program is conducted by fabricating test production NDT. The test specimens are designed to represent the specimens, subsequently inducing flaws and subjecting them to component of interest in that the material and geometry are replicated. Both flawed and unflawed test specimens are used to make the inspection realistic.

as well as production inspectors and the production inspection facilities. The number of flaws detected versus the number of flaws Inspection data is gathered using the appropriate NDT method present are recorded for several inspectors.

usually expressed as 90% probability of detection at a 95% The inspection data is used to estimate the true detection capability through calculation of the probability of detection (POD), confidence level. GP14-0021-486-D/ry

### GP14-0021-483-DACH

# **Probability of Detection (POD)**

Example - Based Upon Binomial Distribution

90/95 for Cracks 0.05 in. Long

Confident That at Least 90% of Cracks 0.05 in. Long Test Results Statistically Demonstrate We Are 95%

Will Be Detected

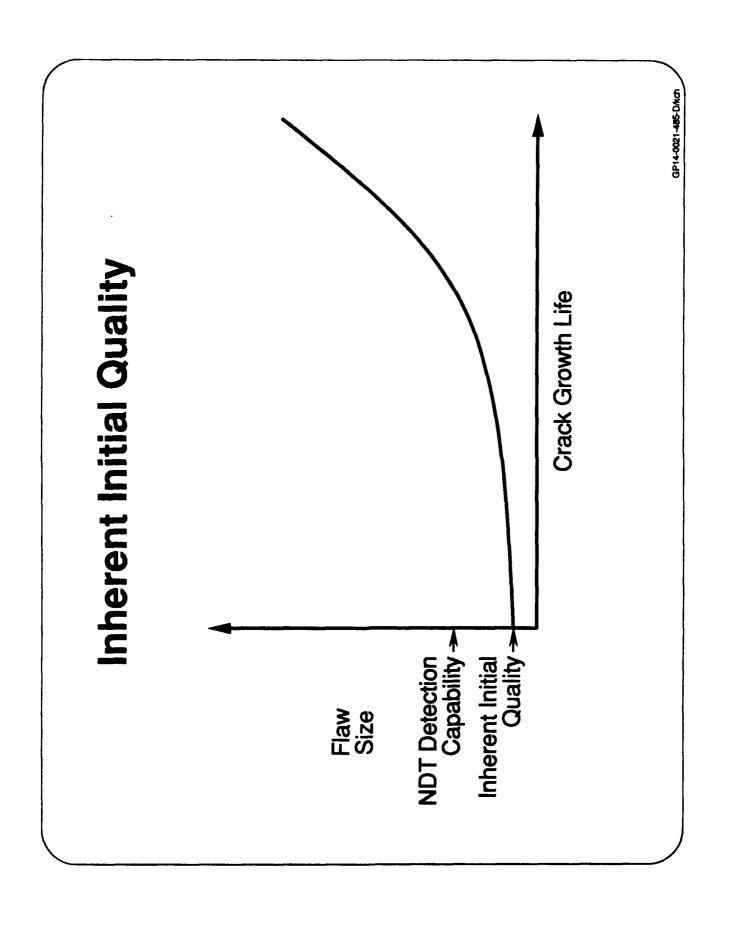
Minimum Number of Tests

-29 of 29

-45 of 46

- 59 of 61

POD, one approach is based upon the binomial distribution where POD can then be calculated using a mathematical relationship the only data considered is whether a flaw is detected or not. The involving number of flaws present, number of flaws detected and Although there is no standardized method for establishing the preselected confidence level desired. The minimum number of tests (sample size) required to demonstrate a 90% POD is a function of the number of existing flaws detected. For example, if 29 flaws are detected without a miss, that is sufficient. If one is missed, however, 45 of 46 must be



GP14-0021-486-DAch

the component. A statistical approach is required, however, to established. Periodic destructive testing could then be used to demonstrate that the material and manufacturing process had not than the detection capability of the NDT methods used to inspect establish the inherent quality. For example, a statistical database of components. In this way the typical inherent flaw size could be In many instances, the inherent component quality is better might be developed through destructive testing of a large number changed with time (i.e., we're in control).

## Structural Integrity of Aircraft Systems

### **Objectives**

- Assess Avionic and Mechanical Subsystem Integrity
- Evaluate Integrity Process

### Approach

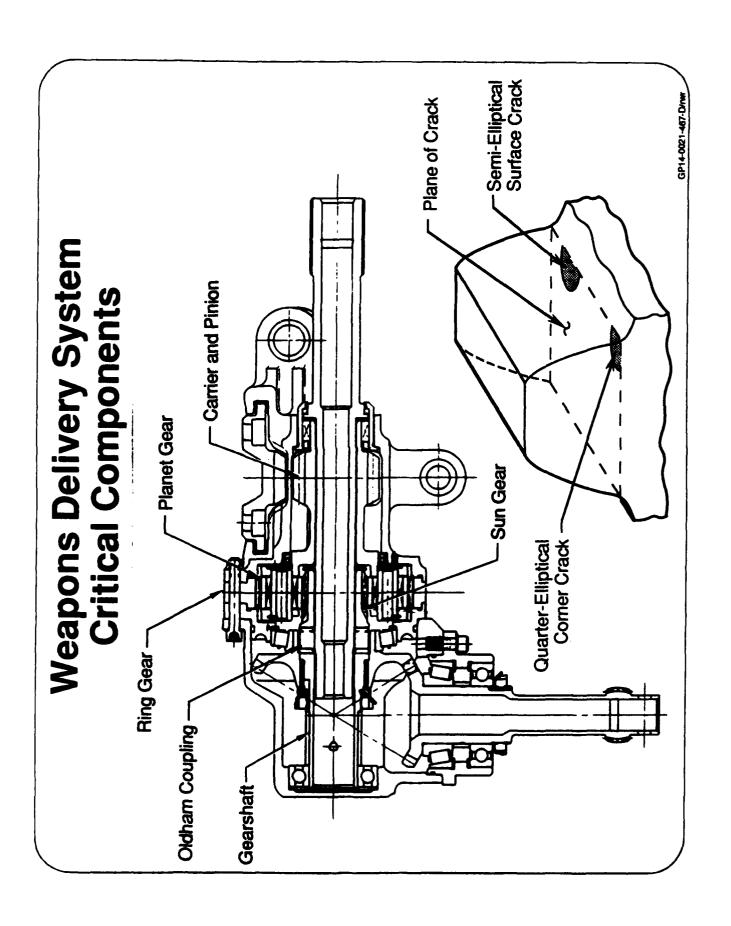
Contracted With Two Avionic and Two System Suppliers

GP14-0021-461-Dynam

GP14-0021-462-D/rwr

A USAF funded program was conducted to gain direct experience in implementing MECSIP and AVIP. Supplier experience and MECSIP/AVIP preparedness also was evaluated.

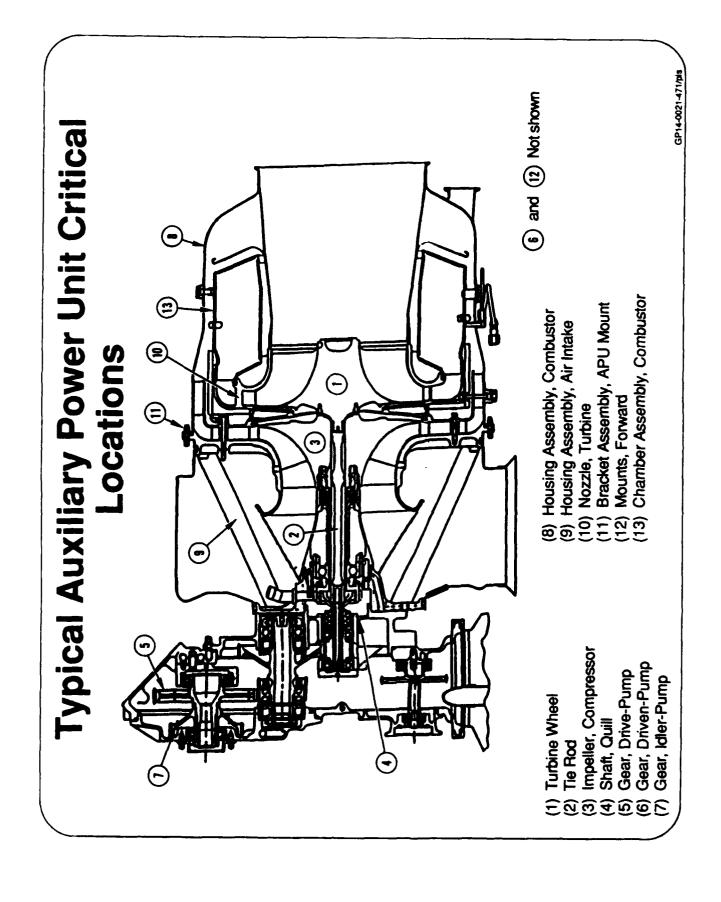
different levels of experience with the integrity assessment process and different component technologies. They are Two avionics and two mechanical system suppliers were contracted to conduct a structural integrity assessment of selected components. These suppliers were selected, in part, to represent considered representative of todays equipment and subsystem suppliers. This paper will concentrate on the mechanical subsystem portion of the program.



440 000 1100

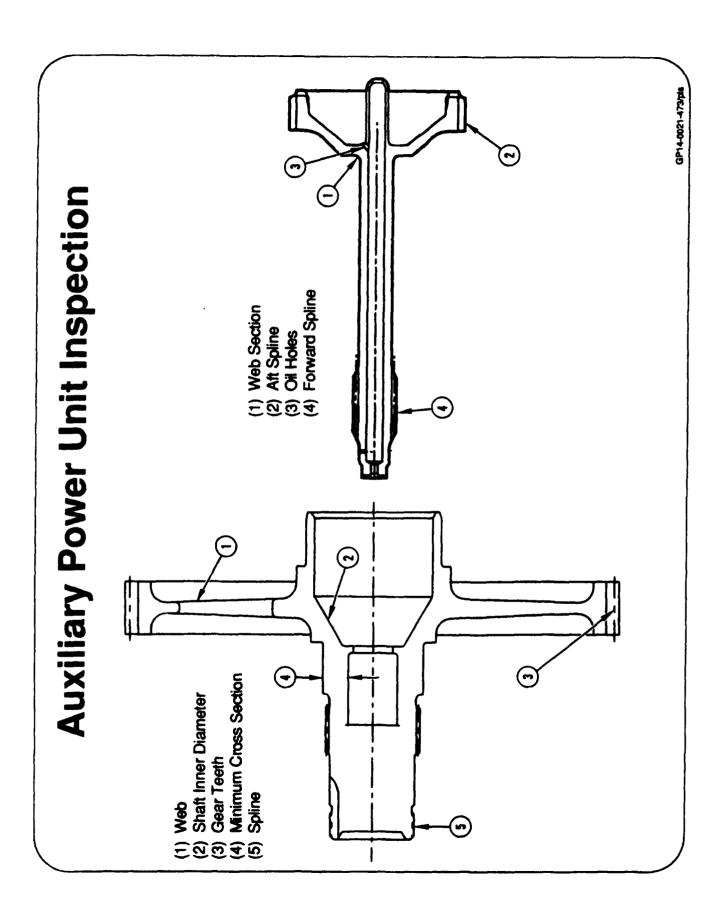
Four gearboxes which use One of two mechanical subsystems assessed during the program carburized gears drive the system. The majority of the critical components selected for integrity analysis were these steel gears. was a weapons delivery system.

The steel gears are inspected by the supplier for cracks in the gear tooth root using magnetic particle inspection.



CD14.0021.472.00mct

which supplies hydraulic and electrical power generation while the The second mechanical subsystem assessed during the program was an auxiliary power unit (APU), a gas turbine unit aircraft is on the ground or main emergency restart while in flight. A variety of APU locations were selected for study. These included gears, tie rods, turbine nozzle and housings.



cracks using magnetic particle inspection. Other components, such The steel gears are inspected by the supplier for gear teeth as the quill shaft, are penetrant inspected.

### Supplier POD Databases Did Not Exist

- Neither Supplier Had In-House POD Databases for Their NDT
- Weapons System
- Estimated Magnetic Particle Inspection Capability (0.12 in. Long)
- Published Data
- Auxiliary Power Unit
- Estimated Magnetic Particle (0.10 in. Long) and Penetrant (0.05 in. Long) Capability
- MIL-SPEC Acceptance Criteria and Published Data

GP14-0021-487-DAM

GD14.0001.488.04.0

Neither supplier had an in-house developed NDT detection capability database. The weapons system supplier estimated penetrant inspection. This was based upon limited published data their magnetic particle inspection capability to be 0.12 inch long based upon limited published data. The auxiliary power unit supplier estimated their capability at 0.10 inch long cracks for magnetic particle inspection and 0.050 inch long cracks for and the acceptance criteria required by the MIL-SPEC.

## Effect of POD Estimates Upon Life

- Some Predicted Lives Were Short Due to Large Initial Flaw
- Use of Smaller Initial Flaw May Be Justified
  - In-House Developed POD
- Alternative NDT Methods
- Inherent Initial Flaw

GP14-0001-489-DAge

estimate, allowing the use of a smaller initial flaw size in the life The predicted lives of some of the weapons systems and was the large initial flaw size used because the NDT detection capability was estimated by the suppliers. A POD study may have revealed that the suppliers detection capability was better than the auxiliary power unit components were relatively short. One factor analysis.

initial flaws. For example, further analysis of several components Use of additional or alternative NDT methods may also have indicated a 30% - 50% predicted life improvement if eddy current increased the detection capability and allowed the use of smaller inspections were to be used.

### CB14,0001,401,040,000

### Summary

### Findings

- Supplier Probability of Detection Databases Do Not Exist
- Inherent Initial Quality Has Not Been Established

### Recommendations

- Prime Contractors Should Require Supplier Probability of Detection Databases
- Statistical Requirements for Determination of Inherent Initial Quality Should Be Established
- Awareness of Impact of Initial Quality on Life Should Be Increased

GP14_0021.402.DAch

plays in the integrity process and the effect it has on predicted This study program brought into focus the significant role NDT component life.

light. Neither supplier had developed in-house NDT detection this program. Although both suppliers recognized the usefulness as a result of these shortcomings, some of the components database for their material and manufacturing processes. Partly However, some shortcomings in the process were brought to capability data and, therefore, had to estimate their capability for of inherent initial quality, neither had developed a statistical analyzed during this program exhibited short predicted life.

## Results From Two MECSIP Studies

Craig L. Brooks
McDonnell Aircraft Co.
McDonnell Douglas Corp.
St. Louis, MO

## Results from Two MECSIP Studies

### Objectives:

- Assess the Operational Service Lives of Two Significantly Different Aircraft Mechanical Subsystems by Applying the USAF Damage Tolerance Philosophy and Using the Mechanical Equipment and Subsystems Integrity Program (MECSIP MIL-STD-1798) Approach.
- Evaluate the Ability of Mechanical Equipment Suppliers to Implement the USAF MECSIP Process.

### **Objectives**

- Assess the Operational Service Lives of Two Significantly Different Aircraft Mechanical Subsystems.
- Evaluate the implementation of the MECSIP Process.

### Integrity Process Used

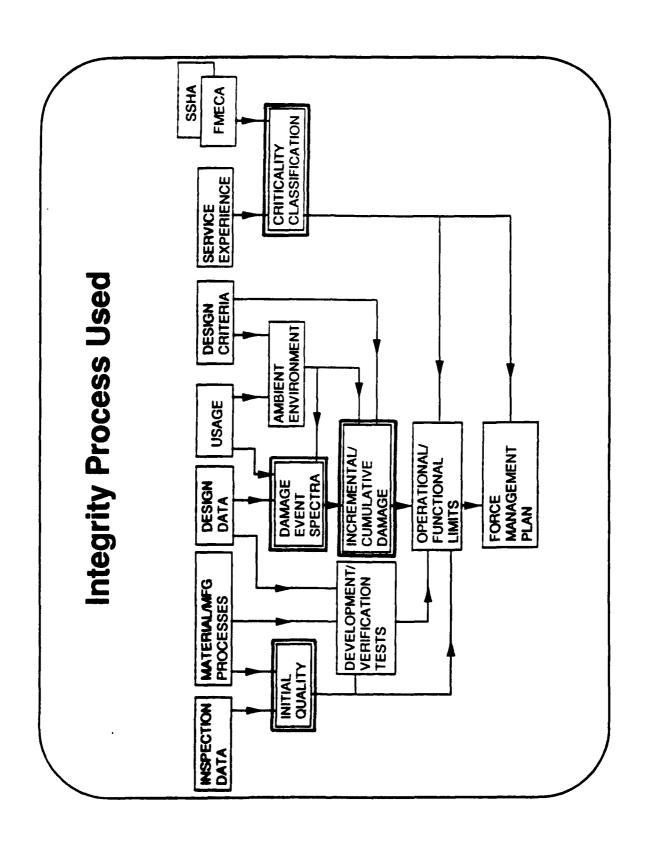
tasks that focused on the highlighted databases shown on the viewgraph. The MECSIP process used by the two suppliers was tailored to four

The four tasks were as follows:

- Component Criticality Assessment
  - Initial Quality Assessment
- Environmental/Stress Spectra Development
  - Integrity Assessment

tolerance. The assessments also provided insight into the inspection By addressing these four tasks, assessments were performed that resulted in an evaluation of the system's durability and damage intervals that would be required for maintaining the system.

The Initial Quality Assessment and the Criticality Assessment were derived from existing data and FMECA's.



## Component Selection Process

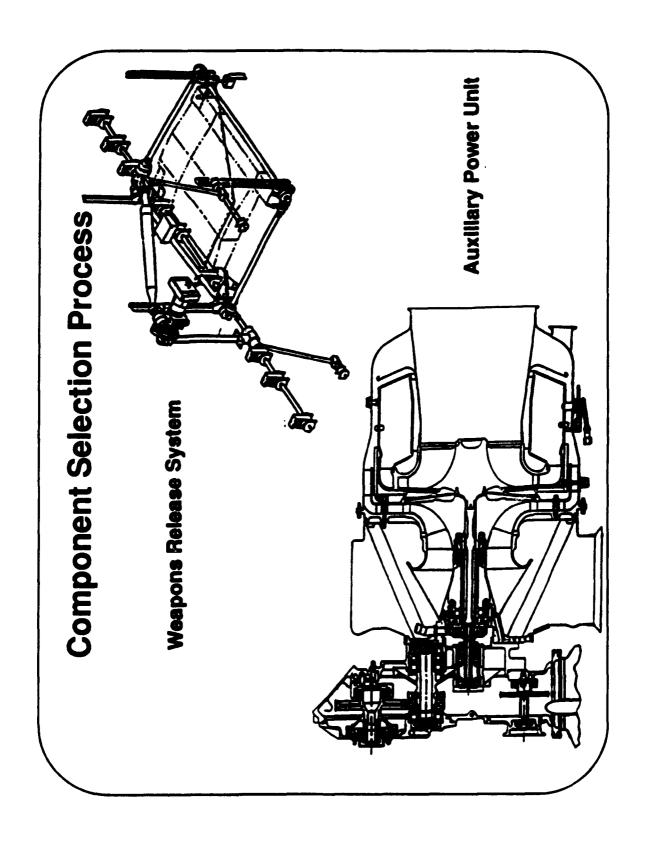
The Weapons Release System and the Auxiliary Power Unit (APU) were selected for this study. They are representative of two fundamentally different systems.

wear and crack growth damage mechanisms occurring each revolution of operation. carburized steel gears. They operate in a vibratory environment combined with The Weapons Release System comprises interconnected gearboxes using

producing centrifugal and thermal stress environments. Additional highly stressed The APU is a small turbine utilizing superalloys operating at high rotational speeds structure included internal gears and attachment lugs, both being exposed to differing fatigue mechanisms and types of loading.

The specific components within each system were selected using engineering judgement and the static design analysis. The emphasis for selection was placed upon criticality and to obtain a variety of geometries, materials and damage mechanisms.

tolerance aspects was presented at the 1990 USAF Structural Integrity Conference. This McDonnell Aircraft Company process is entitled, "An Engineering Procedure to Select and Prioritize Component Evaluation Under USAF Structural Integrity A comprehensive selection process that addresses many of the damage Requirements."



## **Criticality Assessment Process**

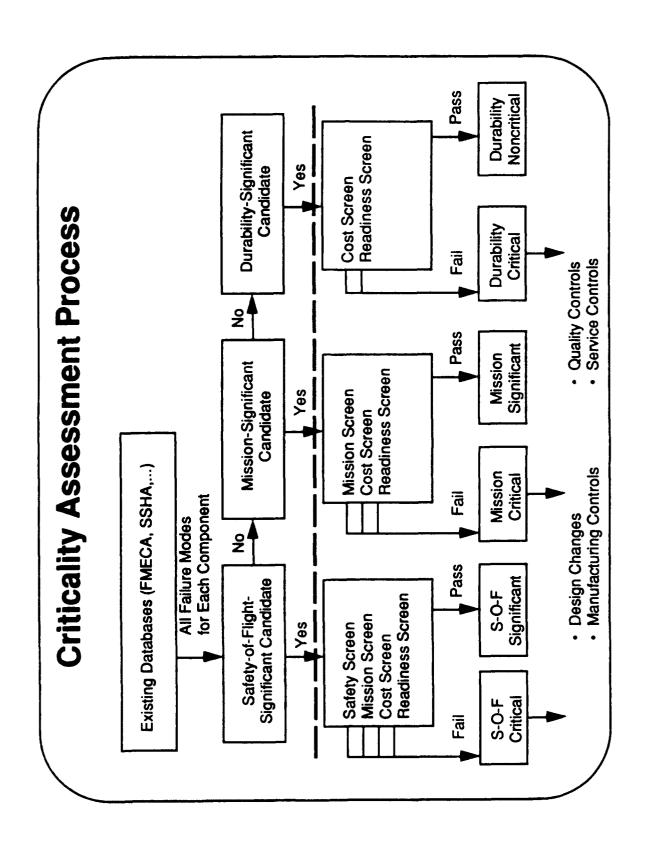
Modes, Effects and Criticality Analysis (FMECA) and the Subsystem Hazard Analysis (SSHA). impose detailed analytical requirements, manufacturing controls, and inspection procedures. The purpose of the Criticality Assessment is to determine the most important parts to A Criticality Assessment was performed using the existing databases such as Failure

The following Criticality definitions were applied:

- A. Safety-of-Flight Significant: A component whose failure could (1) Cause loss of the could severely affect safety of flight, or (3) Cause injury to air or ground personnel. air vehicle, (2) Cause extensive damage to other components which
- B. Mission Significant: A component whose failure could (1) Prohibit the execution of a critical mission, (2) Significantly reduce the operational mission capability, or
  - (3) Significantly increase the system vulnerability.
- impact by requiring costly maintenance, repair, or replacement; which if not performed, C. <u>Durability Significant</u>: A component whose failure may result in a major economic would significantly degrade performance and operational readiness.

indicate that the item is indeed critical. The critical items require design changes to eliminate The candidate items are considered to be significant until the screening analysis results the critical classification or special controls to ensure structural integrity.

Mission Significant. Some APU components were categorized as Safety-of-Flight due to the All components of the weapon release system and most of the APU were categorized as potential for an uncontained failure injuring ground personnel. The screening process for applying special controls based on the probability of a failure was not implemented during this study. This activity is more appropriate for the detail Engineering Manufacturing Development phase.



## **Initial Quality Assessment**

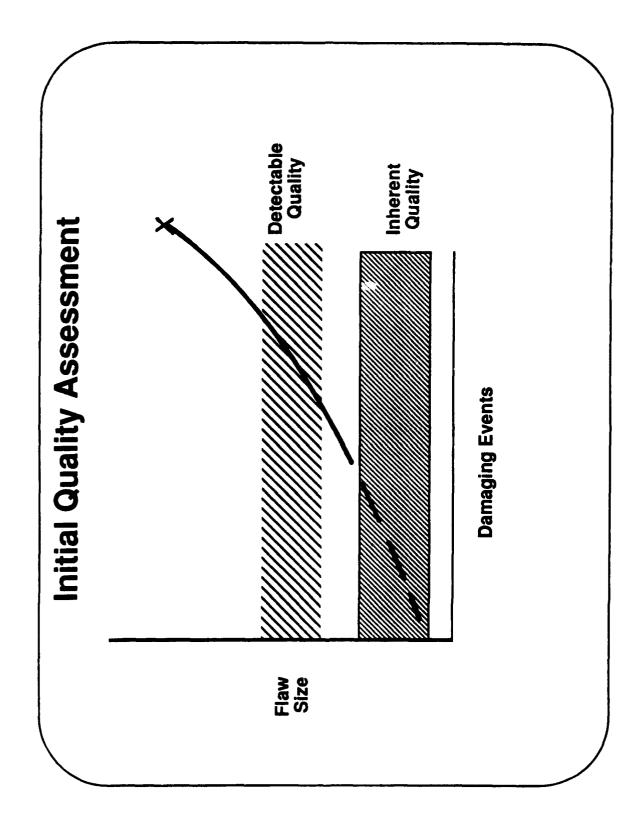
The total life of a component can be expressed in terms of a crack nucleating and growing to failure as a function of the applied damaging events. There are two types of Initial Quality that could be used in a damage tolerance analysis:

- 1. The initial detectable quality that is measurable using Non Destructive Inspection (NDI) techniques
- inclusions, and non-metallic inclusions) and part manufacturing quality (e.g. nicks, The inherent initial quality, comprised of material quality (e.g. micro-porosity, undercuts, mismatch, and machining scratches)

Either Initial Quality may be used providing adequate statistical data is available to provide the required confidence. Safety-of-Flight or Mission Critical Components demand a very low probability of failure, and orientation. The lesser severity of Durability Critical Structure may permit the use hence the initial quality is based upon the detectability of a flaw in a critical location of the initial inherent quality, which is not readily detectable by NDI techniques. However, no inherent initial quality data exists at either supplier.

establish the reliability and confidence in their NDI processes. Both used acceptance Neither of the suppliers performed a Probability of Detection (POD) test program to criteria based on literature search, industry norms, and engineering drawing requirements.

Magnetic Particle and Dye Penetrant Inspection techniques were used almost exclusively.



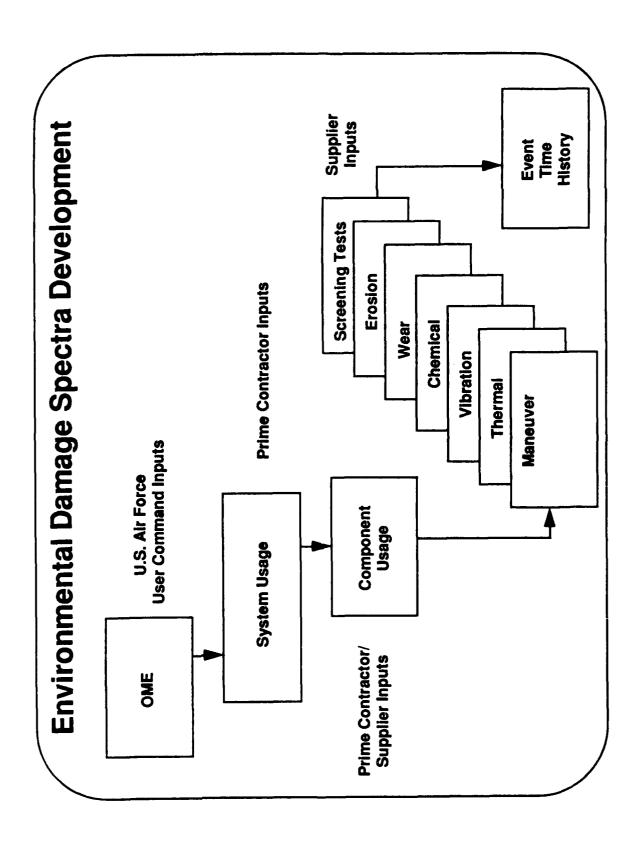
# **Environmental Damage Spectra Development**

An important part of the process for obtaining representative environmental damage spectra is to establish a closely coordinated anticipated usage flow down process from the end user to the subsystem supplier.

The development of the events that constitute the damage event spectrum which is used to ambient environments the aircraft weapon system will encounter. It includes generalized develop component life initiates with the Operational Mission Environment (OME). This document is issued by the Air Force user command to describe the overall usage and mission descriptions, basing scenarios, and ambient climates.

Events which cause insignificant damage can be screened out or combined to avoid unnecessary testing. In addition, the interface environment between the subsystem and the airframe is a joint The prime contractor reduces this data to describe the external environment and usage spectra responsibility. These mission descriptions should also include any screening tests performed. specific knowledge of the environment in which the subsystem operates, and the supplier has developing the usage spectra, important damaging events can be recognized and specified. procurement specification. This negotiation is a key element as the Prime contractor has for each subsystem. This in turn is negotiated with the subsystem supplier through the specific knowledge of what is damaging and the system operational loading. By jointly

It is important to account for all damaging influences and environments in the development damage the suppliers had difficulty in accurately accounting for the vibratory interaction. of spectrum. Although it was recognized by both suppliers that vibratory loading cause Neither supplier had techniques available to define the vibratory environment and its interaction with low frequency loading.

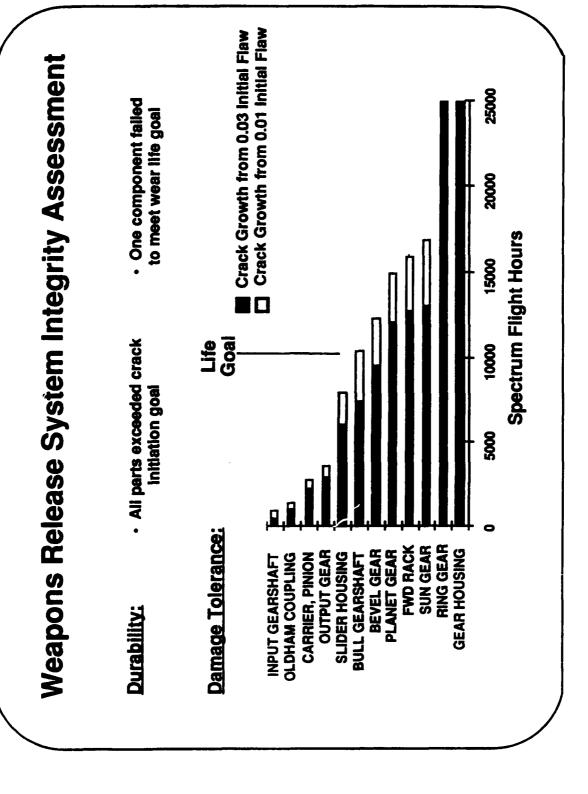


# Weapons Release System Integrity Assessment

The Weapon Release System supplier used three types of life prediction analyses to assess the durability and damage tolerance capabilities of the selected components. The durability analysis consisted of a typical crack initiation prediction using Miner's Linear Damage Rule. The results showed lives for ten of the components to be greater than ten limes the USAF goal. Two components resulted in lives greater than four times the goal.

made to assess durability. One component had a very low wear life prediction of 5% of Abrasive wear computations using linear wear equations and empirical wear data were the life goal. Due to the relatively small amount of wear data available, most wear lives were based upon experience.

smaller flaw sizes. For the carburtzed materials, both representative crack growth rate data and obtained for configurations and components that have processing controls to ensure quality by improved methodology is needed. Some of these components had low damage tolerance lives, results. The short predicted lives are a result of needing to start the analysis at the detectable The crack growth results were not commensurate with field experience nor the crack initiation establishing a database substantiating the initial inherent material and manufacturing quality, The crack growth predictions were performed using a commercially available computer code. and improving inspection techniques to allow conducting the life analysis from significantly detectable flaw size is quite severe. Increases in the usable damage tolerance lives can be even considering a .01" initial flaw size. Reductions in analytical conservatisms could be strength steel gears and similar types of geometries operating at high stress states, the llaw size and/or having compounding analytical conservatisms in the analysis. For high removed by performing verification and correlation test for these type configurations.



## **APU Integrity Assessment**

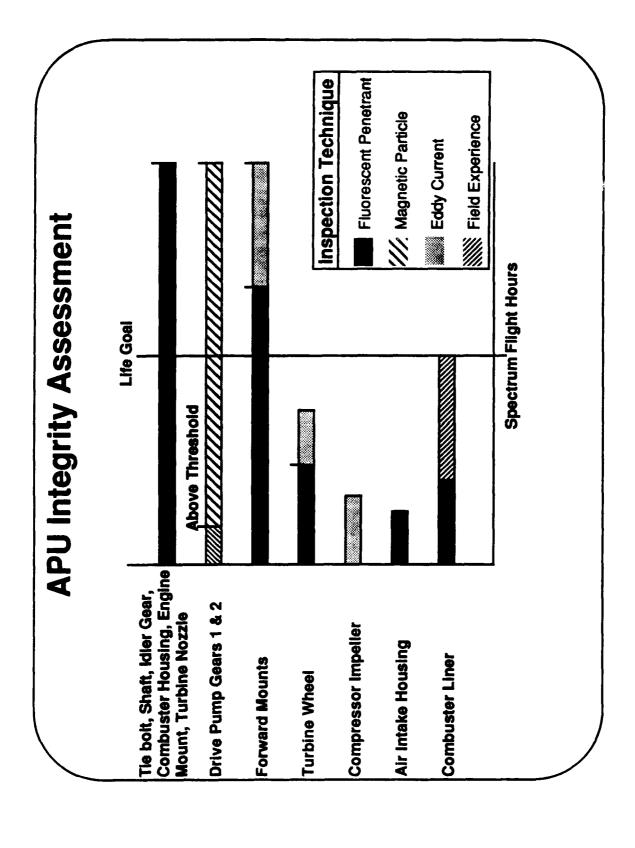
evaluations of the protective coatings, monitoring systems, and other prevention techniques The APU supplier conducted crack growth analysis for a variety of geometries, components durability failure modes, such as corrosion and wear, were addressed through quantitative used. The supplier had no analytical tools for predicting corrosion and wear degradation. components to ensure the most severe crack growth location was determined. Other and environments. A screening analysis approach was used for each of the selected

contained in the spectrum. Although these components meet the goals, analysis showed high detectable size, produced stress intensities that exceeded the long crack growth threshold Eight of the thirteen selected components meet the USAF life goal by more than a factor of two. Two of these, the Drive Pump Gears, had dynamic loads and effects (vibrations) sensitivity to initial flaw size. For example, a flaw .01" larger than the assumed initial and an extremely low life resulted.

Use of Eddy Current procedures as one of the available NDI techniques improved the damage tolerance options for the forward mounts and the turbine wheel.

patterned hole configuration lacked appropriate stress intensity solutions for continuing damage. techniques. The combuster liner operates in an extremely hot environment and the multiple The life used for this part was based upon empirical data, field inspection, and repair data. The analysis for the combuster liner was beyond state-of-the-art crack growth prediction

Implementation of the damage tolerance analysis proved its benefit to this supplier by providing insight into recent hardware failures.



### **Findings**

### Criticality Assessment:

as a means to classify the component as a "significant candidate". The component would not be The criticality Assessment was better understood by considering the consequence of failure Inested as critical until results of the integrity Assessment indicated it was critical.

not just crack growth. The details of component selection and the subsequent Criticality Assessment components should be fully analyzed. This process should examine all potential failure modes and The process can be improved by adding a procedure for component selection, to identify which should be clearly defined in the prime contractor's requirements.

### inklal Quality Assessment:

Suppliers need to develop a Probability of Detection (POD) database that would provide increased confidence, continue quality improvements, and enable in-house improvements.

Statistically establishing inherent material and manufacturing quality would enable increased use of a component's available life. The formation of this database would also enable improvements in Inherent quality.

### **Environmental Spectra:**

through good communications and understanding among the customer, prime contractors and suppliers. Removal of unnecessary conservatisms will avoid cost burdens that may result from subsystem Development of spectra to accurately represent the subsystem usage needs to be achieved

### Integrity Assessment:

maintenance.

tools will need to be tailored toward solving the particular problems associated with their structure Mechanical equipment suppliers need to gain experience using damage tolerance tools. These and operation conditions.

occur for modeling the specific materials used in the mechanical systems, specifically carburized steels. Continued testing and generation of material crack initiation and crack growth databases need to

### Force Management Plan:

This program did not address the Force Management Plan aspects of a MECSIP. The lack of insight into or an example of the final end product posed some difficulty for the supplier in understanding the value of the process and how results are to be used.

### **Findings**

### Criticality Assessment

- Not fully understood
- · Primes need to supply detail requirements

- Initial Quality Assessment
   Statistical inspection capability not characterized
  - Inherent Initial Flaw approach has merit

### **Environmental Spectra**

- Flow down process is crucial
- · Conservative fatigue spectra used

- Integrity Assessment
   Experience and tailored methods are needed
  - Material databases lacking

### Force Management Plan Undefined by user

### Recommendations

- · A model force management plan should be developed with supplier participation to provide insight into the value of the process to the user.
- databases. These databases would consist of statistically significant distributions of flaw sizes Guidelines should be estabilished for standardizing the development and use of Initial quality representing the raw material and the supplier's manufacturing process correlated against life, and flaw size as a function of Probability of Detection.
- · Mechanical equipment suppliers should conduct NDI probability of detection studies to establish realistic initial flaw sizes for use in MECSIP integrity studies.
- · Prime contractors should transfer life prediction practices and methodology to suppliers, certify methodology usage through test correlations, and monitor design analyses.
- companies, including small concerns which may not have the resources to develop design data. · The present public domain, material databases should be supported with data contributions for the materials commonly used in mechanical equipment. These data are accessible by all
- and corrosion degradation. The current practices rely on crude approximations for vibrations, and · Life prediction methodologies need to be developed for vibratory interaction, wear mechanisms, material selection, surface coatings and lubrication to avoid wear and corrosion problems.

the customer, the prime contractors, and the equipment suppliers. They are intended to help evoive The above recommendations are suggested for all parties associated with the integrity process, the NECSIP process to ensure reliable cost efficient weapons systems.

### Recommendations

- Specify Supplier Participation in Force Management Planning
- Establish Guidelines for Inherent Initial Quality and POD Database Development
- Establish Flaw Probability of Detection Databases
- Improve Technology Transfer to Supplier
- Support and Contribute Data to USAF Damage Tolerance Design Handbook and MIL-HDBK-5E
- Develop Vibratory, Wear, and Corrosion Methodologies

## VARIABILITY IN CRACK GROWTH RATE DATA

Eric J. Tuegel, Ph.D.
McDonnell Aircraft Co.
McDonnell Douglas Corp.
St. Louis, MO

#### Outline

tested. Basic crack growth rate tests, and constant amplitude and spectrum tests Approximately 140 specimens of 7050-T7451 plate, 7050-T7452 hand forgings, mill annealed Ti-6Al-4V, recrystallization annealed Ti-6Al-4V and 2124-T851 plate were of open hole and loaded bolt hole specimens were performed by a commercial testing laboratory. When examining the basic crack growth rate data from these tests, the data seemed to be widely scattered in Region I and early Region II. Several causes for this large scatter were identified and will be discussed in this paper. They are:

- (1) Friction between the compact tension specimens C(T), and the loading clevis.
- (2) Decreasing ∆K tests, and
- (3) C(T) specimen data versus center-crack specimen M(T), data.

The objectives of this paper are to:

- (1) Encourage the reader to closely scrutinize the results of standard tests.
- Promote further investigations into the phenomena that were encountered during this test program. 3
- Apprise the reader of the importance of complying with the ASTM E647 standard, and illustrate some potential problems of noncompliance. ල

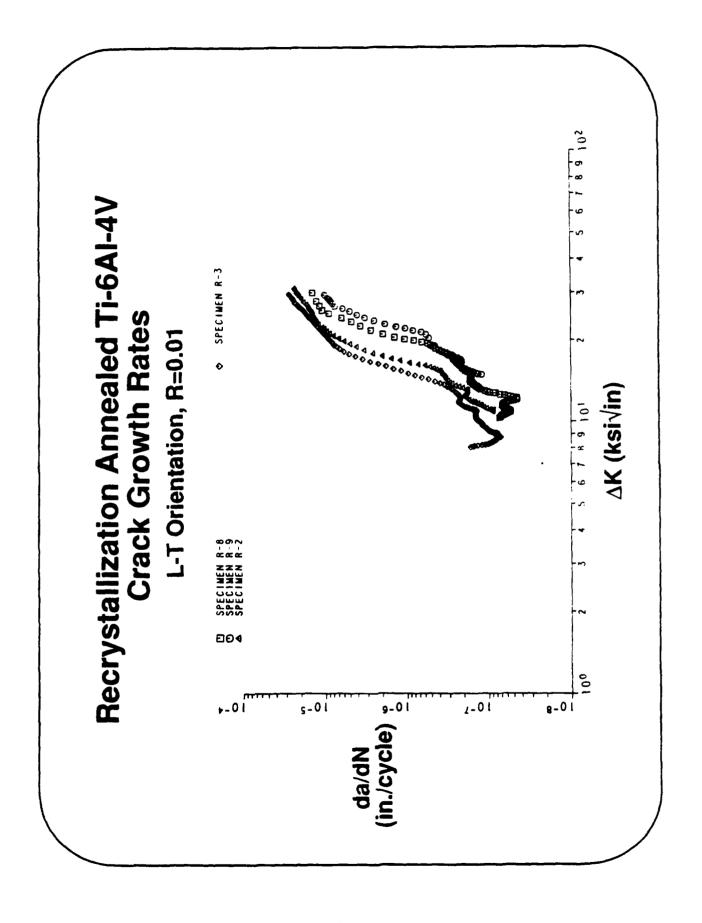
#### Outline

Discuss sources of variation in crack growth rate data.

- Loading clevis rubbing against C(T) specimens
- **Decreasing ∆K tests**
- C(T) specimens vs. M(T) specimens

## Recrystallization Annealed Ti-6AI-4V Crack Growth Rates L-T Orientation, R=0.01

amount of scatter observed in this data. Therefore, an examination of the details The data in the accompanying slide from crack growth rate tests at constant maximum load on recrystallization annealed (R.A.) Ti-6AI-4V is widely scattered. This is particularly evident at crack growth rates less than 1.0E-6 in./cycle. For consistent test conditions, crack growth data does not typically exhibit the of the tests was conducted to identify the causes.



## Example of Galled R.A.Ti-6Al-4V C(T) Specimen

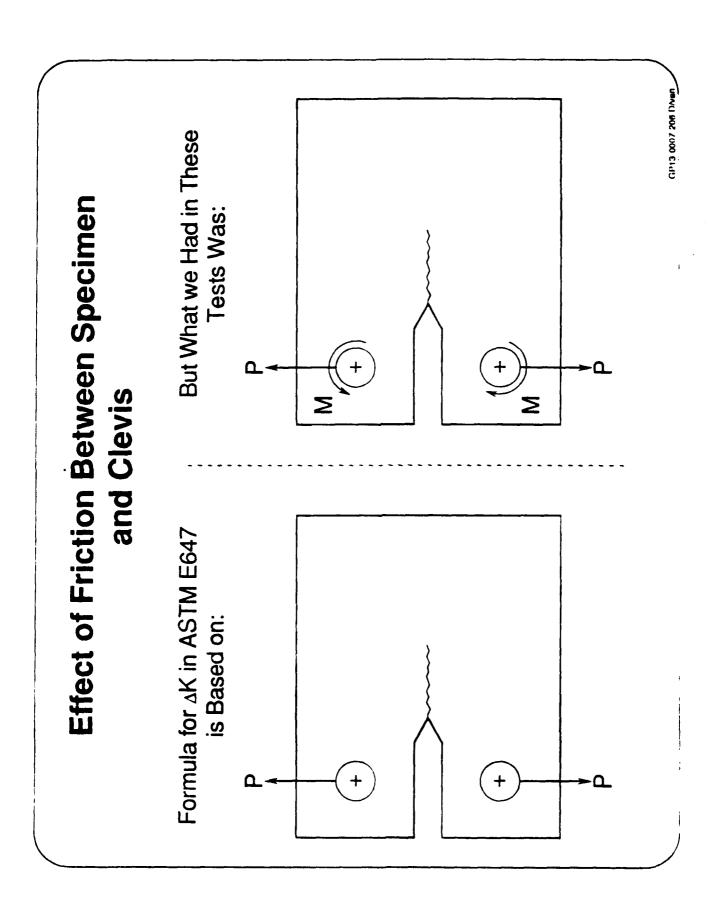
Visual inspection of the C(T) specimens after the tests revealed galling of the specimen around the loading hole. The galling generally formed the outline of the loading clevis indicating that there had been considerable rubbing between the specimen and the loading clevis during the test.



# Effect of Friction Between Specimen and Clevis

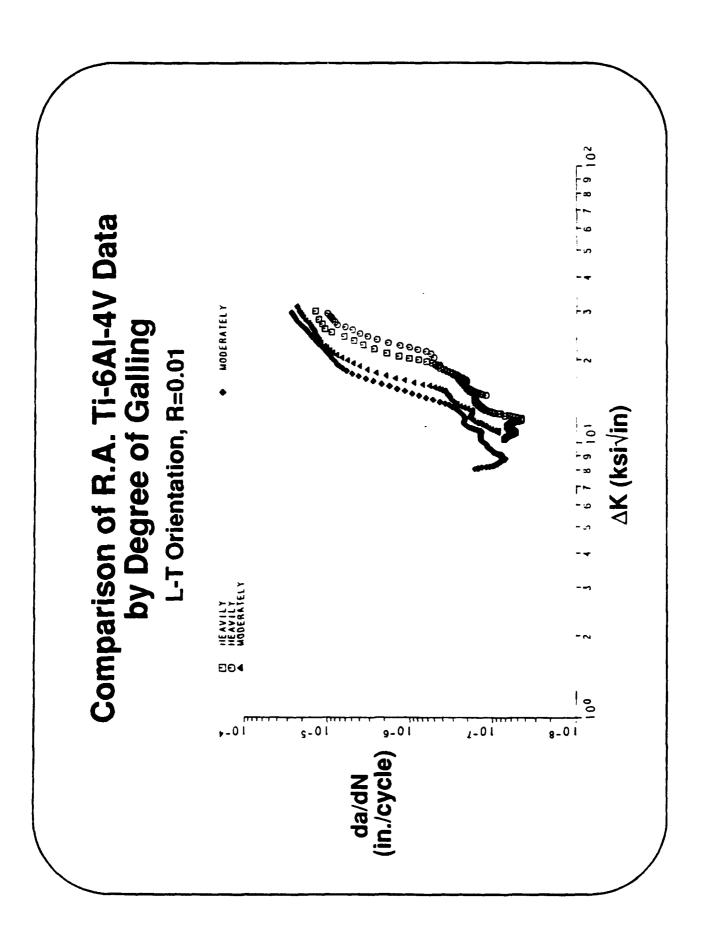
conditions upon which the formula for calculating the stress intensity range, ∆K, is based. The formula in ASTM E647 assumes that a vertical load will be Friction between the specimen and the loading clevis changes the boundary wider than the specimens, the moment is only on one face of the specimen. moment applied about the loading holes. Because the clevises are slightly applied through the loading holes. In our tests, there was an additional The magnitude of this moment is unknown.

specimens are loaded in pure tension and are held in such a way that there can be no relative motion between the specimen and the loading fixture. This situation does not occur for center crack, M(T), specimens. M(T)



# Comparison of R.A. Ti-6A1-4V Data by Degree of Galling

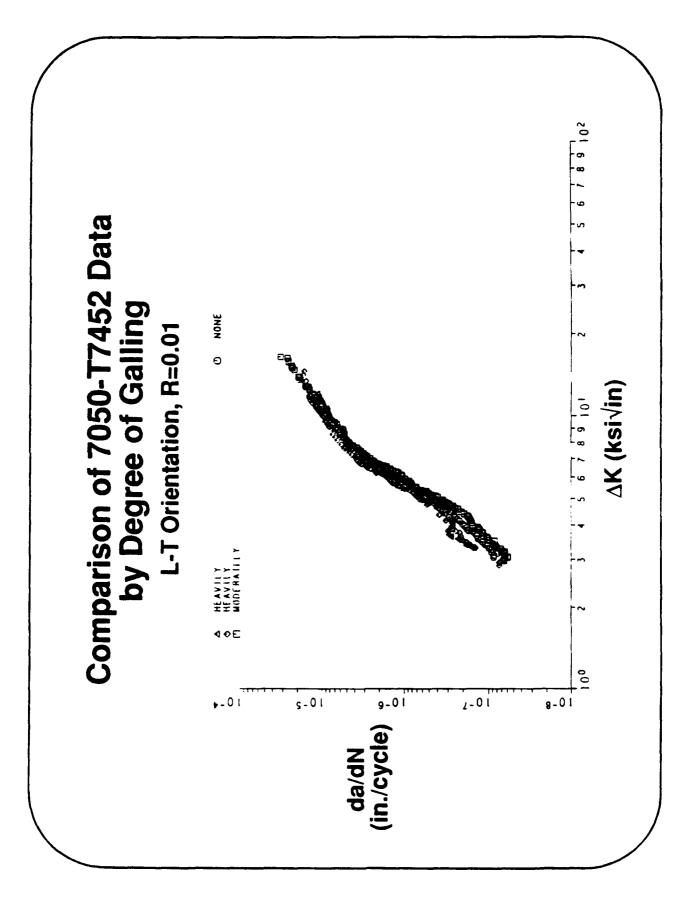
All the compact tension specimens were examined and the degree of galling on each was rated as heavy, moderate, slight, or none. The crack growth rate data from R.A. Ti-6Al-4V C(T) specimens show a distinct banding according to the degree of the galling.



## Comparison of 7050-T7452 Data by Degree of Galling

Data from 7050-T7452 hand forging C(T) specimens did not appear to be affected by the rubbing between the specimen and the loading clevis. The data are less widely scattered and distinct bands related to the degree of galling are not evident.

Perhaps this is because for most materials this rubbing is not a problem. loading clevis. Nor does it contain recommendations on how to avoid it. low friction spacer, be placed on both sides of a C(T) specimen between ASTM E647 does not warn about rubbing of C(T) specimens against the warranted. We would recommend that Teflon washers, or some other However, in light of this recent test data, we feel that caution is it and the loading clevis to minimize the effects of friction.

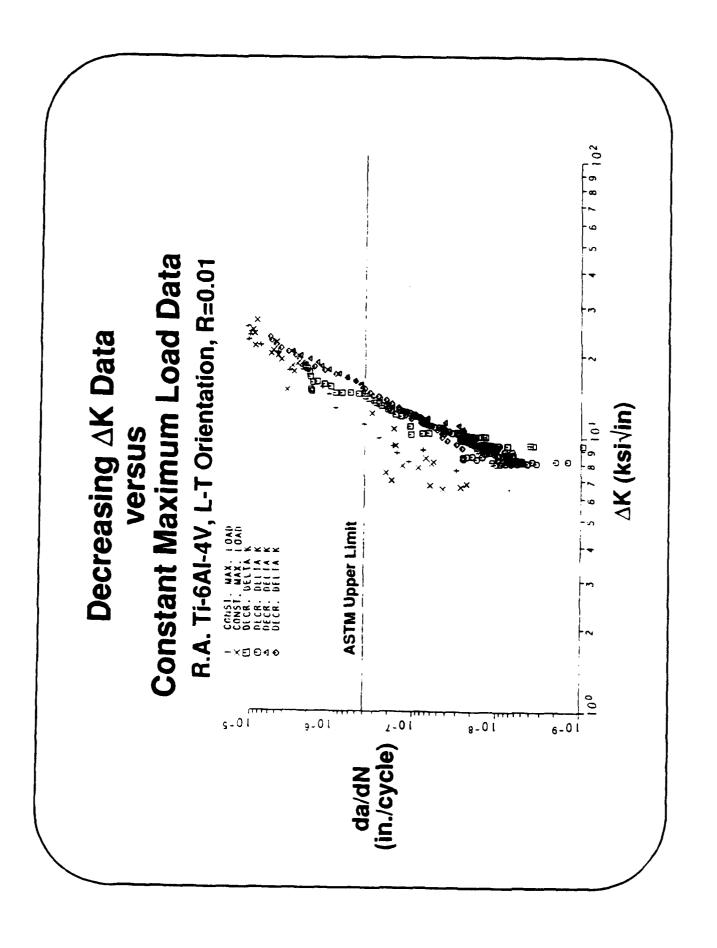


# Decreasing △K Data Versus Constant Maximum Load Data R.A. Ti-6Al-4V, L-T Orientation, R=0.01

prior loading history at the associated low AK's may influence near-threshold AK is reduced throughout the test so that progressively slower crack growth crack growth rate data near the crack growth threshold. In this type of test, crack growth rate behavior. Guidelines for performing this type of test are Decreasing ∆K tests were conducted on C(T) specimens in order to obtain rates are achieved. Decreasing AK tests require careful control, because demonstrate that prior loading history did not influence the crack growth decreasing ∆K tests be compared to data from increasing ∆K tests to included in ASTM E647. One of these guidelines is that all data from

lests and from constant maximum load tests on M(T) specimens at R=0.01. In Because the rubbing between the C(T) specimens and the loading clevis may decreasing ∆K tests was compared to data from constant maximum load showed a difference between crack growth rate data from decreasing ∆K procedures used by the lab conflicted with the guidelines in ASTM E647. tests on M(T) specimens. R.A. Ti-6Al-4V, as well as the other materials, have affected the results of the constant maximum load tests, data for reviewing the details of the tests, it was noted that some of the test

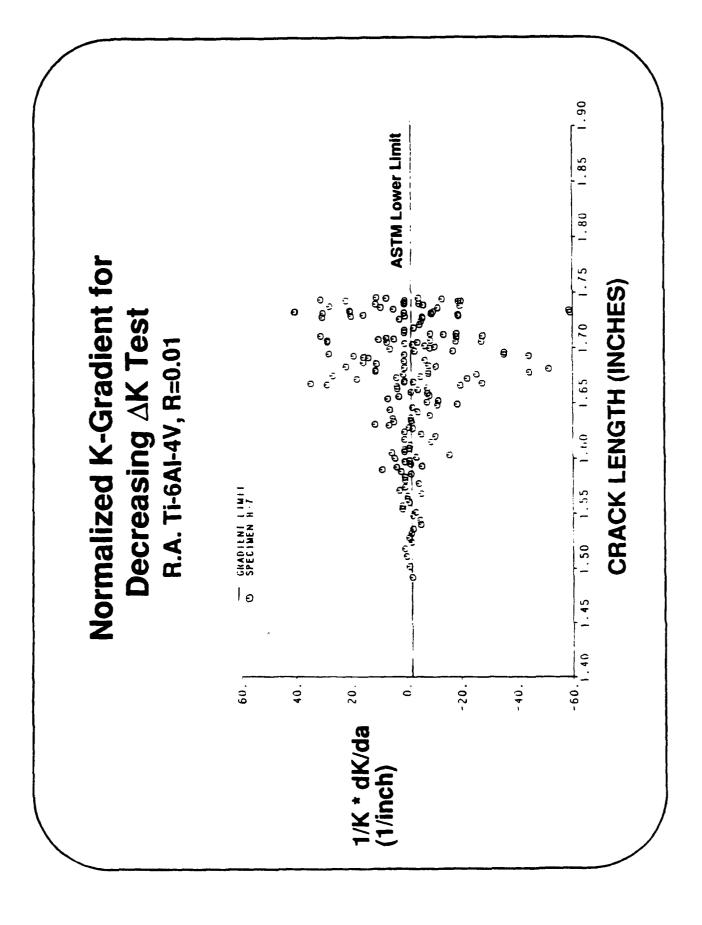
The decreasing ∆K tests were started at crack growth rates of almost 1.0E-5 in./cycle, much faster than the 4.0E-7 in./cycle recommended in ASTM E647.



## Normalized K-Gradient for Decreasing AK Tests R.A. Ti-6Al-4V, R=0.01

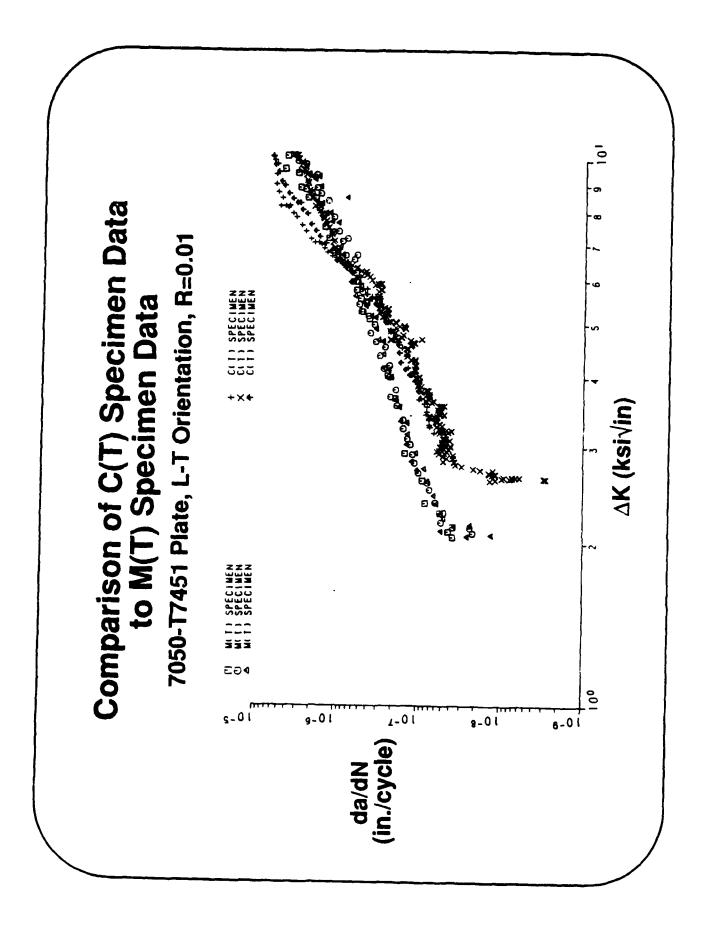
The load was continuously shed during these tests such that on average the normalized K-gradient, 1/K * dK/da, was slightly slower than loads. Prudence would dictate that the normalized K-gradient should be significantly slower than -2/in. so that variations in the value would not compliance crack length measurements and the ability to control the approach the limit. However, as the data in the accompanying graph indicates, it is extremely difficult to meet the normalized K-gradient instantaneous values of the normalized K-gradient were frequently much less than -2/in. because of the limits on the accuracy of the -2/in. lower limit specified in ASTM E647. However, the requirement in ASTM E647 for continuous load shedding:

 $0 / inch \ge 1/K * dK/da \ge -2.0 / inch.$ 



# Comparison of C(T) Specimen Data to M(T) Specimen Data 7050-T7451 Plate, L-T Orientation, R= 0.01

decreasing AK tests, which used C(T) specimens, agreed with data from the load. But, data from C(T) specimens gives a higher crack growth threshold specimens. The near-threshold crack growth rate versus ∆K relationship ives for aircraft structure than will the relationship developed using M(T) concern since most crack growth threshold data is generated using C(T) Further examination of all the data revealed that the differences between developed using C(T) specimens will give significantly longer predicted less severely galled C(T) specimens tested under a constant maximum stress intensity than does data from M(T) specimens. This result is of decreasing ∆K test data and constant maximum load data from M(T) specimens may not be entirely due to test procedures. Data from



# Comparison of C(T) and M(T) Specimens

because a compliance gage can be used to automate measuring the crack specimen and there is a natural place at the end of the specimen to mount a compliance gage. In addition to easing the burden of recording data for long threshold tests, the compliance gage allows the crack opening and Most crack growth threshold data is generated using C(T) specimens length. The compliance solution has been developed for the C(T) closing stresses, and thus the effective ∆K, to be determined

M(T) specimens are frequently used in crack growth rate tests because the specimens are less costly to fabricate and are suitable of tests at negative stress ratios. M(T) specimens, however, gave a lower crack growth threshold stress intensity than C(T) specimens.

this time to determine the effective  $\Delta K$ 's for the M(T) specimen data and to The basis of fracture mechanics is that the crack growth rate depends on specimens has not be developed. As a result, few tests measuring crack ∆K; specimen geometry should not have any effect other than how ∆K is calculated. Using the effective ∆K, that is, accounting for crack closure, closure in M(T) specimens have been reported. So, it is not possible at Unfortunately, a standard method for measuring crack closure in M(T) verify that the crack growth threshold data from the two different should bring the data from the two specimens into agreement. specimens agree. Comparison of C(T) and M(T) Specimens M(T) Specimen + 520 C(T) Specimen

#### Conclusions

lesting. The user needs to be familiar with the standard for crack growth between the testing lab and the user when conducting crack growth rate examined for visual indications of problems with the test method. We This test program demonstrates the importance of close coordination recommend that steps be taken to reduce the possibility of rubbing rate testing, ASTM E647. After the test, the test record should be reviewed for testing irregularities and the specimens need to be between C(T) specimens and the loading clevis.

Be careful when performing decreasing AK tests!!!! The results are very sensitive to the testing conditions; the decreasing AK test requires careful control which may be difficult to properly achieve.

the two different specimens in terms of effective ∆K will then be possible. specimens are lower than those from C(T) specimens. Work needs to be specimen geometries. Comparison of crack growth threshold data from done comparing crack opening and closing stresses for the two Crack growth threshold stress intensities determined with M(T) This should resolve the observed differences in the data.

#### Conclusions

- 1. Crack growth rate data needs to be scrutinized carefully.
- Look at the specimens after the test.
- Be wary of crack growth rate data from decreasing AK
- Decreasing ∆K tests are hard to control.
- 3. Crack growth threshold data from M(T) specimens is more conservative than data from C(T) specimens.
- Crack closure tests on M(T) specimens are needed.

### Selection of Critical Point-in-the-Sky for Navy Aircraft

Darla Y. Crain McDonnell Aircraft McDonnell Douglas Corporation St. Louis, MO

Mike McMahon NAVAIR GP12-0294-1-D/b

25PR-033

## **Detail Specification Requirements**

reads "For determination of loads, the airplane shall be at the critical speed and altitude which include "spectra for analysis and test...shall be supplemented...to ensure that each airplane component is designed and tested to the proper repeated loadings." "Ordering and frequency of loads within the usage spectra shall be random, consistent with flight-by-flight airplane operation..." results in the minimum life on the component being considered." Other specification requirements Military specification, MIL-A-8866B(AS), defines requirements for repeated loads, fatigue, and damage tolerance applicable to Navy procured aircraft. Aircraft detail specifications have similar spectra requirements as they pertain to point-in-the-sky selection. Section 3.5 Maneuver loads,

The method presented here results in a single spectrum which can be used for the entire aircraft. It is based on "minimum life" criteria, but will still allow for combining component loading realistically for analysis and test.

ന

### MIL-A-8866B (AS) Airplane Strength and Rigidity **Detail Specification Requirements**

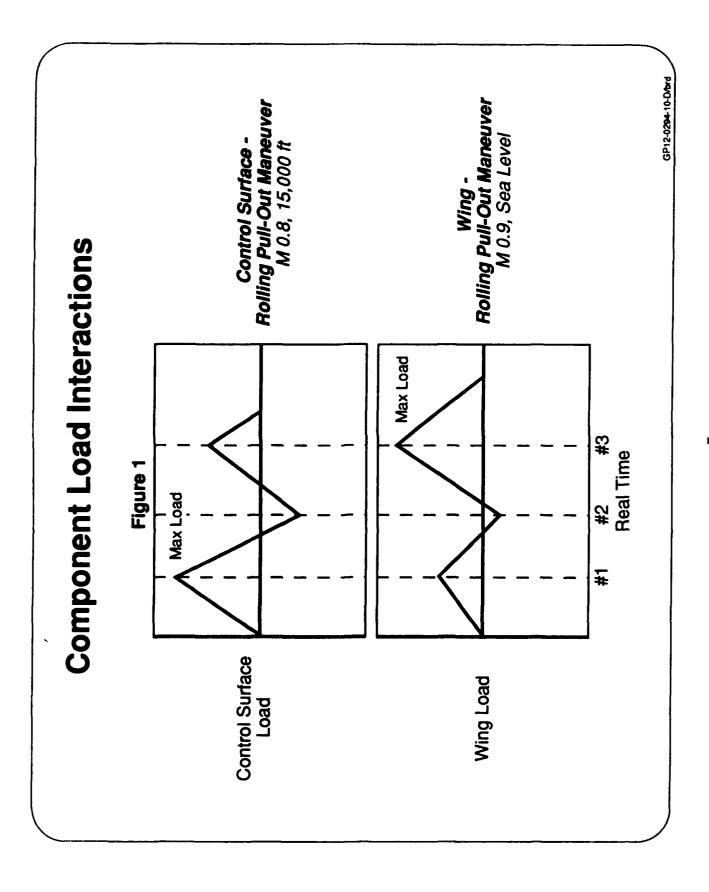
#### 3.5 Maneuver Loads

Critical Speed and Altitude Which Results in the Minimum Life " For Determination of Loads, the Airplane Shall Be at the on the Component Being Considered."

### Component Load Interactions

It and the wing has a peak load that occurs at time slice #3 at M0.9, sea level, it would be overly conservative to combine the peak loads of both the control surface and the wing to design the structure on the wing where the control surface attaches. This is due to two inconsistencies: 1) the The contractor also requires that each component spectra be consistent with flight-by-flight airplane operation in order to avoid over-design or over-test. For example, during a rolling pull-out (RPO), if a control surface on a wing has a peak load that occurs at time slice #1 at M0.8, 15,000 peak loads occur at different points-in-time and 2) the peak loads occur at different points-in-thesky. See Figure 1. Similar load interactions occur throughout an airplane and need to be addressed realistically to avoid weight penalties.

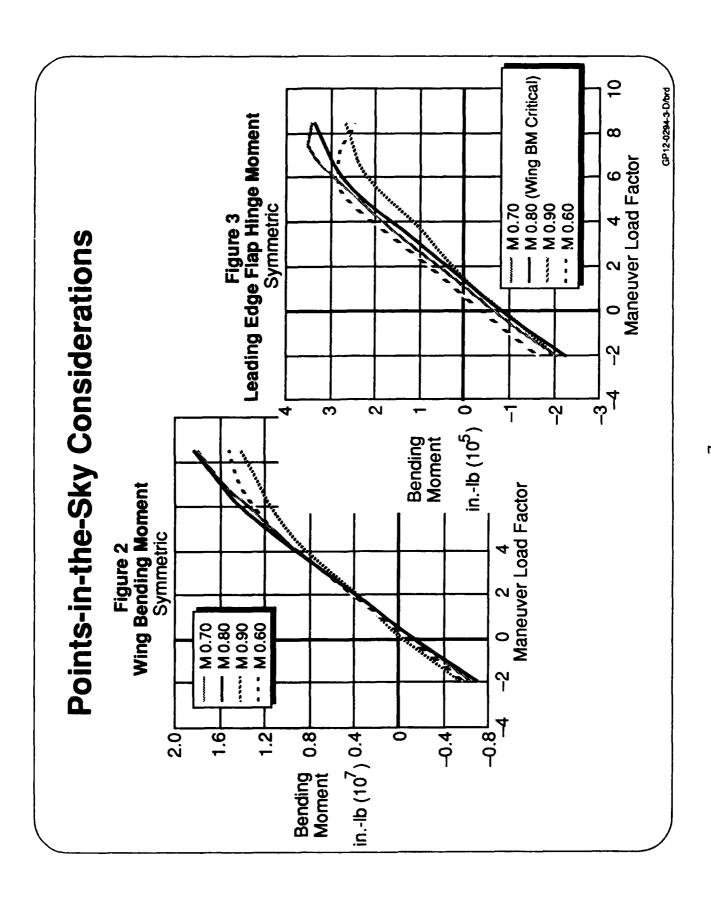
loads described above would also lead to an unbalanced test condition. It is desirable to design and test to the same spectrum. If, as frequently occurs, compromises are made in testing full scale articles, difficulty arises in determining whether the test met requirements. This method eliminates Consideration must be given to both analysis and test spectra Combination of the maximum many of these compromises.



## Points-in-the-Sky Considerations

Historically, critical point-in-the-sky selections have been based only on infrequently occurring maximum loads and not on the more frequently occurring intermediate loads which cause significant damage. The specification criteria, "which results in the minimum life...", may not be met for that selection approach. A method using damage calculations for the selection is preferable. Another consideration, previously discussed, is keeping consistency among component's time slices and points-in-the-sky. One single point-in-the-sky will not result in the minimum life on a component; it can be shown that the minimum life results from a combination of points-in-the-sky. Further, one combination of points-in-the-sky is not critical for all components. For each spectrum event the entire airplane must be at a distinct point-in-the-sky for the purposes of both analysis and

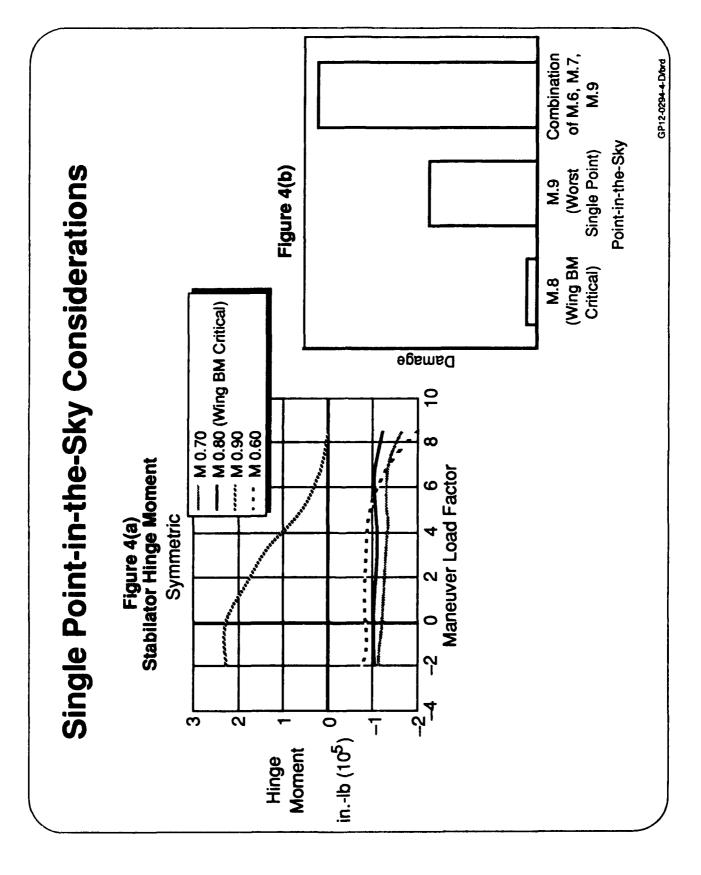
curves for symmetric maneuvers for several points-in-the-sky. Assume a symmetric maneuver is largest peak hinge moments occur at M 0.70 above 6 g's and M 0.60 below 6 g's and the valleys To illustrate these points, an example Navy attack airplane will be used for sample calculations through the rest of this paper. Figure 2 shows the airplane's wing bending moment versus Nz made up of one cycle; a "peak" Nz paired with a "valley" Nz. Note that M 0.80 at sea level will obviously give the most damage for symmetric maneuvers since both the largest peaks and the minimum valleys (greatest ranges) occur at this point-in-the-sky. However, the leading edge flap's are critical at M 0.80 (See Figure 3). The challenge is to develop a single spectrum that can accurately account for the damage on each component.



## Single Point-in-the-Sky Considerations

The stabilator hinge moments in Figure 4 (a) are an example of how one single point-in-thesky may not be critical for a single component.

is not nearly as critical as the damage due to M 0.90 at sea level. However, the damage due to e.g., as the airplane pulls Nz there will be the tendency to slow down; hence, the possible pairing the peak Nz's being at M 0.60 at sea level above 5.6 g's, M 0.70 at sea level below 6.5 g's and the valleys being at M 0.90 at sea level results in even greater damage and is a realistic scenario, As seen in Figure 4[b], the damage to the stabilator at M 0.80 at sea level (the wing critical point) of low Nz's at high Mach with higher Nz's at lower Mach.



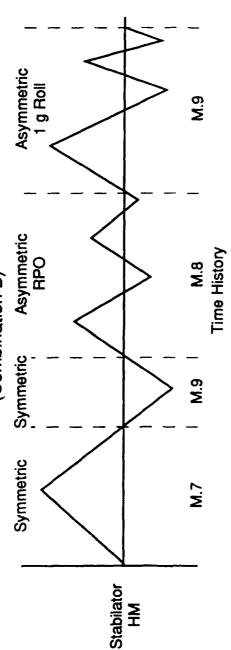
# Master Event Spectrum and Initial Selection

Before selecting the critical points-in-the-sky, a master event spectrum must be created. As required by the specification, it should include all significant events such as symmetric and asymmetric maneuvers, 1g rolls, gusts, speed brake events, store ejections, operations of devices, ground-airground cycles, etc. Some of these maneuvers may be grouped together because they have the damaging cycles occurring at the same point-in-the-sky. The selection process will be simplified by identifying these possible groupings early. It is also important to identify components that will introduce significant damaging loads to surrounding structure. For each of these components, a search on minimum and maximum loads is performed on the different maneuvers to attain the worst points-in-the-sky for the components. In the example, this process resulted in the four points-in-the-sky plotted in Figures 2-4. When the pointsin-the-sky have been down selected to a minimum, loads must be generated for all components performing all manguvers at these points-in-the-sky.

The four points-in-the-sky which resulted from the min-max search on loads were used to determine The table presented in Figure 5 shows the components and maneuvers selected for this example. worst case combinations. When a damaging event consists of only one peak-valley pair, as is the case for the symmetric maneuvers presented previously, the critical points-in-the-sky can be selected by observation (maximum range). When the maneuver is comprised of multiple peak-valley pairs, such as a RPO, it may be necessary to run damage calculations varying the point-in-the-sky for that particular maneuver to determine which is critical. A baseline condition is developed to compare relative damage; this condition is the one single most critical point-in-the-sky for each component. That is, only one point-in-the-sky is used for all maneuver types. The asterisk in Figure 5 indicates the worst single point-in-the-sky condition for the example airplane. Another baseline for comparison purposes is the worst combination of points-in-the-sky for each component, i.e., Combinations A, B, C or D as identified in Figure 5.

# Master Event Spectrum and Initial Selection





## Worst Case Combination of Points-in-the-Sky

742

Points-in-the-Sky	Component	Symr	Symmetric	Asyn	Asymmetric
Combination	Loading	Max Positive	Max Negative	RPO's	RPO's I g Rolls
A	Wing BM	.080	0.80	08.0	06:0
∢	Wing Torque	0.80	0.80	0.80	.06.0
ω	Stabilator HM	≤6.5 g's 0.70	*06.0	0.80	0.90
		>6.5 g's 0.60			
ပ	Vertical Tail BM	•06.0	06.0	0.00	06:0
∢	Rudder HM	0.80	0.80	0.80	.06.0
۵	Leading Edge Flap HM	≤5.5 g's 0.60*	0.80	0.80	0.90
		>5.5 g's 0.70			
Note: All points at sea level		* Worst single point condition			GP12-0294-5-D/brd

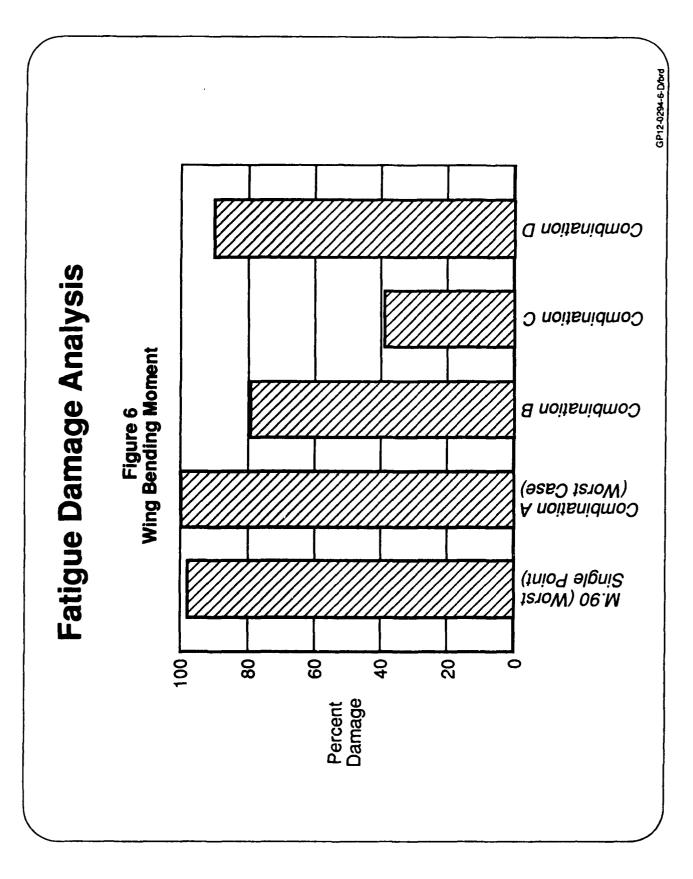
### Fatigue Damage Analysis

the mix of combinations to provide maximum overall aircraft damage must be determined. These Once the combination of critical points-in-the-sky has been determined for each component, steps are readily automated.

of point-in-the-sky combinations and components. Spectra consisting of Combination A (Figure 5) loads need to be created for every component, similarly for Combination B, etc. Note that Combination A is critical for Wing BM, Wing Torque, and Rudder HM, but will be less damaging for the other components. Each combination is assessed to determine what percentage of damage First, damage calculations (similar to Figure 4 [b]) need to be established for the entire matrix is caused by that combination.

tions B, C, and D will have damage percentages less than the single point-in-the-sky and A spectrum with all maneuver loads at the single most critical point-in-the-sky baseline is also created for each component. This assessment is represented graphically in Figure 6. Combina-Combination A will have a greater percentage of damage. This is just an example and the relationships for each component can be different, but the Combination previously determined as being most severe for a specific component will always have the lowest life (or highest percentage of damage).





# Fatigue Damage Due to Worst Combinations

in Figure 5. Note that Wing Torque is not sensitive to point-in-the-sky changes, but the Stabilator is very dependent on the point-in-the-sky chosen. An analysis must be performed with these Figure 7 shows the percentage of damage on each component due to the Combinations identified combinations to identify what mix of conditions will produce maximum overall aircraft damage.

## GP12-0294-7-D/brd

15

# Fatigue Damage Due to Worst Combinations

### Figure 7

		Percent Damage	Damage	
Component Loading	Point	Point-in-the-Sky Combination	y Combina	ıtion
	٧	В	၁	a
Wing BM	100	62	39	06
Wing Torque	100	100	100	100
Stabilator HM	12	100	40	12
Vertical Tail BM	62	34	100	62
Rudder HM	100	13	72	100
LEF HM	09	73	29	100

# Fatigue Damage Comparison to Single Critical Point-in-the-Sky

increments of 10% were used and the top ten are shown in Figure 8. These ratios of Combinations of each set of ratios are calculated to aid in sorting on the maximum overall damage. These values The process to develop the mix of conditions which produce the maximum fatigue damage can easily be automated. All ratios of Combinations must be checked for severity. In this example, A, B, C, and D produced the highest damage on all components. The mean and standard deviation are only used for determining optimization of damage on all components. The last line was the chosen ratio for the master event spectrum. The comparisons for this table are normalized to the baseline single worst point-in-the-sky as a reference; therefore, a combination can actually give more than 100% damage as in the case of the Stabilator HM.

## GP12-0294-8-Drord

# Fatigue Damage Comparison to Single Critical Point-in-the-Sky

### Figure 8

Percent	İ	İ	Perce	Percent of "Worst Single Point" Damage	t Single P	oint" Dan	nage	!	
Combinations BM Torque	<b>D</b>	Wing	D 9	Stabilator HM	Vertical Tail BM	Rudder HM	LEF	Mean	۲
		(M.9)	6	(M.90)	(M.90)	(M.90)	(M.60)		>
10 50 94 100		5	0	125	22	62	111	86	22
0 40 95 100		5	0	125	51	92	106	86	21
10 30 93 100		10	0	147	52	79	103	100	23
0 30 95 100		9	0	125	55	92	101	97	21
10 20 94 100		10	0	147	25	79	86	66	83
10 20 96 100		9	0	125	55	92	26	96 	2
0 10 95 100		9	0	147	52	79	66	86	53
10 10 97 100		9	0	125	55	92	95	8	2
10 0 96 10		<u> </u>	100	147	52	79	68	86	29
10 0 98 10		7	100	125	22	62	<i>2</i> 8	92	21

# Fatigue Damage Comparison to Worst Combination of Points-in-the-Sky

damage percentages will always be less than the worst case combination damage. For example, Figure 9 presents comparisons to the worst case combination of points-in-the-sky. it should be noted that the Stabilator HM damage is much less than this reference.

approximately 45% to correctly design the tail and backup structure. For full scale testing the 9, are at an unacceptable level. For analysis the severity of this component will be increased is used for the evaluation. For example, the Vertical Tail BM damage levels as shown in Figure Some components would not be tested adequately if the worst combination of points-in-the-sky vertical tail would be cycled beyond the rest of the test to complete the necessary damage.

## Fatigue Damage Comparison to Worst Combination of Points-in-the-Sky

### Figure 9

	Percent	ænt			Percent	Percent of "Worst Case Combination" Damage	ase Comb	ination" D	amage		
<b>ස්</b> ර	Distribution of Combinations	ution ratio	of ns	Wing BM	Wing	Stabilator HM	Vertical Tail BM	Rudder	LEF	Mean	۲
A	8	ပ	O	(A)	(A)	(B)	(C)	(A)	(D)		
0	40	10	50	81	100	90	22	85	82	74	18
10	40	10	40	82	100	20	55	62	78	73	17
10	20	10	30	80	100	59	52	22	75	72	17
20	40	10	30	83	100	20	22	62	74	73	17
20	20	10	20	8	100	29	52	\$	71	72	17
30	40	10	20	\$	100	20	55	62	20	72	17
30	20	10	10	82	100	29	52	25	29	71	17
40	40	10	10	85	100	20	22	62	49	72	18
40	50	10	0	83	100	59	52	54	63	71	18
50	40	10	0	98	100	20	22	62	<b>29</b>	1.1	ήŖ

750

GP12-0294-9-D/brd

### DAMAGE TOLERANCE MANAGEMENT OF THE X-29 VERTICAL TAIL

JAMES A. HARTER WL/FIBEC WPAFB OH 45433

### **BACKGROUND**

Many current high performance aircraft have experienced vertical tail buffet at high angle-of-attack (AOA). Under high AOA conditions, turbulent air flow from the aircraft forebody can impinge on the vertical tail causing high frequency loading. This buffeting action has the potential to severely reduce the service life of aft, vertical control surfaces. The X-29 demonstrator aircraft #2 first encountered significant vertical tail buffet on 9 May 1990 during flight #42 at angles-of-attack between 20 and 35 degrees. This buffet condition ocurred for 15 seconds and resulted in fin tip accelerations exceeding 110 g's and a dominant fin first bending mode of 16 Hz. This condition resulted in vertical tail loads approaching their design limits and the decision was made to temporarily avoid this flight region. However, this decision impacted the X-29 flight test program since military utility flights were to be conducted at high AOA to demonstrate the maneuverability of the aircraft. Damage tolerance analyses of the tail were performed for the assumed most critical location to estimate the crack growth life of the vertical tail at various 'g' levels. An initial flaw size of 0.03 inch was chosen based on field experience and confidence with existing non-destructive evaluation (NDE) methods. In this case, an eddy current inspection method was used. Preliminary analyses established inspection intervals at the most critical areas of the tail. These analyses used the limited fin tip acceleration data that was originally available for the tail and a simple transfer function to estimate local stress levels. Additional strain gage instrumentation was installed on the vertical tail while the aircraft was down for it's next scheduled maintenance and stress analyses were performed to determine the actual stresses at several locations on the tail. These analyses were then correlated with subsequent flight test data and more detailed crack growth predictions were performed to more accurately establish the damage tolerance of the vertical tail.

### **APPROACH**

Analysis of the in-flight accelerometer data during buffet revealed that the vertical fin was primarily experiencing the first bending mode at a natural frequency of 16 Hz. There was some indication of the second bending mode and first torsion mode at higher frequencies but at a much lower amplitude. Several areas of the tail were considered as possible areas for crack initiation and growth (see Figure 1.0), but the aft root area (location 4) was considered to be the most critical since the tail was being loaded primarily in pure bending during buffet. The aft fin mount was considered to be most highly loaded due to the fact that the vertical tail is swept backward, shifting the center of mass toward the rear fitting. This was supported by static test data supplied by the

manufacturer (Grumman). Grumman also supplied a transfer function relating fin tip acceleration to stress at the aft fitting. This was accomplished by relating acceleration to deflection and deflection to root bending moment and finally to the gross section stress in the aft attachment fitting. The 15 second fin tip acceleration trace obtained during flight #42 was normalized (Figure 2.0) to be used as a loading spectrum for crack growth analysis. Various maximum 'g' levels were modelled by mutiplying the normalized spectrum by the stress level corresponding to a given acceleration.

Prior to performing any damage tolerance analysis for the aft fin attachment, a reasonable initial crack length must be assumed. The assumed size should, of course, be large enough to have a high probability of being found during inspection. Since NASA/Dyden had safety of flight responsibility for the aircraft, they were responsible for any type of aircraft inspection. It was determined that eddy current inspections would be performed at three locations on the tail (location 3, 4, and 6 - see Figure 1.0). Inspection of areas 1 and 2 would have required the removal of blind fasteners and Location 5 was considered less critical than location 4. The NASA inspector initially claimed to be able to detect flaws larger than .005 inch using a hand held probe inside fastener holes. Air Force experience has indicated that a more realistic size is on the order of 0.03 - 0.05 inch. After discussion with NASA and Grumman engineers, it was decided to use the Air Force crack growth prediction program, MODGRO, assuming an initial 0.03 x 0.03 inch corner flaw at location 4. It was also agreed that an immediate inspection of locations 3, 4, and 6 would be conducted and subsequent inspections would follow if and when the time spent in buffet exceeded one half the predicted time to failure for the highest fin tip acceleration measured since the last inspection. The predicted life (time in buffet) is shown in Figure 3.0 as a function of maximum 'g' level. This approach was very conservative assuming that location 4 was indeed the most critical location, but it was felt that the limited available data waranted a conservative approach to assure safety. In any case, this approach returned the aircraft to flight at high AOA.

While the above approach returned the X-29 to high AOA flight, subsequent flights and frequent inspections demonstrated a need to obtain more data to remove some of the conservatism from the analyses. While the aircraft was nearing the next standard 100 hour overall inspection, Air Force, NASA, and Grumman Engineers decided to install strain gages covering all six critical locations on the right side of the tail during the scheduled down time. These gages would provide detailed stress information for these locations. Grumman was contracted to perform stress analyses for each location and used flight test data from the new gages to calibrate their analyses. Flight 55 was the first flight after the installation of the gages and was flown at low AOA to obtain less dynamic strain data for calibration purposes. Flight 57 was the next flight in which a 25 second buffet event ocurred at high AOA. Table 1.0 shows the maximum strains and calibrated knotch stresses for these flights. As can be seen in Table 1.0, the initial assumption that location 4 was the most critical location was incorrect. In fact, applying the rule-of-thumb that the difference in crack growth life is approximately equal to the cube of the stress ratio

results in a factor of 27 between the life at location 4 compared with location 2. Location 2, which is just above the drag chute bracket, is non-inspectable in practice since blind fasteners must be drilled out for inspection. A detailed view of location 2 is given in Figure 3.0. Grumman engineers performed both crack initiation and crack growth analyses for location 2 using the 25 second buffet event. Constant load amplitude test data for 2024-T851 aluminum (X-29 tail material) coupons with open holes were also available from Grumman. These data provided cycles to failure at several load levels. Since Grumman is primarily a Navy contractor, their aircraft are generally certified by crack initiation analyses. Since the Air Force requires damage tolerance analysis for safety of flight, MODGRO was used to determine an initial corner crack size that would yield a predicted life matching the Grumman test data. The resulting initial crack length was 0.01 inch for the 2024-T851 aluminum skin material. This size also happens to be the same as the generally accepted size defining crack initiation. This was pure coincidence since a much smaller initial crack size is usually required to predict total life with crack growth analysis alone. However, this material is relatively brittle and Grumman had also predicted a short initiation time for the flight #57 buffet event. In lieu of any inspection of location #2, an initial 0.01 inch x 0.01 inch initial corner crack was assumed at the lower fastener hole (see Figure 4.0). Since all locations on the vertical tail are matched on both the left and right side, the event in flight #57 was also inverted to model the loads on both sides of the tail. The mean stress is rarely zero, probably due to the fact that at various AOA, left or right rudder are applied to maintain heading or perhaps the vortices favor one side over the other. The strain trace from flight #57 is given in Figure 5.0. The minimum crack growth life from the initial flaw size was predited to be 330 repeats of the buffet event seen in flight #57 (Figure 6.0). After more discussions between Air Force, Grumman, and NASA, a life of 165 repeats of the event seen in flight #57 was decided in order to provide a safety factor of two (2) for the analysis. Time in buffet prior to flight #57 was counted by using the flight 57 event, correlation between max stress at location #2 and fin tip acceleration, maximum stress ratio between previous events and flight #57, and the time spent in buffet in the previous flights. Once the correlation between stress at location 2 and fin tip acceleration was determined, the equivalent time in buffet (based on flight #57) for each previous flight was determined as follows:

Max Stress 3

Equivalent Time = (-----) x Time in Buffet
Flight #57 Max Stress

A review of previous flight test records resulted in approximately 45 equivalent buffet events up to flight #57. Therefore, after flight #57, approximately 30% of the tail life was used.

A special version of MODGRO was supplied to NASA/Dryden to be used to predict crack extension using actual flight test data. Between flight days, buffet stress data is down loaded to a IBM compatible PC and crack growth predictions are made using both the given and inverted version of the stress spectrum. Crack growth is predicted from the last predicted crack size and each spectrum is input twice to provide the safety factor of

two (2) on life. The most conservative prediction is then used as the new crack size. To provide a metric for percent of life expended, the crack growth curve for flight #57 was used as a reference in that the number of repeats of the flight #57 event corresponding to the current crack size was divided by the life (330 repeats). At present, the aircraft is nearly at 100% of the predicted life. The X-29 was scheduled to end it's flight test program by 1 Oct 1991, but it has been decided to continue to use the aircraft to study the potential of vortex flow control to suppliment the vertical tail yaw control. Work is currently underway to rework certain fastener holes at location #2 by drilling out the old fasteners, eddy current inspecting the holes, reaming out a 0.03 inch radius, re-inspecting, coldworking, and re-installing interference fit fasteners. The Wright Laboratory Fatique and Fracture Facility is performing tests on cold-worked and non-cold-worked fastener specimens supplied by Grumman to verify the life extension for this rework. Grumman is also providing analysis support to determine the number of fasteners to rework at location #2 and will examine the possible impact of a life extension at other locations on the tail.

### CONCLUSIONS

The X-29 demonstrator aircraft was not designed using damage tolerance requirements, but after the tail buffet problem was discovered, it was possible to employ the damage tolerance philosophy to provide a means to continue it's mission safely. Without the use of damage tolerance analysis methods, it is extremely doubtful that the responsible organizations (NASA, Air Force, and Grumman) would have continued operations under high AOA conditions. Although location #4 was not the most critical location, the use of a conservative initial approach quickly led to the discovery of the high knotch stress at location #2. The subsequent detailed analysis of location #2 provided a means to manage future flights. The Air Force and NASA used MODGRO as a tool to manage the X-29 test program after flight #57. More severe flights were conducted earlier than they would have been and experience gained from certain maneuvers allowed them to be modified or deleted to complete other important tests of the aircraft. It is very difficult to quantify the success of the damage tolerant design philosophy by pointing out aircraft that have not experienced a structural failure. However, it's use in the X-29 test program has clearly been invaluable.

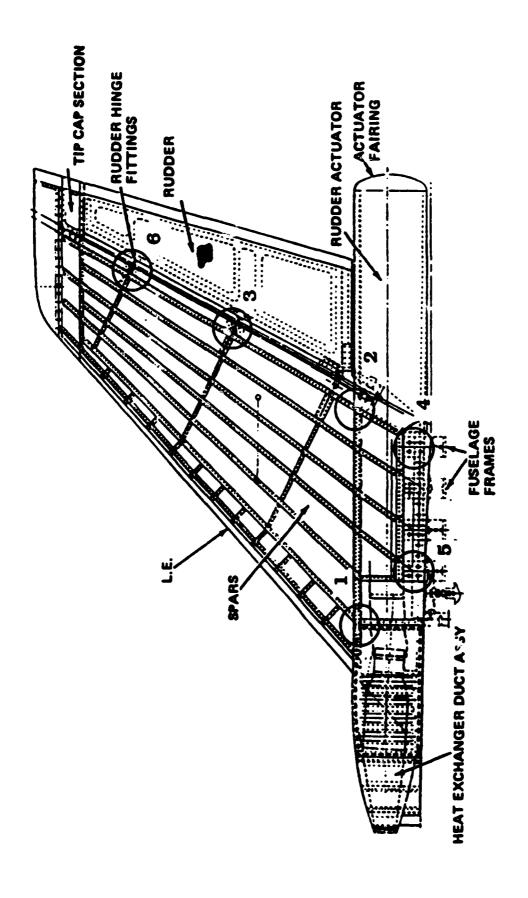
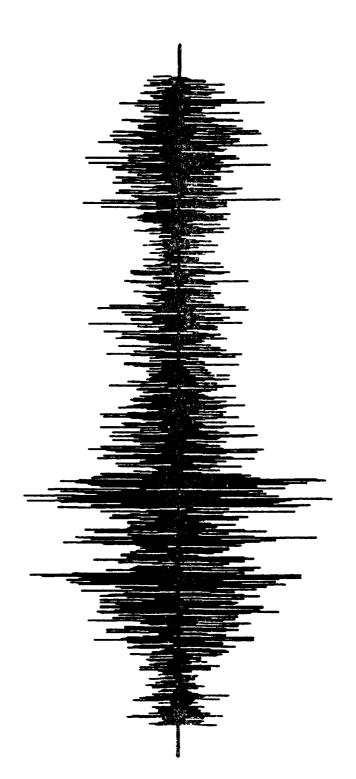


Figure 1.0 : Vertical Tail Critical Locations



1025 Cycles 15 Second Event 68.3 Cycles/Second

Figure 2.0 : Flight #42 Fin Tip Accelerometer

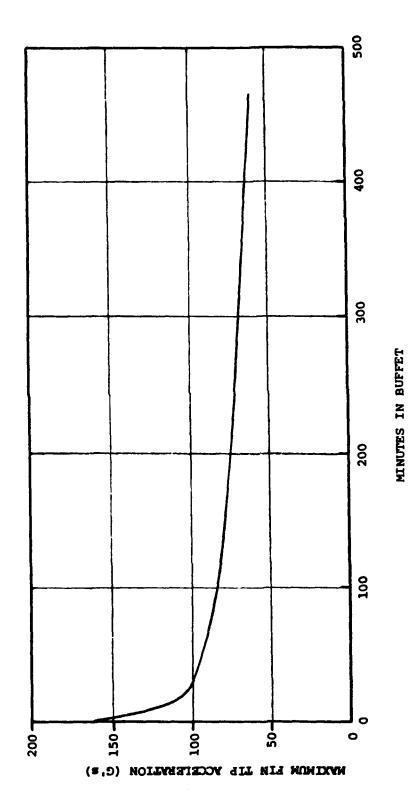


Figure 3.0: Aft Pedestal (Location 4) Crack Growth Life

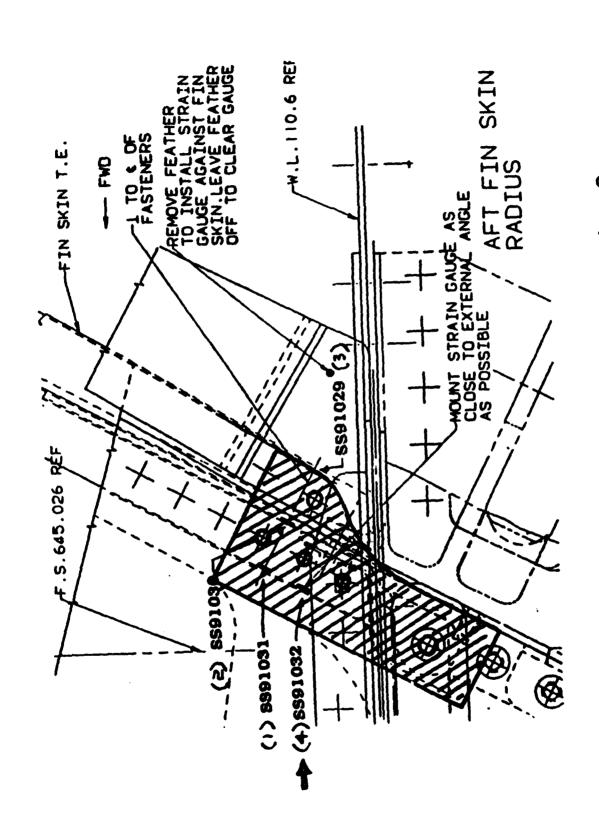
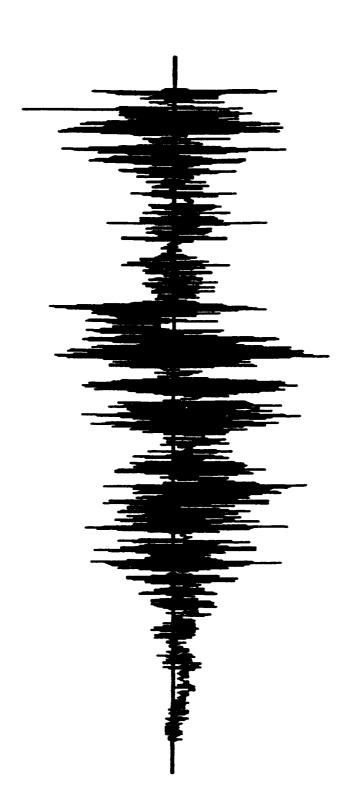


Figure 4.0 : Detailed View of Location 2



532 Cycles 25 Second Event 21.3 Cycles/Second

Figure 5.0 : Flight #57 Strain Gage 91032 Trace

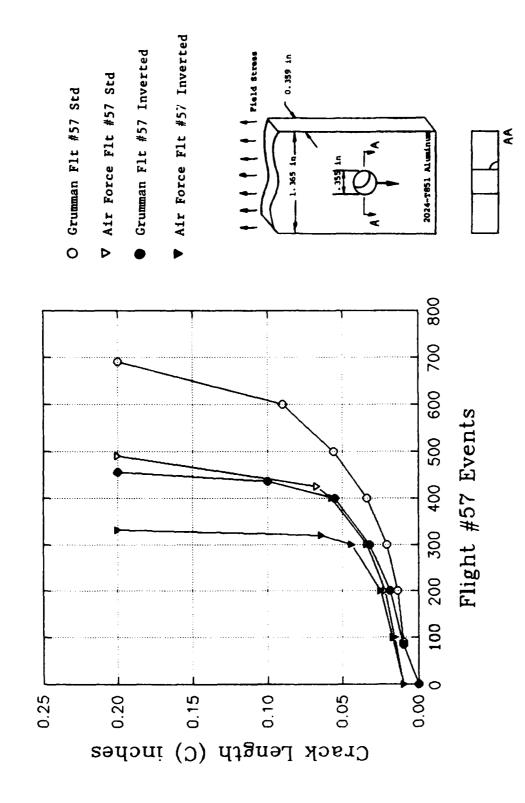


Figure 6.0 : Total Life at Location 2

TABLE 1.0 X-29 Flight Test Results

Location	Str Gage	· ·	ro-inch) Flt 57	
				(1100)
Fwd Skin	91033	680	700	
Radius	91034	610	600	16.1
(1)	91035	580	600	
Aft Skin	91029	170	600	
Radius	91030	820	1500	
(2)	91031	900	1500	77.5
	91032	1160	2000	
Mid Rudder	91026	300	1200	
Hinge	91027	400	1200	19.0
(3)	91028	500	1300	
Aft	91037	650	700	
Pedestal	91038	620	700	24.4
(4)	91039	520	800	
Fwd Pedestal	91040	590	500	
(5)	91041	980	850	17.9
Upper Hinge	91024	290	900	
(6)	91025	200	700	32.0

### A Case History for Assessing Dynamic Environment on the SRAM T Missile



1991 United States Air Force Structural Integrity Program Conference San Antonio, Texas 3-5 December, 1991

W.F. Buckey, Jr. ASD/YGEF WPAFB

A Case History for Assessing Dynamic Environment on the SRAM T Missile

ASIP SLIDES: By William F. Buckey, Jr

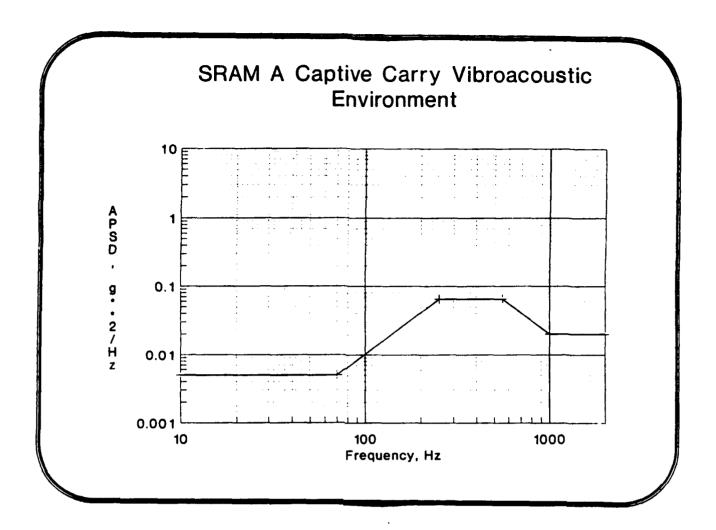
SLIDE 1.) Title Page: Good afternoon, everyone! My name is Bill Buckey and I work in the area of Structural Loads & Dynamics for the Aeronautical Systems Division at Wright Patterson AFB. My paper is entitled: A Case History for Assessing Dynamic Environment on the SRAM T Missile. The goal of this paper is to document the thought process and method used to predict the (current) environment on the SRAM T missile. This environmental data would have been used to redesign the structure, if necessary, and also to assess the risk associated with the program.

### Intro to the SRAM II/T Program

**A Short Program History** 

- * The new generation Short Range Attack Missile (SRAM II) was developed as a replacement for the aging SRAM A currently in use by the USAF. The SRAM II Program was in FSD preparing for the Critical Design Review when the President cancelled the program.
- * In the Fall of 1988 the program began studying a tactical variant of the SRAM II known as the SRAM T. SRAM T was approved by the Defense Acquisition Board in December 1989 and began full scale development in April 1999.
- * The idea was to make as little change as possible to the baseline SRAM II missile. The major changes made were to the warhead and software.
- * The SRAM T system was scheduled for delivery to the Tactical Air Forces in August 1997.

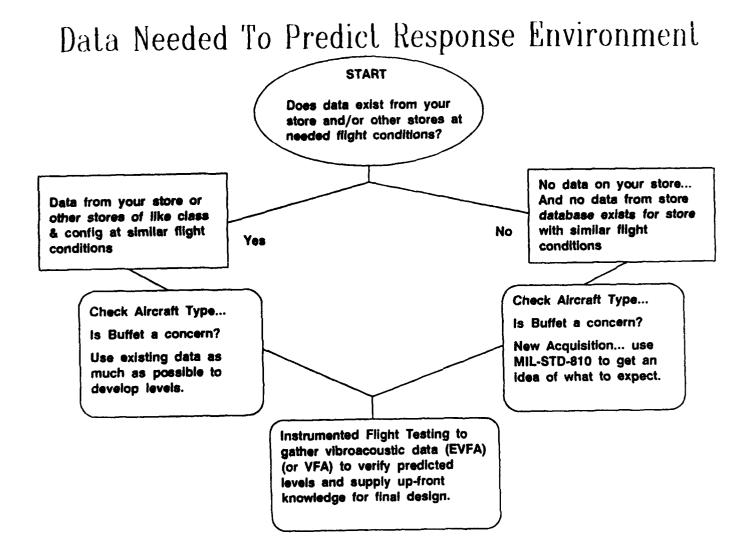
SI.IDE 2.) Intro to the SRAM II/T Program: The new generation Short Range Attack Missile (SRAM II) was developed as a replacement for the aging SRAM A currently in use by the USAF. In the Fall of 1988 the program office began studying a tactical variant of the SRAM II known as the SRAM T. In December of 1989 the Defense Acquisition Board approved the SRAM T program and full scale development began in April 1990. The goal of the program office was to solve the Tactical Air Command's procurement problem by converting the internal carriage SRAM II into an external-carriage "tactical" version with as few changes as possible to the baseline missile. (The major portion of the modification involved replacing the warhead and software). SRAM T was scheduled for delivery to the Tactical Air Forces in August 1997. As you may already know, the President cancelled the SRAM II program in early Fall of this year.



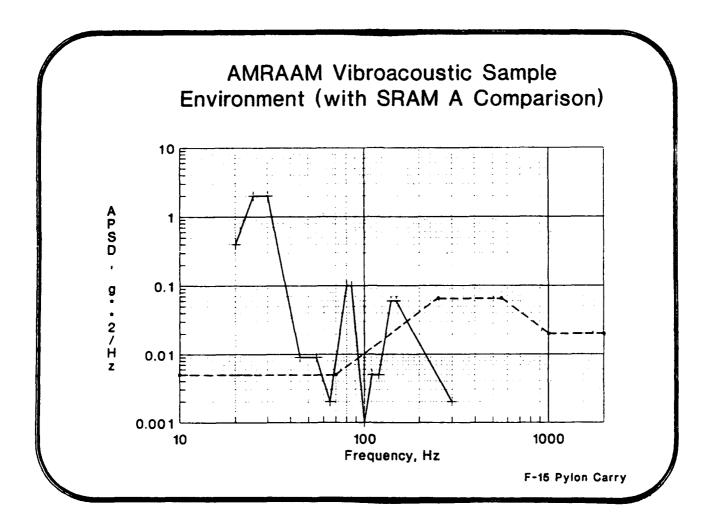
SLIDE 3.) SRAM II Vibration levels: I would like to start off with a chart showing SRAM II vibration levels that were originally derived (adopted) from SRAM A levels. The SRAM A is very similar to the SRAM II (being the same approximate size & weight). The SRAM A was initially designed for internal and external carriage on the B-52G/H and FB-111. Later the SRAM A was certified for carriage on the B-1B with no change to the spec vibration level. The SRAM II was designed for internal carriage and deployment on the Strategic Air Command's B-1B and B-2 aircraft.

F-15E/SRAM T Photos On This Page

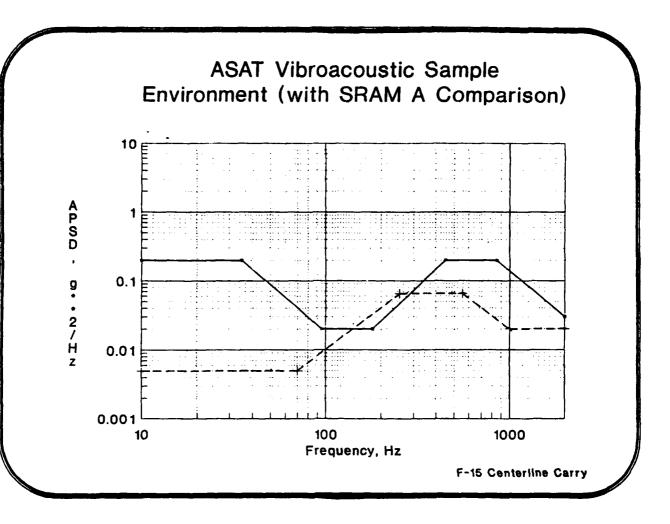
SLIDE 4.) Now the SRAM T Case. The idea here was to satisfy TAC's need for a new tactical missile with very little or no change to the baseline SRAM II missile. The new problem turns out to be: to what level would the SRAM T need to be designed in order to survive the vibroacoustic environment on the F-15E wing and fuselage stations. Our problem here was similar to that of a new store in that we needed to determine what the response of our missile would be in captive flight on the F-15E. This problem is especially significant due to the fact that the F-15's ability to generate severe buffet during maneuvers has caused serious problems on other stores. (slide 4 = Photo of F-15E/SRAM T: station #8)

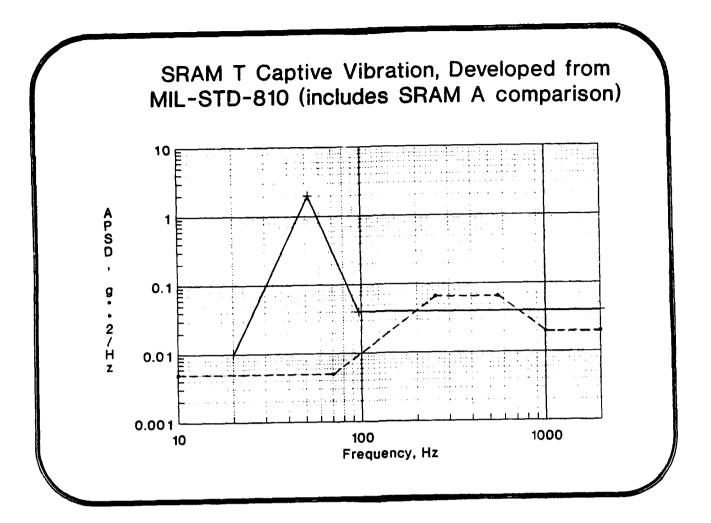


SLIDE 5.) Data needed to predict the response environment. To start the process of gathering data needed to predict the vibroacoustic response of a store like the SRAM T, one must look at whether some (or any) data exists on the store or even data on a similar store (of course at the same flight conditions). A new store with no data from similar or previous type stores is a challenge which requires use of MIL-STD-810. After determining whether the aircraft in question will be able to generate significant buffet, one would then use MIL-STD-810 to get a rough estimate of the vibroacoustic environment. A very worthwhile document that evaluates the methods and practices for qualification and certification of air-launched weapon systems during captive carriage has recently been made available as a Technical Report (TR-90-15) from Amold Engineering Development Center (AEDC), Amold AFB. Tennessee (slide 5 = PP flow chart on procedure for determining environment)

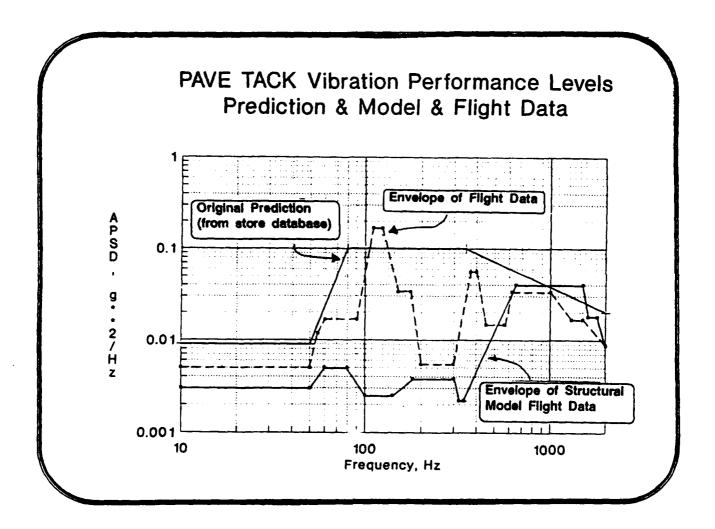


SLIDE 6.) TWO SLIDES: F-15/AMRAAM & F-15/ASAT, Examples of levels from other systems on the F-15E. Since our situation involves a buffet environment, we must stick with stores that have had experience on a buffet producing aircraft. We were able to concentrate on the F-15 due to the large amount of data available. AIM-7 and AIM-9 problems first introduced the community to what effect the buffet environment could really have on a store. We were fortunate to have levels from recent AMRAAM flight testing. Even though AMRAAM was not a very similar store, it was still a useful tool in providing an idea of what was to come. ASAT was a SRAM A derivative store that was flight tested on the F-15 centerline. Data gathered on ASAT was limited but did provide a look into store response on the centerline. These data helped us justify the flight test program to management. (slide 6 = samples of centerline & wing levels... note two slides)

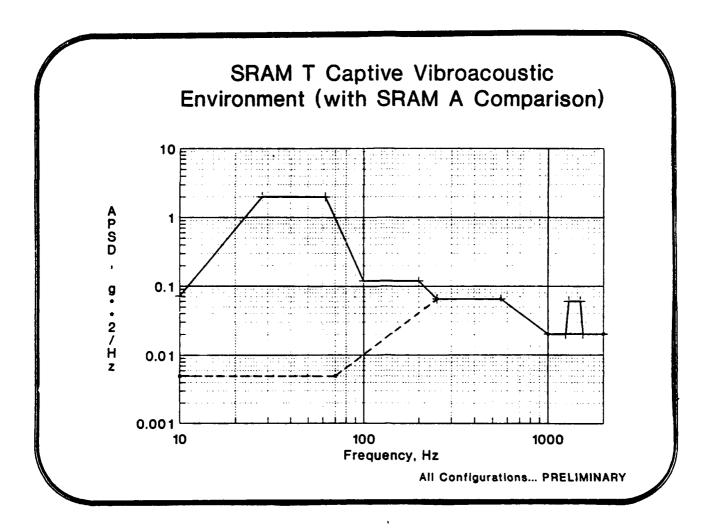




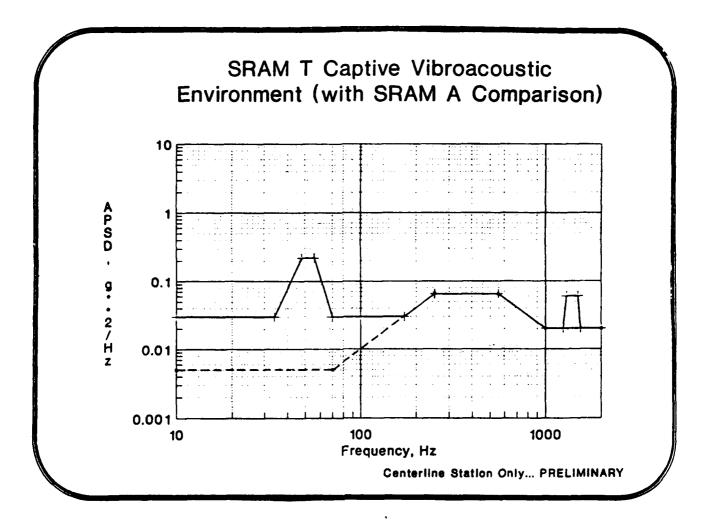
SLIDE 7.) MIL-STD-810 Method for predicting response environment: Method 514.3 Category 7A, allows a rough estimate of levels seen by stores carried externally. The big thing to note here is that the levels provided give a reasonable first-cut to the cycle of predicting store response. The levels shown here are those compiled for SRAM T using the guidelines in MIL-STD-810. (both HI & Low in one)



SLIDE 8.) PAVE TACK Example: This is a program from the mid seventies that was able to "do the right thing" when predicting the environment. This program and others like it formed the basis for conducting the early flight testing on the SRAM T instrumented vehicle. Pave Tack was a centerline only carry on both the F-4E and F-111A and was successful because an updated store configuration was flown at different stages of the program to verify the missile predicted environment. They also flew to the extremes of the aircraft envelope. The vibration specs were rewritten each time, but that was alright because it was early in the program and ECP's could be employed to change the criteria for pre-production and production.



SLIDE 9.) TWO SLIDES: SRAM T Levels from instrumented flight test: Our Early flight Test Program (EVFA) produced some very high levels for the conditions flown. On this chart is an envelope of the flight data measured during the EVFA. Responses below 100 HZ are due mostly to buffet on the wing (station 5&8). Centerline levels were much lower than those at the wing station. The largest centerline levels came from a nose-wheel down condition that occurred at a specific dynamic pressure on the approach to landing condition. (two levels: one all configurations & one centerline only.



### **SRAM T Flight Test Program**

Schedule, Planning, & Summary

### Flight Test Schedule & Planning

- * Early planning began Aug 89 with Technical Interchange Meetings followed by monthly Test Planning & Working Group Meetings.
- * SRAM T FSD Contract finalized July 1990
- * Flight Testing scheduled to begin Sept 15th & actually started Nov 5th, 1990

### **Test Summary**

- * Scheduled 12 Test Flights, test points broken into 3 Phases
- * An additional flight was included to cover a fins-deployed flight regime.
- * 13 Test Flights were accomplished (11/5/90 4/29/91), (6 months)

108 Test Points Flown ... (from 3 Phases)

48 Vibroacoustic, (Phase 1)

36 Moderate Buffet Points, (Phase 2, 1-3 G's)

24 Heavy Buffet Points, (Phase 3, 3-5 G's)

- * Non-production piece of the suspension structure determined to be fatigue critical and monitored throughout the flight test program. Total of 93% life consumed during the testing.
- * Observed different buffet response on the wing compared to centerline.

SLIDE 10.) Flight Test Program: Early planning for our flight test program started in Aug of '89 followed by monthly Test Planning & Working Group Meetings (TPWG). The SRAM T FSD Contract was finalized July 1990 and flight testing was scheduled to begin Sept 15th. Schedule problems didn't allow us to start actual flight testing until Nov 5th. 1990. Summary: We originally scheduled 12 flights, broken into 3 phases. An additional flight was included to cover a fins-deployed flight regime. 108 test points were flown (see breakdown). A non-production piece of suspension structure (an aluminum attach lug) was determined to be fatigue critical and monitored throughout the flight test program. A total of 93% of the component life was consumed during the testing. Missile response was markedly different on the wing as compared to the centerline station. Vibroacoustic levels from straight & level flight were lower than expected. Wing station buffet was very heavy and created extreme vibrations on the internal components of the missile.

### SRAM T Conclusions & Lessons Learned

General Advice on the Conduct of a Timely Early Vibroacoustics Flight Test

### **Good Points:**

- * Technical Interchange Meetings (TIM) began early & were followed by monthly Test Planning & Working Group (TPWG) meetings. These meetings involved all pertinent participants to discuss ideas and plan details of the test.
- * Involved all parties to write a very thorough test plan: Team Approach

### **Bad Points:**

- * Number of flight test points was limited due to a fatigue critical part in the suspension structure.
- * Unknowns involved in predicting fatigue life remaining (through use of critical telemetered data points) created a slow test schedule near the end of testing.
- * Gathering & Data reduction problems early in the flight test program made the program slip approx 4 months. Attributed to: tape speed & cross talk.

SLIDE 11.) Conclusions & Lessons Learned: This chart is intended to pass along some advice and general warnings on the conduct of a timely Early Vibroacoustic Flight Test. The basic idea here is that an early assessment of the vibration environment allows for a properly designed store. The first four bullets on this chart are general rules to follow for a successful test program (we had these conclusions in mind early on in the test program): A vibroacoustic instrumented flight test vehicle should be flown as early as possible in the program. This flight test vehicle should be as close to the production model as possible and be properly instrumented. And assure that the flight conditions proposed are similar to those of an operational mission. The last two bullets are items that were very critical to the success of our program (these items were learned as we progressed through the program): Interchange Meetings were started early (about one year in advance of the planned testing) and then continued on a monthly basis as Test Planning & Working Group meetings. These meetings were especially significant due to the fact that they involved the entire community...aircraft & store contractors, aircraft & store Programs Offices, Test Organizations from Edwards AFB, and store certification people at Eglin AFB. With all of these organizations kept in the loop technically, details & plans for the test program were made suitable to everyone. This Team Approach was a key in our success. Data gathering and reduction problems were not really anticipated in our program, but really caused a major delay in our program (a 2 month slip in gathering useful data!). Advice here would be to anticipate these type of problems and do the best you can.